

TECHNICAL REPORT 02-06

Project Opalinus Clay

Models, Codes and Data for Safety Assessment

Demonstration of disposal feasibility
for spent fuel, vitrified high-level waste
and long-lived intermediate-level waste
(Entsorgungsnachweis)

December 2002

TECHNICAL REPORT 02-06

Project Opalinus Clay

Models, Codes and Data for Safety Assessment

Demonstration of disposal feasibility
for spent fuel, vitrified high-level waste
and long-lived intermediate-level waste
(Entsorgungsnachweis)

December 2002

This report was prepared by a project team consisting of (in alphabetical order): Peter Gribi (Vibro-Consult AG, Brugg), Richard Klos (Aleksandria Sciences, UK), Georg Kosakowski (Paul Scherrer Institut, Villigen), Gerhard Mayer (Colenco Power Engineering AG, Baden), Peter Robinson (Quintessa Ltd., UK), Paul Smith (Safety Assessment Management Ltd., UK), with contributions from many other individuals. The figures were prepared by Bruno Kunz and Claudia Frei (Nagra). The project was managed by Jürg Schneider and Piet Zuidema.

ISSN 1015-2636

"Copyright © 2002 by Nagra, Wetingen (Switzerland) / All rights reserved.

All parts of this work are protected by copyright. Any utilisation outwith the remit of the copyright law is unlawful and liable to prosecution. This applies in particular to translations, storage and processing in electronic systems and programs, microfilms, reproductions, etc."

Summary

The present report is designed to provide readers with the necessary information to perform, if they so wish, independent checks of the results of the evaluation of the "assessment cases" described in the Safety Report (Nagra 2002c) for Project *Entsorgungsnachweis*. It also describes the conceptual models and corresponding codes for the near field, geosphere and biosphere that were used in the safety assessment to evaluate the assessment cases, including the reasons why they are considered adequate for their intended purposes, and the operational elements and procedures that were used to manage the required large number of calculations. Models and codes not described in this report are the *supporting models* used to derive parameter values for the near field, geosphere and biosphere codes, and to support model assumptions. These include, for example, groundwater flow models, mechanistic models of sorption, temperature evolution models, waste dissolution models, etc., and are described in the Project *Entsorgungsnachweis* reference reports.

An assessment case is a specific set of assumptions regarding the broad evolution of the repository and its environment, the conceptualisation of individual features, events and processes (FEPs) relevant to the fate of radionuclides within the disposal system and the parameters used to describe these FEPs. In the safety assessment, a broad range of assessment cases is analysed in order to illustrate the impact of various detrimental FEPs and uncertainties on the level of safety provided by the disposal system. The assessment cases are defined, the underlying reasoning documented and the results of their analysis presented in the Safety Report. In the interests of transparency, the Safety Report presents these descriptions in a mainly qualitative fashion, without exhaustively documenting all relevant formulae and data. The present report complements the Safety Report with a comprehensive description of models, codes and data and thus provides traceability within the safety assessment. The two reports together satisfy the *assessment principle* (see Chapter 2 of the Safety Report) that the development of the safety case and its results should be documented in manner that provides both transparency and traceability.

In the safety assessment for Project *Entsorgungsnachweis*, assessment cases are divided into a number of groups, according to the issues or uncertainties that they address. The main part of the present report focuses, in turn, on groups of assessment cases that explore:

- the consequences of particular *scenario*, *conceptual* and *parameter* uncertainties, where this range can be bounded with reasonable confidence on the basis of available scientific understanding,
- more speculative "what if?" possibilities that are considered in order to test the robustness of the disposal system,
- various design or system options, and
- different stylised possibilities for the characteristics and evolution of the surface environment ("biosphere").

Overviews are given of the conceptual models underlying the assessment cases and the various assumptions and simplifications that are made in order to arrive at sets of mathematical equations and input parameters so that each case can be evaluated using corresponding computer codes, with references to appendices that give detailed descriptions of the codes and the equations that they solve, as well as tables containing the data used and the data source. In the appendices, descriptions are given of the capabilities of each code in terms of the phenomena (or "Super-FEPs") that they address. This is important within the FEP management procedure to allow an evaluation of the suitability of a given code to address a given Super-FEP

(Nagra 2002d). It is shown that the codes used are sufficiently versatile to evaluate all the required assessment cases. There are a few safety-relevant phenomena that the codes are not "qualified" to evaluate, but, in all cases, either significant effects can be ruled out by supplementary studies (e.g. for criticality), effects are intrinsically favourable to safety and can be conservatively neglected (e.g. transport resistances in the SF / HLW near field), or parameters (e.g. canister breaching time) can be chosen to ensure that calculations err on the side of pessimism.

In addition to the models and codes used to analyse the assessment cases, simplified *insight models* are used to examine particular aspects of system performance and sensitivity to key system properties and model assumption. The insight models are described in Chapter 9.

The deterministic evaluation of assessment cases is complemented by probabilistic calculations to build further system understanding and, in particular, to indicate the performance of the system for parameter combinations not analysed by deterministic calculations. The computational tool used to sample input parameters from probability density functions (PDFs) and the PDFs themselves are described in Appendices 2 and 3, respectively.

Except for a few cases, no justifications are given in the present report for the model assumptions made and no final or intermediate results are presented, except where this is considered to help understanding. For a full presentation of results and a justification of assumptions, the reader is referred to the Safety Report and the reference reports.

It is, however, noted that all assessment cases are evaluated using, to some extent, pessimistic or conservative conceptual assumptions, parameters and model simplifications, resulting in calculated doses that should be regarded as upper bounds for, rather than predictions of, expected doses. To assess the degree of bias introduced by such assumptions, the modelling approaches used to evaluate each assessment case are examined systematically in Chapter 10. It first summarises the various assumptions and simplifications made in order to arrive at sets of mathematical equations and input parameters so that each case can be quantitatively evaluated, and then it assesses these assumptions and simplifications in terms of their degree of realism, pessimism or conservatism. This information is then used as a tool to systematically assess the bias that has been introduced into the models ("bias audit").

Zusammenfassung

Der vorliegende Bericht hat zum Ziel, alle Informationen zu dokumentieren, die für den unabhängigen Nachvollzug der in Nagra (2002c) enthaltenen Resultate aller Rechenfälle für das Projekt Entsorgungsnachweis notwendig sind. Er beschreibt die konzeptuellen Modelle und entsprechenden Rechencodes für das Nahfeld, die Geosphäre und die Biosphäre, die in der Sicherheitsanalyse für die Durchführung der Rechenfälle Verwendung fanden, sowie die in der Datenverarbeitung der grossen Anzahl durchzuführender Rechenfälle benutzten Werkzeuge. Der Bericht nennt ferner die Gründe, wieso die eingesetzten Rechencodes als für den vorgesehenen Verwendungszweck geeignet gelten. Nicht im vorliegenden Bericht dokumentiert sind die Modelle und Rechencodes, die für die Herleitung von Parameterwerten für die Nahfeld-, Geosphären- und Biosphären-Rechencodes und für die Begründung von Modellannahmen Verwendung fanden. Hierzu gehören zum Beispiel Grundwassermodelle, mechanistische Sorptionsmodelle, Temperaturverlaufsmodelle und Abfallauflösungsmodelle. Diese Modelle und Rechencodes sind in den Referenzberichten des Projekts Entsorgungsnachweis beschrieben.

Ein Rechenfall ist definiert durch die spezifische Konzeptualisierung bestimmter Vorgänge und Ereignisse (abgekürzt mit der englischen Bezeichnung FEPs für „features, events and processes“), die für den Verbleib der Radionuklide im Lagersystem relevant sind, sowie durch die in der Modellierung dieser FEPs benutzten Parameter. In der Sicherheitsanalyse werden neben dem Referenzfall eine breite Palette von Rechenfällen mit dem Ziel untersucht, den Einfluss von ungünstigen FEPs und Ungewissheiten auf die Sicherheit des Lagersystems zu illustrieren. Die Definition der Rechenfälle, die Dokumentation der zugrundeliegenden Argumentation und die Präsentation der Resultate der Analyse erfolgt im Sicherheitsbericht.

In der Sicherheitsanalyse für das Projekt Entsorgungsnachweis werden die Rechenfälle gemäss dem Typ der untersuchten Fragestellung oder Ungewissheit gruppiert. Der Hauptteil des vorliegenden Berichts befasst sich, in dieser Reihenfolge, mit den Rechenfall-Gruppen zur Untersuchung

- der Konsequenzen von bestimmten Ungewissheiten in Bezug auf Szenarien, Konzeptualisierungen und Parametern, deren Schwankungsbereich sich aufgrund des vorhandenen wissenschaftlichen Verständnisses hinreichend zuverlässig eingrenzen lässt,
- von spekulativen Möglichkeiten (englisch „what if?“ possibilities), die auf das Testen der Robustheit des Lagersystems abzielen,
- von Auslegungs- und System-Optionen,
- verschiedener stilisierter Möglichkeiten der Erscheinungsformen und Entwicklungen der Erdoberfläche (Biosphäre).

Zu Gunsten der Transparenz erfolgt diese Beschreibungen im Sicherheitsbericht in qualitativer Art, d.h. ohne mathematische Gleichungen und unter Verzicht auf eine vollständige Dokumentation aller Eingabeparameter. Der vorliegende Bericht ergänzt den Sicherheitsbericht mit einer umfassenden Beschreibung von Modellen, Rechencodes und Daten und gewährleistet damit die Nachvollziehbarkeit der Sicherheitsanalyse. Zusammen erfüllen diese zwei Bericht das Prinzip der Transparenz und Nachvollziehbarkeit der Dokumentation des Sicherheitsnachweises, wie im Kap. 2 des Sicherheitsberichts gefordert.

Der vorliegende Bericht enthält Beschreibungen der konzeptuellen Modelle, auf denen die Rechenfälle basieren, sowie der getroffenen Annahmen und Vereinfachungen bei der Ableitung der mathematischen Gleichungssysteme und Eingabeparameter, die eine Behandlung der Rechenfälle mit den entsprechenden Rechencodes erlauben. Detaillierte Beschreibungen der

Rechencodes, unter Angabe der zu lösenden mathematischen Gleichungssysteme, und deren Eingabeparameter sind in den Berichtsanhängen enthalten. Besonderes Augenmerk wird aus Sicht des FEP-Managements auf die Anwendungsbereiche der Rechencodes in Bezug auf die modellierbaren Phänomene („Super-FEPs“) gelegt. In Nagra (2002d) wird gezeigt, dass alle identifizierten Rechenfälle mit den verfügbaren Rechencodes in geeigneter Art und Weise analysiert werden können (Eignung der Rechencodes). Einige wenige sicherheits-relevante Phänomene sind mit den verfügbaren Rechencodes nicht angemessen behandelbar. Ergänzende Studien zeigen aber, dass die damit verbundenen Effekte entweder unbedeutend sind (z.B. Kritikalität) oder sich günstig auf die Lagersicherheit auswirken und deswegen konservativ vernachlässigt werden dürfen (z.B. residualer Transportwiderstand der BE/HAA-Behälter nach dem Zeitpunkt ihres Versagens), oder aber es lassen sich Parameterwerte wählen (z.B. Zeitpunkt des Versagens der BE/HAA-Behälter), die gewährleisten, dass die damit erzielten Resultate auf der pessimistischen Seite liegen.

Zusätzlich zu den Modellen und Rechencodes, die bei der Analyse der Rechenfälle zur Anwendung gelangen, wurden vereinfachte Modelle (englisch „insight models“) entwickelt, die das Verständnis spezieller Aspekte des Systemverhaltens verbessern und die es erlauben, Sensitivitäten in Bezug auf Schlüsseigenschaften des Lagersystems oder Modellannahmen aufzuzeigen. Diese vereinfachten Modelle sind im Kapitel 9 beschrieben.

Die deterministischen Untersuchungen der Rechenfälle werden ergänzt durch probabilistische Modellrechnungen. Diese zielen auf ein vertieftes Systemverständnis ab und gewähren einen systematischen Einblick in das Systemverhalten auch für diejenigen Parameterkombinationen, welche durch die deterministischen Modellrechnungen nicht abgedeckt sind. Das verwendete Rechenwerkzeug zur Stichprobenentnahme und die Verteilungsfunktionen sind in den Anhängen 2 und 3 beschrieben.

Die Begründung von Modellannahmen und die Präsentation von Zwischen- und Endresultaten sind nicht Bestandteil des vorliegenden Berichts, ausser wenn dies für das Verständnis der Ausführungen erforderlich ist. Die umfassende Dokumentation der Resultate und die Begründung der Modellannahmen sind im Sicherheitsbericht und in den Referenzberichten zu finden.

Zum Schluss sei darauf hingewiesen, dass alle Rechenfälle teilweise, aber in unterschiedlichem Ausmass, auf pessimistischen oder konservativen Modellannahmen, Parametern und Vereinfachungen beruhen. Um den so eingeführten Grad an Realitätsabweichung festzuhalten, wurden die Modellannahmen systematisch und für jeden Rechenfall individuell auf ihre Realitätsnähe geprüft (Kapitel 10). Dazu wurden die unterschiedlichen Modellannahmen und Vereinfachungen zur Herleitung der mathematischen Gleichungen und Eingabeparameter eines jeden Rechenfalles aufgelistet und sodann auf ihren Grad an Realitätsnähe (realistisch, pessimistisch, konservativ) beurteilt. Diese Informationen dienen als Werkzeug zur systematischen Erfassung der in den Modellen enthaltenen Realitätsabweichung (englische Bezeichnung dieses Prozesses: „bias audit“).

Résumé

Dans ce rapport, le lecteur trouvera l'information lui permettant, s'il le souhaite, de procéder à une vérification indépendante des résultats obtenus pour l'analyse des "situations" (en anglais *assessment cases*, littéralement "cas sur lesquels porte l'évaluation") présentées dans le rapport sur la sûreté radiologique à long terme (*Safety Report* ou Rapport de sûreté, Nagra 2002c), rédigé dans le cadre du projet *Entsorgungsnachweis* sur la démonstration de la faisabilité du stockage géologique. Le présent rapport décrit également les modèles conceptuels et les codes correspondants utilisés dans le cadre de l'analyse de la sûreté pour évaluer les différentes "situations" dans le champ proche, la géosphère et la biosphère. Il justifie le choix de ces codes et modèles, et présente les éléments et procédures opérationnels mis en oeuvre pour gérer l'important volume de calculs nécessaires. En revanche, ce rapport ne traite ni des modèles et codes utilisés pour déduire les paramètres pour le champ proche, la géosphère et la biosphère, ni de ceux sur lesquels reposent les hypothèses de modélisation – tels que par exemple les modèles concernant la circulation des eaux souterraines, les modèles mécanistiques de sorption, les modèles concernant l'évolution de la température, la dissolution des déchets, etc., qui sont présentés dans les rapports annexes du projet *Entsorgungsnachweis*.

Une "situation" est caractérisée par (a) la conceptualisation spécifique d'événements et de processus particuliers (en anglais *Features, Events and Processes* ou FEP) relatifs au comportement des radionucléides dans le système de dépôt, et (b) par les paramètres utilisés pour quantifier ces FEP. L'analyse de la sûreté prend en compte, outre la Situation de référence (en anglais *Reference Case*), une large gamme de situations qui permettent de montrer dans quelle mesure la sûreté à long terme du dépôt peut être affectée par différents FEP potentiellement néfastes, ou encore par les incertitudes qui subsistent. Le Rapport de sûreté comprend la définition des différentes situations, le détail des raisonnements et les résultats de l'analyse.

Dans l'analyse de la sûreté pour le projet *Entsorgungsnachweis*, les situations sont réparties en plusieurs catégories, selon le type de question ou d'incertitude abordée. La majeure partie du présent rapport est consacrée à des groupes de situations qui concernent:

- les conséquences de certaines incertitudes spécifiques relatives à des *scénarios*, des *conceptualisations* ou des *paramètres*, dans les cas où les connaissances scientifiques actuelles permettent d'estimer la marge d'incertitude de manière suffisamment sûre,
- des possibilités de l'ordre de la spéculation ("qu'arriverait-il si...") prises en compte pour tester la robustesse du système de dépôt,
- des variantes relatives à l'architecture ou au système de dépôt,
- des variantes schématisées relatives aux caractéristiques et à l'évolution de l'environnement de surface (la "biosphère").

Par souci de transparence, les descriptions fournies dans le Rapport de sûreté sont essentiellement qualitatives, et ne contiennent ni les équations mathématiques, ni une documentation exhaustive de l'ensemble des données. Le présent rapport vient compléter le Rapport de sûreté en livrant une description détaillée des modèles, codes et données, et contribue ainsi à la traçabilité des résultats obtenus par l'analyse de la sûreté. Complémentaires, les deux rapports permettent de remplir les exigences de transparence et traçabilité, évoquées au chapitre 2 du Rapport de sûreté, qui conditionnent l'élaboration d'une démonstration de la sûreté et ses résultats.

Ce rapport fournit une vue d'ensemble des modèles conceptuels utilisés, ainsi que des diverses hypothèses et simplifications effectuées en vue d'obtenir des ensembles d'équations mathématiques et des paramètres d'entrée, de façon à ce que chaque situation puisse être évaluée en

utilisant les codes informatiques correspondants. Les annexes décrivent en détail les codes, ainsi que les équations auxquels ils sont destinés, et contiennent des tableaux présentant les données et leur provenance. Elles comprennent également une description de chacun des codes en fonction des phénomènes (ou "Super-FEP") auxquels il peut être appliqué. Ceci est un aspect important de la gestion des FEP, qui doit permettre d'estimer si un code donné est adapté au traitement de tel ou tel phénomène (Nagra 2002d). Il est démontré ici que les codes utilisés sont suffisamment souples pour traiter toutes les situations nécessaires. Il existe quelques phénomènes importants pour le traitement desquels les codes ne sont pas "qualifiés", mais dans chacun de ces cas, soit des études supplémentaires permettent d'exclure tout impact de quelque importance (p. ex. la criticité), soit les conséquences sont favorables en elles-mêmes et peuvent par conséquent être ignorées dans un souci d'adopter un point de vue "conservateur" (p. ex. la résistance résiduelle à la migration des radionucléides fournie par les conteneurs AC / DHA après leur perte d'étanchéité), soit enfin les paramètres (p. ex. la durée écoulée jusqu'à la perte d'étanchéité des conteneurs) peuvent être fixés de manière à ce que les calculs reflètent toujours une vision pessimiste des processus.

Outre les modèles et codes utilisés pour analyser les situations, des modèles simplifiés (en anglais *insight models*) ont servi à examiner certains aspects spécifiques du fonctionnement du système, et à faire apparaître des sensibilités particulières en rapport avec les propriétés principales du système ou avec des hypothèses de modélisation. Ces modèles simplifiés sont décrits au chapitre 9.

L'évaluation déterministe des situations est complétée par des calculs probabilistes afin d'améliorer encore la compréhension du système, et de mettre notamment en lumière ses performances en présence de combinaisons de paramètres non analysées par les calculs déterministes. L'outil informatique utilisé pour extraire les paramètres d'entrée des fonctions de densité de probabilité (pdf) et les pdf elles-mêmes sont décrites respectivement dans les annexes 2 et 3.

A quelques exceptions près, ce rapport fournit pas de justifications relatives aux hypothèses de modélisation et ne présente pas de résultats finals ou intermédiaires, sauf dans les cas où ces informations rendent les démonstrations plus compréhensibles. Pour une présentation détaillée des résultats et une justification des hypothèses, le lecteur se reportera au rapport principal (Rapport de sûreté) et aux rapports annexes.

Il faut enfin préciser que, pour l'évaluation de l'ensemble des situations, on a eu recours à des hypothèses conceptuelles, des paramètres et des simplifications de modèles qui étaient, pour une part plus ou moins grande, pessimistes ou conservateurs. Afin d'estimer l'écart ainsi obtenu par rapport à la réalité, les démarches de modélisation utilisées pour évaluer chaque situation sont passées systématiquement en revue au chapitre 10. Dans un premier temps, on énumère les différentes hypothèses et simplifications effectuées pour obtenir les ensembles d'équations mathématiques et les paramètres d'entrée, puis on estime leur degré de réalisme, de pessimisme ou de conservatisme. Ces informations sont ensuite utilisées pour effectuer ce qu'on appelle en anglais un *bias audit*, c'est-à-dire estimer de façon systématique dans quelle mesure les modèles divergent de la réalité.

Table of Contents

Summary	I
Zusammenfassung.....	III
Résumé	V
Table of Contents	VII
List of Tables.....	XVIII
List of Figures	XXVI
1 Introduction	1
1.1 The role of this report within Project <i>Entsorgungsnachweis</i>	1
1.2 Use of quantitative models in this safety assessment	2
1.3 Scope of this report.....	3
1.4 Organisation of this report.....	4
2 System to be modelled and Assessment Cases.....	7
2.1 Overview of the disposal system and the multi-barrier system.....	7
2.2 The list of assessment cases.....	13
3 The Reference Scenario.....	19
3.1 The Reference Conceptualisation	19
3.1.1 Overview	19
3.1.2 The conceptual model and its underlying assumptions	20
3.1.3 Codes used.....	27
3.1.4 Parameters	28
3.2 Solubility-limited dissolution of spent fuel (Case 1.2).....	36
3.2.1 Overview	36
3.2.2 The conceptual model and its underlying assumptions	36
3.2.3 Codes used.....	36
3.2.4 Parameters	37
3.3 Bentonite thermal alteration (Case 1.3).....	38
3.3.1 Overview	38
3.3.2 The conceptual model and its underlying assumptions	38
3.3.3 Codes used.....	38
3.3.4 Parameters	38
3.4 Glacially-induced flow in the Opalinus Clay (Case 1.4).....	39
3.4.1 Overview	39

3.4.2	The conceptual model and its underlying assumptions	39
3.4.3	Codes used	42
3.4.4	Parameters	42
3.5	Additional barrier provided by confining units (Case 1.5)	45
3.5.1	Overview	45
3.5.2	The conceptual model and its underlying assumptions	45
3.5.3	Codes used	46
3.5.4	Parameters	47
3.6	Radionuclide release affected by ramp/shaft (Case 1.6)	53
3.6.1	Overview	53
3.6.2	The conceptual model and its underlying assumptions	53
3.6.2.1	Calculation of water flow rates in the repository system	53
3.6.2.2	Calculation of radionuclide release from near field	61
3.6.2.3	Calculation of radionuclide transport through host rock and access tunnel system	61
3.6.3	Codes used	63
3.6.4	Parameters	63
3.7	Convergence-induced release of radionuclides affected by ramp/shaft (Case 1.7)	76
3.7.1	Overview	76
3.7.2	The conceptual model and its underlying assumptions	76
3.7.2.1	SF/HLW	76
3.7.2.2	ILW	77
3.7.3	Codes used	80
3.7.4	Parameters	80
3.8	Gas-induced release of radionuclides affected by ramp/shaft (Case 1.8)	86
3.8.1	Overview	86
3.8.2	The conceptual model and its underlying assumptions	86
3.8.2.1	Calculation of gas-induced porewater displacement rates	86
3.8.2.2	Calculation of water flow rates in the repository system	88
3.8.2.3	Calculation of radionuclide release from near field	91
3.8.2.4	Calculation of radionuclide transport through host rock and access tunnel system	91
3.8.3	Codes used	91
3.8.4	Parameters	92

4	Modelling Gas Pressure Evolution and the Release of ¹⁴C as Volatile Species in the Gas Phase	97
4.1	Description of the scenario	97
4.2	Evaluation of the scenario using the Gas Model	97
4.3	Pressure evolution and gas migration (as input to Cases 1.8, 2.1, 2.2, 4.5 and 4.6)	97
4.3.1	Overview of the conceptual model	97
4.3.2	Input parameters	98
4.3.3	Results	102
4.3.3.1	ILW	102
4.3.3.2	SF/HLW	107
4.3.3.3	Gas accumulation in Wedelsandstein	110
4.3.3.4	Investigated assessment cases related to the release of ¹⁴ C in volatile form in the gas phase (Cases 2.1, 2.2 and 4.6)	112
4.3.4	Conclusions regarding pressure evolution and gas migration	117
4.4	Dose due to volatile ¹⁴ C in the gas phase (Cases 2.1, 2.2 and 4.6)	118
4.4.1	Overview of the conceptual model	118
4.4.2	Input parameters	118
5	Modelling the Release of Radionuclides Affected by Human Actions	121
5.1	Borehole penetration into the repository (Case 3.1)	121
5.1.1	Overview	121
5.1.2	The conceptual model and its underlying assumptions	121
5.1.3	Codes used	126
5.1.4	Parameters	127
5.2	Deep groundwater extraction from Malm aquifer (Case 3.2)	130
5.2.1	Overview	130
5.2.2	The conceptual model and its underlying assumptions	130
5.2.3	Codes used	130
5.2.4	Parameters	131
5.3	Abandoned repository (Case 3.3)	131
5.3.1	Overview	131
5.3.2	The conceptual model and its underlying assumptions	131
5.3.3	Codes used	134
5.3.4	Parameters	135

6	Modelling "what if?" Cases to Investigate the Robustness of the Disposal System	139
6.1	High water flow rate in geosphere (Case 4.1)	139
6.1.1	Overview	139
6.1.2	Codes used.....	139
6.1.3	Parameters	139
6.2	Transport along transmissive discontinuities (Case 4.2)	139
6.2.1	Overview	139
6.2.2	The conceptual model and its underlying assumptions	140
6.2.3	Codes used.....	141
6.2.4	Parameters	141
6.3	SF: Increased fuel dissolution rate (Case 4.3)	144
6.3.1	Overview	144
6.3.2	The conceptual model and its underlying assumptions	144
6.3.3	Codes used.....	144
6.3.4	Parameters	144
6.4	Redox front penetration in the near field (Case 4.4).....	145
6.4.1	Overview	145
6.4.2	The conceptual model and its underlying assumptions	145
6.4.3	Codes used.....	145
6.4.4	Parameters	145
6.5	Gas-induced release of dissolved radionuclides from ILW through the ramp (Case 4.5).....	146
6.5.1	Overview	146
6.5.2	The conceptual model and its underlying assumptions	146
6.5.3	Codes used.....	147
6.5.4	Parameters	147
6.6	Unretarded transport of volatile radionuclides through the host rock (Case 4.6).....	151
6.7	Poor near field and pessimistic near field / geosphere geochemical dataset (Case 4.7).....	151
6.7.1	Overview	151
6.7.2	The conceptual model and its underlying assumptions	151
6.7.3	Codes used.....	152
6.7.4	Parameters	152
6.8	No advection in the geosphere (diffusive transport only, Case 4.8).....	153
6.8.1	Overview	153

6.8.2	Parameters	153
6.9	Increased cladding corrosion rate in SF (Case 4.9)	153
6.9.1	Overview	153
6.9.2	Parameters	153
6.10	Zero sorption for iodine in the near field and the geosphere (Case 4.10).....	153
6.10.1	Overview	153
6.10.2	Parameters	154
6.11	Decreased transport distance in Opalinus Clay (Case 4.11).....	154
6.11.1	Overview	154
6.11.2	Parameters	154
7	Modelling Design and System Options	155
7.1	Increased waste arisings (Case 5.1).....	155
7.1.1	Overview	155
7.1.2	The conceptual model and the justification of assumptions	155
7.1.3	Codes used.....	155
7.1.4	Parameters	155
7.2	ILW high force compacted waste option (Case 5.2)	155
7.2.1	Overview	155
7.2.2	The conceptual model and the justification of assumptions	156
7.2.3	Codes used.....	156
7.2.4	Parameters	156
7.3	Spent fuel canister with a Cu shell (Case 5.3)	156
7.3.1	Overview	156
7.3.2	The conceptual model and the justification of assumptions	156
7.3.3	Codes used.....	157
7.3.4	Parameters	157
8	Illustration of Effects of Biosphere Uncertainty on Calculated Doses.....	159
8.1	Introduction	159
8.2	Reference Case biosphere (Cases 1.1a, 6.1a and 6.2a).....	159
8.3	Alternative geomorphology (Cases 6.1b-d).....	162
8.4	Alternative climates (Cases 6.2b-d).....	166
8.5	Summary of cases.....	167
8.6	Codes used.....	167
8.7	Input parameters	168

9	Insight Models	169
9.1	Use of insight models in the safety assessment	169
9.2	Model to illustrate the meaning of the timescale for diffusion across the Opalinus Clay	169
9.2.1	Definition of the timescale for diffusion	169
9.2.2	Insight model	171
9.2.3	Application of the insight model in the safety assessment	174
9.3	Barrier efficiency models for non-fractured media	174
9.3.1	Definition of the barrier efficiency	174
9.3.2	Model for the Opalinus Clay plus the SF / HLW bentonite buffer.....	174
9.3.3	Model for the Opalinus Clay alone.....	179
9.3.4	Model for the ramp and shaft.....	180
9.3.5	Application of the insight models in the safety assessment.....	181
9.4	Barrier efficiency model for Opalinus Clay intersected by discontinuities	183
9.4.1	Definition of the barrier efficiency	183
9.4.2	Insight model	184
9.4.3	Application of the insight model in the safety assessment	186
9.5	Model to illustrate dissolution of the SF matrix as a function of canister breaching time	187
9.5.1	Process model.....	187
9.5.2	Application of the process model in the safety assessment	188
9.6	Model to illustrate the transport of ¹⁴ C as volatile species	188
9.6.1	Insight model	188
9.6.2	Application of the insight model in safety assessment	190
10	Evaluation of the Models Used for the Assessment Cases	191
10.1	Aim of this chapter	191
10.2	Types of assumptions	191
10.3	Applicability of assumptions	192
10.4	Categorisation of assumptions.....	192
10.5	Assessment of Reference Case assumptions	193
10.6	Assessment of assumptions for alternative cases	199
10.7	Summary and conclusions	222
11	References	227

Appendix 1: Codes for Modelling Assessment Cases	A-1
A1.1 Introduction	A-1
A1.1.1 Scope of this appendix.....	A-1
A1.1.2 Codes discussed in this appendix	A-1
A1.1.3 Structure of this appendix.....	A-2
A1.2 Qualification of the codes for the treatment of Super-FEPs	A-2
A1.2.1 The need for qualification.....	A-2
A1.2.2 Model domains to which the codes are applied.....	A-2
A1.2.3 The representation of Super-FEPs in safety assessment computer codes.....	A-4
A1.2.4 Approach to verification of codes.....	A-11
A1.3 SPENT	A-12
A1.3.1 Scope and purpose	A-12
A1.3.2 Phenomena included in SPENT.....	A-12
A1.3.2.1 Overview	A-12
A1.3.2.2 Containment and canister breaching.....	A-16
A1.3.2.3 Fuel release mechanisms and the reservoir.....	A-17
A1.3.2.4 Transport through the buffer.....	A-17
A1.3.2.5 Interface with the host rock	A-18
A1.3.3 Mathematical representation.....	A-19
A1.3.3.1 Overview	A-19
A1.3.3.2 Containment and canister breaching.....	A-19
A1.3.3.3 Fuel release mechanisms and the reservoir.....	A-20
A1.3.3.4 Transport through the buffer.....	A-22
A1.3.3.5 Interface with the host rock	A-23
A1.3.4 Input parameters	A-24
A1.3.5 Verification.....	A-28
A1.4 STRENG.....	A-31
A1.4.1 Scope and purpose	A-31
A1.4.2 Phenomena included in STRENG	A-31
A1.4.2.1 Overview	A-31
A1.4.2.2 Containment and canister breaching.....	A-35
A1.4.2.3 Glass release mechanisms and the reservoir.....	A-36
A1.4.2.4 Transport through the buffer and the interface with the host rock	A-36
A1.4.3 Mathematical representation.....	A-36
A1.4.3.1 Glass release mechanisms.....	A-36

A1.4.4	Input parameters	A-38
A1.4.5	Verification	A-39
A1.5	STALLION.....	A-40
A1.5.1	Scope and purpose	A-40
A1.5.2	Phenomena included in STALLION	A-40
A1.5.2.1	Overview	A-40
A1.5.2.2	Containment.....	A-43
A1.5.2.3	The behaviour of radionuclides in the cementitious region.....	A-43
A1.5.2.4	Interface with the host rock	A-44
A1.5.3	Mathematical representation.....	A-44
A1.5.3.1	Cementitious region.....	A-44
A1.5.4	Input parameters	A-45
A1.5.5	Verification	A-46
A1.6	PICNIC	A-48
A1.6.1	Scope and purpose	A-48
A1.6.2	Phenomena included in PICNIC.....	A-49
A1.6.2.1	Overview	A-49
A1.6.2.2	Phenomena in a single leg	A-53
A1.6.2.3	Network structure and properties.....	A-55
A1.6.3	Mathematical representation.....	A-55
A1.6.3.1	Leg areas and porosities.....	A-55
A1.6.3.2	Transport equations in a single leg	A-56
A1.6.3.3	Rock matrix transport equations.....	A-58
A1.6.3.4	Coupling of solute flux at junctions through response functions	A-59
A1.6.3.5	Methods of solution	A-59
A1.6.4	Input parameters	A-60
A1.6.5	Verification	A-62
A1.7	TAME.....	A-63
A1.7.1	Scope and purpose	A-63
A1.7.2	Phenomena included in TAME	A-63
A1.7.2.1	Overview	A-63
A1.7.2.2	Key model assumptions.....	A-65
A1.7.3	Mathematical representation.....	A-66
A1.7.4	Input parameters	A-74
A1.7.5	Verification	A-75

A1.8	FRAC3DVS.....	A-76
A1.8.1	Scope and purpose.....	A-76
A1.8.2	Phenomena included in FRAC3DVS	A-76
A1.8.2.1	Overview	A-76
A1.8.2.2	Geometric features.....	A-79
A1.8.2.3	Flow phenomena.....	A-82
A1.8.2.4	Transport and retention phenomena	A-82
A1.8.3	Mathematical representation.....	A-82
A1.8.3.1	Flow in porous medium.....	A-83
A1.8.3.2	Flow in fractures.....	A-83
A1.8.3.3	Transport in porous medium.....	A-84
A1.8.3.4	Transport in fractures.....	A-85
A1.8.3.5	Boundary conditions.....	A-86
A1.8.3.6	Numerical implementation	A-87
A1.8.3.7	Solution of the flow and transport equations	A-87
A1.8.4	Input parameters	A-87
A1.8.5	Verification.....	A-89
A1.9	The Gas Model	A-90
A1.9.1	Scope and purpose.....	A-90
A1.9.2	Phenomena included in the Gas Model	A-90
A1.9.3	Pressure evolution and gas migration	A-93
A1.9.3.1	Conceptual model.....	A-93
A1.9.3.2	Mathematical Representation	A-98
A1.9.4	Dose due to volatile ¹⁴ C in the gas phase.....	A-105
A1.9.4.1	Conceptual model.....	A-105
A1.9.4.2	Mathematical model	A-108
A1.9.5	Input parameters	A-111
A1.9.6	Verification.....	A-111
A1.10	Execution of model calculations with the Reference Model Chain.....	A-112
A1.10.1	Objectives and tools.....	A-112
A1.10.2	Excel workbooks	A-113
A1.10.2.1	Excel workbook for near field calculations with STMAN	A-114
A1.10.2.2	Excel workbook for geosphere calculations with PICNIC.....	A-119
A1.10.2.3	Excel workbook for biosphere calculations with TAME	A-122
A1.10.3	Job Starter.....	A-124

A1.10.4	Revision Control System.....	A-125
A1.10.5	QA of Excel workbooks and input file generator.....	A-126
Appendix 2: Probabilistic calculations.....		B-1
A2.1	Scope and purpose.....	B-1
A2.2	Methodology (GIPC).....	B-1
A2.2.1	The Control File.....	B-1
A2.2.2	The Processed Files.....	B-3
A2.2.3	The Specification File.....	B-3
A2.3	Mathematical representation.....	B-6
A2.4	Input parameters.....	B-6
A2.5	Post processing of probabilistic sensitivity analysis.....	B-6
A2.6	Verification.....	B-7
Appendix 3: Datasets.....		C-1
A3.1	Introduction.....	C-1
A3.2	Parameter combinations for the evaluation of assessment cases.....	C-1
A3.2.1	Near-field parameter combinations.....	C-1
A3.2.2	Geosphere parameter combinations.....	C-2
A3.2.3	Biosphere parameter combinations.....	C-12
A3.3	Parameter values for the evaluation of assessment cases.....	C-13
A3.3.1	Parameter values for STMAN calculations.....	C-13
A3.3.2	Parameter values for PICNIC calculations.....	C-27
A3.4	Nuclide-dependent parameters.....	C-38
A3.5	Element-dependent parameters.....	C-51
A3.6	Specific explanatory notes on the derivation of parameters.....	C-58
A3.7	Reference Case input parameters for biosphere modelling.....	C-65
A3.8	Input parameters for biosphere modelling of alternative cases.....	C-73
A3.9	Biosphere dose conversion factors.....	C-76
A3.10	Input parameters for probabilistic analysis.....	C-80
A3.10.1	Input PDFs.....	C-80
A3.10.2	Correlations.....	C-81
Appendix 4: Solving the Governing Equations for Steady-State Transport Through Opalinus Clay Intersected by Discontinuities.....		D-1
Appendix 5: Selection of Safety-Relevant Radionuclides.....		E-1

Appendix 6: Semi-Quantitative Dose Estimate for the Periglacial Climate	F-1
A6.1 Introduction	F-1
A6.2 Specific features of arctic biospheres	F-1
A6.3 Comparison of release and biosphere transport processes in the arctic region.....	F-2
A6.4 Comparison of critical groups in a periglacial climate with the reference biosphere.....	F-3
A6.5 Semi-quantitative evaluation	F-3
Appendix 7: The Applicability of the One-Dimensional Approximation for Modelling Transport through the Opalinus Clay	G-1
A7.1 Introduction	G-1
A7.2 Method to evaluate the applicability of the one-dimensional approximation.....	G-1
A7.3 Boundary conditions and data	G-2
A7.4 Results and conclusion	G-3
Appendix 8: Quality Assurance Measures	H-1

List of Tables

Tab. 2.2-1:	List of scenarios, what if cases, design and system options and illustration of biosphere uncertainty with associated conceptualisations and parameter variations that define the different assessment cases, structured according to the categories of uncertainty that they address	15
Tab. 3.1-1:	SPENT/STRENG/STALLION input data for the radionuclides and inventory in the Reference Case	29
Tab. 3.1-2:	SPENT input data for the spent fuel waste form and canister in the Reference Case.....	29
Tab. 3.1-3:	STRENG input data for the vitrified HLW waste form and canister in the Reference Case.....	30
Tab. 3.1-4:	STALLION input data for the ILW waste form and container in the Reference Case.....	31
Tab. 3.1-5:	SPENT/STRENG input data for the bentonite buffer and STMAN near field / geosphere properties in the Reference Case	32
Tab. 3.1-6:	PICNIC input data in the Reference Case.....	33
Tab. 3.1-7:	The deterministic parameter variations that are performed within the Reference Conceptualisation.....	34
Tab. 3.3-1:	SPENT/STRENG input data for the bentonite buffer for the conceptualisation "bentonite thermal alteration" (Case 1.3), where these differ from the Reference Case parameters.....	39
Tab. 3.4-1:	Hydraulic and transport boundary conditions for boundaries A-F.....	40
Tab. 3.4-2:	FRAC3DVS input data differing from the Reference Case.....	43
Tab. 3.4-3:	Sequence of future glaciation periods and derived time-dependent hydraulic heads at boundaries A and B (see Fig. 3.4-1)	44
Tab. 3.5-1:	Network flow data and source term information (Base Case)	48
Tab. 3.5-2:	PICNIC input data for leg L ₁ , which represents upward vertical transport through the Opalinus Clay and upper confining units (Base Case)	48
Tab. 3.5-3:	PICNIC input data for leg L ₂ , which represents downward vertical transport through the Opalinus Clay and lower confining units (Base Case)	49
Tab. 3.5-4:	Network flow data and source term information (model variant).....	49
Tab. 3.5-5:	PICNIC input data for leg L ₁₁ , which represents upward vertical transport through the Opalinus Clay (model variant).....	50
Tab. 3.5-6:	PICNIC input data for leg L ₁₂ , which represents lateral transport through the Wedelsandstein (model variant).....	51
Tab. 3.5-7:	PICNIC input data for leg L ₂₁ , which represents downward vertical transport through the Opalinus Clay and the Lias / Upper Keuper (model variant).....	52
Tab. 3.5-8:	PICNIC input data for leg L ₂₂ , which represents lateral transport through the Sandsteinkeuper (model variant).....	52

Tab. 3.6-1:	Parameter values used for the calculation of water flow rates in the resistor network	65
Tab. 3.6-2:	Network flow data and source term information calculated using the resistor network and the parameter values listed in Tab. 3.6-1	66
Tab. 3.6-3:	PICNIC input data for legs L ₁ , L ₂ , L ₃ and L ₄ which represent axial transport through the backfill of the operations tunnel, construction tunnel and ventilation tunnel.....	67
Tab. 3.6-4:	PICNIC input data for leg L ₅ , which represents upward vertical transport through the EDZ of the shaft.....	68
Tab. 3.6-5:	PICNIC input data for legs L _{6,A} , L _{6,B} , L _{6,C} and L ₇ , which represent upward vertical transport through the Opalinus Clay for SF/HLW and ILW.....	69
Tab. 3.6-6:	Network flow data and source term information	70
Tab. 3.6-7:	PICNIC input data differing from the Base Case.....	71
Tab. 3.6-8:	Parameter value used for the calculation of water flow rates in the resistor network.....	71
Tab. 3.6-9:	Network flow data and source term information	72
Tab. 3.6-10:	PICNIC input data differing from the Base Case.....	73
Tab. 3.7-1:	Void volumes of ILW waste containers (from Schwyn et al. 2003).....	81
Tab. 3.7-2:	Additional parameter value used for the calculation of water flow rates in the resistor network.....	81
Tab. 3.7-3:	Network flow data and source term information (calculated based on parameter values listed in Tabs. 3.6-1 and 3.7-2)	82
Tab. 3.7-4:	PICNIC input data for the leg representing axial transport through the backfill of the operations tunnel to the ramp.....	83
Tab. 3.7-5:	PICNIC input data for leg L ₇ which represents upward vertical transport through the Opalinus Clay for ILW (domain D).....	84
Tab. 3.7-6:	FRAC3DVS input data for a path representing upward vertical transport through the Opalinus Clay	85
Tab. 3.8-1:	Additional parameter values used for the calculation of water flow rates in the resistor network (Base Case).....	93
Tab. 3.8-2:	Network flow data and source term information (Base Case)	93
Tab. 3.8-3:	PICNIC input data for legs L ₁ , L ₂ , L ₃ and L ₄ which represent axial transport through the backfill of the operations tunnel, construction tunnel and ventilation tunnel, and legs L ₅ , L _{6,A} , L _{6,B} , L _{6,C} and L ₇ , which represent upward vertical transport through the EDZ of the shaft (L ₅) and through the Opalinus Clay (L ₆ and L ₇) for PICNIC network structure, see Fig. 3.6-5.....	94
Tab. 3.8-4:	Additional parameter values used for the calculation of water flow rates in the resistor network (parameter variation).....	95
Tab. 3.8-5:	Network flow data and source term information (parameter variation).....	95

Tab. 3.8-6:	PICNIC input data differing from the Base Case, for leg L ₁ , which represents axial transport through the backfill of the operations tunnel, construction tunnel and ventilation tunnel, and leg L ₇ , which represents upward vertical transport through the Opalinus Clay for the PICNIC network structure, see Fig. 3.6-5.....	96
Tab. 4.3-1:	Total gas generation rate for SF/HLW and ILW as a function of time (from Nagra 2003a).....	98
Tab. 4.3-2:	Summary of input parameters for the model calculations related to gas migration in the SF/HLW/ILW repository system.....	99
Tab. 4.3-3:	Justification of chosen values for characteristic lengths of hydraulic gradient and concentration gradient of dissolved hydrogen in Opalinus Clay.....	102
Tab. 4.3-4:	Maximal gas pressure in the SF emplacement tunnels for various gas permeabilities and corrosion rates considering capillary leakage by 2-phase flow and gas diffusion, but no pathway dilation (pressures above the threshold for pathway dilation of 13 MPa in italics).....	108
Tab. 4.3-5:	Maximal radius of free gas phase in the Wedelsandstein and maximal gas flow rate through the low-permeability upper confining units as a function of the steel corrosion rate; both quantities are found to be independent of the gas permeability in the Opalinus Clay.....	111
Tab. 4.3-6:	Pore space available for gas considered in the different assessment cases.....	112
Tab. 4.3-7:	Calculated gas storage volumes.....	113
Tab. 4.4-1:	Data for ¹⁴ C for SF.....	118
Tab. 4.4-2:	Data for ¹⁴ C for ILW.....	119
Tab. 4.4-3:	Summary of input parameters for the model calculations related to the release of volatile ¹⁴ C from SF and ILW.....	119
Tab. 5.1-1:	Parameter values used for the calculation of the water flow rate in the collapsed borehole (Base Case).....	127
Tab. 5.1-2:	Flow data and source term information (Base Case, see Tab. A3.2-1b in App. 3).....	127
Tab. 5.1-3:	Parameter values used for the calculation of water flow rates in the collapsed borehole.....	128
Tab. 5.1-4:	Network flow data and source term information (variant 1).....	128
Tab. 5.1-5:	Network flow data and source term information (variant 2).....	129
Tab. 5.1-6:	Network flow data and source term information (variant 3).....	129
Tab. 5.1-7:	Network flow data and source term information (variants 4-6).....	130
Tab. 5.3-1:	Additional parameter values used for the calculation of water flow rates in the resistor network.....	135
Tab. 5.3-2:	Network flow data and source term information (calculated based on parameter values listed in Tabs. 3.6-1 and 5.3-1).....	136

Tab. 5.3-3:	PICNIC input data for legs L ₁ , L ₂ , L ₃ and L ₄ which represent axial transport through the backfill of the operations tunnel, construction tunnel and ventilation tunnel, and legs L ₅ and L _{6,A} , L _{6,B} , L _{6,C} , L ₇ , which represent upward vertical transport through the EDZ of the shaft (L ₅) and through the Opalinus Clay (L ₆ , L ₇), respectively	137
Tab. 6.2-1:	STMAN near field / geosphere properties differing from the Reference Case.....	142
Tab. 6.2-2:	Network flow data and source term information	142
Tab. 6.2-3:	PICNIC input data for leg L ₂ , which represents transport through a discontinuity.....	143
Tab. 6.5-1:	Additional parameter values used for the calculation of water flow rates (values discussed in the text)	147
Tab. 6.5-2:	Network flow data and source term information calculated based on parameter values listed in Tab. 3.6-1 and 6.5-1	148
Tab. 6.5-3:	PICNIC input data for leg L ₁ which represents axial transport through the backfill of the operations tunnel to the ramp.....	149
Tab. 6.5-4:	Additional parameter values used for the calculation of water flow rates	150
Tab. 6.5-5:	Network flow data and source term information (calculated based on parameter values listed in Tab. 3.6-1 and 6.5-4).....	150
Tab. 6.5-6:	PICNIC input data differing from the Base Case, for leg L ₁ which represents axial transport through the backfill of the operations tunnel to the ramp.....	151
Tab. 6.7-1:	Input parameters for the case "Poor near field and pessimistic near field / geosphere geochemical dataset" (Case 4.7)	152
Tab. 8.2-1:	Abbreviations used in the schematic representations of the considered water fluxes and solid material fluxes in Figs. 8.2-1, 8.3-1 and 8.3-2	161
Tab. 8.5-1:	Overview of investigated biosphere cases	167
Tab. 9.1-1:	Insight models used in specific sections of the Safety Report and the sections of the present chapter where the details of these insight models are described	169
Tab. 9.2-1:	Reference Case parameters used to evaluate the ratio $t_d/t_{1/2}$ in Fig. 6.6-1 of Nagra (2002c).....	171
Tab. 9.2-2:	The percentage breakthrough of a stable nuclide for different values of time t	172
Tab. 9.3-1:	Dimensions and hydraulic properties of the ramp and shaft.....	180
Tab. 9.3-2:	Reference Case parameters used to evaluate advection and dispersion in the Opalinus Clay.....	181
Tab. 9.3-3:	Reference Case parameters used to evaluate diffusion in the bentonite buffer.....	182
Tab. 9.3-4:	Parameters used to evaluate transport along the backfilled ramp	183
Tab. 9.3-5:	Parameters used to evaluate transport along the shaft EDZ.....	183

Tab. 9.6-1: Parameters used to evaluate the transport of ¹⁴ C as volatile species (methane)	190
Tab. 10.5-1: Assessment of the main conceptual assumptions made in the Reference Case.....	194
Tab. 10.6-1: Assessment of the main conceptual assumptions made in the alternative cases within the Reference Scenario: release of dissolved radionuclides	200
Tab. 10.6-2: Assessment of the main conceptual assumptions made in Alternative Scenario 1: Release of volatile radionuclides along gas pathways	206
Tab. 10.6-3: Assessment of the main conceptual assumptions made in Alternative Scenario 2: Release of radionuclides affected by human actions	211
Tab. 10.6-4: Assessment of the main conceptual assumptions made in the "what if?" cases to investigate the robustness of the disposal system.....	216
Tab. 10.6-5: Assessment of the main conceptual assumptions made in the cases addressing design and system options.....	222
Tab. 10.6-6: Assessment of the main conceptual assumptions made in the cases illustrating the effects of biosphere uncertainty	223
Tab. A1.2-1: Model domains to which the assessment codes have been applied	A-3
Tab. A1.2-2: The representation of Super-FEPs and their safety-relevant aspects in safety assessment computer codes	A-6
Tab. A1.3-1: Super-FEPs, their safety-relevant aspects (as taken from Tab. A5.2.1 of Nagra 2002d) and the ways in which they are represented by the code SPENT	A-13
Tab. A1.3-2: Phenomena explicitly included in the SPENT model	A-16
Tab. A1.3-3: STMAN input data requirements for the radionuclides and inventory	A-25
Tab. A1.3-4: SPENT input data requirements for the waste form and canister	A-26
Tab. A1.3-5: STMAN input data requirements for the buffer	A-27
Tab. A1.4-1: Super-FEPs, their safety-relevant aspects (as taken from Tab. A5.2.1 of Nagra 2002d) and the ways in which they are represented by the code STRENG	A-32
Tab. A1.4-2: Phenomena explicitly included in the STRENG model.....	A-35
Tab. A1.4-3: STRENG input data requirements for the glass and canister.....	A-39
Tab. A1.5-1: Super-FEPs, their safety-relevant aspects (as taken from Tab. A5.2.1 of Nagra 2002d) and the ways in which they are represented by the code STALLION	A-41
Tab. A1.5-2: Phenomena explicitly included in the STALLION model	A-42
Tab. A1.5-3: STALLION input data requirements for the cement and container.....	A-46
Tab. A1.5-4: Results of a verification test for slow release with STALLION	A-47
Tab. A1.6-1: Super-FEPs, their safety-relevant aspects (as taken from Tab. A5.2.1 of Nagra 2002d) and the ways in which they are represented by the code PICNIC.....	A-50

Tab. A1.6-2: Phenomena explicitly included in the PICNIC model	A-53
Tab. A1.6-3: PICNIC input data requirements	A-61
Tab. A1.6-4: PICNIC verification steps and codes used for cross-comparisons.....	A-63
Tab. A1.7-1: Super-FEPs, their safety-relevant aspects (as taken from Tab. A5.2.1 of Nagra 2002d) and the ways in which they are represented by the code TAME	A-64
Tab. A1.7-2: Phenomena explicitly included in the TAME model	A-65
Tab. A1.7-3: Summary of exposure pathways modelled in TAME	A-69
Tab. A1.7-4: Parameters used to characterise the dose from the drinking water pathways ..	A-73
Tab. A1.8-1: Super-FEPs, their safety-relevant aspects (as taken from Tab. A5.2.1 of Nagra 2002d) and the ways in which they are represented by the code FRAC3DVS	A-77
Tab. A1.8-2: Phenomena explicitly included in the FRAC3DVS model	A-79
Tab. A1.8-3: FRAC3DVS input data requirements.....	A-88
Tab. A1.8-4: Overview of test cases for FRAC3DVS.....	A-89
Tab. A1.9-1: Super-FEPs, their safety-relevant aspects (as taken from Tab. A5.2.1 of Nagra 2002d) and the ways in which they are represented by the Gas Model	A-91
Tab. A1.9-2: Safety-relevant aspects of the Super-FEPs and other phenomena explicitly included in the Gas Model	A-93
Tab. A1.9-3: Summary of transport processes considered in the conceptual models for the different transport pathways and waste types	A-95
Tab. A1.9-4: Pore space available for gas considered in the different assessment cases (numbering of cases according to Chapter 2)	A-106
Tab. A2.2-1a: Valid sampling controls of the code GIPC.....	B-2
Tab. A2.2-1b: Valid actions in the Control File of the code GIPC	B-2
Tab. A2.2-2: Types of probability density functions available in GIPC	B-4
Tab. A3.2-1a: Parameter combinations in the STMAN calculations for assessment cases within the Reference Scenario	C-3
Tab. A3.2-1b: Parameter combinations in the STMAN calculations for the assessment cases within Alternative Scenario 2 (release of radionuclides affected by human actions)	C-5
Tab. A3.2-1c: Parameter combinations in the STMAN calculations for "what if?" assessment cases	C-6
Tab. A3.2-1d: Parameter combinations in the STMAN calculations to investigate design and system options	C-8
Tab. A3.2-2a: Parameter combinations in the PICNIC calculations for assessment cases within the Reference Scenario	C-9

Tab. A3.2-2b: Parameter combinations in the PICNIC calculations for assessment cases within Alternative Scenario 2 (release of radionuclides affected by human actions)	C-10
Tab. A3.2-2c: Parameter combinations in the PICNIC calculations for "what if?" assessment cases	C-11
Tab. A3.2-3: Parameter combinations in the TAME calculations.....	C-12
Tab. A3.3-1: Parameter values for STMAN calculations.....	C-14
Tab. A3.3-2a: SF near field parameter values.....	C-24
Tab. A3.3-2b: HLW near field parameter values	C-25
Tab. A3.3-2c: ILW near field parameter values.....	C-26
Tab. A3.3-3: Parameter values for PICNIC calculations	C-28
Tab. A3.3-4a: Parameters for host rock	C-32
Tab. A3.3-4b: Key hydrogeological parameters for alternative radionuclide transport pathways within the host rock and confining units.....	C-33
Tab. A3.3-4c: Parameters for alternative radionuclide transport pathways within / along the ramp / shaft.....	C-34
Tab. A3.3-4d: Effective radii for various repository elements	C-36
Tab. A3.3-4e: Parameters used for the gas model.....	C-37
Tab. A3.4-1: Safety-relevant radionuclides and properties related to radioactivity	C-39
Tab. A3.4-2a: Inventories and their distributions – reference SF packages.....	C-41
Tab. A3.4-2b: Inventories and their distributions – alternative SF packages.....	C-45
Tab. A3.4-2c: Reference inventories of HLW packages and ILW tunnels and inventory of ILW-1 for the high force compacted waste option	C-49
Tab. A3.4-2d: IRF values of key radionuclides for BWR and PWR UO ₂ fuel and PWR MOX fuel	C-51
Tab. A3.5-1: Solubility limits and associated uncertainties for the SF / HLW near field, for reference case (pH = 7.25, Eh = -194 mV) and for oxidising conditions ("what if?" case); "high" denotes a solubility limit that is assumed to be never attained	C-52
Tab. A3.5-2: Sorption constants, effective diffusion coefficients and accessible porosities in compacted bentonite.....	C-54
Tab. A3.5-3: Solubility limits and associated uncertainties for the cementitious near field of the waste groups ILW-1 and ILW-2	C-55
Tab. A3.5-4: Sorption constants for the ILW cementitious near field	C-56
Tab. A3.5-5: Sorption coefficients, effective diffusion coefficients and accessible porosities in Opalinus Clay	C-57
Tab. A3.6-1: Fuel matrix fractional dissolution rate as a function of time, evaluated assuming two different canister loadings.....	C-60
Tab. A3.6-2: The effective flowrate per waste package for different combinations of Darcy velocity and effective diffusion coefficient (D _e) in the Opalinus Clay .	C-64

Tab. A3.7-1: Definition of biosphere compartments and input parameters determining water and solid material fluxes between the compartments.....	C-66
Tab. A3.7-2: Biosphere sorption database (K_d).....	C-68
Tab. A3.7-3: Parameter values characterising human diet and practices	C-69
Tab. A3.7-4: Transfer factors and concentration ratios for foodstuffs	C-71
Tab. A3.7-5: Food processing factors, turnover times for weathering losses and other rate factors.....	C-72
Tab. A3.8-1: List of biosphere input parameters for alternative biosphere cases	C-74
Tab. A3.9-1: Biosphere dose conversion factors (BDCFs) in Sv Bq^{-1} for all safety-relevant radionuclides and for the various cases shown in Fig. A3.9-1	C-78
Tab. A3.10-1: Probability density functions (PDF's) for probabilistic analysis	C-83
Tab. A5-1: List of safety-relevant activation and fission products.....	E-3
Tab. A5-2: List of safety-relevant actinide decay chain members for the present assessment.....	E-4
Tab. A5-3: Dose conversion factors (ingestion/inhalation) for activation and fission products and actinide decay chains, compiled from StSV (1994) and supplemented with ICRP (1996).....	E-5
Tab. A6.3-1: Overview of different contamination mechanisms	F-2
Tab. A6.4-1: Characteristics of different communities / critical groups (in the framework of the assessment of radioactive waste disposal)	F-3
Tab. A6.5-1: Relative doses for different populations for the same level of contamination....	F-3
Tab. A6.5-2: Comparison of biosphere scenarios (Strand et al. 2002).....	F-4
Tab. A7.3-1: Boundary conditions and geometrical parameters for FRAC3DVS	G-3
Tab. A7.4-1: Maximum release rates and times of these maxima for some example radionuclides, evaluated using PICNIC and using FRAC3DVS	G-3

List of Figures

Fig. 1.1-1:	Reporting structure for the safety assessment of Project Entsorgungsnachweis.....	2
Fig. 2.1-1:	Possible layout for a deep geological repository for SF/HLW/ILW in Opalinus Clay.....	8
Fig. 2.1-2:	The system of safety barriers in the case of SF.....	9
Fig. 2.1-3:	The system of safety barriers in the case of HLW.....	10
Fig. 2.1-4:	The system of safety barriers in the case of ILW.....	11
Fig. 2.1-5:	Status of the repository during the monitoring phase, when waste emplacement is complete, but before final sealing and closure of the facility.....	12
Fig. 2.1-6:	Status of the repository after final sealing and closure of the facility.....	13
Fig. 2.2-1:	The hierarchy of scenarios, conceptualisations and parameter sets.....	14
Fig. 3.1-1:	Geometrical simplification for modelling of radionuclide transport through the SF/HLW bentonite buffer.....	22
Fig. 3.2-1:	Comparison of the fractional fuel dissolution rates obtained by the radiolytic oxidation model, as used in the Reference Case, and by the solubility-limited dissolution model, as used in the present case.....	37
Fig. 3.4-1:	Conceptual model for the calculation of glacially-induced flow and transport in bentonite and Opalinus Clay.....	41
Fig. 3.5-1:	Illustration of the radionuclide transport pathways in the conceptualisation considering the additional barriers provided by the confining units.....	46
Fig. 3.5-2:	The PICNIC network structure used to model the two variants of the conceptualisation considering the additional barriers provided by the confining units.....	47
Fig. 3.6-1:	a) Resistor network model for hydraulic calculations of water flow through the tunnel system; b) repository domains for modelling radionuclide transport through the host rock and the ramp/shaft.....	54
Fig. 3.6-2:	Comparison of water flow rates obtained from the resistor network model calculations in the Base Case, described in the present section, and the numerical hydrodynamic model calculations for case RLU0, described in Nagra (2002a).....	58
Fig. 3.6-3:	Comparison of water flow rates obtained from the resistor network model calculations for various values of the hydraulic conductivity of the EDZ.....	59
Fig. 3.6-4:	Comparison of the vertical flow rates per SF canister, driven by the hydraulic head difference between the Sandsteinkeuper and Wedelsandstein formations, the vertical effective flow rates, taking diffusion into account, and the horizontal flow rates along the axes of the SF emplacement tunnels.....	60
Fig. 3.6-5:	The PICNIC network structure used to model the conceptualisation "radionuclide release affected by ramp/shaft".....	64

Fig. 3.6-6:	Dose as a function of time for the assessment case considering radionuclide release affected by the ramp / shaft (Base Case).....	74
Fig. 3.6-7:	Dose as a function of time for the assessment case considering radionuclide release affected by the ramp / shaft (model variant related to radionuclide transport through the liner of the operations/construction/ventilation tunnels).....	75
Fig. 3.7-1:	Resistor network model for the calculation of water flow from the ILW-1 part of the repository through the Opalinus Clay and the operations tunnel/ramp	79
Fig. 3.8-1:	Scheme with the conceptual model for gas-induced release of dissolved radionuclides through the Opalinus Clay and through the access tunnel system.....	87
Fig. 3.8-2:	Gas-induced water flow rates.....	90
Fig. 3.8-3:	Transient water flow rates used to calculate the near field radionuclide source term with STMAN (thick lines) and corresponding steady-state "sources of water" assumed in the resistor network calculations, used to derive steady-state water flow rates for PICNIC legs (thin lines).....	92
Fig. 4.3-1:	Evolution of gas pressure in the ILW emplacement tunnels assuming an initial saturation of 50 %.....	103
Fig. 4.3-2:	Upper and middle figure: Evolution of gas pressure in the ILW emplacement tunnels taking into account gas diffusion, porewater displacement and capillary leakage by 2-phase flow, but without consideration of pathway dilation. Lower figure: Gas-induced porewater displacement rates from the ILW emplacement tunnels into the Opalinus Clay (same parameter values as in upper figure).....	105
Fig. 4.3-3:	Propagation of a representative dilatant gas pathway from the ILW emplacement tunnel into the Opalinus Clay ($P = 13$ MPa), taking gas diffusion, porewater displacement and capillary leakage by 2-phase flow from tunnels and horizontal dilatant gas pathways into account	106
Fig. 4.3-4:	Evaluation of the importance of additional gas storage volume for ILW	106
Fig. 4.3-5:	Evolution of gas pressure in the SF emplacement tunnel taking gas diffusion and capillary leakage by 2-phase flow into account, but without consideration of pathway dilation (steel corrosion rate $1 \mu\text{m a}^{-1}$).....	107
Fig. 4.3-6:	Propagation of a representative dilatant gas pathway from the SF emplacement tunnel into the Opalinus Clay, taking gas diffusion and capillary leakage by 2-phase flow from tunnels and horizontal dilatant gas pathways into account ($P = 13$ MPa, corrosion rate $1 \mu\text{m a}^{-1}$).....	109
Fig. 4.3-7:	Propagation of a representative dilatant gas pathway from the SF emplacement tunnel into the Opalinus Clay, taking gas diffusion and capillary leakage by 2-phase flow from tunnels and horizontal dilatant gas pathways into account ($P = 13$ MPa, corrosion rate $0.1 \mu\text{m a}^{-1}$).....	109
Fig. 4.3-8:	Radial propagation of a free gas phase in the Wedelsandstein caused by gas generation in SF/HLW/ILW, taking gas diffusion through the low-permeability upper confining units into account (corrosion rate $1 \mu\text{m a}^{-1}$).....	110

Fig. 4.3-9:	Gas flow rate by diffusion from free gas phase in the Wedelsandstein through the low-permeability upper confining units to the Malm aquifer (corrosion rate $1 \mu\text{m a}^{-1}$).....	111
Fig. 4.3-10:	Results for Case 2.1 (steel corrosion rate $1 \mu\text{m a}^{-1}$)	114
Fig. 4.3-11:	Results for Case 2.2 (steel corrosion rate $1 \mu\text{m a}^{-1}$)	115
Fig. 4.3-12:	Results for Case 4.6 (steel corrosion rate $1 \mu\text{m a}^{-1}$)	116
Fig. 5.1-1:	Steady-state water flow rate in the borehole as a function of the hydraulic conductivity, taken to be identical in the borehole (partially filled with mud and partially collapsed, covering several stages of self-sealing) and in its EDZ.....	122
Fig. 5.1-2:	Scheme of investigated variants of borehole penetration: a) SF/HLW (near hit), b) SF (direct hit), c) ILW-1.....	123
Fig. 5.1-3:	Scheme for calculation of the diffusive fluxes from the ILW-1 emplacement tunnel radially into the Opalinus Clay and axially towards the borehole	126
Fig. 5.3-1:	Water flow rates obtained from the resistor network model calculations for the case of an abandoned repository for different hydraulic conductivities of the abandoned tunnel	133
Fig. 5.3-2:	Comparison of water flow rates obtained from the resistor network model calculations, described in the present section, and the numerical hydrodynamic model calculations for case RLU02, described in Nagra (2002a)	134
Fig. 6.2-1:	The PICNIC network structure used to model the "what if?" case "transport along transmissive discontinuities in the host rock" (Case 4.2).....	141
Fig. 8.2-1:	Schematic representation of water fluxes (F_{ij}) and solid material fluxes (M_{ij}) considered in the Reference Case.....	160
Fig. 8.3-1:	Schematic representation of water fluxes (F_{ij}) and solid material fluxes (M_{ij}) considered in the model variant "Sedimentation Area".....	163
Fig. 8.3-2:	Schematic representation of water fluxes (F_{ij}) and solid material fluxes (M_{ij}) considered in the model variant "Wetland"	165
Fig. 9.2-1:	Simplified view of the disposal system, in which radionuclides undergo one-dimensional diffusion in the vertical direction through the Opalinus Clay from the repository towards the upper and lower confining units.....	170
Fig. 9.2-2:	Concentration at the boundary of the Opalinus Clay with the upper confining units as a function of time if a fixed concentration is imposed at the boundary with the repository near field	173
Fig. 9.3-1:	Geometrical simplification of the bentonite / Opalinus Clay barrier for modelling purposes (upper figure), and transport processes within the model domain (lower figure)	176
Fig. 9.4-1:	"Actual" geometry of the disposal system around one tunnel, and simplified geometry for evaluation of the barrier efficiency, in the case of Opalinus Clay intersected by discontinuities	185

Fig. A1.3-1:	Comparison of SPENT and AMBER results in a code comparison verification test.....	A-29
Fig. A1.3-2:	Doses calculated using SPENT and PICNIC in a code comparison verification test.....	A-30
Fig. A1.3-3:	Doses calculated using AMBER in a code comparison verification test	A-30
Fig. A1.5-1:	Comparison of STALLION and AMBER buffer release rates in a code comparison verification test	A-48
Fig. A1.6-1:	Areas defining the properties of a PICNIC leg.....	A-54
Fig. A1.7-1:	Structure of the TAME transport and accumulation model of the biosphere (Klos et al. 1996).....	A-67
Fig. A1.7-2:	The TAME exposure pathway sub-model showing the relationship between pathways and the physical environment.....	A-68
Fig. A1.7-3:	Comparison of biosphere dose conversion factors (BDCFs) calculated by TAME and by the simplified analytical model discussed in Gribi (2003)	A-76
Fig. A1.8-1:	Input data requirements in a FRAC3DVS model.....	A-80
Fig. A1.8-2:	Modelling strategies with FRAC3DVS.....	A-81
Fig. A1.9-1a:	Scheme of the conceptual model for pressure build-up in the ILW emplacement tunnels, mitigated by gas diffusion, capillary leakage, porewater displacement and by the formation of dilatant gas pathways	A-96
Fig. A1.9-1b:	Scheme of the conceptual model for pressure build-up in the SF/HLW emplacement tunnels, mitigated by gas diffusion, capillary leakage and by the formation of dilatant gas pathways.....	A-97
Fig. A1.9-2:	Scheme of the conceptual model for gas release from the SF/HLW/ILW emplacement tunnels through Opalinus Clay, Wedelsandstein and low-permeability upper confining units.....	A-98
Fig. A1.9-3:	Fit of time-dependent gas generation rate for ILW using an exponential law in the time period $10^4 \text{ a} < t < 10^5 \text{ a}$	A-101
Fig. A1.9-4:	Illustration of the conceptual model for the release of volatile ^{14}C from the SF and ILW parts of the repository in Opalinus Clay	A-107
Fig. A1.9-5:	Scheme of compartment model used for the calculation of the activity concentration in the gas phase and in the biosphere (Quaternary aquifer)..	A-107
Fig. A1.10-1:	Overview of the basic operational elements and procedures of the system implemented to run the model calculations with STMAN, PICNIC and TAME.....	A-113
Fig. A1.10-2a:	Table "release" listing release rates for two spent fuel canister types as a function of time	A-115
Fig. A1.10-2b:	Table "solubility" listing element-dependent solubility limits for various chemical conditions	A-116
Fig. A1.10-3:	Excerpt of table "cases".....	A-117
Fig. A1.10-4:	Excerpt of the table "cases" showing links to certain columns in the data tables as required for the creation of input files	A-118

Fig. A1.10-5:	Section of table "Vorlage" with excerpts of templates for PICNIC input files	A-120
Fig. A1.10-6:	Excerpt of the "GeoCases" table of calculational cases showing a matrix of cases (rows) and parameters (columns)	A-121
Fig. A1.10-7:	Excerpt of the "GeoCases" table of calculational cases showing a matrix of cases (rows) and parameters (columns)	A-122
Fig. A1.10-8:	Excerpt of the table of calculational cases "tamecases" defining all parameters required to create the input files for TAME calculations.....	A-123
Fig. A1.10-9:	Table "Vorlage" is used to create the input file required to run TAME 3c.	A-124
Fig. A1.10-10:	Example of the interactive window of Job Starter	A-126
Fig. A2.2-1:	Typical scatter plot of two (slightly negatively) correlated parameters	B-6
Fig. A3.6-1:	Normalised release, as a function of thickness of the diffusive barrier (Opalinus Clay) around the cementitious ILW-1 tunnel	C-62
Fig. A3.9-1:	Biosphere dose conversion factors (BDCFs) for various cases related to uncertainty in conditions in the surface environment.....	C-77
Fig. A7.2-1:	The two-dimensional domain modelled using FRAC3DVS	G-2

1 Introduction

1.1 The role of this report within Project *Entsorgungsnachweis*

This report describes the models¹, codes and data used in the post-closure radiological safety assessment of a deep geological repository in the Opalinus Clay² in the potential siting area of the Zürcher Weinland in northern Switzerland and designed for the disposal of

- spent fuel (SF³), in the form of fuel assemblies containing UO₂ or mixed-oxide (MOX) fuel,
- vitrified high-level waste (HLW⁴) from the reprocessing of spent fuel, and
- long-lived intermediate-level waste (ILW⁵).

The safety assessment has been carried out as part of the technical basis for Project *Entsorgungsnachweis*⁶. This project is a milestone in the programme for the management of SF, HLW and ILW and represents an evaluation of the feasibility of the disposal of these wastes in Switzerland. It is also a major step on the way towards repository implementation.

Documentation of Project *Entsorgungsnachweis* is presented in a series of reports. At the highest level, there are three key technical project reports, which are primarily aimed at a technical audience (Swiss safety authorities, the Swiss scientific and technical community, technical bodies such as implementers and regulators in other countries, but also the technically interested non-specialist reader). These three reports are:

- a project report providing a synthesis of geological information on Opalinus Clay and on the geology of northern Switzerland and, specifically, on the region of the Zürcher Weinland (Nagra 2002a),
- a project report describing the design, construction, operation and closure of the proposed facilities (Nagra 2002b),
- a safety assessment report, which is divided into two parts: (i) the main report (Nagra 2002c), and (ii) the present report on models, codes and data that provides more detailed information in support of the main report.

The three project reports, in turn, are backed up by more detailed technical "reference reports". This is indicated for the safety assessment in Fig. 1.1-1.

The safety assessment report is divided into two parts to satisfy the two important requirements of transparency and traceability: The main report aims at pulling together as transparently as possible the arguments and analyses that make up the safety case, without, however, giving all the detailed formulae and data used (Nagra 2002c). The present report aims at providing a compilation of detailed, traceable information that should allow the interested reader to re-

¹ Short for "conceptual models".

² Opalinus Clay is a shale (claystone) formation present in large areas of northern Switzerland.

³ The German term, used in Switzerland, is BE (abgebrannte Brennelemente).

⁴ Termed HAA (**h**ochaktive **A**bfälle) in German.

⁵ Termed LMA (**l**anglebige **m**ittelaktive **A**bfälle) in German. This waste form is broadly similar to the waste category sometimes referred to as TRU - transuranic-containing waste - even though the transuranics may not be the most safety-relevant radionuclides in such waste.

⁶ The German term is also used in the English version of this report. The term translates into English as "demonstration of disposal feasibility".

calculate the results shown in the main report independently. The present report itself is in turn complemented by a series of reference reports that give the technical background, as indicated in Fig. 1-1-1. It thus provides the link between the results in the main report and the specific reference reports.

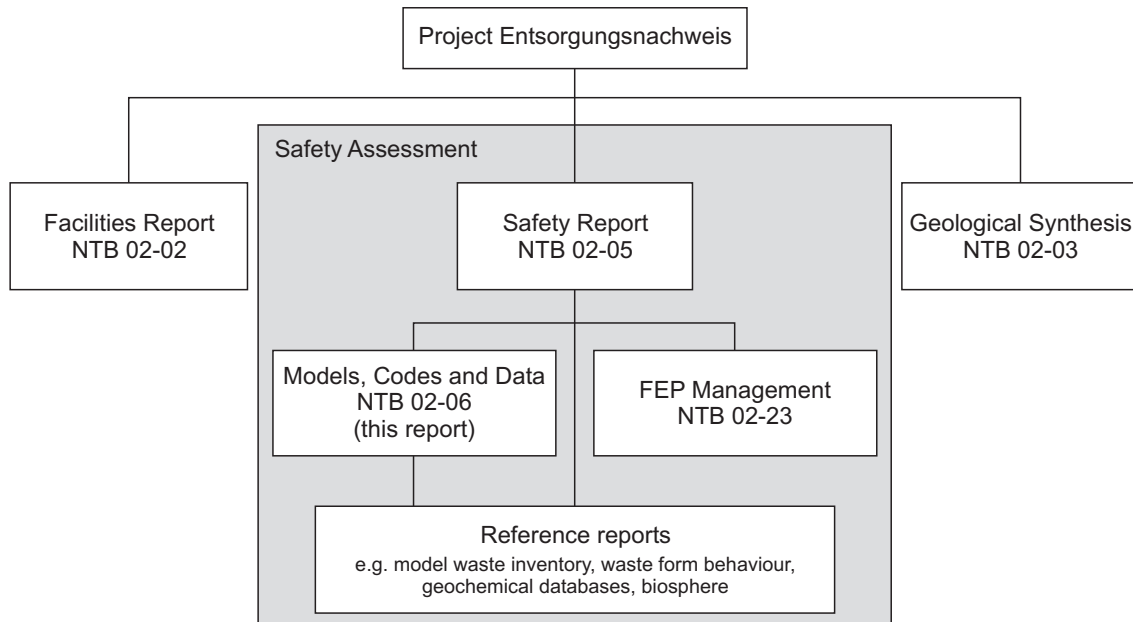


Fig. 1.1-1: Reporting structure for the safety assessment of Project *Entsorgungsnachweis*

1.2 Use of quantitative models in this safety assessment

In this safety assessment, quantitative models are used to test compliance of the proposed disposal system with safety requirements and, in particular, the regulatory guideline for dose and risk. According to Protection Objective 1 of the Swiss regulatory guideline HSK-R-21 (HSK&KSA 1993):

"The release of radionuclides from a sealed repository subsequent upon processes and events reasonably expected to happen shall at no time give rise to individual doses which exceed 0.1 mSv per year".

Protection Objective 2 of the same guideline states:

"The individual radiological risk of fatality from a sealed repository subsequent upon unlikely processes and events not taken into consideration in Protection Objective 1 shall, at no time, exceed one in a million per year."

Protection Objective 2 is used in this safety assessment to derive the regulatory constraint for calculated complementary cumulative density functions (CCDFs) of the dose for the probabilistic analyses (see Chapter 7 of the main report).

Dose is, in general, evaluated using a chain of models and corresponding computer codes and databases, namely:

- *near field models, codes and data*, used to evaluate the release of radionuclides from the waste forms and transport through the engineered barrier system of the repository,
- *geosphere models, codes and data*, used to evaluate the transport of radionuclides through the repository host rock and adjacent geological formations, and
- *biosphere models, codes and data*, used to evaluate the distribution of radionuclides in the surface environment and the exposure pathways that result in an individual dose.

These models, codes and data are not only used to calculate individual dose to test compliance with the Swiss regulatory guideline, but also to provide the alternative safety indicators presented and discussed in the main report.

The characteristics and evolution of the repository is subject to uncertainties. Furthermore, at the current stage of the Swiss programme, various design and system options are kept open. A single model-chain calculation is thus insufficient to show that the safety requirements are met. Rather, a range of *assessment cases* is defined. The starting point is the reference design, the expected characteristics and the expected broad evolutionary path of the disposal system, which, together with certain model assumptions and parameters, defines a Reference Case. A range of additional cases is, however, also defined in order to illustrate the consequences of specific uncertainties and design and system options. The structuring of these cases according to the classification of uncertainties as *scenario uncertainties*, *conceptual uncertainties* and *parameter uncertainties* is described in the main report.

The near field, geosphere and biosphere computer codes used to analyse the Reference Case and most of the additional cases is termed the *reference model chain*⁷. For a few cases, however, alternative conceptualisations are considered that do not fall within the scope of these codes, and alternative codes or analytical solutions are employed. Furthermore, in order to examine particular aspects of system performance in more detail, and to investigate sensitivity to key system properties and model assumption, results using the reference model chain are complemented by the results of simplified models that focus on a limited number of features, events and processes (FEPs). These are termed *insight models*.

Most of the assessment cases are evaluated using deterministic calculations. These are complemented by probabilistic calculations, in which the input parameters of the reference model chain are varied stochastically around their Reference Case values, but considering correlations where appropriate. In carrying out the probabilistic analyses, a computational tool termed GIPC⁸ is used to sample input parameters from probability density functions (PDFs) and to run the reference model chain repeatedly. This code is used, in particular, to indicate the performance of the system for parameter combinations not analysed by deterministic analyses.

1.3 Scope of this report

This report is not intended to be a "stand-alone" report; rather, it should be used together with, and as a complement to, the main report⁹, and, to some extent, the more detailed reference reports. As mentioned above, it is designed to provide a compilation of detailed, traceable information that should allow the interested reader to independently re-calculate the results of all assessment cases discussed in the main report and includes:

⁷ The reference model chain consists of the models STMAN - PICNIC - TAME.

⁸ GIPC: General Input Processing Code, see Appendix 2.

⁹ A certain degree of overlap between the two reports is, however, inevitable.

- a description of the conceptual models used in the safety assessment,
- a description of the corresponding computer codes, and
- the data used to evaluate the assessment cases.

Except for a few cases, it does not include justifications of assumptions; these are given, as a rule, in the main report or in the reference reports.

The models and codes described in this report include:

- the principal models / codes (near field, geosphere and biosphere) that were used to calculate the results presented in Chapter 7 of the main report ("Evaluation of the performance of the disposal system"), including simplified analytical calculations,
- the principal models / codes that were used to calculate the results presented in Chapter 6 of the main report ("The safety concept and the identification of assessment cases"), including insight models, and
- GIPC, the driver for probabilistic analyses that runs codes of the reference model chain in a probabilistic mode (used for calculations presented both in Chapters 6 and 7 of the main report).

The data presented in this report include:

- all Reference Case data and all data for the alternative cases for the codes mentioned above, and
- all input data for the probabilistic analyses.

Models and codes not described in this report are the *supporting models* used to derive parameter values for the near field, geosphere and biosphere models, and to support model assumptions. These include, for example, groundwater flow models, mechanistic models of sorption, temperature evolution models, waste dissolution models, etc. These are described in the reference reports (see Figure 1.1-1).

Generally, no final results are presented in this report; however, in a few cases, where this is considered to help understanding, some final and / or intermediate results are shown. The results of all assessment cases analysed (see Tab. 2.2-1) are given in the main report (Nagra 2002c); in some cases in the form of dose curves, but in the majority of cases only in terms of dose maxima in a number of figures and tables. The detailed, time-dependent results of all cases, including intermediate results, are compiled in a Nagra working report in electronic form (Nagra 2003c).

1.4 Organisation of this report

As mentioned above, this report describes the models, codes and data used in the main report.

Chapter 1 is the introductory chapter, explaining the role of the present report within Project *Entsorgungsnachweis*, the use of quantitative models in this safety assessment and the scope and organisation of the present report.

Chapter 2 presents a brief overview of the disposal system and introduces the list of assessment cases, which are structured according to the methodology described in the main report (Nagra

2002c, Tab. 6.8-2). Also included in the list of assessment cases is information on the codes used to analyse each case.

Chapters 3 to 8 describe the models, codes and data used to analyse the assessment cases. Even though in principle the detailed equations underlying the conceptual models should be included in these early chapters describing how the assessment cases were analysed, they are only given in Appendix 1 to avoid repetition. Chapter 3 addresses the assessment cases that fall within the scope of the Reference Scenario, Chapters 4 and 5 address cases that fall within the scope of alternative scenarios related to the release of radionuclides as volatile species along gas pathways and to the release of dissolved radionuclides affected by human actions, respectively. Chapter 6 covers the models, codes and data for "what if?" cases, which involve assumptions that are outside the range of possibilities supported by scientific evidence and, in order to limit the number of cases, involve perturbations to key properties of the pillars of safety¹⁰. This group of "what if?" cases serves to illustrate the robustness of the system. Cases addressing design and system options are covered in Chapter 7. Cases illustrating the effects of uncertainty in the biosphere on dose are covered in Chapter 8. For each conceptualisation, "what if?" case, design and system option or illustration of biosphere uncertainty, the description includes:

- an overview,
- a description of the model and its underlying assumptions,
- the codes used to solve the governing equations of the model, referring ahead to Appendix 1 for a detailed description of the general-purpose codes, and
- the parameters and variations used (referring ahead to Appendix 3, where appropriate).

For each tool, a qualitative description of its capability in terms of the Super-FEPs¹¹ that it can address is also included, with a corresponding quantitative description given in tabular form in Appendix 1. This is important within the FEP management procedure to allow an evaluation of the suitability of a given tool to address a given Super-FEP (Nagra 2002d). Note, however, that it is beyond the scope of the present report to show that the list of Super-FEPs is comprehensive and adequate to describe the system; this topic is treated in Nagra (2002d).

Chapter 9 discusses the insight models and associated data used in Chapter 6 of the main report to examine particular aspects of Reference Case system performance in more detail, and to investigate sensitivity to key system properties and model assumptions.

Chapter 10 assesses the modelling approaches used to evaluate the assessment cases. It summarises the various assumptions and simplifications made in order to arrive at sets of mathematical equations and input parameters so that each case can be quantitatively evaluated, and it assesses these assumptions and simplifications in terms of their degree of realism, pessimism or conservatism. This information is then used as a tool to systematically assess the bias that has been introduced into the models ("bias audit").

Appendix 1 describes in detail the codes used to model the majority of the assessment cases. Each code is considered in turn, and a discussion is given of:

- the scope and purpose of the code,
- the phenomena included in the code,
- the mathematical representation of these phenomena,

¹⁰ See Nagra (2002c), Appendix 5, for a definition of "what if?" cases, pillars of safety and other key terms.

¹¹ A Super-FEP comprises several FEPs related to a common theme, see Section 6.8.2 of Nagra (2002c).

- the input parameters required by the code,
- verification of the code, and
- the capability of the code in terms of the Super-FEPs that it can address.

Appendix 2 describes the management of probabilistic calculations. In all cases evaluated probabilistically, the model chain STMAN - PICNIC was used to treat near-field and geosphere transport, respectively. In order to convert releases from the host rock to dose, steady-state biosphere dose conversion factors (BDCFs) were used that were evaluated using the biosphere code TAME with reference-case input parameters (see Appendix 3). The input probability density functions for STMAN and PICNIC used in the probabilistic analyses are given in Appendix 3.

Appendix 3 presents a compilation of the various physical, geological, geochemical and biosphere datasets used. It is designed to serve a two-fold purpose: for each assessment case, it should allow the reader (i) to determine with relatively little effort what parameter values were used to evaluate that particular case, and (ii) to identify the source of each parameter value given. In order to achieve this dual purpose, a clear hierarchy is introduced. In a first category of tables, the parameter combinations used for each assessment case are indicated (e.g. Tab. A3.2-1a for STMAN calculations within the Reference Scenario). In a second category of tables (e.g. Tab. 3.3-1 for STMAN calculations), either the values themselves, or, for example in the case of radionuclide inventories, references to tables, are given for all parameter combinations, together with further references to a third category of tables linking the data to the source, which is typically one of the reference reports. An example for this third category is Tab. A3.3-2a for SF near field parameter values. In order to help the reader, input parameters required by the codes are not only given in Appendix 3, but are introduced and listed in tabular form in the chapters where the applications of the codes are first described, with reference to the special tables in Appendix 3 mentioned above.

Appendix 4 discusses an insight model that solves the governing equations for steady-state transport of radionuclides through the Opalinus Clay intersected by discontinuities, as used in Chapter 6 of the main report.

Appendix 5 gives the derivation of the list of safety-relevant radionuclides included in the safety assessment.

Appendix 6 describes the semi-quantitative dose estimate used for the assessment case related to a periglacial climate.

Appendix 7 discusses the applicability of the one-dimensional approximation for modelling radionuclide transport through the Opalinus Clay.

Appendix 8 gives a summary of the quality assurance measures relevant to the development and application of the models, codes and data used in the safety assessment for Project *Entsorgungsnachweis*.

2 System to be modelled and Assessment Cases

2.1 Overview of the disposal system and the multi-barrier system

In the present chapter, the most relevant components of the disposal system, including the repository layout and the system of safety barriers, are discussed. A more detailed description of the disposal system is given in Nagra (2002b, 2002c).

Figure 2.1-1 illustrates a possible layout for the repository, which would be placed in the centre of the Opalinus Clay formation, and Figures 2.1-2, 2.1-3. and 2.1-4 provide overviews of the system of safety barriers for each of the three waste types: spent fuel (SF), high level waste (HLW) and long-lived intermediate level waste (ILW). In each case, the principal components of the multi-barrier system are listed, together with the key attributes that contribute to the safety functions defined in the main report (Chapters 2, 6).

SF assemblies consist of ceramic uranium oxide (UO_2 or MOX) pellets contained in a zirconium alloy (Zircaloy) cladding. The radionuclides of HLW are incorporated into borosilicate glass. The ILW, which contains much lower activity than SF or HLW, is embedded within a cement or, in some cases, a bitumen solidification matrix in steel drums.

In the proposed repository, carbon steel canisters containing either SF or HLW from reprocessing are emplaced co-axially within a system of parallel tunnels that are excavated in the mid-plane of the Opalinus Clay layer. For SF, a design variant of a copper canister with a steel insert is also considered. The tunnels are backfilled with a combination of bentonite granules and bentonite blocks that support the canisters, forming a buffer around the canisters.

The ILW drums are placed within concrete containers. These containers are placed in tunnels with a larger cross-section than those for SF/HLW. Void spaces within and around the containers are filled with cementitious grout.

A plan view of the repository is shown in Figures 2.1-5 (monitoring phase) and 2.1-6 (after final closure). The main elements include:

- an access ramp, construction and operations tunnels, central waste receiving facilities and a shaft,
- pilot and test facilities,
- an array of SF/HLW emplacement tunnels of 800 m length, spaced 40 m apart, and
- three short emplacement tunnels for ILW.

The waste emplacement tunnels and the operations and construction tunnels will be excavated at a depth of ~650 m in the centre of the Opalinus Clay formation, which dips gently to the south-east. Horizontal emplacement in tunnels was selected rather than borehole emplacement because the Opalinus Clay formation is 100 – 125 m thick, thus tunnel emplacement maximises the length of the radionuclide transport path to adjacent formations. Local variations in the dip of the formation mean that the tunnels are not always absolutely centered in the formation, thus the transport path may be less than 50 m in some locations. The maximum principal stress is 21 MPa and is nearly horizontal with a N-S orientation. The minimum stress and lithostatic stress are 15 MPa. The SF/HLW tunnels (diameter = 2.5 m) are oriented in the direction of the maximum stress so as to maximise tunnel stability. These tunnels are expected to be self-supporting, based on experience with excavations in Opalinus Clay (Nagra 2002b). All other tunnels, including the ILW emplacement tunnels and the access ramp, require concrete liners to

ensure tunnel stability. The design and operations of the repository are described in detail in Nagra (2002b).

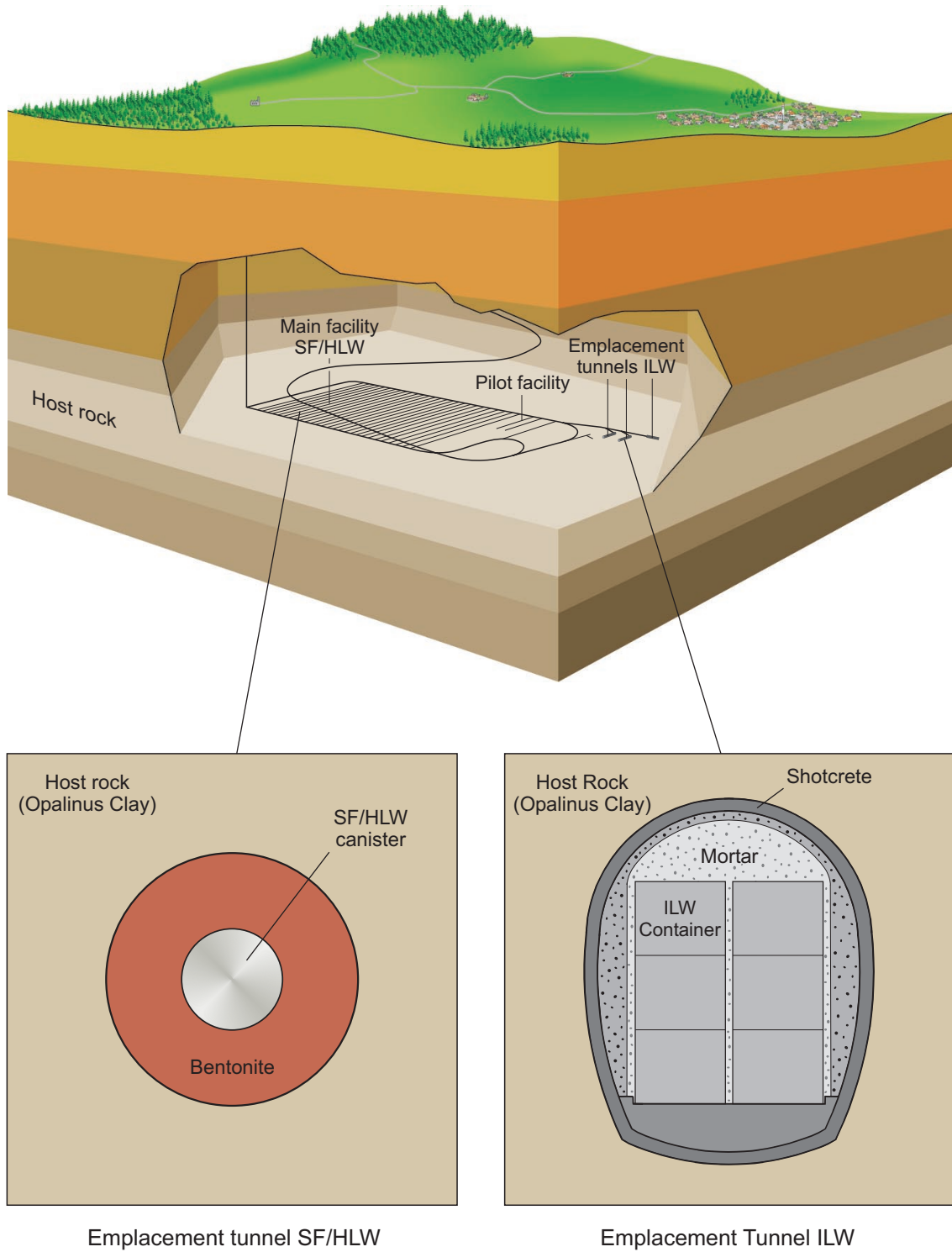


Fig. 2.1-1: Possible layout for a deep geological repository for SF/HLW/ILW in Opalinus Clay

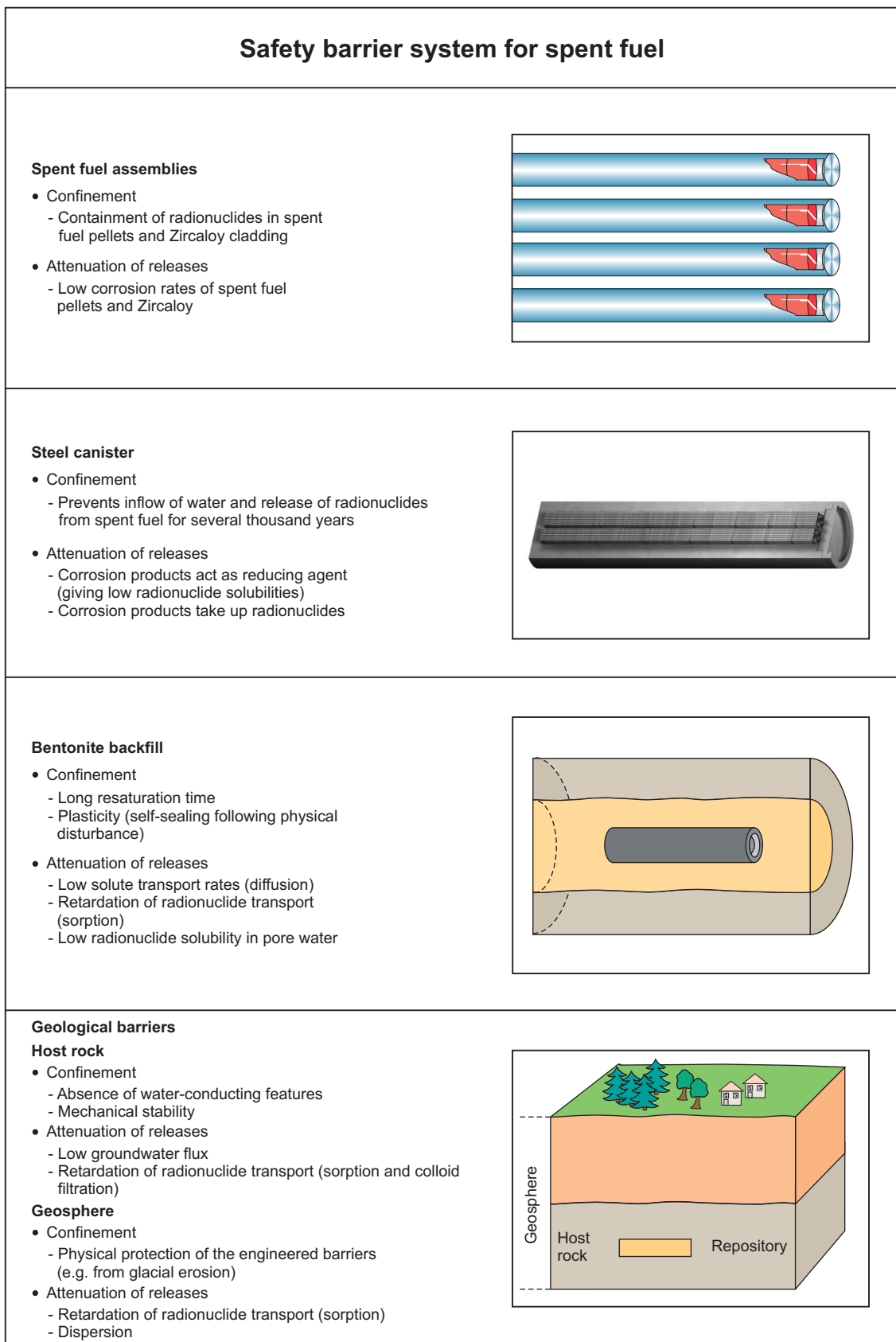


Fig. 2.1-2: The system of safety barriers in the case of SF

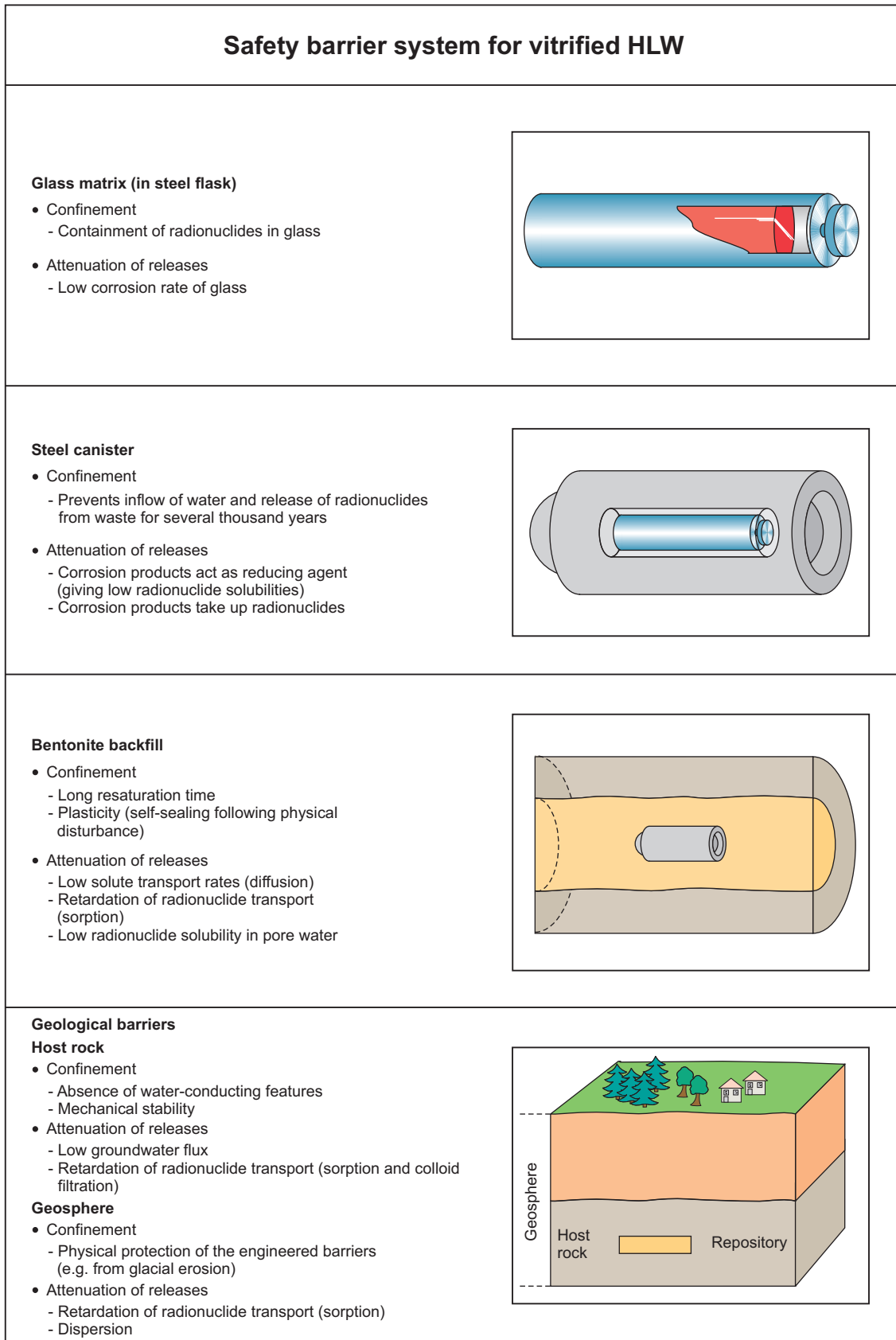


Fig. 2.1-3: The system of safety barriers in the case of HLW

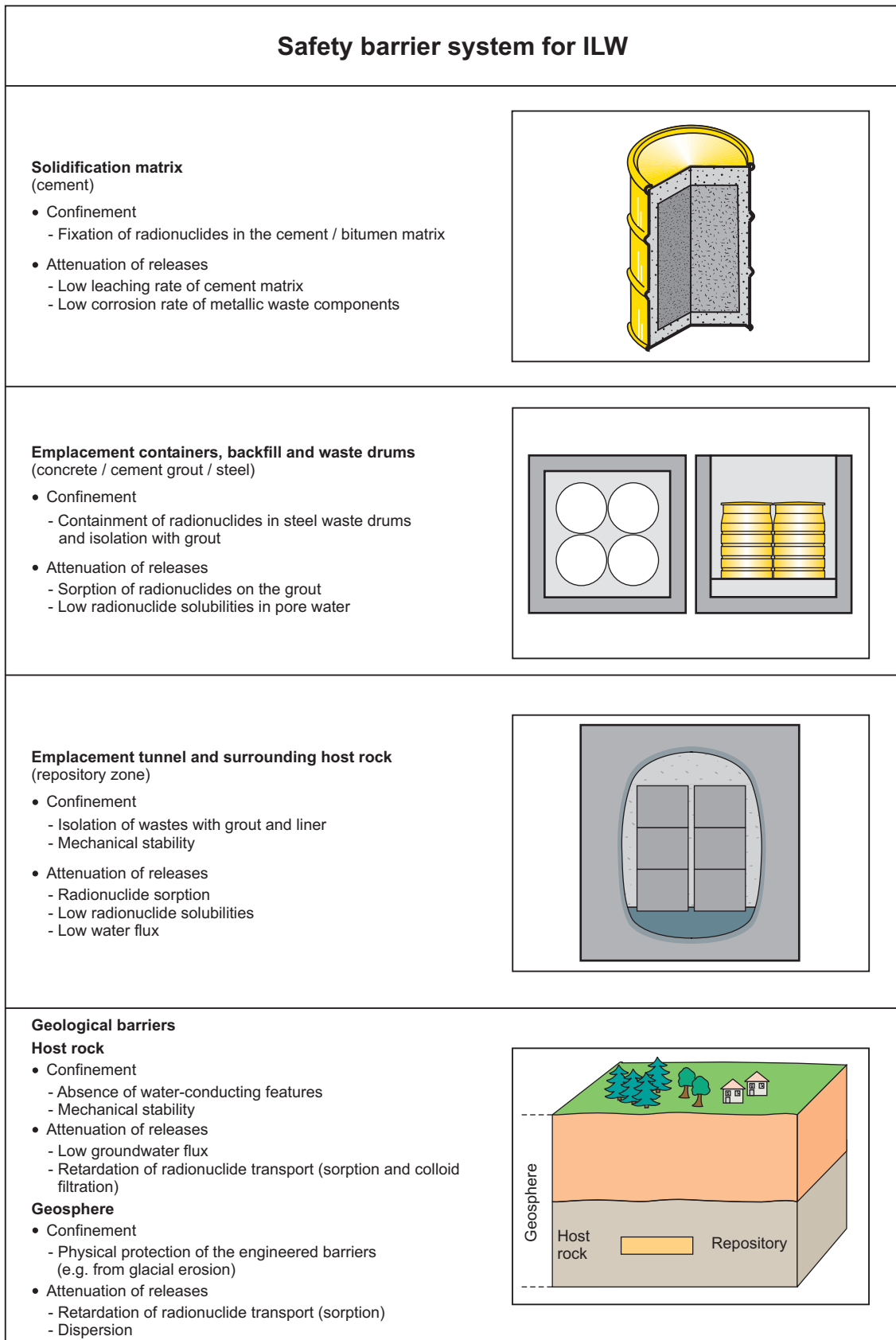


Fig. 2.1-4: The system of safety barriers in the case of ILW

Monitoring phase

The status of the disposal facility after the completion of emplacement of all wastes is shown in Figure 2.1-5. At this time, all wastes are in backfilled and sealed emplacement tunnels and the main operations tunnels are sealed. The wastes in the pilot facility are in backfilled emplacement rooms that are accessible to monitoring using the adjacent observation tunnel and monitoring boreholes.

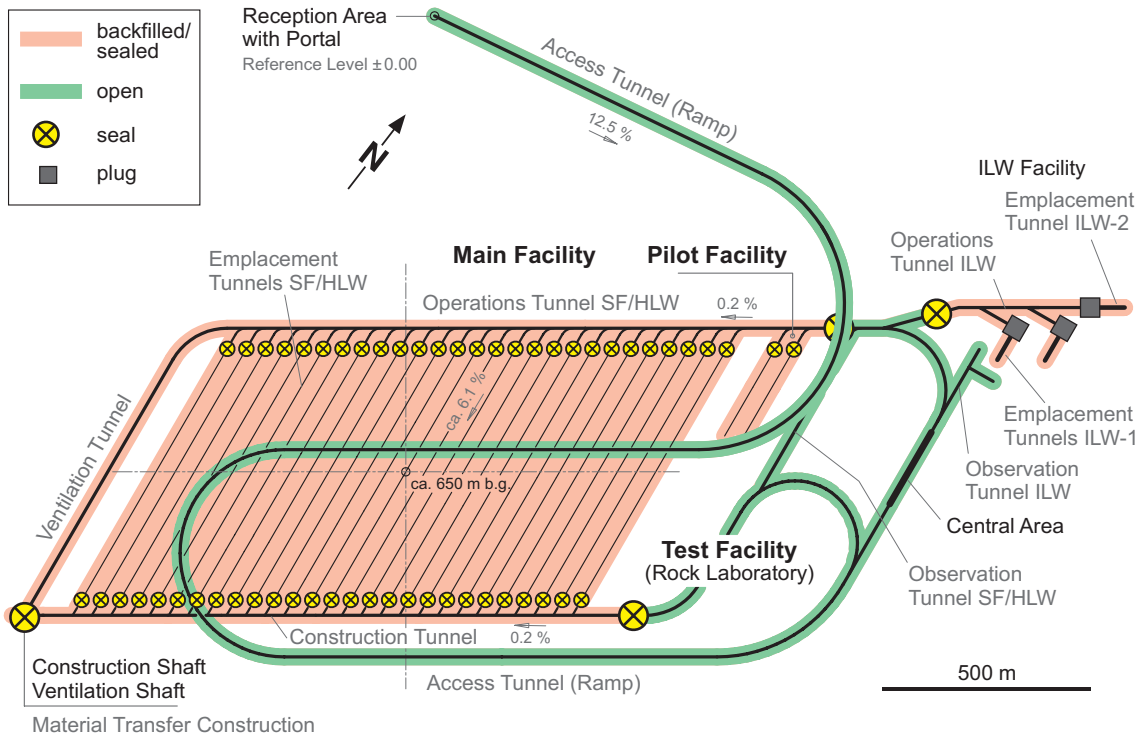


Fig. 2.1-5: Status of the repository during the monitoring phase, when waste emplacement is complete, but before final sealing and closure of the facility

Note that the seals are considered to comprise highly compacted bentonite, along with a concrete bulkhead. Plugs at the entrances to ILW emplacement tunnels are composed of concrete.

Closure and final sealing

Final closure of the facility would involve backfilling the observation tunnels and the ramp with a bentonite/sand mixture and placing seals of highly compacted bentonite contained between bulkheads at the construction branchoff of the access tunnel (Figure 2.1-6), as well as where the ramp intersects the overlying Wedelsandsstein. These long-term seals are designed with the objective of ensuring that the main tunnels and access ramp have hydraulic properties similar to those of the undisturbed host rock.

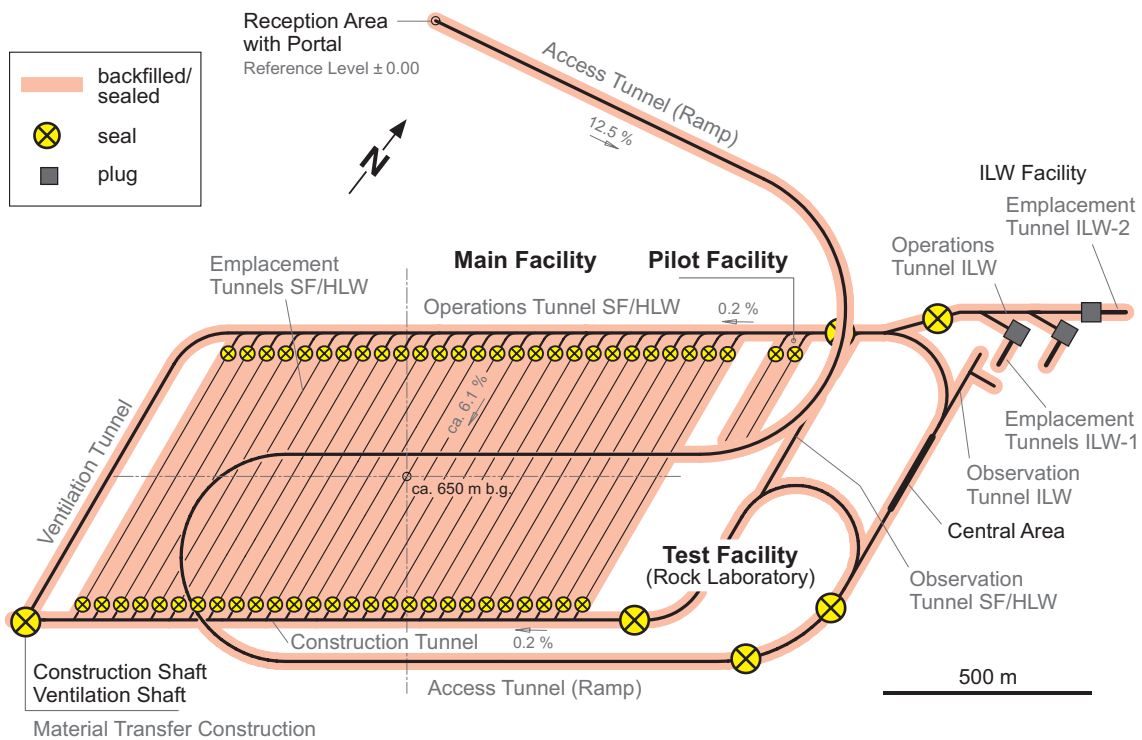


Fig. 2.1-6: Status of the repository after final sealing and closure of the facility

2.2 The list of assessment cases

As described in Chapter 6 of Nagra (2002c), assessment cases are divided into a number of groups, according to the issues or uncertainties that they address. In particular, these groups include:

- cases that explore the range of possibilities arising from particular uncertainties affecting the disposal system, where this range can be bounded with reasonable confidence on the basis of available scientific understanding,
- "what if?" cases to test the robustness of the disposal system,
- cases to address design and system options, and
- cases to scope different (stylised) possibilities for the characteristics and evolution of the surface environment (the biosphere).

Like the Reference Case, each alternative case is defined in terms of a scenario (the broad evolutionary path that the disposal system follows), a number of conceptual assumptions for modelling key FEPs, and a set of parameters. Issues and uncertainties are assessed as to whether they (i), significantly affect the broad path of evolution of the disposal system described by the Reference Scenario, in which case they generate alternative scenarios, or whether they only affect (ii), the conceptualisation of FEPs within a given scenario, or, (iii), the assignment of parameter values within a given conceptualisation of a scenario. The result is a number of scenarios, within each of which there may be alternative conceptualisations of particular FEPs. Furthermore, for each conceptualisation, there may be a range of alternative parameter sets, including a Base Case parameter set. This hierarchy of scenarios, conceptualisations and parameter sets is illustrated in Fig. 2.2-1.

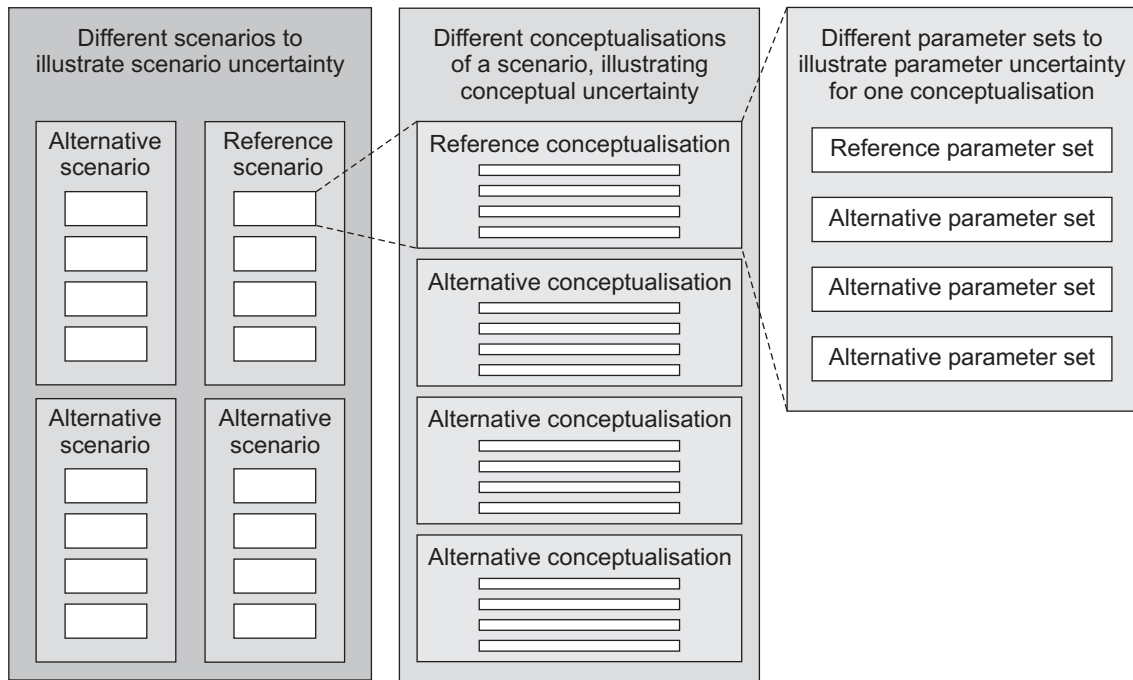


Fig. 2.2-1: The hierarchy of scenarios, conceptualisations and parameter sets

The assessment cases are shown grouped in this manner in Tab. 2.2-1. Each case is defined in terms of the main group (scenarios, "what if?" cases, design and system options, illustrations of biosphere uncertainty), the conceptual assumptions used for modelling specific phenomena, and a set of parameters. The cases are each assigned a number for identification. The first character identifies the scenario, or the fact that it is a "what if?" case, a case addressing design and system options, or a case illustrating biosphere uncertainty. The second character (after the point) indicates differences in conceptual assumptions. The third (alphabetical) character indicates differences in the datasets used. Also indicated are the codes applied to evaluate each assessment case.

Tab. 2.2-1: List of scenarios, what if cases, design and system options and illustration of biosphere uncertainty with associated conceptualisations and parameter variations that define the different assessment cases, structured according to the categories of uncertainty that they address

Also indicated are the codes applied to evaluate each assessment case. Numbers in brackets refer to the sections in the Safety Report (Nagra 2002c) where each scenario is discussed.

Alternative scenarios addressing scenario uncertainty	Alternative conceptualisations addressing conceptual uncertainty	Parameter variations addressing parameter uncertainty	Codes applied							
			SPENT	STRENG	STALLION	PICNIC	TAME	FRAC3DVS	GAS MODEL	Analytical calculations
1. Reference Scenario Release of dissolved radionuclides (7.4)	1.1 Reference conceptualisation	1.1a Reference Case (RC)	x	x	x	x	x			
		1.1b Variability in canister inventory	x	x		x	x			
		1.1c Reduced canister lifetime	x	x		x	x			
		1.1d Pessimistic near field geochemical dataset	x	x	x	x	x			
		1.1e Increased glass dissolution rate in HLW		x		x	x			
		1.1f Increased water flow rate in geosphere (10-fold increase)	x	x	x	x	x			
		1.1g Decreased water flow rate in geosphere (10-fold decrease)	x	x	x	x	x			
		1.1h Pessimistic geosphere sorption constants	x	x	x	x	x			
		1.1i Pessimistic near-field and geosphere geochemical dataset	x	x	x	x	x			
		1.1j Pessimistic geosphere diffusion constants	x	x	x	x	x			
		1.1k Pessimistic treatment of ¹⁴ C (organic) in SF	x			x	x			
	1.2 Solubility-limited dissolution of SF	1.2a Base Case only	x			x	x			
	1.3 Bentonite thermal alteration	1.3a Base Case only	x	x		x	x			
	1.4 Glacially-induced flow in the Opalinus Clay	1.4a Base Case only	x				x	x		
	1.5 Additional barrier provided by confining units	1.5a Vertical transport through confining units	x	x	x	x	x			
		1.5b Horizontal transport in local aquifers	x	x	x	x	x			
	1.6 Radionuclide release affected by ramp / shaft	1.6a Base Case	x	x	x	x	x			
		1.6b Increased hydraulic conductivity of EDZ (100-fold increase)	x	x	x	x	x			
	1.7 Convergence-induced release affected by ramp (ILW)	1.7a Steady-state hydraulics			x	x	x			
		1.7b Water pulse			x		x	x		
	1.8 Gas-induced release of dissolved radionuclides affected by ramp / shaft	1.8a Base Case	x		x	x	x			
		1.8b Increased water flow rate in ILW			x	x	x			

Tab.2.2-1: (Cont.)

Alternative scenarios addressing scenario uncertainty	Alternative conceptualisations addressing conceptual uncertainty	Parameter variations addressing parameter uncertainty	Codes applied								
			SPENT	STRENG	STALLION	PICNIC	TAME	FRAC3DVS	GAS MODEL	Analytical calculations	
	4.6 Unretarded transport of ¹⁴ C released as volatile species through host rock; retardation in confining units taken into account	4.6a-c Three different gas permeability values								x	
	4.7 Poor near field and pessimistic near-field / geosphere geochemical dataset	4.7a RC flow rate	x	x	x	x	x				
		4.7b 10-fold increase of flow rate	x	x	x	x	x				
		4.7c 100-fold increase of flow rate	x	x	x	x	x				
	4.8 No advection in geosphere (diffusive transport only)	4.8a Base Case only	x	x	x	x	x				
	4.9 SF: Increased cladding corrosion rate	4.9a 10-fold increase with respect to RC	x			x	x				
	4.10 K _a (l) for NF and geosphere = 0	4.10a Base Case only	x	x	x	x	x				
	4.11 Decreased transport distance in Opalinus Clay (30 m)	4.11a Base Case only	x	x	x	x	x				
5. Design and system options (7.8)	5.1 Increased waste arisings (300 GWa(e))	5.1a Base Case only	x			x	x				
	5.2 ILW high force compacted waste option	5.2a Base Case only			x	x	x				
	5.3 SF canister with Cu shell	5.3a Canister breaching at 10 ⁵ years	x			x	x				
		5.3b Initial defect (small initial pinhole, full breaching at 10 ⁵ years)	x			x	x				
		5.3c Initial defect (large initial pinhole, full breaching at 10 ⁵ years)	x			x	x				
6. Illustration of effects of biosphere uncertainty (7.9)	6.1 Reference and alternative geomorphology	6.1a Reference area (RC)	x	x	x	x	x				
		6.1b Sedimentation area	x	x	x	x	x				
		6.1c Wetland	x	x	x	x	x				
		6.1d Exfiltration to spring located at valley side	x	x	x	x					x
	6.2 Reference and alternative climates	6.2a Present-day climate (RC)	x	x	x	x	x				
		6.2b Drier / warmer than present-day climate	x	x	x	x	x				
		6.2c Wetter / warmer than present-day climate	x	x	x	x	x				
		6.2d Periglacial climate	x	x	x	x					x

3 The Reference Scenario

3.1 The Reference Conceptualisation

3.1.1 Overview

The Reference Conceptualisation is based on the assumption that the likely / expected broad evolutionary path of the disposal system is followed. In particular, the pillars of safety¹² are assumed to operate as expected:

- *The deep underground location of the repository* is assumed to be maintained over several million years, isolating the waste from the surface environment.
- *The host rock* is assumed to maintain its safety-relevant properties over several million years and these properties are not significantly perturbed by the presence of the repository (e.g. by gas generated within the repository), by geological and climatic events and processes and by any future human activities. The low hydraulic conductivity and the fine, homogeneous pore structure of the host rock, as well as the backfilling and sealing of the access tunnel and shaft, ensure that transport of radionuclides through the near field and host rock is dominated by aqueous diffusion. The sealed access tunnel and shaft are assumed at no time to provide preferential transport pathways, although some limited radionuclide transport along these features may occur.
- *The favourable chemical environment*, which provides a range of geochemical immobilisation and retardation processes, is assumed to be maintained over several million years.
- *The bentonite buffer (for SF and HLW)*, which provides a well-defined interface between the canisters and the host rock, with similar properties as the host rock, is assumed to maintain its favourable properties over several million years.
- *The SF and HLW waste forms* continue to retain most radionuclides after canister breaching. Some ILW components, such as hulls and ends from reprocessing, are also stable and will retain radionuclides, although no credit is taken for this in the reference conceptualisation (see below).
- *The SF and HLW canisters* provide an initial period of complete containment (although the possibility of one or more initial canister defects cannot be excluded). For all waste types, the repository and its surroundings are assumed to be fully resaturated by the time pore-water comes into contact with the wastes and porewater is assumed to have reached chemical equilibrium.

This is the definition of the Reference Scenario (see Nagra 2002c). In addition, in the Reference Conceptualisation of this scenario, a number of assumptions are made regarding the conceptualisation for modelling purposes of key FEPs associated with the various system components, some of which can be justified on the grounds of conservatism, whereas others are explored in alternative scenarios and conceptualisations.

¹² For the definition of the *pillars of safety*, see Appendix 5 in Nagra (2002c).

3.1.2 The conceptual model and its underlying assumptions

In describing the conceptual model and its assumptions, it is convenient to consider the following aspects separately:

- radionuclide inventories,
- the period of complete containment,
- radionuclide release from the waste forms,
- radionuclide transport through the SF/HLW bentonite buffer and ILW cementitious buffer,
- the interface with the host rock,
- radionuclide transport in the host rock,
- radionuclide transport through the overlying and underlying sedimentary layers (the "confining units" and regional aquifers), and
- the surface environment and exposure pathways.

Radionuclide inventories

The radionuclide inventory in the repository is assumed to be initially present in:

- the SF matrix and HLW borosilicate glass, in which radionuclides are homogeneously mixed,
- the SF grain boundaries of the fuel matrix, in fuel pellet cracks and in the gap between the fuel and cladding – this is termed the instant release fraction (IRF) in the SF inventory,
- the SF Zircaloy cladding (which includes a 20 % IRF for ^{14}C), and
- the ILW waste forms.

In the Reference Conceptualisation, all ^{14}C originating from the cladding is considered to be in organic form, whereas all ^{14}C from the fuel matrix is assumed to be inorganic.

The concept of monitored geological disposal (EKRA 2000, Nagra 2002c) involves the disposal of a small but representative amount of SF and HLW in separate waste emplacement tunnels (the pilot facility) for monitoring purposes. The radionuclide inventory contained in the pilot facility is not, however, analysed separately, but is added to the model inventories for SF and HLW of the main facility.

The period of complete containment

SF and HLW are contained within steel canisters. These canisters are emplaced coaxially along the emplacement tunnels of the repository, with the gaps between the canisters, and between the canisters and the tunnel walls, filled with a bentonite buffer. The canisters are assumed to remain in this position over the entire period of the assessment, i.e. canister sinking is assumed to be negligible.

Eventually (after 10 000 years in the Reference Case) it is assumed that the canisters are breached due to mechanical loads, following some degree of weakening by corrosion. Then water contacts the waste forms and radionuclide release begins. In the cases of SF and HLW, prior to canister breaching time, the canister is assumed to be completely intact. The only

significant processes occurring within the canister up to this time are radioactive decay and ingrowth. All SF and HLW canisters are assumed to be breached simultaneously at a reference time of 10 000 years following waste emplacement. No initially defective canisters are present.

In the case of ILW, release of radionuclides to solution is assumed not to begin until a reference time of 100 years after waste emplacement due to incomplete resaturation of the repository and its surroundings at earlier times.

It is conservatively assumed that SF/HLW canister breaching is instant and complete, so the breached canisters provide no physical barrier to water ingress or radionuclide release. Furthermore, no credit is taken for the possible continued integrity of the SF Zircaloy cladding and the HLW fabrication flasks. Sorption onto canister corrosion products and transport resistances provided by cracks in the waste forms are also neglected.

The governing equations describing the period of complete containment are described in Appendix 1. They are Eqs. A1.3-1 and A1.3-2 for all three waste forms.

Radionuclide release from the waste forms

The release rates of radionuclides depend on the location of the radionuclides:

- radionuclides in the SF matrix and HLW borosilicate glass are released congruently as these matrices dissolve,
- radionuclides in the SF IRF and in the ILW waste forms are released immediately following the period of complete containment, and
- radionuclides in the SF cladding (other than the 20 % ^{14}C IRF) are released congruently with cladding corrosion.

The rate of SF matrix dissolution changes with time, since it is assumed here to be controlled by the generation of radiolytic oxidants. The modelling of this process is described in Chapter 9. The overall cladding corrosion rate is assumed to be constant with time, as is the rate of HLW dissolution per unit surface area of wetted glass. At production during cooling of the HLW glass, cracks form so that the surface area of the waste form at the time of emplacement is greater than that of original moulded blocks. Glass fragments are conceptualised as a number of equally sized spheres, with a total volume equal to the total volume of glass, and a total surface area that accounts for the cracking of the glass. The surface area of the spheres decreases with time as they dissolve.

Radionuclides released from the waste forms are conceptualised as entering "reservoirs" of water within the SF and HLW canisters, and within the pore space of the ILW emplacement tunnels, where they are uniformly mixed. Chemical equilibrium is assumed to exist within the reservoirs. Solubility limits appropriate to the chemical conditions constrain the aqueous concentrations of radionuclides, with precipitation occurring if the solubility limits of the corresponding elements are exceeded, and redissolution occurring if concentrations fall. Only the concentrations of isotopes originating from the waste are taken into account in evaluating whether solubility limits are exceeded. The background concentrations of isotopes originating elsewhere are conservatively ignored. In the case of radium, since the necessary data are available and because of the potential significance to safety of ^{226}Ra , co-precipitation with inactive isotopes of chemically similar elements is taken into account. In all other cases, however, immobilisation by co-precipitation is conservatively neglected, as is sorption on the corrosion products of the canisters and waste forms.

Conservatively, no sorption is considered to occur within the reservoirs in the cases of SF and HLW. In the case of ILW, it is assumed that radionuclides released from the waste matrix are partitioned between aqueous, sorbed and precipitated phases. Linear, reversible, equilibrium sorption is assumed, described by an element-dependent sorption coefficient (K_d).

The governing equations describing radionuclide release from the waste forms and the evolution of concentration in the reservoirs are Eqs. A1.3-3 to A1.3-8 for SF, Eqs. A1.4-1 to A1.4-7 for HLW, and Eqs. A1.5-1 to A1.5-5 for ILW.

Radionuclide transport through the SF/HLW bentonite buffer and the ILW cementitious buffer

The buffer surrounding the SF and HLW canisters is an annular region between the canister and the tunnel wall. It is assumed that the bentonite is fully resaturated at the time of canister breaching, with transport-relevant properties that are constant in space and time. In particular, the thermally altered zone in the bentonite around the waste packages is assumed to be of negligible extent and any radiolytic oxidants formed near the wastes are assumed not to migrate significantly into the buffer.

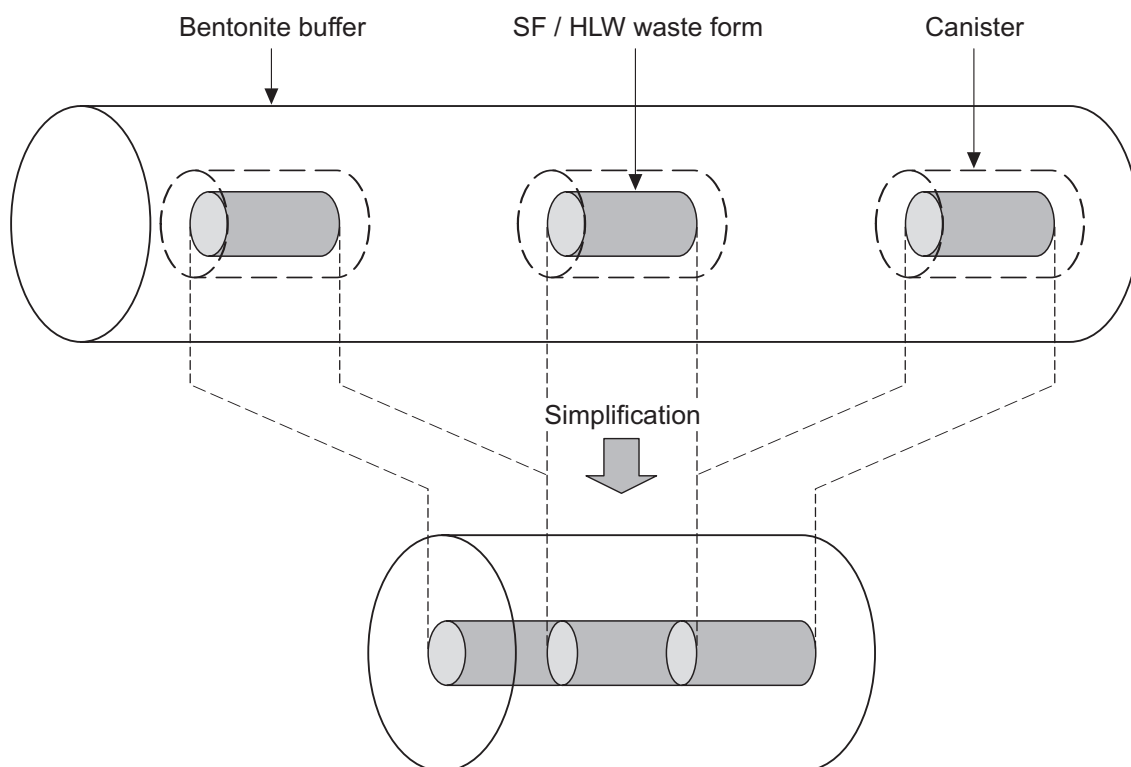


Fig. 3.1-1: Geometrical simplification for modelling of radionuclide transport through the SF/HLW bentonite buffer

Within the buffer, radionuclide transport is assumed to take place by diffusion, described by Fick's laws, and retarded by linear, reversible, equilibrium sorption, described by an element-dependent sorption coefficient (K_d). Some radionuclides are subject to anion exclusion which affects their diffusion coefficients and the effective porosity that they can access. The hydraulic properties are assumed to prevent any significant advective flow. Gas-mediated transport is

assumed to be negligible. Furthermore, any colloids are assumed to be immobile in the bentonite and are, therefore, neglected. As in the reservoir, constant chemical conditions are assumed to prevail within the buffer, with solubility limits constraining radionuclide concentrations.

For the calculation of diffusion through the buffer, the geometry of the system is simplified in such a way that only one-dimensional radial diffusion is considered, i.e. the axial diffusion of radionuclides into the buffer separating the canisters is conservatively neglected. The release of radionuclides from the buffer surrounding the SF and HLW is thus calculated as if the waste forms were arranged end-to-end in a continuous cylinder, as illustrated in Fig. 3.1-1.

The governing equations describing radionuclide transport through the SF/HLW bentonite buffer are Eqs. A1.3-11 to A1.3-14 for both SF and HLW.

In the case of ILW, the waste forms, emplacement containers and surrounding buffer are assumed to be homogeneously mixed in two separate cylindrical volumes, representing two ILW-1 emplacement tunnels on the one hand and the single ILW-2 emplacement tunnel on the other hand. It is assumed that the emplacement tunnels are fully resaturated at the reference time of 100 years (see above), with transport-relevant properties that are constant in space and time. No thermal alteration is expected and any radiolytic oxidants formed near the wastes are assumed not to migrate significantly into the buffer.

After 100 years, instantaneous homogeneous mixing of all radionuclides is assumed within the buffer. The radionuclides are distributed between aqueous and solid phase by linear, reversible, equilibrium sorption, described by an element-dependent sorption coefficient (K_d). The aqueous concentrations of radionuclides are constrained by solubility limits. The model does not include porosity scaling factors since the cement is assumed to be an open structure in which anion exclusion is not important. The hydraulic properties of the host rock are assumed to prevent any significant advective flow in the ILW emplacement tunnels. In the near field calculations, this is modelled by assuming a thin annular region of surrounding Opalinus Clay (thickness 1 cm), in which radionuclide transport is by diffusion only, taking linear, reversible, equilibrium sorption and anion exclusion into account, as in the case of transport through the host rock (see below). It can be readily shown that any further decrease of the diffusion length (say to 1 mm) has no significant impact on radionuclide release rates from the near field (see App. 3.6). Furthermore, gas-mediated transport is assumed to be negligible. Any colloids are assumed to be immobile in the surrounding host rock and are, therefore, neglected.

The governing equations describing mixing, sorption and release of radionuclides in the ILW cementitious buffer are Eqs. A1.5-1 to A1.5-5.

Interface with the host rock

At the interface between the buffer and the host rock it is assumed that the transport processes can be mathematically decoupled. Conceptually, transport processes in the host rock carry radionuclides away from the interface into the host rock at a rate that balances their rate of arrival by diffusion from the bentonite buffer or the cementitious ILW backfill (s. Eq. A1.3-16). In reality (and especially for a host rock where diffusion is the dominant transport process) radionuclides can diffuse back from the host rock into the bentonite buffer or the cementitious ILW backfill, but this is conservatively neglected.

The rate at which transport processes in the host rock carry radionuclides away from the interface into the host rock is described in terms of an effective flow rate at the interface,

Q_{eff} [$\text{m}^3 \text{a}^{-1}$], even though the transport process in question is strongly affected by diffusion. As also discussed in Appendix 3 (Section A3.6), this flow rate is given by:

$$Q_{eff} = Q + \frac{AD_e}{L}, \quad (3.1-1)$$

where Q [$\text{m}^3 \text{a}^{-1}$] is the water flow rate per waste package¹³, D_e [$\text{m}^2 \text{a}^{-1}$] is the effective diffusion coefficient in the host rock, A [m^2] is the area per waste package and L [m] is an equivalent length for diffusion (see below).

The value chosen for the diffusion constant corresponds to non-anionic species, which is larger than the value for anionic species. The area per waste package is calculated as follows:

$$A = 2\pi r_{EDZ} p \quad (3.1-2)$$

where r_{EDZ} [m] is the EDZ radius and p [m] is the length of a waste package (the canister pitch in the case of SF/HLW and the tunnel length in the cases of ILW-1 and ILW-2).

L , the length over which the radionuclide concentration gradient is established, is assumed to be constant and equal for all radionuclides. In reality, L is time-dependent and depends on the properties of radionuclides (diffusion constant, decay rate). In the course of time and for non-decaying species, L increases from nearly zero to 40 m (i.e. the transport path length within Opalinus Clay). A value of 5 m has been chosen, in order not to underestimate the concentration gradient at early times. As shown by simplified analytical calculations, the combined near field and geosphere release rates of those radionuclides that are known to dominate dose are adequately reproduced by this simplified approach (Gribi 2003).

Radionuclide transport processes in the host rock

The host rock consists of the Opalinus Clay and the Murchisonae Beds in Opalinus Clay facies (although, in later sections of this chapter, the term "Opalinus Clay" is used in preference to "host rock", and is taken to include the Murchisonae Beds). It is assumed that its transport-relevant properties are constant in space and time. In particular, uplift and erosion are assumed to have negligible effects on the hydraulic properties of the host rock over the time period of interest, and it is assumed that the host rock contains no discontinuities with significant transmissivities. Furthermore, it is assumed that no radionuclides are transported along the tunnels, ramp and shaft, or their associated excavation-disturbed zones (EDZs). In effect, the transport-relevant properties of the backfilled and sealed tunnels, ramp and shaft are not distinguished from those of the surrounding host rock.

It is assumed that solubility limits are never exceeded within the host rock, so that radionuclides are present either in solution or as sorbed phases, but not as precipitated phases. Dissolved radionuclides are transported by diffusion and advection, with mechanical dispersion¹⁴. Advection is described using Darcy's law and is driven by the currently observed pressure difference between the small aquifers in the lower and upper confining units (Sandsteinkeuper, Wedel-sandstein). Glacial cycling is assumed to have negligible effects on advective transport. Diffusion and longitudinal mechanical dispersion are described using Fick's laws. Transverse

¹³ Note that for ILW, a "waste package" corresponds to 1 m of tunnel length.

¹⁴ Although heterogeneity is not considered explicitly, the mechanical dispersion that is assumed to occur during transport may be considered to arise, in part, from such heterogeneity. The combination of the processes of diffusion and mechanical dispersion is sometimes termed "hydrodynamic dispersion".

dispersion is conservatively neglected. Transport is retarded by linear, reversible, equilibrium sorption, described by an element-dependent sorption coefficient (K_d). Some radionuclides are subject to anion exclusion which affects their diffusion coefficients and the effective porosity that they see. Gas-mediated transport is assumed to be negligible. Any colloids are assumed to be immobile in the host rock and are, therefore, neglected.

For the calculation of transport through the host rock, the geometry of the system is simplified in such a way that only one-dimensional transport is considered. In effect, all transport paths through the host rock are assumed to be identical, so that only one such path needs to be considered. The applicability of the one-dimensional approximation for modelling transport through the Opalinus Clay has been investigated using a two-dimensional model (see Appendix 7). The dispersion caused by the spread of different near field release times of radionuclides from SF/HLW and ILW is taken into account, whereas the spread originating from different waste packages is conservatively neglected.

The generalised equation governing transport through the host rock is Eq. A1.6-4. This equation is formulated for a dual-porosity medium, with water conducting features embedded in a diffusion-accessible matrix. The equation for a homogeneous porous medium can, however, be obtained by setting j_m^n , the solute flux of nuclide n from the fracture to the matrix per unit matrix interface, to zero, thus making the final term in Eq. A1.6-4 irrelevant.

Radionuclide transport through the upper and lower confining units

It is assumed that radionuclides released from the host rock are transferred instantaneously to the biosphere. Transport times through the sedimentary layers overlying and underlying the host rock (the upper and lower confining units) are conservatively neglected. Furthermore, dilution in deep regional aquifers is small compared to that assumed to occur in Quaternary aquifers and in the surface environment, and is neglected.

The surface environment and exposure pathways

The assumptions made in modelling the surface environment and exposure pathways are adopted as part of a "stylised approach", as discussed in Chapter 2 of Nagra (2002c).

It is assumed that any radionuclides that migrate as far as the surface environment are strongly diluted in the Quaternary aquifer and in surface waters and sediments. Present-day climatic and surface environmental conditions are assumed to persist unchanged into the future, and, on this basis, the natural discharge zone for groundwater containing radionuclides originating from the repository is taken to be within some future equivalent of the present-day Rhine valley just below the Rhine Falls. This is a broad valley with high river flow and, moreover, contains substantial gravel deposits. Thus, a large dilution is guaranteed for groundwaters discharging to this valley¹⁵.

The river collects precipitation from a large area so that radionuclide concentrations away from the initial discharge zone are further reduced due to water exchange between the Quaternary aquifer and the river. Some radionuclides are assumed to be sorbed locally on sediments and

¹⁵ Although there are significant uncertainties associated with the climatic and geomorphological changes that are possible in northern Switzerland, key factors that determine the dilution of radionuclides in the surface environment are considered to be robust. One is the continued presence of a major river system, which is to be expected even in the event of drier climate states due to the nearby presence of large areas of high ground receiving precipitation, including the Alps and / or the Black Forest. Another is the continued direction of discharge from the repository towards this major river system under topographic heads imposed by the Alpine massive and foreland.

soils and retained within the surface environment, so that some degree of accumulation is possible. The processes of erosion and biological turnover, however, limit this accumulation so that concentrations in local solid materials cannot exceed levels determined by local and regional fluxes of solid material.

The distribution of radionuclides in the surface environment is analysed by means of a dynamic compartment model consisting of five main compartments¹⁶:

- Quaternary aquifer (gravel aquifer),
- deep soil layer,
- top soil layer,
- river water, and
- aquatic sediment.

The term "dynamic" means that the radionuclide inventory in each compartment is calculated as a function of time.

Transport of radionuclides between compartments occurs as a result of movements of water and diffusion (radionuclides in solution) and movements of solid materials (radionuclides sorbed onto the solid phase). The processes considered are:

- the interaction of the Quaternary aquifer with the river,
- the interaction of the river with the river bed sediments,
- irrigation of crops with water from the Quaternary aquifer or from the river (assuming 100 % from the Quaternary aquifer in the Reference Case),
- the effects of infiltrating meteoric water,
- bioturbation – the effects of soil fauna moving between soil horizons and transporting material (and adsorbed radionuclides),
- the maintenance and evolution of the river, e.g. flooding, dredging, meandering, leading to transport of solid material (and adsorbed radionuclides), and
- surface run-off, flooding and erosion of soil.

Processes operating on short timescales - typically with characteristic time constants of a few years or less, e.g. seasonal effects and episodic flooding, are included implicitly by averaging of the input data.

Average concentrations within the compartments are calculated as the total radionuclide content (time-dependent) divided by the total volume or mass (fixed over the time of the calculations). The concentrations of shorter-lived radionuclides, not treated explicitly in the dynamic model, are assumed to be in equilibrium with their longer-lived parents. The concentrations in the compartments are used to calculate the dose¹⁷ received by an average individual living in the region of discharge.

¹⁶ Note that in Fig. A1.7-1 of Appendix 1, the *Quaternary aquifer* is represented by the compartment *local aquifer*, and the river water is represented by the compartment *surface water*. *Local aquifer* and *surface water* are generic terms, which include other types of aquifers (e.g. non-Quaternary sediments) and surface waters (e.g. lakes).

¹⁷ For the definition of dose, see Appendix 5 in Nagra (2002c).

The population group for which the dose is to be calculated, is assumed to inhabit a region large enough to supply all basic requirements for a small community, and the group is assumed to obtain all its dietary requirements, including vegetables, grain, fruit, eggs, milk, meat and fish, from local sources. Furthermore, it is assumed that drinking water is abstracted from a well in the Quaternary aquifer. The soils in the region are used for agricultural production: arable crops and pasture are grown in a well-mixed rooting zone. Livestock ingest radionuclides via drinking water and fodder as well as by the direct consumption of soil. All foodstuffs for consumption by animals are assumed to be produced in the area of maximum radionuclide concentration. Fish in the river accumulate radionuclides from the water.

Doses are calculated for an adult individual¹⁸ with present-day diet, but assuming local production of all foodstuffs. The doses are received via a range of pathways, as illustrated in Fig. A1.7-2 of Appendix 1, which shows the exposure pathway model. Doses via each pathway depend on the concentrations in corresponding compartments, e.g. doses via foodstuff consumption pathways are proportional to the concentration of radionuclides in the top soil compartment, averaged over the region in which the population group is assumed to live¹⁹, and on average concentrations in the water and foodstuffs consumed. Details of spatial distribution of radionuclides need not, therefore, be represented. Doses are also received due to external radiation from radionuclides in soil and due to inhalation of soil particulates, which may also contain radionuclides.

The governing equations for the compartment model are Eqs. A1.7-1 and A1.7-2. The governing equations for the exposure pathway model are Eqs. A1.7-3 to A1.7-11.

3.1.3 Codes used

The conceptualisation of the key FEPs described above forms the basis of a set of governing equations, with accompanying initial conditions and boundary conditions, that are solved using the computer codes STMAN for the near field, PICNIC for the host rock, and TAME for the biosphere (see Appendix 1). STMAN consists of three modules that are run independently, and are termed SPENT for SF, STRENG for HLW and STALLION for ILW.

The reference model chain of STMAN-PICNIC-TAME is used to model the radionuclide release from the near field, migration through the host rock and distribution in the biosphere. The selection of safety-relevant radionuclides and the treatment of decay chains is discussed in Appendix 5.

¹⁸ The exposed population will include all ages. Whereas doses per unit intake for children and infants are generally greater than doses per unit intake for adults (Greenhalgh *et al.* 1985), this is compensated for by larger dietary intakes by adults. Thus, for adults and children exposed by various pathways to the same concentrations of safety-relevant radionuclides in environmental media, the doses to children typically differ by not more than a factor of three from, and are generally less than, the doses to adults (Bergström & Nordlinder 1990). If it is assumed that an individual spends its entire life in the region, then the dose to an adult can be thought of as an approximation of the annual average dose over a lifetime.

¹⁹ The assumed requirements of the community define a *minimum* area over which it is valid to average radionuclide concentrations, i.e. an area that could supply all the dietary needs of the community. However, consideration of the spatial extent of the zone of geosphere discharge may lead to definition of a larger region as being more appropriate. In the present safety assessment, an area of 2.3 km² is considered; this is derived from a specific section of the Rhine valley below the Rhine Falls where discharge of deep groundwaters from the Malm aquifer takes place.

3.1.4 Parameters

Reference Case (Case 1.1a)

The following reference canister loadings for SF/HLW and ILW waste groups are defined:

In the case of SF,

- 9 BWR UO₂ fuel assemblies
- 4 PWR UO₂ fuel assemblies
- 3 PWR UO₂ assemblies plus 1 PWR MOX fuel assembly,

all with a burnup of 48 GWd/t_{HM}.

For HLW, vitrified waste from COGEMA and BNFL is considered separately. In the case of ILW, the two waste groups ILW-1 and ILW-2 are distinguished.

STMAN input data for the radionuclides and inventory in the Reference Case are listed in Tab. 3.1-1. Input data for the waste forms (SF/HLW canisters and ILW tunnels) are given in Tabs. 3.1-2 to 3.1-4 for the SPENT, STRENG and STALLION modules, respectively. STMAN input data for the SF and HLW bentonite buffer are listed in Tab. 3.1-5. A buffer region is also assumed to exist in the governing equations solved by the STALLION code for ILW, although the ILW part of the repository has no buffer (the STALLION code was originally conceived for a different repository design). Thus, for numerical reasons, a thin annulus of Opalinus Clay around each tunnel is treated as the "buffer" for ILW. Numerical experiments have been performed to confirm that the thickness of this annulus is not a sensitive parameter (App. 3.6).

PICNIC input data for the Reference Case are listed in Tab. 3.1-6. For SF (and similarly for HLW), a single PICNIC run is performed with a near field source term collecting the radionuclide release rates from all reference canister types, followed by a single TAME run. In the case of ILW, different PICNIC and TAME runs are performed for ILW-1 and ILW-2.

The complete TAME input data for the Reference Case is given in Tabs. A3.7-1 to A3.7-5 in Appendix 3.

Tab. 3.1-1: SPENT/STRENG/STALLION input data for the radionuclides and inventory in the Reference Case

Input	Units	Values	Source
<i>Nuclides and Decays</i>			
Nuclides and decays to be used.	Half lives are specified in years.	Tab. A3.2-1a, Parameter 1, Value A	
<i>Total Inventory</i>			
Inventory of each nuclide for a single package (SF/HLW) or ILW-1 / ILW-2 tunnels.	moles or TBq	Tab. A3.2-1a, Parameter 2, Value A	

Tab. 3.1-2: SPENT input data for the spent fuel waste form and canister in the Reference Case

Input	Units	Values	Source
<i>Inventory Fractions</i>			
Percentage of the inventory for each nuclide for matrix, cladding and instant release.	dimensionless (%)	Tab. A3.2-1a, Parameter 3, Value A	
<i>Canister Properties</i>			
Containment time	years	10 000	Tab. A3.2-1a, Parameter 5, Value A
Number of canisters	dimensionless	Tab. A3.2-1a, Parameter 6, Value A	
Canister length	m	Tab. A3.2-1a, Parameter 7, Value A	
Initial diameter of waste	m	This is only used to calculate a reservoir volume if none is set explicitly. In the study, the reservoir volume is set directly and so the waste diameter is not used.	
<i>Release Properties</i>			
Matrix release rate	per year	Tab. A3.2-1a, Parameter 9, Value A	
Grain (or cladding) release rate	per year	Tab. A3.2-1a, Parameter 10, Value A	
Reservoir volume	m ³	This is calculated from the reservoir thickness (Tab. A3.2-1a, Parameter 15, Value A), using the relationship given in Section A3.6.	
Solubility limits	mol l ⁻¹	Tab. A3.2-1a, Parameter 16, Value A	
Pinhole radius	m	Not used in the Reference Case	
Number of pinholes	dimensionless	Not used in the Reference Case	

Tab. 3.1-3: STRENG input data for the vitrified HLW waste form and canister in the Reference Case

Input	Units	Values	Source
<i>Canister Properties</i>			
Containment time	years	10 000	Tab. A3.2-1a, Parameter 5, Value A
Number of canisters	dimensionless	Tab. A3.2-1a, Parameter 6, Value A	
Canister length	m	Tab. A3.2-1a, Parameter 7, Value A	
Initial diameter of waste	m	This is only used to calculate a reservoir volume if none is set explicitly. In the study, the reservoir volume is set directly and so the waste diameter is not used.	
<i>Release Properties</i>			
Glass grain density	kg m ⁻³	Tab. A3.2-1a, Parameter 11, Value A	
Glass dissolution rate	kg m ⁻² a ⁻¹	Tab. A3.2-1a, Parameter 12, Value A	
Equivalent spherical radius	m	Tab. A3.2-1a, Parameter 13, Value A	
Reservoir volume	m ³	This is calculated from the reservoir thickness (Tab. A3.2-1a, Parameter 15, Value A), using the relationship given in Section A3.6.	
Solubility limits	mol l ⁻¹	Tab. A3.2-1a, Parameter 16, Value A	
Pinhole radius	m	Not used in the Reference Case	
Number of pinholes	dimensionless	Not used in the Reference Case	

Tab. 3.1-4: STALLION input data for the ILW waste form and container in the Reference Case

Input	Units	Values	Source
<i>Slow Release Properties</i>			
Fraction of the inventory that is subject to slow release	dimensionless	Not used in any of the assessment cases.	
Slow release rate	per year	Not used in any of the assessment cases.	
<i>Waste Package Properties</i>			
Containment time	years	100	Tab. A3.2-1a, Parameter 5, Value A
Number of waste packages	dimensionless	Tab. A3.2-1a, Parameter 6, Value A	
Waste package length	m	Tab. A3.2-1a, Parameter 7, Value A	
<i>Cementitious Region Properties</i>			
Porosity	dimensionless	0.3	Tab. A3.2-1a, Parameter 19, Value A
Grain density	kg m ⁻³	Tab. A3.2-1a, Parameter 20, Value A	
Sorption K_d	m ³ kg ⁻¹	Tab. A3.2-1a, Parameter 21, Value A	
Solubility limits	mol l ⁻¹	Tab. A3.2-1a, Parameter 22, Value A	

Tab. 3.1-5: SPENT/STRENG input data for the bentonite buffer and STMAN near field / geosphere properties in the Reference Case

Input	Units	Values	Source
<i>Buffer Properties</i>			
Inner radius	m	0.525 (SF) 0.47 (HLW)	Tab. A3.2-1a, Parameter 23, Value A
Outer radius	m	1.15	Tab. A3.2-1a, Parameter 24, Value A
Split radius	m	The radius separating an inner and outer buffer region which have different properties; not used in the Reference Case.	
Porosity	dimensionless	0.36	Tab. A3.2-1a, Parameters 26/27, Value A
Porosity Factors	dimensionless	0.14 (anions) 1 (non-anions)	
Grain density	kg m ⁻³	Tab. A3.2-1a, Parameter 28, Value A	
Sorption K_d	m ³ kg ⁻¹	Tab. A3.2-1a, Parameter 29/30, Value A	
Solubility limits	mol l ⁻¹	Tab. A3.2-1a, Parameter 31/32, Value A	
Effective diffusion coefficient	m ² a ⁻¹	Tab. A3.2-1a, Parameter 33/34, Value A	
<i>Interface Near field / Geosphere Properties</i>			
Mixing cell flow rate per waste package	m ³ a ⁻¹	Tab. A3.2-1a, Parameter 35, Value A	
Incoming water concentrations	TBq m ⁻³ or mol m ⁻³	Set to zero in all assessment cases.	

Tab. 3.1-6: PICNIC input data in the Reference Case

Input	Units	Values	Source
<i>Nuclides and Decays</i>			
Nuclides and decays to be used.	Half lives are specified in years.	Tab. A3.2-2a, Parameter 1, Value A	
<i>Network Structure</i>			
List of junction names. Inlet and outlet junctions for each leg.	-	Only a single PICNIC leg is considered in the Reference Case, representing a single transport path through the Opalinus Clay.	
<i>Leg Data – Basic Data</i>			
Length	m	40	Tab. A3.2-2a, Parameter 3, Value A
Cross-sectional area	m ²	Irrelevant	
Darcy velocity	m a ⁻¹	6.3×10^{-7}	Tab. A3.2-2a, Parameter 5, Value A
Hydraulic conductivity	m a ⁻¹	Omitted since specific flow is specified by Darcy velocity.	
Peclet number	dimensionless	Tab. A3.2-2a, Parameter 6, Value A	
Effective diffusion coefficient	m ² a ⁻¹	Tab. A3.2-2a, Parameter 7, Value A	
<i>Leg Data – Properties of Flowing Region</i>			
Retardation	dimensionless	Calculated from the other parameters.	
Grain density	kg m ⁻³	Tab. A3.2-2a, Parameter 8, Value A	
Flow porosity	dimensionless	This is set equal to the infill porosity.	
Infill Porosity	dimensionless	0.12	Tab. A3.2-2a, Parameter 10, Value A
Porosity Factors	dimensionless	0.5 (anions) 1 (non-anions)	
Sorption K_d	m ³ kg ⁻¹	Tab. A3.2-2a, Parameter 11, Value A	
<i>Leg Data – Properties of Matrix</i>			
There is no "matrix" in the Reference Case – the Opalinus Clay is a homogeneous porous medium. The matrix penetration depth and surface sorption coefficients are thus set equal to zero, and all other parameters are irrelevant.			
<i>Network Flow Data</i>			
There is no "network" in the Reference Case.			
<i>Source Term Information</i>			
Source flux	mol a ⁻¹	Output from STMAN.	
Fraction to each leg	dimensionless	Only a single PICNIC leg is considered in the Reference Case.	

Deterministic parameter variations to the Reference Case (Cases 1.1a – 1.1k)

Tab. 3.1-7 shows the deterministic parameter variations that are performed within the Reference Conceptualisation, highlighting any differences to the Reference Case parameter set.

Tab. 3.1-7: The deterministic parameter variations that are performed within the Reference Conceptualisation

Deterministic parameter variation	Input parameters differing from Reference Case	Values	Source
Variability in canister inventory (Case 1.1b)	Canister inventory (including instant release fraction)	9 BWR UO ₂ -48' 4 PWR UO ₂ -48' 3 PWR UO ₂ -48 + 1 PWR MOX-48' 4 PWR UO ₂ -55 3 PWR UO ₂ -55 + 1 PWR UO ₂ -65 3 PWR UO ₂ -55 + 1 PWR UO ₂ -75 3 PWR UO ₂ -48 + 1 PWR MOX-65 COGEMA' (HLW) BNFL' (HLW)	Tab. A3.2-1a: Parameter 2 (inventory per canister) given in Tab. A3.4-2a/b Parameter 3, Value B Parameter 6, Value C Parameter 9, Value B
Reduced canister lifetime (Case 1.1c)	Containment time	1 000 a	Tab. A3.2-1a, Parameter 5, Value C
Pessimistic near field geochemical dataset (Case 1.1d)	Sorption constants and solubility limits	Pessimistic values	Tab. A3.2-1a: various Parameters
Increased glass dissolution rate in HLW (Case 1.1e)	Glass dissolution rate	$4.0 \times 10^{-2} \text{ kg m}^{-2} \text{ a}^{-1}$ (BNFL and COGEMA glasses)	Tab. A3.2-1a: Parameter 12, Value B
Increased water flow rate in geosphere (Case 1.1f)	Water flow rate in geosphere	10-fold increase	Tab. A3.2-1a: Parameter 35, Value D Tab. A3.2.2a: Parameter 5, Value D
Decreased water flow rate in geosphere (Case 1.1g)	Water flow rate in geosphere	10-fold decrease	Tab. A3.2-1a: Parameter 35, Value C Tab. A3.2.2a: Parameter 5, Value C
Pessimistic geosphere sorption constants (Case 1.1h)	Sorption constants	Pessimistic values	Tab. A3.2-2a: Parameter 11, Value B
Pessimistic near field and geosphere geochemical dataset (Case 1.1i)	Sorption constants and solubility limits in the near field, sorption constants in the geosphere	Pessimistic values	Tab. A3.2-1a: various parameters, Tab. A3.2-2a: Parameter 11, Value B

Tab. 3.1-7: (Cont.)

Deterministic parameter variation	Input parameters differing from Reference Case	Values	Source
Pessimistic geosphere diffusion constants (Case 1.1j)	Effective diffusion constants in the geosphere	Pessimistic values ²	Tab. A3.2-1a: Parameter 35, Value F, Tab. A3.2-2a: Parameter 7, Value B
Pessimistic treatment of ¹⁴ C (organic) in SF (Case 1.1k)	Chemical form of ¹⁴ C (inorganic, organic)	All ¹⁴ C in SF is pessimistically assumed to be organic.	Tab. A3.2-1a: Parameter 2, Value B

¹ Reference canister loadings (abbreviation stands for reactor type and burnup in GWd/t_{HM})

² Note that for neutral species, e.g. ¹⁴C_{org}, the pessimistic value for the effective diffusion constant in the Opalinus Clay (10⁻¹⁰ m² s⁻¹) is assumed to be identical to the pessimistic value for cationic species. This assumption is considered to be very pessimistic.

Probabilistic parameter variations to the Reference Case

As discussed in Chapter 6 in Nagra (2002c), probabilistic analyses are performed in addition to the deterministic analyses in order to investigate the sensitivity to reference model chain input parameters in a comprehensive manner. This specifically includes scoping the effects of varying all parameters at the same time to further enhance confidence that no critical parameter combination has been overlooked. In these probabilistic calculations, the conceptual model assumptions are identical to those used in the deterministic calculations of the Reference Conceptualisation.

The input PDFs and the correlations between different parameters are listed and discussed in detail in Appendix 3 (Section A3.10). Note that in contrast to the deterministic Reference Case parameter variations, the PDFs also contain increased cladding corrosion rates and that for all parameters varied, values more optimistic than reference values are also included. Moreover, in the probabilistic calculations the upper truncation for the effective diffusion constant in the Opalinus Clay has been set to three times the Reference Case value, whereas in the deterministic calculations, the pessimistic value for the effective diffusion constant is increased by a factor of 3 (anions) and 10 (non-anions), see Tab. A3.5-5.

The probabilistic results are presented by means of complementary cumulative density functions of the dose (CCDF²⁰, see Fig. 7.4-3a in Nagra 2002c) and by comparison of the evolution with time of the median, the 95th percentile and the highest / lowest dose maxima of all samples (see Fig. 7.4-3b in Nagra 2002c).

²⁰ The CCDF is the probability of exceeding a given dose, as a function of that dose.

3.2 Solubility-limited dissolution of spent fuel (Case²¹ 1.2)

3.2.1 Overview

In the conceptualisation "solubility-limited dissolution of spent fuel", the likely/expected broad evolutionary path of the disposal system is followed, as in the Reference Conceptualisation. It differs from the Reference Conceptualisation, however, in the chemical conditions that are assumed to prevail at the surfaces of the SF matrix. These conditions affect the rate at which the matrix dissolves. In the Reference Conceptualisation, the rate of SF matrix dissolution is assumed to be controlled by the generation of radiolytic oxidants (see Sections 3.1.2 and 9.5). In the conceptualisation "solubility-limited dissolution of spent fuel", however, reducing conditions are assumed to prevail also at the surfaces of the SF matrix, irrespective of the generation of radiolytic oxidants. The rate of dissolution is assumed to be controlled by the solubility of the matrix under reducing conditions. This is a more favourable situation than that of the Reference Conceptualisation, since it gives rise to much lower rates of dissolution, and is actually considered more realistic (see Chapter 5 of Nagra 2002c). The treatment of the instant release fraction and of the SF cladding are the same as in the Reference Conceptualisation.

3.2.2 The conceptual model and its underlying assumptions

The conceptual model and its underlying assumptions are identical to those of the Reference Conceptualisation except in treatment of radionuclide release from the SF matrix. Following canister breaching, dissolution of the UO₂ fuel matrix continually supplies aqueous U(IV) to the "reservoir" of water that is assumed to exist within the SF canisters. At the same time, U(IV) is continuously transported from the reservoir into the bentonite by aqueous diffusion, which is described by Fick's laws, with retardation by linear, reversible, equilibrium sorption, described by the sorption coefficient (K_d) for uranium. Dissolution is assumed to occur at a rate sufficient to maintain the aqueous concentration of U(IV) in the "reservoir" of water within the SF canisters at the solubility limit for reducing conditions.

3.2.3 Codes used

As in the Reference Conceptualisation, the reference model chain of STMAN-PICNIC-TAME is used to model the radionuclide release, migration and distribution in the biosphere. The SPENT module of STMAN is, however, run twice:

- In the first run, only ²³⁸U is considered. The release and transport of ²³⁸U is calculated by assigning the entire ²³⁸U inventory to the instant release fraction. This then either precipitates as solid UO₂ (corresponding to the SF matrix) or enters solution in the pore space adjacent to the fuel matrix as aqueous U(IV). The transport of U(IV) into the bentonite is evaluated as in the Reference Conceptualisation. The time-dependent rate of transport of U(IV) into the bentonite gives the rate of SF matrix dissolution, which is used as input in the second run.
- In the second run, all safety-relevant radionuclides are considered. This run differs from the Reference Case in that the time-dependent spent fuel matrix dissolution rate is taken from the results of the first run, rather than from the output of the radiolysis model described in Chapter 9.

²¹ "Case x.y" is short for "alternative conceptualisation x.y" (see Tab. 2.2-1).

3.2.4 Parameters

Base Case

In the first run, the parameters are as in the Reference Case, but with 100 % of the ^{238}U SF inventory assigned to the instant release fraction. In Fig. 3.2-1, the fractional fuel dissolution rates calculated in this way are shown to be more than two orders of magnitudes lower than the fractional fuel dissolution rates obtained by the radiolytic oxidation model, as used in the Reference Case.

In the second run, the parameters are as in the Reference Case, except for the fractional fuel dissolution rates obtained from the results of the first run, as described in Section 3.2.3, above.

Parameter variations

No parameters variations are performed for this conceptualisation.

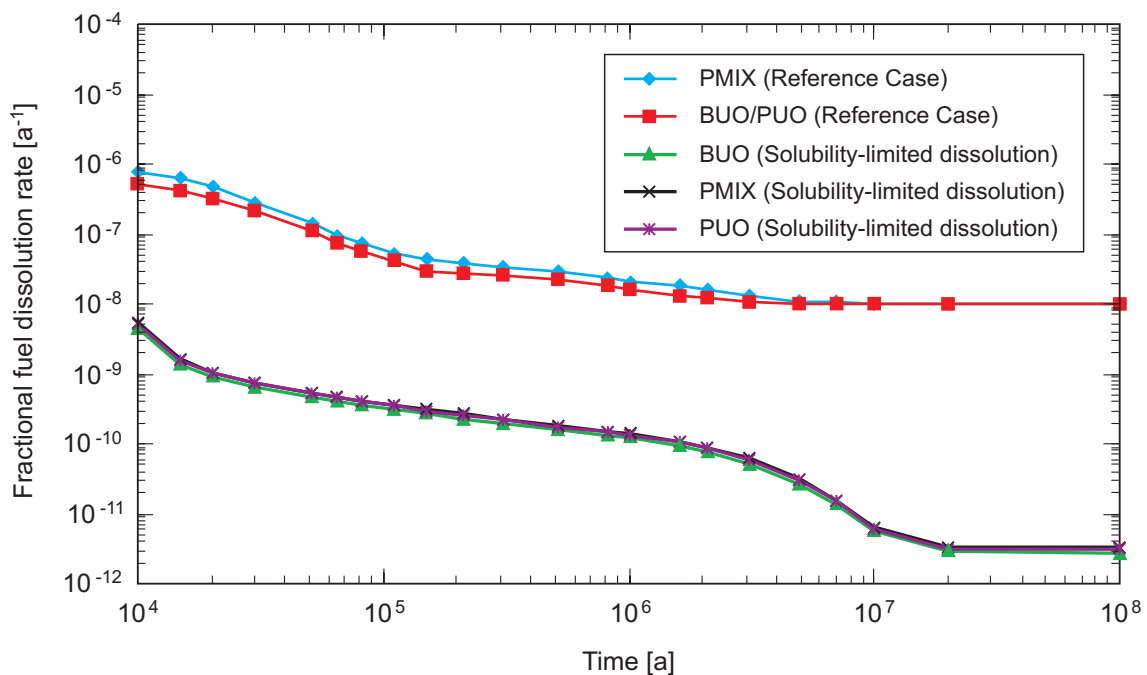


Fig. 3.2-1: Comparison of the fractional fuel dissolution rates obtained by the radiolytic oxidation model, as used in the Reference Case, and by the solubility-limited dissolution model, as used in the present case

BUO: 9 BWR UO_2 -48 fuel elements per canister; PUO: 4 PWR UO_2 -48 fuel elements per canister; PMIX: 3 PWR UO_2 -48 + 1 PWR MOX-48 fuel elements per canister. The curves for the three canister types are not identical because the fractional fuel dissolution rate is calculated by dividing the flux of ^{238}U into bentonite [mol a^{-1}] (identical) by the inventory of ^{238}U [mol] (not identical, see Tab. A3.4-2a).

3.3 Bentonite thermal alteration (Case 1.3)

3.3.1 Overview

In the conceptualisation "bentonite thermal alteration", the likely/expected broad evolutionary path of the disposal system is followed, as in the Reference Conceptualisation. It differs from the Reference Conceptualisation, however, in that a thermally altered bentonite zone of significant spatial extent is assumed to exist around the SF and HLW waste packages, due to heat generation by the wastes. Increased temperatures above 125 °C due to radioactive decay in SF/HLW canisters are known to be limited to the inner half of the bentonite buffer. Thermal alteration is thus assumed to be confined to this part of the bentonite (Section 5.3.2 of Nagra 2002c). Thermal alteration is assumed to enhance radionuclide diffusion, but the sorption properties of bentonite are taken to be unaffected by thermal effects. The outer half of the bentonite functions according to design, i.e. its swelling pressure is fully developed, colloids are filtered by its micro-porous structure, and transport is diffusion dominated.

3.3.2 The conceptual model and its underlying assumptions

The conceptual model and its underlying assumptions are identical to those of the Reference Conceptualisation except in the treatment of radionuclide transport through the SF and HLW bentonite buffer. As discussed above, in the conceptualisation "bentonite thermal alteration", it is pessimistically assumed that increased temperatures lead to the thermal degradation of the inner half of the bentonite buffer surrounding the SF and HLW canisters. The buffer is thus considered to consist of two concentric annular regions between the canister and the tunnel wall. Within both regions, radionuclide transport is assumed to take place by diffusion, described by Fick's laws, and retarded by linear, reversible, equilibrium sorption, described by an element-dependent sorption coefficient (K_d). The K_d values are the same in both regions. The diffusion coefficient, however, is pessimistically assumed to be that of free water in the inner region, whereas in the outer region the effects of the pore structure of the unaltered bentonite reduce the rates of diffusion.

3.3.3 Codes used

As in the Reference Conceptualisation, the reference model chain of STMAN-PICNIC-TAME is used to model the radionuclide release, migration and distribution in the biosphere.

3.3.4 Parameters

Base Case

The parameters are as in the Reference Case, except for the STMAN input data for the buffer. Parameters that differ from those of the Reference Case are given in Tab. 3.3-1.

Tab. 3.3-1: SPENT/STRENG input data for the bentonite buffer for the conceptualisation "bentonite thermal alteration" (Case 1.3), where these differ from the Reference Case parameters

Input	Units	Values	Source
<i>Buffer Properties</i>			
Split radius	m	Set at half distance between canister surface and tunnel wall.	Tab. A3.2-1a, Parameter 25, Value B
Pore diffusion coefficient	m ² a ⁻¹	Inner buffer region: 6.3 × 10 ⁻² m ² a ⁻¹	Tab. A3.2-1a, Parameter 33, Value B
		Outer buffer region: Identical to Reference Case	

Parameter variations

No parameters variations are performed for this conceptualisation.

3.4 Glacially-induced flow in the Opalinus Clay (Case 1.4)

3.4.1 Overview

In the conceptualisation "glacially-induced flow in the Opalinus Clay", the likely/expected broad evolutionary path of the disposal system is followed as in the Reference Conceptualisation. It differs from the Reference Conceptualisation, however, in that compaction and decompaction of the Opalinus Clay due to glacial loading and unloading, and the resulting flow of water out of and into the Opalinus Clay, is taken into account in evaluating the transport of radionuclides through the host rock. In the Reference Conceptualisation, advection is assumed to be driven solely by the currently observed pressure difference between the lower and upper confining units, directed upwards. The conceptualisation "glacially-induced flow in the Opalinus Clay" is investigated in order to test the assumption of the Reference Conceptualisation that glacial cycling has a minor effect on overall radionuclide transport.

3.4.2 The conceptual model and its underlying assumptions

The conceptual model and its underlying assumptions are identical to those of the Reference Conceptualisation except in the treatment of radionuclide transport through the bentonite and Opalinus Clay. Advective transport is driven by glacially-induced flow, evaluated over a one million year period. In the course of the next million years, a periodic series of 10 glaciations is assumed to occur (with an assumed frequency of one glaciation every 10⁵ years), starting at 50 000 years from today. The duration of each glaciation is taken to be 20 000 years, with an assumed ice shield thickness of 200 m for eight glaciations and 400 m for two glaciations (fourth and tenth event).

As a result of these glaciations, periodic elastic compaction and rebound of the clay barrier (bentonite and Opalinus Clay) occurs, leading to spatial and temporal changes in the ground-water flow in the clay barrier. The clay barrier is assumed to remain homogeneous, i.e. no frac-

turing occurs before, during or after ice loading. Flow and transport modelling is based on a 2D vertical cross-section through the repository representing a single SF emplacement tunnel and the surrounding Opalinus Clay (Fig. 3.4-1). The presence of neighbouring emplacement tunnels is taken into account by requiring zero flow and transport over the vertical boundaries (Tab. 3.4-1). Water flows along the access tunnel system are neglected in the calculations. This is shown to be a valid assumption for a number of different situations (see discussion in Sections 3.6, 3.7 and 3.8), and is, therefore, also expected to be a valid assumption in the present context of glaciation-induced flow.

Tab. 3.4-1: Hydraulic and transport boundary conditions for boundaries A-F

Parameter	Unit	Value	Comment
Hydraulic head at boundaries A and B	m	time-dependent (see Tab. 3.4-3)	Step-wise time-dependent head mimics the periodic glacial loading/unloading, while the hydraulic gradient is assumed to be constant in time (1 m m^{-1} , as in the Reference Case).
Concentration at boundaries A and B	mol m^{-3}	0	zero concentration boundary
Boundaries C and D	-	-	no-flow boundary for both flow and transport
Boundary E	-	-	no-flow boundary for both flow and transport
Boundary F	mol s^{-1}	-	radionuclide release rate from canister to bentonite (Reference Case)

The conceptual model for glacially-induced flow in the Opalinus Clay is based on the assumption that the aquifers bounding the host rock provide a direct connection to a discharge area not influenced by glaciation. The discharge area acts therefore as a constant pressure boundary. After the onset of a glaciation, the Opalinus Clay under load finds a new equilibrium via an outflow of water contained in the rock formation. The time needed for equilibration is directly related to the hydraulic conductivity of the medium. Because the bounding aquifers have a hydraulic conductivity which is 4-6 orders of magnitude higher than that of the Opalinus Clay (see Tab. A3.3-4b), the pressure in these aquifers will equilibrate much faster, even if one takes into account the long distance to the discharge area. It is thus conservatively assumed that the bounding aquifers are, compared to the Opalinus Clay, equilibrated instantaneously. This assumption leads to the following idealised situation: At the onset of a glaciation, the hydraulic pressure is instantaneously increased in the Opalinus Clay, but remains as before in the bounding aquifers. For modelling purposes, this situation is equivalent to an instantaneous pressure reduction at the start of a glaciation cycle at the upper (A) and the lower (B) boundary (Fig. 3.4-1). When the load is removed at the end of a glaciation, the reverse process is applied. Again, the bounding aquifers equilibrate much faster and an instantaneous increase of the reference pressure at the boundaries is implemented in the model.

The assumed sequence of future glaciations and the applied time-dependent hydraulic heads at the boundaries are listed in Tab. 3.4-3. In order to minimise manipulations during simulation runs, the changes of pressure were implemented with a "numerical trick": The flow field was

solved with hydraulic heads with respect to a reference level. For the stationary Reference Case the reference level was chosen to be at the upper model boundary (A). At the start of a glaciation the hydraulic head at the boundaries is decreased (see last paragraph) in order to simulate the pressure difference between the Opalinus Clay and the bounding aquifers, leading to negative hydraulic head values in Tab. 3.4-3. At the end of a glaciation cycle the hydraulic heads at the boundaries are restored to their original values.

Because of the dominant contribution of SF to calculated doses, the analysis is conducted for SF only and is limited to those radionuclides that dominate the summed dose maximum of the Reference Case (organic ^{14}C , ^{36}Cl , ^{41}Ca , ^{79}Se , ^{129}I). The rate of radionuclide release from the SF canisters to the bentonite as a function of time is imposed at boundary F in Fig. 3.4-1 and is taken to be identical to that of the Reference Case.

For comparison purposes with the calculated doses for the Reference Case, the reference biosphere model is employed, although biosphere conditions will be drastically changed during glaciations (very low population density, sparse vegetation, lower dilution rates). Alternative climatic conditions with the potential to affect the calculated doses are considered in a separate conceptualisation (see Chapter 8).

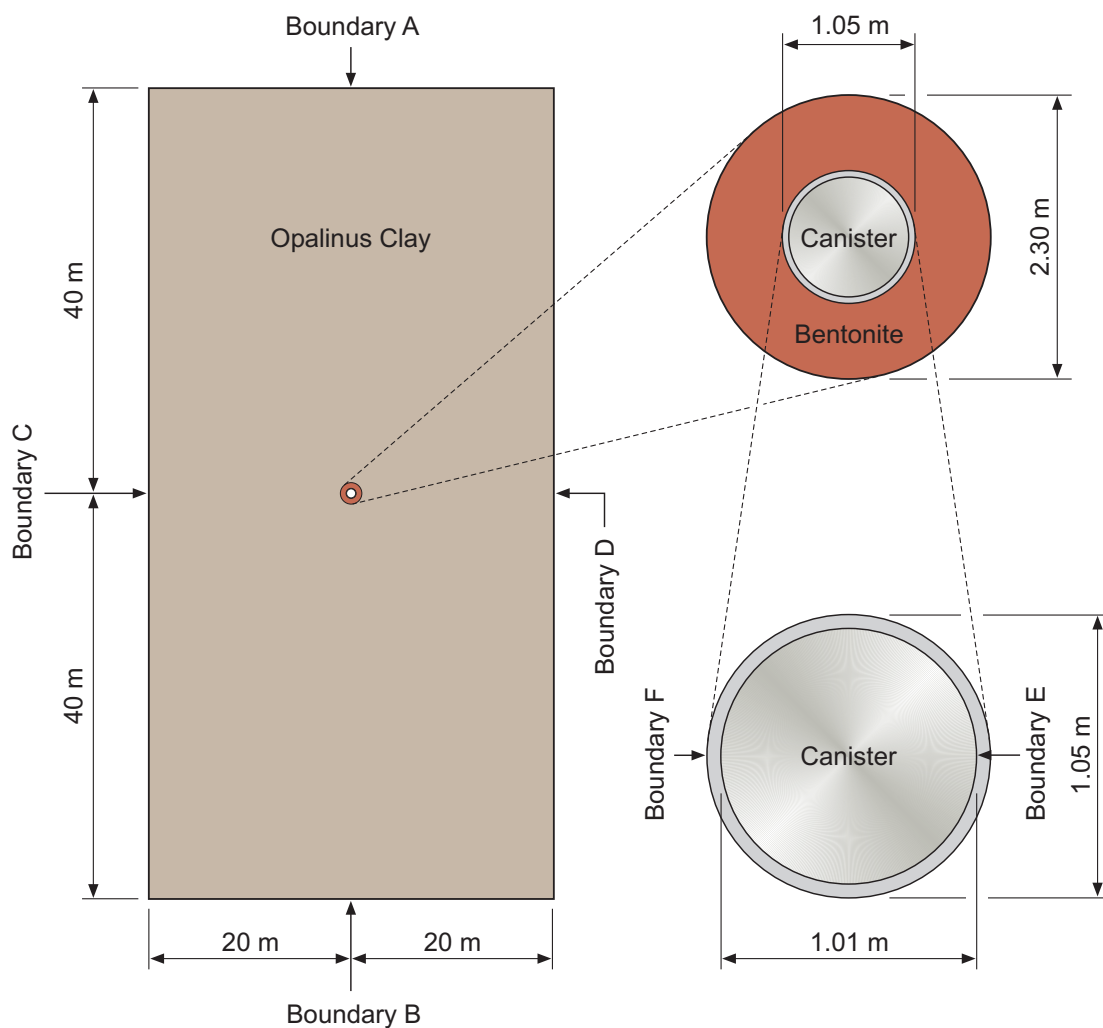


Fig. 3.4-1: Conceptual model for the calculation of glacially-induced flow and transport in bentonite and Opalinus Clay

3.4.3 Codes used

The model chain of SPENT-FRAC3DVS-TAME is used to model the radionuclide release, migration and distribution in the biosphere. FRAC3DVS is used instead of PICNIC because the transient nature of glacial loading leads to a time- and space-dependent flow field in the clay barrier (Eq. A1.8-1, with the source term q_s set to zero). The flow field is modelled both for bentonite and Opalinus Clay in a two-dimensional model (Fig. 3.4-1). According to Terzaghi's theory of consolidation (De Marsily 1986), the specific storage, S_s [m^{-1}], for the two domains can be approximated by:

$$S_s = \rho_f g \alpha \quad (3.4-1)$$

where α compressibility of relevant domains (bentonite, Opalinus Clay) [Pa^{-1}]
 ρ_f fluid density [kg m^{-3}]
 g gravitational acceleration [m s^{-2}].

The coupled flow and transport equations Eq. A1.8-1 and A1.8-8 are solved in FRAC3DVS for a composite 2D porous medium, representing the bentonite buffer and the Opalinus Clay (Fig. 3.4-1).

3.4.4 Parameters

Base Case

FRAC3DVS input data for the Base Case related to glacially-induced flow are listed in Tab. 3.4-2, including radionuclide-dependent data, source term information and data on bentonite and Opalinus Clay. The assumed sequence of future glaciations is listed in Tab. 3.4-3.

Tab. 3.4-2: FRAC3DVS input data differing from the Reference Case

Input	Units	Values	Source/comment
<i>Nuclides and Decays</i>			
Nuclides and decays to be used.	Half lives are specified in years.	Analysed nuclides: organic ^{14}C , ^{36}Cl , ^{41}Ca , ^{79}Se , ^{129}I Half lives: Tab. A3.2-1a, Parameter 1, Value C	
<i>Data for bentonite</i>			
Hydraulic conductivity	m s^{-1}	1.0×10^{-13}	Tab. 3.6-1
Peclet number	dimensionless	dispersion neglected	
Specific storage coefficient	m^{-1}	2.0×10^{-4}	Based on data reported in ENRESA (1999, 2000)
<i>Data for Opalinus Clay</i>			
Thickness of Opalinus Clay	m	80	Extent of model domain (see Fig. 3.4-1)
Peclet number	dimensionless	dispersion neglected	
Retardation	dimensionless	Calculated from the other parameters.	
Specific storage coefficient	m^{-1}	10^{-5}	Tab. A.3.3-4a
<i>Source Term Information</i>			
Source flux	mol s^{-1}	Output from SPENT: Radionuclide release rate from canister to bentonite (Reference Case)	

Tab. 3.4-3: Sequence of future glaciation periods and derived time-dependent hydraulic heads at boundaries A and B (see Fig. 3.4-1)

The "start of period", "end of period" and glacial overburden thickness values are based on Nagra (2002a, Section 9.4.8); the times of maximal overburden of 400 m were conservatively chosen in such a way that one of these occurs towards the end of the one million year period considered, where releases from the Opalinus Clay are highest. The absolute values of the hydraulic heads were calculated assuming a density of ice of 917 kg m⁻³; the negative signs are discussed in Section 3.4-2.

Start of period [a]	End of period [a]	Glacial overburden (ice thickness at surface) [m]	Hydraulic head at boundary A [m] ¹	Hydraulic head at boundary B [m] ¹
0	50 000	0	0	80
50 000	70 000	200	-183.4	-103.4
70 000	150 000	0	0	80
150 000	170 000	200	-183.4	-103.4
170 000	250 000	0	0	80
250 000	270 000	200	-183.4	-103.4
270 000	350 000	0	0	80
350 000	370 000	400	-366.8	-286.8
370 000	450 000	0	0	80
450 000	470 000	200	-183.4	-103.4
470 000	550 000	0	0	80
550 000	570 000	200	-183.4	-103.4
570 000	650 000	0	0	80
650 000	670 000	200	-183.4	-103.4
670 000	750 000	0	0	80
750 000	770 000	200	-183.4	-103.4
770 000	850 000	0	0	80
850 000	870 000	200	-183.4	-103.4
870 000	950 000	0	0	80
950 000	970 000	400	-366.8	-286.8
970 000	1 000 000	0	0	80

¹ Calculated assuming a density of ice of 917 kg m⁻³.

Parameter variations

No parameters variations – other than the variation of the glacial overburden - are analysed for this conceptualisation.

3.5 Additional barrier provided by confining units (Case 1.5)

3.5.1 Overview

In the conceptualisation "additional barrier provided by confining units", the likely/expected broad evolutionary path of the disposal system is followed, as in the Reference Conceptualisation. It differs from the Reference Conceptualisation, however, in that the barrier to radionuclide transport provided by the sedimentary layers overlying and underlying the host rock (the upper and lower confining units) are taken into account in transport modelling. In the Reference Conceptualisation, it is assumed that radionuclides released from the host rock are transferred instantaneously to the biosphere, conservatively neglecting additional retention and decay during transport through the upper and lower confining units.

3.5.2 The conceptual model and its underlying assumptions

The conceptual model and its underlying assumptions are identical to those of the Reference Conceptualisation except in the treatment of radionuclide transport through the upper and lower confining units. In the Reference Conceptualisation, the portion of the transport path through the confining units is not taken into account in transport modelling. In the conceptualisation "additional barrier provided by confining units", two model variants are envisaged:

- **Base case** – vertical transport through Opalinus Clay (40 m), followed by vertical transport through the entire upper and lower confining units (Fig. 3.5-2, path a); this case represents the possibility that the local aquifers (Wedelsandstein, Sandsteinkeuper) are not hydraulically connected over long distances and, therefore, do not convey radionuclides to the biosphere. After assumed instantaneous transport along the Malm / Muschelkalk aquifers, discharge occurs in the equivalent of the present-day Rhine valley just below the Rhine Falls for transport of radionuclides through the overlying Malm aquifer and further downstream in the equivalent of the present-day confluence of the Rhine and Aare river for transport through the underlying Muschelkalk aquifer.
- **Model variant** – vertical transport through Opalinus Clay (40 m) and Lias / Upper Keuper below the Opalinus Clay (60 m), followed by lateral transport in the local aquifers (Wedelsandstein, Sandsteinkeuper) within the confining units (Fig. 3.5-2, path b). In the upper confining units, additional retardation is provided by advective/dispersive transport in a segment of 25 km length within the fractured Wedelsandstein formation and by considering diffusion from the fractures into the intact rock matrix. In the lower confining units, advective/dispersive transport takes place in a segment of 15 km length within the Sandsteinkeuper formation, which is treated as an equivalent porous medium (no matrix diffusion). The Darcy flows within the local aquifers are derived from observed hydraulic heads and conductivities: $5 \times 10^{-13} \text{ m s}^{-1}$ (Wedelsandstein) and $10^{-10} \text{ m s}^{-1}$ (Sandsteinkeuper). Discharge is assumed to occur in the equivalent of the present-day Rhine valley at different locations downstream of the reference biosphere area.

Biosphere conditions in the equivalent of the present-day Rhine valley just below the Rhine Falls (Reference Case) and lower downstream are similar. The biosphere model is, therefore, taken to be identical to the Reference Case for all discharge areas described above. Furthermore, the calculated doses at different discharge areas are added. This is conservative since in reality, different population groups would be affected.

The governing equation for transport through all of these media is Eq. A1.6-4. This equation is formulated for a dual-porosity medium, with water conducting features (or fractures) embedded in a diffusion-accessible matrix. However, for those media that are considered to be homoge-

neous, i.e. the Opalinus Clay, Lias / Upper Keuper, Sandsteinkeuper, j_m^n , the solute flux of nuclide n from the fracture to the matrix per unit matrix interface, is set to zero, making the final term in Eq. A1.6-4 irrelevant.

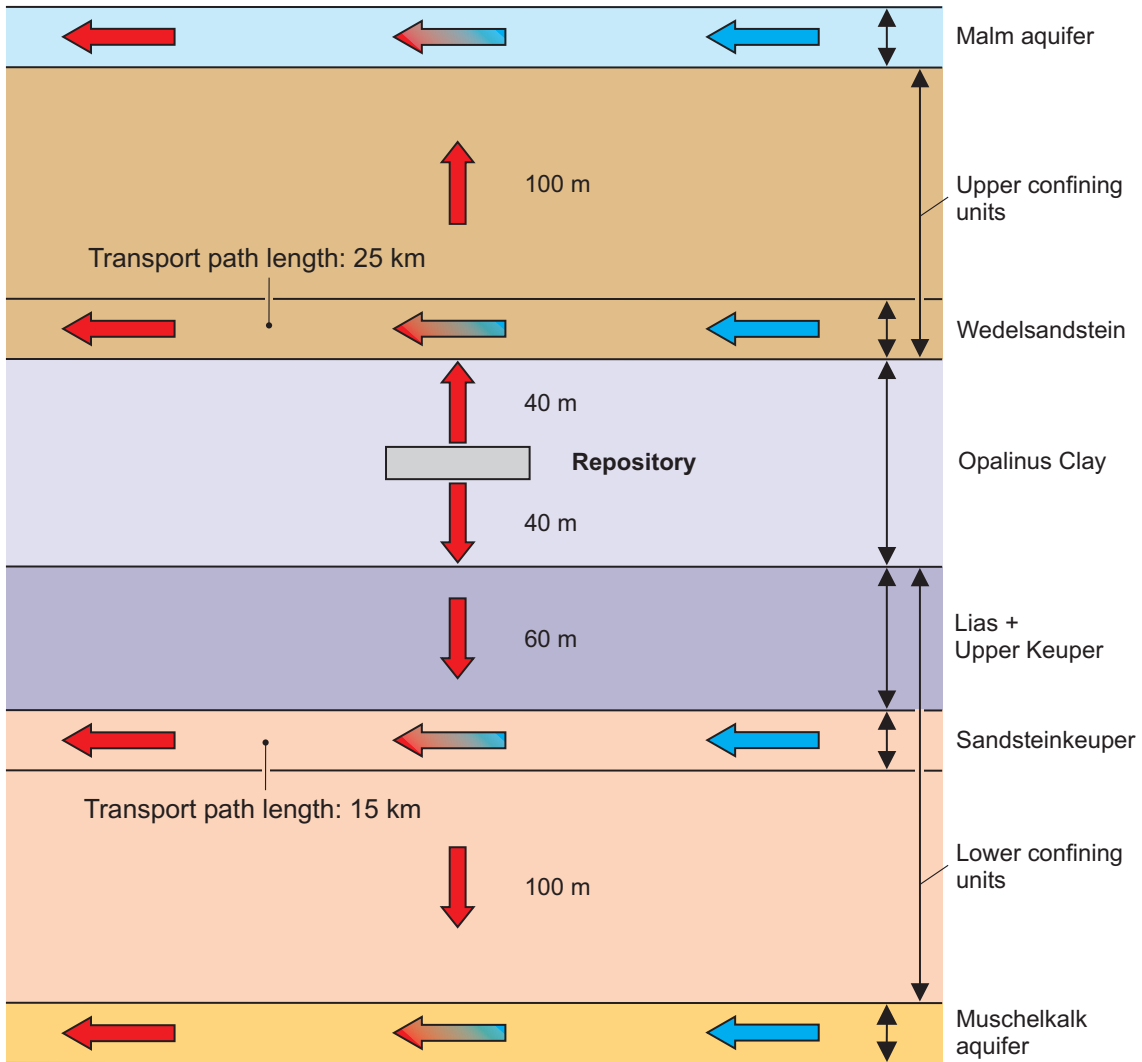


Fig. 3.5-1: Illustration of the radionuclide transport pathways in the conceptualisation considering the additional barriers provided by the confining units

3.5.3 Codes used

As in the Reference Conceptualisation, the reference model chain of STMAN-PICNIC-TAME is used to model the radionuclide release, migration and distribution in the biosphere. However, rather than employing a single PICNIC "leg" (see Appendix 1) to model a single transport path through the homogeneous host rock, the network capabilities of PICNIC are employed to model the two transport paths described above.

The network structures used for these conceptualisations are depicted in Fig. 3.5-2. In the Base Case, the leg L_1 (upward vertical transport through Opalinus Clay and upper confining units) and L_2 (downward vertical transport through the Opalinus Clay and lower confining units) represent the paths for vertical radionuclide transport through the geosphere.

In a model variant, the legs L_{11} (upward vertical transport through the Opalinus Clay) and L_{12} (lateral transport through the Wedelsandstein) represent the upper path. The legs L_{21} (downward vertical transport through the Opalinus Clay and the Lias / Upper Keuper) and L_{22} (lateral transport through the Sandsteinkeuper) represent the lower path. q_1 and q_2 represent the diluting water in which radionuclides are mixed when they enter the Wedelsandstein and Sandsteinkeuper at junctions J_{11} and J_{21} , respectively.

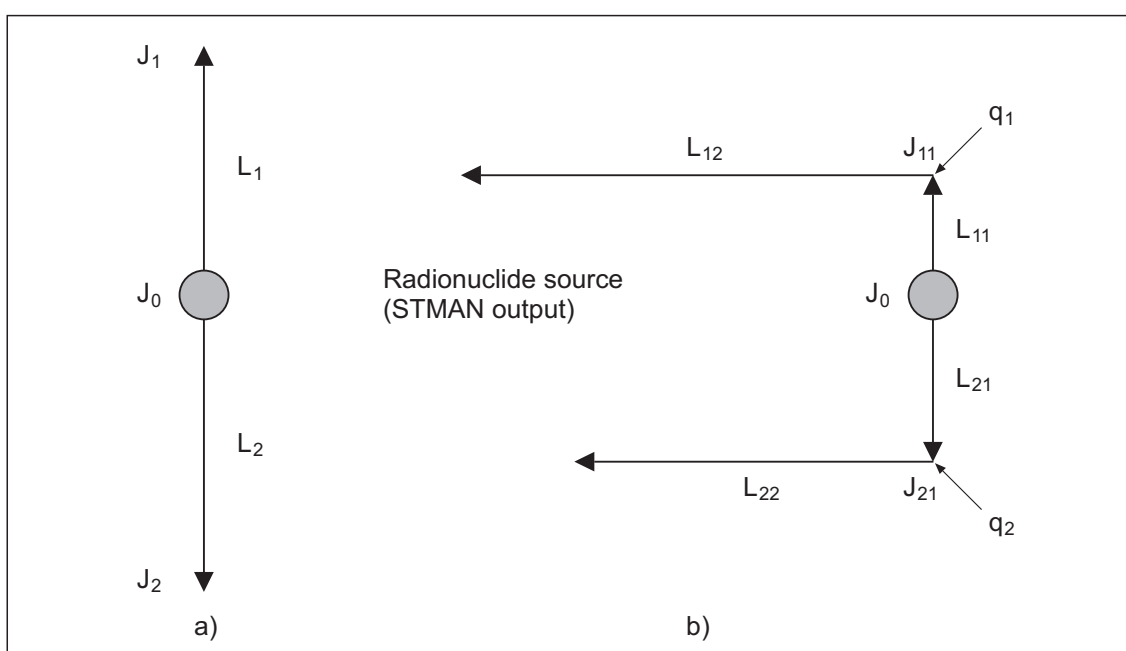


Fig. 3.5-2: The PICNIC network structure used to model the two variants of the conceptualisation considering the additional barriers provided by the confining units

a) Base Case (left), b) model variant (right).

3.5.4 Parameters

Base Case

The parameters are as in the Reference Case, except for the PICNIC input data for the legs illustrated in Fig. 3.5-2a. Network flow data and source term information are given in Tab. 3.5-1. Transport parameters for legs L_1 and L_2 are given in Tabs. 3.5-2 to 3.5-3, respectively.

Tab. 3.5-1: Network flow data and source term information (Base Case)

Input	Units	Values	Source
Network Structure			
List of junction names. Inlet and outlet junctions for each leg.	-	Fig. 3.5-2a	
Network Flow Data			
Head at Junction J ₀ at Junction J ₁ at Junction J ₂	m	504 364 304	Derived from a hydraulic gradient of 1 m m ⁻¹ (upwards and downwards), pessimistically assuming overpressures in the host rock (Tab. A3.3-4b)
Source Term Information			
Source flux	mol a ⁻¹	Radionuclide releases to host rock obtained from the output of code STMAN (Reference Case).	
Fraction to each leg	-	0.5	Radionuclide transport assumed identical upwards and downwards

Tab. 3.5-2: PICNIC input data for leg L₁, which represents upward vertical transport through the Opalinus Clay and upper confining units (Base Case)

Input	Units	Values	Source
Leg Data – Basic Data			
Length	m	140	Tab. A3.2-2a, Parameter 3, Value D
Darcy velocity	m a ⁻¹	3.2×10^{-6}	Tab. A3.2-2a, Parameter 5, Value F (based on a vertical hydraulic conductivity of 10 ⁻¹³ m s ⁻¹ , see Tab. A3.3-4b)
Leg Data – Properties of Flowing Region			
Identical to Reference Case.			
Leg Data – Properties of Matrix			
There is no "matrix" for this leg – the Opalinus Clay and the upper confining units are a homogeneous porous medium. The matrix penetration depth and surface sorption coefficients are thus set equal to zero, and all other parameters are irrelevant.			

Tab. 3.5-3: PICNIC input data for leg L₂, which represents downward vertical transport through the Opalinus Clay and lower confining units (Base Case)

Input	Units	Values	Source
Leg Data – Basic Data			
Length	m	200	Tab. A3.2-2a, Parameter 3, Value D
Darcy velocity	m a ⁻¹	6.3×10^{-7}	Tab. A3.2-2a, Parameter 5, Value F (identical to Reference Case)
Leg Data – Properties of Flowing Region			
Identical to Reference Case.			
Leg Data – Properties of Matrix			
There is no "matrix" for this leg – the Opalinus Clay and the lower confining units are a homogeneous porous medium. The matrix penetration depth and surface sorption coefficients are thus set equal to zero, and all other parameters are irrelevant.			

Model variant

The parameters are as in the Reference Case, except for the PICNIC input data for the legs illustrated in Fig. 3.5-2b. Network flow data and source term information are given in Tab. 3.5-4. Transport parameters for legs L₁₁, L₁₂, L₂₁ and L₂₂ are given in Tabs. 3.5-5 to 3.5-8, respectively.

Tab. 3.5-4: Network flow data and source term information (model variant)

Input	Units	Values	Source
Network Structure			
List of junction names. Inlet and outlet junctions for each leg.	-	Fig. 3.5-2b	
Network Flow Data			
Head at Junction J ₀	m	504	Derived from a hydraulic gradient of 1 m m ⁻¹ (upwards and downwards), pessimistically assuming overpressures in the host rock (Tab. A3.3-4b)
at Junction J ₁₁		464	
at Junction J ₂₁		404	
Source Term Information			
Source flux	mol a ⁻¹	Radionuclide releases to host rock obtained from the output of code STMAN (Reference Case).	
Fraction to each leg	-	0.5	Radionuclide transport assumed identical upwards and downwards

Tab. 3.5-5: PICNIC input data for leg L₁₁, which represents upward vertical transport through the Opalinus Clay (model variant)

Input	Units	Values	Source
<p><i>Leg Data – Basic Data</i> Identical to Reference Case.</p>			
<p><i>Leg Data – Properties of Flowing Region</i> Identical to Reference Case.</p>			
<p><i>Leg Data – Properties of Matrix</i> There is no "matrix" for this leg – the Opalinus Clay is a homogeneous porous medium. The matrix penetration depth and surface sorption coefficients are thus set equal to zero, and all other parameters are irrelevant.</p>			

Tab. 3.5-6: PICNIC input data for leg L₁₂, which represents lateral transport through the Wedelsandstein (model variant)

Input	Units	Values	Source
Leg Data – Basic Data			
Length	m	25 000	Tab. A3.2-2a, Parameter 3, Value F
Cross sectional area	m ²	irrelevant	
Darcy velocity ¹	m a ⁻¹	1.6×10^{-5}	Tab. A3.2-2a, Parameter 5, Value G
Pore diffusion coefficient	m ² a ⁻¹	6.3×10^{-2}	Tab. A3.2-2a, Parameter 7, Value C
Leg Data – Properties of Flowing Region			
Retardation	dimensionless	Calculated from the parameters below.	
Grain density	kg m ⁻³	irrelevant	Tab. A3.2-2a, Parameter 8, Value B
Flow porosity	dimensionless	This is set equal the infill porosity.	
Infill porosity	dimensionless	1	Tab. A3.2-2a, Parameter 10, Value B
Porosity factors	dimensionless	irrelevant	
Sorption K_d	m ³ kg ⁻¹	irrelevant	Tab. A3.2-2a, Parameter 11, Value D
Leg Data – Properties of Matrix			
Specific surface area	m ⁻¹	2 000	Tab. A3.2-2a, Parameter 12, Value B
Maximum penetration depth	m	0.5	Tab. A3.2-2a, Parameter 13, Value B
Surface Sorption K_a	m	Set to zero (sorption on fracture surfaces conservatively neglected)	
Retention	dimensionless	Calculated from parameters below.	
Grain density	kg m ⁻³	Tab. A3.2-2a, Parameter 15, Value B	
Matrix porosity	dimensionless	0.12 × porosity factors	Tab. A3.2-2a, Parameter 16, Value B
Porosity factors	dimensionless		
Sorption K_d	m ³ kg ⁻¹	0.1 × K_d (OPA)	Tab. A3.2-2a, Parameter 17, Value B
Pore diffusion coefficients	m ² a ⁻¹	anions: 2.6×10^{-3} (8.3×10^{-11} m ² s ⁻¹) non-anions: 1.3×10^{-3} (4.2×10^{-11} m ² s ⁻¹)	Tab. A3.2-2a, Parameter 18, Value B

¹ The Darcy velocity for the Wedelsandstein is based on a hydraulic conductivity of 5.0×10^{-10} m s⁻¹ and a hydraulic gradient of 0.001 m m⁻¹ (see Tab. A3.3-4b).

Tab. 3.5-7: PICNIC input data for leg L₂₁, which represents downward vertical transport through the Opalinus Clay and the Lias / Upper Keuper (model variant)

Input	Units	Values	Source
Leg Data – Basic Data			
Length	m	100	Tab. A3.2-2a, Parameter 3, Value F
Darcy velocity	m a ⁻¹	1.6×10^{-6}	Tab. A3.2-2a, Parameter 5, Value G (based on a vertical hydraulic conductivity of 5×10^{-14} m s ⁻¹ , see Tab. A3.3-4b)
Leg Data – Properties of Flowing Region			
Identical to Reference Case.			
Leg Data – Properties of Matrix			
There is no "matrix" for this leg – the Opalinus Clay and the Lias / Keuper is a homogeneous porous medium. The matrix penetration depth and surface sorption coefficients are thus set equal to zero, and all other parameters are irrelevant.			

Tab. 3.5-8: PICNIC input data for leg L₂₂, which represents lateral transport through the Sandsteinkeuper (model variant)

Input	Units	Values	Source
Leg Data – Basic Data			
Length	m	15 000	Tab. A3.2-2a, Parameter 3, Value F
Cross sectional area	m ²	irrelevant	
Darcy velocity ¹	m a ⁻¹	3.2×10^{-3}	Tab. A3.2-2a, Parameter 5, Value G
Pore diffusion coefficient	m ² a ⁻¹	6.3×10^{-2}	Tab. A3.2-2a, Parameter 7, Value C
Leg Data – Properties of Flowing Region			
Retardation	dimensionless	Calculated from the parameters below.	
Grain density	kg m ⁻³	irrelevant	Tab. A3.2-2a, Parameter 8, Value B
Flow porosity	dimensionless	This is set equal the infill porosity.	
Infill Porosity	dimensionless	0.05 × porosity factors in Tab. A3.5-5	Tab. A3.2-2a, Parameter 10, Value C
Porosity Factors	dimensionless	see Tab. A3.5-5	
Sorption K_d	m ³ kg ⁻¹	$0.05 \times K_d$ (OPA)	Tab. A3.2-2a, Parameter 11, Value C
Leg Data – Properties of Matrix			
There is no "matrix" for this leg – the Sandsteinkeuper is a homogeneous porous medium. The matrix penetration depth and surface sorption coefficients are thus set equal to zero, and all other parameters are irrelevant.			

¹ The Darcy velocity for the Sandsteinkeuper is based on a hydraulic conductivity of 2.0×10^{-8} m s⁻¹ and a hydraulic gradient of 0.005 m m⁻¹ (see Tab. A3.3-4b).

3.6 Radionuclide release affected by ramp/shaft (Case 1.6)

3.6.1 Overview

One of the basic assumptions in the Reference Conceptualisation is that transport along the operations and construction tunnels is negligible compared with transport through the host rock. In this alternative conceptualisation, the validity of this assumption is tested by calculating the radionuclide release through host rock and access tunnel system in parallel.

3.6.2 The conceptual model and its underlying assumptions

The status of the repository after final sealing and closure of the facility is shown in Fig. 2.1-6. The calculations of radionuclide release affected by ramp/shaft are performed in three distinct steps:

- In a first step, the water flow rates in the repository system are calculated using a simplified resistor network model that is compared with the results of the 3D hydrodynamic finite element model (Nagra 2002a).
- In a second step, the near field release rates are calculated taking into account the hydraulic boundary conditions calculated in the first step.
- In a third step, the simultaneous radionuclide release through host rock and access tunnel system is calculated based on the flow field and source term calculated in the previous steps.

As in the Reference Conceptualisation, the effectiveness of the confining units as a barrier to radionuclide transport is conservatively neglected. Once the radionuclides enter the confining units they are assumed to be instantaneously transported to the reference discharge area where dilution takes place by mixing with flowing groundwater in the Quaternary aquifer.

3.6.2.1 Calculation of water flow rates in the repository system

The water fluxes in the repository are calculated analytically by means of a steady-state resistor network model, assuming sealing zones to be located as indicated in Fig. 3.6-1a and to be functioning as-designed. Note that in these simplified model calculations, only the inner sealing zone in the ramp (located near the construction branch off) is taken into account. Inflow of water into the emplacement tunnels and flow of water along the tunnels is driven by the hydraulic head difference between the Sandsteinkeuper and Wedelsandstein formations. In the resistor network model, the SF/HLW emplacement tunnels are represented as continuous resistors, i.e. the continuous head profile along the axis of the emplacement tunnels is calculated explicitly. The hydraulic head in the ILW emplacement tunnels, branch galleries and operations tunnel is assumed to be uniform (H_{n3}). The sealing zones are treated as discrete resistors. Hydraulic heads between sealing zones are assumed to be uniform (H_{n1} , H_{s1} , H_1 , H_2). The hydraulic conductivities of Opalinus Clay (vertical direction), EDZ, sealing zones (bentonite) and tunnel backfill (bentonite / sand mixture) are assumed to be 2×10^{-14} , 1×10^{-12} , 1×10^{-13} and $5 \times 10^{-11} \text{ m s}^{-1}$, respectively (Base Case, data from Nagra 2002a). This means that water flow through the sealing zones takes place predominantly through the EDZ²², whereas water flow in tunnel sections backfilled with a bentonite / sand mixture is assumed to occur mainly in

²² Note that prior to the emplacement of the sealing plugs, the EDZ is partially removed. As a consequence, the hydraulic conductivity of the EDZ in sealing sections is expected to be lower than $1 \times 10^{-12} \text{ m s}^{-1}$, but this is not taken into account in the present calculations.

the tunnel backfill. While water flows between emplacement tunnels (by far the largest part of the repository) and the Opalinus Clay is explicitly taken into account, water flows between operations, construction and ventilation tunnels on one hand and the Opalinus Clay on the other hand are neglected. The hydraulic resistance of backfilled sections in the operations, construction and ventilation tunnels are assigned to the up-stream sealing sections.

In a parameter variation, the hydraulic conductivity of the EDZ is increased by a factor of 100 ($1 \times 10^{-10} \text{ m s}^{-1}$, value applied to emplacement tunnels and sealing sections). In a further model variant, the water flow and radionuclide transport in tunnel sections backfilled with a bentonite / sand mixture is assumed to occur in the tunnel liner (shotcrete). These alternative cases are discussed below.

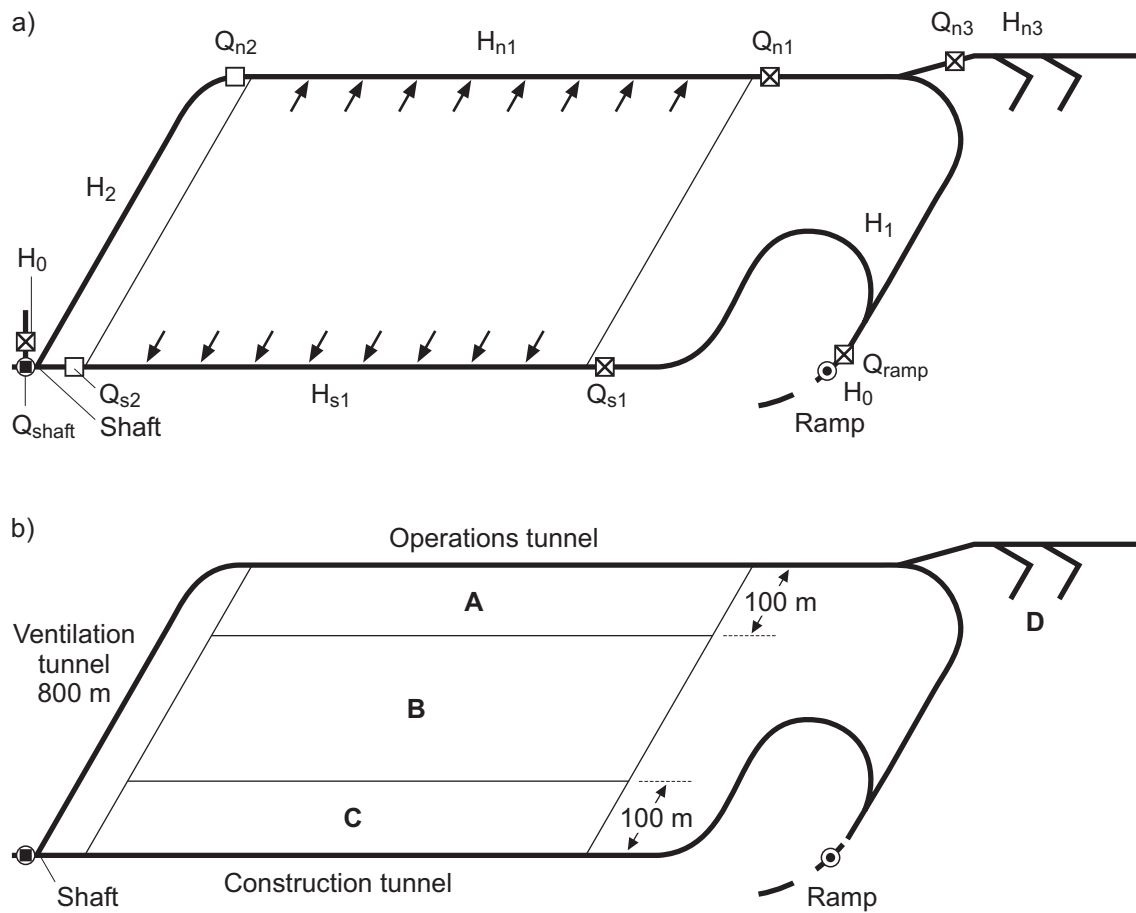


Fig. 3.6-1: a) Resistor network model for hydraulic calculations of water flow through the tunnel system; b) repository domains for modelling radionuclide transport through the host rock and the ramp/shaft

H denotes the hydraulic heads between sealing zones and Q the water fluxes through sealing zones (squares with crosses) and control points (empty squares). A/B/C: SF/HLW part of the repository; D: ILW part of the repository.

In the Base Case, the water inflow rate from the host rock to the SF/HLW emplacement tunnels, q [$\text{m}^3 \text{s}^{-1}$], can be calculated from²³:

$$\frac{dq}{dx} = 4\gamma r K_{HR} \left(\frac{H_l - h(x)}{L_l} + \frac{H_u - h(x)}{L_u} \right) \quad (3.6-1)$$

where

K_{HR}	hydraulic conductivity of host rock [m s^{-1}]
r	radius of the SF/HLW emplacement tunnel [m]
γ	ratio of radii EDZ/emplacement tunnel [-]
x	coordinate along axis of emplacement tunnel [m]
$h(x)$	hydraulic head within emplacement tunnel at location x [m]
H_l	hydraulic head in Sandsteinkeuper (lower confining unit) [m]
H_u	hydraulic head in Wedelsandstein (upper confining unit) [m]
L_l	distance from mid Opalinus Clay to Sandsteinkeuper [m]
L_u	distance from mid Opalinus Clay to Wedelsandstein [m]

On the other hand, the flow of water along the SF/HLW emplacement tunnel (predominantly within EDZ, but also within bentonite) is:

$$q = -\pi r^2 (K_B + (\gamma^2 - 1)K_{EDZ}) \frac{dh}{dx} \quad (3.6-2)$$

with

K_B	hydraulic conductivity of bentonite [m s^{-1}]
K_{EDZ}	axial hydraulic conductivity of EDZ [m s^{-1}]

²³ Eq. 3.6-1 is derived for steady-state conditions, in which case the water flow is linear and takes place predominantly in the vertical direction. Explanation for factor $4\gamma r$ in Eq. 3.6-1: Diameter of tunnel and EDZ is $2\gamma r$. The convergence of vertical flow lines towards the tunnels is accounted for by a factor of 2. Note that in a transient regime following backfilling and sealing of the emplacement tunnels, inflow to the tunnels is expected to occur predominantly in the radial direction.

From Eq. 3.6-1 and 3.6-2 one obtains:

$$\frac{d^2 h}{dx^2} = \kappa^2 (h(x) - H_A)$$

with

$$\kappa^2 = \frac{4\gamma K_{HR}}{\pi r (K_B + (\gamma^2 - 1)K_{EDZ})} \left(\frac{1}{L_l} + \frac{1}{L_u} \right) \quad (3.6-3)$$

$$H_A = \frac{\frac{H_l}{L_l} + \frac{H_u}{L_u}}{\frac{1}{L_l} + \frac{1}{L_u}}$$

The boundary conditions at the ends of each emplacement tunnel (with l [m] denoting the length of a SF/HLW emplacement tunnel) are:

$$h\left(\frac{l}{2}\right) = H_{n1} \quad \text{and} \quad h\left(-\frac{l}{2}\right) = H_{s1} \quad (3.6-4)$$

The solution to Eq. 3.6-3 and 3.6-4 is:

$$h(x) = \frac{H_{n1} - H_{s1}}{2 \sinh\left(\frac{\kappa l}{2}\right)} \sinh(\kappa x) + \frac{H_{n1} + H_{s1} - 2H_A}{2 \cosh\left(\frac{\kappa l}{2}\right)} \cosh(\kappa x) + H_A \quad (3.6-5)$$

The total water flow from N SF/HLW emplacement tunnels to the operations tunnel (northern branch), Q_n [$\text{m}^3 \text{a}^{-1}$], and construction tunnel (southern branch), Q_s [$\text{m}^3 \text{a}^{-1}$], are:

$$Q_n = -\alpha^+ H_{n1} + \alpha^- H_{s1} + \alpha H_A \tanh\left(\frac{\kappa l}{2}\right) \quad (3.6-6)$$

$$Q_s = \alpha^- H_{n1} - \alpha^+ H_{s1} + \alpha H_A \tanh\left(\frac{\kappa l}{2}\right)$$

with

$$\alpha = \pi r^2 N \kappa (K_B + (\gamma^2 - 1)K_{EDZ})$$

$$\alpha^\pm = \alpha \left(\frac{1}{2 \tanh\left(\frac{\kappa l}{2}\right)} \pm \frac{1}{2} \tanh\left(\frac{\kappa l}{2}\right) \right) \quad (3.6-7)$$

The total water flow rate from the ILW emplacement tunnels to the operations tunnel, Q_{n3} [$\text{m}^3 \text{a}^{-1}$], is estimated as (see footnote to Eq. 3.6-1):

$$Q_{n3} = \alpha_1 (H_A - H_{n3}) \quad \text{with} \quad \alpha_1 = A_D K_{HR} \left(\frac{1}{L_l} + \frac{1}{L_u} \right); \quad A_D = 4\gamma_{ILW} r_{ILW} A_{ILW} \quad (3.6-8)$$

with

A_D	effective drainage area of the ILW emplacement tunnels [m^2]
r_{ILW}	radius of the ILW emplacement tunnel [m]
γ_{ILW}	ratio of radii EDZ/emplacement tunnel [-]
A_{ILW}	total length of ILW emplacement tunnels [m]

The mass balance of all water fluxes in Fig. 3.6-1a yields an algebraic system of equations for the five unknown hydraulic heads H_1 , H_2 , H_{n1} , H_{n3} and H_{s1} , from which the individual water fluxes can be calculated:

$$\begin{aligned} Q_{ramp} &= \beta_r (H_1 - H_0) \\ Q_{shaft} &= \beta_s (H_2 - H_0) \\ Q_{n1} &= \beta_{n1} (H_{n1} - H_1) \\ Q_{n2} &= \beta_{n2} (H_{n1} - H_2) \\ Q_{n3} &= \alpha_1 (H_A - H_{n3}) \\ Q_{s1} &= \beta_{s1} (H_{s1} - H_1) \\ Q_{s2} &= \beta_{s2} (H_{s1} - H_2) \\ Q_{OPA} &= 4\gamma r N K_{HR} ((H_A - H_u)l + (H_{n1} + H_{s1} - 2H_A) \tanh(\kappa l / 2) / \kappa) / L_u \quad (SF / HLW) \\ Q_{OPA} &= A_D K_{HR} (H_{n3} - H_u) / L_u \quad (ILW) \end{aligned} \quad (3.6-9)$$

with

$$\beta_i = \frac{\pi R_i^2}{\frac{l_i}{K_i + (\gamma_i^2 - 1)K_{i,EDZ}} + \frac{l_{i,BF}}{K_{i,BF}}} \quad (3.6-10)$$

$H_0 (=H_u)$ hydraulic head at intersection of ramp/shaft and Wedelsandstein formation [m]

R_i, l_i radius and length of sealing zone i [m]

γ_i ratio of radii EDZ/tunnel [-]

K_i hydraulic conductivity of sealing zone i [m s^{-1}]

$K_{i,EDZ}$ hydraulic conductivity of EDZ around sealing zone i [m s^{-1}]

$K_{i,BF}$ hydraulic conductivity of backfilled tunnel downstream of sealing zone i [m s^{-1}]

$l_{i,BF}$ Length of backfilled tunnel downstream from sealing zone i [m]

The Base Case results of the resistor network model are compared with the results from a 3D hydrodynamic finite element model (Nagra 2002a). Analytical and numerical water flow rates, calculated at several different locations in the repository, are compared in Fig. 3.6-2. The numerical analysis is based on the case RLU0²⁴. Clearly, the water flow occurs predominantly vertically from the Sandsteinkeuper formation to the Wedelsandstein formation, i.e. from the bottom to the top of the Opalinus Clay. Only small amounts of water are deviated axially along the various tunnels. The numerical and analytical water flow rates are generally in good agreement. An exception is location *n2*, where the numerically calculated flow is directed towards the SF/HLW emplacement tunnels, whereas the analytically calculated flow direction is towards the shaft. This difference is due to variability of the head distribution within the plane of the repository caused by small variations of the distance from the tunnels to the (non-planar) top of the Opalinus Clay. This small variability in the external head distribution is not taken into account in the analytical model.

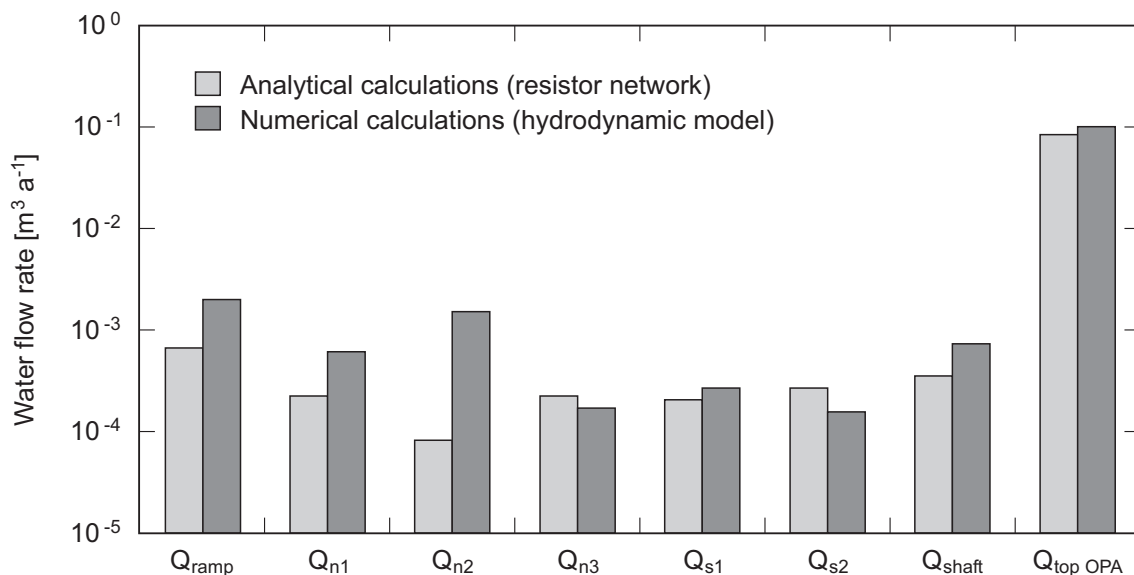


Fig. 3.6-2: Comparison of water flow rates obtained from the resistor network model calculations in the Base Case, described in the present section, and the numerical hydrodynamic model calculations for case RLU0, described in Nagra (2002a)

The various locations in the repository are labelled according to Fig. 3.6-1a. Note that the numerical and analytical fluxes at node *n2* point in opposite directions (see text).

In Fig. 3.6-3, the effect of an increase in the hydraulic conductivity of the EDZ (emplacement tunnels, sealing sections) on the water flow rates in the tunnel system is shown. A value of $1 \times 10^{-12} \text{ m s}^{-1}$ corresponds to the Base Case. The water flow rates level off at conductivities of about $1 \times 10^{-10} \text{ m s}^{-1}$, because of the limited water inflow from the Opalinus Clay. In the framework of a parameter variation, a value of the $1 \times 10^{-10} \text{ m s}^{-1}$ is therefore investigated.

²⁴ The case RLU0 involves vertical groundwater movement driven by the hydraulic head difference between the Sandsteinkeuper and Wedelsandstein formations, without considering overpressures in the near field and the geosphere and assuming that the seals/EDZ function as expected.

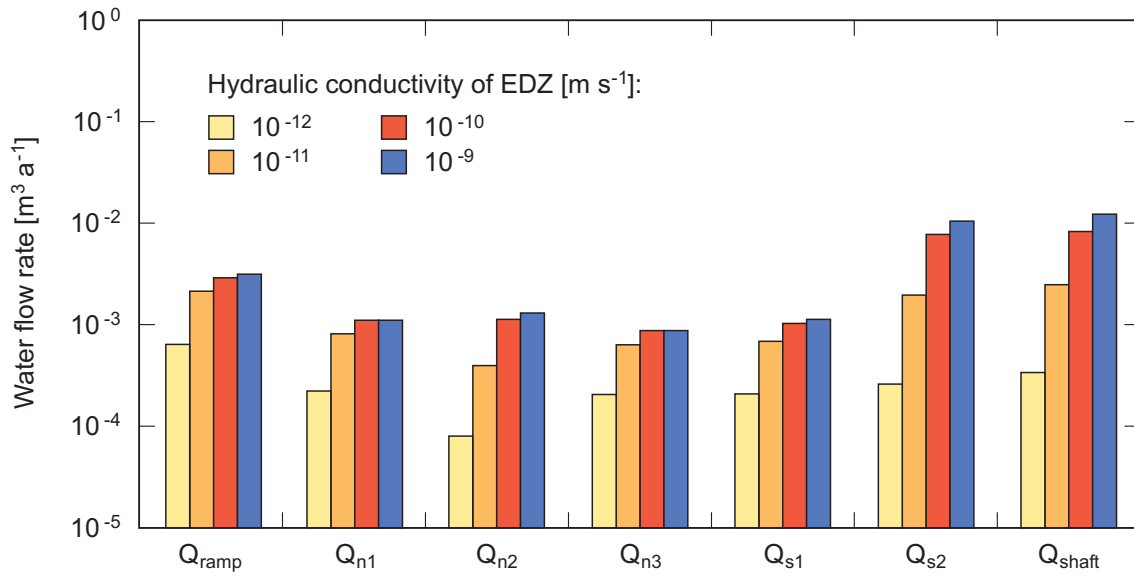


Fig. 3.6-3: Comparison of water flow rates obtained from the resistor network model calculations for various values of the hydraulic conductivity of the EDZ

The various locations in the repository are labelled according to Fig. 3.6-1a.

In a model variant, the flow of water along the operations/construction/ventilation tunnels is assumed to occur in the liner (shotcrete with a thickness of $d = 0.3$ m and an assumed hydraulic conductivity of $K_{i,liner} = 1 \times 10^{-9} \text{ m s}^{-1}$), instead of occurring in the tunnel backfill (sand/bentonite mixture with a tunnel radius of $R = 2.7$ m and a hydraulic conductivity of $K_{i,BF} = 5 \times 10^{-11} \text{ m s}^{-1}$) as assumed in the Base Case. The water flow rates for the model variant are calculated as in the Base Case, but replacing $K_{i,BF}$ with $K_{i,BF,eff}$ in Eq. 3.6-10, as follows:

$$K_{i,BF,eff} = \left[\left(\frac{R+d}{R} \right)^2 - 1 \right] K_{i,liner} \quad (3.6-11)$$

With the above values for R , d and $K_{i,liner}$, one obtains $K_{i,BF,eff} = 2.3 \times 10^{-10} \text{ m s}^{-1}$. This effective hydraulic conductivity is about a factor of 5 higher than the value for the sand/bentonite mixture ($K_{i,BF} = 5 \times 10^{-11} \text{ m s}^{-1}$) used in the Base Case.

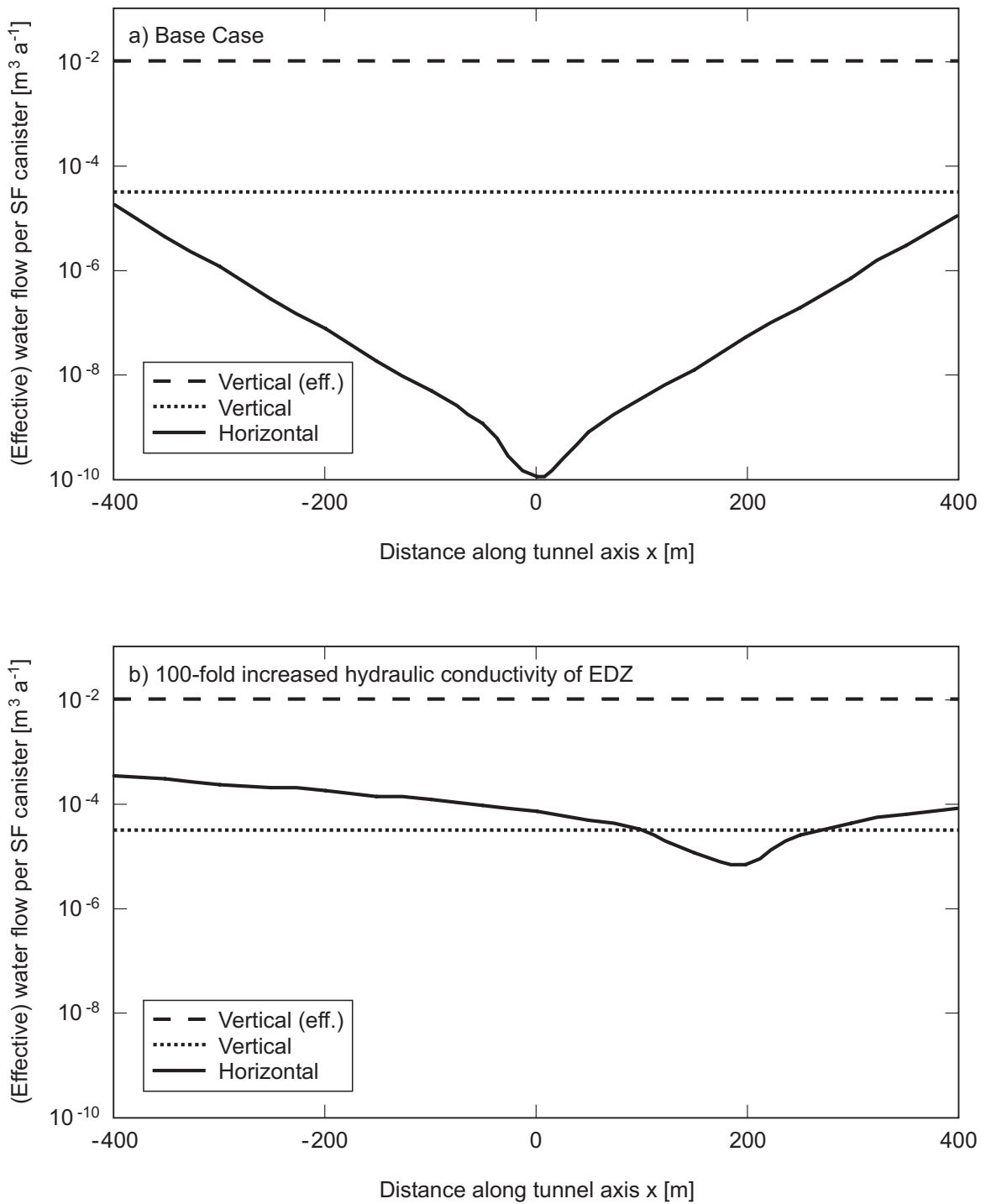


Fig. 3.6-4: Comparison of the vertical flow rates per SF canister, driven by the hydraulic head difference between the Sandsteinkeuper and Wedelsandstein formations, the vertical effective flow rates, taking diffusion into account, and the horizontal flow rates along the axes of the SF emplacement tunnels

a) EDZ/seals functioning as-designed (Base Case), b) 100-fold increased hydraulic conductivity of EDZ ($10^{-10} \text{ m s}^{-1}$; value applied to emplacement tunnels and sealing zones).

3.6.2.2 Calculation of radionuclide release from near field

In the case of SF/HLW, the vertical water flow rate per canister, driven by the hydraulic head difference between the Sandsteinkeuper and Wedelsandstein formations, dominates over the horizontal flow rate along the axis of the emplacement tunnel, except for the tunnel sections in the vicinity of the operations/construction tunnels. This is demonstrated in Fig. 3.6-4a for the case of sealings functioning as-designed (with a hydraulic conductivity of $10^{-13} \text{ m s}^{-1}$), in which the vertical water flow per SF canister and the axial water flow are compared. In addition, Fig. 3.6-4a also shows the effective vertical water flow rate, which includes the contribution of diffusion in the Opalinus Clay (see Eq. 3.1-1). Note that the effective horizontal water flow rate (not shown in Fig. 3.6-4), which includes a diffusive contribution to transport along the tunnels axis, is nearly identical to the horizontal water flow rate, because the horizontal concentration gradient is close to zero. Fig. 3.6-4a demonstrates that for the majority of the canisters, the near field release rate is not significantly affected by the axial flow rate. Only at the ends of the emplacement tunnels is the axial water flow rate in the same order of magnitude as the vertical water flow rate. Fig. 3.6-4b shows that, for the case of a 100-fold increased hydraulic conductivity of the EDZ ($1 \times 10^{-10} \text{ m s}^{-1}$), the axial flow rate exceeds the vertical flux by maximally a factor of 10. The effective vertical water flow rate is, however, still considerably higher than the horizontal water flow rate.

For this reason, in all investigated cases related to the release of radionuclides affected by the ramp/shaft, the SF/HLW near field is split up into three domains, labelled A, B and C in Fig. 3.6-1b. The length of the domains A and C, measured along the emplacement tunnels, is 100 m, whereas the length of domain B is 600 m. Within segment B (75 % of the SF/HLW facility), the near field release terms for SF/HLW are taken to be identical to the Reference Case²⁵. The calculation of the near field release terms for domains A and C is also based on the Reference Case, but with a 10-fold increased groundwater flow rate. By similar arguments, the near field release term for ILW (domain D) is also modelled in the same way as for the Reference Case, but with a 10-fold increased groundwater flow rate.

3.6.2.3 Calculation of radionuclide transport through host rock and access tunnel system

For the calculation of radionuclide transport affected by the ramp and shaft, the waste is split up in four domains, as shown in Fig. 3.6-1b. For the sake of simplicity, the radionuclide inventory contained in the pilot facility is included in the SF/HLW main facility. This simplification is justified because also for the main facility, only a reduced path length for radionuclide transport within the tunnel of 1 000 m, corresponding to the length of the tunnel segment in between the seal emplaced nearest to the pilot facility and the seal of the ramp, is considered (see Fig. 2.1-6 for the location of these seals).

The inventory of domain B (corresponding to 75 % of the SF/HLW part of the repository) is released through the Opalinus Clay only, and the geosphere model calculations are performed as in the Reference Case. For domains A/C (both SF/HLW) and D (ILW), radionuclide transport occurs in parallel through the host rock and through the ramp/shaft. For each of the waste

²⁵ By doing so, the near field release rate for the case with an increased hydraulic conductivity of the EDZ may be slightly underestimated. But this has no significant effect on the resulting dose.

domains A/C/D, the flux of radionuclides is, therefore, split up between the host rock and the access tunnel system, using fixed branching ratios defined by²⁶:

$$\begin{aligned}
 f_{A,HR} &= \frac{Q_{HR,eff}^A}{Q_{HR,eff}^A + Q_{n1} + Q_{n2}} & f_{A,n1} &= \frac{Q_{n1}}{Q_{HR,eff}^A + Q_{n1} + Q_{n2}} & f_{A,n2} &= 1 - f_{A,HR} - f_{A,n1} \\
 f_{C,HR} &= \frac{Q_{HR,eff}^C}{Q_{HR,eff}^C + Q_{s1} + Q_{s2}} & f_{C,s1} &= \frac{Q_{s1}}{Q_{HR,eff}^C + Q_{s1} + Q_{s2}} & f_{C,s2} &= 1 - f_{C,HR} - f_{C,s1} \\
 f_{D,HR} &= \frac{Q_{HR,eff}^D}{Q_{HR,eff}^D + Q_{n3}} & f_{D,n3} &= 1 - f_{D,HR}
 \end{aligned} \quad (3.6-12)$$

where

$f_{\alpha,HR/ni/si}$	branching ratios for waste domains $\alpha = A, C, D$, used to split the flux of radionuclides at branching nodes into different transport legs [-]
$Q_{HR,eff}^{\alpha}$	effective water flow rate through the host rock for waste domains $\alpha = A, C, D$, including the diffusive contribution to transport [$m^3 a^{-1}$]
$Q_{ni,si}$	water flow rate through the access tunnel system calculated analytically at different locations using the resistor network model [$m^3 a^{-1}$]

The effective water flow rate through the host rock is calculated as in the Reference Case (see Eq. 3.1-1). The cross-sectional areas of the various legs (see Fig. 3.6-5) used in the calculation of radionuclide transport in the Base Case (1.6a) and in the parameter variation (1.6b) are given by:

$$A_i = \begin{cases} \pi R_i^2 & i = n1, n2, n3, s1, s2, ramp \\ \pi R_i^2 (\gamma_i^2 - 1) & i = shaft \\ 4\gamma r \Lambda_i & i = A, B, C (SF / HLW) \\ 4\gamma_{ILW} r_{ILW} \Lambda_{ILW} & i = D (ILW) \end{cases} \quad (3.6-13)$$

where

R_i	radius of tunnel segment i (taken to be equal to radius of sealing zone i located upstream of tunnel segment i) [m]
γ_i	ratio of radii EDZ/tunnel of tunnel segment i [-]
r	radius of the SF/HLW emplacement tunnel [m]
γ	ratio of radii EDZ/emplacement tunnel for SF/HLW [-]
$A_{A,B,C}$	total length of SF/HLW emplacement tunnels of domains A, B, C [m]
r_{ILW}	radius of the ILW emplacement tunnel [m]
γ_{ILW}	ratio of radii EDZ/emplacement tunnel for ILW [-]
A_{ILW}	total length of ILW emplacement tunnels [m]

²⁶ Transport in Opalinus Clay is strongly affected by diffusion. In PICNIC, however, radionuclide transport at branching points is divided according to the water fluxes involved. This is dealt with by using the effective water flux through the host rock which includes an effective contribution of diffusion, instead of the real water flux (see Eq. 3.1-1).

Retardation in the various segments in the operations/construction/ventilation tunnels is explicitly considered, assuming advection, dispersion, diffusion, decay and sorption in the bulk of the tunnel backfill (mixture of 30 % bentonite and 70 % quartz sand). Note that only sorption on bentonite is taken into account, whereas sorption on quartz sand is conservatively neglected. No transport and no matrix diffusion is considered, neither within the liner nor within the EDZ of the backfilled tunnels. In contrast, radionuclide transport in the shaft is assumed to occur in the EDZ only, but no matrix diffusion is considered.

In the model variant related to flow and transport in the tunnel liner, retardation in the various segments in the operations/construction/ventilation tunnels is explicitly considered, assuming advection, dispersion, diffusion, decay and sorption in the tunnel liner (shotcrete). In this case, no transport and no matrix diffusion is considered, neither within the sand/bentonite backfill of the tunnels nor within the EDZ. The cross-sectional areas of the various legs representing transport in the liner are given by

$$A_i = \pi \left((R_i + d)^2 - R_i^2 \right) \quad i = n1, n2, n3, s1, s2, ramp \quad (3.6-14)$$

with d [m] being the liner thickness. All other cross sectional areas are identical to those given in Eq. 3.6-13. Radionuclide transport in the shaft and in the Opalinus Clay is treated as in the Base Case.

3.6.3 Codes used

As in the Reference Conceptualisation, the reference model chain of STMAN-PICNIC-TAME is used to model the radionuclide release, migration and distribution in the biosphere. However, rather than employing a single PICNIC "leg" (see Appendix 1) to model a single transport path through the homogeneous host rock, the network capabilities of PICNIC are employed to model the simultaneous transport of radionuclides through Opalinus Clay, ramp and shaft.

The network structure used for this case is depicted in Fig. 3.6-5. The legs L_1 - L_5 represent the transport path through the access tunnel system. The legs $L_{6,A}$, $L_{6,B}$, $L_{6,C}$ and L_7 represent upward vertical transport through the Opalinus Clay from SF/HLW (domains A, B, C) and ILW (domain D), respectively. The water flow rates, Q_i , and cross sectional areas, A_i , ($i = n1, n2, n3, s1, s2, ramp, shaft, A, B, C, D$), are calculated using Eqs. 3.6-9 and 3.6-13/14, respectively.

3.6.4 Parameters

Base Case

In the Base Case, the repository is assumed to be fully backfilled and all sealing zones functioning as-designed. The parameter values used for the calculation of water flow rates (resistor network) are summarised in Tab. 3.6-1. Network flow data and source term information are given in Tab. 3.6-2. Note that most of the radionuclide inventory is released through the Opalinus Clay. Transport parameters for legs L_1 to L_7 are given in Tabs. 3.6-3 to 3.6-5.

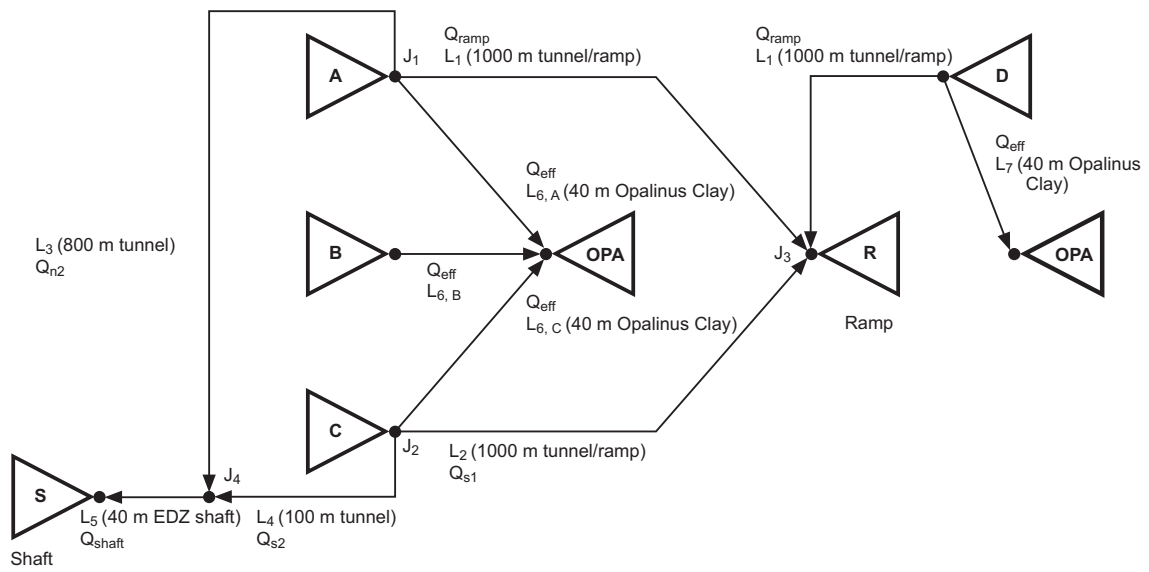


Fig. 3.6-5: The PICNIC network structure used to model the conceptualisation "radionuclide release affected by ramp/shaft"

Tab. 3.6-1: Parameter values used for the calculation of water flow rates in the resistor network
 Values taken from Tabs. A3.3-2 to A3.3-4 and Nagra 2002a.

Parameter	Symbol	Unit	Value
Host rock and EDZ			
Hydraulic head in Sandsteinkeuper	H_l	m	465
Hydraulic head in Wedelsandstein	H_u	m	342
Hydraulic head at ramp/shaft exit	$H_0 (=H_u)$	m	342
Hydraulic conductivity of host rock	K_{HR}	m s^{-1}	2×10^{-14}
Hydraulic conductivity of EDZ	K_{EDZ}	m s^{-1}	10^{-12}
Distance from mid Opalinus Clay to Sandsteinkeuper	L_l	m	100
Distance from mid Opalinus Clay to Wedelsandstein	L_u	m	40
SF/HLW emplacement tunnels			
Hydraulic conductivity of bentonite	K_B	m s^{-1}	10^{-13}
Radius	r	m	1.15
Ratio of radii EDZ/tunnel	γ	-	1.61
Length	l	m	800
Number	N	-	27
ILW emplacement tunnels			
Radius	r_{ILW}	m	4.5
Ratio of radii EDZ/tunnel	γ_{ILW}	-	1.22
Total length	L_{ILW}	m	180
Sealing zones (incl. backfilled tunnel segments downstream)			
Hydraulic conductivity of sealing	K_i	m s^{-1}	10^{-13}
Hydraulic conductivity of EDZ	$K_{i,EDZ}$	m s^{-1}	10^{-12}
Hydraulic conductivity of backfilled tunnel downstream of sealing	$K_{i,BF}$	m s^{-1}	5×10^{-11}
Radius (not including liner): Ramp Shaft all others	R_i	m	3.1 1.8 2.7
Ratio of radii EDZ/tunnel: Ramp Shaft all others	γ_i	-	1.42 1.50 1.44
Length of sealing: Ramp Shaft all others	l_i	m	40 40 10
Length of backfilled tunnel segments downstream of sealing: n1, n3,s1 n2 s2 shaft, ramp	$l_{i,BF}$	m	1 000 800 100 0

Tab. 3.6-2: Network flow data and source term information calculated using the resistor network and the parameter values listed in Tab. 3.6-1

Input	Units	Values
Network Structure		
List of junction names. Inlet and outlet junctions for each leg.	-	Fig. 3.6-5
Network Flow Data		
Flows		
Q_{ramp}		6.5×10^{-4}
Q_{n1}		2.3×10^{-4}
Q_{n2}		7.9×10^{-5}
Q_{n3}		2.1×10^{-4}
Q_{s1}	$m^3 a^{-1}$	2.0×10^{-4}
Q_{s2}		2.6×10^{-4}
Q_{shaft}		3.4×10^{-4}
SF/HLW Q_{OPA}		8.8×10^{-2} (upwards, summed over domains A, B and C)
ILW Q_{OPA}		2.0×10^{-3} (upwards, domain D)
Source Term Information		
Source flux	$mol a^{-1}$	Radionuclide releases obtained from the output of code STMAN (Reference Case source term for domain B, 10-fold increased groundwater flow rate for domains A,C,D)
Fraction to each leg:		Fraction to each leg (including diffusion, see Eq. 3.6-12):
$f_{A,HR}$		0.99992
$f_{A,n1}$		6×10^{-5}
$f_{A,n2}$		2×10^{-5}
$f_{C,HR}$	dimensionless	0.99988
$f_{C,s1}$		5×10^{-5}
$f_{C,s2}$		7×10^{-5}
$f_{D,HR}$		0.99974
$f_{D,n3}$		2.6×10^{-4}

Tab. 3.6-3: PICNIC input data for legs L₁, L₂, L₃ and L₄ which represent axial transport through the backfill of the operations tunnel, construction tunnel and ventilation tunnel

Input	Units	Values	Source
Leg Data – Basic Data			
Length L ₁ , L ₂ L ₃ L ₄	m	1 000 800 100	Tab. A3.2-2a, Parameter 3, Value G
Cross sectional area L ₁ , L ₂ , L ₃ , L ₄	m ²	23	Tab. A3.2-2a, Parameter 4, Value C
Darcy velocity L ₁ L ₂ L ₃ L ₄	m a ⁻¹	2.8 × 10 ⁻⁵ 8.7 × 10 ⁻⁶ 3.4 × 10 ⁻⁶ 1.1 × 10 ⁻⁵	Calculated from water flow rates in Tab. 3.6-2 and cross sectional areas (see also Tab. A3.2-2a, Parameter 5, Value H)
Pore diffusion constant for backfill	m ² a ⁻¹	1.6 × 10 ⁻²	Tab. A3.2-2a, Parameter 7, Value D
Leg Data – Properties of Flowing Region			
Retardation	dimensionless	Calculated from the parameters below.	
Bulk dry density (mass of bentonite per m ³ of backfill material, sorption on quartz sand neglected)	kg m ⁻³	558	Tab. A3.2-2a, Parameter 8, Value C
Flow porosity	dimensionless	This is set equal to the infill porosity.	
Infill Porosity	dimensionless	0.3	Tab. A3.2-2a, Parameter 10, Value E
Porosity Factors	dimensionless	none	
Sorption K _d	m ³ kg ⁻¹	values for bentonite	Tab. A3.2-2a, Parameter 11, Value E
Leg Data – Properties of Matrix			
There is no "matrix" for this leg – the tunnel backfill is a homogeneous porous medium. The matrix penetration depth and surface sorption coefficients are thus set equal to zero, and all other parameters are irrelevant.			

Tab. 3.6-4: PICNIC input data for leg L₅, which represents upward vertical transport through the EDZ of the shaft

Input	Units	Values	Source
<i>Leg Data – Basic Data</i>			
Length	m	40	Tab. A3.2-2a, Parameter 3, Value G
Cross sectional area	m ²	13	Tab. A3.2-2a, Parameter 4, Value C
Darcy velocity	m a ⁻¹	2.6×10^{-5}	Calculated from water flow rate in Tab. 3.6-2 and cross sectional area (see also Tab. A3.2-2a, Parameter 5, Value H)
Pore diffusion constant for shaft EDZ	m ² a ⁻¹	1.6×10^{-3}	Tab. A3.2-2a, Parameter 7, Value E
<i>Leg Data – Properties of Flowing Region</i>			
Retardation	dimensionless	Calculated from the parameters below.	
Dry density	kg m ⁻³	2 120	Tab. A3.2-2a, Parameter 8, Value D
Flow porosity	dimensionless	This is set equal to the infill porosity.	
Infill porosity	dimensionless	0.22	Tab. A3.2-2a, Parameter 10, Value D
Porosity factors	dimensionless	none	
Sorption K_d	m ³ kg ⁻¹	values for Opalinus Clay	Tab. A3.2-2a, Parameter 11, Value A
<i>Leg Data – Properties of Matrix</i>			
There is no "matrix" for this leg – the shaft EDZ is a homogeneous porous medium. The matrix penetration depth and surface sorption coefficients are thus set equal to zero, and all other parameters are irrelevant.			

Tab. 3.6-5: PICNIC input data for legs $L_{6,A}$, $L_{6,B}$, $L_{6,C}$ and L_7 , which represent upward vertical transport through the Opalinus Clay for SF/HLW (domains A, B, C) and ILW (domain D)

Input	Units	Values	Source
Leg Data – Basic Data			
Length $L_{6,A}$, $L_{6,B}$, $L_{6,C}$, L_7	m	40	Tab. A3.2-2a, Parameter 3, Value G
Cross sectional area $L_{6,A}$, $L_{6,C}$ $L_{6,B}$ L_7	m ²	2.0×10^4 1.2×10^5 4.0×10^3	Tab. A3.2-2a, Parameter 4, Value C
Darcy velocity $L_{6,A}$, $L_{6,B}$, $L_{6,C}$ L_7	m a ⁻¹	5.5×10^{-7} 5.0×10^{-7}	Calculated from water flow rates in Tab. 3.6-2 and cross sectional areas (see also Tab. A3.2-2a, Parameter 5, Value H)
Leg Data – Properties of Flowing Region			
Identical to Reference Case.			
Leg Data – Properties of Matrix			
There is no "matrix" for this leg – the Opalinus Clay is a homogeneous porous medium. The matrix penetration depth and surface sorption coefficients are thus set equal to zero, and all other parameters are irrelevant.			

Parameter variation

In a parameter variation, the hydraulic conductivity of the EDZ is increased by a factor of 100 ($1 \times 10^{-10} \text{ m s}^{-1}$). All other parameter values used for the calculation of water flow rates (resistor network) are identical to those of the Base Case (Tab. 3.6-1). Network flow data and source term information are given in Tab. 3.6-6. Note that even for a 100-fold increased hydraulic conductivity of the EDZ, most of the radionuclide inventory is released through the Opalinus Clay. Transport parameters for legs L_1 to L_7 are given in Tab. 3.6-7.

Tab. 3.6-6: Network flow data and source term information

Calculated based on 100-fold increased hydraulic conductivity of EDZ and parameter values listed in Tab. 3.6-1.

Input	Units	Values	Source
Network Structure			
List of junction names. Inlet and outlet junctions for each leg.	-	Fig. 3.6-5	
Network Flow Data			
Flows			
Q_{ramp}		3.0×10^{-3}	
Q_{n1}		1.1×10^{-3}	
Q_{n2}		1.1×10^{-3}	
Q_{n3}		8.6×10^{-4}	
Q_{s1}	$m^3 a^{-1}$	1.0×10^{-3}	
Q_{s2}		7.4×10^{-3}	
Q_{shaft}		8.4×10^{-3}	
SF/HLW Q_{OPA}		8.1×10^{-2} (upwards, summed over domains A, B and C)	
ILW Q_{OPA}		1.6×10^{-3} (upwards, domain D)	
Source Term Information			
Source flux	$mol a^{-1}$	Radionuclide releases obtained from the output of code STMAN (Reference Case source term for domain B, 10-fold increased groundwater flow rate for domains A,C,D)	
Fraction to each leg:		Fraction to each leg (including diffusion, see Eq. 3.6-12):	
$f_{A,HR}$		0.99944	
$f_{A,n1}$		2.8×10^{-4}	
$f_{A,n2}$		2.8×10^{-4}	
$f_{C,HR}$	dimensionless	0.99789	
$f_{C,s1}$		2.5×10^{-4}	
$f_{C,s2}$		1.86×10^{-3}	
$f_{D,HR}$		0.9989	
$f_{D,n3}$		1.1×10^{-3}	

Tab. 3.6-7: PICNIC input data differing from the Base Case

Data for legs L₁, L₂, L₃ and L₄ which represent axial transport through the backfill of the operations tunnel, construction tunnel and ventilation tunnel, and legs L₅, L_{6,A}, L_{6,B}, L_{6,C} and L₇, which represent upward vertical transport through the EDZ of the shaft and through the Opalinus Clay, respectively.

Input	Units	Values	Source
Leg Data – Basic Data			
Darcy velocity			Calculated from water flow rates in Tab. 3.6-6 and cross sectional areas (see also Tab. A3.2-2a, Parameter 5, Value I)
L ₁	m a ⁻¹	1.3×10^{-4}	
L ₂		4.3×10^{-5}	
L ₃		4.8×10^{-5}	
L ₄		3.2×10^{-4}	
L ₅ (shaft EDZ)		6.5×10^{-4}	
L _{6,A} , L _{6,C} (SF-OPA)		5.1×10^{-7}	
L _{6,B} (SF-OPA)		5.1×10^{-7}	
L ₇ (ILW-OPA)		4.0×10^{-7}	
All other leg parameters		Identical to parameter values in Tabs. 3.6-3, 3.6-4 and 3.6-5	

Model variant

In a model variant, in which the size of the domains A, B, C and D in Fig. 3.6-1b is assumed to be the same as in the Base Case, water flow and radionuclide transport along the operations/-construction/ventilation tunnels are assumed to occur in the liner (shotcrete). The effective hydraulic conductivity of the tunnel backfill, used to mimic water flow within the liner, is given in Tab. 3.6-8. All other parameter values used for the calculation of water flow rates (resistor network) are identical to those of the Base Case (Tab. 3.6-1). Network flow data and source term information are given in Tab. 3.6-9. The cross-sectional area and the Darcy velocities are calculated for an annulus representing the shotcrete liner (5.4 m²). Transport parameters for leg L₁ to L₇ are given in Tab. 3.6-10.

Tab. 3.6-8: Parameter value used for the calculation of water flow rates in the resistor network
Value calculated with Eq. 3.6-11.

Parameter	Symbol	Unit	Value
Sealing zones (incl. backfilled tunnel segments downstream)			
Hydraulic conductivity of backfilled tunnel downstream of sealing	$K_{i,BF,eff}$	m s ⁻¹	2.3×10^{-10}

Tab. 3.6-9: Network flow data and source term information

Calculated based on flow through liner and parameter values listed in Tab. 3.6-1.

Input	Units	Values	Source
Network Structure			
List of junction names. Inlet and outlet junctions for each leg.	-	Fig. 3.6-5	
Network Flow Data			
Flows			
Q_{ramp}		7.5×10^{-4}	
Q_{n1}		2.6×10^{-4}	
Q_{n2}		1.3×10^{-4}	
Q_{n3}		2.4×10^{-4}	
Q_{s1}	$m^3 a^{-1}$	2.4×10^{-4}	
Q_{s2}		2.2×10^{-4}	
Q_{shaft}		3.5×10^{-4}	
SF/HLW Q_{OPA}		8.8×10^{-2} (upwards, summed over domains A, B and C)	
ILW Q_{OPA}		2.0×10^{-3} (upwards, domain D)	
Source Term Information			
Source flux	$mol a^{-1}$	Radionuclide releases obtained from the output of code STMAN (Reference Case source term for domain B, 10-fold increased groundwater flow rate for domains A,C,D)	
Fraction to each leg:	dimensionless	Fraction to each leg (including diffusion, see Eq. 3.6-12):	
$f_{A,HR}$		0.99990	
$f_{A,n1}$		7×10^{-5}	
$f_{A,n2}$		3×10^{-5}	
$f_{C,HR}$		0.99988	
$f_{C,s1}$		6×10^{-5}	
$f_{C,s2}$		6×10^{-5}	
$f_{D,HR}$		0.99970	
$f_{D,n3}$		3.0×10^{-4}	

Tab. 3.6-10: PICNIC input data differing from the Base Case

Data for legs L_1 , L_2 , L_3 and L_4 which represent axial transport through the liner of the operations tunnel, construction tunnel and ventilation tunnel, and legs L_5 , $L_{6,A}$, $L_{6,B}$, $L_{6,C}$ and L_7 , which represent upward vertical transport through the EDZ of the shaft and through the Opalinus Clay, respectively.

Input	Units	Values	Source
Leg Data – Basic Data			
Cross sectional area $L_1 - L_4$	m^2	5.4	Calculated from tunnel radius of 2.7 m and liner thickness of 0.3 m.
Darcy velocity L_1 L_2 L_3 L_4 L_5 (shaft EDZ) $L_{6,A}, L_{6,C}$ (SF-OPA) $L_{6,B}$ (SF-OPA) L_7 (ILW-OPA)	$m a^{-1}$	1.4×10^{-4} 4.4×10^{-5} 2.4×10^{-5} 4.1×10^{-5} 2.7×10^{-5} 5.5×10^{-7} 5.5×10^{-7} 5.0×10^{-7}	Calculated from water flow rates in Tab. 3.6-9 and cross sectional areas
Pore diffusion constant	$m^2 s^{-1}$	10^{-10}	Nagra (1994c), value for concrete liner
Leg Data – Properties of Flowing Region (Legs L1 and L2)			
Retardation	dimensionless	Calculated from the parameters below.	
Dry density of concrete liner	$kg m^{-3}$	700	Identical value as for ILW-1
Flow porosity	dimensionless	This is set equal the infill porosity.	
Infill Porosity	dimensionless	0.2	Typical value for shotcrete
Porosity Factors	dimensionless	not used	
Sorption K_d	$m^3 kg^{-1}$	values for cement	Identical values as for ILW-1
All other leg parameters		Identical to parameter values in Tabs. 3.6-3, 3.6-4 and 3.6-5	

Comparison of results for the Base Case and the model variant

In Figs. 3.6-6 and 3.6-7, the dose as a function of time for the assessment cases considering radionuclide release affected by the ramp / shaft in the Base Case (Fig. 3.6-6 is identical to Fig. 7.4-6 in Nagra 2002c) and the model variant related to radionuclide transport through the liner of the operations/construction/ventilation tunnels are compared. Clearly, the details of the transport path along the tunnel system have a marginal impact on the resulting doses. This is because most of the radionuclides released from the near field are transported through the Opalinus Clay, not through the access tunnel system.

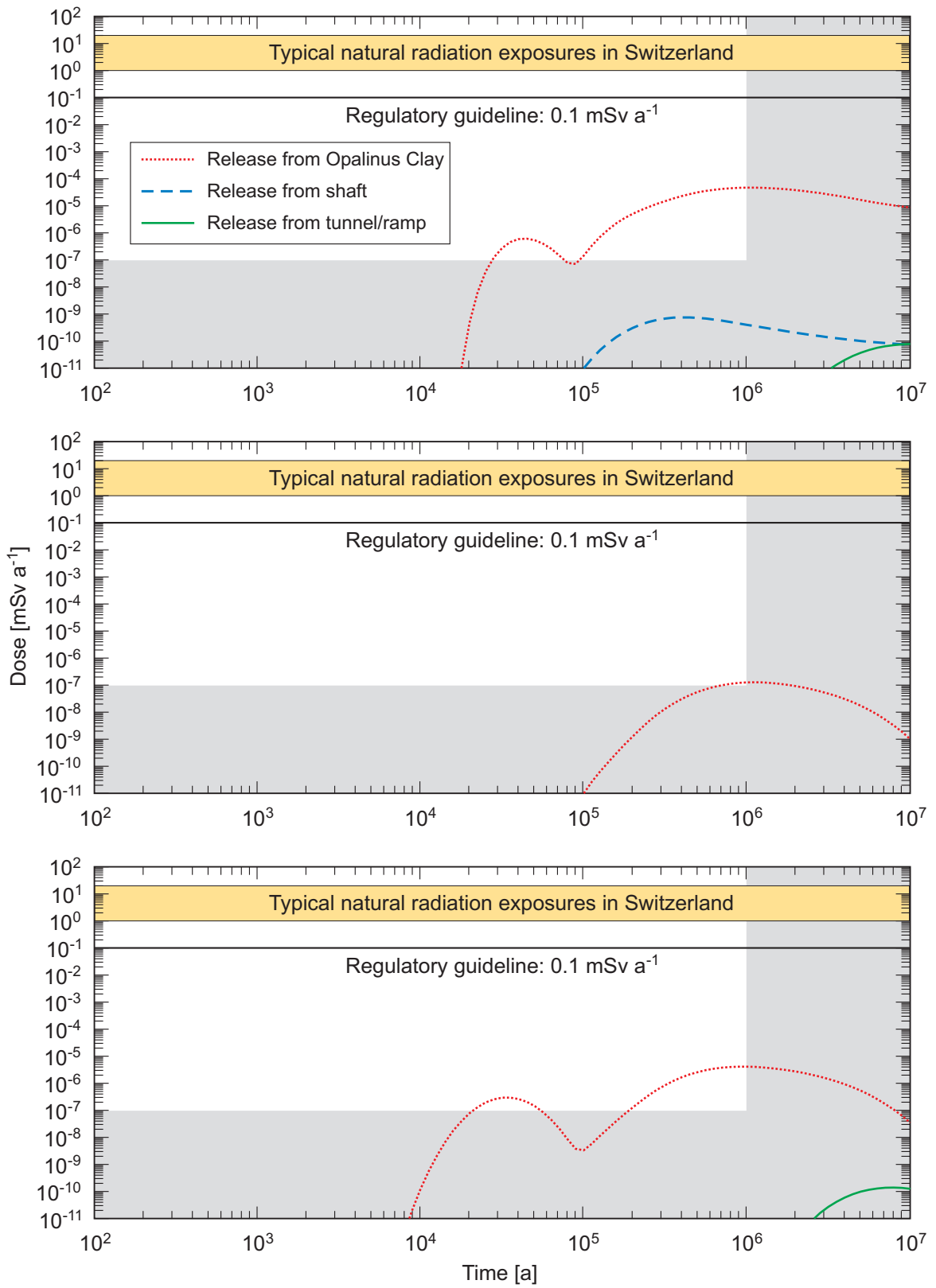


Fig. 3.6-6: Dose as a function of time for the assessment case considering radionuclide release affected by the ramp / shaft (Base Case)

Upper figure: SF, middle figure: HLW, lower figure: ILW.

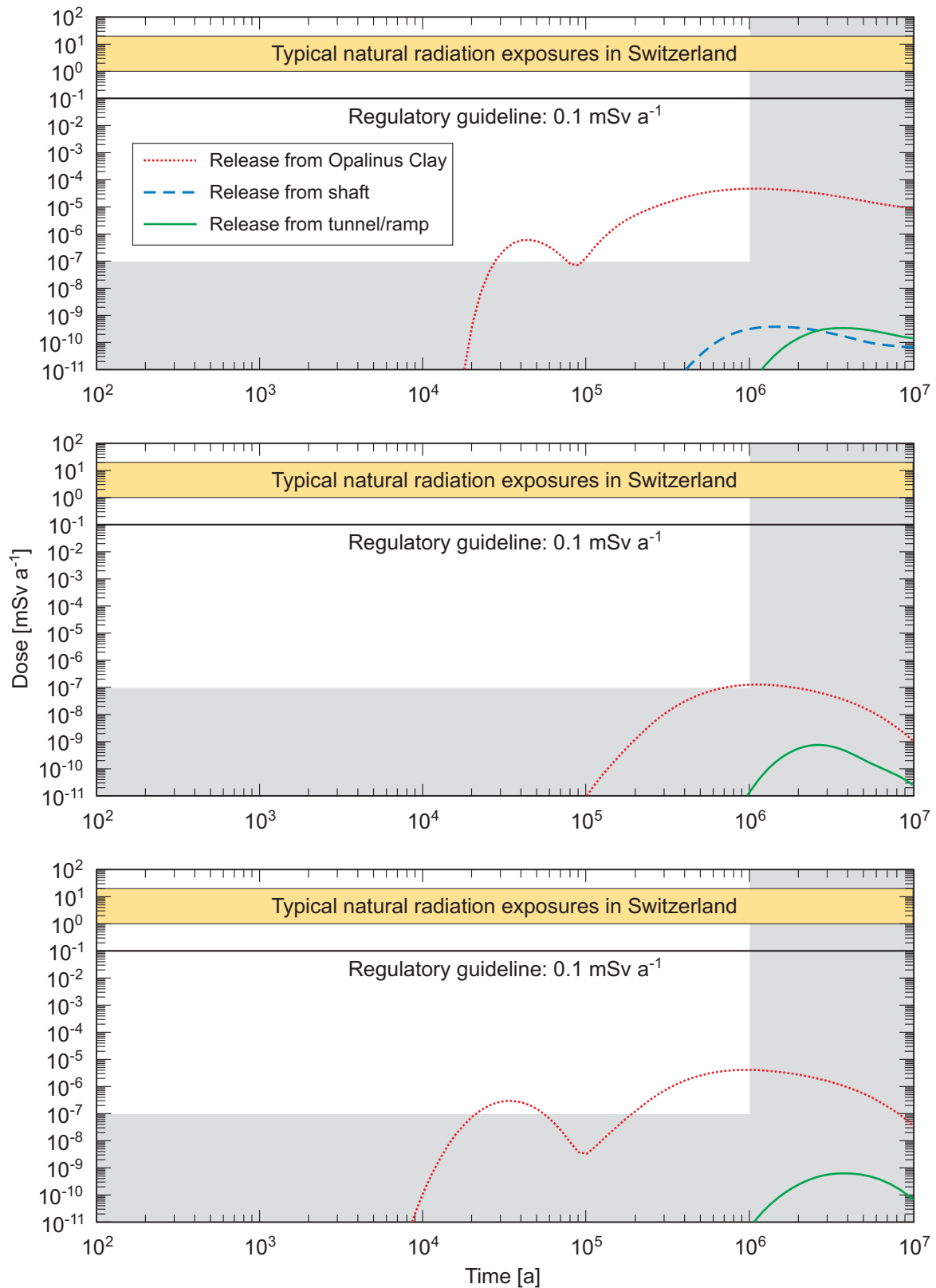


Fig. 3.6-7: Dose as a function of time for the assessment case considering radionuclide release affected by the ramp / shaft (model variant related to radionuclide transport through the liner of the operations/construction/ventilation tunnels)

Upper figure: SF, middle figure: HLW, lower figure: ILW.

3.7 Convergence-induced release of radionuclides affected by ramp/shaft (Case 1.7)

3.7.1 Overview

In the Reference Case for SF/HLW, tunnel convergence induced by creep of the Opalinus Clay is considered to be completed before canister breaching, with no effect on radionuclide release. In the Reference Case for ILW, tunnel convergence is assumed to occur during repository construction and resaturation, with little or no deformations of the tunnel cross-section occurring after resaturation of the emplacement tunnels, i.e. after the start of radionuclide release. The current conceptualisation differs from the Reference Case in that alternative assumptions regarding the extent and duration of tunnel convergence are considered, that may lead to enhanced water flow either through the host rock or through the access tunnel system.

3.7.2 The conceptual model and its underlying assumptions

3.7.2.1 SF/HLW

Due to creep of Opalinus Clay, the bentonite buffer of the SF/HLW emplacement tunnels may be compacted and its porosity reduced. There is some uncertainty in the degree of compaction and the time-scales involved. The range of uncertainty is considered to be bounded by the following limiting cases:

1. The swelling pressure of bentonite (2 – 4 MPa) is sufficient to prevent tunnel convergence and compaction of bentonite. This view is supported by the evidence that an anisotropic stress field is observed in the Opalinus Clay (with an anisotropy factor of ca. 1.3) which indicates that creep of Opalinus Clay is not an efficient process for completely removing stress heterogeneities or anisotropies, such as those induced by the repository. This case is not modelled in the current safety assessment.
2. The rock surrounding the bentonite will deform, compacting the bentonite and increasing its swelling pressure until it is balanced by the external stress field, and, at the same time, reducing the bentonite porosity from 45 % to ca. 36 % and the tunnel radius from 1.25 m to 1.15 m. The time period over which these processes take place may be in the order of
 - a) a few decades to hundreds of years (if full bentonite compaction develops in parallel with near field saturation); this is assumed in the Reference Case for SF/HLW
 - b) tens of thousands to hundreds of thousands of years (long-term hydromechanical evolution of near field conditions); this is considered in the present conceptualisation.

In cases 1 and 2a), no significant effects on radionuclide release are expected because bentonite compaction is either absent (case 1) or is fully developed before canister breaching (case 2a). In case 2b, there seems to be a possibility that tunnel convergence can lead to the displacement of contaminated water from the near field either along the EDZ of the emplacement tunnels or through the Opalinus Clay.

Squeezing of porewater through the Opalinus Clay is possible if the increased hydraulic head and the corresponding hydraulic gradient balances the water flow induced by porosity reduction

in the bentonite. In a one-dimensional approximation, the hydraulic gradient increase can be estimated as follows²⁷:

$$i = \frac{Q}{2pdK} \quad (3.7-1)$$

with

$$Q = \frac{(r_0^2 - r_\infty^2)\pi p}{\tau} \quad (3.7-2)$$

- i hydraulic gradient increase caused by tunnel convergence [m m^{-1}]
- Q water flow rate per canister driven by tunnel convergence [$\text{m}^3 \text{a}^{-1}$]
- p canister pitch [m]
- d separation of SF/HLW emplacement tunnels [m]
- K hydraulic conductivity of Opalinus Clay [m a^{-1}]
- r_0 initial tunnel radius (before convergence) [m]
- r_∞ tunnel radius after convergence [m]
- τ duration of tunnel convergence [a].

For a hydraulic conductivity of the Opalinus Clay of $2 \times 10^{-14} \text{ m s}^{-1}$ and an assumed duration of bentonite compaction of 10^4 (10^5) years, an increase of the hydraulic gradient in the order of 1.5 (0.15) m m^{-1} is sufficient for the displacement of convergence-induced water through the Opalinus Clay. This corresponds to an increase of the Darcy velocity in the Opalinus Clay by a factor of 2.5 (1.15). As shown in Chapter 6 (Figs. 6.7-6 and 6.7-8) in Nagra (2002c) and in Section 3.1 (Case 1.1f), such small increases of the Darcy velocity have no safety-relevant impact on the release of radionuclides.

Even if an initially defective canister were present, negligible water displacement is expected during tunnel convergence in case 2a, due to the prevailing unsaturated conditions in the near field. Therefore, convergence-induced release of dissolved radionuclides from the SF/HLW repository is considered to be negligible and is not further analysed.

3.7.2.2 ILW

In the case of ILW, little convergence is expected after backfilling and (partial) resaturation of the emplacement tunnel due to the strength of the aggregates contained in the cementitious materials (concrete, mortar). There is, however, some uncertainty related to the compaction of void volumes present in the waste containers. In the present conceptualisation, it is assumed that the corroded waste containers (and the structural material) will be partially compacted, leading to tunnel convergence and water displacement (Section 5.4.3 in Nagra 2002c). Because of the strength of the backfill and the low corrosion rates of much of this material (e.g. stainless steel and Zircaloy) and the relatively low initial porosity, it is expected that the containers will experience limited deformation. Here, it is assumed that the deformation will reduce the porosity by about half. The total reduction in void volume per unit length of ILW-1 tunnel is

²⁷ Eq. 3.7-1 is derived for steady-state conditions, in which case the water flow is one-dimensional and takes place predominantly in the vertical direction. Note that in a transient regime after the onset of tunnel convergence, outflow from the tunnels is expected to occur predominantly in the radial direction.

estimated to be $0.6 \text{ m}^3 \text{ m}^{-1}$, resulting in a maximal cumulated water displacement for ILW-1 of roughly 100 m^3 (rounded values, see Tab. 3.7-1). Tunnel convergence is assumed to take place within 1 000 years following waste emplacement, in parallel with tunnel saturation. This leads to a convergence-induced water flux of ca. $0.1 \text{ m}^3 \text{ a}^{-1}$. No calculations are performed for ILW-2, because the total void volume per unit tunnel length and the overall inventory are much lower than for ILW-1 (Tab. 3.7-1).

The aim of the following steady-state model is to show that the displacement of water will occur predominantly through the Opalinus Clay if the seals operate as expected. In a one-dimensional approximation, the total water flow rate is given by (see Fig. 3.7-1):

$$Q = Q_u + Q_l + Q_T = \frac{V_w}{T} \quad (3.7-3)$$

where²⁸

$$Q_j = 4\gamma_{ILW} r_{ILW} \Lambda_{ILW} K_{HR} \frac{H - H_j}{L_j}; \quad j = u, l \quad (3.7-4)$$

$$Q_T = \left(\frac{l_{BF}}{\pi R_T^2 K_{BF}} + \sum_{i=1}^2 \frac{l_i}{\pi R_i^2 (K_i + (\gamma_i^2 - 1) K_{i,EDZ})} \right)^{-1} (H - H_0) \quad (3.7-5)$$

Q_l	water flow rate from ILW-1 downwards to Sandsteinkeuper [$\text{m}^3 \text{ a}^{-1}$]
Q_u	water flow rate from ILW-1 upwards to Wedelsandstein [$\text{m}^3 \text{ a}^{-1}$]
Q_T	water flow rate from ILW-1 through operations tunnel [$\text{m}^3 \text{ a}^{-1}$]
V_w	cumulated water displacement caused by tunnel convergence [m^3]
τ	duration of tunnel convergence [a]
r_{ILW}, Λ_{ILW}	radius and length of ILW-1 emplacement tunnels [m]
γ_{ILW}	ratio of radii of EDZ and ILW-1 emplacement tunnel [-]
K_{HR}	hydraulic conductivity of Opalinus Clay [m a^{-1}]
L_u, L_l	distance from mid Opalinus Clay to Wedelsandstein and Sandsteinkeuper, respectively [m]
H	hydraulic head in ILW-1 emplacement tunnel [m]
H_u, H_l	hydraulic head in Wedelsandstein and Sandsteinkeuper [m]
R_i, l_i	radius and length of sealing zones [m]
l_{BF}	length of backfilled tunnel section between sealing sections [m]
R_T	radius of operations tunnel [m]
$K_i, K_{i,EDZ}$	hydraulic conductivity of sealing zones i and adjacent EDZ [m a^{-1}]
K_{BF}	hydraulic conductivity of backfill [m a^{-1}]

²⁸ As in the case of SF/HLW, Eq. 3.7-4 is derived for steady-state conditions, in which case the water flow is one-dimensional and takes place predominantly in the vertical direction. Explanation for factor $4 \gamma_{ILW} r_{ILW}$ in Eq. 3.7-4: Diameter of tunnel and EDZ is $2 \gamma_{ILW} r_{ILW}$. The spread of vertical flow lines away from the tunnel is accounted for by a factor of 2. Note that in a transient regime after the onset of tunnel convergence, outflow from the tunnels is expected to occur predominantly in the radial direction.

Defining

$$Q_{OPA} = Q_u + Q_l = \alpha(H - H_A)$$

$$\alpha = 4\gamma_{ILW}r_{ILW}\Lambda_{ILW}K_{HR}\left(\frac{1}{L_u} + \frac{1}{L_l}\right); \quad H_A = \frac{\frac{H_l}{L_l} + \frac{H_u}{L_u}}{\frac{1}{L_l} + \frac{1}{L_u}} \quad (3.7-6)$$

$$Q_T = \beta(H - H_0)$$

$$\beta = \left(\frac{l_{BF}}{\pi R_T^2 K_{BF}} + \sum_{i=1}^2 \frac{l_i}{\pi R_i^2 (K_i + (\gamma_i^2 - 1)K_{i,EDZ})} \right)^{-1} \quad (3.7-7)$$

one obtains for the hydraulic head in the ILW part of the repository:

$$H = \frac{\frac{V_w}{T} + \alpha H_A + \beta H_0}{\alpha + \beta} \quad (3.7-8)$$

As shown in Tab. 3.7-3, the water flow rate through the Opalinus Clay is indeed a factor of five higher than the water flow rate through the operations tunnel.

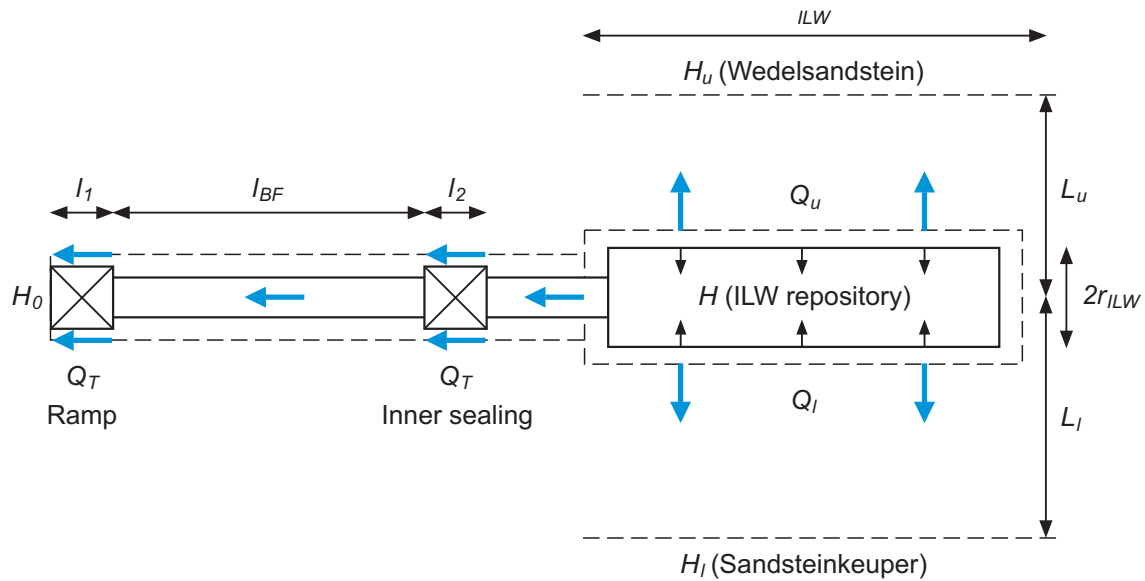


Fig. 3.7-1: Resistor network model for the calculation of water flow from the ILW-1 part of the repository through the Opalinus Clay and the operations tunnel/ramp

The modelling of simultaneous release of radionuclides through host rock and access tunnel system is performed in the same way as for the case described in Section 3.6. The near field release rate for ILW-1 is assumed to be a pulse of dissolved radionuclides conveyed by water squeezed out of the tunnels. Transport properties of the host rock and the access tunnel system are identical to the case treated in Section 3.6, assuming steady-state water flows to simplify calculations.

In the framework of a model variant for ILW-1, a pulse of water containing dissolved radionuclides is assumed to be released from the ILW emplacement tunnels through the Opalinus Clay due to tunnel convergence (transient water flows in the Opalinus Clay assumed). In this calculation, radionuclide transport is assumed through the Opalinus Clay only, i.e. the sealings are taken to be impermeable. An upward directed hydraulic gradient of 1 m m^{-1} is imposed in the Opalinus Clay, generated by the hydraulic heads in the Sandsteinkeuper and the Wedelsandstein. In addition, a source of water, maintained for 1 000 years and with a constant water flow rate of $0.1 \text{ m}^3 \text{ a}^{-1}$, is assumed in a plane corresponding to the horizontal cross-sectional area of two ILW-1 emplacement tunnels ($9 \text{ m} \times 180 \text{ m}$, see Section 3.7.4). Radionuclide transport is assumed to occur by advection and diffusion from the ILW-1 emplacement tunnels both upwards and downwards through the Opalinus Clay, considering transient water flow rates. The analysis is limited to those radionuclides that dominate the summed dose maximum of the Reference Case (organic ^{14}C , ^{129}I).

3.7.3 Codes used

As in the Reference Conceptualisation for ILW, the reference model chain of STALLION-PICNIC-TAME is used to model the radionuclide release, migration and distribution in the biosphere in the Base Case. The solution technique used in STALLION for modelling a pulse of radionuclides released from the near field is discussed in Appendix 1. The network capabilities of PICNIC are employed to model the simultaneous transport of radionuclides from the ILW-1 emplacement tunnel through the Opalinus Clay and the operations tunnel/ramp under steady-state flow conditions (Base Case). Note that in the model calculations, transport through the Opalinus Clay is pessimistically assumed to occur upwards only.

In the transient model variant considering a pulse of water conveying dissolved radionuclides from the ILW-1 emplacement tunnels through the Opalinus Clay only, the model chain STALLION-FRAC3DVS-TAME is employed. The source term, calculated by STALLION, is identical to the one used in the Base Case. For geosphere transport, FRAC3DVS is employed instead of PICNIC because the transient nature of tunnel convergence leads to a time-dependent flow field in the Opalinus Clay (Eq. A1.8-1, with a non-zero source term q_s). The coupled flow and transport equations Eq. A1.8-1 and A1.8-8 are solved in FRAC3DVS for a 1D porous medium representing the Opalinus Clay.

3.7.4 Parameters

Base Case

In the case of SF/HLW, the effect of tunnel convergence on radionuclide release is negligible, as previously discussed. No calculations have, therefore, been performed.

For ILW-1, a slow reduction of about 50 % of the void volume within the waste containers is considered, yielding a cumulated amount of displaced water of about 100 m^3 (Tab. 3.7-1). No calculations are performed for ILW-2, because the total void volume per unit tunnel length and the overall inventory are much lower than for ILW-1.

Tab. 3.7-1: Void volumes of ILW waste containers (from Schwyn et al. 2003)

Container type	Waste group	Number of containers	Void volume per container [m ³]	Total void volume [m ³]	Total void volume per unit tunnel length [m ³]
WA-BNF-2	ILW-1	33	0.013	0.4	-
WA-BNF-4	ILW-1	266	0.014	3.7	-
WA-BNF-7	ILW-1	167	0.013	2.2	-
WA-COG-4	ILW-1	323	0.215	69.4	-
WA-COG-6	ILW-1	514	0.248	127.5	-
Total	ILW-1	1303	-	203.2	1.13
Value considered in present case (half of total void volume, rounded values)				100	0.6
WA-COG-2	ILW-2	383	0.063	24.1	0.40

In the model calculations for the Base Case, an increased steady-state water flow rate in the host rock is conservatively considered, and radionuclide transport occurs simultaneously through the host rock and through the access tunnel system. The parameter values used for the calculation of convergence-induced water flow rates (resistor network) in the Base Case are identical to those listed in Tab. 3.6-1, with the exception of the convergence-induced porewater displacement rate from the ILW-1 emplacement tunnels, listed in Tab. 3.7-2. Network flow data and source term information are given in Tab. 3.7-3. Note that most of the radionuclide inventory is released through the Opalinus Clay. Transport parameters for PICNIC legs are given in Tabs. 3.7-4 and 3.7-5.

Tab. 3.7-2: Additional parameter value used for the calculation of water flow rates in the resistor network

Parameter	Symbol	Unit	Value
ILW-1 emplacement tunnels			
Cumulated water displacement caused by tunnel convergence	V_w	m ³	100
All other parameters	Identical to parameter values in Tab. 3.6-1		

Tab. 3.7-3: Network flow data and source term information (calculated based on parameter values listed in Tabs. 3.6-1 and 3.7-2)

Input	Units	Values
Network Structure		
List of junction names. Inlet and outlet junctions for each leg.	-	Fig. 3.6-5 (ILW-1 part of repository only, including PICNIC legs L ₁ and L ₇)
Network Flow Data		
Flows Q_T Q_{OPA}	$m^3 a^{-1}$	0.013 0.064 (upwards)
Source Term Information		
Source flux	$mol a^{-1}$	Radionuclide release obtained from the output of code STALLION ¹ : - Reference Case release rates - release of 3 % of dissolved radionuclide inventory ($\approx 0.6 m^3$ water per m tunnel length) within a period of 1 000 a (plug flow)
Fraction to each leg: $f_{D,HR}$ $f_{D,n3}$	dimensionless	Fraction to each leg (including diffusion, see Eq. 3.6-12): 0.9958 4.2×10^{-3}

¹ These source terms are conservatively superposed, thereby double counting the 3 % fraction of the dissolved radionuclide inventory corresponding to about half the void volume within the ILW-1 waste containers ($100 m^3$).

Tab. 3.7-4: PICNIC input data for the leg representing axial transport through the backfill of the operations tunnel to the ramp

Input	Units	Values	Source
<i>Leg Data – Basic Data</i>			
Length	m	1 000	Tab. A3.2-2a, Parameter 3, Value I
Cross sectional area	m ²	23	Tab. A3.2-2a, Parameter 4, Value D
Darcy velocity	m a ⁻¹	5.7×10^{-4}	Calculated from water flow rates in Tab. 3.7-3 and cross sectional areas (see also Tab. A3.2-2a, Parameter 5, Value M)
Pore diffusion constant for backfill	m ² a ⁻¹	1.6×10^{-2}	Tab. A3.2-2a, Parameter 7, Value D
<i>Leg Data – Properties of Flowing Region</i>			
Retardation	dimensionless	Calculated from the parameters below.	
Bulk dry density (mass of bentonite per m ³ of backfill material, sorption on quartz sand neglected)	kg m ⁻³	558	Tab. A3.2-2a, Parameter 8, Value C
Flow porosity	dimensionless	This is set equal to the infill porosity.	
Infill Porosity	dimensionless	0.3	Tab. A3.2-2a, Parameter 10, Value E
Porosity Factors	dimensionless	none	
Sorption K_d	m ³ kg ⁻¹	values for bentonite	Tab. A3.2-2a, Parameter 11, Value E
<i>Leg Data – Properties of Matrix</i>			
There is no "matrix" for this leg – the tunnel backfill is a homogeneous porous medium. The matrix penetration depth and surface sorption coefficients are thus set equal to zero, and all other parameters are irrelevant.			

Tab. 3.7-5: PICNIC input data for leg L₇ which represents upward vertical transport through the Opalinus Clay for ILW (domain D)

Input	Units	Values	Source
<i>Leg Data – Basic Data</i>			
Length	m	40	Tab. A3.2-2a, Parameter 3, Value H
Cross sectional area	m	4.0×10^3	Tab. A3.2-2a, Parameter 4, Value D
Darcy velocity	m a ⁻¹	1.6×10^{-5} (upwards)	Calculated from water flow rates in Tab. 3.7-3 and cross sectional area (see also Tab. A3.2-2a, Parameter 5, Value M)
<i>Leg Data – Properties of Flowing Region</i>			
Identical to Reference Case,			
<i>Leg Data – Properties of Matrix</i>			
There is no "matrix" for this leg – the Opalinus Clay is a homogeneous porous medium. The matrix penetration depth and surface sorption coefficients are thus set equal to zero, and all other parameters are irrelevant.			

Model variant

In a model variant for ILW-1, a pulse of water containing dissolved radionuclides is assumed to be released due to tunnel convergence through the host rock only (impermeable seals). The cumulated amount of radionuclide-containing water displaced (ca. 100 m³) corresponds to ca. 3 % of the total initial pore volume in the ILW-1 emplacement tunnels. It is therefore assumed that 3 % of the radionuclide inventory dissolved in the porewater is released within a time span of 1 000 years, starting at 100 years and ending at 1 100 years, at a rate of ca. 0.1 m³ a⁻¹ (Tab. 3.7-6). The remainder of the radionuclide inventory is released and transported as in the Reference Case. The boundary conditions for FRAC3DVS are listed in Tab. 3.7-7.

Tab. 3.7-6: FRAC3DVS input data for a path representing upward vertical transport through the Opalinus Clay

Input	Units	Values
<i>Nuclides and Decays</i>		
Nuclides and decays to be used.	Half lives are specified in years.	Analysed nuclides: organic ^{14}C , ^{129}I Half lives: Tab. A3.2-1a, Parameter 1, Value D
<i>Data for Opalinus Clay</i>		
Cross sectional area	m^2	1.6×10^3 (= 9 m \times 180 m)
Darcy velocity	m a^{-1}	calculated by FRAC3DVS based on boundary conditions in Tab. 3.7-7
all other parameters		identical to Reference Case
<i>Source Term Information</i>		
Source flux	mol s^{-1}	Output from STALLION: Radionuclide release rate from tunnel into Opalinus Clay (see Tab. 3.7-7)

Tab. 3.7-7: Hydraulic and transport boundary conditions for FRAC3DVS set at the top and the bottom of the Opalinus Clay

Parameter	Unit	Value	Comment
Hydraulic head at top the OPA	m	0	fixed head, resulting in a hydraulic gradient of 1 m m^{-1} (Reference Case)
Hydraulic head at bottom the OPA	m	80	
Concentration at top the OPA	mol m^{-3}	0	zero concentration boundary
Concentration at bottom the OPA	mol m^{-3}	0	zero concentration boundary
Hydraulic source term at mid the OPA	$\text{m}^3 \text{ m}^{-2} \text{ a}^{-1}$	6.2×10^{-5}	planar source (9 m \times 180 m), maintained for 1 000 a, yielding a cumulative fluid volume of $0.1 \text{ m}^3 \text{ a}^{-1}$.
Radionuclide source term at mid the OPA	mol s^{-1}	Output from STALLION: planar source (9 m \times 180 m) representing radionuclide release from tunnel into Opalinus Clay ¹ : - Reference Case release rates - release of 3 % of dissolved radionuclides ($\approx 0.6 \text{ m}^3$ water per m tunnel length) within 1 000 a	

¹ these source terms are conservatively superposed, thereby double counting the 3 % fraction of the dissolved radionuclide inventory

3.8 Gas-induced release of radionuclides affected by ramp/shaft (Case 1.8)

3.8.1 Overview

In the Reference Case, little or no displacement of contaminated porewater is assumed to occur as a consequence of gas pressure build-up following gas generation in the emplacement tunnels. Case 1.8 differs from the Reference Case in that the possibility of accelerated release of dissolved radionuclides through the Opalinus Clay and through the access tunnel system is considered (gas-induced displacement of contaminated porewater).

3.8.2 The conceptual model and its underlying assumptions

3.8.2.1 Calculation of gas-induced porewater displacement rates

SF/HLW

Gas generation from anaerobic metal corrosion (SF/HLW/ILW) and microbial degradation of organic material (ILW) leads to the generation of hydrogen gas, carbon dioxide and methane. In the case of SF/HLW, steel corrosion takes place upon contact with water at a rate of $1 \mu\text{m a}^{-1}$ or less, which corresponds to a hydrogen gas generation rate at external canister surfaces of about $7.4 \times 10^{-2} \text{ m}^3 \text{ (STP) a}^{-1}$ per canister (STP = Standard Temperature and Pressure). There is the possibility that hydrogen may be reduced to methane by microbial activity, leading to a reduction in the total gas volume, but this process is not considered in the calculations (Rodwell 2000).

Initially, the generated gas dissolves in the near field porewater until the gas solubility is reached. Thereafter, a free gas phase is formed and sustained and gas pressure starts to build up.

After breaching of the SF canisters, the possibility is considered that accelerated radionuclide release could arise from hydrogen gas production due to corrosion of internal canister surfaces, at a similar rate to the gas generation rate at external canister surfaces (the available surfaces are roughly equal). This could expel water from the canister if the defect were in an unfavourable location (e.g. the underside of the canister, see Fig. 3.8-1). In reality, a canister is likely to be breached at several locations, or it may already be pressurised with hydrogen gas diffusing into the canister before full breaching. Both of these processes significantly reduce the maximum amount of water displaced. This is taken into account by assuming that only 10 % of all canisters are subject to water displacement from the canister interior. In all other canisters, gas may escape without displacing significant amounts of water. Furthermore, the inflow and outflow of water may be limited by the hydraulic resistivity of the pinholes, but this effect is neglected. Instead, it is pessimistically assumed that the entire canister void volume of 0.7 m^3 is filled with water before the internal gas generation starts. Assuming a uniform probability density function for the location of a single pinhole around the canister circumference, the mean water volume displaced per canister is 0.35 m^3 .

This effect is potentially significant for SF, since the instant release fraction of the inventory would be available for expulsion by gas, whereas HLW radionuclides would be immobilised almost entirely within the glass matrix. The effects of gas-induced porewater displacement from the HLW part of the repository is thus considered to be small and is not considered further.

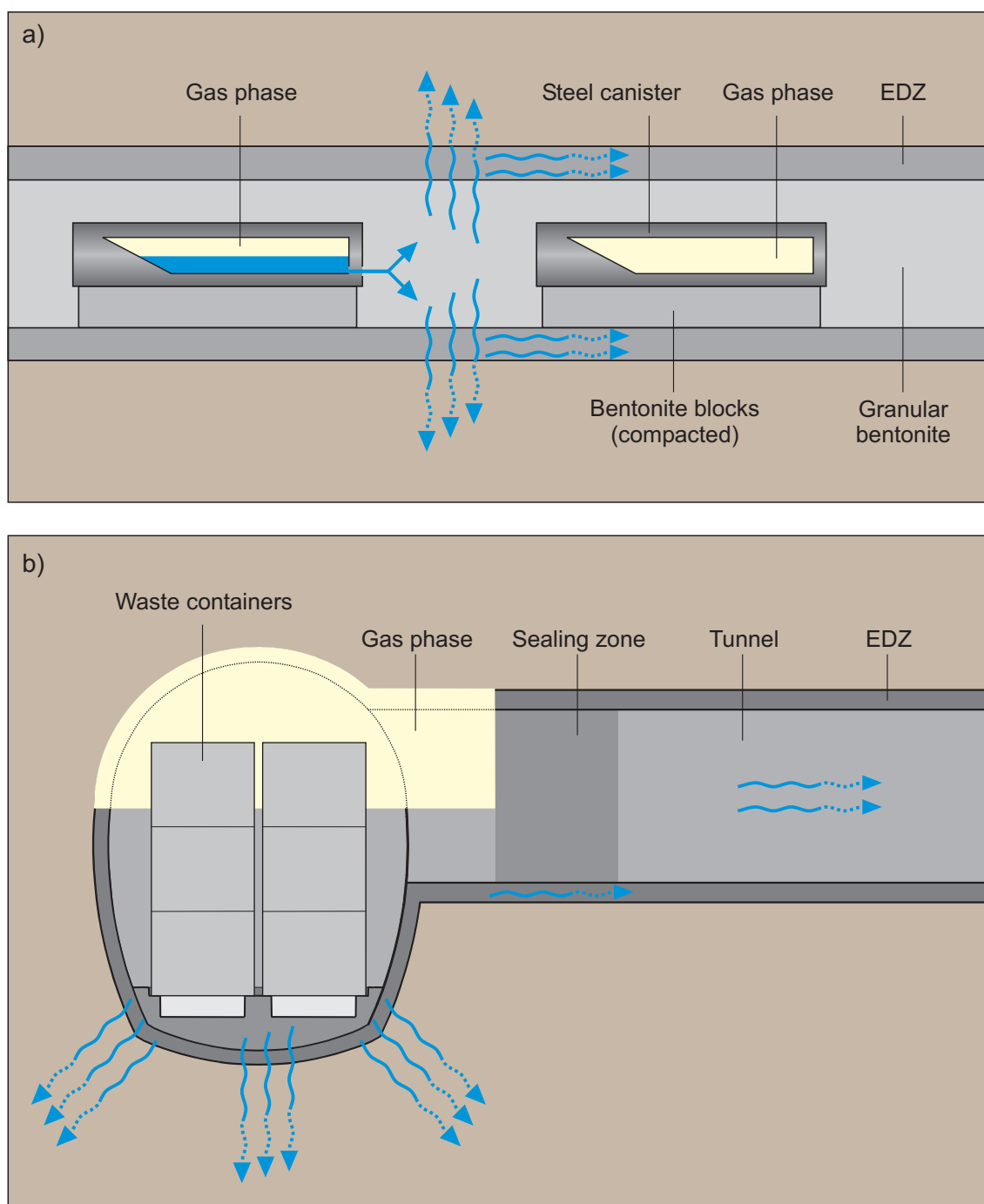


Fig. 3.8-1: Scheme with the conceptual model for gas-induced release of dissolved radionuclides through the Opalinus Clay and through the access tunnel system

a) SF, b) ILW.

ILW

In the case of ILW, the total gas generation rate is about $700 \text{ m}^3 \text{ (STP) a}^{-1}$ for the first few years after the onset of gas generation, declining rapidly to about $100 \text{ m}^3 \text{ (STP) a}^{-1}$ after 10 years and gradually to about $10 \text{ m}^3 \text{ (STP) a}^{-1}$ after 10 000 years (Tab. 4.3-1).

As discussed in Chapter 4, it takes 5 000 – 10 000 years for the pressure to reach values in the order of 10 MPa where significant porewater displacement from the ILW emplacement tunnels into the formation occurs. By then, the gas generation rate is reduced to roughly $10 \text{ m}^3 \text{ (STP) a}^{-1}$, corresponding to $0.1 \text{ m}^3 \text{ a}^{-1}$ at a pressure of 10 MPa. Assuming a volume balance between generated gas and displaced water, the rate of water displacement is thus estimated to be $0.1 \text{ m}^3 \text{ a}^{-1}$.

As shown by more detailed calculations in Section 4.3 (Fig. 4.3-2), the rate of water displacement is indeed in the order of $0.05 \text{ m}^3 \text{ a}^{-1}$, starting at 10 000 years and maintained for a time period of about 30 000 years. The cumulated amount of displaced water is assumed to be $1\,500 \text{ m}^3$, corresponding to 50 % of the available pore space in the ILW part of the repository.

In a pessimistic variant, it is assumed that an amount of water corresponding to 100 % of the available pore space is displaced within 10 000 years, starting at 1 000 years, at a rate of $0.3 \text{ m}^3 \text{ a}^{-1}$.

3.8.2.2 Calculation of water flow rates in the repository system

The gas-induced water fluxes in the SF/ILW parts of the repository are calculated analytically by means of a steady-state resistor network model, which is very similar to the model described in Section 3.6 (Fig. 3.6-1). By mass balance considerations, the axial water flow rate in the SF emplacement tunnels including EDZ, $q \text{ [m}^3 \text{ s}^{-1}\text{]}$, can be calculated from²⁹:

$$\frac{dq}{dx} = 4\gamma r K_{HR} \left(\frac{H_l - h(x)}{L_l} + \frac{H_u - h(x)}{L_u} \right) + q^* \quad (3.8-1)$$

where

K_{HR}	hydraulic conductivity of host rock [m s^{-1}]
r	radius of the SF emplacement tunnel [m]
γ	ratio of radii EDZ/emplacement tunnel [-]
x	coordinate along axis of emplacement tunnel [m]
$h(x)$	hydraulic head within emplacement tunnel [m]
H_l	hydraulic head in Sandsteinkeuper (lower confining unit) [m]
H_u	hydraulic head in Wedelsandstein (upper confining unit) [m]
L_l	distance from mid Opalinus Clay to Sandsteinkeuper [m]
L_u	distance from mid Opalinus Clay to Wedelsandstein [m]
q^*	gas-induced porewater displacement rate from SF canisters [$\text{m}^3 \text{ s}^{-1} \text{ m}^{-1}$].

²⁹ Eq. 3.8-1 is derived for steady-state conditions, in which case the water flow is one-dimensional and takes place predominantly in the vertical direction. Explanation for factor $4\gamma r$ in Eq. 3.8-1: Diameter of tunnel and EDZ is $2\gamma r$. The spread of vertical flow lines away from the tunnel is accounted for by a factor of 2. Note that in a transient regime after the onset of gas generation, outflow from the tunnels is expected to occur predominantly in the radial direction.

In the framework of the steady-state hydraulic calculations presented in this section, the transient nature of the gas-induced porewater displacement rate, q^* , squeezed from the SF canisters by corrosion of internal surfaces, is neglected (conservative simplification). The source term and the calculation of radionuclide transport in the different parts of the repository, however, will be time-dependent (see Sections 3.8.2.3 and 3.8.2.4).

The flow of water along the SF emplacement tunnel (predominantly within the EDZ, but also within the bentonite) is:

$$q = -\pi r^2 (K_B + (\gamma^2 - 1)K_{EDZ}) \frac{dh}{dx} \quad (3.8-2)$$

with

$$\begin{aligned} K_B & \text{ hydraulic conductivity of bentonite [m s}^{-1}\text{]} \\ K_{EDZ} & \text{ axial hydraulic conductivity of EDZ [m s}^{-1}\text{]} \end{aligned}$$

Combining Eqs. 3.8-1 and 3.8-2 yields:

$$\begin{aligned} \frac{d^2 h}{dx^2} &= \kappa^2 (h(x) - H_A) \\ \text{with } \kappa^2 &= \frac{4\gamma K_{HR}}{\pi r (K_B + (\gamma^2 - 1)K_{EDZ})} \left(\frac{1}{L_l} + \frac{1}{L_u} \right); \quad H_A = \frac{\frac{H_l}{L_l} + \frac{H_u}{L_u} + \frac{q^*}{4\gamma r K_{HR}}}{\frac{1}{L_l} + \frac{1}{L_u}} \end{aligned} \quad (3.8-3)$$

The boundary conditions at the ends of each emplacement tunnel are:

$$h\left(\frac{l}{2}\right) = H_{n1} \quad \text{and} \quad h\left(-\frac{l}{2}\right) = H_{s1} \quad (3.8-4)$$

The solution to Eqs. 3.8-3 and 3.8-4 is identical to the solution given in Eq. 3.6-5, using the modified definitions of the parameter H_A in Eq. 3.8-3. In the same way, the water fluxes from N emplacement tunnels to the operations tunnel (northern branch), Q_n , and construction tunnel (southern branch), Q_s , are calculated using Eqs. 3.6-6 and 3.6-7.

The total water flow rate from the ILW emplacement tunnels to the operations tunnel, Q_{n3} [$\text{m}^3 \text{s}^{-1}$], is estimated as:

$$\begin{aligned} Q_{n3} &= \alpha_1 (\bar{H}_A - H_{n3}) \\ \text{with } \alpha_1 &= A_D K_{HR} \left(\frac{1}{L_l} + \frac{1}{L_u} \right); \quad \bar{H}_A = \frac{\frac{H_l}{L_l} + \frac{H_u}{L_u} + \frac{q^* A_{ILW}}{A_D K_{HR}}}{\frac{1}{L_l} + \frac{1}{L_u}}; \quad A_D = 4\gamma_{ILW} r_{ILW} A_{ILW} \end{aligned} \quad (3.8-5)$$

with

A_D	effective drainage area of the ILW emplacement tunnels [m^2]
r_{ILW}	radius of the ILW emplacement tunnel [m]
γ_{ILW}	ratio of radii EDZ/emplacement tunnel [-]
A_{ILW}	total length of ILW emplacement tunnels [m]
q^*	gas-induced porewater displacement rate from ILW tunnels [$\text{m}^3 \text{s}^{-1} \text{m}^{-1}$].

As discussed in Section 3.6, the mass balance of all water fluxes in Fig. 3.6-1a (including those through the Opalinus Clay) yields an algebraic system of equations from which the individual water fluxes can be calculated using Eqs. 3.6-9 and 3.8-1 to 3.8-5.

The water flow rates calculated by the resistor network model are shown in Fig. 3.8-2 for different values of the water displacement rate from the ILW part of the repository (0.05 and $0.3 \text{ m}^3 \text{ a}^{-1}$). The water displacement rate from the SF part of the repository is fixed at $0.07 \text{ m}^3 \text{ a}^{-1}$, corresponding to a corrosion rate of $1 \mu\text{m a}^{-1}$ (200, i.e. 10 % of all canisters affected, a mean water volume displacement of 0.35 m^3 per canister, and a duration of the water displacement of 1 000 a following canister breaching at 10 000 a, see Section 3.8.2.1). Note that the water fluxes at nodes n1 and s1 are directed towards the SF/HLW emplacement tunnels, driven by the hydraulic head gradient between the ILW and SF/HLW part of the repository. All other water fluxes are directed from the inside to the outside of the repository, i.e. towards the ramp and shaft. As a consequence, radionuclide transport from the SF/HLW emplacement tunnels through the access tunnel system takes place through the shaft only. On the other hand, in the model calculations for ILW, radionuclide transport is assumed to occur along the operations tunnel to the ramp only, i.e. transport from the ILW to the SF/HLW part of the repository and further to the shaft, is not taken into account in the calculations because of the long transport distances involved.

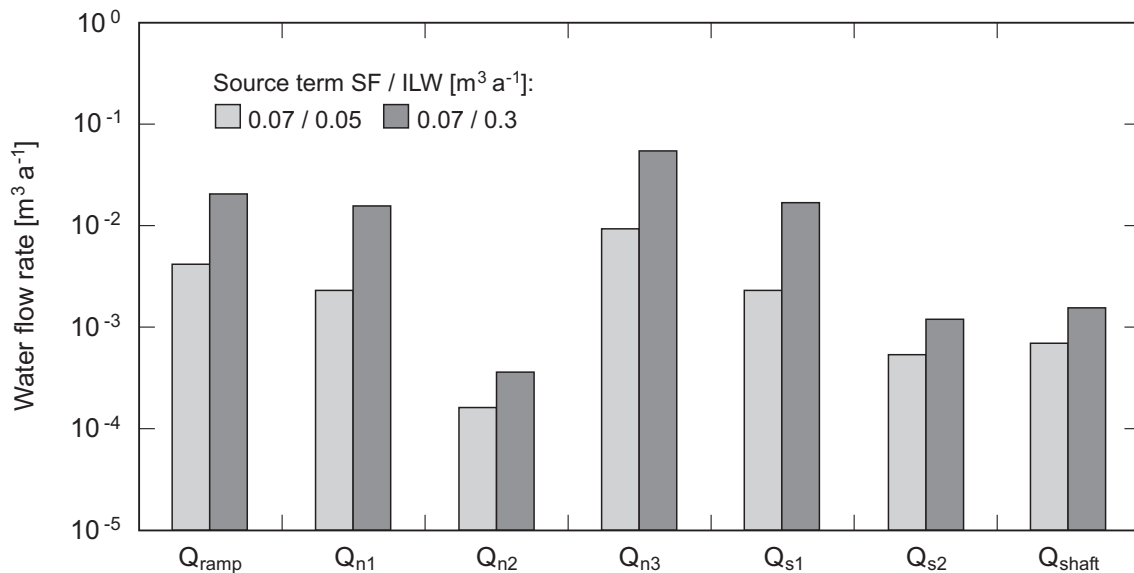


Fig. 3.8-2: Gas-induced water flow rates

Obtained from the resistor network model calculations for two different water displacement rates for ILW (0.05 and $0.3 \text{ m}^3 \text{ a}^{-1}$) and for a constant water displacement rate for SF ($0.07 \text{ m}^3 \text{ a}^{-1}$); the various locations in the repository are labelled according to Fig. 3.6-1a.

3.8.2.3 Calculation of radionuclide release from near field

In the Base Case for SF, it is assumed that the instant release fraction is expelled by gas into the Opalinus Clay and the access tunnel system over a 1 000 years period following canister breaching, based on a corrosion rate $1 \mu\text{m a}^{-1}$. The total water flow rate from 10 % of all canisters is $0.07 \text{ m}^3 \text{ a}^{-1}$. The dose contribution of the remainder of the radionuclides (cladding, fuel matrix) is not taken into account.

In the Base Case for ILW, a pulse release, starting at 10 000 years and lasting for 30 000 years, with a mean water flow rate of $0.05 \text{ m}^3 \text{ a}^{-1}$ is assumed, conveying 50 % of the total mobile radionuclide inventory from ILW. The dose contribution of the remainder of the radionuclides (rest of mobile inventory and sorbed inventory) is not taken into account. In a parameter variation, a mean water flow rate of $0.3 \text{ m}^3 \text{ a}^{-1}$ is assumed, starting at 1 000 years and lasting 10 000 years, conveying 100 % of the total mobile radionuclide inventory from ILW. Again, the dose contribution of the remainder radionuclides (sorbed inventory) is neglected.

3.8.2.4 Calculation of radionuclide transport through host rock and access tunnel system

Gas-induced displacement of contaminated water from the SF and ILW parts of the repository takes place through the Opalinus Clay and the access tunnel system in parallel. As in the treatment in Section 3.6 (Case 1.6), the SF near field is split up into three domains, labelled A, B and C in Fig. 3.6-1b. A, B and C are assumed to have the same size as in Case 1.6. The same cross sectional areas but different Darcy velocities are used for each leg (calculated according to Eqs. 3.6-9 and 3.8-1 to 3.8-5). The branching ratios for radionuclide transport are calculated in the same way as in the assessment case considering radionuclide release affected by the ramp/shaft (Eq. 3.6-12), using the axial water flow rates calculated in Section 3.8.2.2 and the Reference Case effective water flow rates for the Opalinus Clay. As discussed in Section 3.8.2.2, radionuclide transport from the SF emplacement tunnels to the ramp is negligible, due to the reversed water fluxes in this part of the repository, and radionuclide transport from the ILW emplacement tunnels to the shaft is inhibited in the calculations.

3.8.3 Codes used

As in the Reference Conceptualisation, the reference model chain of STMAN-PICNIC-TAME is used to model the radionuclide release, migration and distribution in the biosphere. STMAN is used to model the pulse release of dissolved radionuclides from the near field, based on transient water flow rates induced by gas pressure build-up (see Fig. 3.8-3). The network capabilities of PICNIC are employed to model the simultaneous transport of radionuclides through the Opalinus Clay, the ramp and the shaft. The network structure is similar to the one illustrated in Fig. 3.6-5, with the exception of the legs L_1 (from node J_1 to J_3) and L_2 (from node J_2 to J_3), which are omitted. The water flow rates calculated by means of the resistor network and used in PICNIC are based on the same gas-induced water displacement rates from the near field as those used in the STMAN calculations, but are interpreted as steady-state water fluxes (Fig. 3.8-3).

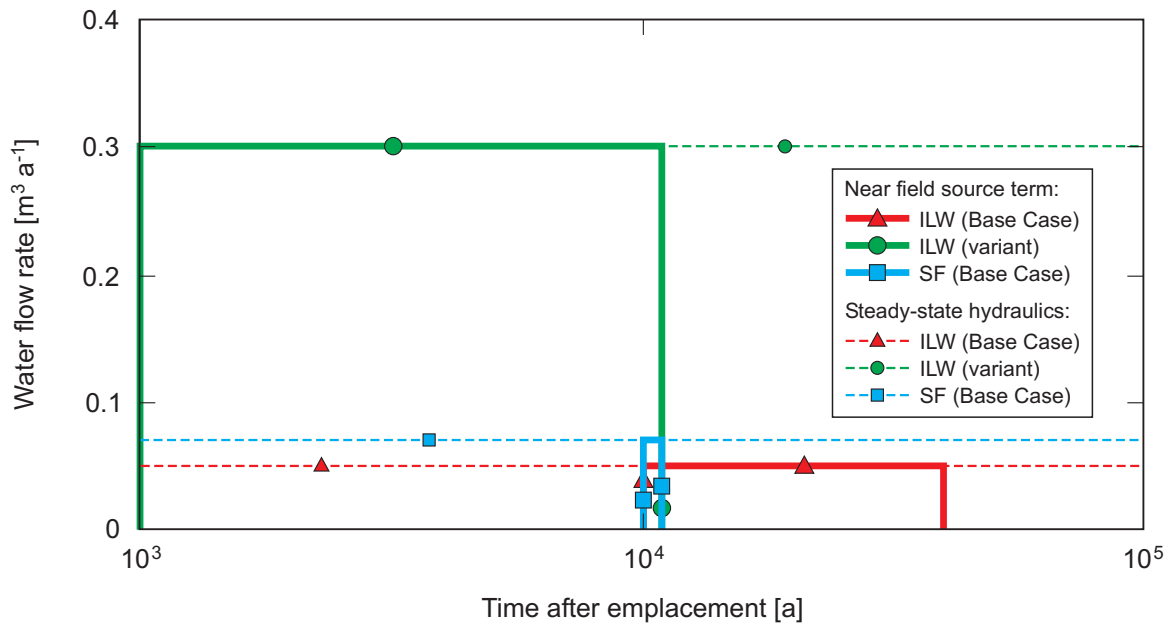


Fig. 3.8-3: Transient water flow rates used to calculate the near field radionuclide source term with STMAN (thick lines) and corresponding steady-state "sources of water" assumed in the resistor network calculations, used to derive steady-state water flow rates for PICNIC legs (thin dashed lines)

3.8.4 Parameters

Base Case

The parameter values used for the calculation of gas-induced water flow rates (resistor network) in the Base Case are identical to those listed in Tab. 3.6-1, with the exception of the gas-induced porewater displacement rates from the SF and ILW near field. These are listed in Tab. 3.8-1. Network flow data and source term information are given in Tab. 3.8-2. Note that most of the radionuclide inventory is released through the Opalinus Clay. Radionuclide release into the Opalinus Clay is assumed to occur upwards only. This is a conservative assumption, because the Darcy velocity is higher and the transport path length shorter than for the downwards transport path. Legs with negative water flows are not taken into account in the transport calculations, because they do not significantly contribute to radionuclide release along the access tunnel system. Release fractions to such legs are thus set to zero. Transport parameters for legs L_1 to L_7 are identical to those listed in Tabs. 3.6-3 to 3.6-5, with the exception of the Darcy velocities (Tab. 3.8-3).

Tab. 3.8-1: Additional parameter values used for the calculation of water flow rates in the resistor network (Base Case)

The values are discussed in the text.

Parameter	Symbol	Unit	Value
Near field			
Gas-induced porewater displacement rates	q^*	$\text{m}^3 \text{a}^{-1}$ (total repository)	0.07
SF			
ILW			
All other parameters	Identical to parameter values in Tab. 3.6-1		

Tab. 3.8-2: Network flow data and source term information (Base Case)

Calculated using resistor network and parameter values listed in Tabs. 3.6-1 and 3.8-1.

Input	Units	Values
Network Structure		
List of junction names. Inlet and outlet junctions for each leg.	-	Fig. 3.6-5
Network Flow Data		
Flows	$\text{m}^3 \text{a}^{-1}$	4.2×10^{-3}
Q_{ramp}		-2.3×10^{-3}
Q_{n1}		1.6×10^{-4}
Q_{n2}		8.8×10^{-3}
Q_{n3}		-2.3×10^{-3}
Q_{s1}		5.4×10^{-4}
Q_{s2}		7.0×10^{-4}
Q_{shaft}		0.14 (upwards, summed over domains A, B and C)
SF Q_{OPA}		0.032 (upwards, domain D)
ILW Q_{OPA}		
Source Term Information		
Source flux	mol a^{-1}	Radionuclide releases to host rock obtained from the output of code STMAN (plug flow): Start: 10 000 a / End: 11 000 a; 100 % IRF Start: 10 000 a / End: 40 000 a; 50 % of mobile inventory
SF ILW		
Fraction to each leg:	dimensionless	Fraction to each leg (including diffusion, see Eq. 3.6-12):
$f_{A,HR}$		0.99996
$f_{A,n1}$		0
$f_{A,n2}$		4×10^{-5}
$f_{C,HR}$		0.99986
$f_{C,s1}$		0
$f_{C,s2}$		1.4×10^{-4}
$f_{D,HR}$		0.989
$f_{D,n3}$	1.1×10^{-2}	

Tab. 3.8-3: PICNIC input data for legs L_1 , L_2 , L_3 and L_4 which represent axial transport through the backfill of the operations tunnel, construction tunnel and ventilation tunnel, and legs L_5 , $L_{6,A}$, $L_{6,B}$, $L_{6,C}$ and L_7 , which represent upward vertical transport through the EDZ of the shaft (L_5) and through the Opalinus Clay (L_6 and L_7) for PICNIC network structure, see Fig. 3.6-5

Input	Units	Values ¹	Source
Leg Data – Basic Data			
Darcy velocity			Calculated from water flow rates in Tab. 3.8-2 and cross sectional areas (see also Tab. A3.2-2a, Parameter 5, Value J)
L_1 (ILW)		1.8×10^{-4}	
L_1 (SF)		-1.0×10^{-4}	
L_2		-1.0×10^{-4}	
L_3	m a ⁻¹	7.0×10^{-6}	
L_4		2.3×10^{-5}	
L_5 (shaft EDZ)		5.4×10^{-5}	
$L_{6,A}, L_{6,C}$ (SF-OPA)		8.8×10^{-7}	
$L_{6,B}$ (SF-OPA)		8.8×10^{-7}	
L_7 (ILW-OPA)		8.0×10^{-6}	
All other leg parameters		Identical to parameter values in Tabs. 3.6-3, 3.6-4 and 3.6-5	

¹ Legs with negative water flows are not taken into account in the transport calculations; the release fractions to such legs are set to zero.

Parameter variation (ILW only)

The parameter values used for the calculation of gas-induced water flow rates (resistor network) in the parameter variation are identical to those listed in Tab. 3.6-1, with the exception of the gas-induced porewater displacement rates from the ILW near field. These are listed in Tab. 3.8-4. Network flow data and source term information are given in Tab. 3.8-5. As in the Base Case, most of the radionuclides are released through the Opalinus Clay. Radionuclide release in the Opalinus Clay is assumed to occur upwards only. Legs with negative water flows are not taken into account in the transport calculations (release fractions to such legs are set to zero). Transport parameters for legs L_1 and L_7 are identical to those listed in Tabs. 3.6-3 to 3.6-5, respectively, with the exception of the Darcy velocities (Tab. 3.8-6). Note that in order to calculate the Darcy velocities for these two legs, the whole network needs to be considered (Tabs. 3.8-4 and 3.8-5). For transport calculations, only legs L_1 and L_7 are considered (Tab. 3.8-6).

Tab. 3.8-4: Additional parameter values used for the calculation of water flow rates in the resistor network (parameter variation)

The values are discussed in the text.

Parameter	Symbol	Unit	Value
Near field			
Gas-induced porewater displacement rates	q^*	$\text{m}^3 \text{a}^{-1}$	
SF		(total repository)	0.07
ILW			0.3
All other parameters	Identical to parameter values in Tab. 3.8-1		

Tab. 3.8-5: Network flow data and source term information (parameter variation)

Calculated using resistor network and parameter values listed in Tabs. 3.6-1 and 3.8-4.

Input	Units	Values
Network Structure		
List of junction names. Inlet and outlet junctions for each leg.	-	Fig. 3.6-5
Network Flow Data		
Flows		
Q_{ramp}		2.1×10^{-2}
Q_{n1}		-1.6×10^{-2}
Q_{n2}		3.6×10^{-4}
Q_{n3}		5.3×10^{-2}
Q_{s1}		-1.6×10^{-2}
Q_{s2}		1.2×10^{-3}
Q_{shaft}		1.5×10^{-3}
SF		0.16 (upwards, summed over domains A, B and C)
ILW		0.18 (upwards, domain D)
Source Term Information		
Source flux (ILW)	mol a^{-1}	Radionuclide releases to host rock obtained from the output of code STMAN (plug flow): Start: 1 000 a / End: 11 000 a; 100 % mobile inventory
Fraction to each leg:	dimensionless	Fraction to each leg (including diffusion, see Eq. 3.6-12):
$f_{D,HR}$		0.948
$f_{D,n3}$		5.2×10^{-2}

Tab. 3.8-6: PICNIC input data differing from the Base Case, for leg L₁, which represents axial transport through the backfill of the operations tunnel, construction tunnel and ventilation tunnel, and leg L₇, which represents upward vertical transport through the Opalinus Clay for the PICNIC network structure, see Fig. 3.6-5

Input	Units	Values	Source
<i>Leg Data – Basic Data</i>			
Darcy velocity L ₁ (ILW) L ₇ (ILW-OPA)	m a ⁻¹	9.1 × 10 ⁻⁴ 4.5 × 10 ⁻⁵	Calculated from water flow rates in Tab. 3.8-5 and cross sectional areas (see also Tab. A3.2-2a, Parameter 5, Value K)
All other leg parameters for L₁ and L₇		Identical to parameter values in Tab. 3.8-3	

4 Modelling Gas Pressure Evolution and the Release of ^{14}C as Volatile Species in the Gas Phase

4.1 Description of the scenario

In this scenario, repository-induced gasses convey ^{14}C in volatile form from the near field to the upper confining units where all gasses are completely dissolved and transported to the Malm aquifer by diffusion in the aqueous phase. Transport of ^{14}C from the Malm aquifer to the biosphere is conservatively assumed to occur instantaneously. ^{14}C is then further diluted in the Quaternary aquifer (without degassing into the atmosphere), which is used as a source of drinking water.

4.2 Evaluation of the scenario using the Gas Model

The scenario is evaluated using the "Gas Model", which consists of two parts:

1. Evaluation of pressure evolution and gas migration, as input to the calculations for gas-induced release of dissolved radionuclides (Cases 1.8 and 4.5, see Sections 3.8 and 6.5) and for the release of ^{14}C as volatile species in the gas phase (Cases 2.1, 2.2 and 4.6, see subsequent sections).
2. Evaluation of dose due to the release of ^{14}C as volatile species in the gas phase (Cases 2.1, 2.2 and 4.6).

The conceptual models and mathematical representations underlying the calculations using the Gas Model are described in detail in Appendix 1. In the following, an overview of the conceptual models followed by a description of the input parameters and results are given. A synthesis of all investigations undertaken and calculations performed on issues related to the fate of gas in the SF/HLW/ILW repository in Opalinus Clay is given in Nagra (2003a).

4.3 Pressure evolution and gas migration (as input to Cases 1.8, 2.1, 2.2, 4.5 and 4.6)

4.3.1 Overview of the conceptual model

Gas is generated by anaerobic corrosion of steel and - for ILW - other metals, generating hydrogen, and, by microbial degradation of organic compounds, generating CH_4 and CO_2 . The pressure build-up caused by gas generation is mitigated by gas dissolution and gas diffusion³⁰, gas-induced porewater displacement and capillary leakage³¹ from the emplacement tunnel walls into the Opalinus Clay or along the EDZ into the access tunnel system. If the gas pressure exceeds the threshold pressure of ca. 13 MPa, dilatant gas pathways³² in the Opalinus Clay are created, which increase the efficiency of gas release and limit the maximal gas pressure in the repository. Upon gas breakthrough through the host rock, gas will accumulate in the Wedelsandstein formation (lateral extension due to higher permeability compared to Opalinus Clay and low-permeability upper confining units), from which gas release takes place through the low-

³⁰ *Gas diffusion* is an abbreviation for diffusive transport of dissolved gas in the aqueous phase.

³¹ *Capillary leakage* is an abbreviation for advective transport of gas in the gas phase under two-phase conditions (no structural changes in pore space involved).

³² *Dilatant gas pathway* is an abbreviation of gas-induced microscopic pathway dilation (which involves mechanical deformation of the pore space).

permeability upper confining units to the Malm aquifer and further to the biosphere. In the model calculations, gas transport through the Malm aquifer to the biosphere is conservatively assumed to be instantaneous.

4.3.2 Input parameters

The gas generation rates for a steel corrosion rate of $1 \mu\text{m a}^{-1}$ (SF/HLW) and for base case assumptions (ILW) are listed in Tab. 4.3-1. In the case of SF/HLW, the gas generation rate does not include contributions from additional steel in the emplacement tunnels (mesh, rock bolts, rails). These materials may increase the gas generation rate by up to a factor of 3, but are likely to be corroded away after a few thousand years. As a consequence, these additional steels have no significant long-term effect on the migration of gas. For ILW, the calculations of gas generation rates have been performed for a time period of up to 10^4 a. The gas generation rates for times beyond 10^4 a have been extrapolated (see Fig. A1.9-3). In the model calculations, all generated gas is assumed to be hydrogen. The total generated gas is estimated to be $4 \times 10^7 \text{ m}^3$ (STP) for SF/HLW and $5 \times 10^5 \text{ m}^3$ (STP) for ILW, the latter including the contribution from Zircaloy. Resaturation of the ILW tunnels at the onset of gas generation is assumed to be 50 %. In the case of SF/HLW, the mean gas saturation of the bentonite pore space is set to an arbitrary small value. All input parameters used in the model calculations are summarised in Tab. 4.3-2.

Tab. 4.3-1: Total gas generation rate for SF/HLW and ILW as a function of time (from Nagra 2003a)

Time	Total gas generation rate [m^3 (STP) a^{-1}]	
	SF/HLW (gas generated at external canister surface for a corrosion rate of $1 \mu\text{m a}^{-1}$)	ILW (base case)
1.0	240	690
3.0	240	670
10	240	110
30	240	110
100	240	98
300	240	79
1000	240	45
3000	240	20
1×10^4	240	10
3×10^4	240	< 10
1×10^5	240	< 10
1.7×10^5	240	0
2×10^5	0	0
Total	$4 \times 10^7 \text{ m}^3$ (STP)	$5 \times 10^5 \text{ m}^3$ (STP)

Data for gas-related properties of the near field and the geosphere are discussed in Nagra (2003a). The measured gas entry pressure for Opalinus Clay (threshold pressure for capillary leakage) is 5 MPa. The threshold pressure for microscopic pathway dilation in the Opalinus Clay is 13 MPa (which is slightly lower than the minimum stress component). The gas entry pressure in the EDZ is assumed to be 2 MPa. This is particularly relevant to the ILW part of the repository, because it allows gas to escape around the plug into the backfill of the operations tunnel, which significantly reduces the maximal gas pressure in the emplacement tunnels.

The measured intrinsic gas permeability in the Opalinus Clay is 10^{-20} m^2 (horizontal) and $2 \times 10^{-21} \text{ m}^2$ (vertical). The relative gas permeability depends on the gas saturation in the formation, which is a varying function in time and space. A broad range is, therefore, considered for the gas permeability (defined as the product of intrinsic and relative gas permeabilities) of the Opalinus Clay: 10^{-21} to 10^{-24} m^2 .

In the Gas Model, the large number of microscopic dilatant gas pathways, originating from the emplacement tunnels and creeping horizontally into the Opalinus Clay, are described by means of a single representative gas pathway. The effective aperture of the representative gas pathway is determined by the dilatancy of Opalinus Clay (elastic and plastic deformations due to gas-induced overpressure) as well as by the extent of a representative desaturated zone along the dilatant gas pathways. This desaturated zone represents the gas-filled pore space along a large number of microscopic dilatant gas pathways, and its formation is assumed to occur in equilibrium with the propagation of the dilatant gas pathways (Eq. A1.9-9). The dilatancy of Opalinus Clay is in the order of 0.01. The extent of the representative desaturated zone, where a fraction of 5 % of the pore space is assumed gas-filled, is assumed to be 2 m, roughly corresponding to the diameter of the SF/HLW emplacement tunnel. The same value is also used for ILW, representing a layer of Opalinus Clay at the top of the emplacement tunnels, where preferential formation of dilatant gas pathways may occur (favourable stress conditions due to low lithostatic load). From this, the effective aperture of the representative gas pathway, w , is calculated to be 0.03 m, using Eq. A1.9-9.

Only part of the Wedelsandstein formation (5 m) is taken to be hydraulically active (Tab. 9.4-4a in Nagra 2002a). This zone is modelled as a fractured medium with a flow porosity of 0.1 %, which is fully accessible for gas at a low gas entry pressure (0.2 MPa). The input parameters for the overlying low-permeability confining units are chosen by analogy to the input parameters for the Opalinus Clay (porosity, pore diffusion constant, gas entry pressure, characteristic length for concentration gradient).

Tab. 4.3-2: Summary of input parameters for the model calculations related to gas migration in the SF/HLW/ILW repository system

Parameter	Symbol	Unit	Value	Comment/source	
ILW	Gas generation rate	\dot{n}_p	mol a ⁻¹ (total)	Tab. 4.3-1	Nagra (2003a)
	Tunnel radius	r	m	4.5	Tab. A3.3-2
	Tunnel length	H	m	180	
	Tunnel separation	d_{sep}	m	100	
	Bulk porosity (near field)	ε_{ILW}	-	0.3	
	Initial gas saturation (near field)	S_{ILW}	-	0.5	

Tab. 4.3-2: (Cont.)

Parameter		Symbol	Unit	Value	Comment/source	
SF/HLW	Gas generation rate (per canister) SF HLW	\dot{n}_p	mol a ⁻¹ per canister	4 (0.4) 2 (0.2)	corrosion rates of 1 $\mu\text{m a}^{-1}$ (0.1 $\mu\text{m a}^{-1}$), see Nagra (2003a); value for HLW scaled from SF by ratio of canister lengths.	
	Number of canisters: BWR-UO ₂ -48 PWR UO ₂ -48 + PWR MOX-48 PWR-UO ₂ -48 COGEMA BNFL			-		-
	Canister breaching time	t_0	a	10 000	Tab. A3.3-1, Parameter 5, Value A	
	Tunnel radius	r	m	1.15	Tab. A3.3-2	
	Tunnel separation	d_{sep}	m	40		
	Canister pitch SF HLW	p	m	7.6 5		
	Bentonite porosity			ε_{ben}		-
	Mean gas saturation (bentonite)	S_{ben}	-	0.06		Nagra (2003a)
	Opalinus Clay	Thickness	d_{OPA}	m	100	Nagra (2002a)
		Pore pressure at repository depth	P_s	MPa	6.5 (absolute pressure)	Tab. A3.3-4
Gas entry pressure (2-phase flow)		P_a	MPa	5 (relative pressure)		
Threshold pressure for creation of dilatant gas pathways through Opalinus Clay		P_g	MPa	13 (absolute pressure)		
Gas entry pressure for EDZ (2-phase flow)		$P_{a,EDZ}$	MPa	2 (relative pressure)		
Distance over which concentration gradient of dissolved H ₂ is maintained		l_d	m	20	see text	
Distance over which hydraulic gradient is maintained		l_l	m	40	see text	
Dilatancy		$\Delta\varepsilon$	-	0.01	Nagra (2002a)	

Tab. 4.3-2: (Cont.)

Parameter		Symbol	Unit	Value	Comment/source
Opalinus Clay	Extent of gas saturated zone assumed to be in equilibrium with dilatant gas pathways	W	m	2	assumed value, roughly corresponding to the diameter of the SF/HLW emplacement tunnels
	Gas permeability	k_g	m^2	$10^{-24} - 10^{-21}$	Tab. A3.3-4
	Hydraulic conductivity	K	$m\ s^{-1}$	6×10^{-14}	$= (K_v + K_h)/2$, Tab. A3.3-4
	Porosity	ε_{OPA}	-	0.12	Tab. A3.3-4
	Gas accessible porosity fraction in Opalinus Clay	S_{OPA}	-	0.05*	(* derived from pessimistic value for gas accessible porosity in Opalinus Clay)
	Pore diffusion constant (vertical)	D_p	$m^2\ s^{-1}$	8.3×10^{-11}	
Wedelsandstein	Hydraulically active thickness	d_w	m	5	Tab. A3.3-4
	Gas entry pressure for horizontal gas migration (2-phase flow)	$P_{a,w}$	MPa	0.2 (relative pressure)	
	Pore pressure	$P_{s,w}$	MPa	5.4 (absolute pressure)	
	Gas accessible porosity	ε_w	-	0.001	
	Gas saturation of gas accessible porosity	S_w	-	1	see text
Low-permeability upper confining units	Distance over which concentration gradient of dissolved H_2 is maintained	$l_{cu,d}$	m	20	same as in Opalinus Clay
	Distance over which hydraulic gradient is maintained	$l_{cu,t}$	m	100	see text
	Gas entry pressure (2-phase flow)	$P_{a,cu}$	MPa	5 (relative pressure)	same as in Opalinus Clay
	Pore pressure	$P_{s,cu}$	MPa	5.4 (absolute pressure)	derived from Tab. A3.3-4
	Porosity	ε_{cu}	-	0.12	same as in Opalinus Clay
	Pore diffusion constant	$D_{p,cu}$	$m^2\ s^{-1}$	8.3×10^{-11}	same as in Opalinus Clay
General	Solubility of hydrogen (at 0.1 MPa)	C	$mol\ m^{-3}$	0.847	Nagra (2003a)
	Dynamic viscosity of hydrogen gas	μ_g	Pa·s	10^{-5}	

The lengths over which the gas-induced hydraulic gradient and the concentration gradient for dissolved gas in the Opalinus Clay are non-zero are assumed to be time-independent. The values for the characteristic lengths listed in Tab. 4.3-2 are justified by the estimates presented in Tab. 4.3-3. For the characteristic diffusion length, l_d , a representative value of 20 m is chosen. In the case of the characteristic hydraulic length, l_l , a value of 40 m is chosen. This is a bounding value which roughly corresponds to the distance from mid-Opalinus Clay to the Wedelsandstein. For the case of the low-permeability upper confining units, the corresponding values are 20 m (diffusion length) and 100 m (hydraulic length, bounding value corresponding to thickness of upper confining units).

Tab. 4.3-3: Justification of chosen values for characteristic lengths of hydraulic gradient and concentration gradient of dissolved hydrogen in Opalinus Clay

K is the hydraulic conductivity, averaged over horizontal/vertical directions ($6 \times 10^{-14} \text{ m s}^{-1}$) and S_s is the specific storativity (10^{-5} m^{-1}).

Time t [a]	$l_d = \sqrt{\pi D_p t}$ [m] (hydrogen concentration gradient)	$l_l = \sqrt{\pi \frac{K}{S_s} t}$ [m] (hydraulic gradient)
10^2	0.9	7.7
10^3	2.9	24
10^4	9.0	77
10^5	29	240
Choice	20	40 (bounding value, see text)

4.3.3 Results

4.3.3.1 ILW

The calculated pressure evolution in the ILW emplacement tunnels in the absence of capillary leakage by 2-phase flow through the tunnel walls is shown in Fig. 4.3-1. Within roughly 6 000 and 8 000 years after the end of waste emplacement the pressure rises to the capillary leakage threshold (11.5 MPa) and to the threshold pressure for the formation of dilatant pathways (13 MPa), respectively.

In the absence of any transport of gas and water and assuming a resaturation of 50 % at the start of gas generation, the gas pressure reaches a hypothetical maximum of about 30 MPa after several hundred thousand years. The effects of gas dissolution in the near field porewater and aqueous gas diffusion through the tunnel walls on the pressure evolution are small up to one hundred thousand years, but get more important at a later stage when the gas generation is reduced to nearly zero. Gas-induced porewater displacement from the emplacement tunnels into the Opalinus Clay reduces the hypothetical pressure maximum from 30 MPa to a maximum of about 14 MPa occurring at 15 000 years (Fig. 4.3-1).

When diffusion of dissolved gas, porewater displacement and capillary leakage by 2-phase flow from the tunnel walls into the Opalinus Clay are taken into account (Fig. 4.3-2), the pressure

risers to a maximum occurring within about 15 000 years and declines thereafter due to pore-water displacement from the tunnels. As soon as the porewater has been completely displaced from the tunnels, the pressure rises again because the rate of capillary leakage and gas diffusion is smaller than the gas generation rate. For gas permeabilities of 10^{-23} m^2 or lower, the threshold pressure for the formation of dilatant pathways (13 MPa) is exceeded. Also shown in Fig. 4.3-2 is the rate of gas-induced porewater displacement from the ILW emplacement tunnels into the Opalinus Clay, also used as input in the assessment case 1.8 and 4.5, related to the gas-induced release of dissolved radionuclides from the ILW tunnels (see Sections 3.8 and 6.5). Significant displacement of water starts at roughly 10 000 years, at a maximal rate of approximately $0.05 \text{ m}^3 \text{ a}^{-1}$. For pressures lower than the formation pore pressure at the beginning of the pressure build-up, inflow to the emplacement tunnels occurs, but these (negative) flow rates are not shown in Fig. 4.3-2.

When the threshold pressure (13 MPa) is exceeded, gas pathways are created by pathway dilation. The most likely situation is that dilatant gas pathways propagate from the upper part of the tunnel (lowest lithostatic load) laterally along the bedding planes (minimal tensile strength). A network of dilatant gas pathways is created representing a perturbation of the host rock limited to a horizontal layer at the level of the upper part of the waste emplacement tunnels, thus creating additional volume for gas and surface area for capillary leakage by 2-phase flow and diffusion of dissolved gas. In the model, this network is represented by a single representative pathway with an effective aperture of 0.03 m (see Section 4.3.2).

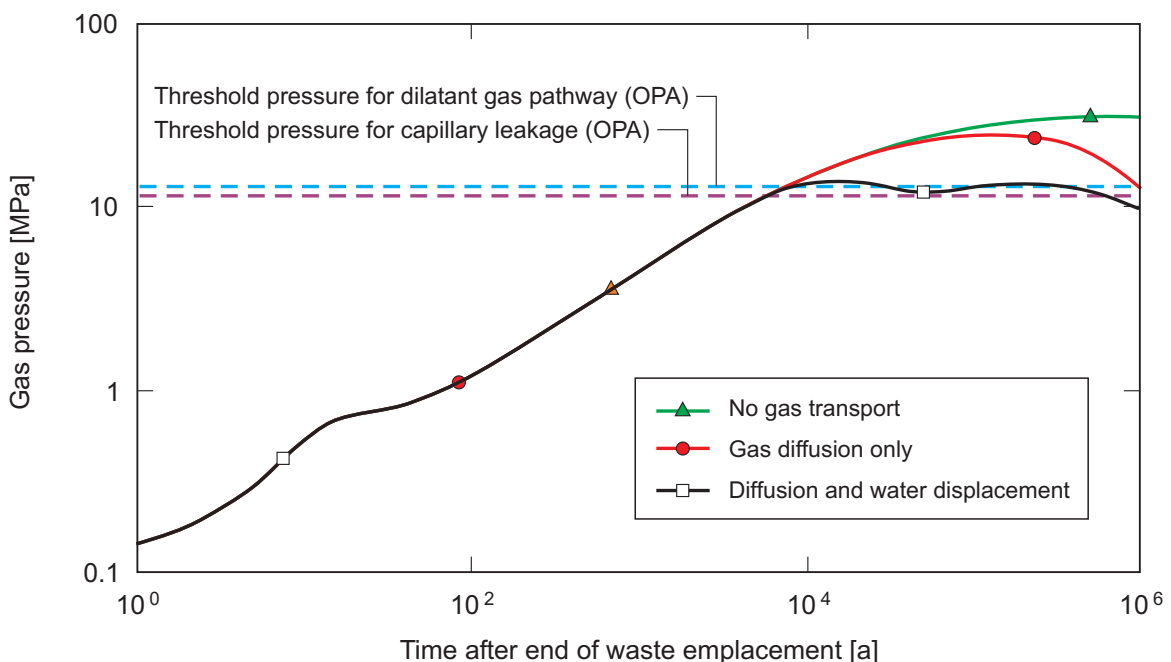


Fig. 4.3-1: Evolution of gas pressure in the ILW emplacement tunnels assuming an initial saturation of 50 %

Gas diffusion and porewater displacement is taken into account, but capillary leakage by 2-phase flow and pathway dilation are not considered.

The time-dependent length (tunnel to tip) of the representative dilatant pathway is shown in Fig. 4.3-3 for the case of ILW as a function of time and gas permeability. The maximal length of the dilatant pathway depends on the assumed value for the gas permeability for capillary leakage into the Opalinus Clay matrix. The highest value of less than 10 m (from tunnel to tip) is obtained in the absence of any capillary leakage ($k_g = 0$, i.e. gas diffusion only) at roughly 15 000 years. When the combined effect of capillary leakage by 2-phase flow, diffusion of dissolved gas and porewater displacement exceeds the gas generation rate, the fracture length is reduced and the dilatant pathway eventually closes. The maximal creep rate of the representative gas pathway is found to be 2.5 mm a^{-1} . The issue of creep rates is discussed in more detail in Nagra (2003a).

In an attempt to illustrate the effect of additional porosity for gas storage in the access tunnel system, the tunnel length has been doubled from 180 m to 360 m (Fig. 4.3-4). All other input parameters are left identical to the ones used to produce the results in Fig. 4.3-2. The maximum pressure in the absence of any gas and water escape is reduced to 16 MPa. Taking porewater displacement from the 360 m long tunnel into account, the pressure rises to approximately 9 MPa. In this case, no capillary leakage by 2-phase flow and no pathway dilation takes place, because the corresponding threshold pressures are not exceeded.

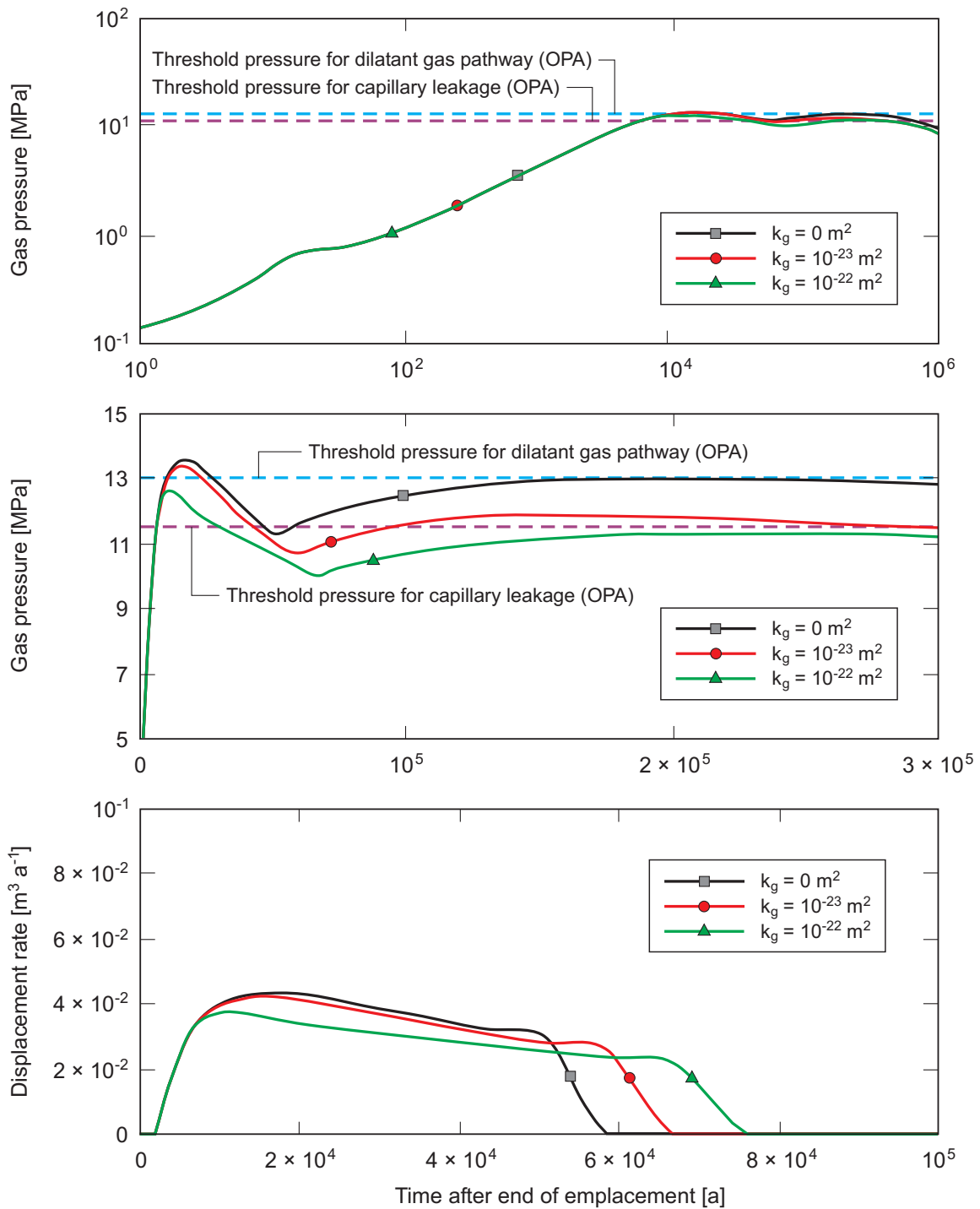


Fig. 4.3-2: Upper and middle figure: Evolution of gas pressure in the ILW emplacement tunnels taking into account gas diffusion, porewater displacement and capillary leakage by 2-phase flow, but without consideration of pathway dilation. Lower figure: Gas-induced porewater displacement rates from the ILW emplacement tunnels into the Opalinus Clay (same parameter values as in upper figure)

For better visibility of the details of the curves, linear-linear plots are shown in the middle and lower figure. The displacement rates in the lower figure are also used as input in the assessment cases 1.8 and 4.5, related to the gas-induced release of dissolved radionuclides from the ILW tunnels (see Sections 3.8 and 6.5).

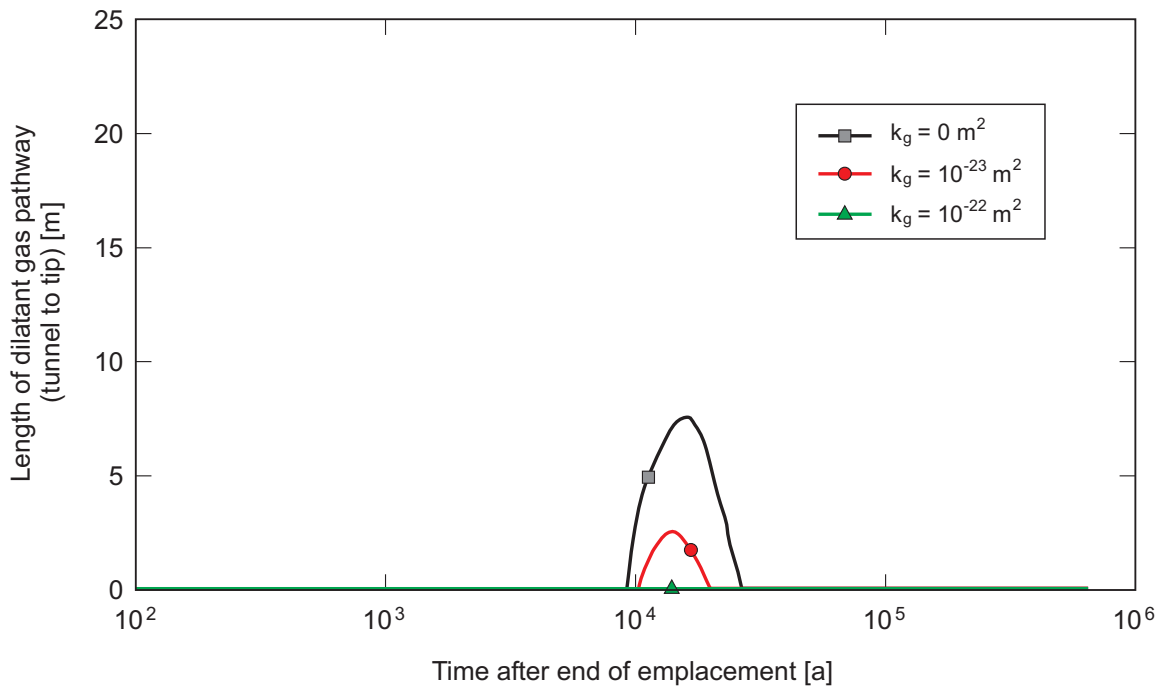


Fig. 4.3-3: Propagation of a representative dilatant gas pathway from the ILW emplacement tunnel into the Opalinus Clay ($P = 13$ MPa), taking gas diffusion, porewater displacement and capillary leakage by 2-phase flow from tunnels and horizontal dilatant gas pathways into account

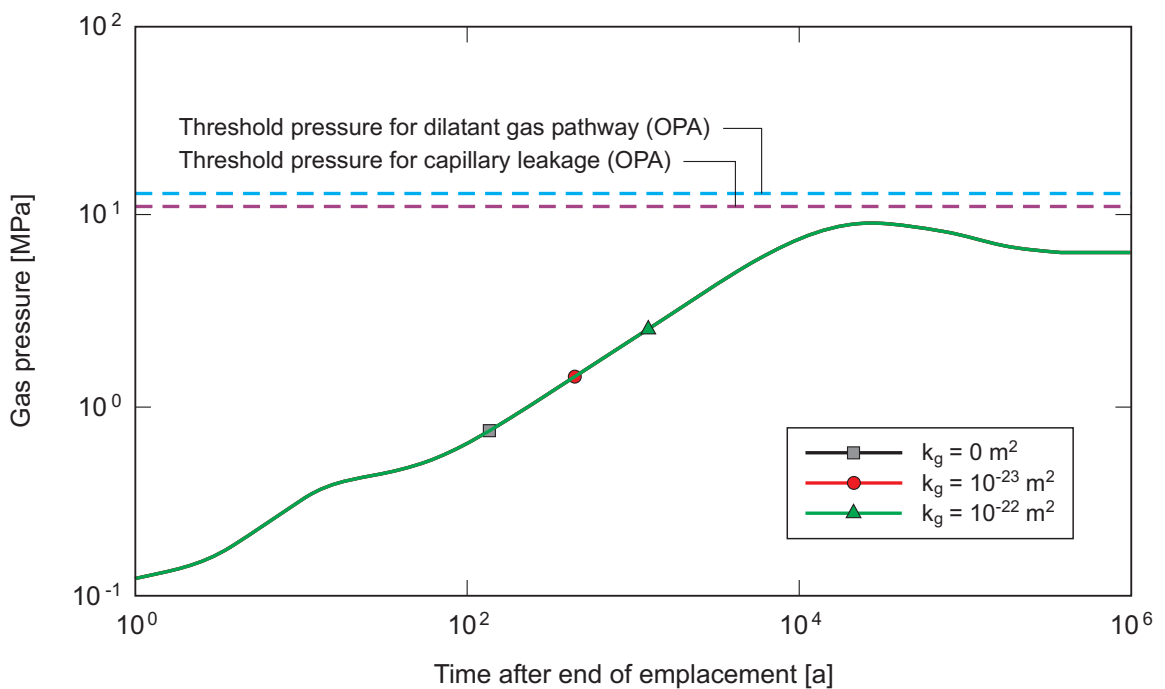


Fig. 4.3-4: Evaluation of the importance of additional gas storage volume for ILW

The total tunnel length is increased from 180 m to 360 m to include additional volume provided by the operations tunnel. The evolution of gas pressure in the ILW facility is taking into account gas diffusion and porewater displacement; all pressure curves are identical.

4.3.3.2 SF/HLW

The calculated pressure evolution in the SF emplacement tunnels is shown in Fig. 4.3-5 for a steel corrosion rate of $1 \mu\text{m a}^{-1}$. In the absence of capillary leakage by 2-phase flow, the pressure rises to the capillary leakage threshold (11.5 MPa) and to the threshold pressure for the formation of dilatant gas pathways (13 MPa) within roughly 1 000 years after the end of waste emplacement. For HLW, the pressures are expected to be lower than for SF, due to the lower canister length-to-pitch ratio (lower gas generation rate per unit tunnel length).

In the absence of any transport processes and assuming a gas storage volume corresponding to 6 % gas saturation in the bentonite (arbitrary small volume), the gas pressure reaches extremely high values. The effects of gas dissolution in the near field porewater and aqueous gas diffusion through the tunnel walls on the pressure evolution are significant only at very high pressures.

When capillary leakage by 2-phase flow and gas diffusion from the SF tunnel walls into the Opalinus Clay are taken into account (Fig. 4.3-5), the pressure reaches a steady state, which corresponds to an equilibrium between gas generation and gas escape. In Tab. 4.3-4, the maximum gas pressure in the SF tunnels is listed as a function of gas permeability and corrosion rate.

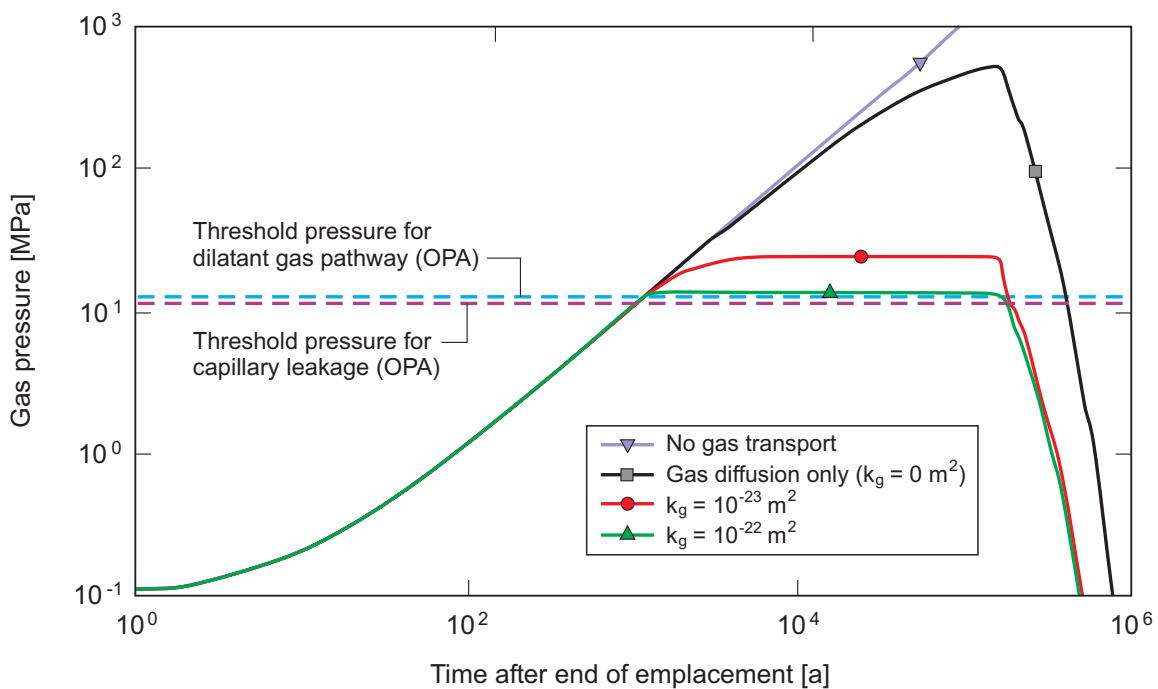


Fig. 4.3-5: Evolution of gas pressure in the SF emplacement tunnel taking gas diffusion and capillary leakage by 2-phase flow into account, but without consideration of pathway dilation (steel corrosion rate $1 \mu\text{m a}^{-1}$)

Tab. 4.3-4: Maximal gas pressure in the SF emplacement tunnels for various gas permeabilities and corrosion rates considering capillary leakage by 2-phase flow and gas diffusion, but no pathway dilation (pressures above the threshold for pathway dilation of 13 MPa in italics)

Gas permeability of Opalinus Clay [m ²]	Maximal gas pressure [MPa] vs. steel corrosion rate [$\mu\text{m a}^{-1}$]	
	0.1	1
0	<i>54.7</i>	<i>520</i>
10 ⁻²³	12.9	<i>23.7</i>
10 ⁻²²	11.9	<i>13.3</i>
10 ⁻²¹	11.9	12.0

For the case considering the formation of dilatant pathways into the Opalinus Clay ($P = 13$ MPa), the time-dependent length (tunnel to tip) of the representative pathway is shown in Fig. 4.3-6 as a function of time and gas permeability for leakage into the Opalinus Clay matrix (corrosion rate $1 \mu\text{m a}^{-1}$). In the absence of any capillary leakage by 2-phase flow, the networks of pathways of two adjacent emplacement tunnels overlap, i.e. a connected horizontal network of dilatant gas pathways would develop covering the SF/HLW repository plane. In this situation, the length of the discrete pathway in Fig. 4.3-6 is truncated to 20 m, which corresponds to half of the tunnel separation of 40 m. Note that the effective aperture of the representative pathway only influences the growth rate of the feature, but not the maximum length. The maximal creep rate of the representative gas pathway is found to be 1.5 mm a^{-1} . For gas permeabilities equal or larger than 10^{-22} m^2 , the generated gas is able to escape by gas diffusion and capillary leakage into the Opalinus Clay (insignificant or no pathway dilation).

Fig. 4.3-7 shows the propagation of the representative gas pathway in the case of a decreased steel corrosion rate of $0.1 \mu\text{m a}^{-1}$. Clearly, the rate of capillary leakage by 2-phase flow is sufficient for transporting away all the gas generated by the slow corrosion of steel. In the absence of capillary leakage, the maximal creep rate of the representative gas pathway is found to be approximately 0.1 mm a^{-1} .

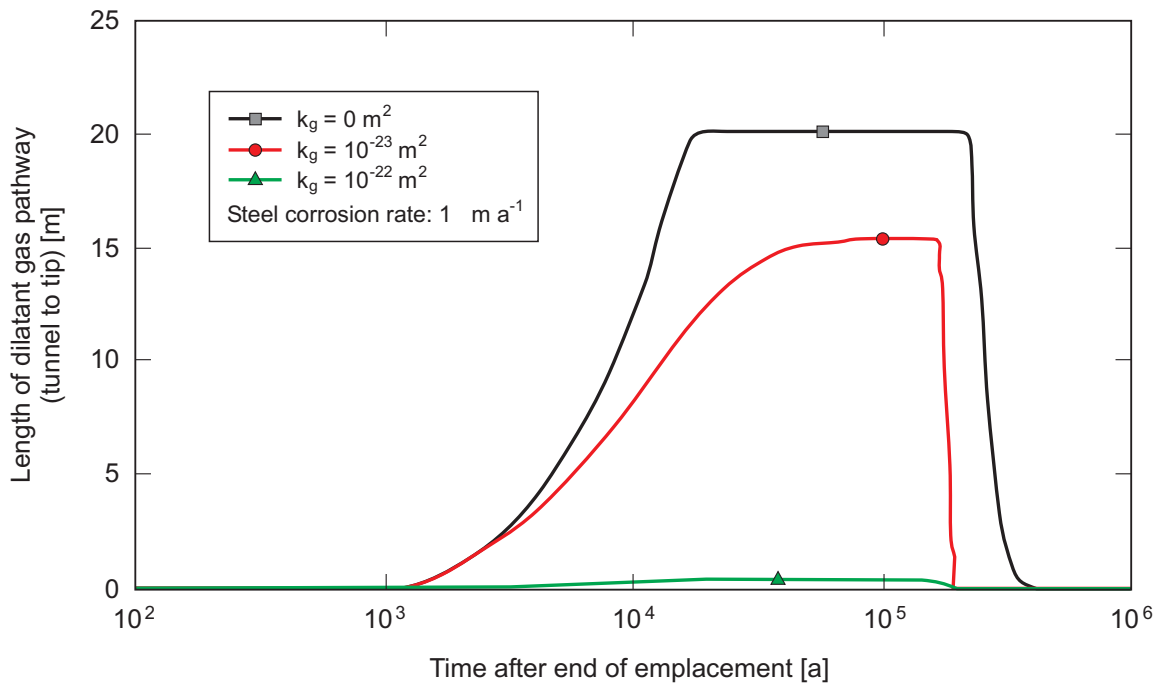


Fig. 4.3-6: Propagation of a representative dilatant gas pathway from the SF emplacement tunnel into the Opalinus Clay, taking gas diffusion and capillary leakage by 2-phase flow from tunnels and horizontal dilatant gas pathways into account ($P = 13 \text{ MPa}$, corrosion rate $1 \text{ } \mu\text{m a}^{-1}$)

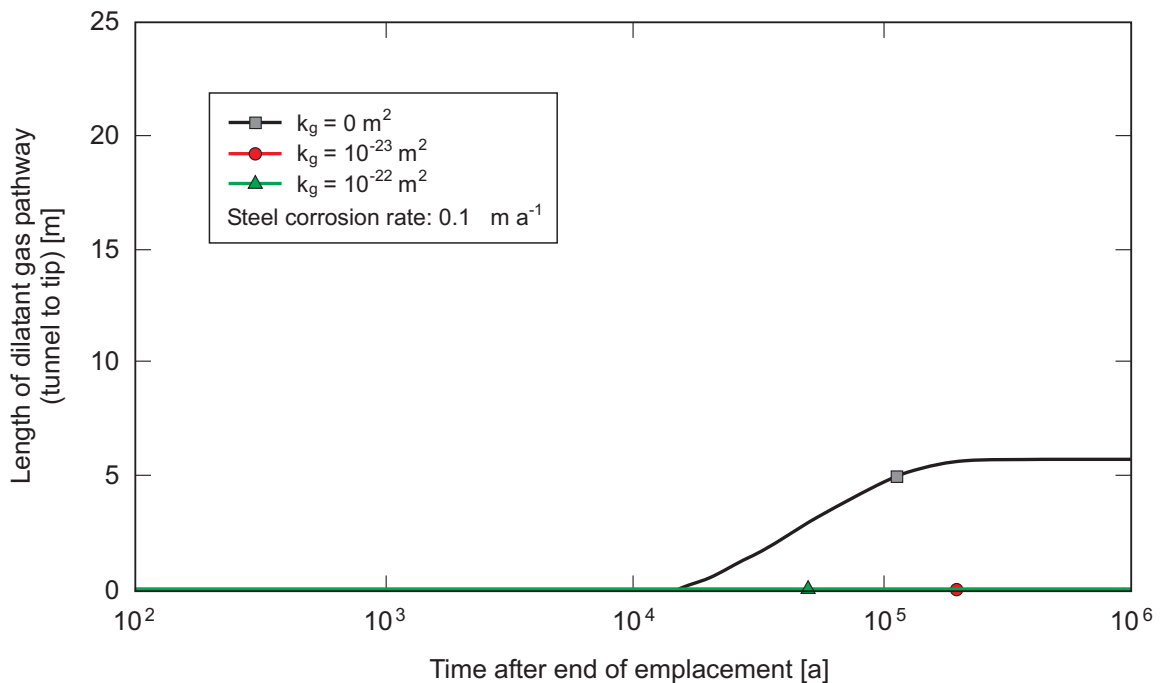


Fig. 4.3-7: Propagation of a representative dilatant gas pathway from the SF emplacement tunnel into the Opalinus Clay, taking gas diffusion and capillary leakage by 2-phase flow from tunnels and horizontal dilatant gas pathways into account ($P = 13 \text{ MPa}$, corrosion rate $0.1 \text{ } \mu\text{m a}^{-1}$)

4.3.3.3 Gas accumulation in Wedelsandstein

Gas transported through the host rock and/or through the ramp/shaft will accumulate in the Wedelsandstein, due to its higher permeability compared to Opalinus Clay and low-permeability upper confining units. The free gas phase will develop radially at a rate controlled by the gas inflow to the Wedelsandstein and by the gas loss from the Wedelsandstein through the low-permeability upper confining units into the Malm aquifer, see Fig. 4.3-8. The size of the gas-filled volume is independent of the gas permeability of the low-permeability upper confining units, because the gas entry pressure is never exceeded and, therefore, gas loss through the low-permeability upper confining units is by diffusion only. The dependency on gas permeability stems from capillary leakage by 2-phase flow within the Opalinus Clay. In Fig. 4.3-9, the gas transport rate through the low-permeability upper confining units is compared to the gas generation rate in the repository (with contributions from SF, HLW and ILW). Again, the release curves are nearly independent of the gas permeability. In the calculations, it has been assumed that gas diffusion from the Wedelsandstein takes place both upwards through the low-permeability upper confining units and downwards back into the Opalinus Clay³³. For this reason, the maximal gas transport rate in Fig. 4.3-9 amounts to only half the gas generation rate shown in Fig. 4.3-13.

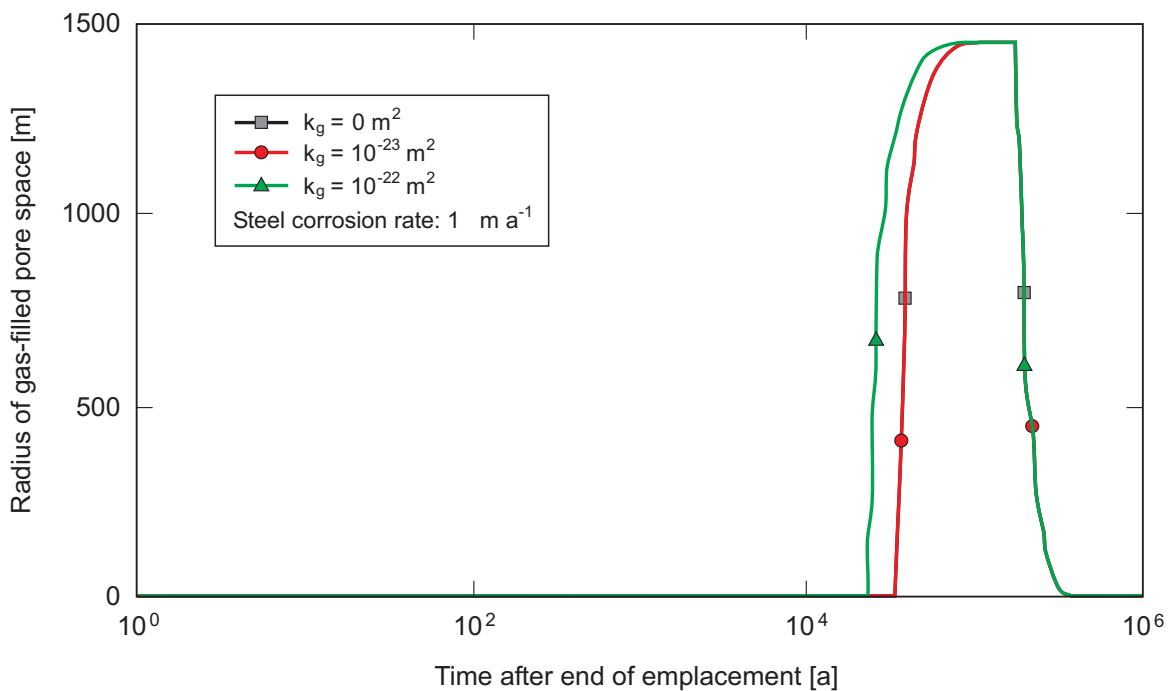


Fig. 4.3-8: Radial propagation of a free gas phase in the Wedelsandstein caused by gas generation in SF/HLW/ILW, taking gas diffusion through the low-permeability upper confining units into account (corrosion rate $1 \mu\text{m a}^{-1}$)

The curves for gas permeabilities in the Opalinus Clay of $k_g = 0$ and 10^{-23} m^2 are identical.

³³ This assumption is justified by the fact that only 10 % of the gas accessible pore space of the Opalinus Clay above the repository has been assumed to be filled with gas before gas breakthrough to the Wedelsandstein occurs (overflow criterion, see Eq. A1.9-13). The remainder of the pore space is filled with water and the gas solubility limit is not expected to be exceeded. Moreover, the gas accumulation area in the Wedelsandstein at the time of its maximal extent is significantly larger than the repository area.

The maximal radius of the gas-filled pore volume and the maximal gas flow rates are listed in Tab. 4.3-5 as a function of the steel corrosion rate. Both quantities decrease with decreasing steel corrosion rate, but are found to be independent of the gas permeability in the Opalinus Clay (not shown in Tab. 4.3-5). Due to the gradual accumulation of gas in the various parts of the repository system, the release of gas to the Malm aquifer is retarded by several tens of thousands of years (confinement) and lasts for about 2×10^5 years.

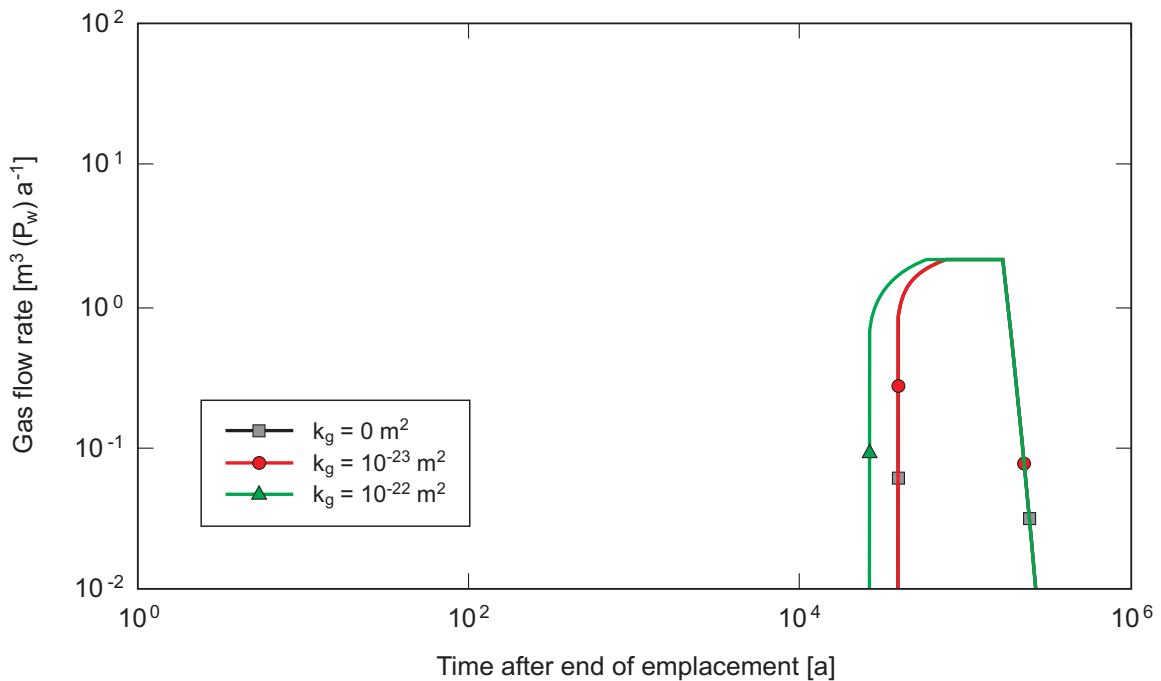


Fig. 4.3-9: Gas flow rate by diffusion from free gas phase in the Wedelsandstein through the low-permeability upper confining units to the Malm aquifer (corrosion rate $1 \mu\text{m a}^{-1}$)

The curves for gas permeabilities in the Opalinus Clay of $k_g = 0$ and 10^{-23} m^2 are identical. $\text{m}^3 (\text{P}_w)$: gas volume at gas pressure in the Wedelsandstein.

Tab. 4.3-5: Maximal radius of free gas phase in the Wedelsandstein and maximal gas flow rate through the low-permeability upper confining units as a function of the steel corrosion rate; both quantities are found to be independent of the gas permeability in the Opalinus Clay

Steel corrosion rate [$\mu\text{m a}^{-1}$]	Maximal radius of free gas phase [m]	Maximal gas flow rate [$\text{m}^3 (\text{P}_w) \text{ a}^{-1}$]
0.1	460	0.21
1	1 400	2.1

4.3.3.4 Investigated assessment cases related to the release of ^{14}C in volatile form in the gas phase (Cases 2.1, 2.2 and 4.6)

The different assessment cases related to the gaseous release of radionuclides as volatile species from SF and ILW through the Opalinus Clay or, alternatively, through the access tunnel system are summarised in Tab. 4.3-6. These assessment cases are characterised by the release pathway for gas from the near field to the biosphere and by the corresponding pore space available for gas accumulation:

- In **Case 2.1**, gas migrates from the SF and ILW tunnels through the Opalinus Clay to the Wedelsandstein and further to the Malm aquifer. Contributions to the gas accumulation volume are provided by the backfill of the emplacement tunnels, the EDZ, the dilatant gas pathways in the Opalinus Clay and by the Wedelsandstein. Conceptual assumptions, data and results for this assessment case are discussed in detail in the previous sections (Sections 4.3.3.1 to 4.3.3.3).
- In **Case 2.2**, gas migrates from the SF and ILW tunnels through the access tunnel system to the Wedelsandstein and further to the Malm aquifer. Contributions to the gas accumulation volume are provided by the backfill of the emplacement tunnels, the EDZ, the backfill of the access tunnel system and by the Wedelsandstein.
- In **Case 4.6**, gas migrates without retardation from the SF and ILW tunnels through the Opalinus Clay to the Wedelsandstein and further to the Malm aquifer. Contributions to the gas accumulation volume are provided by the backfill of the emplacement tunnels, the EDZ and by the Wedelsandstein.

Tab. 4.3-6: Pore space available for gas considered in the different assessment cases

Values for gas storage volumes are given in Tab. 4.3-7.

Assessment case	Backfill	EDZ	Dilatant gas pathways in Opalinus Clay	Access tunnels	Wedel-sandstein
Case 2.1 Release of volatile ^{14}C from SF and ILW in the gas phase not affected by ramp/shaft ("tight seals")	✓	✓	✓	-	✓
Case 2.2 Release of volatile ^{14}C from SF and ILW in the gas phase affected by ramp/shaft ("leaky seals")	✓	✓	-	✓	✓
Case 4.6 Unretarded transport of volatile ^{14}C from SF and ILW through host rock ("what if?")	✓	✓	-	-	✓

For each of these assessment cases, the accumulation volumes of the free gas phase in the different parts of the repository system and the gas flow rate from the Wedelsandstein to the Malm aquifer are plotted as a function of time in Figs. 4.3-10 to 4.3-12. These results are shown for different gas permeabilities of the Opalinus Clay and for a steel corrosion rate of $1 \mu\text{m a}^{-1}$. In all investigated cases, the Wedelsandstein provides the largest contribution to the total gas

volume. Other significant contributions stem from the near field (which, in Case 2.2, include the gas-filled pore space in the access tunnel system) and/or from the dilatant gas pathways in the Opalinus Clay (Case 2.1, SF).

Tab. 4.3-7: Calculated gas storage volumes

System component	Bulk volume [m ³]	Porosity [-]	Gas saturation [-]	Gas storage volume [m ³]
SF				
Bentonite	61 900	0.36	0.065	1 450
EDZ	98 600	0.22	0.05	1 080
Opalinus Clay (dilatant gas pathways only)	time-dependent modelling (see Figs. 4.3-10,11,12)			
Access tunnel system	149 000	0.3	0.2	8 940
Total SF ¹	-	-	-	11 470
ILW				
Waste + tunnel backfill	11 500	0.3	1	3 450
EDZ	5 590	0.22	0.05	60
Opalinus Clay (dilatant gas pathways only)	time-dependent modelling (see Figs. 4.3-10,11,12)			
Access tunnel system	149 000	0.3	0.2	8 940
Total ILW ¹				12 450
Wedelsandstein (V_w)	time-dependent modelling (see Figs. 4.3-10,11,12)			

¹ excluding contributions from dilatant gas pathways in Opalinus Clay and gas-filled pore space in Wedelsandstein.

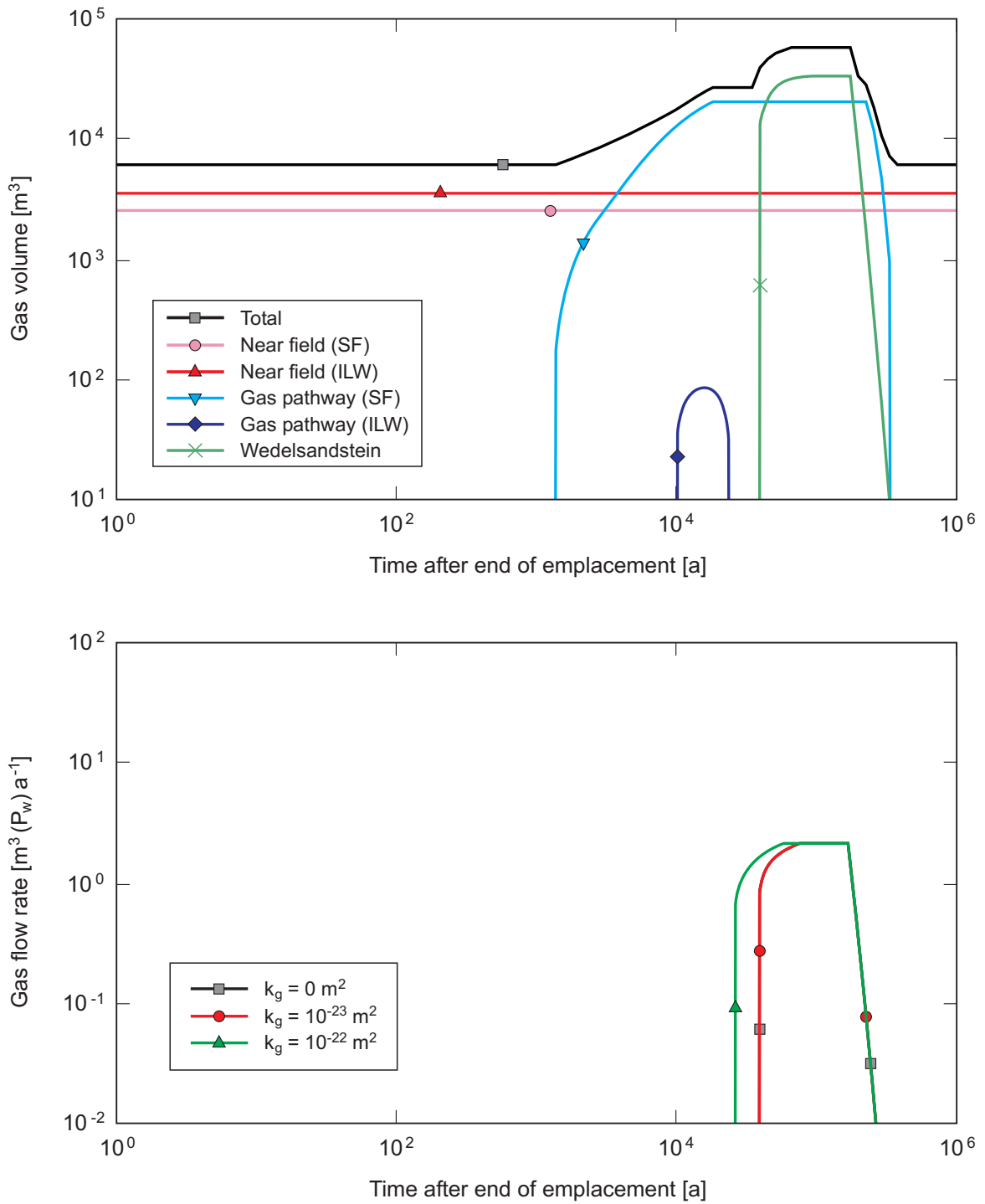


Fig. 4.3-10: Results for Case 2.1 (steel corrosion rate 1 μm a⁻¹)

Upper figure: Volume of free gas phase in the different parts of the repository system.
 Lower figure: Gas flow rate from Wedelsandstein to Malm aquifer as a function of time and of gas permeability in the Opalinus Clay (duplicate of Fig. 4.3-9).

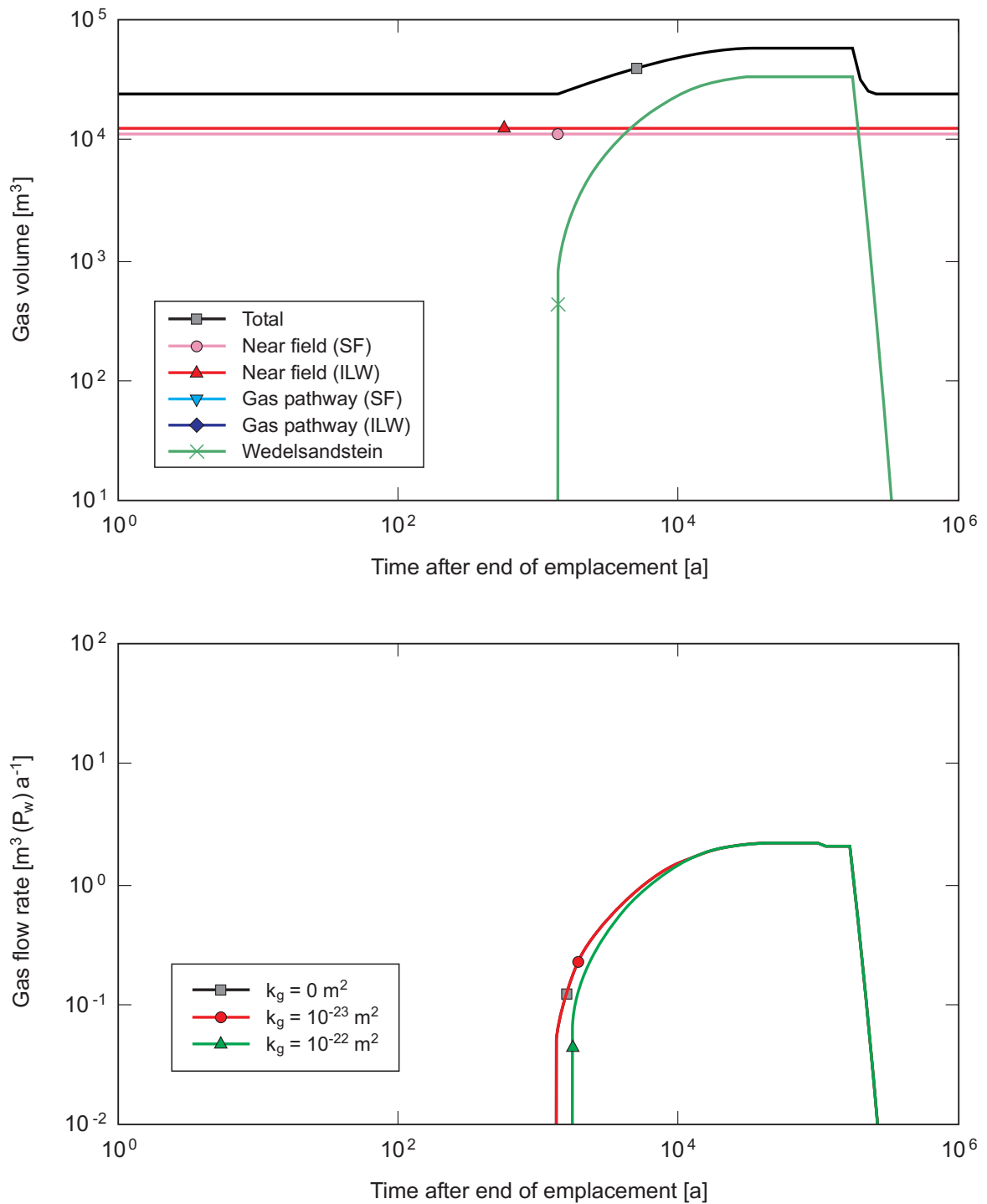


Fig. 4.3-11: Results for Case 2.2 (steel corrosion rate $1 \mu\text{m a}^{-1}$)

Upper figure: Volume of free gas phase in the different parts of the repository system.
 Lower figure: Gas flow rate from Wedelsandstein to Malm aquifer as a function of time and of gas permeability in the Opalinus Clay.

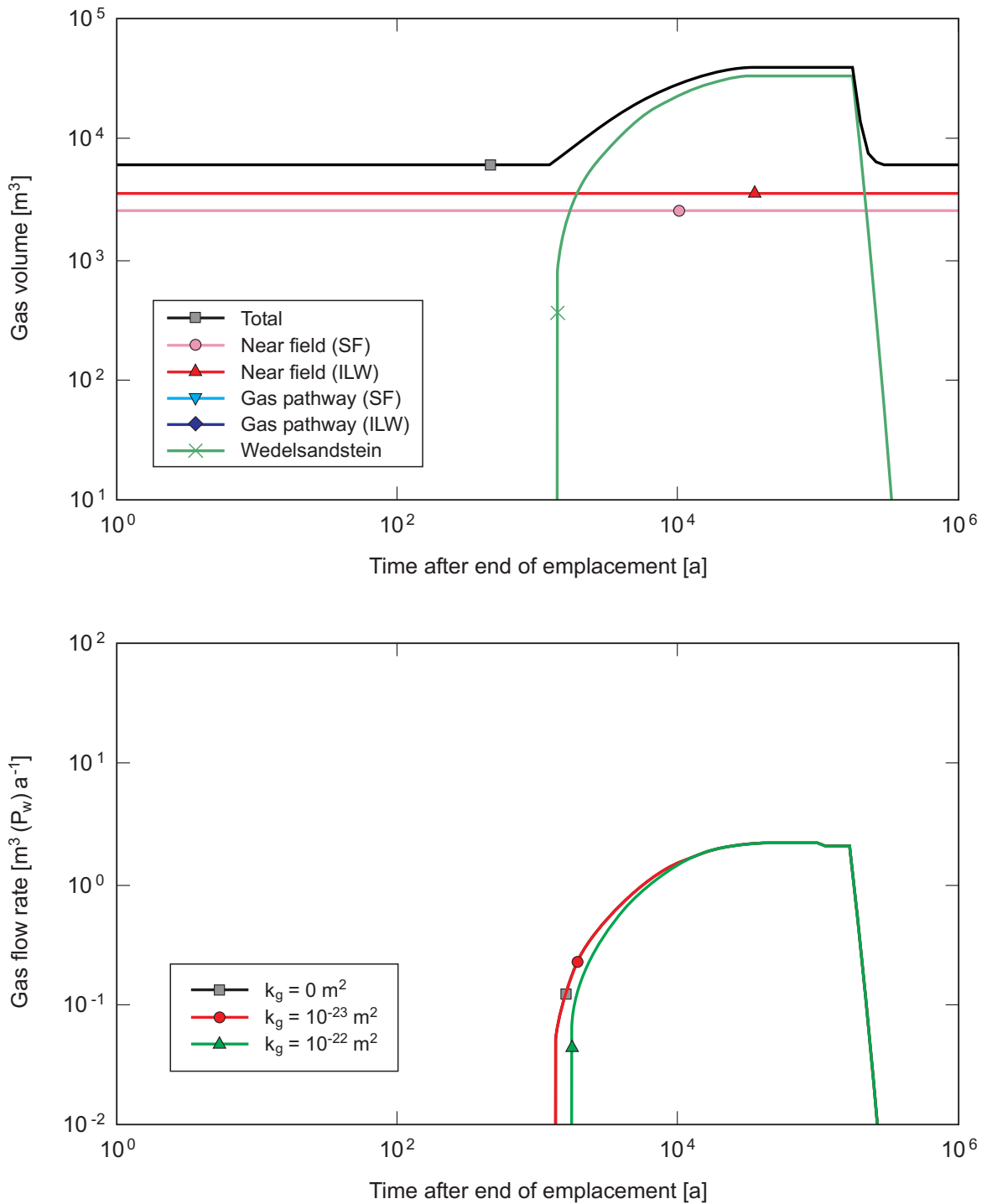


Fig. 4.3-12: Results for Case 4.6 (steel corrosion rate 1 μm a⁻¹)

Upper figure: Volume of free gas phase in the different parts of the repository system. Lower figure: Gas flow rate from Wedelsandstein to Malm aquifer as a function of time and of gas permeability in the Opalinus Clay. This figure is identical to the lower figure in Fig. 4.3-11 because identical criteria were used for the onset of gas flow to the Wedelsandstein for the two cases 2.2 (Fig. 4.3-11) and 4.6 (Fig. 4.3-12), see paragraph after Eq. A1.9-13 or Nagra (2003a) for a more detailed discussion.

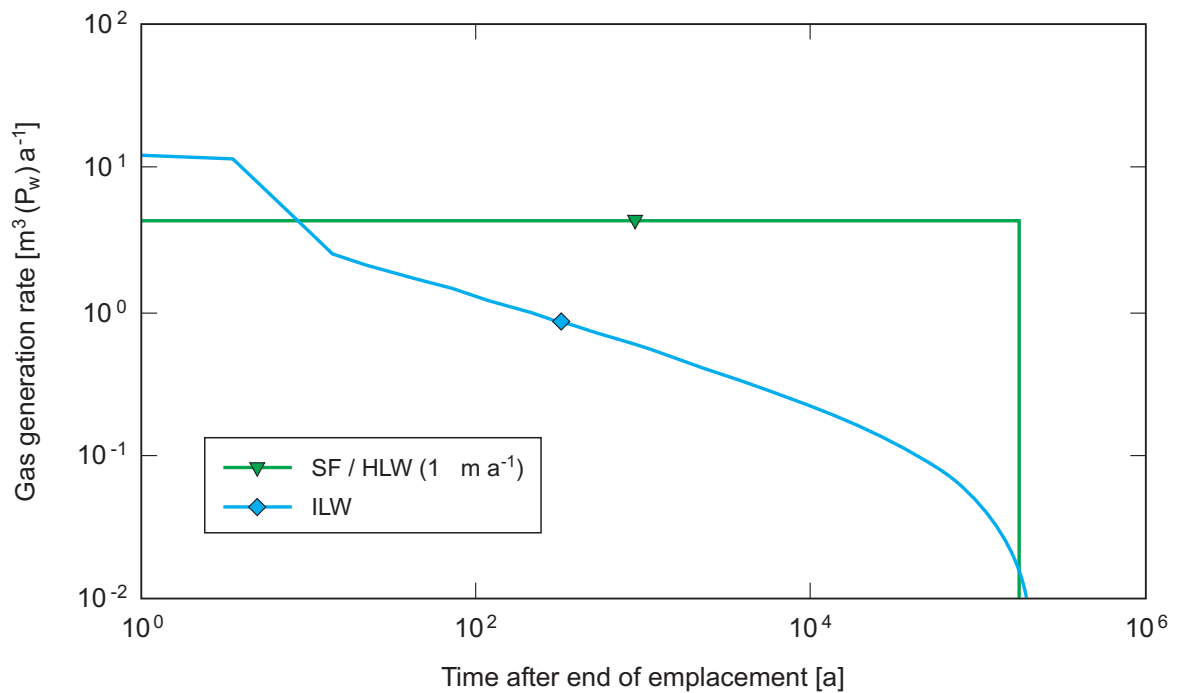


Fig. 4.3-13: Gas generation rate for SF / HLW (corrosion rate $1 \mu\text{m a}^{-1}$) and for ILW

4.3.4 Conclusions regarding pressure evolution and gas migration

- The calculations show that porewater displacement, capillary leakage by 2-phase flow and dilatant gas pathways in the Opalinus Clay mitigate the effects of gas pressure build-up in the SF/HLW/ILW repository. Gas dissolution in the near field and diffusion of dissolved gas are less efficient transport processes.
- Taking the gas accessible pore space available in the access tunnels of the ILW facility into account, it can be concluded that the gas pressure stays well below the thresholds for capillary leakage by 2-phase flow (11.5 MPa) and for pathway dilation (13 MPa).
- In the case of SF/HLW, the calculations show that the generated gas may be able to escape due to gas diffusion and capillary leakage by 2-phase flow through the tunnel walls, if the gas permeability of the Opalinus Clay is not too small ($\geq 10^{-22} \text{ m}^2$). For gas permeabilities $< 10^{-22} \text{ m}^2$ a significant network of dilatant gas pathways in the Opalinus Clay is likely to develop in the horizontal plane of the SF/HLW repository.
- After gas transport through the Opalinus Clay or, alternatively, through the access tunnel system, gas accumulates within the Wedelsandstein formation (with a radius of the free gas phase of up to 1.4 km). Gas diffusion through the low-permeability upper confining units leads to gas migration to the overlying Malm aquifer, where all gases are assumed to remain completely dissolved in the aqueous phase.

4.4 Dose due to volatile ^{14}C in the gas phase (Cases 2.1, 2.2 and 4.6)

4.4.1 Overview of the conceptual model

The objective of this model is to calculate doses for the release of radionuclides as volatile species in the gas phase from the repository to the biosphere. Calculations are performed for ^{14}C only, because ^{14}C is the only relevant volatile radionuclide in SF and ILW. For HLW, the contribution of volatile radionuclides to the total dose is insignificant.

After canister breaching, volatile ^{14}C is assumed to be instantaneously mixed with non-radioactive gases, the pressure evolution and migration of which are described in the previous sections. ^{14}C is thus distributed throughout a "gas storage volume", consisting of gas-filled pore space present in the near field (backfill), in the EDZ, in and around dilatant gas pathways created in the Opalinus Clay, in the access tunnel system and in the Wedelsandstein formation. The spatial distribution and evolution of gas-filled pore space in the repository system is modelled in a simplified way by considering three characteristic assessment cases (Tabs. 4.3-6 and 4.3-7). For each assessment case, the gas release rate to the Malm aquifer is calculated separately, considering vertical gas diffusion through the low-permeability formations of the upper confining units, but neglecting horizontal transport of dissolved gas by advection and diffusion within the Wedelsandstein formation. ^{14}C is then further diluted in the Quaternary aquifer, which is used as a source of drinking water.

4.4.2 Input parameters

The input parameters used in the model calculations related to the release of ^{14}C from the repository into the biosphere are summarised in the following tables. In Tabs. 4.4-1 and 4.4-2, the inventory for ^{14}C is given for SF and ILW, indicating the fraction of radionuclides that may be transformed into volatile species and that may be released instantaneously (IRF). Note that all ^{14}C contained in the SF waste matrix is assumed to be present in inorganic form, whereas all ^{14}C in the cladding is assumed to be in organic form. For both SF and ILW, the IRF corresponds to 20 % of the total cladding inventory, the remaining 80 % being released by congruent cladding dissolution³⁴. Tab. 4.4-3 gives an overview of all input parameters used in the model calculations.

Tab. 4.4-1: Data for ^{14}C for SF

Inventories from Tab. A3.4-2a, half life and dose coefficient from Tab. A3.4-1.

Radio-nuclide	Half life [a]	Dose coefficient for ingestion, DF^{ing} [mSv Bq ⁻¹]	Waste sort	Inventory after 40 years decay [Bq per canister]			Volatile fraction [-]
				BWR: 9 UO ₂	PWR: 3 UO ₂ +1 MOX	PWR: 4 UO ₂	
^{14}C	5.7×10^3	5.8×10^{-7}	Fuel matrix	inorganic ^{14}C only			0
			Cladding	4.6×10^{10}	2.5×10^{10}	2.9×10^{10}	1
			IRF	1.1×10^{10}	6.3×10^9	7.1×10^9	1
			Total (volatile fraction only)	5.7×10^{10}	3.1×10^{10}	3.6×10^{10}	

³⁴ Note that in the Reference Case, the dissolution of cladding contained in the ILW is assumed to occur instantaneously after containment failure.

Tab. 4.4-2: Data for ^{14}C for ILW

Inventories from McGinnes 2002, half life and dose coefficient from Tab. A3.4-1.

Radio-nuclide	Half life [a]	Dose coefficient for ingestion, DF_i^{ing} [mSv Bq ⁻¹]	Inventory after 40 years of decay		Volatile fraction [-]	IRF [-]
			Waste sort	Inventory [Bq]		
^{14}C	5.7×10^3	5.8×10^{-7}	WA-BNF-2	9.2×10^{12}	0	-
			WA-BNF-4	5.9×10^{12}	1	0.2
			WA-COG-4	3.2×10^{12}	1	0.2
			Total (volatile fraction only)	9.1×10^{12}		

Tab. 4.4-3: Summary of input parameters for the model calculations related to the release of volatile ^{14}C from SF and ILW

Parameter	Symbol	Unit	Value	Source
Volatile ^{14}C inventory	I_i, IRF_i $F_{i,m}, F_{i,c}$	Bq, -	Tab. 4.4-1 and 4.4-2	Tab. A3.4-2a McGinnes (2002)
Number of SF canisters				
BWR UO ₂ -48			935	Tab. A3.3-1, Parameter 6, Value A
PWR UO ₂ -48 + PWR MOX-48			450	
PWR UO ₂ -48			680	
SF canister breaching time	-	a	10^4	Tab. A3.3-1, Parameter 5, Value A
Corrosion rate of cladding	r_c	m a ⁻¹	1×10^{-8}	Tab. A3.3-2
Thickness of cladding	d_c	m	6×10^{-4}	
Gas storage volumes	V_g, V_w	m ³	time-dependent	Figs. 4.3-10, 4.3-11, 4.3-12
Gas generation rate in near field	$Q_{g,in}$	m ³ (STP) a ⁻¹	Tab. 4.3-1	Nagra (2003a)
Dilution rate in Quaternary aquifer	Q_B	m ³ a ⁻¹	1.5×10^6	Tab. A3.7-1
Pore volume of Quaternary aquifer	V_B	m ³	9.1×10^6	calculated from Tab. A3.7-1
Degassing factor	δ_i	-	1	No degassing assumed
Drinking water consumption rate	U	m ³ a ⁻¹	0.73	Tab. A3.7-3
Decay constant for ^{14}C	λ_i	a ⁻¹	1.2×10^{-4}	derived from Tab. A3.4-1
Dose coefficient for ingestion for ^{14}C	DF_i^{ing}	mSv Bq ⁻¹	5.8×10^{-7}	Tab. A3.4-1

5 Modelling the Release of Radionuclides Affected by Human Actions

5.1 Borehole penetration into the repository (Case 3.1)

5.1.1 Overview

The Reference Case is based on the assumption that there will be no future boreholes within or near the repository affecting the safety of the repository. This conceptualisation addresses the effects of a hypothetical borehole penetrating one of the emplacement tunnels, or, in the most extreme case, a spent fuel canister.

5.1.2 The conceptual model and its underlying assumptions

In the course of some future exploratory activity at the repository site in the Zürcher Weinland, an inadvertent borehole penetration of the repository is postulated. Besides the exposure of drilling personnel³⁵, long-term safety will be affected due to the fact that a direct pathway from the repository (or, in an extreme case, from a spent fuel canister) to the biosphere will exist for some period of time.

When drilling boreholes through rocks such as the Opalinus Clay, casings are required to stabilise the borehole. In the present assessment case, a single borehole, passing all the way through the Opalinus Clay, is assumed to penetrate an emplacement tunnel. The borehole is assumed to be abandoned without proper sealing and without removing the casing. Initially, the casing may be regarded as being impermeable to water inflow from the formation, preventing radionuclides to be released into the borehole. As corrosion progresses, the casing becomes leaky and the borehole will partially collapse, filling up with sedimented mud. At that time, radionuclides may enter, and migrate within, the borehole. When the casing is completely corroded, the borehole will collapse and finally self-seal due to swelling / disintegration of the Opalinus Clay. Short-term experiments show that the hydraulic conductivity of mud-filled boreholes may be in the order of 10^{-7} to 10^{-8} m s⁻¹ or even lower (Nagra 2002e). In the model calculations, it is pessimistically assumed that complete self-sealing of the borehole does not occur and that a steady-state water flux through the borehole is established.

Water flow in the borehole is driven by the hydraulic gradient between the local aquifers (directed upwards from the Sandsteinkeuper to the Wedelsandstein formation). No overpressure is assumed in the Opalinus Clay. Thus, the flow rate is primarily determined by the hydraulic conductivity of the borehole (partially filled with drilling mud and partially collapsed), assumed to be time-independent. The flow rate is estimated as:

$$Q_{BH} = \pi r_{BH}^2 (K_{BH} + (\gamma^2 - 1)K_{EDZ}) \frac{H_l - H_u}{L_l + L_u} \quad (5.1-1)$$

Q_{BH} water flow rate along the borehole (incl. EDZ) [m³ s⁻¹]

K_{BH} hydraulic conductivity of collapsed borehole [m s⁻¹]

K_{EDZ} hydraulic conductivity of the EDZ of the collapsed borehole [m s⁻¹]

³⁵ The calculation of the radiological consequences of the exposure of drilling personnel is outside the scope of this safety assessment, see Chapter 2 of Nagra (2002c).

r_{BH}	borehole radius [m]
γ	ratio of radii EDZ/borehole [-]
H_l	hydraulic head in Sandsteinkeuper (lower confining unit) [m]
H_u	hydraulic head in Wedelsandstein (upper confining unit) [m]
L_l	distance between repository and Sandsteinkeuper [m]
L_u	distance between repository and Wedelsandstein [m]

A wide range of hydraulic conductivities of the borehole is considered, ranging from 2×10^{-14} to 10^{-6} m s^{-1} (Fig. 5.1-1). This wide range represents the temporal variation of the hydraulic conductivities at different stages of self-sealing (Nagra 2002e), including the final state of a perfectly sealed borehole with identical hydraulic properties as in the Opalinus Clay matrix. The hydraulic conductivities of the borehole and of its EDZ are taken to be identical. Furthermore, unlimited availability of water in the penetrated Sandsteinkeuper formation is pessimistically assumed. In the model calculations for radionuclide release, steady-state borehole water flow rates of $10^{-4} - 1 \text{ m}^3 \text{ a}^{-1}$ are considered, corresponding to hydraulic conductivities in the borehole of $10^{-10} - 10^{-6} \text{ m s}^{-1}$.

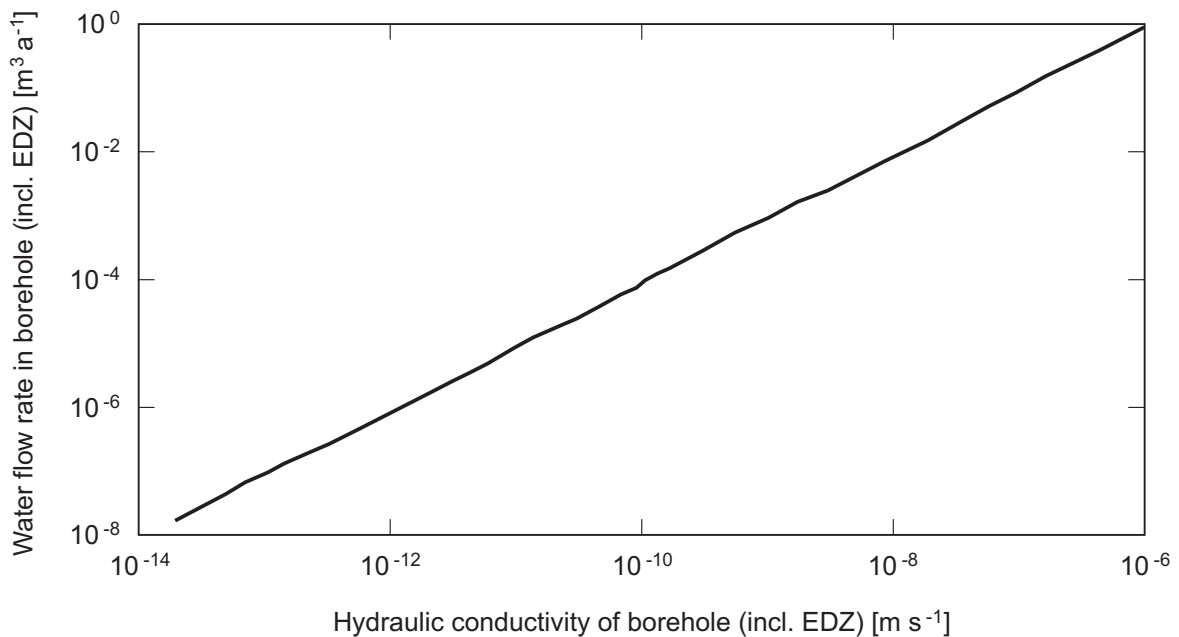


Fig. 5.1-1: Steady-state water flow rate in the borehole as a function of the hydraulic conductivity, taken to be identical in the borehole (partially filled with mud and partially collapsed, covering several stages of self-sealing) and in its EDZ

Instantaneous transport of radionuclides is assumed to take place upwards along the borehole into the Malm aquifer, and from there to the reference biosphere area.

Three cases are considered (Fig. 5.1-2):

- the borehole penetrates a SF/HLW emplacement tunnel between two canisters
- the borehole penetrates a SF canister (direct hit)
- the borehole penetrates an ILW-1 emplacement tunnel (direct hit).

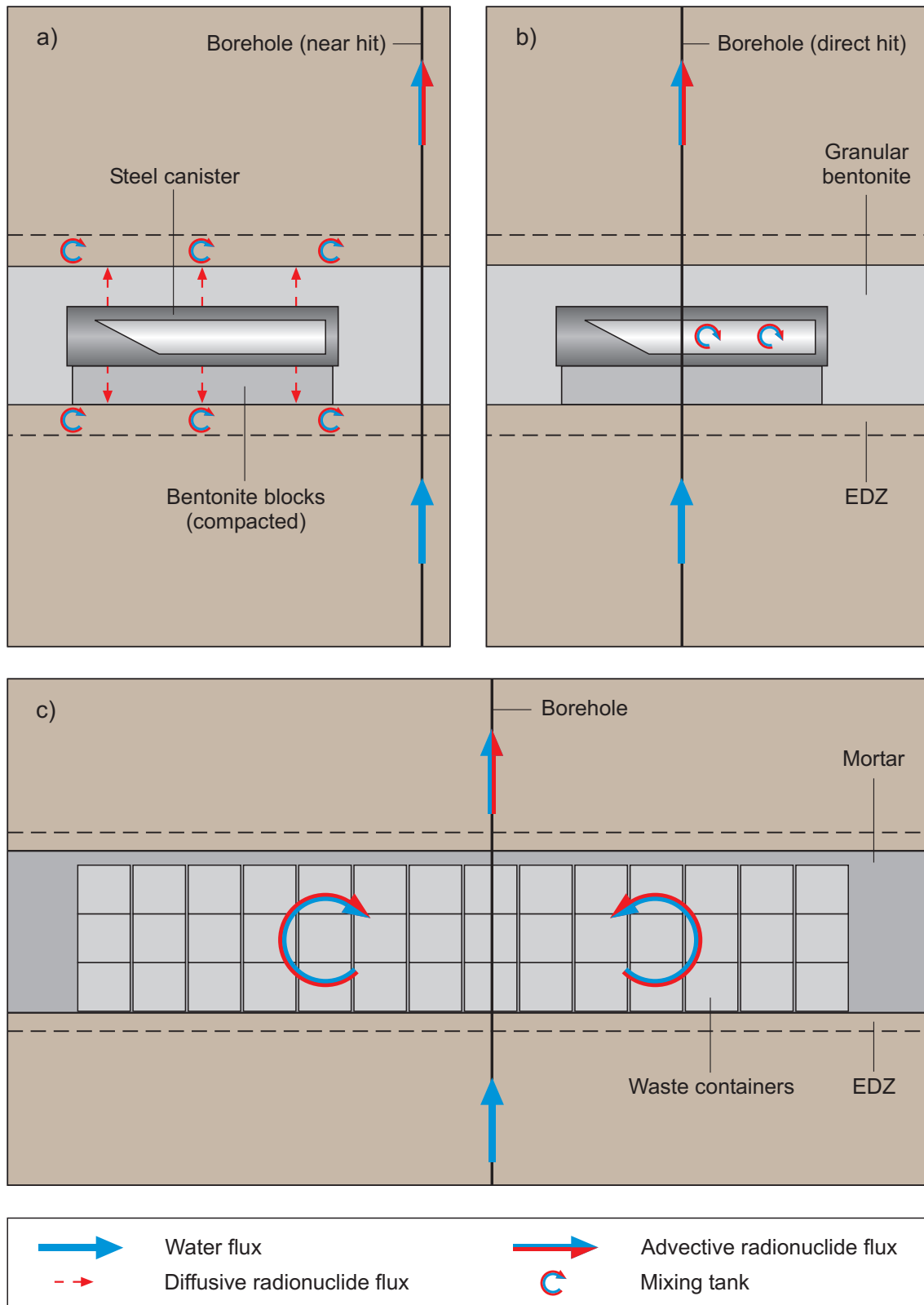


Fig. 5.1-2: Scheme of investigated variants of borehole penetration: a) SF/HLW (near hit), b) SF (direct hit), c) ILW-1

Base Case and parameter variations

Penetration of a SF/HLW emplacement tunnel between two canisters – near hit (Cases 3.1a-d)

The borehole is assumed to penetrate a SF/HLW emplacement tunnel midway between 2 canisters, shortly after canister failure. Based on current drilling technology, a borehole casing would be immediately emplaced in such a situation, thus limiting the extent of bentonite erosion. To span the range of possibilities, two cases are considered: i) The near field release of 2 canisters is discharged directly into the borehole (Base Case); ii) the near field release of 4 canisters is discharged directly into the borehole. Radionuclide retardation along the axis of the emplacement tunnel is pessimistically neglected. In both cases, the remainder of the radionuclides from the SF part of the repository is assumed to be released to the unperturbed clay matrix, but this dose contribution is not taken into account in the present case.

For the SF/HLW source term, a reference near field is assumed, with the exception of a changed boundary condition at the interface near field / geosphere using a range of flow rates (Base Case: $10^{-2} \text{ m}^3 \text{ a}^{-1}$, parameter variations of 10^{-4} and $1 \text{ m}^3 \text{ a}^{-1}$). These water fluxes are shared between the affected canisters. This boundary condition realistically represents the hydraulic conditions for the two SF/HLW canisters in the vicinity of the borehole, whereas it is considered to be pessimistic for the canisters further away from the borehole. Solubility limitations and sorption constants for reducing conditions are employed in the calculations. Radionuclides released from the near field are directly transported to the Reference Case biosphere, conservatively neglecting retardation in the partially collapsed borehole and during lateral transport to the biosphere.

Penetration of a SF canister - direct hit (Cases 3.1e-g)

The most severe case is that of a borehole drilled directly into a spent fuel canister. As long as the steel canister walls are entirely or partially intact, it is not considered feasible, with current drilling technology, to drill through the walls without detection. A direct hit is, therefore, not to be expected before about 10^5 years, i.e. before a substantial part of the canister wall has been corroded away. In the model calculations, a mixed PWR canister (3 PWR UO_2 -48 fuel elements + 1 PWR MOX-48 fuel element) is assumed to be penetrated at 10^5 years. It is conservatively assumed that no release of radionuclides takes place before the perforation of the canister by the borehole, and, after perforation, the release of dissolved radionuclides occurs directly from the canister to the reference biosphere area. The bentonite is assumed not to function as a diffusion barrier (zero diffusion length, no sorption). Solubility limitation in the reservoir and in the bentonite is neglected. For the hydraulic boundary condition between near field and host rock, water flow rates of 10^{-4} , 10^{-2} and $1 \text{ m}^3 \text{ a}^{-1}$ are used. Retardation of radionuclides along the partially collapsed borehole by sorption on the borehole infill and by diffusion / sorption in the Opalinus Clay matrix is neglected, as is retardation during lateral transport to the biosphere. The remainder of the SF/HLW part of the repository is assumed not to be affected by the borehole and its dose contribution is neglected in the present case.

Penetration of an ILW-1 emplacement tunnel (Cases 3.1a, 3.1c and 3.1d)

The borehole is assumed to penetrate an ILW-1 emplacement tunnel 500 years after the end of emplacement, i.e. when the information record on the repository may have been lost. Due to the connected pore space of the cementitious backfill, the entire emplacement tunnel is affected by the borehole, corresponding to half of the ILW-1 inventory. The dose contribution of the

remaining radionuclides from the other emplacement tunnels is not taken into account in the present case.

In the calculation of the ILW source term, a loss of the diffusion barrier is postulated. As in the Reference Case, instantaneous mixing of radionuclides within the entire emplacement tunnel is conservatively assumed. Solubility limitations and sorption constants for reducing conditions are employed in the calculations. The release of radionuclides from the near field is assumed to take place by advection through the borehole only, at a rate controlled by the flow rate in the borehole. The contributions of advection and diffusion to transport of radionuclides through the Opalinus Clay is neglected.

In reality, only a fraction of the radionuclide inventory contained in the ILW-1 emplacement tunnel is transported towards and released through the borehole, as shown by the following calculations (Fig. 5.1-3). The diffusive radionuclide fluxes from the ILW-1 emplacement tunnel radially into the Opalinus Clay, F_{HR} [mol a⁻¹], and axially towards the borehole, F_{BH} [mol a⁻¹], can be estimated as:

$$F_{HR} = 2\pi r_{ILW} (\Lambda_{ILW} - 2R_{BH}) D_{HR} \frac{C_0}{l_d} \quad (5.1-2)$$

$$F_{BH} = 2\pi r_{ILW}^2 D_C \frac{C_0}{R_{BH}}$$

with

r_{ILW}, A_{ILW}	radius and length of ILW-1 emplacement tunnel [m]
R_{BH}	distance of non-zero (axial) radionuclide concentration gradient in emplacement tunnel towards the borehole [m]
l_d	distance of non-zero (radial) radionuclide concentration gradient in Opalinus Clay [m]
D_{HR}	effective diffusion constant in Opalinus Clay [m ² s ⁻¹]
D_C	average effective diffusion constant of cementitious materials in emplacement tunnel [m ² s ⁻¹]
C_0	initial aqueous radionuclide concentration in emplacement tunnel [mol m ⁻³]

The fraction of the diffusive flux directed towards the borehole to the total diffusive flux, f [-], is thus:

$$f = \frac{F_{BH}}{F_{BH} + F_{HR}} = \frac{1}{1 + \frac{F_{HR}}{F_{BH}}} = \frac{1}{1 + \frac{(\Lambda_{ILW} - 2R_{BH}) R_{BH} D_{HR}}{r_{ILW} l_d D_C}} \quad (5.1-3)$$

Note that Eqs. 5.1-2 and 5.1-3 are valid for sorbing and non-sorbing radionuclides. Sorption in the Opalinus Clay and in the cementitious materials within the ILW-1 tunnel does, however, affect the magnitudes of the parameters l_d and R_{BH} , respectively.

For a realistic set of parameter values³⁶, $f \approx 0.5$. In the model calculations, it is therefore assumed that only half of the radionuclide inventory in the penetrated ILW-1 emplacement tunnel is actually available for release through the borehole.

The water flux in the borehole is varied over a broad range: $10^{-2} \text{ m}^3 \text{ a}^{-1}$ (Base Case) and 10^{-4} and $1 \text{ m}^3 \text{ a}^{-1}$ (parameter variations). Radionuclides released to the borehole are assumed to be directly transported to the Reference Case biosphere without considering any retention. Retardation of radionuclides along the partially collapsed borehole by sorption on the borehole infill and by diffusion into and sorption in the Opalinus Clay matrix is conservatively neglected, as is retardation during lateral transport to the biosphere.

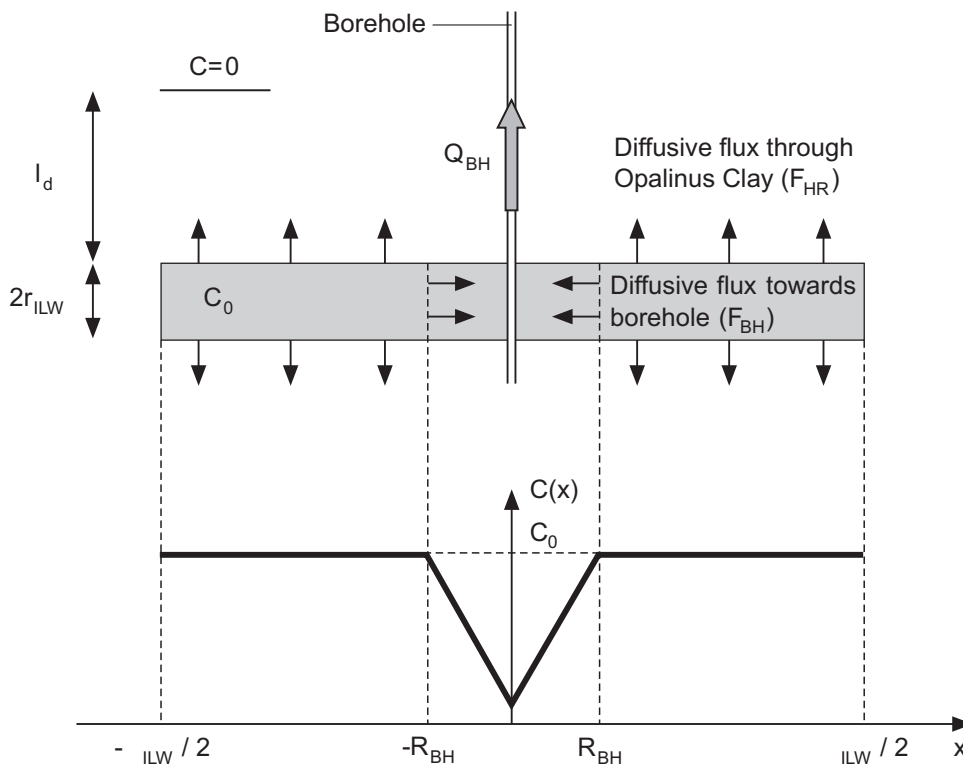


Fig. 5.1-3: Scheme for calculation of the diffusive fluxes from the ILW-1 emplacement tunnel radially into the Opalinus Clay and axially towards the borehole

5.1.3 Codes used

For the near field release and biosphere transport and dose calculations, the codes STMAN and TAME are used, as in the Reference Conceptualisation. No geosphere transport calculations are performed due to the assumed instantaneous transport of radionuclides through the borehole to the Malm aquifer, and from there to the reference biosphere.

³⁶ The following values have been assumed in the estimate for f : $r_{ILW} = 4.5 \text{ m}$, $A_{ILW} = 90 \text{ m}$, $R_{BH} = 4.5 \text{ m}$ (i.e. assuming that the radius of diffusive influence of the borehole is about equal to the tunnel radius), $l_d = 10 \text{ m}$, $D_{HR} = 10^{-11} \text{ m}^2 \text{ s}^{-1}$ (diffusion of non-anionic species perpendicular to bedding planes, see Tab. A3.5-5) and $D_C = 10^{-10} \text{ m}^2 \text{ s}^{-1}$. Note that for a large range of R_{BH} ($6 \text{ m} \leq R_{BH} \leq 35 \text{ m}$), $f < 0.5$.

5.1.4 Parameters

Base Case

In the Base Case, the borehole penetrates a SF/HLW emplacement tunnel midway between two canisters (near hit, 2 canisters affected), or, alternatively, an ILW-1 emplacement tunnel (direct hit). The Base Case water flow rate in the collapsed borehole is estimated using the input data in Tab. 5.1-1. Flow data and source term information for the Base Case are given in Tab. 5.1-2.

Tab. 5.1-1: Parameter values used for the calculation of the water flow rate in the collapsed borehole (Base Case)

Parameter	Symbol	Unit	Value	Source
Host rock				
Hydraulic head in Sandsteinkeuper	H_l	m	465	Tab. A3.3-4b
Hydraulic head in Wedelsandstein	H_u	m	342	
Distance from repository to Sandsteinkeuper	L_l	m	100	
Distance from repository to Wedelsandstein	L_u	m	40	
Borehole				
Radius	r_{BH}	m	0.05	assumed value
Ratio of radii EDZ/borehole	γ	-	2.0	assumed value
Hydraulic conductivity of collapsed borehole	K_{BH}	m s^{-1}	10^{-8}	Nagra (2002e)
Hydraulic conductivity of borehole EDZ	K_{EDZ}	m s^{-1}	$= K_{BH}$	assumed value

Tab. 5.1-2: Flow data and source term information (Base Case, see Tab. A3.2-1b in App. 3)

Input	Units	Values	Source
Flow Data			
Flow in borehole (Q_{BH})	$\text{m}^3 \text{a}^{-1}$	10^{-2}	calculated using Eq. 5.1-1 and $K_{BH} = 10^{-8} \text{m s}^{-1}$
Source term information			
Source flux	mol a^{-1}	Radionuclide releases obtained from the output of code STMAN as in Reference Case, except groundwater flow rate for mixing tank boundary condition (Q_{BH}) to be used for 2 SF canisters, or alternatively 2 HLW canisters, and for the entire ILW-1 emplacement tunnel, respectively.	
Fraction to each leg	dimensionless	SF/HLW: Release from 2 canisters directly to borehole (starting at 10 000 years), remainder of inventory not taken into account. ILW-1: Release of half of the inventory contained in a single ILW-1 tunnel to borehole (starting at 500 years), remainder of inventory not taken into account.	

Model variants (see Tab. A3.2-1b in Appendix 3):

- Variant 1: Near hit, 4 SF canisters, or alternatively 4 HLW canisters affected by borehole, Base Case flow rate (Tab. 5.1-4)
- Variant 2: Near hit, 2 SF canisters, or alternatively 2 HLW canisters or entire ILW-1 tunnel affected by borehole, increased flow rate in borehole (Tab. 5.1-5)
- Variant 3: Near hit, 2 SF canisters, or alternatively 2 HLW canisters or entire ILW-1 tunnel affected by borehole, decreased flow rate in borehole (Tab. 5.1-6)
- Variants 4–6: Direct hit, 1 SF canister affected, Base Case flow rate, increased flow rate and decreased flow rate in borehole, respectively (Tab. 5.1-7).

The water flow rates in the collapsed borehole are estimated using the input data in Tab. 5.1-3. Network flow data and source term information for the variants 1-6 are given in Tab. 5.1-4 to 5.1-7.

Tab. 5.1-3: Parameter values used for the calculation of water flow rates in the collapsed borehole

See text for a discussion of the parameter variations.

Parameter	Symbol	Unit	Value
Borehole			
Hydraulic conductivity of collapsed borehole	K_{BH}	$m s^{-1}$	10^{-8} (variants 1 and 4) 10^{-6} (variants 2 and 5) 10^{-10} (variants 3 and 6)
All other parameters as in Base Case.			

Tab. 5.1-4: Network flow data and source term information (variant 1)

Input	Units	Values	Source
Network Flow Data			
Flow in borehole (Q_{BH})	$m^3 a^{-1}$	10^{-2}	calculated using Eq. 5.1-1 and $K_{BH} = 10^{-8} m s^{-1}$
Source term information			
Source flux	$mol a^{-1}$	Radionuclide releases obtained from the output of code STMAN as in Reference Case, except groundwater flow rate for mixing tank boundary condition (Q_{BH}) to be used for 4 SF canisters.	
Fraction to each leg	dimensionless	SF: Release from 4 canisters directly to borehole (starting at 10 000 years), remainder of inventory to Reference Case geosphere leg.	

Tab. 5.1-5: Network flow data and source term information (variant 2)

Input	Units	Values	Source
Network Flow Data			
Flow in borehole (Q_{BH})	$m^3 a^{-1}$	1	calculated using Eq. 5.1-1 and $K_{BH} = 10^{-6} m s^{-1}$
Source term information			
Source flux	$mol a^{-1}$	Radionuclide releases obtained from the output of code STMAN as in Reference Case, except groundwater flow rate for mixing tank boundary condition (Q_{BH}) to be used for 2 SF canisters, or alternatively for 2 HLW canisters or for the entire ILW-1 emplacement tunnel, respectively.	
Fraction to each leg	dimensionless	SF/HLW: Release from 2 canisters directly to borehole (starting at 10 000 years), remainder of inventory not taken into account. ILW-1: Release of half of the inventory contained in a single ILW-1 tunnel to borehole (starting at 500 years), remainder of inventory not taken into account.	

Tab. 5.1-6: Network flow data and source term information (variant 3)

Input	Units	Values	Source
Network Flow Data			
Flow in borehole (Q_{BH})	$m^3 a^{-1}$	10^{-4}	calculated using Eq. 5.1-1 and $K_{BH} = 10^{-10} m s^{-1}$
Source term information			
Source flux	$mol a^{-1}$	Radionuclide releases obtained from the output of code STMAN as in Reference Case, except groundwater flow rate for mixing tank boundary condition (Q_{BH}) to be used for 2 SF canisters, or alternatively for 2 HLW canisters or for the entire ILW-1 emplacement tunnel, respectively.	
Fraction to each leg	dimensionless	SF/HLW: Release from 2 canisters directly to borehole (starting at 10 000 years), remainder of inventory not taken into account. ILW-1: Release of half of the inventory contained in a single ILW-1 tunnel to borehole (starting at 500 years), remainder of inventory not taken into account.	

Tab. 5.1-7: Network flow data and source term information (variants 4-6)

Input	Units	Values	Source
Network Flow Data			
Flow in borehole (Q_{BH})	$\text{m}^3 \text{a}^{-1}$		calculated using Eq. 5.1-1 and $K_{BH} = 10^{-8}, 10^{-6}, 10^{-10} \text{ m s}^{-1}$, respectively
variant 4		10^{-2}	
variant 5		1	
variant 6		10^{-4}	
Source term information			
Source flux	mol a^{-1}	Radionuclide releases obtained from the output of code STMAN: Zero bentonite thickness, no solubility limitation, no sorption, groundwater flow rate for mixing tank boundary condition (Q_{BH}) to be used for 1 SF canister.	
Fraction to each leg	dimensionless	SF: Release from 1 canister directly to borehole (starting at 100 000 years), remainder of inventory not taken into account.	

5.2 Deep groundwater extraction from Malm aquifer (Case 3.2)

5.2.1 Overview

In the conceptualisation "deep groundwater extraction from the Malm aquifer", the likely / expected broad evolutionary path of the disposal system is followed, as in the Reference Conceptualisation of the Reference Scenario. This conceptualisation differs from the Reference Conceptualisation, however, in that, rather than migrating to the Quaternary aquifer, radionuclides released from the host rock are captured by a deep well in the Malm aquifer used for the extraction of drinking water.

5.2.2 The conceptual model and its underlying assumptions

The conceptual model and its underlying assumptions are identical to those of the Reference Conceptualisation except in the treatment of radionuclides following their release to the confining units. In particular, a fraction of the radionuclides released to the upper confining units are assumed to enter the catchment area of a deep well located in the Malm aquifer that is used for drinking water, conservatively neglecting radionuclide retention and decay within the confining units. The resulting drinking water doses are calculated on the assumption that the well provides all the drinking water needed by the individuals the exposure of which is evaluated.

5.2.3 Codes used

The reference near field / geosphere model chain of STMAN-PICNIC is used to model the release and migration to the confining units. Drinking water doses arising from the consumption of water from the well are calculated using the equation:

$$D_{water} = \eta_{well} D_{ing} I_{water} \frac{J}{Q_{abs}} \quad (5.2-1)$$

where J [Bq a^{-1}] is the radionuclide release rate from the Opalinus Clay to the confining units calculated using PICNIC. The other symbols used are defined below. It is assumed that a proportion η_{well} of radionuclides reaching the upper confining units is captured by the well (the capture efficiency). It is further assumed that no sorption on the borehole walls occurs and that the water is not filtered.

5.2.4 Parameters

Base Case

The release of radionuclides from the near field and the geosphere are taken to be identical to those of the Reference Case. The dose per unit intake D_{ing} [Sv Bq^{-1}] is taken from Tab. A3.4-1 and the rate of ingestion of water I_{water} [$\text{m}^3 \text{a}^{-1}$] is set to 2 l d^{-1} (Tab. A3.7-3).

The pumping rate, Q_{abs} [$\text{m}^3 \text{a}^{-1}$], is taken to be $1.6 \times 10^5 \text{ m}^3 \text{a}^{-1}$ (300 l min^{-1}), which is considered to be a reasonable minimum rate for a viable drinking water well. For comparison, the lowest pumping rate from the Malm aquifer in a range of hydrogeothermal boreholes in southern Germany is 160 l min^{-1} , but that particular borehole is only used as a sampling point. All other boreholes have substantially larger pumping rates (Bertleff et al. 1988).

There is significant uncertainty related to the capture efficiency of the deep well. Because the source of radionuclides released to the Malm aquifer is distributed over an area approximately as large as the repository area (plane source resulting from predominantly vertical release of radionuclides through the Opalinus Clay and confining units), the well is likely to catch only a small fraction of all radionuclides released. A 10 % capture efficiency is assumed in the Base Case. The dose contribution of the remainder of the radionuclides is not taken into account in the present conceptualisation.

Parameter variation

In a parameter variation, a capture efficiency of 100 % is chosen. This is an extremely pessimistic assumption and covers all conceivable situations.

5.3 Abandoned repository (Case 3.3)

5.3.1 Overview

This conceptualisation differs from the Reference Case in that the repository is assumed to be abandoned in the observational period without proper backfilling/sealing of the access tunnel system. All emplacement tunnels and part of the operations/construction tunnels are, however, assumed to be fully backfilled/sealed during or shortly after emplacement, respectively.

5.3.2 The conceptual model and its underlying assumptions

After the abandonment of the repository, it is assumed that no maintenance activity of the open part of the access tunnel system will be undertaken (see Fig. 2.1-5). As a result of saturation and creep of the Opalinus Clay, the initially open lined tunnels collapse. This causes a triangular shaped progressive damage zone above the abandoned tunnels, with debris of rock and liner falling down into the tunnel (Nagra 2002a).

The minimal transport distance (within properly backfilled/sealed tunnel segments) between any waste package, emplaced in the main facility or pilot facility, and the abandoned part of the tunnel is 100 m (Fig. 2.1-5). This minimal transport distance provides an efficient barrier against water flows (hydraulic barrier) and radionuclide migration (transport barrier), so that most radionuclides decay before they reach the abandoned part of the access tunnel system. Any non-decayed radionuclides arriving in the abandoned tunnel segments are conservatively assumed to be instantaneously released to the Wedelsandstein formation via the pathway through the damage zone around or through the abandoned tunnels.

The model calculations of radionuclide transport are performed in the same way as in Section 3.6 (case related to the release of radionuclides affected by ramp/shaft), except for the transport barrier provided by the tunnel segments between sealing zones n1, n3 and s1 and the ramp (the abandoned tunnel sections), which is conservatively neglected in the present transport calculations (see Fig. 3.6-1). Thus, the backfilled/sealed tunnel segments and the EDZ of the shaft are modelled as equivalent porous media, where radionuclide transport occurs at a rate controlled by the water flows in the tunnel system (calculated below) and by sorption. Once the radionuclides arrive in the non-sealed ramp and subsequently in the Wedelsandstein formation, instantaneous transport to the Reference Case biosphere is conservatively assumed.

The water fluxes in the abandoned SF/HLW/ILW repository are calculated analytically by means of a steady-state resistor network model, which is very similar to the model employed in Section 3.6 (Fig. 3.6-1). The major conceptual difference is that the inflow of water from the Opalinus Clay to the higher permeable collapsed tunnel segments is taken into account as follows:

$$Q_Z = \eta \left(\frac{H_l - H_1}{L_l} + \frac{H_u - H_1}{L_u} \right) \quad \text{with} \quad \eta = 4\gamma r K_{HR} l_Z \quad (5.3-1)$$

K_{HR}	hydraulic conductivity of host rock [m s^{-1}]
r	radius of abandoned tunnel segments [m]
l_Z	total length of abandoned tunnel segments [m]
γ	ratio of radii EDZ/tunnels [-]
H_1	hydraulic head in abandoned tunnel segments [m]
H_l	hydraulic head in Sandsteinkeuper (lower confining unit) [m]
H_u	hydraulic head in Wedelsandstein (upper confining unit) [m]
L_l	distance from mid Opalinus Clay to Sandsteinkeuper [m]
L_u	distance from mid Opalinus Clay to Wedelsandstein [m]

The water flow rates calculated by the resistor network model are shown in Fig. 5.3-1 for a wide range of hydraulic conductivities of the collapsed tunnels. Fig. 5.3-1 clearly shows that for conductivities above 10^{-9} m s^{-1} , the water fluxes in the tunnel system are insensitive to any further increase of the conductivity. The conductivity of 10^{-9} m s^{-1} can be interpreted as a threshold value, above and below which the water fluxes in the tunnel system are controlled either by the inflow of water from the Opalinus Clay or by the resistance of the tunnel system. For the purpose of the hydraulic calculations presented in this section, it is assumed that the residual hydraulic conductivity of the collapsed tunnels is 10^{-8} m s^{-1} , and that the water flow rates in the tunnel system are not affected by the damage zone around the collapsed tunnels.

The results of the resistor network model are compared with the results from a 3D hydro-dynamic finite element model, for a hydraulic conductivity of the abandoned tunnel segments of 10^{-8} m s^{-1} (see Section 7.8 in Nagra 2002a). Analytical and numerical water flow rates, calculated at several different locations in the repository, are compared in Fig. 5.3-2. The numerical analysis is based on the case RLU02 (Tab. 7.8-2 in Nagra 2002a)³⁷. The water flow occurs at the same time vertically from the Sandsteinkeuper formation to the Wedelsandstein formation (top of Opalinus Clay) and along the abandoned tunnels through the ramp. Only small amounts of water are deviated towards the shaft. The numerical and analytical water flow rates are in fair agreement. An exception is location *n2*, where the numerically calculated flow is directed towards the SF/HLW emplacement tunnels, whereas the analytically calculated flow is directed towards the shaft. As in case RLU0, this difference is due to variability of the head distribution within the plane of the repository caused by small variations of the distance from the tunnels to the (non-planar) top of the Opalinus Clay. This small variability in the external head distribution is not taken into account in the analytical model.

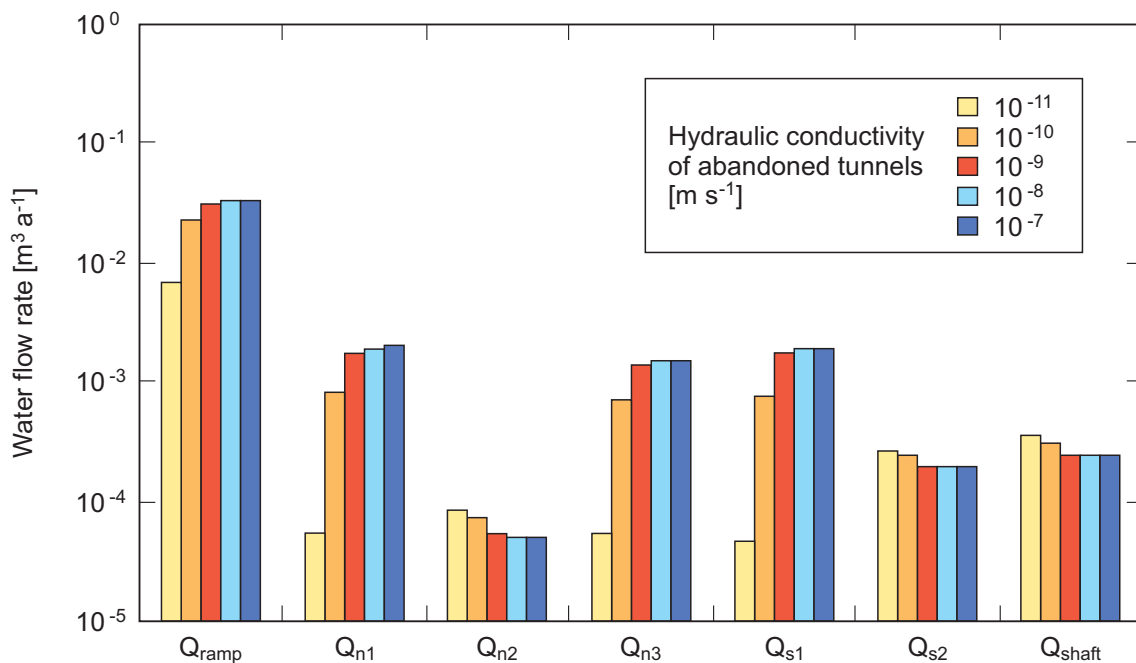


Fig. 5.3-1: Water flow rates obtained from the resistor network model calculations for the case of an abandoned repository for different hydraulic conductivities of the abandoned tunnel

The various locations in the repository are labelled according to Fig. 3.6-1a.

³⁷ The case RLU02 involves vertical groundwater movement driven by the hydraulic head difference between the Sandsteinkeuper and the Wedelsandstein formation and takes into account higher permeable tunnel sections (10^{-8} m s^{-1}) representing partially collapsed tunnels as a consequence of an abandonment of the repository.

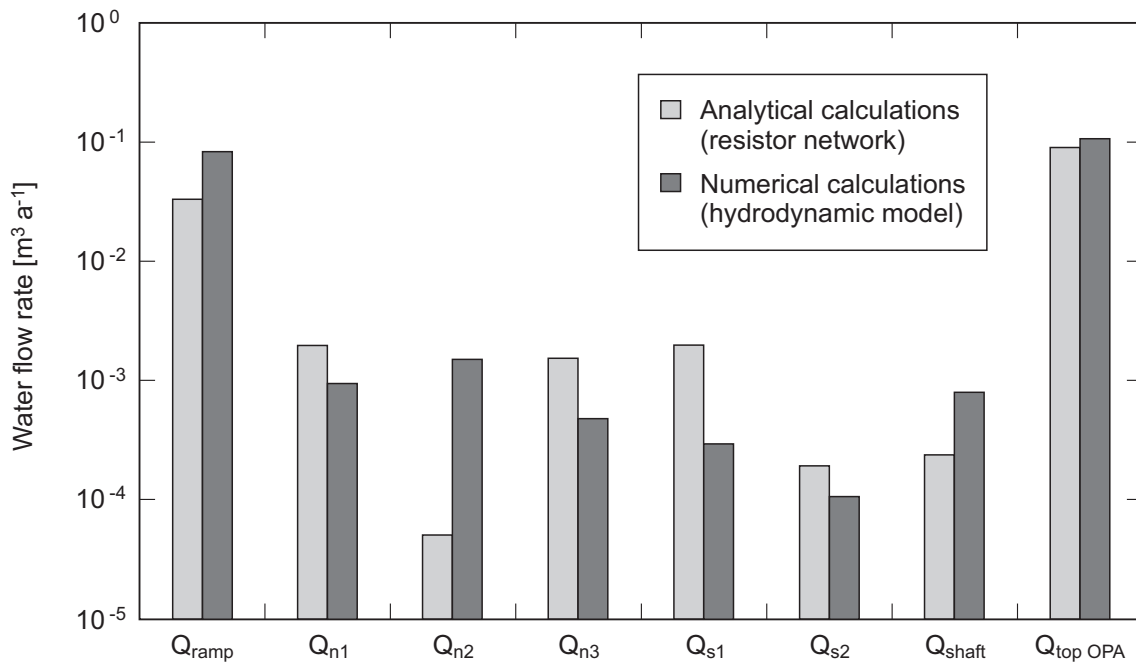


Fig. 5.3-2: Comparison of water flow rates obtained from the resistor network model calculations, described in the present section, and the numerical hydrodynamic model calculations for case RLU02, described in Nagra (2002a)

The various locations in the repository are labelled according to Fig. 3.6-1a. In both cases, the hydraulic conductivity of the higher permeable tunnel sections is 10^{-8} m s^{-1} , and the effect of the damage zone around these tunnel sections is neglected. Note that the numerical and analytical fluxes at node n2 point in opposite directions.

5.3.3 Codes used

As in the Reference Conceptualisation, the reference model chain of STMAN-PICNIC-TAME is used to model the radionuclide release, migration and distribution in the biosphere. The network capabilities of PICNIC are employed to model the simultaneous transport of radionuclides through the Opalinus Clay, the ramp and the shaft.

The PICNIC network structure used for this problem is similar to the structure depicted in Fig. 3.6-5. Again, the legs L_1 - L_5 represent the transport path through the access tunnel system, with the only difference that legs L_1 and L_2 represent here the backfilled tunnel segments (with a length of 100 m instead of 1 000 m) located inside the sealing zones n1, n3 and s1. As in Section 3.6, the legs $L_{6,A}$, $L_{6,B}$, $L_{6,C}$ and L_7 represent upward vertical transport through the Opalinus Clay from SF/HLW (domains A, B, C) and ILW (domain D), respectively. The water flow rates Q_i ($i = n1, n2, n3, s1, s2, \text{ramp, shaft, A, B, C, D}$) are calculated using Eq. 3.6-9, taking Eq. 5.3-1 into account.

5.3.4 Parameters

Base Case

The parameter values used for the calculation of water flow rates (resistor network) in the Base Case are identical to those listed in Tab. 3.6-1, with the exception of the hydraulic conductivity of the abandoned tunnel segments set at 10^{-8} m s^{-1} (Tab. 5.3-1). Network flow data and source term information are given in Tab. 5.3-2. Note that even in the present case related to the abandonment of the repository, most of the radionuclide inventory still is released through the Opalinus Clay. Transport parameters for leg L_1 to L_7 are identical to those listed in Tabs. 3.6-3 to 3.6-5, with the exception of the Darcy velocities (all legs) and lengths (legs L_1 and L_2 only), see Tab. 5.3-3.

Tab. 5.3-1: Additional parameter values used for the calculation of water flow rates in the resistor network

Parameter	Symbol	Unit	Value
Hydraulic conductivity of abandoned tunnel ($i =$ abandoned tunnel segments only)	$K_{i,BF}$	m s^{-1}	10^{-8} (10^{-7} to 10^{-11})
All other parameters			Identical to parameter values in Tab. 3.6-1

Tab. 5.3-2: Network flow data and source term information (calculated based on parameter values listed in Tabs. 3.6-1 and 5.3-1)

Input	Units	Values
Network Structure		
List of junction names. Inlet and outlet junctions for each leg.	-	Similar to Fig. 3.6-5, but legs L ₁ and L ₂ represent here the backfilled tunnel segments (with a length of 100 m instead of 1 000 m) located inside the sealing zones n1, n3 and s1.
Network Flow Data		
Flows		
Q _{ramp}		3.3×10^{-2}
Q _{n1}		1.9×10^{-3}
Q _{n2}		5.0×10^{-5}
Q _{n3}		1.5×10^{-3}
Q _{s1}		1.9×10^{-3}
Q _{s2}		1.9×10^{-4}
Q _{shaft}		2.4×10^{-4}
SF/HLW Q _{OPA}		8.6×10^{-2} (upwards, summed over domains A, B and C)
ILW Q _{OPA}		1.1×10^{-3} (upwards, domain D)
Source term information		
Source flux	mol a ⁻¹	Radionuclide releases obtained from the output of code STMAN (Reference Case source term for domain B, 10-fold increased groundwater flow rate for domains A,C,D)
Fraction to each leg:		Fraction to each leg (including diffusion, see Eq. 3.6-12):
f _{A,HR}		0.99951
f _{A,n1}		4.8×10^{-4}
f _{A,n2}		1×10^{-5}
f _{C,HR}		0.99947
f _{C,s1}		4.8×10^{-4}
f _{C,s2}		5×10^{-5}
f _{D,HR}		0.9981
f _{D,n3}		1.9×10^{-3}

Tab. 5.3-3: PICNIC input data for legs L_1 , L_2 , L_3 and L_4 which represent axial transport through the backfill of the operations tunnel, construction tunnel and ventilation tunnel, and legs L_5 and $L_{6,A}$, $L_{6,B}$, $L_{6,C}$, L_7 , which represent upward vertical transport through the EDZ of the shaft (L_5) and through the Opalinus Clay (L_6 , L_7), respectively

Input	Units	Values	Source
<i>Leg Data – Basic Data</i>			
Length L_1 , L_2	m	100	Tab. A3.2-2b, Parameter 3, Value H
Darcy velocity L_1 (SF/HLW) L_1 (ILW) L_2 L_3 L_4 L_5 (shaft EDZ) $L_{6,A}$, $L_{6,B}$, $L_{6,C}$ (OPA) L_7 (OPA)	m a^{-1}	8.3×10^{-5} 6.5×10^{-5} 8.3×10^{-5} 2.2×10^{-6} 8.3×10^{-6} 1.8×10^{-5} 5.4×10^{-7} 2.8×10^{-7}	Calculated from water flow rates in Tab. 5.3-2 and cross sectional areas (see also Tab. A3.2-2b, Parameter 5, Value L)
All other leg parameters		Identical to parameter values in Tabs. 3.6-3, 3.6-4 and 3.6-5	

Parameter variations

No parameter variations are performed.

6 Modelling "what if?" Cases to Investigate the Robustness of the Disposal System

6.1 High water flow rate in geosphere (Case 4.1)

6.1.1 Overview

In the "what if?" case "high water flow rate in the geosphere", the upwardly directed water flow rate in the Opalinus Clay is hypothetically increased by a factor of 100 with respect to the Reference Case. Such an increase is not supported by scientific evidence. The present assessment case is, therefore, regarded as a "what if?" case.

6.1.2 Codes used

As in the Reference Case, the reference model chain of STMAN-PICNIC-TAME is used to model the radionuclide release, migration and distribution in the biosphere.

6.1.3 Parameters

Base Case

The Base Case parameters are the same as those of the Reference Case, except for a 100-fold increase in the groundwater flow used in the near field and geosphere model calculations (Tab. A3.2-1c, Parameter 35, Value E and Tab. A3.2-2c, Parameter 5, Value E).

Deterministic parameter variations

No deterministic parameters variations are performed for this "what if?" case.

Probabilistic parameter variations

The present "what if?" case has also been analysed probabilistically. The water flow rate in the Opalinus Clay has been set to $2 \times 10^{-12} \text{ m s}^{-1}$ (i.e. a 100-fold increase with respect to the Reference Case), while all other parameters have been sampled from their PDFs as in the probabilistic analysis of the Reference Conceptualisation (see Tab. A3.10-1 in Appendix 3).

6.2 Transport along transmissive discontinuities (Case 4.2)

6.2.1 Overview

In the Reference Case, any discontinuities present in the Opalinus Clay are considered not to be significantly hydraulically different from the intact Opalinus Clay rock matrix. In the present conceptualisation a small number of permeable discontinuities are hypothetically postulated to be present in the Opalinus Clay. These permeable features result in advective transport of radionuclides predominantly along the plane of the discontinuities, with matrix diffusion into the rock matrix. As discussed in Sections 5.2.2 and 5.5.3.2 of Nagra (2002c), no credible mechanism has been identified that could lead to discontinuities with enhanced hydraulic transmissivity. The present assessment case is, therefore, regarded as a "what if?" case.

6.2.2 The conceptual model and its underlying assumptions

The near field model and its underlying assumptions are identical to those of the Reference Case, except that a more pessimistic boundary condition is imposed at the outer boundary of the near field in the vicinity of the discontinuity. In the case of SF/HLW, a zero concentration condition is imposed at the outer boundary of the bentonite for the canisters near to the discontinuity: i.e. $C_{GW}^n = 0$ in Eq. A1.3-15 of Appendix 1. This boundary condition represents the relatively high flow hydraulic conditions near to where a discontinuity intersects the outer boundary of the bentonite. In the case of ILW, a mixing tank boundary condition is imposed with a flow rate, Q [$\text{m}^3 \text{s}^{-1}$], calculated as follows:

$$Q = 2T i D n \quad (6.2-1)$$

T [$\text{m}^2 \text{s}^{-1}$] denotes the transmissivity of the intersecting discontinuity, i [m m^{-1}] is the hydraulic gradient, D [m] is the diameter of the EDZ (inner zone), and n is the number of ILW tunnels intersected ($n = 2$ for ILW-1 and $n = 1$ for ILW-2). A factor of 2 is included to take account of the convergence of flow lines towards the emplacement tunnels.

The geosphere model differs from that of the Reference Case in that the effects of the discontinuities on radionuclide transport through the host rock are taken into account. The transmissivities of the discontinuities are assumed to be constant in space and time; i.e. self-sealing is postulated not to occur. One or more vertical discontinuities are assumed to intersect all the SF/HLW emplacement tunnels, and a single discontinuity is assumed to intersect the ILW tunnels. The hydraulic gradient along the discontinuities is assumed to be the same as that within the Opalinus Clay matrix in the Reference Case.

In the case of SF/HLW, radionuclide release from the near field is partitioned into different fractions that are treated independently in the geosphere transport model. These are:

- the fraction of the release that occurs near to where the repository tunnels are intersected by particular discontinuities, and is captured by these discontinuities and transported along them by flowing groundwater, and
- the remaining fraction that is released from the near field further away from discontinuities, which is treated as in the Reference Case (near field and geosphere).

Each discontinuity is assumed to affect all 27 SF/HLW emplacement tunnels, and is assumed to capture the release from one canister in each tunnel, i.e. the release from a total of 22 PWR mixed UO_2/MOX canisters and 5 BNFL HLW canisters is assumed to be captured by each discontinuity. In the Case of ILW, because of the greater degree of mixing within the cementitious buffer compared to the bentonite, all radionuclides are assumed to be captured by a discontinuity.

Radionuclide transport along the discontinuities takes place by advection / dispersion and is retarded by matrix diffusion and sorption in the matrix. Matrix diffusion from the discontinuities laterally into the Opalinus Clay matrix is limited to approximately half the canister pitch in the case of SF/HLW and is unlimited in the case of ILW. The governing equation for radionuclide transport along the discontinuities is Eq. A1.6-4, and the equation for matrix diffusion is Eq. A1.6-8.

6.2.3 Codes used

As in the Reference Case, the reference model chain of STMAN-PICNIC-TAME is used to model the radionuclide release, migration and distribution in the biosphere. The network capabilities of PICNIC are employed to model transport through the undisturbed Opalinus Clay and through the discontinuities.

The network structure used for this problem is depicted in Fig. 6.2-1. The leg L_1 represents the path through the undisturbed Opalinus Clay that conveys the fraction of the SF/HLW release that is not captured by discontinuities ($R_{SF,1} + R_{HLW,1}$), and is modelled as in the Reference Case. The leg L_2 represents the path through the discontinuities that conveys the fraction of the SF/HLW release that is captured ($R_{SF,2} + R_{HLW,2}$), and also the ILW release (R_{ILW}). All discontinuities are assumed to be identical and can be modelled using a single leg. The number of discontinuities only affects the fraction of the SF/HLW release that is captured.

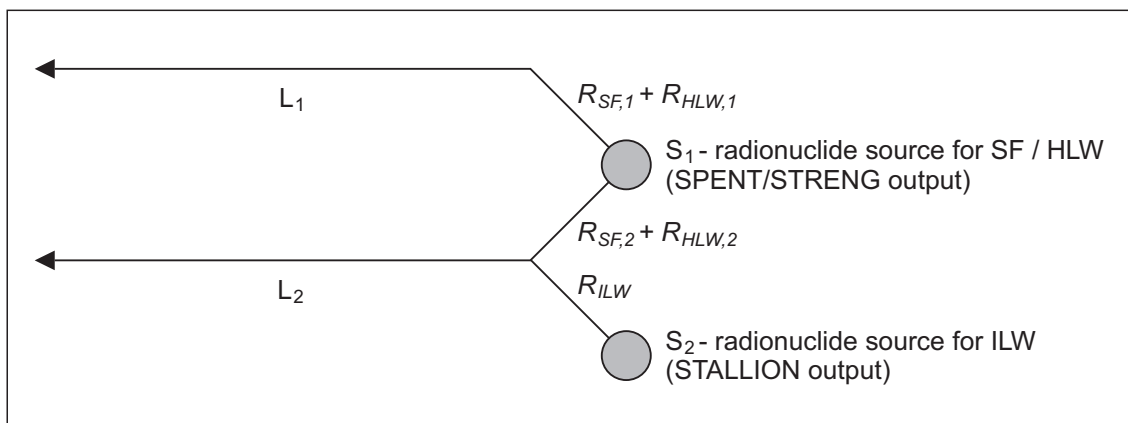


Fig. 6.2-1: The PICNIC network structure used to model the "what if?" case "transport along transmissive discontinuities in the host rock" (Case 4.2)

SPENT, STRENG and STALLION are the components of the near-field code STMAN used to calculate SF, HLW and ILW near field releases, respectively.

6.2.4 Parameters

Base Case

The Base Case parameters for STMAN are the same as those of the Reference Case. For the canisters located nearest to the discontinuity (one canister per emplacement tunnel), however, a zero concentration condition is imposed at the outer boundary of the bentonite (Tab. 6.2-1). Network flow data and source term information for PICNIC are given in Tab. 6.2-2. The release calculations for SF/HLW are based on the assumption that there is a single discontinuity capturing the release from one canister in each of the 27 intersected tunnels, the remainder of the SF/HLW near field release being transported through the Opalinus Clay, as in the Reference Case.

In the case of the ILW part of the repository, a mixing tank boundary condition is assumed, with a water flow rate of 0.14 m³ a⁻¹ (ILW-1) and 0.05 m³ a⁻¹ (ILW-2), calculated using Eq. 6.2-1. These water flow rates are based on a hydraulic transmissivity of $T = 10^{-10} \text{ m}^2 \text{ s}^{-1}$, a hydraulic gradient of 1 m m⁻¹ and a trace length of the discontinuity corresponding to twice the EDZ inner zone diameter of 11 m (ILW-1) and 7.8 m (ILW-2).

PICNIC input data for leg L₁ are the same as in the Reference Case. Input data for leg L₂, which represents the discontinuities, are given in Tab. 6.2-3. The discontinuities are treated as parallel walled fractures of aperture $2b = 10^{-3} \text{ m}$ (arbitrary assumption). The hydraulic conductivity of the leg L₂, $K \text{ [m a}^{-1}\text{]}$, is obtained from the equation:

$$\frac{K}{\varepsilon} = \frac{T}{2b}, \tag{6.2-2}$$

where $T = 10^{-10} \text{ m}^2 \text{ s}^{-1}$ is the transmissivity of the discontinuity and ε is the flow porosity of the leg (set to 1). The specific surface of the leg is equal to $1/b$.

Tab. 6.2-1: STMAN near field / geosphere properties differing from the Reference Case

Input	Units	Values	Source
Interface Near field / Geosphere Properties			
Mixing cell flow rate per waste package	m ³ a ⁻¹	Tab. A3.2-1c, Parameter 35, Value G (applied to 22 SF canisters and 5 HLW canisters) Tab. A3.2-1c, Parameter 35, Value L (applied to ILW)	

Tab. 6.2-2: Network flow data and source term information

Input	Units	Values	Source
Network Structure			
List of junction names. Inlet and outlet junctions for each leg.	-		Fig. 6.2-1
Network Flow Data			
Hydraulic head	m m ⁻¹	1	Tab. A3.3-4a
Hydraulic transmissivity	m ² s ⁻¹	10 ⁻¹⁰	Tab. A3.3-4b
Source Term Information			
Source flux	mol a ⁻¹	S ₁ – radionuclide releases to host rock obtained from the output of codes SPENT and STRENG. S ₂ – radionuclide releases to host rock obtained from the output of codes STALLION	
Fraction to each leg	dimensionless	S ₁ – release of 22 SF canisters and 5 HLW canisters to leg L ₂ (Base Case); remainder to leg L ₁ S ₂ – all release to leg L ₂	

Tab. 6.2-3: PICNIC input data for leg L₂, which represents transport through a discontinuity

Input	Units	Values	Source
Leg Data – Basic Data			
Length	m	40	Tab. A3.2-2c, Parameter 3, Value E
Darcy velocity	m a ⁻¹	3.2	Calculated from Eq. 6.2-1, assuming a hydraulic gradient of 1 m m ⁻¹ and a transmissivity of 10 ⁻¹⁰ m ² s ⁻¹ (see also Tab. A3.2-2c, Parameter 5, Value X)
Pore diffusion coefficient	m ² a ⁻¹	6.3 × 10 ⁻²	Tab. A3.2-2c, Parameter 7, Value C (free water)
Leg Data – Properties of Flowing Region			
Retardation	dimensionless	Irrelevant (no infill in discontinuity)	
Grain density	kg m ⁻³		
Flow porosity	dimensionless	1	Tab. A3.2-2c, Parameter 9, Value C (no infill)
Infill porosity	dimensionless	Irrelevant (no infill in discontinuity)	
Porosity factors	dimensionless		
Sorption K _d	m ³ kg ⁻¹		
Leg Data – Properties of Matrix			
Specific surface area	m ² m ⁻³	2 000	Tab. A3.2-2c, Parameter 12, Value B
Maximum penetration depth	m	Limited to half the canister pitch in the case of SF/HLW and unlimited in the case of ILW	Tab. A3.2-2c, Parameter 13, Value C
Surface sorption K _d	m ³ m ⁻²	Set to zero (sorption on fracture surfaces conservatively neglected)	
Retention	dimensionless	Calculated from the parameters below.	
Grain density	kg m ⁻³	2 720	Tab. A3.2-2c, Parameter 15, Value B
Matrix porosity	dimensionless	0.12 × porosity factors	Tab. A3.2-2c, Parameter 16, Value C
Porosity factors	dimensionless		
Sorption K _d	m ³ kg ⁻¹	Values for Opalinus Clay	Tab. A3.2-2c, Parameter 17, Value C
Pore diffusion coefficients	m ² a ⁻¹	anions: 2.6 × 10 ⁻³ (8.3 × 10 ⁻¹¹ m ² s ⁻¹) non-anions: 1.3 × 10 ⁻² (4.2 × 10 ⁻¹⁰ m ² s ⁻¹)	Tab. A3.2-2c, Parameter 18, Value B (Identical to pore diffusion constant parallel to strata in Opalinus Clay)

Deterministic parameter variations

In a deterministic parameter variation, the effect of two discontinuities rather than one intersecting all SF and HLW is investigated. It is also assumed that the release from two rather than one canister in each tunnel is captured by each discontinuity. In further deterministic parameter variations, the transmissivity of the discontinuities is hypothetically increased to $T = 10^{-9} \text{ m}^2 \text{ s}^{-1}$ (Tab. 3.3-4b) corresponding to a Darcy velocity of 32 m a^{-1} .

Probabilistic calculations

The present "what if?" case has also been analysed probabilistically. The transmissivity of the discontinuity has been set to $10^{-10} \text{ m}^2 \text{ s}^{-1}$ and the hydraulic gradient within the discontinuity kept constant at its Reference Case value of 1 m m^{-1} . The geometry of the discontinuity is left unchanged, with the exception of the transport path length, which is varied as in the probabilistic analysis of the Reference Conceptualisation. The effective diffusion constant parallel to the bedding planes of the Opalinus Clay matrix, used in leg L_2 (Fig. 6.2-1), is sampled probabilistically, while it is assumed to be strongly correlated with the effective diffusion constant perpendicular to the bedding planes, used in leg L_1 (correlation coefficient equal to 1). Likewise, the K_d values for the Opalinus Clay used in legs L_1 and L_2 are probabilistically sampled, but are taken to be fully correlated.

All other parameters have been sampled from their PDFs as in the probabilistic analysis of the Reference Conceptualisation (see Tab. A3.10-1 in Appendix 3).

6.3 SF: Increased fuel dissolution rate (Case 4.3)

6.3.1 Overview

In the "what if?" case "increased fuel dissolution in spent fuel", the rate of fuel dissolution is increased by a factor of 10 and 100 with respect to the Reference Case.

6.3.2 The conceptual model and its underlying assumptions

The conceptual model and its underlying assumptions are identical to those of the Reference Case, except for the rate assumed for spent fuel dissolution. The increased rate is outside the range supported by scientific evidence, which is why this is classified as a "what if?" case.

6.3.3 Codes used

As in the Reference Case, the reference model chain of STMAN-PICNIC-TAME is used to model the radionuclide release, migration and distribution in the biosphere.

6.3.4 Parameters

Base Case

The Base Case parameters are the same as those of the Reference Case, except that the reference fuel matrix release rate, which is specified as a tabulated function of time, is increased by a factor of 10 (Tab. 3.2-1c, Parameter 9, Value C).

Parameter variations

In a parameter variation, the fuel matrix release rate is increased by a factor of 100 (Tab. 3.2-1c, Parameter 9, Value D).

6.4 Redox front penetration in the near field (Case 4.4)

6.4.1 Overview

In the Reference Case, radiolytic oxidants generated around the spent fuel and ILW waste forms are assumed not to affect redox conditions in the surrounding bentonite buffer or cementitious backfill. Reducing conditions prevail in these regions and in the host rock. In the present conceptualisation, radiolytic oxidants are assumed to affect redox conditions throughout the SF and ILW near fields. The assumption of a complete penetration of the redox front throughout the bentonite is not supported by scientific evidence. The present assessment case is, therefore, regarded as a "what if?" case.

6.4.2 The conceptual model and its underlying assumptions

The conceptual model and its underlying assumptions are identical to those of the Reference Case, except for the values assigned to

- the SF dissolution rates and cladding dissolution rates
- the solubility limits applied to radionuclides entering the "reservoirs" of water within the SF canisters following canister breaching
- the solubility limits and sorption constants applied to radionuclides in the bentonite surrounding the SF waste packages and the ILW cementitious backfill
- the ILW inventory, for which only the high force compacted waste option is considered, because of its increased production of radiolytic oxidants compared to the cemented waste option.

In the case of HLW, the generation of radiolytic oxidants is assumed to have negligible effects.

In the Opalinus Clay, reducing conditions are assumed to prevail. This will most probably lead to precipitation of some redox-sensitive radionuclides at the redox front at the near-field / geosphere interface. This precipitation is, however, conservatively neglected. Rather, it is assumed that precipitation does not occur within the host rock, or at the near-field / geosphere interface.

6.4.3 Codes used

As in the Reference Case, the reference model chain of STMAN-PICNIC-TAME is used to model the radionuclide release, migration and distribution in the biosphere.

6.4.4 Parameters

Base Case

The Base Case parameters are the same as those of the Reference Case, with the exception of a 10-fold increase in SF dissolution rate and cladding dissolution rate and except for solubility

limits and sorption constants applied to radionuclides in the bentonite surrounding the SF waste packages and the ILW cementitious backfill (see Tab. A3.2-1c). These values are taken from Tabs. A3.5-1 through A3.5-4 of Appendix 3 (note that the values for ILW-2 may also be used as conservative estimates for oxidising conditions in ILW-1). For the ILW inventory, the high force compacted waste option is considered (Tab. A3.4-2c). Note that in this case the total length of the ILW-1 emplacement tunnels is reduced from 180 m to 150 m.

Deterministic parameter variations

No deterministic parameter variations are performed for this "what if?" case.

Probabilistic parameter variations

For spent fuel, the present "what if?" case has also been analysed probabilistically. The near field sorption and solubility limit parameters for the redox-sensitive elements have been set to their values for oxidising conditions and the spent fuel and cladding dissolution rate have been increased by a factor of 10, while all other parameters have been sampled from their PDFs as in the probabilistic analysis of the Reference Conceptualisation (see Tab. A3.10-1 in Appendix 3).

6.5 Gas-induced release of dissolved radionuclides from ILW through the ramp (Case 4.5)

6.5.1 Overview

In the Reference Case, little or no displacement of contaminated porewater is assumed to occur along the emplacement tunnels and the ramp/shaft as a consequence of gas pressure build-up following gas generation. This conceptualisation for ILW differs from the Reference Case in that the possibility of accelerated release of dissolved radionuclides through the operations tunnel and along the ramp is considered (gas-induced displacement of contaminated porewater). To increase the calculated release along the ramp, the host rock is postulated to be impermeable, and thus the assessment case must be qualified as a "what if?" case.

6.5.2 The conceptual model and its underlying assumptions

The modelling for this case is performed much in the same way as in the case "gas-induced release of radionuclides affected by ramp/shaft" (Section 3.8). The main difference is that the host rock is hypothetically assumed to be impermeable, i.e. water flow and radionuclide transport from the ILW emplacement tunnels takes place through the operations tunnel and ramp exclusively.

The gas-induced radionuclide release rates from the ILW near field are identical to those calculated in Section 3.8.2.3: In the Base Case for ILW, a pulse release, starting at 10 000 years and lasting for 30 000 years, with a mean water flow rate of $0.05 \text{ m}^3 \text{ a}^{-1}$ is assumed, conveying 50 % of the total mobile radionuclide inventory from ILW (see also Fig. 4.3-2). The dose contribution of the remaining radionuclides (rest of mobile inventory and sorbed inventory) is not taken into account. In a parameter variation, a mean water flow rate of $0.3 \text{ m}^3 \text{ a}^{-1}$ is assumed, starting at 1 000 years and lasting 10 000 years, conveying 100 % of the total mobile radionuclide inventory from the ILW part of the repository. Again, the dose contribution of the remaining radionuclides (sorbed inventory) is neglected.

In the calculation of radionuclide transport, the branching ratio for ILW is set to zero, i.e. the source term from the near field is released entirely through the operations tunnel and ramp (no release through the Opalinus Clay).

6.5.3 Codes used

The codes used for ILW are identical to those used in the case "gas-induced release of radionuclides affected by ramp/shaft" (Section 3.8). A single PICNIC leg is used to model the transport of radionuclides through the operations tunnel and ramp.

6.5.4 Parameters

Base Case

The parameter values used for the calculation of water flow rates in the Base Case are identical to those listed in Tab. 3.6-1, with the exception of the parameters listed in Tab. 6.5-1. Network flow data and source term information are given in Tab. 6.5-2. Transport parameters for leg L₁ are listed in Tab. 6.5-3.

Tab. 6.5-1: Additional parameter values used for the calculation of water flow rates (values discussed in the text)

Parameter	Symbol	Unit	Value
Host rock			
Hydraulic conductivity of host rock	K_{HR}	m s ⁻¹	0
Near field			
Gas-induced porewater displacement rate (ILW)	q^*	m ³ a ⁻¹ (total repository)	0.05
Sealing zones			
Hydraulic conductivity of sealings n1 and s1	K_i	m s ⁻¹	0
Hydraulic conductivity of EDZ (n1 and s1)	$K_{i,EDZ}$	m s ⁻¹	0
All other parameters	Identical to parameter values in Tab. 3.6-1		

Tab. 6.5-2: Network flow data and source term information calculated based on parameter values listed in Tab. 3.6-1 and 6.5-1

For the location of the points where flow is calculated, see Fig. 3.6-1.

Input	Units	Values
<i>Network Structure</i>		
List of junction names. Inlet and outlet junctions for each leg.	-	Fig. 3.6-5 (Operations tunnel ILW and ramp only, leg L ₁)
<i>Network Flow Data</i>		
Flows (ILW)		
Q _{ramp}	m ³ a ⁻¹	5.0 × 10 ⁻²
Q _{n3}		5.0 × 10 ⁻²
Q _{OPA}		0
<i>Source Term Information</i>		
Source flux (ILW)	mol a ⁻¹	Radionuclide releases obtained from the output of code STALLION (plug flow): Start: 10 000 a / End: 40 000 a; 50 % of mobile inventory
Fraction to leg	dimensionless	1 (L ₁)

Tab. 6.5-3: PICNIC input data for leg L₁ which represents axial transport through the backfill of the operations tunnel to the ramp

Input	Units	Values	Source
Leg Data – Basic Data			
Length	m	1 000	Tab. A3.2-2c, Parameter 3, Value C
Cross sectional area (L ₁)	m ²	23	Tab. A3.2-2c, Parameter 4, Value A
Darcy velocity (L ₁)	m a ⁻¹	2.2 × 10 ⁻³	Calculated from water flow rates in Tab. 6.5 2 and cross sectional areas (see also Tab. A3.2-2c, Parameter 5, Value V)
Pore diffusion constant for backfill	m ² a ⁻¹	1.6 × 10 ⁻²	Tab. A3.2-2c, Parameter 7, Value D
Leg Data – Properties of Flowing Region			
Retardation	dimensionless	calculated from the parameters below	
Bulk dry density (mass of bentonite per m ³ of backfill material, sorption on quartz sand neglected)	kg m ⁻³	558	Tab. A3.2-2c, Parameter 8, Value C
Flow porosity	dimensionless	this is set equal the infill porosity	
Infill Porosity	dimensionless	0.3	Tab. A3.2-2c, Parameter 10, Value E
Porosity Factors	dimensionless	none	
Sorption K _d	m ³ kg ⁻¹	values for bentonite	Tab. A3.2-2c, Parameter 11, Value E
Leg Data – Properties of Matrix			
There is no "matrix" for this leg – the tunnel backfill is a homogeneous porous medium. The matrix penetration depth and surface sorption coefficients are thus set equal to zero, and all other parameters are irrelevant.			

Parameter variation

The parameter values used for the calculation of water flow rates in the parameter variation are identical to those listed in Tab. 3.6-1, with the exception of the gas-induced porewater displacement rate for ILW, listed in Tab. 6.5-4. Network flow data and source term information are given in Tab. 6.5-5. Transport parameters for leg L₁ are listed in Tab. 6.5-6.

Tab. 6.5-4: Additional parameter values used for the calculation of water flow rates
Values discussed in the text.

Parameter	Symbol	Unit	Value
Host rock			
Hydraulic conductivity of host rock	K_{HR}	m s^{-1}	0
Near field			
Gas-induced porewater displacement rate (ILW)	q^*	$\text{m}^3 \text{a}^{-1}$ (total repository)	0.3
Sealing zones			
Hydraulic conductivity of sealings n1 and s1	K_i	m s^{-1}	0
Hydraulic conductivity of EDZ (n1 and s1)	$K_{i,EDZ}$	m s^{-1}	0
All other parameters	Identical to parameter values in Tab. 3.6-1		

Tab. 6.5-5: Network flow data and source term information (calculated based on parameter values listed in Tab. 3.6-1 and 6.5-4)

Input	Units	Values
Network Structure		
List of junction names. Inlet and outlet junctions for each leg.	-	Fig. 3.6-5 (Operations tunnel ILW and ramp only, leg L_1)
Network Flow Data		
Flows (ILW)		
Q_{ramp}	$\text{m}^3 \text{a}^{-1}$	0.3
Q_{n3}		0.3
Q_{OPA}		0
Source Term Information		
Source flux (ILW)	mol a^{-1}	Radionuclide releases obtained from the output of code STALLION (plug flow): Start: 1 000 a / End: 11 000 a; 100 % mobile inventory
Fraction to leg	dimensionless	1 (L_1)

Tab. 6.5-6: PICNIC input data differing from the Base Case, for leg L₁ which represents axial transport through the backfill of the operations tunnel to the ramp

Input	Units	Values	Source
<i>Leg Data – Basic Data</i>			
Darcy velocity (L ₁)	m a ⁻¹	1.3 × 10 ⁻²	Calculated from water flow rates in Tab. 6.5 5 and cross sectional areas (see also Tab. A3.2-2c, Parameter 5, Value W)
<i>All other parameters</i>	Identical to parameter values in Tab. 6.5-3		

6.6 Unretarded transport of volatile radionuclides through the host rock (Case 4.6)

In the Reference Case, organic and inorganic ¹⁴C is assumed to dissolve in the porewater and to be transported through the Opalinus Clay by advection/diffusion. In the present conceptualisation, organic ¹⁴C is assumed to be volatile and – after the available pore space in the near field has been filled with gas – to escape rapidly to the Wedelsandstein formation, due to the postulated existence of a continuous gas pathway leading to instantaneous release through the Opalinus Clay. Gas accumulation in the Wedelsandstein formation is taken into account.

The conceptual model and its underlying assumptions, the solution techniques and the parameters are discussed in the context of the Alternative Scenario "Release of volatile ¹⁴C along gas pathways" (see Chapter 4). The differences between the three conceptualisations involving release and transport of ¹⁴C as volatile species (i.e. Cases 2.1, 2.2 and 4.6) are related to the pore space available for gas and are summarised in Tab. 4.3-6.

6.7 Poor near field and pessimistic near field / geosphere geochemical dataset (Case 4.7)

6.7.1 Overview

The objective of the present conceptualisation is to test the robustness of the repository system by considering a number of cumulated pessimistic assumptions, many of which are outside the range supported by scientific evidence: short canister life-time, high waste dissolution rates, pessimistic near field and geosphere geochemical dataset. Furthermore, the effect of increased water flow rates in the geosphere is considered.

6.7.2 The conceptual model and its underlying assumptions

In the framework of the present "what if?" case, pessimistic assumptions are considered simultaneously for several pillars of safety:

- it is hypothetically assumed that the SF/HLW canister lifetime is reduced from 10 000 to 100 years and the containment time for ILW is reduced from 100 years to zero,
- the dissolution rates for the spent fuel matrix, cladding and glass are all increased by a factor of 10 in comparison with the Reference Case values,

- pessimistic near field and geosphere geochemical data (solubility limits, sorption constants) are used,
- the water flow rate in the geosphere is set at its Reference Case value (Base Case) and increased by factors of 10 and 100 (parameter variations).

6.7.3 Codes used

As in the Reference Case, the reference model chain of STMAN-PICNIC-TAME is used to model the radionuclide release, migration and distribution in the biosphere.

6.7.4 Parameters

Base Case

The Base Case parameters are the same as those of the Reference Case, except for the parameters listed in Tab. 6.7-1.

Tab. 6.7-1: Input parameters for the case "Poor near field and pessimistic near field / geosphere geochemical dataset" (Case 4.7)

Parameter	Unit	Value	Source
Near field			
SF/HLW canister lifetime	a	100	Tab. A3.2-1c, Parameter 5, Value E
ILW containment time	a	0	
SF fuel dissolution rate	a ⁻¹	10-fold increase	Tab. A3.2-1c, Parameter 9, Value C
SF cladding dissolution rate	a ⁻¹	10-fold increase	Tab. A3.2-1c, Parameter 10, Value B
HLW glass dissolution rate	kg m ⁻² a ⁻¹	10-fold increase	Tab. A3.2-1c, Parameter 12, Value C
Sorption constants (K _d)	m ³ kg ⁻¹	pessimistic	Tab. A3.2-1c, Parameters 21, 29 and 30, Value B
Solubility limits	mol l ⁻¹	pessimistic	Tab. A3.2-1c, Parameters 16, 22, 31 and 32, Value B
Geosphere			
Sorption constants (K _d)	m ³ kg ⁻¹	pessimistic	Tab. A3.2-2c, Parameter 11, Value B
Specific water flow rate (Darcy velocity)	m s ⁻¹	2 × 10 ⁻¹⁴	Tab. A3.2-2c, Parameter 5, Value A
		2 × 10 ⁻¹³	Tab. A3.2-2c, Parameter 5, Value D
		2 × 10 ⁻¹²	Tab. A3.2-2c, Parameter 5, Value E

Parameter variations

As a parameter variation, the specific water flow rate in the Opalinus Clay is increased by a factor of 10 (2 × 10⁻¹³ m s⁻¹) and 100 (2 × 10⁻¹² m s⁻¹), see Tab. 6.7-1.

6.8 No advection in the geosphere (diffusive transport only, Case 4.8)

6.8.1 Overview

In the present conceptualisation the Darcy flow rate in the geosphere is set to zero, so that radionuclide transport in the near field and the geosphere is by diffusion only. The codes used are identical to those of the Reference Case.

6.8.2 Parameters

Base Case

The Base Case parameters are the same as those of the Reference Case, except for the Darcy velocity in the geosphere which is set to zero in both near field and geosphere model calculations (Tab. A3.2-1c, Parameter 35, Value B and Tab. A3.2-2c, Parameter 5, Value B).

Parameter variations

No parameters variations are performed for this "what if?" case.

6.9 Increased cladding corrosion rate in SF (Case 4.9)

6.9.1 Overview

This conceptualisation differs from the Reference Case in that the cladding corrosion rate for SF is hypothetically increased by a factor of 10, which is considered to be outside the range of scientific evidence ("what if?"). The codes used are identical to those of the Reference Case.

6.9.2 Parameters

Base Case

The Base Case parameters are the same as those of the Reference Case, except for the cladding corrosion rate which is increased by a factor of 10 with respect to the Reference Case (Tab. A3.2-1c, Parameter 10, Value B).

Parameter variations

No parameters variations are performed for this "what if?" case.

6.10 Zero sorption for iodine in the near field and the geosphere (Case 4.10)

6.10.1 Overview

In contrast to the Reference Case, where the assumed sorption values (K_d) for iodine in bentonite, cement and Opalinus Clay are 5×10^{-4} , 1×10^{-3} and $3 \times 10^{-5} \text{ m}^3 \text{ kg}^{-1}$ respectively, in the present conceptualisation the sorption values for iodine are set to zero both in the near field

and in the geosphere. This is outside the range of scientific evidence ("what if?" case). The codes used are identical to those of the Reference Case.

6.10.2 Parameters

Base Case

The Base Case parameters are the same as those for the Reference Case, except for the sorption values for iodine in bentonite, cement and Opalinus Clay, which are set to zero (Tab. A3.2-1c, Parameters 21, 29 and 30, Value D and Tab. A3.2-2c, Parameter 11, Value F).

Parameter variations

No parameters variations are performed for this "what if?" case.

6.11 Decreased transport distance in Opalinus Clay (Case 4.11)

6.11.1 Overview

In the Reference Case, the transport distance in the Opalinus Clay is assumed to be 40 m. While this value is pessimistic for the overwhelming part of the repository, it may be a realistic value for a limited number of waste packages emplaced. To test the robustness of the disposal system, the transport distance is reduced to 30 m in the present conceptualisation, which is outside the range of scientific evidence for all waste packages emplaced ("what if?"). The codes used are identical to those of the Reference Case.

6.11.2 Parameters

Base Case

The Base Case parameters are the same as those of the Reference Case, except for the transport distance in Opalinus Clay which is reduced from 40 m to 30 m (Tab. A3.2-2c, Parameter 3, Value B).

Parameter variations

No parameters variations are performed for this "what if?" case.

7 Modelling Design and System Options

7.1 Increased waste arisings (Case 5.1)

7.1.1 Overview

The Reference Case is based on a 192 GWa(e) nuclear power generation scenario, postulating a lifetime of 60 years for the existing nuclear power plants. The alternative conceptualisation, corresponding to an assumed 300 GWa(e) scenario, serves to demonstrate the flexibility of the repository system with respect to increased amounts of radioactive waste.

7.1.2 The conceptual model and the justification of assumptions

The assumed amount of waste arising as spent fuel and vitrified high-level waste in the 192 GWa(e) scenario for Switzerland is 3217 t_{IHM} and 292 t of glass, representing reprocessing of 1195 t_{IHM} of spent fuel (Reference Case). In the case of the 300 GWa(e) scenario, the extra spent fuel is assumed to be directly disposed of without reprocessing, yielding 5576 t_{IHM} as spent fuel, which is a factor of about 1.7 more spent fuel than in the case of the 192 GWa(e) scenario. The mass of vitrified high-level waste is identical in the two scenarios.

7.1.3 Codes used

As in the Reference Case, the reference model chain of STMAN-PICNIC-TAME is used to model the radionuclide release, migration and distribution in the biosphere.

7.1.4 Parameters

Base Case

The Base Case parameters are the same as those of the Reference Case, except for the increased number of spent fuel canisters: 1630 canisters with BWR UO₂ fuel, 1500 with PWR UO₂ fuel, 450 with PWR UO₂/MOX fuel (rounded numbers), all with a burnup of 48 GWd/t_{IHM} (see Tab. A3.2-1d, Parameter 6, Value B).

Parameter variations

No parameters variations are performed for this design and system option.

7.2 ILW high force compacted waste option (Case 5.2)

7.2.1 Overview

This conceptualisation differs from the Reference Case in that an alternative waste conditioning method for part of the ILW is considered, in which the hulls and end-pieces and ILW technological wastes from COGEMA are treated by high-force compaction.

7.2.2 The conceptual model and the justification of assumptions

The conceptual model and its underlying assumptions are identical to those of the Reference Case, except for a modified ILW radionuclide inventory. Note that in reality, the radionuclide concentration in the vicinity of the compacted wastes will be higher than the average concentration in the ILW tunnels, leading to increased precipitation. This effect is conservatively neglected.

7.2.3 Codes used

As in the Reference Case, the reference model chain of STMAN-PICNIC-TAME is used to model the radionuclide release, migration and distribution in the biosphere.

7.2.4 Parameters

Base Case

The Base Case parameters are the same as those of the Reference Case, except for the modified ILW radionuclide inventory, which is given in Tab. A3.4-2c of Appendix 3. Note that in this case the total length of the ILW-1 emplacement tunnels is reduced from 180 m to 150 m.

Parameter variations

No parameter variations are performed for this design / system option.

7.3 Spent fuel canister with a Cu shell (Case 5.3)

7.3.1 Overview

In the Reference Case, spent fuel is contained within steel canisters. In the design / system option "spent fuel canister with a Cu shell", an alternative canister design is considered consisting of a cast steel insert inside a Cu shell. The cast iron insert provides mechanical stability and the Cu shell protects against corrosion in the repository environment. The canister has a design lifetime of 100 000 years and is thus expected to give a longer period of complete containment than the reference design.

7.3.2 The conceptual model and the justification of assumptions

The conceptual model and its underlying assumptions are identical to those of the Reference Case, except in the duration of the period of complete containment, and in the consideration of the possibility of initial manufacturing defects, although such defects are considered to be extremely unlikely.

In the Base Case it is conservatively assumed (as in the Reference Case) that spent fuel canister breaching is instant and complete immediately after the specified canister lifetime has been reached, so that the breached canisters provides no physical barrier to water ingress or radionuclide release. In the variant case, it is assumed that a single spent fuel canister containing 3 PWR UO₂ assemblies and 1 PWR MOX assembly, all with a burnup of 48 GWd/t_{IHM}, has an undetected manufacturing defect (e.g. a through-wall welding defect).

In the variant case, it is conservatively assumed that the defect allows water ingress and radionuclide release instantaneously upon repository closure, and that the repository and its surroundings are already resaturated by this time. The transport resistance of the defect is, however, taken into account. In particular, for the affected canister, Eq. A1.3-9 of Appendix 1 describing release to the buffer through a defect is used in place of Eq. A1.3-8, until such a time as the canister becomes fully breached. All other canisters are modelled as in the Base Case.

7.3.3 Codes used

The reference model chain of STMAN-PICNIC-TAME is used to model the radionuclide release, migration and distribution in the biosphere. The STMAN "pinhole release" option described in Appendix 1 is used to model the canister with an undetected manufacturing defect.

7.3.4 Parameters

Base Case

In the Base Case, all spent fuel canisters are assumed to be breached simultaneously at a time of 100 000 years following waste emplacement (Tab. A3.2-1d, Parameter 5, Value D). No initially defective canisters are present.

Parameter variants

In the parameter variant, the canister with an undetected manufacturing defect is assumed to be perforated by a single hole with a cross-sectional area of 4 mm². In the SPENT module of STMAN (see Appendix 1), the "pinhole radius", r_{pin} , is set to $\sqrt{4/\pi} = 1.1$ mm and the number of pinholes, N_{pin} , to 1. Full breaching of the defective canister occurs at 100 000 years, along with all the remaining, initially intact canisters (see Tab. A3.2-1d, Parameters 5, 6, 17, 18).

In a parameter variation, the size of the defect is increased to 50 mm², i.e. a pinhole radius of $\sqrt{50/\pi} = 4.0$ mm (see Tab. A3.2-1d, Parameters 5, 6, 17, 18).

8 Illustration of Effects of Biosphere Uncertainty on Calculated Doses

8.1 Introduction

In Nagra (2002c), four climate states and six local geomorphological units³⁸ were identified that are relevant for biosphere modelling. In the following sections, a selection of six alternative cases is discussed that cover the range of possible situations with respect to the resulting doses. The focus is on conceptual aspects, but in order to illustrate the cases, some data on water fluxes and solid material fluxes are included in the discussion.

As a rule, discharge of deep groundwater occurs at the lowest points of terrain, i.e. in valley bottoms. In the derivation of biosphere cases, the focus is therefore on the conditions in the valley bottoms. This means that the gravel aquifer or the river is, as a rule, the recipient compartment for radionuclide release from the geosphere to the biosphere. For comparison, a case is considered where discharge of radionuclides occurs in a spring at the side of a larger river valley (Section 8.3).

8.2 Reference Case biosphere (Cases 1.1a, 6.1a and 6.2a)

The Reference Case biosphere is characterised by the climate state "present-day climate" and the local geomorphological unit "eroding river". Precipitation is 1.0 m a^{-1} and evapotranspiration 0.6 m a^{-1} . Discharge of contaminated deep groundwater is assumed to occur into the Quaternary gravel aquifer in the Rhine valley. Because eroding rivers cut into the gravel aquifer or the underlying rock, and because the river level and the groundwater table are connected, the groundwater table is relatively low (more than 10 m below ground level). The groundwater zone (i.e. the saturated part of the gravel aquifer) is assumed to be 20 m deep.

Groundwater flow from upstream, lateral inflow from the valley sides and precipitation lead to a dilution in the gravel aquifer. Groundwater containing radionuclides reaches the top soil by irrigation with pumped water from the gravel aquifer (0.5 m a^{-1}). This is a pessimistic assumption because irrigation water is normally taken from a nearby river. Capillary rise can be excluded, because the separation between groundwater table and rooting zone is too large. The erosion rate is assumed to compensate an uplift rate of 0.1 mm a^{-1} and the sedimentation rate is set to zero, i.e. net erosion takes place. In this report, all solid material fluxes due to erosion and sedimentation are based on erosion and sedimentation rates given in mm a^{-1} , with an assumed solid density of the hard rock underground of 2700 kg m^{-3} .

To investigate the radionuclide transport in the area of interest, all relevant water fluxes and solid material fluxes have to be considered, satisfying the corresponding mass balances. Fig. 8.2-1 gives a schematic representation of the considered fluxes in the Reference Case.

It is assumed that the food is grown in local agriculture. All exposure pathways are taken into account (drinking water, food, soil ingestion, inhalation, external radiation). Agricultural practices and exposure pathways are discussed further in Section A1.7 of Appendix 1 and in Nagra (2003b).

³⁸ For the purpose of biosphere description in the present report, local geomorphological units are defined to be those valley types in northern Switzerland where discharge of deep groundwaters occurs today and may continue to occur in the future.

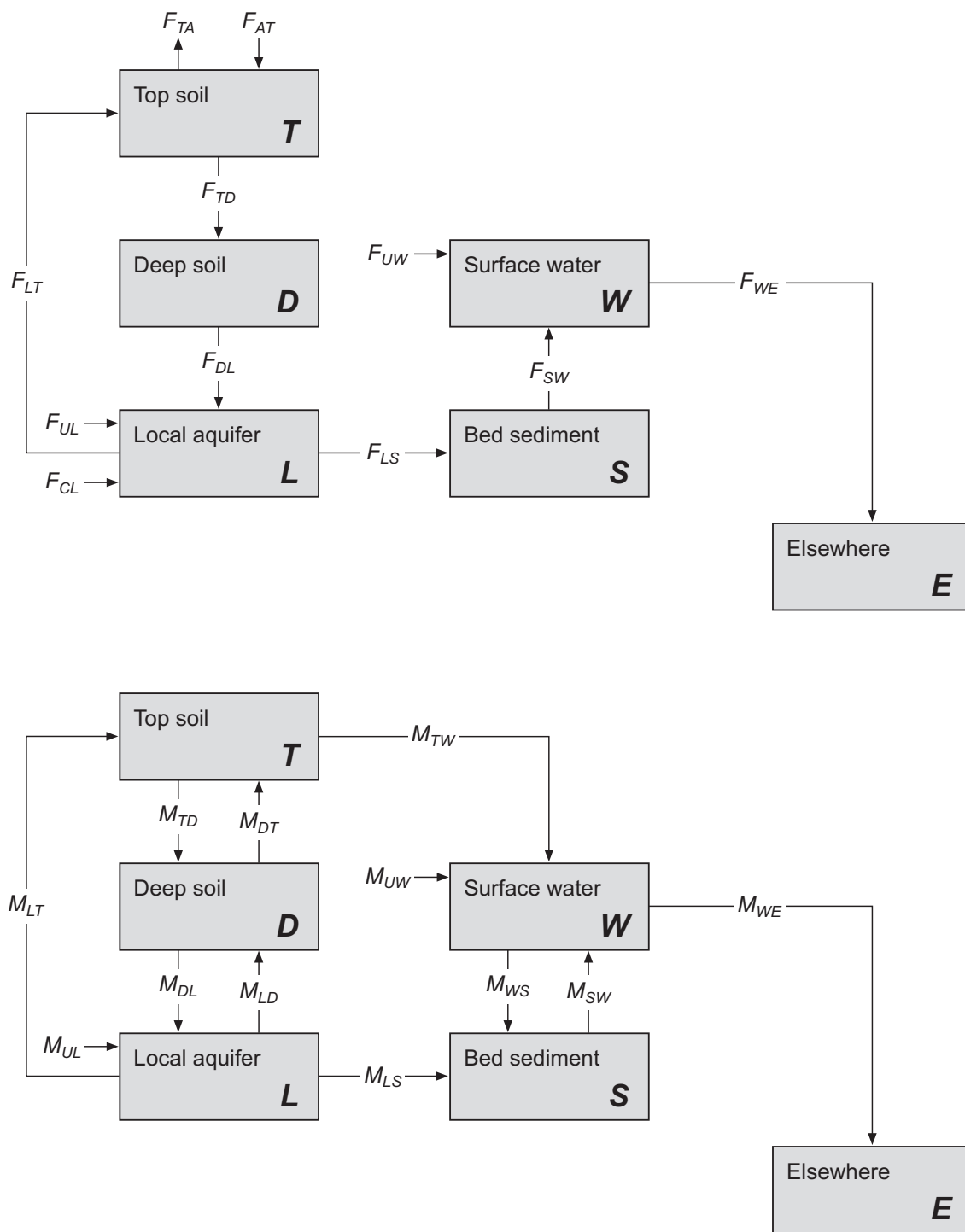


Fig. 8.2-1: Schematic representation of water fluxes (F_{ij}) and solid material fluxes (M_{ij}) considered in the Reference Case

The abbreviations are explained in Tab. 8.2-1.

Tab. 8.2-1: Abbreviations used in the schematic representations of the considered water fluxes and solid material fluxes in Figs. 8.2-1, 8.3-1 and 8.3-2

Indices:	
<i>A</i>	Atmosphere
<i>C</i>	Contaminated
<i>D</i>	Deep soil
<i>E</i>	Elsewhere (sink)
<i>L</i>	Local aquifer (gravel aquifer)
<i>S</i>	Bed sediment (river bed sediments)
<i>T</i>	Top soil
<i>U</i>	Uncontaminated
<i>W</i>	Surface water (river)
Water fluxes:	
F_{AT}	Precipitation
F_{TA}	Evapotranspiration
F_{LT}	Irrigation with groundwater (from gravel aquifer)
F_{WT}	Flooding and irrigation with river water
F_{TD}	Percolation from top soil to deep soil
F_{DT}	Water flux from deep soil to top soil (e.g. capillary rise)
F_{DL}	Percolation from deep soil to gravel aquifer
F_{LD}	Water flux from gravel aquifer to deep soil (e.g. capillary rise)
F_{UL}	Flux of uncontaminated water into gravel aquifer
F_{CL}	Discharge of contaminated deep groundwater into gravel aquifer
F_{LS}	Water flux from gravel aquifer to river bed sediments
F_{SW}	Water flux from river bed sediments to river
F_{UW}	Flux of uncontaminated water into river (mainly from previous river section)
F_{CW}	Flux of contaminated water into river
F_{WE}	Water flux from river to sink (out of the model area)
Solid material fluxes:	
M_{LT}	Solid material flux by irrigation with groundwater
M_{WT}	Solid material flux from river to top soil by flooding and irrigation with river water
M_{TW}	Solid material flux from top soil to river by erosion
M_{TD}	Solid material flux from top soil to deep soil (e.g. bioturbation and percolation)
M_{DT}	Solid material flux from deep soil to top soil (e.g. bioturbation)
M_{DL}	Solid material flux from deep soil to gravel aquifer (e.g. percolation)
M_{LD}	Solid material flux from gravel aquifer to deep soil
M_{UL}	Flux of uncontaminated solid material into gravel aquifer
M_{LS}	Solid material flux from gravel aquifer to river bed sediments
M_{LE}	Solid material flux from gravel aquifer to sink (used for mass balance reasons so that dimensions of gravel aquifer compartment stay constant in case of net deposition)
M_{WS}	Deposition of river bed sediments
M_{SW}	Resuspension of river bed sediments
M_{UW}	Flux of uncontaminated solid material into river (mainly from previous river section)
M_{WE}	Solid material flux from river to sink

8.3 Alternative geomorphology (Cases 6.1b-d)

The starting point in the derivation of alternative biosphere cases is the Reference Case. In a first step, the climate state is kept constant and the local geomorphological unit is varied (this section). Variations to the climate state are discussed in Section 8.4, with the geomorphological unit kept constant (eroding river).

The term "alternative" does not mean that the respective cases are unlikely but simply expresses the fact that discharge can occur under different conditions, for example in different local geomorphological units. Varying the local geomorphological unit thus serves to illustrate the effects of variability in the biosphere and of uncertainty in the exact location of discharge.

It is not necessary to investigate all six local geomorphological units described in the safety assessment (Nagra 2002c). Lakes need not to be considered because 1) the low permeability of lake sediments inhibits the discharge of deep groundwaters, and 2) lakes involve large dilution and, therefore, lead to lower doses than river systems. Braided rivers, meandering rivers, and river deltas in lakes show similar hydrological characteristics (dilution by mixing with uncontaminated water and solid materials, depth of groundwater table) and can be represented by a single unit, termed "Sedimentation Area". Therefore three local geomorphological units remain, namely "Eroding River" (Reference Case, Section 8.2), "Sedimentation Area", and "Wetland".

Sedimentation Area (Case 6.1b)

In this model variant, the river is an equivalent to a tributary river to the Rhine. It carries a significant amount of solid material, which has not been removed by sedimentation in a lake further upstream, as is the case for the Rhine. This model variant differs from the Reference Case mainly by the smaller potential of the river to transport solid material. More specifically, net deposition caused by the river is assumed. This has several consequences:

The river level is higher than in the Reference Case. When river discharge is above average, river water infiltrates into the gravel aquifer, and when it is very high, flooding occurs (at an assumed rate of 0.5 m a^{-1}). Infiltration and flooding lead to dilution of potentially released radionuclides in the gravel aquifer. Furthermore, flooding usually causes a large turnover of solid material, with erosion at some places, sedimentation at other places, and an overall positive mass balance (i.e. net deposition). The erosion rate is assumed to be 0.60 mm a^{-1} and the sedimentation rate 0.65 mm a^{-1} . These numbers indicate a rather large mass turnover with a slight surplus of sedimentation.

The groundwater table, in connection with the river level, is also higher than in the Reference Case (typically less than 2 m below ground). A higher groundwater table enables capillary rise from the aquifer to the rooting zone (0.1 m a^{-1}). Capillary rise and flooding reduce the demand for irrigation (0.25 m a^{-1}).

Fig. 8.3-1 gives a schematic representation of the considered fluxes in the model variant "Sedimentation Area".

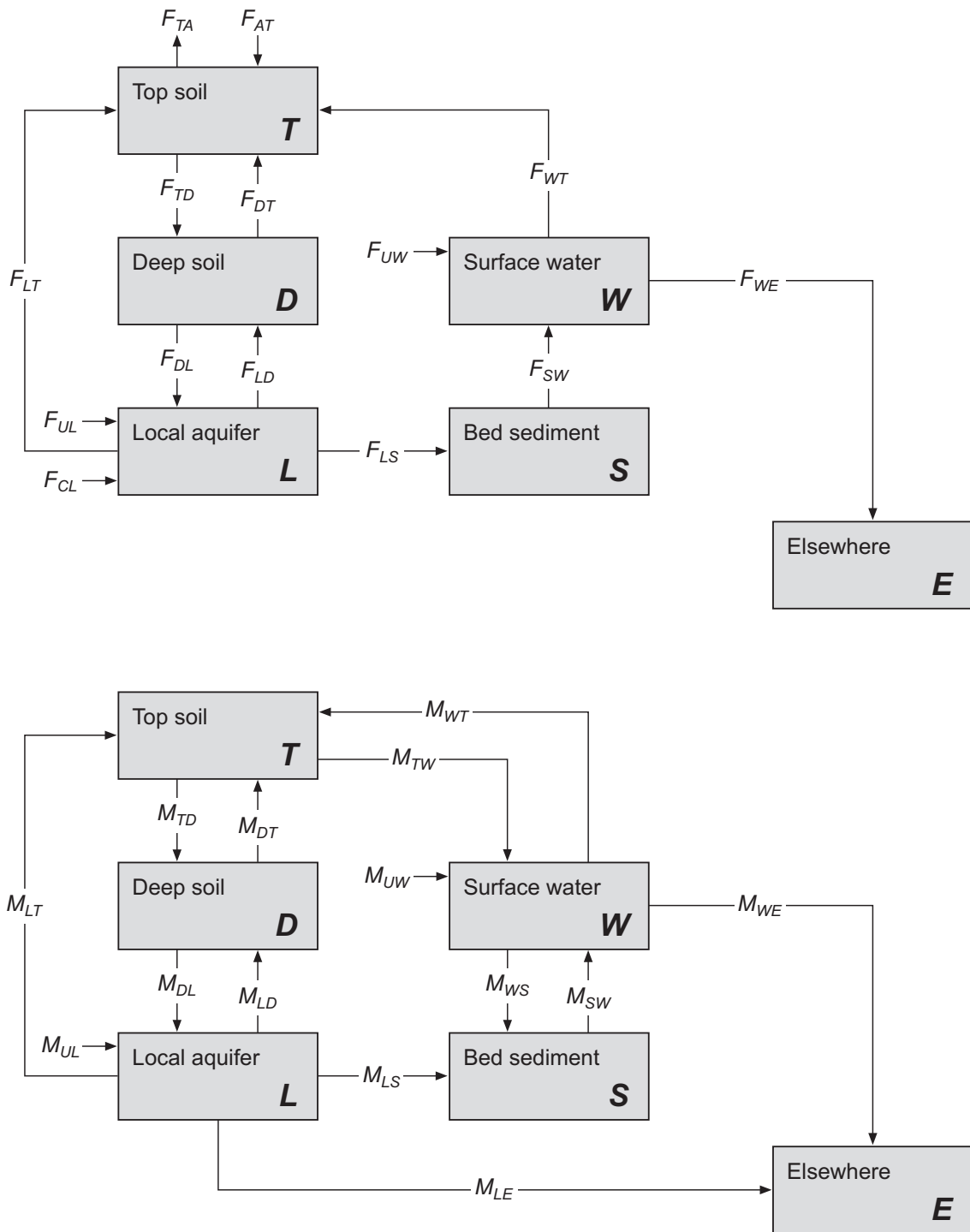


Fig. 8.3-1: Schematic representation of water fluxes (F_{ij}) and solid material fluxes (M_{ij}) considered in the model variant "Sedimentation Area"

The abbreviations are explained in Tab. 8.2-1.

Wetland (Case 6.1c)

In a second model variant, the effects of discharge of radionuclides to a river with subsequent flooding in an area of wetlands is investigated. The biosphere area is assumed to consist of open water (small river), marsh, and agricultural land.

The main difference between this model variant and the Reference Case consists in the significantly higher groundwater table. Here, the groundwater table is assumed to be less than 1 m below ground, so that there is always ample water available in the soil. As a consequence, irrigation is not applied.

It is assumed that the release of radionuclides from the geosphere takes place further upstream from the investigated biosphere area directly into the river. Flooding is, therefore, the essential process that carries released radionuclides into the soil. Because of the high water level, the river frequently causes significant flooding (at an assumed rate of 1.0 m a^{-1}).

The erosion rate is assumed to be zero. Sedimentation occurs mainly by deposition of organic material (from decayed, locally produced plants) and, to a lesser extent, of inorganic material (sand, loam, and clay). The high content of organic matter (more than 10 % of organics) causes strong radionuclide sorption in the soil.

Due to the very wet conditions involved, the land is only suitable for a restricted number of agricultural practices. The agricultural productivity depends on various factors, including type and water content of soils, human activities (active drainage, use of fertilisers, etc.). In wetter areas, straw production and pasture land is predominant and the productivity is low while in more desaturated areas a wider range of agricultural production with higher yields is possible, as in the Reference Case. In this conceptualisation, the agricultural practices are restricted to cattle raising and milk production. For this reason, the calculation of doses is performed for the exposure pathways milk/dairy products and meat only.

Fig. 8.3-2 gives a schematic representation of the considered fluxes in the model variant "Wetland".

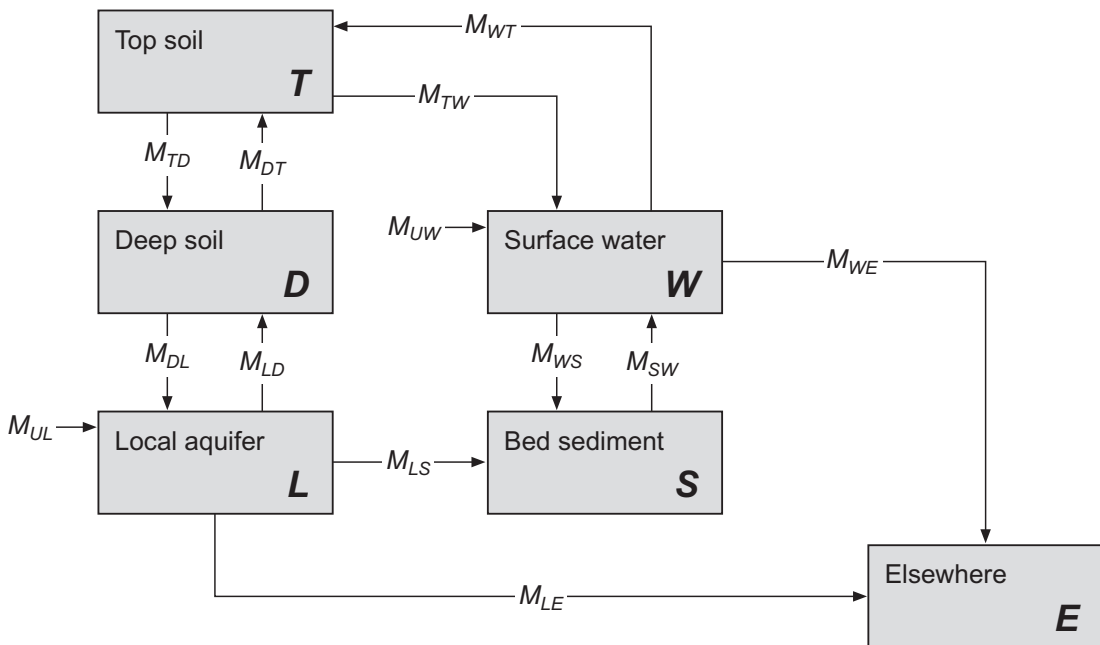
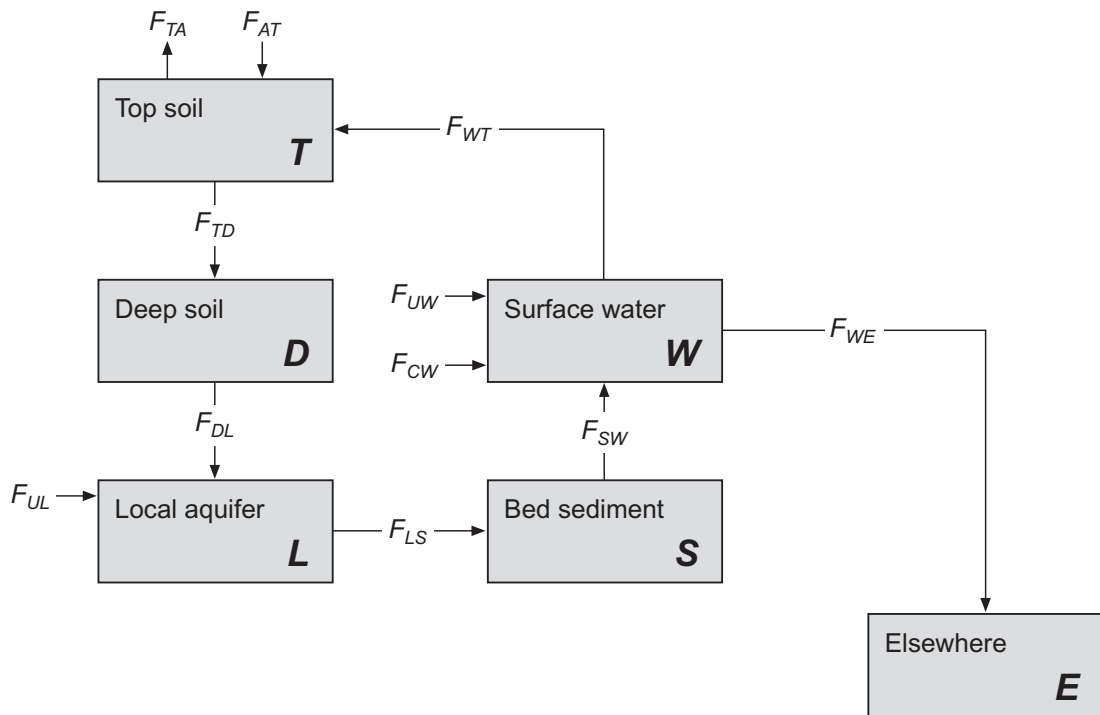


Fig. 8.3-2: Schematic representation of water fluxes (F_{ij}) and solid material fluxes (M_{ij}) considered in the model variant "Wetland"

The abbreviations are explained in Tab. 8.2-1.

Exfiltration to spring at valley side (Case 6.1d)

In this model variant, it is assumed that the release of radionuclides occurs to a spring located at a valley side, which is fed by deep groundwater from the Malm aquifer. Although such a situation can be ruled out for present-day hydrogeological conditions, it cannot be completely excluded in the long term. The well is assumed to be used for drinking water, although the salinity of groundwater from the Malm aquifer in the Zürcher Weinland is known to be substantial (Nagra 2002a). The production rate is taken to be $10^{-3} \text{ m}^3 \text{ s}^{-1}$, a conceivable value for natural discharge of Malm groundwater from the south in the area of interest. It is assumed that 100 % of the discharged water is deep groundwater, i.e. no mixing with near-surface (meteoric) water is assumed. The capture efficiency of the spring (the fraction of radionuclides released from the repository to the Malm aquifer that is captured by the spring) is assumed to be 10 %. The dose is calculated for the drinking water exposure pathway only, other exposure pathways (other use of water) are considered unlikely and are neglected.

8.4 Alternative climates (Cases 6.2b-d)

Starting point in the derivation of alternative biosphere cases with other than present-day climates is again the Reference Case. The illustration includes a wet climate, a dry climate and a periglacial climate.

Dry Climate (Case 6.2b)

The climate in this model variant is drier and warmer than the present-day climate in northern Switzerland. With respect to the water budget, it is similar to the present-day climate around Sion in the Canton of Valais. It is characterised by a precipitation rate of 0.5 m a^{-1} and an evapotranspiration rate of 1.0 m a^{-1} . The latter value is close to the potential evapotranspiration rate for the considered climate (i.e. to the rate that is controlled by the climatic conditions and not limited by water supply). In other words, the high evapotranspiration rate requires that there is sufficient water available in the soil. This condition is warranted in spite of low precipitation, because of plentiful irrigation with groundwater (0.6 m a^{-1}).

The schematic representations of the considered fluxes in the model variant "Dry Climate" is identical to the Reference Case (Fig. 8.2-1).

Wet Climate (Case 6.2c)

The climate in this model variant is wetter and warmer than the present-day climate in northern Switzerland. With respect to the water budget, it is similar to the present-day climate around Lugano in the Canton of Ticino. It is characterised by a precipitation rate of 2.0 m a^{-1} and an evapotranspiration rate of 1.0 m a^{-1} . Although precipitation is high, dry spells can occur. These are bridged by irrigation (0.25 m a^{-1}). Consequently, there is always plentiful water in the soil, so that actual evapotranspiration almost reaches potential evapotranspiration, as in the model variant "Dry Climate".

The schematic representations of the considered fluxes in the model variant "Wet Climate" is identical to the Reference Case (Fig. 8.2-1).

Periglacial climate (Case 6.2d)

The periglacial climate is a tundra climate, comparable to the present-day climate in Lapland or the southern parts of the Canadian Arctic. In tundra regions, low temperatures prevent agricultural practices like those assumed in the other biosphere cases. The diet of locally produced food is derived from natural and semi-natural environments (no agricultural activity, diet based on berries, mushrooms, fish and reindeer), in which activity accumulation is significantly higher than in food from agricultural land. However, in such environments a larger area is required for food production, leading to lower average activity concentrations in the food.

Detailed dose calculations are not performed for the periglacial climate, because, except for the case of Cs, the available data is scarce and unreliable. Instead, a simplified model to estimate dose making use of the available data on the fate of Cs in arctic regions originating from radioactive fallout is used. The conceptual assumptions and data used for the dose estimate are summarised in Appendix 6.

8.5 Summary of cases

As a summary, the investigated biosphere cases are listed in Tab. 8.5-1. The case with a discharge of radionuclides to a spring at the side of a river valley can, in principal, be allocated to any one of the geomorphological units, but this has no effect on the calculated drinking water dose. The semi-quantitative dose estimate performed for the periglacial climate does not refer to any particular geomorphological unit or discharge area.

Tab. 8.5-1: Overview of investigated biosphere cases

Shaded area indicates Reference Case biosphere assumptions.

Climate / Case		Local geomorphological unit		
		Eroding river	Sedimentation area	Wetland
		Discharge from geosphere into:		
		Gravel aquifer	Gravel aquifer	River (located upstream from area of wetland)
Interglacial	Present-day	Cases 6.1a, 6.2a	Case 6.1b	Case 6.1c
	Dry	Case 6.2b		
	Wet	Case 6.2c		
Periglacial		Case 6.2d		
Spring at valley side		Case 6.1d		

8.6 Codes used

All biosphere model calculations are performed using the code TAME (see Appendix 1, Section A1.7), with the exception of the model variants related to the discharge of radionuclides to a spring at a valley side (drinking water dose) and to periglacial climatic conditions (see the semi-quantitative dose estimate described in Appendix 6).

8.7 Input parameters

The complete set of input parameters for TAME for the Reference Case is listed in Appendix 3 (Tabs. A3.7-1 to A3.7-5). Tab. A3.8-1 in Appendix 3 gives an overview of TAME input parameters used for the biosphere model variants that differ from the Reference Case input parameters. A detailed justification of these input parameters is given in (Nagra 2003b).

For the variant considering consumption of drinking water from a spring, the dose coefficients are taken from Tab. A3.4-1, the production rate of the spring is taken to be 1 l s^{-1} and the rate of ingestion of water is set to 2 l d^{-1} (Tab. A3.7-3).

For the variant related to a periglacial climate, the biosphere parameter values used for the dose estimate are summarised in Appendix 6.

9 Insight Models

9.1 Use of insight models in the safety assessment

Insight models are used to complement more comprehensive models used to analyse the assessment cases. More specifically, they are used to:

- develop a better understanding of particular aspects of the behaviour of the system (or components of the system) in a specific case (the Reference Case), and
- investigate sensitivity to key system properties.

The insight models that are used in specific sections (and to generate specific figures) of the Safety Report (Nagra 2002c) are listed in Tab. 9.1-1. The table also shows the sections of the present chapter where the details of these insight models are described.

Tab. 9.1-1: Insight models used in specific sections of the Safety Report and the sections of the present chapter where the details of these insight models are described

Insight model	Sections / figures of the Safety Report (Nagra 2002c) where the model is used	Description of the model in the present report
Model to illustrate the meaning of the timescale for diffusion across the Opalinus Clay	Section 6.6.2 (Figs. 6.6-1 and 6.6-3)	Section 9.2
Barrier efficiency model for non-fractured media:		Section 9.3
- Opalinus Clay plus the bentonite buffer	Section 6.6.2 (Figs. 6.6-2 and 6.6-4), Section 6.7.3 (Figs. 6.7-7 and 6.7-8)	(9.3.2)
- The Opalinus Clay alone	Section 6.7.3 (Fig. 6.7-9)	(9.3.3)
- Ramp and shaft	Section 6.7.2 (Fig. 6.7-3)	(9.3.4)
Barrier efficiency for Opalinus Clay intersected by discontinuities	Section 6.7.2 (Fig. 6.7-1)	Section 9.4
Dissolution of the fuel matrix	Section 6.7.3 (Fig. 6.7-5)	Section 9.5
Transport of radionuclides as volatile species	Section 6.7.2 (Fig. 6.7-2)	Section 9.6

9.2 Model to illustrate the meaning of the timescale for diffusion across the Opalinus Clay

9.2.1 Definition of the timescale for diffusion

Diffusion is expected to significantly contribute to radionuclide transport in the Opalinus Clay under the expected hydraulic conditions (see Sections 4.2.5 and 5.5.3.2 of Nagra 2002c). The time required for a radionuclide to diffuse across the clay varies between migrating species due to differences in the degree of sorption that they undergo, differences in the amount of accessible porosity, and differences in their diffusion coefficients. Furthermore, due to the random

nature of the movement of diffusing particles, different particles of the same species take different amounts of time to diffuse across the clay, giving rise to a spreading in time during diffusive transport. It is, however, possible to define a typical timescale, t_d [a], that characterises diffusion across the clay for a particular species.

As a simplifying assumption, one-dimensional diffusion is considered in the vertical direction from the repository through the Opalinus Clay towards the upper and lower confining units (Fig. 9.2-1), with L [m] being the diffusion distance within the Opalinus Clay.

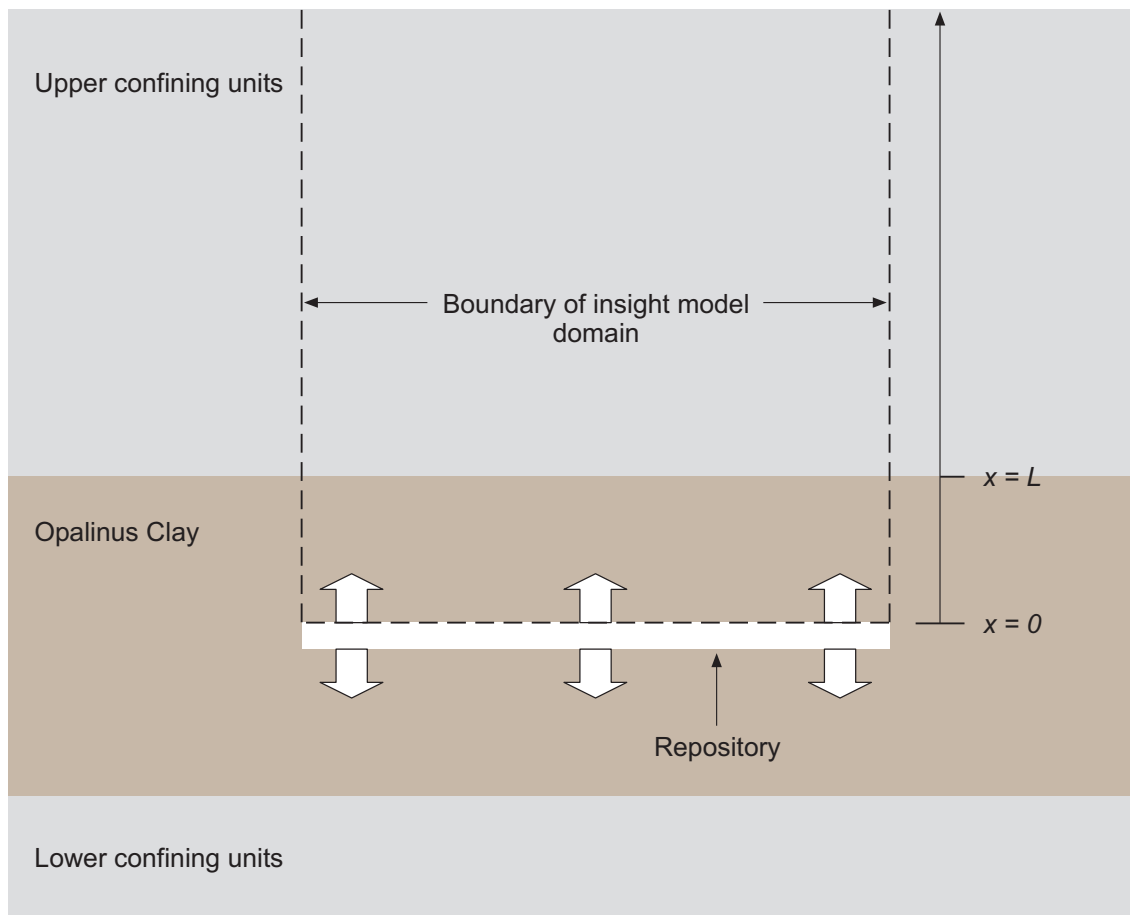


Fig. 9.2-1: Simplified view of the disposal system, in which radionuclides undergo one-dimensional diffusion in the vertical direction through the Opalinus Clay from the repository towards the upper and lower confining units

If the pore diffusion coefficient for a diffusing species is D [$\text{m}^2 \text{a}^{-1}$], the diffusion-accessible porosity within the Opalinus Clay is ε [-], the dry density of the Opalinus Clay is ρ [kg m^{-3}] and the sorption constant is K_d [$\text{m}^3 \text{kg}^{-1}$], then the timescale that characterises diffusion across the layer is given by:

$$t_d = \frac{L^2 R}{D}, \quad (9.2-1)$$

where R is a retardation factor defined as:

$$R = 1 + \frac{\rho K_d}{\varepsilon}. \quad (9.2-2)$$

The ratio $t_d / t_{1/2}$ is plotted in Fig. 6.6-1 of Nagra (2002c) for the different radionuclides considered in the safety assessment, with t_d calculated using Reference Case parameter values (Tab. 9.2-1).

Tab. 9.2-1: Reference Case parameters used to evaluate the ratio $t_d/t_{1/2}$ in Fig. 6.6-1 of Nagra (2002c)

Parameter	Symbol	Value	Source
Diffusion distance within the Opalinus Clay	L	40 m	Tab. A3.3-3, Parameter 3, Value A
Dry density of Opalinus Clay	ρ	2 394 kg m ⁻³	from Tab. A3.3-3, Parameter 8, Value A (grain density ρ_g): $\rho = \rho_g \times (1 - \varepsilon)$, with $\varepsilon = 0.12$
Porosity of Opalinus Clay	ε	0.06 for anions 0.12 for other species	Tab. A3.3-3, Parameter 10, Value A
Effective diffusion coefficient for Opalinus Clay	εD	10 ⁻¹² m ² s ⁻¹ for anions 10 ⁻¹¹ m ² s ⁻¹ for other species	Tab. A3.3-3, Parameter 7, Value A
Distribution coefficient	K_d	Element dependent [m ³ kg ⁻¹]	Tab. A3.3-3, Parameter 11, Value A
Half life	$t_{1/2}$	Radionuclide dependent [s]	Tab. A3.3-3, Parameter 1, Value A

It is argued (based on the insight model, below) that large values of the ratio $t_d/t_{1/2}$ are indicative of highly attenuated releases due to decay during diffusive transport.

9.2.2 Insight model

The timescale t_d provides an indication of the time required for a diffusing species to migrate across the clay. Significant breakthrough does not occur if the elapsed time is much less than t_d . Furthermore, if t_d is much greater than the half life of the diffusing species, then substantial decay will occur during migration.

A simple insight model can be used to illustrate the meaning of t_d . Consider the case of one-dimensional diffusion within a semi-infinite medium. The medium can be considered to be analogous to the Opalinus Clay, with the boundary $x = 0$ representing the boundary with the repository near field and $x = L$ representing the boundary of the Opalinus Clay with the upper confining units (which here are assumed to have the same properties as the Opalinus Clay itself). The boundary of the insight model domain is shown by the dotted line in Fig. 9.2-1. The governing diffusion equation is:

$$\frac{\partial C}{\partial t} = \frac{D}{R} \frac{d^2 C}{dx^2} - \lambda C \tag{9.2-3}$$

where λ [a⁻¹] is the decay constant of the diffusing radionuclide, i.e.:

$$\lambda = \ln 2 / t_{1/2}, \tag{9.2-4}$$

and $t_{1/2}$ [a] is the half life.

The concentration $C(x,t)$ of the diffusing radionuclide is assumed to be zero everywhere initially, and, at times $t > 0$, is held at constant value C_0 at $x = 0$ (this is analogous, say, to solubility-limited radionuclide release). The concentration can be calculated analytically as a function of t and x . The analytical solution of the diffusion equation for this system is given, for example, in Chapter 4.2 of Carslaw & Jaeger (1959) and is:

$$C(x,t) = \frac{C_0}{2} \left[e^{-x\sqrt{\lambda R/D}} \operatorname{erfc} \left(\frac{x}{2} \sqrt{\frac{R}{Dt}} - \sqrt{\lambda t} \right) + e^{x\sqrt{\lambda R/D}} \operatorname{erfc} \left(\frac{x}{2} \sqrt{\frac{R}{Dt}} + \sqrt{\lambda t} \right) \right], \tag{9.2-5}$$

where erfc is the complementary error function. At $x = L$, the concentration is:

$$C(L,t) = \frac{C_0}{2} \left[\exp \left(-\sqrt{\frac{t_d}{t_{1/2}} \log_e(2)} \right) \operatorname{erfc} \left(\frac{1}{2} \sqrt{\frac{t_d}{t}} - \sqrt{\frac{t}{t_{1/2}} \log_e(2)} \right) + \exp \left(\sqrt{\frac{t_d}{t_{1/2}} \log_e(2)} \right) \operatorname{erfc} \left(\frac{1}{2} \sqrt{\frac{t_d}{t}} + \sqrt{\frac{t}{t_{1/2}} \log_e(2)} \right) \right] \tag{9.2-6}$$

Fig. 9.2-2 shows the analytical solution (Eq. 9.2-6) for different hypothetical example radionuclides with different half lives. Tab. 9.2-2 shows the percentage of the final steady-state breakthrough rate of a stable nuclide achieved by different times (t).

Tab. 9.2-2: The percentage breakthrough of a stable nuclide for different values of time t

Percentage breakthrough [100 × C(L,t)/C ₀]	Time t
1.5 × 10 ⁻¹⁰	0.01 t_d
4.5 × 10 ⁻³	0.03 t_d
2.5	0.10 t_d
20	0.30 t_d
48	t_d

There is practically no breakthrough at $t = 0.01 t_d$, compared to a breakthrough of about 2.5 % at $t = 0.1 t_d$. A rough estimate of the time of "first arrival" of a stable nuclide is thus:

$$t \approx 0.03 t_d = 0.03 \frac{L^2 R}{D},$$

i.e. a time by which the breakthrough rate is about 0.005 % of its final steady-state value.

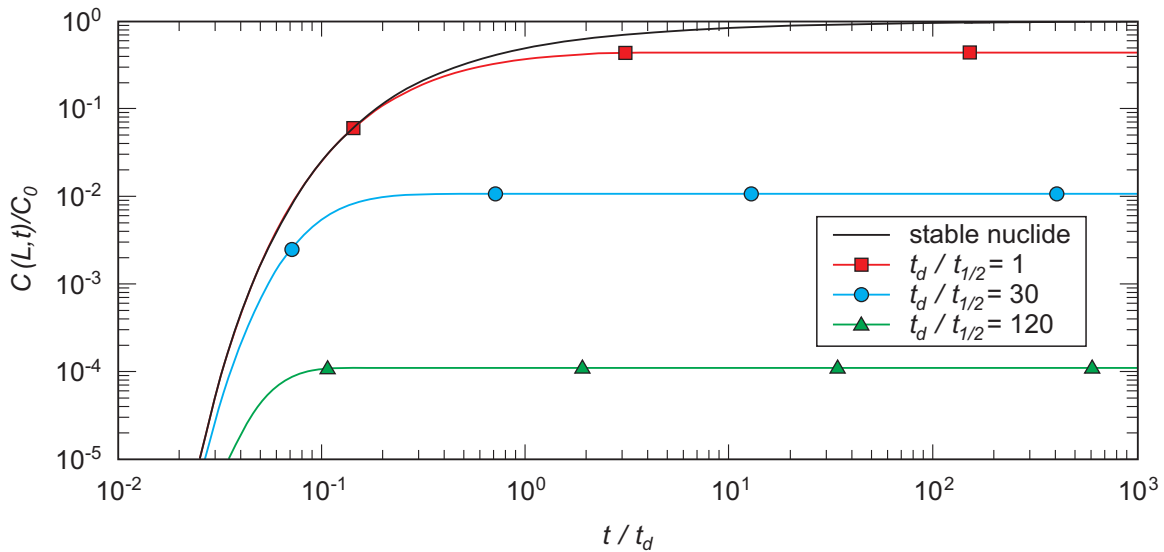


Fig. 9.2-2: Concentration at the boundary of the Opalinus Clay with the upper confining units as a function of time if a fixed concentration is imposed at the boundary with the repository near field

The analytical solution is shown for a stable nuclide, and for hypothetical example radionuclides with different half lives. Algebraic symbols are defined in the main text. By symmetry, these results are also applicable to the interface between Opalinus Clay and lower confining units ($L = -40$ m).

Fig. 9.2-2 also shows C/C_0 as a function of t/t_d for radionuclides with different half lives. The steady-state value of C/C_0 can be obtained from Eq. 9.2-6:

$$\frac{C(L,t)}{C_0} \rightarrow \exp\left(-\sqrt{\frac{t_d}{t_{1/2}} \log_e(2)}\right) \quad \text{as } t \rightarrow \infty . \quad (9.2-7)$$

If, for example, $t_d/t_{1/2}$ is equal to 30, then a concentration reduction across the clay of about 99 % occurs due to decay during diffusive transport once a steady state is reached. If $t_d/t_{1/2}$ is equal to 120, then a concentration reduction across the clay of about 99.99 % occurs. Thus, if the timescale t_d exceeds the radionuclide half life by about an order of magnitude or more, then significant decay during diffusive transport will occur.

9.2.3 Application of the insight model in the safety assessment

Fig. 6.6-3 of Nagra (2002c) shows profiles of the concentration of very long-lived isotopes of U and Th within the Opalinus Clay, represented as a semi-infinite medium, after one million years. The profiles are calculated using Eq. 9.2-5 and Reference Case parameter values, and illustrate the very limited distance into the Opalinus Clay that the isotopes migrate in one million years.

9.3 Barrier efficiency models for non-fractured media

9.3.1 Definition of the barrier efficiency

The degree of decay of different radionuclides during transport by aqueous diffusion and advection through different components of the disposal system can be illustrated using the concept of "barrier efficiency". In defining the barrier efficiency, radionuclides are assumed to enter the component under consideration (component i , which could be the Opalinus Clay, say) at a steady state rate of $F_{0,i}$ [Bq a⁻¹], and to leave the component at a steady state rate of $F_{1,i}$ [Bq a⁻¹]. The barrier efficiency, η , is given by:

$$\eta = 1 - \frac{F_{1,i}}{F_{0,i}}. \quad (9.3-1)$$

The barrier efficiency provides a measure of attenuation of releases by decay during transport on the assumptions (i), that radioactive ingrowth can be neglected and (ii) that releases to the component under consideration are only slowly varying with respect to the timescale for transport across the component (i.e. that a steady-state has been reached). A barrier efficiency of *one* thus corresponds to the ideal situation of complete decay during transport. A barrier efficiency of *zero* indicates that no decay occurs.

Insight models are used to evaluate the barrier efficiency for:

- the Opalinus Clay plus the SF / HLW bentonite buffer,
- the Opalinus Clay alone, and
- the ramp and shaft.

These models entail geometrical simplifications to allow analytical solutions to be obtained. They also assume that the different media are homogeneous. The special case of the Opalinus Clay intersected by discontinuities is considered in Section 9.4.

9.3.2 Model for the Opalinus Clay plus the SF / HLW bentonite buffer

General description

An analytical solution for the barrier efficiency can be obtained for the clay barrier, which comprises the Opalinus Clay and the bentonite buffer that surrounds the SF and HLW canisters.

Fig. 9.3-1 (upper figure) shows the geometrical simplifications that allow analytical solutions to be obtained. All SF / HLW tunnels are assumed to be identical, and the clay barrier within and around one tunnel is considered for modelling purposes. The bentonite is modelled as an annular region, with its axis lying along the centre of the SF / HLW emplacement tunnel. The

Opalinus Clay is treated as a 1-D layer, with releases from the bentonite occurring along one boundary. The boundary of the insight model domain is shown by the dotted line.

Radial diffusion through the bentonite is assumed (Fig. 9.3-1, lower figure). A steady-state concentration C_s [mol m^{-3}] is maintained at the inner boundary of the bentonite buffer. The pore diffusion coefficient in the buffer is D_b [$\text{m}^2 \text{a}^{-1}$], the porosity is ε_b , the solid density is ρ_b [kg m^{-3}], the sorption coefficient for the radionuclide under consideration is K_b [$\text{m}^3 \text{kg}^{-1}$], and the inner and outer radii are r_a [m] and r_b [m], respectively.

The mass passing across the outer boundary of the bentonite is assumed to be equal to that passing across the lower boundary of the model domain within the Opalinus Clay (the line AA' in Fig 9.3-2, lower figure). Furthermore, the radionuclide concentration at the outer boundary of the bentonite is assumed to be equal to that at the lower boundary of the model domain within the Opalinus Clay, and to take a value C_o [mol m^{-3}]. The width of the model domain within the Opalinus Clay is assumed to be equal to the tunnel perimeter ($2\pi r_b$).

One-dimensional, vertically directed aqueous diffusion, advection and dispersion are assumed in the Opalinus Clay. The applicability of the one-dimensional approximation for modelling transport through the Opalinus Clay has been investigated using a two-dimensional model (see Appendix 7). In addition to the parameters introduced in Section 9.2, the hydraulic conductivity in the Opalinus Clay is K [m a^{-1}], the hydraulic gradient is i , and the longitudinal dispersion length is a_L [m]. As in Section 9.2, the confining units are assumed to have the same properties as the Opalinus Clay.

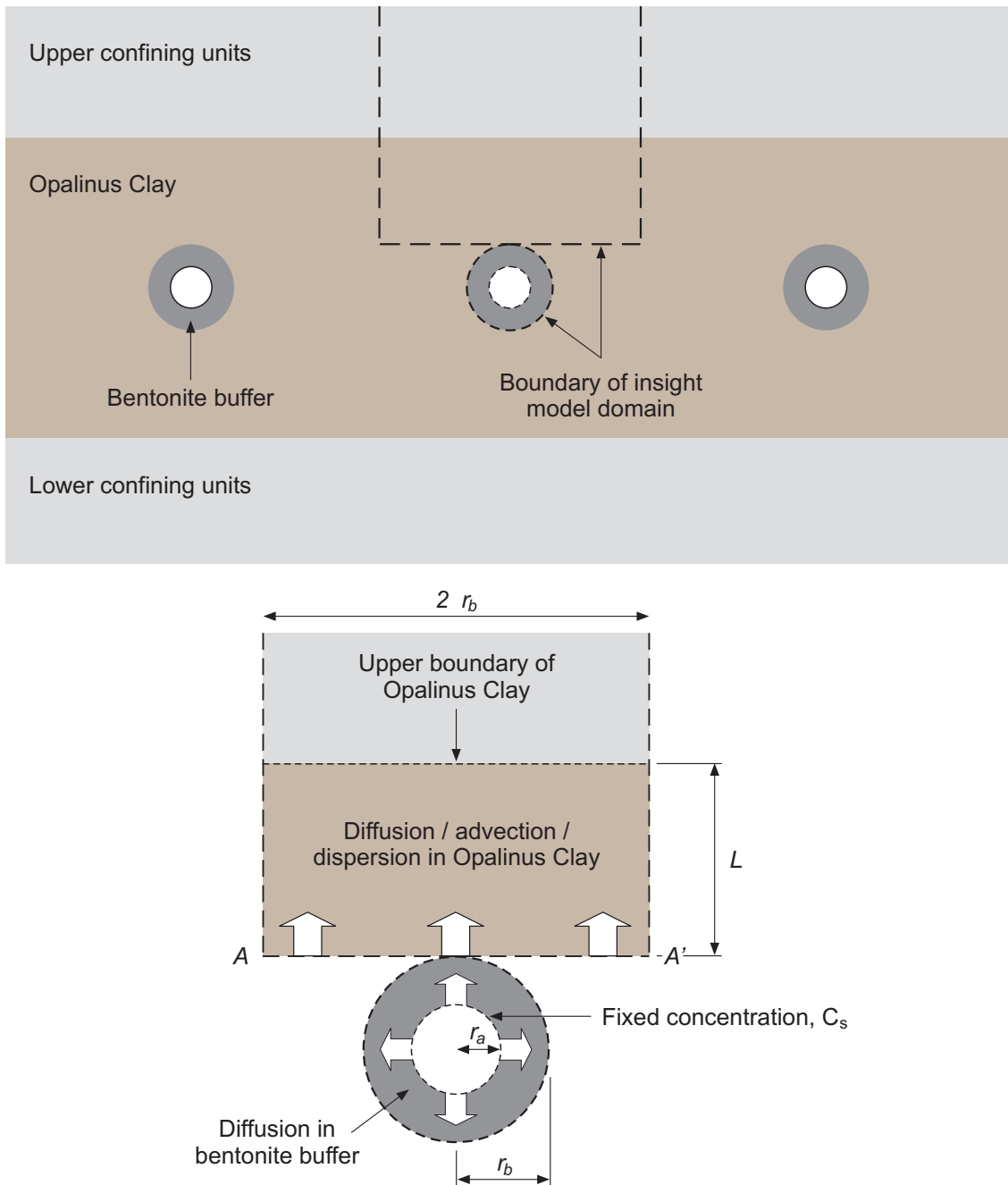


Fig. 9.3-1: Geometrical simplification of the bentonite / Opalinus Clay barrier for modelling purposes (upper figure), and transport processes within the model domain (lower figure)

Diffusion in the bentonite

The steady state equation governing diffusion of radionuclides in the bentonite is:

$$0 = \frac{1}{r} \frac{d}{dr} \left(r \frac{dC}{dr} \right) - \frac{\lambda R_b}{D_b} C, \quad (9.3-2)$$

where,

$$R_b = 1 + \frac{\rho_b K_b}{\varepsilon_b} \quad (9.3-3)$$

Eq. 9.3-2 has boundary conditions:

$$C = C_s \text{ at } r = r_a \quad (9.3-4)$$

and

$$C = C_0 \text{ at } r = r_b. \quad (9.3-5)$$

It can be rewritten in the form:

$$0 = r'^2 \frac{d^2 C}{dr'^2} + r' \frac{dC}{dr'} - r'^2 C, \quad (9.3-6)$$

with r' denoting the dimensionless radius:

$$r' = r \sqrt{\frac{\lambda R_b}{D_b}}. \quad (9.3-7)$$

This has the solution:

$$C = \frac{I_0(r') [C_0 K_0(r'_a) - C_s K_0(r'_b)] - K_0(r') [C_0 I_0(r'_a) - C_s I_0(r'_b)]}{K_0(r'_a) I_0(r'_b) - K_0(r'_b) I_0(r'_a)}. \quad (9.3-8)$$

where I_0 and K_0 are modified Bessel functions of order zero.

The radionuclide release per unit length of tunnel $f_b(r)$ [$\text{mol a}^{-1} \text{m}^{-1}$] through a circular cylindrical surface of radius r [m] within the bentonite is:

$$f_b(r) = -2\pi r \varepsilon_b D_b \frac{dC}{dr}. \quad (9.3-9)$$

From Eqs. 9.3-8 and 9.3-9:

$$f_b(r) = -2\pi r \varepsilon_b \sqrt{\lambda R_b D_b} \left\{ \frac{I_1(r') [C_0 K_0(r'_a) - C_s K_0(r'_b)] + K_1(r') [C_0 I_0(r'_a) - C_s I_0(r'_b)]}{K_0(r'_a) I_0(r'_b) - K_0(r'_b) I_0(r'_a)} \right\} \quad (9.3-10)$$

Advection and diffusion in the Opalinus Clay

The steady state equation governing diffusion and advection / dispersion in the Opalinus Clay is:

$$0 = -u \frac{dC}{dx} + (a_L u + D) \frac{d^2 C}{dx^2} - \lambda R C, \quad (9.3-11)$$

where R is given by Eq. 9.2-2 and

$$u = \frac{Ki}{\varepsilon}. \quad (9.3-12)$$

Eq. 9.3-11 has boundary conditions:

$$C = C_0 \text{ at } x = 0 \quad (9.3-13)$$

and

$$C \rightarrow 0 \text{ as } x \rightarrow \infty. \quad (9.3-14)$$

and has the solution:

$$\frac{C}{C_0} = e^{-ax}, \quad (9.3-15)$$

where

$$a = u \left[\frac{\sqrt{1 + 4(a_L u + D)\lambda R / u^2} - 1}{2(a_L u + D)} \right]. \quad (9.3-16)$$

The radionuclide release through a plane within the Opalinus Clay at a distance x [m] from the lower boundary of the model domain per unit length of tunnel, $f_c(x)$ [mol a⁻¹ m⁻¹], is:

$$f_c = 2\pi r_b \varepsilon \left[uC - (a_L u + D) \frac{dC}{dx} \right] = 2\pi r_b \varepsilon C_0 e^{-ax} [u + a(a_L u + D)] \quad (9.3-17)$$

Continuity at the near-field / geosphere interface

Continuity of mass transport at the interface, i.e.:

$$f_b \Big|_{r=r_b} = f_c \Big|_{x=0}, \quad (9.3-18)$$

is the condition used to fix the unknown concentration, C_0 . From Eq. 9.3-17:

$$f_c \Big|_{x=0} = \chi C_0, \quad (9.3-19)$$

where

$$\chi = 2\pi r_b \varepsilon [u + a(a_L u + D)] \quad (9.3-20)$$

From Eqs. 9.3-10, 9.3-19 and 9.3-20:

$$f_b|_{r=r_b} = \chi C_0 = -2\pi r_b \varepsilon_b \sqrt{\lambda R_b D_b} \left\{ \frac{I_1(r'_b)[C_0 K_0(r'_a) - C_s K_0(r'_b)] + K_1(r'_b)[C_0 I_0(r'_a) - C_s I_0(r'_b)]}{K_0(r'_a) I_0(r'_b) - K_0(r'_b) I_0(r'_a)} \right\} \quad (9.3-21)$$

Eq. 9.3-21 can be rearranged to give the required expression for C_0 :

$$C_0 = C_s \frac{[K_0(r'_b) I_1(r'_b) + I_0(r'_b) K_1(r'_b)]}{[K_0(r'_a) I_1(r'_b) + I_0(r'_a) K_1(r'_b)] + \frac{\chi}{2\pi r_b \varepsilon_b \sqrt{\lambda R_b D_b}} [K_0(r'_a) I_0(r'_b) - I_0(r'_a) K_0(r'_b)]} \quad (9.3-22)$$

Barrier efficiency

From Eq. 9.3-1, the combined barrier efficiency of the Opalinus Clay and SF / HLW bentonite buffer is:

$$\eta_{bc} = 1 - \frac{1}{f_b|_{r=r_a}} \times \begin{cases} f_b & r < r_b \text{ (i.e. at points inside the bentonite buffer)} \\ f_c & x \geq 0 \text{ (i.e. at points inside the Opalinus Clay)} \end{cases} \quad (9.3-23)$$

From Eq. 9.3-10 and 9.3-17:

$$\eta_{bc} = 1 - \begin{cases} \frac{r \{ I_1(r') [C_0 K_0(r'_a) - C_s K_0(r'_b)] + K_1(r') [C_0 I_0(r'_a) - C_s I_0(r'_b)] \}}{r_a \{ I_1(r'_a) [C_0 K_0(r'_a) - C_s K_0(r'_b)] + K_1(r'_a) [C_0 I_0(r'_a) - C_s I_0(r'_b)] \}} & \text{for } r < r_b \\ \text{or} \\ \frac{-r_b \varepsilon C_0 e^{-ax} [u + a(a_L u + D)]}{r_a \varepsilon_b \sqrt{\lambda R_b D_b} \left\{ \frac{I_1(r'_a) [C_0 K_0(r'_a) - C_s K_0(r'_b)] + K_1(r'_a) [C_0 I_0(r'_a) - C_s I_0(r'_b)]}{K_0(r'_a) I_0(r'_b) - K_0(r'_b) I_0(r'_a)} \right\}} & \text{for } r = r_b; x \geq 0 \end{cases} \quad (9.3-24)$$

where C_0 is given by Eq. 9.3-22.

9.3.3 Model for the Opalinus Clay alone

The barrier efficiency of the Opalinus Clay alone is defined as follows (using Eq. 9.3-17):

$$\eta_c = 1 - \frac{f_c}{f_c|_{x=0}} = 1 - e^{-ax} \quad (9.3-25)$$

9.3.4 Model for the ramp and shaft

The status of the repository after final sealing and closure of the facility is shown in Fig. 2.1-6. Tab. 9.3-1 gives the dimensions and hydraulic properties of the ramp and shaft and their surrounding excavation-disturbed zones (EDZ). The table shows that (neglecting the presence of seals) the flow per unit head difference along the length of the ramp, which is backfilled with a 30 % / 70 % bentonite / sand mixture³⁹, is greater through the backfill than through the EDZ, whereas the reverse is true for the shaft which is backfilled with pure bentonite. Thus, in the case of the ramp, in order to define a barrier efficiency, it is assumed that water flow and advective / diffusive transport occur predominantly through the backfill material and that flow and radionuclide transport through the EDZ can be neglected. Conversely, in the case of the shaft, it is assumed that water flow and advective / diffusive transport occur predominantly through the EDZ and that flow and transport through the backfill can be neglected. Both the ramp and the shaft are lined with cementitious material, although the liner is removed where the sealing plugs are emplaced. However, as has been shown in Section 3.6, radionuclide transport takes place predominantly through the host rock, thus the detailed release path within the tunnel system is largely irrelevant.

Tab. 9.3-1: Dimensions and hydraulic properties of the ramp and shaft

Property	Symbol	Units	Value		Source
			Ramp	Shaft	
Length of flow / transport path	L	m	1 000	40	Tab. A3.3-3, Parameter 3, Value G (Legs 1 and 5)
Inner radius of ramp / shaft (not including liner)	r_1	m	3.1	1.8	Tab. A3.3-4c and d
Outer radius of ramp / shaft (including liner)	r_2	m	3.4	2.0	
Outer radius of EDZ	r_3	m	4.4	2.7	
Hydraulic conductivity of backfill	K	m s^{-1}	5×10^{-11}	10^{-13}	
Hydraulic conductivity of EDZ	K_{EDZ}	m s^{-1}	1.0×10^{-12}		
Flow per unit head difference through backfill along length of ramp / shaft	$\pi K r_1^2 / L$	$\text{m}^2 \text{s}^{-1}$	1.5×10^{-12}	2.5×10^{-14}	calculated
Flow per unit head difference through EDZ along length of ramp / shaft	$\pi K_{EDZ} (r_3^2 - r_2^2) / L$	$\text{m}^2 \text{s}^{-1}$	2.5×10^{-14}	2.6×10^{-13}	calculated

The barrier efficiency of the backfilled ramp, η_r , and that of the EDZ surrounding the shaft, η_s , can be defined in an analogous way to that of the Opalinus Clay, if it is further assumed that these pathways are also homogeneous and no mass transfer occurs between these pathways and the surrounding rock. The efficiencies are then given by:

³⁹ Except for sealing zones, where pure bentonite is used.

$$\eta_r = 1 - e^{-a_r x} \quad (9.3-26)$$

and

$$\eta_s = 1 - e^{-a_s x}, \quad (9.3-27)$$

where a_r [m^{-1}] and a_s [m^{-1}] are defined in an analogous way to a in Eq. 9.3-16.

9.3.5 Application of the insight models in the safety assessment

Figs. 6.6-2, 6.6-4, 6.7-7 and 6.7-8 of Nagra (2002c) are based on Eq. 9.3-24 for the combined barrier efficiency of the Opalinus Clay and SF / HLW bentonite buffer, and parameter values for the Reference Case. Reference Case parameters for diffusion in Opalinus Clay are given in Tab. 9.2-1. Additional parameters for advection and dispersion in Opalinus Clay are given in Tab. 9.3-2 and parameters for diffusion in bentonite are given in Tab. 9.3-3.

Tab. 9.3-2: Reference Case parameters used to evaluate advection and dispersion in the Opalinus Clay

Parameter	Symbol	Value	Source
Peclet number for dispersion in Opalinus Clay	$Pe = L/a_L$	10	Tab. A3.3-3, Parameter 6, Value A
Hydraulic conductivity of Opalinus Clay	K	$2 \times 10^{-14} \text{ m s}^{-1}$	Tab. A3.3-3, Parameter 5, Value A (for Ki)
Hydraulic gradient	i	1	

Fig. 6.6-2 of Nagra (2002c) shows the distance into the bentonite buffer and host rock at which, if a steady state is reached, radionuclide transport rates are attenuated by 99 % and 99.99 %; i.e. distances at which the barrier efficiency of the combined Opalinus Clay and SF / HLW bentonite buffer, η_{bc} , is equal 0.99 and 0.9999, respectively. The distances are calculated by solving Eq. 9.3-24 for r or x . The method used is to increase r in a step-wise manner, starting from $r = r_a$ until either η_{bc} reaches a pre-set value (0.99 or 0.9999), or $r = r_b$. In the latter case, x is then increased in a step-wise manner, starting from $x = 0$ until η_{bc} finally does reach the pre-set value. Fig. 6.6-4 of Nagra (2002c) shows the combined efficiency of the Opalinus Clay and SF / HLW bentonite buffer as a function of distance of radionuclide penetration into the clay barrier, i.e. η_{bc} as a function of r and x . The efficiency is calculated directly from Eq. 9.3-24. Fig. 6.7-7 of Nagra (2002c) shows the distance into the bentonite buffer and Opalinus Clay at which, if steady state is reached, radionuclide transport rates are attenuated by 99 %. The distances are calculated as in Fig. 6.6-2, above, assuming Reference Case parameter values, and also the cases of 100 fold and a 1000 fold increases in the specific flow rate through the Opalinus Clay (the product of K and i). Fig. 6.7-8 shows the combined efficiency of the Opalinus Clay and bentonite buffer as a function of specific flow rate through the Opalinus Clay. The efficiency is calculated directly from Eq. 9.3-24, again using Reference Case parameter values and setting $x = L$.

Tab. 9.3-3: Reference Case parameters used to evaluate diffusion in the bentonite buffer

Parameter	Symbol	Value	Source
Inner and outer radii of bentonite	r_a and r_b	0.525 m and 1.15 m	Tab. A3.3-1, Parameters 23 and 24, Values A
Dry density of bentonite	ρ_b	1 766 kg m ⁻³	Tab. A3.3-1, Parameter 28, Value A \times (1 - 0.36)
Porosity of bentonite	ε_b	0.05 for anions 0.36 for other species	Tab. A3.3-1, Parameters 26 and 27, Values A
Effective diffusion coefficient for bentonite	$\varepsilon_b D_b$	3×10^{-12} m ² s ⁻¹ for anions 2×10^{-10} m ² s ⁻¹ for other species	Tab. A3.3-1, Parameters 33 and 34, Values A
Distribution coefficient for bentonite	K_b	Element dependent	Tab. A3.3-1, Parameters 29 and 30, Values A

Fig. 6.7-9 of Nagra (2002c) is based on Eq. 9.3-25 for the barrier efficiency of the Opalinus Clay alone, and parameter values for the Reference Case (Tabs. 9.2-1 and 9.3-1). The figure shows scatter plots of half life ($t_{1/2}$) vs. Reference Case K_d , showing regions in which the barrier efficiency of the Opalinus Clay is less than 0.99 (i.e. less than 99 % decay during steady-state transport), greater than 0.99 and less than 0.9999, and greater than 0.9999.

Fig. 6.7-3 of Nagra (2002c) is based on Eq. 9.3-26 and Eq. 9.3-27 for the barrier efficiencies of the backfilled ramp and the EDZ of the shaft. Parameter values are given in Tabs. 9.3-1, 9.3-4 and 9.3-5. The figure shows the barrier efficiencies of the shaft excavation disturbed zone (EDZ) and the bentonite / sand backfilled ramp as a function of water flow rates, Q_r [m³ a⁻¹] and Q_s [m³ a⁻¹] along these potential radionuclide transport pathways.

The advection velocities along the pathways, u_r [m a⁻¹] and u_s [m a⁻¹], which are required in order to evaluate a_r and a_s (see Eq. 9.3-16), are related to the flow rates via the equations:

$$u_r = \frac{Q_r}{\varepsilon_r \pi r_1^2} \quad (9.3-28)$$

$$u_s = \frac{Q_s}{\varepsilon_s \pi (r_3^2 - r_2^2)} \quad (9.3-29)$$

The symbols not yet defined required to evaluate a_r and a_s are given in Tabs. 9.3-4 and 9.3-5.

Tab. 9.3-4: Parameters used to evaluate transport along the backfilled ramp

Parameter	Symbol	Value	Source
Dry density of ramp backfill ¹	ρ_r	558 kg m ⁻³	Tab. A3.3-3, Parameter 8, Value C
Porosity of ramp backfill	ε_r	0.30	Tab. A3.3-3, Parameter 10, Value E
Pore diffusion coefficient for ramp backfill	D_r	5×10^{-10} m ² s ⁻¹	Tab. A3.3-3, Parameter 7, Value D
Peclet number	Pe	10	Tab. A3.3-3, Parameter 6, Value A
Distribution coefficient	K_b	Element dependent	Tab. A3.3-1, Parameters 29 and 30, Values A (i.e. assumed equal to those of the bentonite buffer)

¹ The backfill of the ramp consists of a 30 % / 70 % bentonite / sand mixture. Sorption on bentonite is taken into account, whereas the aggregates are pessimistically assumed to be non-sorbing.

Tab. 9.3-5: Parameters used to evaluate transport along the shaft EDZ

Parameter	Symbol	Value	Source
Dry density of shaft EDZ	ρ_s	2 394 kg m ⁻³	Tab. A3.3-3, Parameter 8, Value A \times (1 – 0.12)
Porosity of shaft EDZ	ε_s	0.06 for anions 0.12 for other species	Tab. A3.3-3, Parameter 10, Value A
Pore diffusion coefficient for shaft EDZ	D_s	5×10^{-11} m ² s ⁻¹	Tab. A3.3-3, Parameter 7, Value E
Peclet number	Pe	10	Tab. A3.3-3, Parameter 6, Value A
Distribution coefficient	K_d	Element dependent	Tab. A3.3-3, Parameter 11, Value A (i.e. assumed equal to those of undisturbed Opalinus Clay)

9.4 Barrier efficiency model for Opalinus Clay intersected by discontinuities

9.4.1 Definition of the barrier efficiency

If, rather than being homogeneous, the Opalinus Clay is assumed to be intersected by one or more discontinuities, the barrier efficiency of the Opalinus Clay can be defined as:

$$\eta'_c = 1 - \frac{f'_c}{f'_c|_{x=0}}, \quad (9.4-1)$$

where the primes indicate values for a non-homogeneous medium. The radionuclide release rate per unit length of tunnel, f'_c [mol a⁻¹ m⁻¹], consists of two parts: a part due to transport through

the discontinuities, $f_d(x)$ [mol a⁻¹ m⁻¹], and a part due to transport through the undisturbed Opalinus Clay, $f_u(x)$ [mol a⁻¹ m⁻¹]:

$$f'_c = f_d + f_u. \quad (9.4-2)$$

An insight model is used to evaluate f_d and f_u , and hence the barrier efficiency for Opalinus Clay intersected by discontinuities. This model again entails geometrical simplifications to allow a semi-analytical solution to be obtained.

9.4.2 Insight model

Fig. 9.4-1 shows the geometrical simplifications that allow (semi-)analytical solutions to be obtained. Again, all tunnels are assumed to be identical, and the Opalinus Clay around one tunnel is considered for modelling purposes. Discontinuities are assumed to be vertical features, with a regular spacing of $2B$ [m]. The release rate of radionuclides along a single discontinuity is therefore $2Bf_d$ and the release rate of radionuclides through the matrix between two fractures is $2Bf_u$. The boundary of the insight model domain is shown by the dotted line.

Radionuclide transport is assumed to occur by one dimensional advection / dispersion in the x -direction along discontinuities and by two-dimensional diffusion in the Opalinus Clay matrix, i.e. vertical diffusion parallel to the direction of groundwater flow in the discontinuities, and horizontal diffusion normal to the surfaces of the discontinuities (the z -direction). No flow is assumed to occur in the matrix and sorption on the walls of the discontinuities is not taken into account. Radionuclides may, however, pass between the discontinuities and the matrix by diffusion. Mixing is assumed to take place at the interface between the buffer inside the tunnels and the Opalinus Clay, so that, as in the model described in Section 9.3.2, a fixed concentration C_0 exists there.

In addition to the parameters introduced in Sections 9.2 and 9.3, the transmissivity of the discontinuities is T [m² a⁻¹] and their aperture is $2b$ [m], the longitudinal dispersion length for transport within the discontinuities is a'_L [m] and the diffusion coefficient within the fractures is D' [m² a⁻¹]. As in Sections 9.2 and 9.3, the confining units are assumed to have the same properties as the Opalinus Clay.

The steady state equation governing the concentration $P(x)$ of a radionuclide within in the discontinuities is:

$$0 = -u' \frac{dP}{dx} + (a'_L u' + D') \frac{d^2 P}{dx^2} - \lambda P + \frac{\varepsilon D}{b} \frac{\partial C}{\partial z} \Big|_{z=b}, \quad (9.4-3)$$

where

$$u' = \frac{Ti}{2b}, \quad (9.4-4)$$

$C(x,z)$ is the concentration in the matrix and i [m m⁻¹] is the hydraulic head gradient.

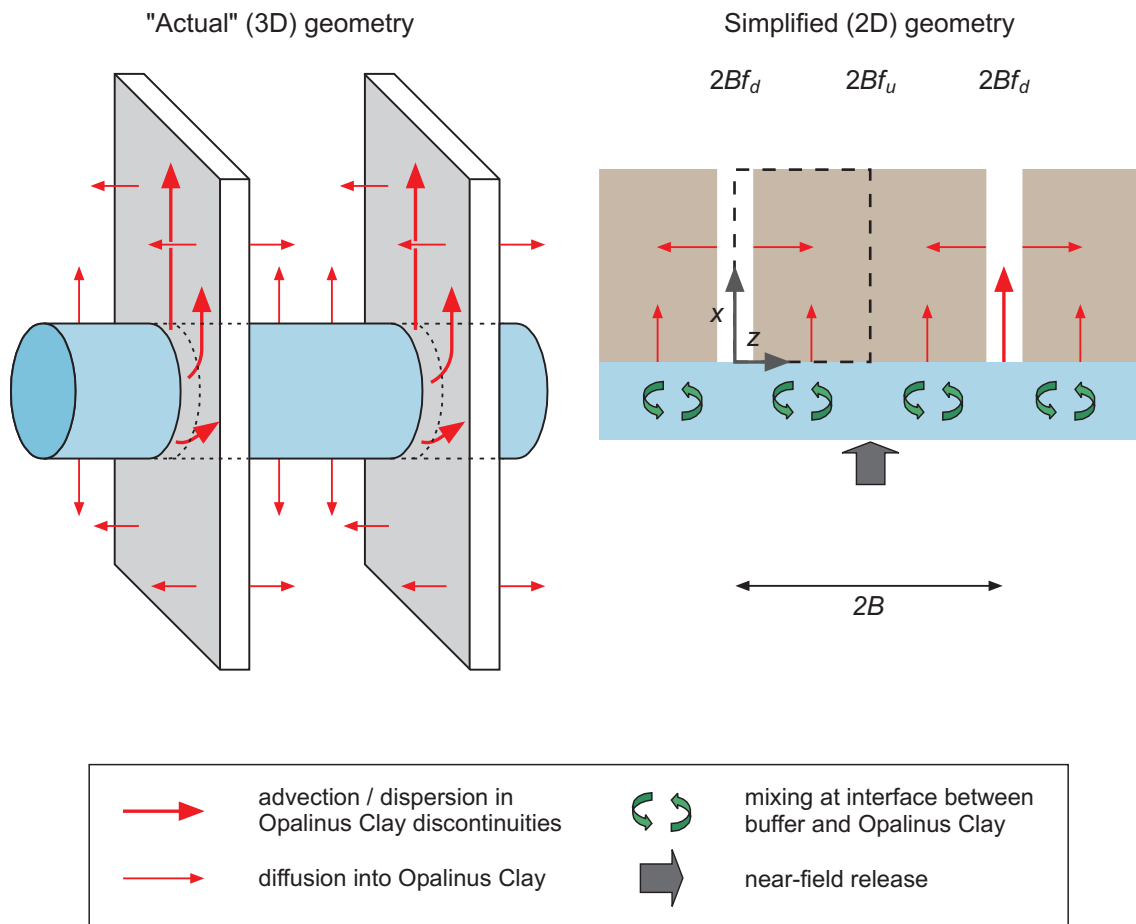


Fig. 9.4-1: "Actual" geometry of the disposal system around one tunnel, and simplified geometry for evaluation of the barrier efficiency, in the case of Opalinus Clay intersected by discontinuities

The steady state equation governing the concentration within the matrix is:

$$0 = \frac{d^2C}{dx^2} + \frac{d^2C}{dz^2} - \frac{\lambda R}{D} C \tag{9.4-5}$$

where R is given by Eq. 9.2-2.

Eq. 9.4-3 has boundary conditions:

$$P = C_0 \text{ as } x = 0 \tag{9.4-6}$$

and

$$P \rightarrow 0 \text{ as } x \rightarrow \infty. \tag{9.4-7}$$

Similarly, Eq. 9.4-5 has boundary conditions:

$$C = C_0 \text{ at } x = 0 \tag{9.4-8}$$

and

$$C \rightarrow 0 \text{ as } x \rightarrow \infty. \quad (9.4-9)$$

The radionuclide concentration is continuous across the boundary between the discontinuities and the rock matrix:

$$C = P \text{ at } z = b. \quad (9.4-10)$$

Finally, the system is periodic in the z -direction. The symmetry of the model system means that:

$$\left. \frac{\partial C}{\partial z} \right|_{z=B} = 0. \quad (9.4-11)$$

The solution of this set of governing equations and boundary conditions is obtained by a semi-analytical approach, as described in Appendix 4.

Having obtained this solution, the release rate of radionuclides along a single discontinuity can be evaluated using:

$$2Bf_d = Y \left[TiP - (a_L Ti + 2bD') \frac{dP}{dx} \right], \quad (9.4-12)$$

where Y [m] is a notional fracture length (normal to the plane shown in the right-hand side of Fig. 9.4-1) through which radionuclides are conveyed. The release rate of radionuclides through the matrix between two fractures is:

$$2Bf_u = -2(B-b)Y\epsilon D \frac{dC}{dx}. \quad (9.4-13)$$

From these equations, together with Eqs. 9.4-1 and 9.4-2, the barrier efficiency is given by:

$$\eta'_c = 1 - \frac{TiP - (a_L Ti + 2bD') \frac{dP}{dx} - 2(B-b)\epsilon D \frac{dC}{dx}}{TiC_0 - (a_L Ti + 2bD') \frac{dP}{dx} \Big|_{x=0} - 2(B-b)\epsilon D \frac{dC}{dx} \Big|_{x=0}}. \quad (9.4-14)$$

9.4.3 Application of the insight model in the safety assessment

Fig. 6.7-1 of Nagra (2002c) is based on Eq. 9.4-14 for the barrier efficiency of the Opalinus Clay intersected by discontinuities, and parameter values for the Reference Case (Tabs. 9.2-1 and 9.3-1), but setting the hydraulic conductivity of the Opalinus Clay matrix to zero, and evaluating the sensitivity of the barrier efficiency to the transmissivity and separation of the discontinuities. The figure shows the efficiency of the Opalinus Clay as a function of transmissivity, T , assuming the discontinuities to have spacings of either 10 m or 100 m throughout the clay. Additional parameters are the aperture of the discontinuities, $2b$, which is set to 1 mm, the longitudinal dispersion length for transport within the discontinuities, a'_L , which is set to 4 m (i.e. a Peclet Number of 10) and the diffusion coefficient within the discontinuities, D' , which is set equal to that of the Opalinus Clay matrix.

9.5 Model to illustrate dissolution of the SF matrix as a function of canister breaching time

9.5.1 Process model

The model used to illustrate dissolution of the SF matrix as a function of canister breaching time is also described in Johnson & Smith (2000). This model serves two purposes: (i) as a process model, it is used to derive the time-dependent fuel dissolution rates for the various fuel types required as input functions for the full near-field model (SPENT); and (ii) as an insight model, it is used to develop and demonstrate system understanding. In this model, dissolution is considered to be the result of an interaction of the matrix with radiolysis products (assumed to be principally H_2O_2), which oxidise the less soluble U(IV) to more soluble U(VI). Conservatively, it is assumed that the supply of water to the fuel surfaces is unlimited and the supply of reductants from repository materials (e.g. Fe^{2+} release from canister-corrosion processes) is neglected.

Since one mole of radiolytically-generated H_2O_2 oxidises one mole of U(IV) to U(VI), the fractional dissolution rate of the fuel, D [a^{-1}], is:

$$D = 10^{-6} P_C W_{U238} \quad (9.5-1)$$

where P_C [$\text{mol a}^{-1} \text{t}_{\text{HM}}^{-1}$] is the production rate of radiolytic H_2O_2 and W_{U238} is the atomic weight of ^{238}U (238 g mol^{-1}).

Radiolytic H_2O_2 is produced as a result of the α -flux experienced by water at the wetted fuel surfaces. This α -flux comes mainly from the top $d = 1.1 \times 10^{-5} \text{ m}$ of the fuel, as a result of the limited mean free path of the α -particles in solid UO_2 (Nitzki & Matzke 1973). The fraction of the fuel that can give rise to α -particles penetrating the wetted surfaces and causing radiolysis is:

$$F_f = \frac{3}{16} \frac{dw}{\pi a^2} \quad (9.5-2)$$

where w [m^2 per m of fuel rod] is the wetted surface area of the fuel and a [m] is the fuel rod radius. The factor of 3/16 is included to take account of the random direction of α -particles generated near the fuel surfaces (Liu & Neretnieks 1995). It is assumed that the wetted surface area of the fuel is 0.15 m^2 per metre of fuel rod (taking into account fracturing), and the fuel-rod radius is 0.5 cm. Thus, $F_f = 0.004$, i.e. only 0.4 % of the α -activity of the fuel gives rise to radiolysis, with the remainder of the energy being directly absorbed by the fuel.

The production rate, P_C , of radiolytic H_2O_2 is given by:

$$P_C = \frac{QG_{\text{eff}}F_f s}{pN_A} \quad (9.5-3)$$

where Q [$\text{W t}_{\text{HM}}^{-1}$] is the heat output of the fuel, G_{eff} is a so-called "effective G value" (Johnson & Smith 2000), s is the number of seconds in a year (3.156×10^7), p is the number of Joules corresponding to 100 eV (1.6×10^{-17}) and N_A is the Avogadro number (6.02×10^{23}). Thus:

$$P_C = 0.013QG_{eff}. \quad (9.5-4)$$

Johnson & Smith (2000) present a critical review of spent-fuel dissolution and radiolysis studies in order to derive an effective G value for radiolytic oxidant production, taking into account the partial recombination of radiolytic oxidants and reductants. It is concluded that a pessimistic value for safety assessment calculations is 0.01.

Using Eqs. 9.5-1 to 9.5-4, as well as data for the heat output of UO_2 and MOX fuels with different burn-ups as a function of time, Johnson & Smith (2000) tabulated fractional dissolution rates of different spent fuels, also as functions of time (see, in particular, Tab. 2 of Johnson & Smith 2000).

Fuel dissolution only occurs once a canister has been breached. In order to calculate the proportion of the fuel matrix that has dissolved as a function of time, $p(t)$, Eq. 9.5-1 is integrated numerically from the time of canister breaching, t_c [a]:

$$p(t) = \int_{t_c}^t D dt. \quad (9.5-5)$$

9.5.2 Application of the process model in the safety assessment

Fig. 6.7-5 of Nagra (2002c) shows the proportion of SF matrix that is corroded as a function of time for different canister breaching times. This is calculated from Eq. 9.5-5 using fractional dissolution rates from column (2) of Tab. A3.6-1 of Appendix 3. These values correspond to a weighted average of 1 MOX fuel element and 3 UO_2 fuel elements, each with a burnup of 48 GWd/ t_{HM} . Values for the individual fuel types and burn-ups are given in Tab. 2 of Johnson & Smith (2000).

9.6 Model to illustrate the transport of ^{14}C as volatile species

9.6.1 Insight model

In the Reference Case, it is assumed that radionuclides are released to solution, and subsequently migrate by aqueous diffusion and advection. Some radionuclides, however, and in particular ^{14}C , have the potential to form volatile species that could become mixed with gas generated within the repository and migrate in the gas phase through the Opalinus Clay and confining units, and hence to the surface environment.

In a simple insight model, a steady state model is considered for the calculation of drinking water doses related to the release of ^{14}C as volatile species. In this model it is assumed that ^{14}C migrates from the repository to the Malm aquifer in the form of methane, where it is dissolved and transported immediately to the Quaternary aquifer, which is used as a source of drinking water. The gas migration path from the repository to the surface environment includes a relatively large "storage volume" provided by gas-filled pore space in the different parts of the repository system. Following a period of complete containment (assumed to last 10 000 years for both SF and ILW)⁴⁰, ^{14}C instantly released from SF and ILW is mixed with repository-

⁴⁰ For both SF and ILW, it takes several tens of thousands of years until breakthrough of gas through the Opalinus Clay to the Wedelsandstein occurs (see Chapter 4). For HLW, transport of ^{14}C as volatile species is not an issue.

generated gas within the "storage volume". In the framework of this simple insight model, the rate at which ^{14}C reaches the surface environment depends on:

- the rate of generation of gas within the repository (principally hydrogen generated by corrosion of the SF / HLW steel canisters, and, less important, gases generated by ILW)⁴¹,
- the magnitude of the "storage volume" provided by the gas-filled pore space in the emplacement tunnels, especially in the cementitious backfill in the ILW tunnels, in the EDZ, in the access tunnel system, in the Opalinus Clay (layer of gas filled porosity in the vicinity of emplacement tunnels), and in the Wedelsandstein.

In the time period following containment, the rate of gas generation in the repository is assumed to be balanced at all times by the rate of gas transported through the low-permeability formations of the upper confining units.

Upon reaching the Malm aquifer, the radioactive methane is assumed to dissolve completely and to be transported instantaneously into the Quaternary aquifer, which is used as a source of drinking water. Degassing and atmospheric dilution of methane is conservatively neglected in the model calculations. The maximal drinking water dose is calculated as follows:

$$D = \frac{IRF}{V_g + V_w} \frac{Q_g}{Q_B} \frac{P_0}{P_w} \exp(-\lambda t_c) \delta U DF^{ing} \quad (9.6-1)$$

where:

IRF	instant release fraction of ^{14}C from SF/ILW, released as methane [Bq]
$V_g + V_w$	gas "storage volume" (see Chapter 4) [m^3]
Q_g	gas generation rate in repository [$\text{m}^3(\text{STP}) \text{a}^{-1}$]
Q_B	dilution rate in the Quaternary aquifer [$\text{m}^3 \text{a}^{-1}$]
P_w	gas pressure in Wedelsandstein [MPa]
P_0	atmospheric pressure [MPa]
λ	decay constant for ^{14}C [a^{-1}]
t_c	containment time [a]
δ	degassing factor [-]
U	drinking water consumption rate [$\text{m}^3 \text{a}^{-1}$]
DF^{ing}	dose conversion factor for ingestion [mSv Bq^{-1}].

The minimal gas "storage volume", provided by the gas-filled pore space in the SF tunnels and the cementitious backfill in the ILW tunnels is about $6\,000 \text{ m}^3$ (including the EDZ, see Tab. 4.3-7). The major contribution to the gas "storage volume" at the time of its maximum is from the gas-filled pore space in the Wedelsandstein. Based on a radius of the reservoir of $1\,400 \text{ m}$ (Tab. 4.3-5), the maximal gas "storage volume" is about $50\,000 \text{ m}^3$, including contributions from near field, gas layer in the Opalinus Clay and the Wedelsandstein formation.

⁴¹ The formation rate of volatile radioactive species is many orders of magnitude lower than the generation rate of non-radioactive gases.

9.6.2 Application of the insight model in safety assessment

Fig. 6.7-2 of Nagra (2002c) shows the drinking water dose as a function of the gas "storage volume" and the steel corrosion rate. Steel corrosion is the principal source of repository-generated gas. The doses associated with the release of volatile ^{14}C are calculated using the data given in Tab. 9.6-1.

Tab. 9.6-1: Parameters used to evaluate the transport of ^{14}C as volatile species (methane)

Parameter	Symbol	Value	Source
Instant release fraction of ^{14}C from SF and ILW at end of waste emplacement	IRF	$2 \times 10^{13} \text{ Bq}$	Tab. A3.3-1, Parameters 2 and 3, Values A, and Parameter 6, Values A
Dilution rate in the Quaternary aquifer	Q_B	$1.5 \times 10^6 \text{ m}^3 \text{ a}^{-1}$	Tab. A3.7-1, Parameter F_UL
Gas pressure in Wedelsandstein	P_w	5.6 MPa	Tab. 4.3-2 ($P_{s,w} + P_{a,w}$)
Atmospheric pressure	P_0	0.1 MPa	standard value
Containment time	t_c	10 000 a	Tab. A3.3-1, Parameter 5, Value A
Degassing factor	δ	1 (no degassing)	pessimistic assumption
Drinking water consumption rate	U	$0.73 \text{ m}^3 \text{ a}^{-1}$	Tab. A3.7-3
Decay constant for ^{14}C	λ	$1.2 \times 10^{-4} \text{ a}^{-1}$	derived from Tab. A3.4-1 (Half life)
Dose conversion factor for ingestion of ^{14}C	DF^{ing}	$5.8 \times 10^{-7} \text{ mSv Bq}^{-1}$	Tab. A3.4-1

10 Evaluation of the Models Used for the Assessment Cases

10.1 Aim of this chapter

Chapters 3 to 8 of this report describe the conceptual models underlying the various scenarios and associated assessment cases evaluated in the safety assessment and the various assumptions⁴² and simplifications that are made in order to arrive at sets of mathematical equations and input parameters so that each case can be quantitatively evaluated using the available computer codes. The aim of this chapter is to summarise these assumptions and to assess them in terms of their degree of realism, pessimism or conservatism⁴³. Although this assessment is to some extent a matter of judgement, and a different categorisation of particular phenomena might also be reasonable in some cases, the assessment is used as a tool to systematically assess the bias that has been introduced into the models – on purpose or inadvertently – by way of conceptual assumptions, parameter values and model simplifications (bias audit).

10.2 Types of assumptions

Each assessment case is based on a range of assumptions that define:

- the scenario considered for the broad evolution of the repository and its environment and the design or system options on which the case is based;
- the conceptual models used to represent the scenario; and
- parameter values used to describe the magnitude of features, the rates of processes and the timing of events.

Some assumptions are common to all or most assessment cases. This includes assumptions that are well supported by the scientific database and so prone to little uncertainty (e.g. the assumption that criticality does not occur), as well as pessimistic or conservative conceptual assumptions and parameters that are used to handle uncertainties that are neither avoidable nor amenable to reduction. Other assumptions vary from case to case, in order to explore the consequences of particular uncertainties or design / system options. These range from assumptions of likely or expected behaviour to more pessimistic or conservative conceptualisations and parameters.

All of these assumptions, whether they are realistic or more pessimistic, are based on current scientific understanding of the characteristics and evolution of the system. There are in addition some "what if?" assumptions made in a small number of assessment cases that are outside the range of possibilities that is reasonably to be expected and are to test the robustness of the system. There are also stylised assumptions made, particularly related to the evolution of the surface environment, where the full range of possibilities that may arise is a matter of speculation over the long time periods of interest in safety assessment. Finally, there are assumptions or simplifications that are made in order make the system amenable to mathematical modelling.

⁴² Assumptions are here defined as the statements that precisely define the assessment cases and the models used for their evaluation. The term should not be taken to imply that the statements are in any way arbitrary or poorly supported by the scientific database.

⁴³ Pessimism is here defined as the use of conceptual assumptions and parameter choices that give rise to calculated radiological consequences that are towards the high end of the range of possibilities supported by current understanding. Conservatism is defined as the use of conceptual assumptions and parameter choices that over-predict radiological consequences, and are known to lie outside the range of possibilities.

These simplifications are generally argued to have a negligible effect or to be conservative, i.e. to lead to an over-prediction of radiological consequences.

10.3 Applicability of assumptions

Some assumptions are considered applicable for all times, whereas others, such as the assumption of complete containment by the SF and HLW canisters, are applicable only over a restricted period, and this is reflected in the choice of parameter values (e.g. canister breaching time). Some other assumptions that are initially well supported by the scientific database but become questionable over timescales that are longer than the million years that is of primary interest in the safety assessment,⁴⁴ and so models and parameter values do not need to reflect the uncertainties for times greater than a few million years.

The applicability of some assumptions can also depend on that of others. It is, for example, assumed that the transport-relevant properties of the SF / HLW buffer are constant in space and time. This assumption is, however, inapplicable during the transient phase during which SF and HLW generate significant heat and the repository and its surroundings are not fully saturated. Its applicability in radionuclide transport calculations depends on the assumption that the SF / HLW canisters remain unbreached throughout the transient phase, so that no radionuclides are present in the buffer at times when its properties are affected by significant temperature and moisture gradients. By incorporating long-lived canisters for SF / HLW in the repository design, it is ensured that the considerable uncertainties associated with transient thermal, hydraulic and mechanical (THM) processes in the buffer do not need to be taken into account in safety assessment calculations, since these uncertainties relate to a period when complete containment of radionuclides in the canisters is assured and since they are not expected to affect the properties of the buffer in the long term.

10.4 Categorisation of assumptions

In the following sections, assumptions relating to the broad characteristics and evolutionary path followed by the system, the conceptualisation of phenomena, the magnitude of features, the rates of processes and the timing of events are categorised in terms of their relationship to current scientific understanding. The following abbreviations are used:

Categorisation of assumptions for the broad characteristics and evolutionary path followed by the system and the conceptualisation of phenomena:	
LE:	Conceptual assumption corresponds to the <u>l</u> ikely/ <u>e</u> xpected characteristics and evolution of the system - any deviations are expected to be unimportant
PCA:	<u>P</u> essimistic <u>c</u> onceptual <u>a</u> ssumption within the range of possibilities that is reasonably to be expected
WRP:	<u>W</u> ithin the <u>r</u> ange of <u>p</u> ossibilities, but likelihood not currently possible to evaluate – other (and sometimes more pessimistic) assumptions may not be unreasonable

⁴⁴ Although, after more than a few million years, the assumptions underlying the conceptualisation of some key FEPs may no longer hold, calculations are continued over a period up to 10 million years, in order to illustrate the behaviour of the model system (rather than the actual system) at these distant future times.

WI:	<u>W</u> hat <u>i</u> f? assumption for system evolution that is outside the range of possibilities that is reasonably to be expected
ST:	<u>S</u> tylised conceptualisation of system characteristics and evolution
Categorisation of assumptions regarding the magnitude of features, the rates of processes and the timing of events:	
BE:	<u>B</u> est <u>e</u> stimate value
WRV:	<u>W</u> ithin the <u>r</u> ange of possible <u>v</u> alues, but likelihood not currently possible to evaluate – other (and sometimes more pessimistic) assumptions may not be unreasonable
PV:	<u>P</u> essimistic <u>v</u> alue within the range of possibilities that is reasonably to be expected
WIV:	<u>W</u> hat <u>i</u> f? <u>v</u> alue that is outside the range of possibilities that is reasonably to be expected

In addition, model simplifications are categorised as follows:

Categorisation of simplifications made for modelling purposes:	
MS:	<u>M</u> odel <u>s</u> implification that does not significantly affect calculational results
CS, CS(R):	Model simplification that is intrinsically <u>c</u> onservative, e.g. favourable feature or process not included in model. (R) indicates reserve FEP (see Tab. 6.8-3 of NAGRA 2002c)
CP:	Model simplification that is <u>c</u> onservative given the model <u>p</u> arameters that are also assumed

10.5 Assessment of Reference Case assumptions

Tab. 10.5-1 lists the assumptions underlying the Reference Case, and categorises them according to the system described in the previous section. In the Reference Case, the assumptions are generally based on the expected evolution of the system components (category LE) and the parameter values used correspond to best estimate values (category BE). However, some pessimistic or conservative conceptual assumptions, parameters and model simplifications (categories PCA, WRP, WRV, PV, MS, CS, CP) and stylised biosphere conceptualisations (ST) are also used, but no "what if?" assumptions and values are adopted (categories WI and WIV).

Tab. 10.5-1: Assessment of the main conceptual assumptions made in the Reference Case

Main conceptual assumptions in the Reference Case	Cat.	Cases addressing alternative assumptions and related uncertainties
General assumptions of the Reference Scenario: release of dissolved radionuclides		
The deep underground location of the repository is maintained over several million years, isolating the waste from the surface environment.	LE	
The host rock maintains its safety-relevant properties over several million years and these properties are not significantly perturbed by the presence of the repository (e.g. by gas generated within the repository), by geological and climatic events and processes and by any future human activities. The low hydraulic conductivity and the fine, homogeneous pore structure of the host rock, as well as the backfilling and sealing of the access tunnels and shafts, ensures very small radionuclide transport rates through the near field and host rock. The sealed access tunnels and shafts are assumed at no time to provide preferential transport pathways, although some limited radionuclide transport along these features may occur.	LE	1.6a-b, 2.1a-c, 2.2a-c, 3.1a-g, 3.2a-b, 3.3a, 4.6a-c
The favourable chemical environment, which provides a range of geochemical immobilisation and retardation processes, is maintained over several million years.	LE	
The bentonite buffer (for SF and HLW) maintains its favourable properties over several million years.	LE	
The SF and HLW waste forms continue to retain most radionuclides after canister breaching.	LE	
The SF and HLW canisters provide an initial period of complete containment. For all waste streams, the repository and its surroundings are assumed to be fully resaturated by the time pore water comes into contact with the wastes and porewater is assumed to have reached chemical equilibrium.	LE	
Criticality does not occur.	LE	
Radionuclide inventories		
The radionuclide inventory contained in the pilot facility is added to the inventories for SF and HLW of the main facility.	MS	
SF waste inventory is based on 192 GWa(e) scenario, corresponding to a 60 year lifetime for current nuclear power plants.	PCA	5.1a
SF waste inventory is based on a burnup of 48 GWd/t _{IHM} .	WRV	1.1b
Best estimate values for the SF IRF are used	BE	1.1b
HLW inventory is based on specified compositions.	BE	
ILW inventory is based on cemented waste option.	BE	4.4a, 5.2a
All ¹⁴ C originating from the cladding is in organic form (20 % of which is assigned to the IRF), whereas all ¹⁴ C from the fuel matrix is assumed to be inorganic.	PV	1.1k
The period of complete containment		
The design option of steel SF/HLW canisters is adopted; no initial defects are present.	LE	5.3a-c
No significant SF/HLW canister sinking takes place.	LE	
No account is taken of the delay in the commencement of SF/HLW corrosion and dissolution processes due to the long resaturation time of the repository.	CS (R)	
A pessimistic canister breaching time of 10 ⁴ years for SF/HLW is assumed.	PV	1.1c
The spreading of radionuclide releases in time due to the fact that SF/HLW canisters would not be breached simultaneously is neglected.	CS	
The SF cladding and HLW fabrication flasks provide no additional period of complete containment following canister breaching.	CS	

Tab. 10.5-1: (Cont.)

Main conceptual assumptions in the Reference Case	Cat.	Cases addressing alternative assumptions and related uncertainties
SF/HLW canister breaching is instant and complete, so the breached canisters provide no physical barrier to water ingress.	CS	
No account is taken of a period of complete containment by ILW steel drums and emplacement containers.	CS	
Radionuclides in ILW are completely contained until the ILW near field is resaturated (resaturation period chosen to assure conservatism).	CP	4.7a-c
Radionuclide release from the waste forms		
Radionuclides in the SF matrix and HLW borosilicate glass are released congruently as the SF matrix and HLW glass dissolve.	LE	
The rate of matrix dissolution is controlled by the rate of production of radiolytic oxidants.	PCA	1.2a, 4.3a-b
The SF cladding inventory is released congruently with cladding corrosion (see, however, below).	LE	4.9a
The cladding corrosion rate is constant with time (cladding corrosion rate chosen to ensure conservatism).	CP	
Radionuclides in the SF IRF are released immediately following the period of complete containment.	PCA	
Some cladding inventory of ¹⁴ C (organic) is assigned to the IRF.	CS	
The rate of HLW dissolution per unit surface area of wetted glass is constant with time.	WRP	1.1e, 4.7a-c
HLW glass is fractured.	LE	
The effects of HLW glass fracturing on dissolution can be represented in terms of equivalent spheres.	MS	
The transport resistance provided by internal spaces (fractures) within the waste forms, by the breached SF/HLW canisters and by corrosion products is neglected.	CS	5.3b-c
ILW radionuclides are released to near-field porewater immediately following the containment period; no account is taken of the delayed release of radionuclides due to the slow corrosion rate of ILW metallic materials (e.g. hulls and ends).	CS (R)	
Radionuclides released from the waste forms enter "reservoirs" of water within the SF and HLW canisters, and within the pore space of the ILW emplacement tunnels, where they are uniformly mixed. Chemical equilibrium is assumed to exist within the reservoirs.	LE	2.1, 2.2, 4.6
Solubility limits constrain the aqueous concentrations of radionuclides, with precipitation occurring if the solubility limits of the corresponding elements are exceeded, and redissolution occurring if concentrations fall.	LE	
Solubility limits are based on realistically estimated chemical conditions.	BE	1.1d, 1.1i, 4.7a-c
Only the concentrations of isotopes originating from the waste are taken into account in evaluating whether solubility limits are exceeded in the reservoirs; the background concentrations of isotopes originating elsewhere are conservatively ignored.	CS (R)	
Immobilisation by co-precipitation with secondary minerals derived from SF, glass and canister corrosion is conservatively neglected (except in the case of ²²⁶ Ra), as is sorption on the corrosion products of the canisters and waste forms.	CS (R)	
No sorption occurs within the reservoirs in the cases of SF and HLW; sorption on canister corrosion products is neglected.	CS	

Tab. 10.5-1: (Cont.)

Main conceptual assumptions in the Reference Case	Cat.	Cases addressing alternative assumptions and related uncertainties
Radionuclide transport through the SF/HLW bentonite buffer and ILW cementitious buffer		
Following resaturation, the transport-relevant properties of the SF/HLW buffer and ILW near field are constant in space and time.	LE	
Tunnel convergence reduces the SF/HLW tunnel diameter; it occurs concurrently with resaturation and so does not affect radionuclide transport (resaturation completed before canister breaching).	LE	1.7a
The thermally altered zone in the buffer around the SF/HLW waste packages is of negligible extent.	LE	1.3a
Radiolytic oxidants produced by SF and HLW are consumed by reaction with steel and do not affect the retention properties of the buffer.	LE	4.4a
Radionuclide transport in the SF/HLW buffer is assumed to take place by diffusion (Fick's laws) and retarded by linear, equilibrium sorption.	LE	3.1e-g
No account taken of irreversible sorption in the SF/HLW buffer.	CS (R)	
Some radionuclides are subject to anion exclusion in the SF/HLW buffer, affecting their diffusion coefficients and the effective porosity that they see.	LE	
The hydraulic properties of the SF/HLW buffer prevent any significant advective transport.	LE	
Axial diffusion of radionuclides into the SL/HLW buffer separating the canisters is conservatively neglected.	CP	
Solubility limits constrain radionuclide concentrations in the SF/HLW buffer; any colloids are immobile.	LE	
Only the concentrations of isotopes originating from the waste are taken into account in evaluating whether solubility limits are exceeded in the reservoirs; the background concentrations of isotopes originating elsewhere are conservatively ignored.	CS (R)	
The hydraulic properties of the host rock prevent any significant advective flow in the ILW emplacement tunnels.	LE	3.1a,c-d, 4.2c,f
Radionuclides released from the ILW waste matrix are partitioned between aqueous, sorbed and precipitated phases; linear, equilibrium sorption is assumed; any radionuclide-bearing colloids do not migrate beyond the cementitious buffer.	LE	
No account taken of irreversible sorption in ILW near field.	CS (R)	
The ILW cement is an open structure in which anion exclusion is not important.	LE	
Tunnel convergence and compaction of ILW waste/mortar does not affect radionuclide transport in the ILW near field.	LE	1.7a-b
The build-up of repository gas pressure does not expel water and dissolved radionuclides from the SF/HLW and ILW near field.	LE	1.8a-b, 4.5a-b
Solubility limits and sorption coefficients in the SF/HLW buffer and ILW near field are based on a realistic geochemical dataset.	BE	1.1d, 1.1i, 4.4a, 4.7a-c, 4.10a
Organic carbon is non-sorbing.	CS	
Interface with the host rock		
Radionuclides that enter the Opalinus Clay cannot diffuse back into the near field; the boundary condition at the near-field/Opalinus Clay interface is modelled via an effective groundwater flow rate at the boundary.	CP	

Tab. 10.5-1: (Cont.)

Main conceptual assumptions in the Reference Case	Cat.	Cases addressing alternative assumptions and related uncertainties
Radionuclide transport processes in the host rock		
All transport paths from the repository through the host rock are assumed to be identical in their transport-relevant properties.	LE	
A single, representative transport path through the Opalinus Clay is considered (40 m long); the spreading of radionuclide releases in space and time due to the lateral extent of the repository, transverse dispersion and the three-dimensional nature of diffusive transport is neglected.	PCA	4.11a
Fick's laws describe diffusion in the Opalinus Clay.	LE	
Diffusion coefficients are based on a realistic geochemical dataset.	BE	1.1j
Advective/dispersive transport in the Opalinus Clay is described by Darcy's Law, and is driven by the currently observed pressure difference between the local aquifers in the lower and upper confining unit (specific flowrate = 2×10^{-14} m s ⁻¹); glacial cycling and other environmental and repository-induced driving forces for flow have a negligible effect on radionuclide transport through the clay.	WRP	1.1f-g, 1.4a 4.1a, 4.7b-c, 4.8a
Any colloids are assumed to be immobile in the Opalinus Clay.	LE	
Some radionuclides are subject to anion exclusion in the Opalinus Clay, affecting their diffusion coefficients and the effective porosity that they see.	LE	
The Opalinus Clay is homogeneous, and contains no discontinuities that are relevant to radionuclide transport and retention.	LE	3.1a-g, 4.2a-f
Transport in the Opalinus Clay is retarded by linear, equilibrium sorption.	LE	
No account taken of irreversible sorption or long-term immobilisation processes (precipitation/co-precipitation) in the host rock.	CS (R) ¹	
Sorption coefficients in the Opalinus Clay are based on a realistic geochemical dataset.	BE	1.1h, 1.1i, 4.7a-c, 4.10a
Organic carbon is non-sorbing.	CS	
Following resaturation, the transport-relevant properties of the Opalinus Clay are constant in space and time, being unaffected by geological and climatic processes, and by the presence of the repository (e.g. no significant impact from high-pH originating from the ILW backfill).	LE	
The sealed tunnel/ramp/shaft and their surrounding excavation disturbed zones do not provide preferential paths for radionuclide transport.	LE	1.6a-b, 1.8a-b, 2.2a-c
The tunnel/ramp/shaft seals remain effective throughout the period addressed, and are not by-passed by relatively permeable excavation-disturbed zones.	LE	1.7a-b, 4.5a-b, 3.3a
Radionuclide transport through the upper and lower confining units		
Radionuclides released from the host rock are transferred instantaneously to the biosphere. Transport times through the sedimentary layers overlying and underlying the host rock (the upper and lower confining units) are conservatively neglected.	CS	1.5a-b
Dilution in deep regional aquifers is small compared to that assumed to occur in Quaternary aquifers and in the surface environment, and is neglected.	MS	3.2a-b

Tab. 10.5-1: (Cont.)

Main conceptual assumptions in the Reference Case	Cat.	Cases addressing alternative assumptions and related uncertainties
The surface environment and exposure pathways		
Discharge of contaminated deep groundwater is assumed to occur into the Quaternary gravel aquifer in the Rhine valley.	LE	3.2a-b, 6.1d
Radionuclides are greatly diluted in the Quaternary aquifer and surface waters and sediments.	LE	
The Reference Case Biosphere is characterised by the climate state "present-day climate" and the local geomorphological unit "eroding river".	ST	
Present day climatic and surface environmental conditions are assumed to persist for all calculated times.	ST	6.2b-d
Exfiltration, and hence radionuclide release, takes place to a section of the Rhine valley where the groundwater table is at some distance from the soil.	ST	6.1b-d
No account is taken of degassing of volatile $^{14}\text{CH}_4$ in the biosphere.	CS (R) ²	
The population group for which dose is calculated is assumed to inhabit a region large enough to supply all its basic requirements, and dietary requirements are obtained from local sources.	ST	

- Notes:
- ¹ Conservative, unless a change in geochemical conditions leads to remobilisation of previously immobilised radionuclides.
 - ² Conservative, unless methane accumulates e.g. in basements.

10.6 Assessment of assumptions for alternative cases

Tabs. 10.6-1 to 10.6-6 list the assumptions made in each of the alternative cases where these differ from the assumptions of the Reference Case, and again categorises them according to the system described in Section 10.4. The following additional abbreviations are used to describe also aspects of the repository and the geological and surface environments:

Key to abbreviations used in the tables in Chapter 10 (continued):

GAS:	Gas generation, dissolution, storage and migration
INV:	Radionuclide in ventories
RELEASE:	Radionuclide re lease from the waste forms
BUFFER:	Radionuclide transport through the SF/HLW bentonite bu ffer and ILW cementitious bu ffer
INT:	The in terface with the host rock, including the emplacement tunnel excavation disturbed zones (EDZs)
ROCK:	Radionuclide transport in the host ro ck (but including also transport through the tunnel / ramp / shaft and their excavation disturbed zones, where these are relevant to the assessment case under consideration)
BH:	Bore hole
SED	Radionuclide transport through the overlying and underlying se dimentary layers (the "confining units" and regional aquifers)
SURF:	The surface environment and exposure pathways

It was noted in Section 10.3 that the applicability of some assumptions is dependent on the characteristics and broad evolutionary path of the system (i.e. on the scenario and design / system options considered). This is true also of the categorisation of assumptions, i.e. the categorisation applied to one assumption can, in principle, depend on that applied to another. For example, the table indicates that the assumption in Case 4.2a that "Radionuclide transport along discontinuities takes place by advection / dispersion and is retarded by matrix diffusion and sorption on matrix pore surfaces" corresponds to the likely / expected characteristics and evolution of the system (**LE**), provided that the existence of transmissive discontinuities is postulated (**WI**).

Tab. 10.6-1: Assessment of the main conceptual assumptions made in the alternative cases within the Reference Scenario: release of dissolved radionuclides

Case (Categorisation of main issues)	Main issues addressed	Key conceptual assumptions where these differ from those of the Reference Case (Case 1.1a)							
		Description	Categorisation of assumptions						
			INV	CONT	RELEASE	BUFFER	INT	ROCK	SED
1.1 Reference Conceptualisation									
1.1b (PCA)	The possibility of a higher SF burnup than assumed in the Reference Case.	SF waste inventory is based on burnups of up to 75 GWd/t _{HM} .	PV						
	Uncertainty in the size of the IRF for UO ₂ and MOX fuels.	A pessimistically assigned IRF inventory for SF is assumed.	PV						
1.1c (PCA)	Uncertainty in the conditions under which mechanical failure of corroded canisters will occur and in the significance of localised corrosion processes.	A pessimistically assigned canister breaching time of 10 ³ years is assumed.		PV					
1.1d (PCA)	Uncertainty in geochemical data and near-field porewater composition.	Solubility limits and sorption coefficients in the SF / HLW buffer and ILW near field are based on a pessimistic geochemical dataset.				PV			
1.1e (PCA)	Uncertainty in the rate of glass dissolution.	Glass dissolution occurs at a higher rate than in the Reference Case.			PV				
1.1f (PCA)	Uncertainty in the rate of groundwater flow in the Opalinus Clay (see also 4.1a, 4.7a-c).	Specific groundwater flow rate increased 10-fold with respect to the Reference Case.						PV	
1.1g (WRP)	Possibility that groundwater flow is less than predicted by Darcy's Law; uncertainty regarding the existence of a "threshold hydraulic gradient" (see also 4.8a).	Specific groundwater flow rate decreased 10-fold with respect to the Reference Case.							WRV

Tab. 10.6-1: (Cont.)

Case (Categorisation of main issues)	Main issues addressed	Key conceptual assumptions where these differ from those of the Reference Case (Case 1.1a)							
		Description	Categorisation of assumptions						
			INV	CONT	RELEASE	BUFFER	INT	ROCK	SED
1.1 Reference Conceptualisation									
1.1h (PCA)	Uncertainty in geochemical data and geosphere porewater composition.	Sorption coefficients in the Opalinus Clay are based on a pessimistic geochemical dataset.						PV	
1.1i (PCA)	Uncertainty in geochemical data and near-field and Opalinus Clay porewater composition.	Solubility limits and sorption coefficients in the near field and sorption coefficients in the Opalinus Clay are based on a pessimistic geochemical dataset.				PV		PV	
1.1j (PCA)	Uncertainty in the geochemical dataset with respect to diffusion in the Opalinus Clay.	Diffusion constants in the Opalinus Clay are based on a pessimistic geochemical dataset.						PV	
1.1k (PCA)	Uncertainty in the chemical state of ¹⁴ C released from SF.	All ¹⁴ C originating from both the cladding and the fuel matrix is in organic form.	PV						
1.2 Solubility-limited dissolution of SF									
1.2a (LE)	Whether the rate of dissolution is controlled by the rate of production of radiolytic oxidants or by the solubility of U(IV).	Reducing conditions prevail at the fuel surface, irrespective of the generation of radiolytic oxidants, and the rate of dissolution of the fuel (and hence the release rate of radionuclides from the fuel matrix) is controlled by the solubility of U(IV) and the rate of diffusion of U(IV) in solution away from the fuel surface.				LE			
1.3 Bentonite thermal alteration									
1.3a (PCA)	The extent and consequences of thermal alteration of the buffer adjacent to SF / HLW canisters.	Increased temperatures lead to the thermal degradation of the inner half of the buffer surrounding the SF / HLW canisters.				PCA			
		The diffusion coefficient is assumed to be that of free water in the altered part of the buffer.				CS			

Tab. 10.6-1: (Cont.)

Case (Categorisation of main issues)	Main issues addressed	Key conceptual assumptions where these differ from those of the Reference Case (Case 1.1a)								
		Description	Categorisation of assumptions							
			INV	CONT	RELEASE	BUFFER	INT	ROCK	SED	SURF
1.4 Glacially-induced flow in the Opalinus Clay										
1.4a (WRP)	The impact of ice loads during future glaciations on the flow through the Opalinus Clay.	No transmissive discontinuities in Opalinus Clay created during glacial loading and unloading.						LE		
		Advective /dispersive transport in the Opalinus Clay is driven by glacial loading and unloading.						WRP		
		A 2-D transport model is used.						MS		
		The reference biosphere model is employed, although biosphere conditions will be drastically changed during glaciations (very low population density, sparse vegetation, lower dilution rates).								ST
1.5 Additional barrier provided by confining units										
1.5a (LE)	The barrier to radionuclide transport provided by the sedimentary layers overlying and underlying the host rock, with the possibility that the local aquifers are not hydraulically connected over long distances and, therefore, do not convey radionuclides with flowing groundwater.	The geosphere transport model includes (in addition to vertical transport through the Opalinus Clay) vertical transport through the entire upper and lower confining units.						LE		
1.5b (WRP)	As above, but with the possibility that the local aquifers are hydraulically connected over long distances.	The geosphere transport includes (in addition to vertical transport through Opalinus Clay) vertical transport through the Lias / Upper Keuper below the Opalinus Clay, and also lateral transport in the local aquifers within the confining units.						WRP		
		In the fractured Wedelsandstein formation of the upper confining units, additional retardation is provided by matrix diffusion.						LE		

Tab. 10.6-1: (Cont.)

Case (Categorisation of main issues)	Main issues addressed	Key conceptual assumptions where these differ from those of the Reference Case (Case 1.1a)								
		Description	Categorisation of assumptions							
			INV	CONT	RELEASE	BUFFER	INT	ROCK	SED	SURF
1.6 Radionuclide release affected by ramp / shaft										
1.6a (WRP)	The possibility that the tunnels/ ramp / shaft and their associated excavation-disturbed zones (EDZs) provide preferential transport paths; best estimate hydraulic parameters assumed.	The SF / HLW near field is split up in three domains. In the two domains adjacent to the operations and construction tunnels (A & C), the effective flow rate at the near-field / host rock interface is increased 10-fold with respect to the Reference Case. In the remaining zone (B), the Reference Case flow rate is used.					PCA			
		The near field release term for ILW (domain D) is also modelled in the same way as for the Reference Case, but with a 10-fold increase in groundwater flow rate.					PCA			
		The inventory of domain B (corresponding to 75 % of the SF / HLW repository) is released through the Opalinus Clay only. The geosphere model calculations for this release are performed in an identical way as in the Reference Case.						LE		
		For domains A/C (both SF / HLW) and D (ILW), radionuclide transport occurs in parallel through the host rock and through the ramp / shaft. For each of the waste domains A/C/D, the flux of radionuclides is split between the host rock and the access tunnel system, with flow rates and branching ratios evaluated using a resistor network model.						LE		
		Transport in the various segments in the operations / construction / ventilation tunnels takes place by advection, dispersion, diffusion, decay and sorption in the bulk of the tunnel backfill (mixture of 30 % bentonite and 70 % quartz sand).						WRV		
		No transport and no matrix diffusion are considered within the EDZ of the backfilled tunnels.						CS		

Tab. 10.6-1: (Cont.)

Case (Categorisation of main issues)	Main issues addressed	Key conceptual assumptions where these differ from those of the Reference Case (Case 1.1a)								
		Description	Categorisation of assumptions							
			INV	CONT	RELEASE	BUFFER	INT	ROCK	SED	SURF
1.8 Gas-induced release affected by ramp										
1.8a (WRP)	The possibility that the build-up of repository gas pressure expels water and dissolved radionuclides from the repository near field.	10 % of the SF canisters are breached at unfavourable locations, so that gas from internal corrosion expels water from the canisters; gas escapes from the other canisters without displacing significant amounts of water.		WRP						
		The mean water volume displaced from this 10 % of SF canisters is 0.35 m ³ ; this volume is assumed to contain the SF IRF.			PV					
		The SF IRF is expelled into the unperturbed Opalinus Clay and the access tunnel system over a 1000 years period following canister breaching.			WRP					
		The effect of gas-induced porewater displacement from the HLW part of the repository is negligible.				LE				
		An amount of water (with dissolved radionuclides) corresponding to 50 % of the available ILW pore space is displaced within 30 000 years, starting at 10 000 years, at a rate of 0.05 m ³ a ⁻¹ .			WRV	WRV				
		Gas-induced displacement of contaminated water from the SF and ILW repository takes place through the unperturbed host rock and the access tunnel system in parallel – see Case 1.6a.						see 1.6a		
		Radionuclides not expelled by repository gas are neglected.			MS					
1.8b (PCA)	As above, but including an increased water flow rate driven by ILW gas.	An amount of water corresponding to 100 % of the available ILW pore space is displaced within 10 000 years, starting at 1000 years, at a rate of 0.3 m ³ a ⁻¹ .			PCA	PCA				

Tab. 10.6-2: (Cont.)

Case (Categorisation of main issues)	Main issues addressed	Key conceptual assumptions where these differ from those of the Reference Case (Case 1.1a)								
		Description	Categorisation of assumptions							
			Gas	INV	CONT	RELEASE	BUFFER	INT	ROCK	SED
2.1	Release of ¹⁴C from SF and ILW as volatile species in the gas phase not affected by ramp / shaft ("tight seals")									
2.1a (PCA)	The possibility that repository gasses will migrate through the host rock and confining units and convey certain radionuclides as volatile species.	If the gas generation rate exceeds the rate of gas removal (dissolution / diffusion) and gas volume increases (ILW porewater displacement), then the gas pressure further rises until capillary leakage by two-phase flow and/or pathway dilation occurs.	LE							
		Leakage of gas into the Opalinus Clay is neglected (gas permeability of zero).	CS							
		The sealing zone being very tight, the ramp / shaft do not provide a gas pathway and the pore volume for gas storage in the operations tunnel is unavailable.	PCA							
		If the threshold pressure for the formation of gas pathways in the Opalinus Clay is reached, gas pathways penetrate from the top of the tunnels along bedding planes into the formation, thus increasing the surface over which capillary leakage / gas diffusion take place.	LE							
		Gas pathway propagation stops when the combined effect of capillary leakage / porewater displacement / gas diffusion over the available surface (tunnel wall and gas pathway) balances the gas generation rate.	LE							
		Upon gas breakthrough through the host rock, a gas reservoir in the Wedelsandstein develops radially at a rate determined by the gas release rate to the reservoir and by gas diffusion from the reservoir through the low-permeability upper confining units to the Malm aquifer.	LE							

Tab. 10.6-2: (Cont.)

Case (Categorisation of main issues)	Main issues addressed	Key conceptual assumptions where these differ from those of the Reference Case (Case 1.1a)								
		Description	Categorisation of assumptions							
			Gas	INV	CONT	RELEASE	BUFFER	INT	ROCK	SED
2.1	Release of ¹⁴C from SF and ILW as volatile species in the gas phase not affected by ramp / shaft ("tight seals")									
2.1a (PCA)	The possibility that repository gasses will migrate through the host rock and confining units and convey certain radionuclides as volatile species.	The formation of macroscopic gas fracs in the Opalinus Clay is not considered.	LE							
		¹⁴ C is the only radionuclide in SF and ILW with the potential to be conveyed as volatile species that is significant to dose.		LE						
		HLW contains no radionuclides with the potential to be conveyed as volatile species that are significant to dose.		LE						
		The release of volatile species from SF begins at the time of canister breaching.			LE					
		The release of volatile species from ILW begins at the end of waste emplacement (no credit taken for a period of complete containment).			CS					
		All the ¹⁴ C inventory in the SF cladding and in ILW hulls and ends is released in the form of volatile compounds (CH ₄).				PCA				
		None of the ¹⁴ C inventory in the SF matrix or in the ILW waste form WA-BNF-2 (MEB crud, barium carbonate slurry) is released in the form of volatile compounds.				WRP				
		¹⁴ C released as volatile species is instantaneously mixed with non-radioactive repository generated gasses that form a time-dependent "storage volume" within the backfill material, the emplacement tunnel excavation disturbed zones, the gas pathways in the Opalinus Clay, and the Wedelsandstein.				PCA	PCA	PCA	PCA	PCA

Tab. 10.6-2: (Cont.)

Case (Categorisation of main issues)	Main issues addressed	Key conceptual assumptions where these differ from those of the Reference Case (Case 1.1a)								
		Description	Categorisation of assumptions							
			Gas	INV	CONT	RELEASE	BUFFER	INT	ROCK	SED
2.2	Release of ¹⁴C from SF and ILW as volatile species in the gas phase affected by ramp / shaft ("leaky seals")									
2.2a (PCA)	The possibility that repository gasses will migrate through the ramp / shaft to the confining units and convey certain radionuclides as volatile species.	As in 2.1a, except that the ramp / shaft (rather than gas pathways in the Opalinus Clay) contributes to the gas "storage volume".	WRP							
2.2b (PCA)	As above, but with leakage of gas into the Opalinus Clay taken into account, assuming low gas permeability.	If the gas pressure exceeds the threshold for capillary leakage, leakage of gas into the Opalinus Clay takes place, described by Darcy's law, with a gas permeability of 10 ⁻²³ m ² .						WRP WRV		
2.2c (PCA)	As above, but with leakage of gas into the Opalinus Clay taken into account, assuming higher gas permeability.	If the gas pressure exceeds the threshold for capillary leakage, leakage of gas into the Opalinus Clay takes place, described by Darcy's law, with a gas permeability of 10 ⁻²² m ² .						WRP WRV		

Tab. 10.6-3: Assessment of the main conceptual assumptions made in Alternative Scenario 2: Release of radionuclides affected by human actions

Case (Categorisation of main issues)	Main issues addressed	Key conceptual assumptions where these differ from those of the Reference Case (Case 1.1a)									
		Description	Categorisation of assumptions								
			INV	CONT	RELEASE	BUFFER	INT	ROCK	BH	SED	SURF
3.1 Borehole penetration											
3.1a (WRP)	The possibility that future drilling creates a borehole that penetrates a SF / HLW or ILW emplacement tunnel.	In the course of some future exploratory activity, an inadvertent borehole penetration of the repository is assumed, creating a direct pathway from the repository to the biosphere.							ST		
		The borehole penetrates all the way through the Opalinus Clay and is abandoned without proper sealing and without removing the casing.							ST		
		Initially, the casing is impermeable to water inflow from the formation, preventing radionuclide release to and transport along the borehole.							LE		
		At later times, the casing becomes leaky and weakens until the borehole collapses. The borehole and its EDZ provide a preferential path for radionuclide transport until they self-seal due to swelling of the Opalinus Clay.							LE		
		The borehole is assumed to penetrate a SF / HLW emplacement tunnel midway between two canisters, shortly after canister breaching and the release of 2 canisters is discharged directly into the borehole. Alternatively, an ILW-1 emplacement tunnel is penetrated.							ST		
		Radionuclide retardation along the axis of the SF / HLW emplacement tunnel is pessimistically neglected.				CS	CS				
		Releases from the remainder of the SF / HLW canisters are disregarded.			MS						

Tab. 10.6-3: (Cont.)

Case (Categorisation of main issues)	Main issues addressed	Key conceptual assumptions where these differ from those of the Reference Case (Case 1.1a)									
		Description	Categorisation of assumptions								
			INV	CONT	RELEASE	BUFFER	INT	ROCK	BH	SED	SURF
3.1 Borehole penetration											
3.1a (WRP)	The possibility that future drilling creates a borehole that penetrates a SF / HLW or ILW emplacement tunnel.	Due to the connected pore space of the cementitious materials the entire ILW emplacement tunnel is affected by the borehole, but only half of the radionuclide inventory is assumed available for transport through the borehole. In total, this corresponds to 25 % of the ILW-1 inventory.							PCA		
		Releases from the remainder of the ILW are disregarded.			MS						
		Water flow in the borehole is driven by the hydraulic gradient between the local aquifers, and is unaffected by the overpressure in the Opalinus Clay.							WRP		
		The time window during which radionuclide transport through the borehole takes place is assumed to be unlimited.			CS						
		The hydraulic conductivities of the collapsed borehole and of its EDZ are taken to be identical.							MS		
		There is unlimited availability of water in the penetrated local aquifers.								CS	
		The release of radionuclides from the near field is assumed to take place by advection through the borehole only, at a rate controlled by the flow rate in the borehole.								CP	
		Instantaneous transport of radionuclides is assumed to take place upwards along the borehole into the Malm aquifer, and from there to the reference biosphere area.								CS	
		Advective and diffusive transport of radionuclides through the Opalinus Clay is neglected.							MS		

Tab. 10.6-4: (Cont.)

Case (Categorisation of main issues)	Main issues addressed	Key conceptual assumptions where these differ from those of the Reference Case (Case 1.1a)								
		Description	Categorisation of assumptions							
			Gas	INV	CONT	RELEASE	BUFFER	INT	ROCK	SED
4.2 Transport along transmissive discontinuities										
4.2b (WI)	As in 4.2a, but with more SF / HLW canisters affected.	Two vertical discontinuities are assumed to intersect all the SF / HLW emplacement tunnels.							WI	
		Each discontinuity is assumed to capture the release from two canisters in each SF / HLW tunnel.				WI				
4.2c (WI)	As in 4.2a, except that the discontinuity affects the ILW tunnels only.	A single discontinuity is assumed to intersect the ILW tunnels.							WI	
4.2d (WI)	As in 4.2a, but with a higher transmissivity discontinuity.	The transmissivity of the discontinuity is constant in space and time, with a value of $10^{-9} \text{ m}^2 \text{ s}^{-1}$.							WIV	
4.2e (WI)	As in 4.2b, but with a higher transmissivity discontinuity.	The transmissivity of the discontinuity is constant in space and time, with a value of $10^{-9} \text{ m}^2 \text{ s}^{-1}$.							WIV	
4.2f (WI)	As in 4.2c, but with a higher transmissivity discontinuity.	The transmissivity of the discontinuity is constant in space and time, with a value of $10^{-9} \text{ m}^2 \text{ s}^{-1}$.							WIV	
4.3 SF: Increased fuel dissolution rate										
4.3a (WI)	Uncertainty in the proportion of radiolytic oxidants that is available for reaction at the fuel surface.	Fuel matrix dissolution occurs at a rate $\times 10$ higher than in the Reference Case.				WIV				
4.3b (WI)	As in 4.3a, but with a still higher propor- tion available.	Fuel matrix dissolution occurs at a rate $\times 100$ higher than in the Reference Case.				WIV				

Tab. 10.6-4: (Cont.)

Case (Categorisation of main issues)	Main issues addressed	Key conceptual assumptions where these differ from those of the Reference Case (Case 1.1a)								
		Description	Categorisation of assumptions							
			Gas	INV	CONT	RELEASE	BUFFER	INT	ROCK	SED
4.5	ILW: Gas-induced release of dissolved radionuclides through the ramp only									
4.5b (WI)	As above, but including an increased water flow rate driven by ILW gas.	An amount of water corresponding to 100 % of the available ILW pore space is displaced within 10 000 years, starting at 1000 years, at a rate of $0.3 \text{ m}^3 \text{ a}^{-1}$.				PCA	PCA			
4.6	Unretarded transport of ^{14}C released as volatile species through host rock; retardation in confining units taken into account									
4.6a (WI)	As in 2.1a (i.e. the possibility that repository gasses will migrate through the host rock and confining units and convey certain radionuclides as volatile species), but with a continuous pathway formed through the host rock.	As in 2.1a, except that neither the ramp / shaft nor gas pathways in the Opalinus Clay contribute to the gas "storage volume".	WI							
4.6b (WI)	As above, but with leakage of gas into the Opalinus Clay taken into account, assuming low gas permeability.	If the gas pressure exceeds the threshold for capillary leakage, leakage of gas into the Opalinus Clay takes place, described by Darcy's law, with a gas permeability of 10^{-23} m^2 .	WI							
4.6c (WI)	As above, but with leakage of gas into the Opalinus Clay taken into account, assuming higher gas permeability.	If the gas pressure exceeds the threshold for capillary leakage, leakage of gas into the Opalinus Clay takes place, described by Darcy's law, with a gas permeability of 10^{-22} m^2 .	WI							

Tab. 10.6-4: (Cont.)

Case (Categorisation of main issues)	Main issues addressed	Key conceptual assumptions where these differ from those of the Reference Case (Case 1.1a)									
		Description	Categorisation of assumptions								
			Gas	INV	CONT	RELEASE	BUFFER	INT	ROCK	SED	SURF
4.7 Poor near field and pessimistic near field / geosphere geochemical dataset											
4.7a (WI)	Unfavourable possibilities arising simultaneously for several pillars of safety.	The SF / HLW canister life-time is 100 years.			WIV						
		The fuel dissolution rate is increased by a factor of 10 with respect to the Reference Case.				WIV					
		The HLW glass dissolution rate is increased by a factor of 10 with respect to the Reference Case.				PV					
		The ILW containment time is zero.			CS						
		Solubility limits appropriate to the pessimistically estimated chemical conditions constrain the aqueous concentrations of radionuclides in the SF / HLW "reservoirs".				PV					
		Solubility limits and sorption coefficients in the SF / HLW buffer and ILW near field are based on a pessimistic geochemical dataset.					PV				
		Sorption coefficients in the Opalinus Clay are based on a pessimistic geochemical dataset.							PV		
4.7b (WI)	As above, but with increased groundwater flow rate.	The groundwater flowrate is increased by a factor of 10 with respect to the Reference Case.						PV			
4.7c (WI)	As above, but with further increased groundwater flow rate.	The groundwater flow rate is increased by a factor of 100 with respect to the Reference Case.						WIV			

Tab. 10.6-5: Assessment of the main conceptual assumptions made in the cases addressing design and system options

Case (Categorisation of main issues)	Main issues addressed	Key conceptual assumptions where these differ from those of the Reference Case (Case 1.1a)							
		Description	Categorisation of assumptions						
			INV	CONT	RELEASE	BUFFER	INT	ROCK	SED
5.1 Increased waste arisings [300 Gwa(e)]									
5.1a (PCA)	The possibility of increased nuclear power production.	SF waste inventory is based on a 300 Gwa(e) scenario.	PCA						
5.2 ILW high force compacted waste option									
5.2a (WRP)	The possibility of adopting the high force compacted waste option (see also 4.4a).	An alternative waste form is included in the ILW, namely hulls and end-pieces from COGEMA that are treated by high-force compaction during reprocessing.	WRP						
5.3 SF canister with Cu shell									
5.3a (WRP)	The design option of a copper canister with steel insert for SF.	A pessimistic canister breaching time of 10 ⁵ years for SF / HLW is assumed, based on this design option.		PV					
5.3b (PCA)	As above, but with the possibility of an initial manufacturing defect.	A single SF canister containing 3 PWR UO ₂ -48 assemblies and 1 MOX-48 assembly is breached prematurely as a result of an undetected manufacturing defect, allowing immediate water ingress and radionuclide release.		PCA					
		The transport resistance of the defect remains constant until such a time as the canister becomes fully breached (10 ⁵ years).			WRP				
5.3c (PCA)	As above, but a larger initial defect is considered.	The defect is larger than in 5.3b and provides less transport resistance for released radionuclides.				CS			

10.7 Summary and conclusions

In this chapter, a summary of assumptions for all assessment cases has been given. Each of these assumptions has been assessed in terms of its degree of realism, pessimism or conservatism. In this sense, the assessment is used as a tool for identifying bias that has been introduced – on purpose or inadvertently – into the models.

The assumptions made and parameter values used in the Reference Case are generally based on the expected evolution of the system components, but some pessimistic or conservative conceptual assumptions, parameters and model simplifications are also used. However, no "what if?" assumptions and values are adopted in the Reference Case.

In the alternative cases of the Reference Scenario and of the Alternative Scenarios 1 and 2, related to the release of volatile radionuclides along gas pathways and to the release of radionuclides affected by human actions, as well as in the alternative cases related to design and system options, the main issues addressed primarily involve pessimistic conceptual assumptions. In some of these cases, however, assumptions are made that are actually more realistic than in the Reference Case (for example Case 1.2a addressing "solubility-limited dissolution of SF"). In other cases, the assumptions are within the range of possibilities, while their likelihood is not currently possible to be evaluated (for example Case 1.4a addressing "Glacially-induced flow in the Opalinus Clay"). In all these alternative cases, the models may involve key conceptual assumptions of any category, with the exception of "what if?" assumptions and values.

In the assessment cases dedicated to testing the robustness of the disposal system, the main issues addressed are, by definition, of the "what if?" type. Here, the models may involve key conceptual assumptions of any category, including "what if?" assumptions and values.

Finally, in the alternative cases illustrating the effects of biosphere uncertainty, stylised conceptualisations of the main issues are adopted. Again, in all these cases, the models may involve key conceptual assumptions of any category, with the exception of "what if?" assumptions and values. In fact, some of the key conceptual assumptions correspond to the likely/expected characteristics and evolution of the surface environment.

In summary, the assessment performed in the present chapter demonstrates that all assessment cases are evaluated using, to some extent, pessimistic or conservative conceptual assumptions, parameters and model simplifications. The models and parameter values vary considerably between cases in their degree of pessimism or conservatism, but are nevertheless adequate to address issues appropriate to the current phase of the Swiss HLW programme, which are: (i) the assessment of feasibility of safe disposal of SF / HLW / ILW in Switzerland and (ii) the guidance of future work by providing a platform for discussion, e.g. with respect to Nagra's proposal to focus future work on the Opalinus Clay in the potential siting area in the region of the Zürcher Weinland. In future project stages, however, additional effort may be needed to elaborate more realistic model approaches and to better balance the degree of realism between the various investigated cases.

11 References

- Aidun, C.K., Bloom, S.G. & Raines, G.E. (1998): Radionuclide Transport Through Penetrations in Nuclear Waste Containers. Scientific Basis for Nuclear Waste Management XI. Mat. Res. Soc. Symp. Proc. Vol 112, pp. 261-272. Materials Research Society, Boston.
- Andra (2001): Référentiel géologique du site de Meuse / Haute-Marne. Rapp. A RP ADS 99-005 de l'Agence nationale pour la gestion des déchets radioactifs, Châtenay-Malabry, France.
- Barten, W. & Robinson, P.C. (2001): Contaminant transport in fracture networks with heterogeneous rock matrices: The PICNIC code. Nagra Technical Report NTB 01-03, Nagra, Wettingen, Switzerland.
- Bear, J. (1972): Dynamics of fluids in porous media. Dover Publications, New York.
- Beazley, D.M. (1999): Python Essential Reference, New Riders Publishing, Indianapolis (IN), USA.
- Bergström, U., Edlund, O., Evans, S. & Rojder, B. (1982): "BIOPATH – A computer code for calculation of the turnover of nuclides in the biosphere and the resulting doses to man". STUDSVIK/NW-82/261, Studsvik AB, Nyköping, Sweden.
- Bergström, U. & Nordlinder, S. (1990): Individual Radiation Doses from Unit Releases of Long-Lived Radionuclides. SKB Technical Report 90-09, Stockholm, Sweden
- Berner, U. (2002): Project Opalinus Clay: Radionuclide concentration limits in the near field of a repository for spent fuel and vitrified high-level waste. Nagra Technical Report NTB 02-10. Nagra, Wettingen, Switzerland.
- Berner, U. (2003): Project Opalinus Clay: Radionuclide concentration limits in the near field of a repository for long-lived intermediate-level waste. Nagra Technical Report NTB 02-22. Nagra, Wettingen, Switzerland.
- Bertleff, B., Joachim, H., Kozirowski, G., Leiber, J., Ohmert, W., Prestel, R., Stober, I., Strayle, G., Villinger, E. & Werner, J. (1988): Ergebnisse der Hydrogeothermiebohrungen in Baden-Württemberg. Jh. geol. Landesamt Baden-Württemberg 30, 27-116. Landesamt für Geologie, Rohstoffe und Bergbau Baden-Württemberg (LGRB), Freiburg i.Br., Germany.
- BIOMASS (2001): International Atomic Energy Agency, BIOMASS: "Reference biospheres" for solid radioactive waste disposal: Volume II - Methodology. Biomass Theme 1: Final Output, Version 3.0: Draft Tecdoc, IAEA, Vienna.
- BIOMOVS II (1996): Representations of the Biosphere in Dose Assessments of Radioactive Waste Repositories: Final Report of the BIOMOVS II Working Group on Complementary Studies, ed. R.A. Klos, ISBN 91-972958-1-7. Swedish Radiation Protection Institute, Stockholm, Sweden.
- Bradbury, M.H. & Baeyens, B. (2003a): Near-field sorption data bases for compacted MX-80 bentonite for performance assessment of a high level radioactive waste repository in Opalinus Clay host rock. Nagra Technical Report NTB 02-18. Nagra, Wettingen, Switzerland.
- Bradbury, M.H. & Baeyens, B. (2003b): Far-field sorption data base for performance assessment of a high level radioactive waste repository in an undisturbed Opalinus Clay host rock. Nagra Technical Report NTB 02-19. Nagra, Wettingen, Switzerland.
- Burga, C.A. & Perret, R. (1998): Vegetation und Klima der Schweiz seit dem jüngeren Eiszeitalter. Ott Verlag + Druck AG, Thun, Switzerland.
- Carslaw, H. S. & Jaeger, J. C. (1959): Conduction of heat in solids. 2nd Ed., Oxford Science Publications, Clarendon Press, Oxford, UK.
- Chambré, P.L., Lee, W., Kim, C.L. & Pigford, T.H. (1986): Steady-state and transient radionuclide transport through penetrations in nuclear waste containers, Lawrence Berkeley Laboratories Report LBL-21806, Berkeley, CA, USA.

- Curti, E. (2003): Glass dissolution parameters: Update for Entsorgungsnachweis. Nagra Technical Report NTB 02-21. Nagra, Wettingen, Switzerland.
- De Marsily, G. (1986): Quantitative hydrogeology. Academic Press, San Diego, USA.
- EKRA (2000): Disposal concepts for radioactive waste: Final report. Expertengruppe Entsorgungskonzepte für radioaktive Abfälle / Expert group on disposal concepts for radioactive waste (EKRA). On behalf of the Federal Department for the Environment, Transport, Energy and Communication.
- ENRESA (1999): CATSIUS Clay Project. Calculation and testing of behaviour of unsaturated clay as barrier in radioactive waste repositories. Stage 3: Validation exercises at a large in-situ scale. Compiled by E.E. Alonso and A. Alcoverro. ENRESA Technical Report 12/99, ENRESA, Madrid, Spain.
- ENRESA (2000): FEBEX Project. Full-scale engineered barriers experiment for a deep geological repository for high level radioactive waste in crystalline rock. Final report. ENRESA Technical Report 1/2000, ENRESA, Madrid, Spain.
- EVEREST (1997): Evaluation of Elements Responsible for the effective Engaged dose rates associated with the final Storage of radioactive waste: Everest project. Vol. 1-4. Office for Official Publications of the European Communities, Brussels, Luxembourg.
- Fetter, C.F. (1993): Contaminant Hydrogeology, Chapter 2, Macmillan Publishing Company, New York, USA.
- Gelhar, L.W., Welty, C. & Rehfeldt, K.R. (1992): A Critical Review of Data on Field-Scale Dispersion in Aquifers; Water Resources Research, Vol. 28, no. 7., pp 1955-1974.
- Greenhalgh, J.R., Fell, T.P. & Adams, N. (1985): Doses from Intakes of Radionuclides by Adults and Young People. NRPB R-162, NRPB Chilton, U.K., available through HMSO, London, U.K.
- Gribi, P. (2003): Analytical calculations of the Reference Case results for the safety assessment for Project Opalinus Clay (Entsorgungsnachweis). Unpubl. Nagra Internal Report, Nagra, Wettingen, Switzerland.
- Grindrod, P., Williams, M., Grogan, H. & Impey, M. (1990): STRENG, A source term model for vitrified high level waste. Nagra Technical Report NTB 90-48, Nagra, Wettingen, Switzerland.
- Hartley, R.W. (1985): Release of radionuclides to the geosphere from a repository for high-level waste. Nagra Technical Report NTB 85-41, Nagra, Wettingen, Switzerland.
- Hoch, A.R. & Rodwell, W.R. (1998): Scoping Studies of Gas Migration from a Repository in Opalinus Clay. AEAT-4516. AEA Technology Environment, UK.
- Howard, B.J., Wright, S.M., Barnett, C.L., Skuterud, L. & Strand, P. (2002): Estimation of critical loads for radiocesium in Fennoscandia and Northwest Russia, Journal of Environmental Radioactivity 60 (2002) 209-220.
- HSK & KSA (1993): Protection objectives for the disposal of radioactive waste, HSK-R-21/e. Swiss Federal Nuclear Safety Inspectorate (HSK) and Federal Commission for the Safety of Nuclear Installations (KSA), Villigen-HSK, Switzerland.
- ICRP (1996): International Commission on Radiological Protection: Age-dependent doses to members of the public from intake of radionuclides, Part 5: Compilation of ingestion and inhalation dose coefficients. ICRP Publication 72, Annals of the ICRP 26. Pergamon Press, Oxford and New York.
- JNC (1999): H12 project to establish technical basis for HLW disposal in Japan - Project overview report. Japan Nuclear Cycle Development Institute JNC TN1400 99-010. JNC, Japan.
- Johnson, L.H. & Smith, P.A. (2000): The interaction of radiolysis products and canister corrosion products and the implications for radionuclide transport in the near field of a repository for spent fuel. Nagra Technical Report NTB 00-04. Nagra, Wettingen, Switzerland.

- Johnson, L.H. & McGinnes, D.F. (2002): Partitioning of radionuclides in Swiss power reactor fuels. Nagra Technical Report NTB 02-07. Nagra, Wettingen, Switzerland.
- Johnson, L.H., Niemeyer, M., Klubertanz, G., Siegel, P. & Gribi, P. (2002): Calculations of the temperature evolution of a repository for spent fuel, vitrified high-level waste and intermediate level waste in Opalinus Clay. Nagra Technical Report NTB 01-04. Nagra, Wettingen, Switzerland.
- Johnson, L.H. & King, F. (2003): Canister options for the direct disposal of spent fuel. Nagra Technical Report NTB 02-11. Nagra, Wettingen, Switzerland.
- Kinzelbach, W. (1992): Numerische Methoden zur Modellierung des Transports von Schadstoffen im Grundwasser. 2. Auflage, gwf-Schriftenreihe Wasser-Abwasser, Oldenbourg Verlag, München / Wien.
- Klos, R.A., Müller-Lemans, H., Van Dorp, F. & Gribi, P. (1996). TAME - The Terrestrial-Aquatic Model of the Environment: Model Definition, Nagra Technical Report NTB 93-04, Nagra, Wettingen, Switzerland.
- Kosakowski, G. (2000): Numerical modelling of transient flow due to consolidation, AN-44-00-17, Paul Scherrer Institute, Villigen, Switzerland.
- Langguth, H.-R. & Voigt, R. (1980): Hydrogeologische Methoden. Springer Verlag, Berlin.
- Liu, J. & Neretnieks, I. (1995): Some evidence of radiolysis in a uranium ore body - quantification and interpretation. In Proc. Mat. Res. Soc. Symp. Vol. 353, pp 1179-1186, Kyoto, ed. T. Murakami and R.C. Ewing, Materials Research Society.
- Lutz, M. & Ascher, D. (1999): Learning Python, O'Reilly & Associates, Sebastopol (CA), USA.
- McGinnes, D.F. (2000): Review of the origin of half-life values and an analysis of the effect of uncertainties on decayed inventories. Unpubl. Nagra Internal Report. Nagra, Wettingen, Switzerland.
- McGinnes, D.F. (2002): Model radioactive waste inventory for reprocessing waste and spent fuel. Nagra Technical Report NTB 01-01. Nagra, Wettingen, Switzerland.
- Nagra (1985): Projekt Gewähr 1985. Endlager für hochaktive Abfälle: Sicherheitsbericht. Nagra Project Report NGB 85-05, Nagra, Wettingen, Switzerland.
- Nagra (1991): Sicherheitstechnische Beurteilung der langlebigen mittelaktiven Abfälle aus der Wiederaufarbeitung bei BNFL. Nagra Internal Report. Nagra, Wettingen, Switzerland.
- Nagra (1994a): Kristallin-I safety assessment report. Nagra Technical Report NTB 93-22. Nagra, Wettingen, Switzerland.
- Nagra (1994c): Bericht zur Langzeitsicherheit des Endlagers SMA am Standort Wellenberg. Nagra Technical Report NTB 94-06. Nagra, Wettingen, Switzerland.
- Nagra (2002a): Projekt Opalinuston – Synthese der geowissenschaftlichen Untersuchungsergebnisse. Entsorgungsnachweis für abgebrannte Brennelemente, verglaste hochaktive sowie langlebige mittelaktive Abfälle. Nagra Technical Report NTB 02-03. Nagra, Wettingen, Switzerland.
- Nagra (2002b): Projekt Opalinuston – Konzept für die Anlage und den Betrieb eines geologischen Tiefenlagers. Entsorgungsnachweis für abgebrannte Brennelemente, verglaste hochaktive sowie langlebige mittelaktive Abfälle. Nagra Technical Report NTB 02-02. Nagra, Wettingen, Switzerland.
- Nagra (2002c): Project Opalinus Clay: Safety Report. Demonstration of disposal feasibility for spent fuel, vitrified high-level waste and long-lived intermediate-level waste (Entsorgungsnachweis). Nagra Technical Report NTB 02-05. Nagra, Wettingen, Switzerland.
- Nagra (2002d): Project Opalinus Clay: FEP Management for Safety Assessment. Demonstration of disposal feasibility for spent fuel, vitrified high-level waste and long-lived intermediate-level waste (Entsorgungsnachweis). Nagra Technical Report NTB 02-23. Nagra, Wettingen, Switzerland.

- Nagra (2002e): SMA/WLB: Bohrlochversiegelung/-verfüllung SB4a/s. Nagra Technical Report NTB 02-24. Nagra, Wettingen, Switzerland.
- Nagra (2003a): Effects of post-disposal gas generation in a repository for spent fuel, high level waste and long lived intermediate level waste sited in Opalinus Clay. Unpubl. Nagra Internal Report. Nagra, Wettingen, Switzerland.
- Nagra (2003b): Biosphere modelling for the Opalinus Clay safety assessment - concepts and data. Unpubl. Nagra Internal Report. Nagra, Wettingen, Switzerland.
- Nagra (2003c): Project Opalinus Clay - Evaluation of assessment cases: Results of model calculations. Demonstration of disposal feasibility for spent fuel, vitrified high-level waste and long-lived intermediate-level waste (Entsorgungsnachweis). Unpubl. Nagra Internal Report. Nagra, Wettingen, Switzerland.
- NIREX (1997): An Assessment of the Post-closure Performance of a Deep Waste Repository at Sellafield. NIREX Science Report S/97/012, NIREX, United Kingdom.
- Nitzki & Matzke (1973): Stopping power of 1-9 meV He⁺⁺ ions in UO₂, (U,Pu)O₂, and ThO₂. Physical Review B, 8, pp 1894-1900.
- Pfingsten, W. (2000): FRAC3DVS, RANCHMD, PICNIC and MOCTAC code comparison for advective-dispersive-diffusive systems - verification tests and applications, AN-44-00-14, Paul Scherrer Institut, Villigen, Switzerland.
- POSIVA (1999): Safety assessment of spent fuel disposal in Hästholmen, Kivetty, Olkiluoto and Romuvaara, TILA-99. POSIVA 99-07, POSIVA, Helsinki, Finland.
- Robinson, P. & Benbow, S. (2003): GIPC: General Input Processor Code - User guide for version 1.0.1. Unpubl. Nagra Internal Report. Nagra, Wettingen, Switzerland.
- Rodwell, W. R. (ed.). (2000): Research into Gas Generation and Migration in Radioactive Waste Repository Systems. European Commission Report EUR 19133 EN.
- Schneider, W. & Göttner, J.-J. (1991): Schadstofftransport in mineralischen Tonabdichtungen und natürlichen Tonschichten. Geologisches Jahrbuch Reihe C, 58, 3-132.
- Schwyn, B., Wersin, P., Berner, U., Wieland, E. & Neall, F. (2003): Near-field chemistry of an ILW repository in Opalinus Clay. Unpubl. Nagra Internal Report. Nagra, Wettingen, Switzerland.
- SKB (1999a): Deep repository for spent nuclear fuel: SR 97 - Post-closure safety. Technical Report TR-99-06, Main report Vol. II, Svensk Kärnbränslehantering AB, Stockholm, Sweden.
- SKB (1999b): Analysis of radionuclide migration from SFL 3-5. Report R-99-14, Svensk Kärnbränslehantering AB, Stockholm, Sweden.
- Smith, P.A. (2003): Gas Model verification. Unpubl. Nagra Internal Report. Nagra, Wettingen, Switzerland.
- Strand P., Howard, B.J., Aarkrog, A., Balanov, M., Tsaturov, Y., Bewers, J.M., Salo, A., Sickel, M., Bergman, R. & Rissanen, K. (2002): Radioactive contamination in the Arctic - sources, dose assessment and potential risks, Journal of Environmental Radioactivity 60 (2002) 5-21.
- StSV (1994): Strahlenschutzverordnung vom 22.6.1994 (Stand 4.4.2000), StSV, SR 814.501, Switzerland.
- Svensson, L. (1979): Dose conversion factors for external photon radiation. FOA Report C 40060-A3, Försvarets Forskningsanstalt (FOA), Sundbyberg, Sweden.
- Therrien, R. & Sudicky, E.A. (1996): Three-dimensional analysis of variably-saturated flow and transport in porous media. Journal of Contaminant Hydrology, 23, 1-44.

- Therrien, R., Sudicky, E.A. & McLaren, R.G. (1999): User's Guide for NP 3.49 - A preprocessor for FRAC3DVS 3.49: An efficient simulator for three-dimensional, saturated-unsaturated groundwater flow and chain-decay solute transport in porous or discretely-fractured porous formations, University of Waterloo, Canada.
- Travnikova, I.G., Shutov, V.N., Ya Bruk, G., Balanov, M.I., Skuterud, I., Strand, P., Pogorely, Ju.A. & Burkova, T.F. (2002): Assessment of current exposure levels in different population groups of the Kola Peninsula, *Journal of Environmental Radioactivity* 60 (2002) 235-248.
- Tichy, W.F. (1985): RCS - A System for Version Control, *Software - Practice & Experience (SPE)* 15, 7, pp. 637-654.
- Vigfusson, J. (2000): Kristallin I: Korrosion von HAA-Glas und Endlagerbehälter. HSK 23/50, Hauptabteilung für die Sicherheit der Kernanlagen, Villigen, Switzerland.
- Wicker, F.W. & Pinder, J.E. (2002): Food chains and biogeochemical pathways: contributions of fallout and other radionuclides, *Health Physics* 82 (2002) 5: 680-689.
- Wieland, E. & Van Loon, L. (2002): Cementitious near-field sorption data base for performance assessment of an ILW repository in Opalinus Clay. Nagra Technical Report NTB 02-20. Nagra, Wettingen, Switzerland.
- YMP (1998): Viability assessment of a repository at Yucca Mountain, DOE Report DOE/RW-0508/V3.
- Yu, J.-W. & Neretnieks, I. (1997): Diffusion and sorption properties of radionuclides in compacted bentonite. SKB TR 97-12. Swedish Nuclear Fuel and Waste Management Co., Stockholm, Sweden.

Appendix 1: Codes for Modelling Assessment Cases

A1.1 Introduction

A1.1.1 Scope of this appendix

This appendix describes the codes used for the numerical analysis of assessment cases in the safety assessment. In line with the aims of the present report within Project *Entsorgungsnachweis* (Chapter 1), the information provided on the codes, together with descriptions of the conceptual models given in Chapters 3 to 8 and the data given in Appendix 3, should allow the interested reader to recalculate the results shown in the main report independently. This requires the full mathematical description of the models that the codes implement, including governing equations, boundary conditions and input parameters, which is given in this appendix⁴⁵.

This appendix also discusses why the suite of codes is adequate for its intended purpose and, in particular:

- how safety-relevant aspects of the various Super-FEPs identified in the safety assessment are represented by the codes; and
- how the codes have been verified to the extent required by the safety assessment.

These points are an aspect of quality assurance, and are among the quality assurance measures for *tools for PA calculations* that are listed in Appendix 8. The system of operational elements and procedures that is used to perform the required large number of calculational cases is also described. These are designed to meet requirements regarding quality management for *performing PA calculations*, including the storing / archiving of files, listed in Appendix 8. Quality assurance measures related to *checking PA calculations* and to *maintenance of PA computer programmes* are also incorporated within the operational framework of the safety assessment, but are not described in detail in the assessment documentation.

A1.1.2 Codes discussed in this appendix

The codes covered in detail in this appendix are the *Reference Model Chain* codes, namely:

- the STMAN family of codes for modelling the release of radionuclides from the waste forms, transport through the engineered barriers and release to the geosphere, comprising:
 - SPENT, which is applicable to directly disposed spent fuel (SF);
 - STRENG, which is applicable to the vitrified high-level waste form (HLW); and
 - STALLION, which is applicable to long-lived intermediate-level waste (ILW);
- the PICNIC geosphere transport code; and
- the TAME biosphere code.

The general-purpose transport code, FRAC3DVS, and the Gas Model referred to in Chapter 4 are also described. The general-purpose probabilistic code, GIPC, is discussed in Appendix 2.

⁴⁵ The appendix does not, however, give details of the approaches used to solve the equations.

A1.1.3 Structure of this appendix

Section A1.2 gives an assessment of the safety-relevant aspects of the various Super-FEPs that are represented by the different codes. This can be seen as an evaluation of the *qualification* of the codes to treat Super-FEPs, since the inapplicability (or lack of qualification) of a particular code to treat a Super-FEP or one of its safety-relevant aspects, including associated uncertainties and design / system options, gives rise to the need to employ an alternative code.

Sections A1.3 to A1.9 describe each of the individual codes in detail. For each code:

- the phenomena that it treats are described;
- the mathematical representation is given;
- the input parameters are listed; and
- measures taken to verify the code are described.

In the case of the STMAN suite of codes, these differ only in their treatment of the waste form. A full description is thus given of the SPENT code, while the descriptions of STRENG and STALLION focus on their specific aspects.

Section A1.10 describes the system of operational elements and procedures used to perform the required large number of calculational cases.

A1.2 Qualification of the codes for the treatment of Super-FEPs

A1.2.1 The need for qualification

In this section, the codes are audited against the Super-FEPs that have been identified in the safety assessment (see Tab. 6.8-1 of Nagra 2002c). Some of these Super-FEPs have several safety-relevant aspects (features and processes, many of which are subject to uncertainty or may have alternative realisations depending on the design / system options that are chosen), and each of these must be taken into account in selecting and applying the codes for assessment calculations. This does not mean that a code must explicitly represent a Super-FEP, with all its safety-relevant aspects, in order to be "qualified" for use in assessment cases involving that particular Super-FEP. It may be sufficient to represent the FEP implicitly via, for example, a conservative model simplification. In practice, the Reference Model Chain is adequate for most of the assessment cases. Where, however, a code cannot treat a safety-relevant aspect of a Super-FEP, or incorporates an assumption of negligible impact while scientific understanding cannot currently exclude significant impact, the need can arise to replace one or more codes in the Reference Model Chain with alternatives for the assessment cases that are affected.

A1.2.2 Model domains to which the codes are applied

In discussing the qualification of codes for the treatment of Super-FEPs, it is first necessary briefly to mention the parts of the system (model domains) to which the codes are applied. The STMAN family of codes as well as TAME and the Gas Model are purpose-built to model the features and processes occurring in specific parts of the disposal system and the biosphere. PICNIC and FRAC3DVS, although they were designed as geosphere transport codes, are however more versatile. PICNIC, for example, can model transport paths through the EDZ of the repository tunnel system, as well as through the undisturbed host rock. FRAC3DVS can model transport through the SF / HLW bentonite buffer as well as the host rock. Tab. A1.2-1 shows the

model domains in which the various assessment codes have been applied in the present assessment. It is emphasised that this does not necessarily represent the limits to the capabilities of the codes. In particular, FRAC3DVS could, in principle, be applied to the confining units and regional aquifers. However, all the assessment cases that required transport in this domain to be modelled explicitly could be dealt with adequately using PICNIC. The qualification of FRAC3DVS to model Super-FEPs related to the confining units and regional aquifers is thus not considered further.

Tab. A1.2-1: Model domains to which the assessment codes have been applied

Model domain	Reference Chain					Alternative Codes	
	STMAN family of codes			PICNIC	TAME	FRAC3DVS	Gas Model
	SPENT	STRENG	STALLION				
SF near field	✓					✓ [1]	✓
HLW near field		✓				✓ [1]	[2]
ILW near field			✓				✓
Access tunnels / ramp / shaft and their associated excavation disturbed zones				✓ [3]			✓ [3]
Undisturbed Opalinus Clay				✓		✓	✓
Confining units and regional aquifers				✓		[4]	✓ [5]
Biosphere					✓		✓

- Notes
- [1] FRAC3DVS can be applied to model retention and transport in the SF and HLW buffer, as well as in the surrounding host rock.
 - [2] It is assumed that radionuclides originating from the HLW near field are not released and transported in the gas phase. Gas generation in the HLW near field does, however, contribute to overall gas generation in the repository and thus provides input to the Gas Model.
 - [3] PICNIC and the Gas Model can be applied to this domain where the seals are assumed to be ineffective or "leaky", so that access tunnels / ramp / shaft and their associated excavation disturbed zones provide preferential paths for aqueous-phase or gas-phase transport.
 - [4] Although FRAC3DVS has not been applied in this domain in the current assessment, this would, in principle, have been possible, as in the case of PICNIC.
 - [5] Accumulation of gas in the Wedelsandstein formation is considered in the Gas Model, as well as diffusion of gas out of the formation and into the upper confining units (gas pressure is never sufficient for capillary leakage to occur out of the Wedelsandstein).

A1.2.3 The representation of Super-FEPs in safety assessment computer codes

The Super-FEPs and their associated uncertainties and design / system options are identified in Tab. 6.8-1 of Nagra (2002c). Each of the Super-FEPs has associated with it certain safety-relevant aspects (e.g. the timing or likelihood of an event, the rate of a process, the magnitude of a feature) that must be taken into account in modelling the Super-FEP. Each aspect is assigned an identification code (e.g. SF1). The ways in which these aspects are taken into account can be affected by the uncertainties or the choice of design / system options. Some, such as the number of waste packages (an aspect of the SF Super-FEP "Quantities and burnup of fuel and associated radionuclide inventories, including the instant release fraction (IRF)"), directly determines an input parameter value, the value of which is affected by, for example, the possibility of increased nuclear power production. As mentioned above, however, a code does not necessarily need to explicitly represent a Super-FEP, with all its safety-relevant aspects, in order to be "qualified" for use in assessment cases. Safety-relevant aspects of the Super-FEPs can be addressed in a number of different ways by the codes, as shown using the following symbols used in Tab. A1.2-2:

- ✓ *A safety-relevant aspect of a Super-FEP is fully represented by a code: either a process modelled explicitly, or the magnitude, timing, rate or spatial extent of a process, or the performance of a feature, directly determines one or more input parameters.*
- ✓ *A safety-relevant aspect of a Super-FEP is only partially represented by a code: either only some limited aspect of a feature is modelled explicitly, or assumptions regarding the (non-negligible) impact of a process on the properties of the system are built into the code, but no parameter values are directly affected that can be used to vary these assumptions.*
- *A safety-relevant aspect of a Super-FEP is not represented by a code, but gives rise time-dependent system properties that can be treated indirectly: parameter sets can be chosen that represent steady-state system properties corresponding, for example, to the end-state of the system once the process is complete or to one of a number of possible transient states.*

Shading indicates where a Super-FEP is irrelevant to the domain modelled by the code. The table confirms that the Reference Model Chain is adequate to represent most of the Super-FEPs and their safety-relevant aspects.

Where a code of the Reference Model Chain cannot treat a safety-relevant aspect of a Super-FEP or incorporates an assumption of negligible impact, but an alternative code exists that can treat this aspect quantitatively, this is indicated using the symbol ► in the table. The symbol appears:

- in the STMAN and PICNIC columns, where safety relevant aspects concern gas production and migration and radionuclides that can be transported as volatile species - these aspects are addressed by replacing the Reference Model Chain with the Gas Model;
- in the PICNIC column, where safety relevant aspects concern the transient effects on groundwater movement of, for example, the compaction of ILW and ice loading during glacial periods - these aspects are addressed using FRAC3DVS in place of PICNIC, and
- in the TAME column, where safety relevant aspects concern drinking water extraction from the Malm aquifer - these aspects are addressed using a simple analytical formula for dose in place of TAME.

Where no qualified code exists, this is indicated using the symbol ●. The symbol appears in rows addressing:

- criticality;
- the requirement for a tunnel liner in the SF / HLW near field;
- the distribution of breaching times for SF / HLW canisters;
- the extent of sorption on canister corrosion products;
- the effects on solubility limitation of the natural concentrations of isotopes;
- the magnitude and time-dependence of transport resistances in the SF / HLW near field;
- long-term changes in the Opalinus Clay and confining units (e.g. due to erosion of overburden); and
- immobilisation processes in the Opalinus Clay and confining units.

For all of these aspects, however, significant effects can be ruled out by supplementary studies (e.g. for criticality), effects are intrinsically favourable to safety and can be conservatively neglected (e.g. transport resistances in the SF / HLW near field), or parameters (e.g. canister breaching time) can be chosen to ensure that calculations err on the side of pessimism.

Tables in the following sections of this appendix explain in more details the allocation of symbols in Tab. A1.2-2. These tables address each code in turn, and indicate the features of the code affected by the various aspects of the Super-FEPs.

Tab. A1.2-2: The representation of Super-FEPs and their safety-relevant aspects in safety assessment computer codes

These Super-FEPs and the safety-relevant aspects are taken from Tab. A5.2.1 of Nagra (2002d).

Super-FEPs	Safety-relevant aspects represented by models		Reference Chain					Alternative codes	
			STMAN codes			PICNIC	TAME	FRAC3DVS	Gas Model
			SPENT	STRENG	STALLION				
SF									
Quantities and burnup of fuel and associated radionuclide inventories, including the instant release fraction (IRF)	SF1	Waste inventory in a single package and number of packages	✓						✓
	SF2	Partitioning between fuel matrix, cladding and IRF	✓						✓
	SF3	¹⁴ C in organic and inorganic form upon release	✓						✓
	SF4	Proportion of organic ¹⁴ C in volatile form upon release	▶						✓
Corrosion of cladding	SF5	Corrosion rate	✓						✓
Breaching of cladding	SF6	Timing	✓						
Dissolution of fuel matrix	SF7	Dissolution rate	✓						✓
Criticality	SF8	None - ruled out by design and supporting calculations	●						
HLW									
Quantities of glass and associated radionuclide inventories	HL1	Waste inventory in a single package and number of packages		✓					✓
Dissolution rate of glass	HL2	Dissolution rate		✓					
SF / HLW canisters									
Breaching of steel canisters	CN1	Distribution of breaching times	●	●					
	CN2	Time of occurrence of breaching	✓	✓					✓
Gas generation by steel canister corrosion	CN3	Gas generation rate for SF / HLW	▶	▶					✓
Canister material	CN4	Time of occurrence of breaching (time of occurrence affected by canister material)	✓	✓					
	CN5	Presence of initial defects (likelihood affected by canister material)	✓	✓					

Tab. A1.2-2: (Cont.)

Super-FEPs	Safety-relevant aspects represented by models		Reference Chain					Alternative codes	
			STMAN codes			PICNIC	TAME	FRAC3DVS	Gas Model
			SPENT	STRENG	STALLION				
SF / HLW near field									
The long resaturation time of the repository and its surroundings	NF1	The rate of the resaturation process	✓	✓					✓
Geochemical immobilisation and retardation in the near field	NF2	Solubility limitation (reservoir)	✓	✓					
	NF3	Solubility limitation (buffer)	✓	✓					
	NF4	Linear, equilibrium sorption	✓	✓				✓	
	NF5	Colloid filtration by bentonite	✓	✓					
	NF6	The extent of co-precipitation with secondary minerals	✓	✓					
	NF7	The extent of sorption on canister corrosion products	●	●					
	NF8	The effects on solubility limitation of the natural concentrations of isotopes	●	●					
Migration of radiolytic oxidants generated at SF surfaces into bentonite buffer	NF9	Proportion of the buffer affected and the magnitude of the effects on geochemical immobilisation	○						
Thermal alteration of the bentonite buffer adjacent to the SF / HLW canisters	NF10	Proportion of the buffer affected and the magnitude of the effects on buffer transport properties	○	○					
Transport resistances provided by internal spaces (fractures) within the waste forms, by the breached SF / HLW canisters and by corrosion products	NF11	The magnitude of transport resistance of initial defects	✓	✓					
	NF12	The magnitude and time-dependence of other transport resistances	●	●					
Tunnel liner	NF13	Requirement for a liner	●	●					

Tab. A1.2-2: (Cont.)

Super-FEPs	Safety-relevant aspects represented by models		Reference Chain					Alternative codes	
			STMAN codes			PICNIC	TAME	FRAC3DVS	Gas Model
			SPENT	STRENG	STALLION				
SF / HLW near field									
Hydraulic transport characteristics of bentonite	NF14	Stationary flow						✓	
	NF15	Transient flow						✓	
	NF16	Advection / dispersion						✓	
	NF17	Aqueous diffusion	✓	✓				✓	
	NF18	Effective flow rate at outer boundary	✓	✓					
	NF19	Compaction of bentonite by tunnel convergence	○	○					
Gas transport characteristics of bentonite	NF20	Gas-induced release of dissolved radionuclides	○						
	NF21	Dilatant gas pathway formation (SF / HLW near field)	▶	▶					✓
	NF22	Gas dissolution and diffusion	▶	▶					✓
ILW									
Quantities of waste and associated radionuclide inventories	IL1	Waste inventory in a single package and number of packages			✓				✓
Breaching of ILW steel drums and emplacement containers	IL2	Time of occurrence of breaching			✓				
Corrosion / dissolution of ILW	IL3	Corrosion rate of metallic components			✓				
	IL4	Corrosion / dissolution rate of remaining ILW components			●				
Immobilisation and retardation in the ILW near field	IL5	Linear, equilibrium sorption and solubility limitation			✓				
Gas generation	IL6	Gas generation rates for ILW			▶				✓
Hydraulic and gas transport characteristics of the ILW near field	IL7	Effective flow rate at outer boundary			✓				
	IL8	Gas dissolution and diffusion			▶				✓
	IL9	Porewater displacement by gas			▶ or ○				✓

Tab. A1.2-2: (Cont.)

Super-FEPs	Safety-relevant aspects represented by models		Reference Chain					Alternative codes	
			STMAN codes			PICNIC	TAME	FRAC3DVS	Gas Model
			SPENT	STRENG	STALLION				
ILW									
Compaction of waste / mortar	IL10	Timing of convergence arising from void reduction of breached, corroded canisters			○				
The long resaturation time of the ILW tunnels	IL11	The rate of the resaturation process			✓				
Tunnels / ramp / shaft and seals									
Low groundwater flow rate along the sealed tunnels / ramp / shaft, and through the surrounding excavation disturbed zones (EDZs)	TS1	Transport paths provided by the tunnels / ramp / shaft				✓			
	TS2	Stationary flow				✓			
	TS3	Transient flow				○			
	TS4	Advection / dispersion				✓			
	TS5	Aqueous diffusion				✓			
The seals and the surrounding rock	TS6	Formation of dilatant gas pathways through the sealing zone							✓
	TS7	Transport resistance of the seals and the surrounding rock				✓			
Opalinus Clay and confining units									
Low groundwater flow rate through undisturbed Opalinus Clay	OP1	Stationary flow				✓		✓	
	OP2	Transient flow				▶ or ○		✓	
	OP3	Advection / dispersion				✓		✓	
	OP4	Aqueous diffusion				✓		✓	
	OP5	Long-term changes (e.g. due to erosion of overburden)				●		●	
Length of vertical transport path from emplacement tunnels to overlying and underlying formations	OP6	Transport paths provided by the Opalinus Clay and confining units				✓		✓	✓
Geochemical immobilisation and retardation in the Opalinus Clay and confining units	OP7	Linear, equilibrium sorption				✓		✓	
	OP8	Immobilisation processes				●		●	

Tab. A1.2-2: (Cont.)

Super-FEPs	Safety-relevant aspects represented by models		Reference Chain					Alternative codes	
			STMAN codes			PICNIC	TAME	FRAC3DVS	Gas Model
			SPENT	STRENG	STALLION				
Opalinus Clay and confining units									
Homogeneity	OP9	Transport paths provided by transmissive discontinuities, faults and repository-induced fractures in the clay				✓		✓	
Migration of high-pH plume from ILW backfill into Opalinus Clay	OP10	The depth of migration, and associated physical and chemical changes in the clay				○			
Radionuclide transport through the confining units and regional aquifers	OP11	Transport paths provided by the confining units and regional aquifers				✓			
The barrier system (general)									
The migration of repository induced gas	BS1	Gas dissolution and diffusion in the Opalinus Clay (incl. tunnel EDZs)				▶			✓
	BS2	Capillary leakage in the Opalinus Clay				▶			✓
	BS3	Pathway dilation in the Opalinus Clay				▶			✓
	BS4	Porewater displacement in the Wedelsandstein				▶			✓
	BS5	Gas dissolution and diffusion in the low-permeability upper confining units				▶			✓
	BS6	Capillary leakage through low-permeability upper confining units				▶			✓
Future human actions	BS7	Borehole penetration of the repository	○	○	○		○		
	BS8	Drinking water extraction from the Malm aquifer					▶		
	BS9	Abandonment of repository before backfilling / sealing				○			
The surface environment									
Climatic evolution	SE1	The nature and timing of climate change					○		
Geomorphological evolution	SE2	Properties of the exfiltration area for groundwater conveying radionuclides					○		

A1.2.4 Approach to verification of codes

Computer codes that are in use for several years are usually updated periodically, for example to add new features or to make them more user-friendly. In view of this situation, the question arises how to deal with code verification. Ideally, a full cross-comparison with one or more well-established, similar code(s) is performed after each update, even if the update involves only minor changes. In practice, however, this is often not feasible. The approach chosen to verify the computer codes used to evaluate the assessment cases of the present safety assessment involves the following steps:

- At least at one point in the life cycle of a code, a cross-comparison with at least one other, well-established code and/or with analytical solutions is performed. This step is described for each of the codes individually under the heading "Verification"; e.g. for SPENT in Section A1.3.5.
- In order to ensure that also the new version of a code can be regarded as verified, two steps are performed routinely: (i) Detailed tests of the behaviour of new capabilities are being carried out to check whether these new features function correctly, and (ii) at least one calculational case, including the Reference Case, is evaluated both with the old and the new version of the code and a cross-comparison is made. It is only after the new version of a code has passed tests (i) and (ii) successfully that it may be used in safety assessment.

A1.3 SPENT

A1.3.1 Scope and purpose

SPENT is that part of the STMAN suite of codes for near field release and transport of radionuclides from a SF canister. SPENT represents the cylindrical canister containing the SF and an annular buffer region around this as a radially symmetric system. The outer boundary of the region considered in SPENT is the interface to the geosphere and is handled through the use of an appropriate boundary condition (generally a mixing cell condition).

The STMAN suite of codes all treat the buffer and outer boundary in the same way, differing only in their treatment of the waste form. Thus, these aspects of the description given here apply also to the other codes (STRENG and STALLION).

In the context of Project *Entsorgungsnachweis* the choice of appropriate conditions at the outer boundary required some careful study. The original conceptualisation of this boundary was as an interface to a hard rock where advective transport dominates, whereas diffusive transport is also important in the Opalinus Clay considered in Project *Entsorgungsnachweis*.

The primary output is a flux to the near field for use in the geosphere but current concentrations and other intermediate results can also be output for use in other calculations, for example human intrusion consequence analysis.

A1.3.2 Phenomena included in SPENT

A1.3.2.1 Overview

An overview of the representation of Super-FEPs in the various safety assessment computer codes is given in Section A1.2.3 (Tab. A1.2-2). Tab. A1.3-1 describes in more detail how SPENT represents the different Super-FEPs that fall into its model domain, namely the SF near field. The symbols used in Tab. A1.3-1 are explained in Section A1.2.3. The following model features are considered separately:

- The containment period and canister breaching modes;
- The release mechanisms for radionuclides from the fuel and the canister;
- Transport through the buffer; and
- The interface with the host rock.

The final two aspects are common to all codes in the STMAN family.

Some safety-relevant aspects of the Super-FEPs (indicated by large bold ticks in Tab. A1.3-1) are either modelled explicitly by SPENT, or their magnitude, timing, rate, spatial extent and performance directly determine one or more input parameters. These aspects or phenomena are summarised in Tab. A1.3-2 and discussed in more detail in the following sections, where they are highlighted in bold. The table also notes radioactive decay and ingrowth as included phenomena. Shaded boxes are used since these phenomena are not directly related to the Super-FEPs. SPENT (and the other STMAN codes) models these phenomena, including the branching and rejoining of chains, in all parts of the system. The suite of radionuclides considered is specified as part of the input so that the STMAN codes can be configured to any situation.

Tab. A1.3-1: Super-FEPs, their safety-relevant aspects (as taken from Tab. A5.2.1 of Nagra 2002d) and the ways in which they are represented by the code SPENT

Symbols: see Section A1.2.3

Super-FEPs	Safety-relevant aspects to be represented by models	Model features				Explanatory comments
		Containment period and breaching modes	Fuel release mechanisms and the reservoir	Transport through the buffer	Interface with the host rock	
SF						
Quantities and burnup of fuel and associated radionuclide inventories, including the instant release fraction (IRF)	Waste inventory in a single package and number of packages	✓				Directly provides input parameters.
	Partitioning between fuel matrix, cladding and IRF		✓			Directly provides input parameters.
	Proportion of ¹⁴ C in organic and inorganic form upon release		✓			Solubility limits and sorption coefficients for ¹⁴ C depend on whether it is in organic or inorganic form.
	Proportion of organic ¹⁴ C in volatile form upon release		▶			Release of organic ¹⁴ C in volatile form not considered (see Gas Model).
Corrosion of cladding	Corrosion rate		✓			Directly provides input parameter.
Breaching of cladding	Timing	✓				Cladding is breached at or before the time of canister breaching. The possibility of a period of complete containment by cladding following canister breaching cannot be modelled with the existing version of SPENT, since release of cladding inventory is assumed to begin simultaneously with the release from the fuel matrix and release of IRF.
Dissolution of fuel matrix	Dissolution rate		✓			Fuel matrix dissolution rate as a function of time is input as a list of parameter values.
Criticality	-	●	●	●	●	Ruled out by design and supporting calculations.
SF canisters						
Breaching of steel canisters	Distribution of breaching times	●				Not included, but canister breaching time can be selected such that results err on the side of pessimism.
	Time of occurrence of breaching	✓				Time of breaching (containment) time is input as a parameter value – see, however, "the long resaturation time of the repository and its surroundings", below.
Gas generation by steel canister corrosion	Gas generation rate for SF / HLW			▶	▶	No transport of radionuclides in volatile form considered; gas generation assumed to be irrelevant (see Gas Model).
Canister material	Time of occurrence of breaching (time of occurrence affected by canister material)	✓				Canister material affects evaluation of breaching time, which must be input as parameter.
	Presence of initial defects (likelihood affected by canister material)	✓				Canister material affects the possibility of localised defects, with associated transport resistances, which are characterised by input parameters.

Tab. A1.3-1: (Cont.)

Super-FEPs	Safety-relevant aspects to be represented by models	Model features				Explanatory comments
		Containment period and breaching modes	Fuel release mechanisms and the reservoir	Transport through the buffer	Interface with the host rock	
SF near field						
The long resaturation time of the repository and its surroundings	The rate of the resaturation process	✓				The resaturation process and its transient effects on the transport-relevant properties of the buffer are not modelled by SPENT. However, the period of complete containment can, if required, be extended beyond canister breaching time to account for a long resaturation time (this is not done in the present assessment).
Geochemical immobilisation and retardation in the near field	Solubility limitation (reservoir)		✓			Solubility limits for the reservoir are input as parameter values.
	Solubility limitation (buffer)			✓		Solubility limits for the buffer are input as parameter values.
	Linear, equilibrium sorption			✓		Sorption coefficients for the buffer are input as parameter values.
	Colloid filtration by bentonite			✓		Precipitated solids are assumed to be immobile.
	The extent of co-precipitation with secondary minerals		✓	✓		Can be taken into account via the setting of the solubility limits.
	The extent of sorption on canister corrosion products		●			Sorption on canister corrosion products not included, but omission is conservative.
	The effects on solubility limitation of the natural concentrations of isotopes		●	●		Natural background concentrations not included, but omission is conservative.
Migration of radiolytic oxidants generated at SF surfaces into bentonite buffer	Proportion of the buffer affected and the magnitude of the effects on geochemical immobilisation			○		Penetration (if any) of oxidants into the buffer must be evaluated separately. Sorption coefficients and solubility appropriate to oxidising conditions can be input, if required, as parameter values for the reservoir and all or part of the buffer.
Thermal alteration of the bentonite buffer adjacent to the SF canisters	Proportion of the buffer affected and the magnitude of the effects on buffer transport properties			○		Extent of thermal alteration must be evaluated separately. Diffusion coefficients appropriate to altered buffer can be input, if required, as parameter values for all or part of the buffer.
Transport resistances provided by internal spaces (fractures) within the waste forms, by the breached SF canisters and by corrosion products	The magnitude of transport resistance of initial defects		✓			Transport resistance of breached canisters can be considered via the "pinhole model" built into SPENT – in practice, this is only used in cases that consider the alternative composite copper / steel canister.
	The magnitude and time-dependence of other transport resistances		●			Other transport resistances not included, but omission is conservative.
Tunnel liner	The requirement for a liner				●	Requirement for a liner ruled out by supplementary studies.

Tab. A1.3-1: (Cont.)

Super-FEPs	Safety-relevant aspects to be represented by models	Model features				Explanatory comments
		Containment period and breaching modes	Fuel release mechanisms and the reservoir	Transport through the buffer	Interface with the host rock	
SF near field						
Hydraulic transport characteristics of bentonite	Effective flow rate at outer boundary				✓	Input parameter.
	Aqueous diffusion			✓		Aqueous diffusion is assumed to convey radionuclides across the bentonite buffer; element-specific diffusion coefficients are input as parameter values.
	Compaction of bentonite by tunnel convergence			○		Compaction during tunnel convergence can be taken into account in setting the tunnel radius and bentonite transport properties.
Gas transport characteristics of bentonite	Gas-induced release of dissolved radionuclides			○		Expulsion of the IRF by repository gas can be simulated, if required, by neglecting the transport resistance of the bentonite for the IRF.
	Dilatant gas pathway formation (SF / HLW near field)			▶		Not considered in SPENT (see Gas Model).
	Gas dissolution and diffusion			▶		See above.
The barrier system (general)						
Future human actions	Borehole penetration of the repository				○	The nature and timing of future human actions cannot be evaluated using SPENT. The consequences of hypothetical actions that may influence the near field can, however, be bounded in some cases (e.g. the possibility of future drilling of a borehole inadvertently affecting the barrier system can be modelled by interfacing SPENT directly with the biosphere model).

Tab. A1.3-2: Phenomena explicitly included in the SPENT model

Model features	Phenomena explicitly included in the SPENT model
All	Radionuclide decay and ingrowth
The containment period and canister breaching modes	Waste inventory in a single package and number of packages
	Time of occurrence of SF canister breaching
	Presence of initial defects
	Transport resistance of initial defects
Fuel release mechanisms and the reservoir	Partitioning between fuel matrix, cladding and IRF
	Proportion of ¹⁴ C in organic form upon release
	Corrosion rate of cladding
	Dissolution rate of fuel matrix
	Solubility limitation
Transport through the buffer	Aqueous diffusion
	Linear equilibrium sorption
	Solubility limitation
Interface with the host rock	Effective flow rate at outer boundary

Some other safety-relevant aspects of the Super-FEPs (indicated by smaller ticks in Tab. A1.3-1) are only partly represented or are built into the SPENT model assumptions (e.g. the assumption of colloid filtration by bentonite). These aspects are also described in detail in later sections.

The possibility of time dependent system properties associated with some Super-FEPs cannot be directly represented by the code (as indicated by the symbol ○ in Tab. A1.3-1). Parameter sets can, however, be chosen that represent steady-state system properties corresponding, for example, to the end-state of the system once the process is complete or one of a number of possible transient states, as explained in the discussions of individual conceptualisations in Chapters 3 to 8.

Phenomena indicated by the symbol ► require the use of an alternative code if they are to be modelled. In particular, SPENT (like all the STMAN codes) only treats radionuclide transport in aqueous solution and only consider processes that are directly relevant to this. It does not consider gas generation and transport and the transport of radionuclides as volatile species. The phenomena are treated by the Gas Model. Where no qualified code exists, this is indicated using the symbol ●.

A1.3.2.2 Containment and canister breaching

Prior to some specified **time of occurrence of SF canister breaching**, the canister is assumed to be completely intact. Complete containment of radionuclides is provided up to this time, although the initial inventory, specified via the **waste inventory in a single package and the number of packages**, is altered by **radioactive decay and ingrowth**.

When the canister is breached, the usual assumption is that the canister breaching is instant and complete, so the canister plays no further role in preventing water ingress or radionuclide release. Releases are then controlled by the behaviour of the fuel and the properties of the radionuclides and the buffer. An alternative breaching mode can also be modelled, where the possible **presence of initial defects**, termed **pinholes**, is considered. In this situation, the **transport resistance of the defects** also affect release rates. Processes leading to breaching are not modelled in SPENT; the breaching time is an input parameter.

A1.3.2.3 Fuel release mechanisms and the reservoir

Following canister breaching, water is assumed to enter the canister and instantly saturate any void spaces in the canister interior. These saturated void spaces are collectively termed the reservoir.

Radionuclides contained in fuel grain boundaries, in fuel pellet cracks and in the gap between the fuel and the cladding are assumed to dissolve instantly in the reservoir – these are termed the instant release fraction (IRF). Note that calculating the instant release fraction of each radionuclide is outside the scope of SPENT. The **partitioning between fuel matrix, cladding and IRF** is specified via input parameters. If required, organic and inorganic ^{14}C can be treated separately - the **proportion of ^{14}C in organic form upon release** is important if organic and inorganic ^{14}C have different properties with respect to subsequent transport and geochemical immobilisation.

Water entering the reservoir comes into contact with the fuel matrix and fuel cladding surfaces, and fuel matrix dissolution and cladding corrosion begin. Radionuclides and stable isotopes are considered to be uniformly distributed within the fuel matrix and within the fuel cladding, and thus release from these media to the reservoir occurs congruently with dissolution and corrosion. In SPENT, the **dissolution rate of the fuel matrix** and the **corrosion rate of cladding** are supplied as input parameters. These rates can change with time to allow, for example, for the effects of radiolytic processes on matrix dissolution.

Radionuclides and stable isotopes are assumed to be uniformly mixed within the reservoir. The transport resistances experienced by radionuclides migrating through the reservoir (including, for example, the transport resistances of cracks within the fuel pellets) are thus neglected. Sorption on the solid surfaces with which reservoir water is in contact (including the canister and canister corrosion products) is also not modelled by SPENT. Aqueous concentrations are, however, constrained by **solubility limitation**; the solubility limits of each element in the reservoir are input as parameters. Concentrations of all isotopes of the same element, including stable isotopes, are taken into account when evaluating whether the solubility limit has been reached. Co-precipitation with, for example, corrosion products, is not modelled explicitly, but can be taken into account if the necessary data are available when setting solubility limits. Solids are precipitated or re-dissolved at rates that maintain aqueous concentrations at or below the solubility limits. Dissolved radionuclides and stable isotopes can diffuse from the reservoir into the buffer (via the pinhole if that model is used), but solids, including colloids, are assumed to be retained within the reservoir (filtration by the buffer).

A1.3.2.4 Transport through the buffer

In cross section, the buffer is represented in SPENT as an annular region bounded by the outer surface of the canister and by the tunnel wall. The length of this region in the axial direction is equal to the canister length, multiplied by the number of canisters. The buffer between canisters

is not taken into account in SPENT. The buffer can be modelled as one or two annular zones; if two are chosen then each can be assigned a different set of homogeneous and isotropic properties. This facility can be used, for example, to account for thermal alteration of the buffer adjacent to the canister.

Properties of the buffer that are taken into account in SPENT include those that quantify radionuclide transport, retardation and immobilisation processes.

Radionuclide transport within the buffer (and also transport of stable isotopes) occurs by **aqueous diffusion** through pore spaces. All pores are assumed to be water saturated and advective transport through the pores is assumed to be negligible. The porosity that is accessible to particular transported species may be less than the overall porosity, due to size and charge effects (anion exclusion), and element-specific accessible porosities are specified. Diffusion coefficients that are element-specific are also specified. Gas-mediated radionuclide transport is not modelled by SPENT.

Diffusion is driven by aqueous concentration gradients in the buffer, which are radially directed in the usual case of no account being taken of the transport resistance of breached canisters. Axial diffusion into the buffer between canisters is neglected and concentrations are assumed to be uniform along the inner and outer⁴⁶ boundaries of the buffer. In the case of pinhole canister breaching (see above), the concentration gradient near the canister is modified by the presence of the pinhole defects.

Linear equilibrium sorption in the buffer retards radionuclide transport; i.e. sorption is represented as an instantaneous, reversible process, with the amount sorbed proportional to aqueous concentration. The constant of proportionality is the element-specific sorption coefficient K_d . The quantification of retardation also requires the overall porosity and density of the buffer to be specified. Density can be expressed either as grain density, i.e. the mass of solid material per unit volume of buffer, not including the volume occupied by pores, or bulk dry density, i.e. the mass of solid material per unit volume of buffer, including pore volume.

Aqueous concentrations are, however, constrained by **solubility limitation**; the solubility limits of each element in the reservoir are input as parameters. Concentrations of all isotopes of the same element, including stable isotopes, are taken into account when evaluating whether the solubility limit has been reached. Solids, including colloids, are precipitated or re-dissolved at rates that maintain aqueous concentrations at or below the solubility limits, and are assumed to be immobile in the buffer (filtration).

A1.3.2.5 Interface with the host rock

It is assumed that, whereas radionuclides can diffuse from the buffer across the interface with the surrounding host rock (including any excavation disturbed zone), the reverse does not take place, i.e. there is no transport of radionuclides from the host rock into the buffer⁴⁷. Conceptually, transport processes in the host rock carry radionuclides away from the interface at a rate that balances their arrival by diffusion. The concentration at the boundary is determined by the relative rates of these processes. In an extreme case, the transport in the host rock is sufficiently rapid that the buffer sees a fixed outer boundary concentration (zero unless there is a

⁴⁶ The effects of non-uniformity around the outer boundary of the buffer at a given position along a tunnel are likely to be small, as discussed in Appendix 9 of Nagra (1994a).

⁴⁷ This assumption allows near field and geosphere modelling to be carried out using separate models, with the results of the near field model (SPENT output) providing the source term for the geosphere model.

background concentration of the radionuclide in the groundwater). In this study, this situation does not arise except in a few special cases.

For the current study, the host rock, like the buffer, is a low conductivity medium and diffusive transport dominates. In principle, this means that radionuclides can be transported back from the host rock to the buffer. This is, however, not included in the model. Rather, the transport rate into the host rock is described via an **effective flow rate**, the calculation of which is outside the scope of STMAN and is described as part of the justification for the choice of input data that is made (Appendix 3).

A1.3.3 Mathematical representation

A1.3.3.1 Overview

Mathematically, the same split of the code into various aspects applies. In the equations presented here only a single radionuclide is used, with a single parent. The full system is created by solving a set of such equations simultaneously. In cases where a radionuclide has no parents the ingrowth term is omitted and in cases where there are multiple parents there are several ingrowth terms.

STMAN is a numerical code that discretises the system spatially in order to solve it. The full details of the solution approaches are not given here.

A1.3.3.2 Containment and canister breaching

Prior to the specified breaching time, the canister is assumed to be completely intact. The only processes occurring within the canister up to this time are radioactive decay and ingrowth. Given the assumptions of complete containment of no interchange between inventory components, it is simply necessary to evaluate the decayed inventory as a function of time. This is done separately for the three components: the instant release fraction (denoted by the subscript b); cladding (denoted by the subscript c); and fuel matrix (denoted by the subscript m). The subscript s is used to denote any of the three components.

The initial inventories are given by

$$N_b^n(0) = F_b I^n, \quad (\text{A1.3-1a})$$

$$N_c^n(0) = F_c I^n, \quad (\text{A1.3-1b})$$

$$N_m^n(0) = F_m I^n, \quad (\text{A1.3-1c})$$

where I^n [mol] is the total initial inventory for radionuclide n and the F factors are the relevant fractions, which sum to unity.

The inventory at later times is governed by the decay and ingrowth equation

$$\frac{dN_s^n}{dt} = -\lambda^n N_s^n + \lambda^{n-1} N_s^{n-1}, \quad (\text{A1.3-2})$$

where $n-1$ denotes the parent radionuclide. Note that N_s^n is not the actual inventory in the decreasing volume of cladding or matrix, but simply an updated total inventory. This is calculated for mathematical convenience, as it allows the release rate from the cladding and matrix to be expressed in a simple form.

A1.3.3.3 Fuel release mechanisms and the reservoir

Following canister breaching, the release of radionuclides to the reservoir begins. At the same time losses from the reservoir to the buffer also begin. The radionuclide amounts in the reservoir, denoted M^n [mol] are governed by

$$\frac{dM^n}{dt} = -\lambda^n M^n + \lambda^{n-1} M^{n-1} + \mu_c N_c^n + \mu_m N_m^n - B^n, \quad (\text{A1.3-3})$$

where

μ_c [a^{-1}] and μ_m [a^{-1}] are the time-dependent congruent release rates for the cladding and matrix respectively and B^n [mol a^{-1}] is the rate at which radionuclides are lost from the reservoir to the buffer. The congruent release rates are defined in terms of fractions of the initial volume, so the rate of change of volume, $\frac{dV}{dt}$, is given by $-\mu V_0$, where V_0 [m^3] is the initial volume.

This equation applies for times after the canister breaching time, t_c [a]. At this time the instant release fraction enters the reservoir,

$$M^n(t_c) = N_b^n(t_c). \quad (\text{A1.3-4})$$

Note that the release rates must integrate to unity in order for mass to be conserved. SPENT calculates a time when each release must stop. The constraints

$$\int_{t_c}^{t_{exh,m}} \mu_m(t) dt = \int_{t_c}^{t_{exh,c}} \mu_c(t) dt = 1 \quad (\text{A1.3-5})$$

define these exhaustion times, $t_{exh,m}$ and $t_{exh,c}$.

Given the amounts of each radionuclide, the concentrations can be calculated for the reservoir. These are subject to solubility limitation. Two cases must be considered, depending on whether the total over all isotopes of a given element exceeds a solubility limiting value for that element or not.

Let m^e be the total mass, summed over isotopes of element e (one of which is radionuclide n). Then, the concentration is given by

$$C^n = M^n / V_R \quad \text{if } m^e \leq V_R C_{sol}^e, \quad (\text{A1.3-6a})$$

$$C^n = \frac{M^n}{m^e} C_{sol}^e \quad \text{if } m^e > V_R C_{sol}^e. \quad (\text{A1.3-6b})$$

Here, V_R [m^3] is the reservoir volume and C_{sol}^e [mol m^{-3}] is the solubility limit for element e in the reservoir.

In the usual case of a fully breached canister, the loss to the buffer is governed by the diffusive flux, with the inner buffer concentration set to the reservoir concentration. So,

$$C_B^n \Big|_{r=r_0} = C^n, \quad (\text{A1.3-7})$$

and

$$B^n = -2\pi r_0 L D_B^n \frac{\partial C_B^n}{\partial r} \Big|_{r=r_0}. \quad (\text{A1.3-8})$$

Here, r_0 [m] is the inner radius of the buffer, L [m] is the canister length and D_B^n [$\text{m}^2 \text{a}^{-1}$] is the effective diffusion coefficient for the buffer.

For the case where a pinhole release is used, the release rate is calculated from the model proposed by Chambré et al. (1986). This gives the release directly as

$$B^n = N_{pin} D_B^n r_{pin} C^n S^n(t), \quad (\text{A1.3-9})$$

where N_{pin} is the number of pinholes in a canister, r_{pin} [m] is their radius, and $S^n(t)$ is a time-dependent shape factor given by

$$S^n = 4 \left[1 + \frac{2r_{pin}}{\pi} \left(\frac{\varepsilon_B^n R_B^n}{\pi D_B^n t} \right)^{1/2} \right]. \quad (\text{A1.3-10})$$

Here ε_B^n [-] is the effective porosity of the buffer and R_B^n [-] is the retardation factor, that accounts for sorption in the buffer. Both of these are the values applying at the inner buffer

boundary. Note that the model of Chambré et al. (1986) assumes pessimistically that the concentration at the surface of the canister (at the outlet of the pinhole) is the same as that within the canister. In contrast to this approach, Aidun et al. (1988) assume that the concentration in the pinhole is controlled by the concentration within the canister (at the inside end of the pinhole). Thus, they include the diffusion resistance of the pinhole itself, which leads to lower radionuclide release rates through the pinhole. This process is pessimistically neglected in STMAN (reserve FEP).

A1.3.3.4 Transport through the buffer

The buffer surrounding the canister is an annular region between the canister and the tunnel wall. It is treated as a one-dimensional radial system. The governing transport equation, in the absence of any solubility limitation, for diffusion in the buffer water is

$$\varepsilon_B^n R_B^n \frac{\partial C_B^n}{\partial t} = D_B^n \nabla_r^2 C_B^n - \lambda^n \varepsilon_B^n R_B^n C_B^n + \lambda^{n-1} \varepsilon_B^{n-1} R_B^{n-1} C_B^{n-1}, \quad (\text{A1.3-11})$$

where C_B^n [mol m⁻³] is the concentration of the radionuclide n in the water, R_B^n [-] the retardation factor, D_B^n [m² a⁻¹] the effective diffusion coefficient, ε_B^n is the porosity including a radionuclide-specific factor, and λ^n the decay constant. Note that R_B^n , ε_B^n , D_B^n and λ^n are all specific for each radionuclide. The effective diffusion coefficient is either specified directly or calculated from the pore diffusion coefficient as $D_B^n = \varepsilon_B^n D_{B,pore}$. The term $\lambda^{n-1} R_B^{n-1} C_B^{n-1}$ is an ingrowth term, which originates from the coupling between different radionuclides of a decay chain. The superscript $n-1$ indicates the parent radionuclide (it is assumed here that there is a single parent; there may be none, in which case the term is omitted, or more than one, in which case there are several such terms).

To handle solubility limitation in the buffer, the governing equation is rewritten as

$$\frac{\partial U_B^n}{\partial t} = D_B^n \nabla_r^2 C_B^n - \lambda^n \varepsilon_B^n R_B^n C_B^n + \lambda^{n-1} \varepsilon_B^{n-1} R_B^{n-1} C_B^{n-1}, \quad (\text{A1.3-12})$$

where U_B^n [mol] is the total concentration of radionuclide n , including aqueous, sorbed and precipitated phases. Then, the relationship between the aqueous and total concentration depends on whether the total over all isotopes of the same element exceeds a solubility limiting value or not.

Let U_B^e be the total concentration summed over isotopes of element e (one of which is radionuclide n). Then, the aqueous concentration is given by

$$C_B^n = U_B^n / (\varepsilon_B^n R_B^n) \quad \text{if } U_B^n \leq \varepsilon_B^e R_B^e C_{B,sol}^e, \quad (\text{A1.3-13a})$$

$$C_B^n = \frac{U_B^n}{U_B^e} C_{B,sol}^e \quad \text{if } U_B^e > \varepsilon_B^e R_B^e C_{B,sol}^e. \quad (\text{A1.3-13b})$$

Here, $C_{B,sol}^e$ [mol m⁻³] is the solubility limit for element e in the buffer. Note that the retardation coefficient is denoted by an element superscript here. In STMAN, the transport properties that vary from radionuclide to radionuclide are in fact entered and stored by element. The porosity is also denoted as being element-dependent. This is to allow exclusion effects to be modelled. A physical porosity, ε_B , is defined with porosity factors set to give the element-dependent value ε_B^e .

Retardation factors are derived from specified sorption coefficients

$$R_B^e = 1 + \frac{(1 - \varepsilon_B) \rho_B K_{d,B}^e}{\varepsilon_B^e}, \quad (\text{A1.3-14})$$

with ρ_B [kg m⁻³] the solid density of matrix (mass per volume of solid matrix in the accessible region), $K_{d,B}^e$ [m³/kg] the buffer sorption coefficient, and ε_B the buffer porosity as defined above (with the extra superscript e denoting the porosity-factor scaled value). Note that the porosity in the factor multiplying density is the physical porosity as this represents the fraction of solid in the system.

STMAN allows that the buffer may have different properties in two regions. An inner and outer region may be defined and separate values given for diffusion coefficients, solubility, sorption coefficients, density, porosity and porosity factors.

The boundary condition for the buffer transport equation on the inner boundary is generally a specified concentration (equation A1.3-7). The exception is when the pinhole release model is used, in which case the total diffusive flux is set (equation A1.3-9).

The outer boundary condition can be a fixed concentration (commonly zero) or a mixing cell condition. These are discussed in the next section.

A1.3.3.5 Interface with the host rock

At the interface between the buffer and the host rock, at radius r_I , two types of boundary condition can be selected. The simplest is a fixed concentration condition,

$$C_B^n(r_I) = C_{GW}^n, \quad (\text{A1.3-15})$$

where C_{GW}^n is a specified concentration in the groundwater, which is often taken to be zero.

Alternatively, a mixing cell condition can be used. This specifies that the diffusive flux to the interface through the buffer is balanced by an effective advective flux in the host rock (even

though in reality transport in the host rock may be diffusion dominated). The concentration on the boundary is set dynamically to maintain the balance. The general form in STMAN allows that the incoming groundwater may already contain dissolved radionuclides. The balance equation is

$$Q_{GW} C_B^n(r_1) = Q_{GW} C_{GW}^n - 2\pi r_1 L D_B^n \left. \frac{\partial C_B^n}{\partial r} \right|_{r=r_1} \quad (\text{A1.3-16})$$

Again, the radionuclide concentration in the incoming water is often set to zero as a conservative value. The only new parameter here is Q_{GW} [$\text{m}^3 \text{a}^{-1}$] which is the effective flow rate (volume per unit time) of the groundwater that is included in the mixing processes. Note that this boundary condition tends to be equivalent to the fixed concentration condition for effective high flow cases. Note also that radial symmetry is preserved in the model, even though the concentration in reality will vary around and along the boundary. In the low effective flow case, this approximation is realistic, while in the high effective flow case, the concentrations are all low compared to that at the canister boundary and so the details are irrelevant.

In the situation of relevance for the current study, where the host rock is itself a diffusive barrier, the basis for selecting a value for Q_{GW} is difficult. The term $Q_{GW} C_B^n(r_1)$ in the boundary condition represents the rate at which radionuclides move away from the boundary and so it is natural in a diffusive system to replace this with a diffusive term of the form

$$\frac{D_{HR} A_{HR}}{L_{HR}} C_B^n(r_1)$$

where the diffusion coefficient, area and length scale in the host rock are combined to give an effective flow rate. The area will simply be the contact area of the buffer and host rock. Justification for the length scale chosen will be part of the description of input parameters for any particular case.

A1.3.4 Input parameters

The input parameters required to specify a SPENT calculation can be split into categories:

- Nuclides and decays;
- Inventory data;
- Physical data for the waste-form and canister;
- Chemical data for the waste-form and canister;
- Physical data for the buffer, including the outer boundary condition;
- Chemical data for the buffer.

Of these, only the physical and chemical properties of the waste-form are specific to SPENT, the others applying to all STMAN codes. To reflect this, the inputs are presented in three separate tables.

In addition, output specifications are needed and control parameters may be modified. These do not form part of the input data listed here, but will be commented on in the description of the individual cases.

The units of input parameters for STMAN are fixed within the code and are quoted here.

Tab. A1.3-3: STMAN input data requirements for the radionuclides and inventory

Input	Units	Requirements
<i>Radionuclides and Decays</i>		
Radionuclides and decays to be used, λ^n	Half lives are specified in years.	Table of parents, daughters and half-lives. Where a parent has more than one daughter, the half-life for each decay is the total half-life of the parent divided by the fraction decaying to the particular daughter.
<i>Total Inventory</i>		
Inventory for each radionuclide for a single package, I_n	moles or TBq	Either the activity in TBq or the amount in moles can be specified.

Tab. A1.3-4: SPENT input data requirements for the waste form and canister

Input	Units	Requirements
<i>Inventory Fractions</i>		
Percentage of the inventory for each radionuclide present in the matrix, cladding (referred to as grain in the code), instant release fraction, F	dimensionless (%)	Must sum to 100 %.
<i>Canister Properties</i>		
Breaching time	a	
Number of containers	dimensionless	This is used to scale the relevant outputs.
Length, L	m	
Initial diameter of waste form	m	This is generally set to be twice the inner buffer radius, but can be less than this. It is only used to calculate a reservoir volume if none is set explicitly. In the present study, the reservoir volume is set directly and so the waste diameter is not used.
<i>Release Properties</i>		
Matrix release rate, μ_m	a ⁻¹	Time-dependent congruent release rate for the matrix fraction of the inventory.
Cladding (or grain) release rate, μ_c	a ⁻¹	Time-dependent congruent release rate for the cladding fraction of the inventory. Referred to as grain fraction in output files.
Reservoir volume, V_R	m ³	A non-zero volume is needed, but this can be set to be small if required.
Solubility limits, C_{sol}^e	mol l ⁻¹	For each element in the reservoir. Note that the units are molar in the input.
Pinhole radius, r_{pin}	m	If the pinhole option is used.
Number of pinholes, N_{pin}	dimensionless	If the pinhole option is used.

Tab. A1.3-5: STMAN input data requirements for the buffer

Input	Units	Requirements
Buffer Properties		
Inner radius, r_0	m	The radial co-ordinate of the inside of the buffer (at the canister).
Outer radius, r_1	m	The radial co-ordinate of the outside of the buffer (at the host rock).
Split radius	m	The radius separating an inner and outer buffer region which can have different properties.
Porosity, ϵ_B^n	dimensionless	Separate inner and outer buffer values may be set
Porosity Factors	dimensionless	Factor to scale porosity for some radionuclides. Default is 1, so only needed for radionuclides that are affected. The factors are less than one and represent constraints on the accessible porosity for some radionuclides (e.g. due to anion exclusion). The scaled porosities are denoted by ϵ_B^n . Separate values can be given for the inner and outer buffer regions.
Density, ρ_B	kg m ⁻³	Either solid density, ρ_B , or bulk dry density, ρ_B^{dry} , may be specified for the buffer material.
Sorption coefficient, $K_{d,B}^e$	m ³ kg ⁻¹	Equilibrium sorption coefficients, for each element in the buffer. Separate values can be given for the inner and outer buffer regions.
Solubility limits, $C_{B,sol}^e$	mol l ⁻¹	For each element in the buffer. Note that the units are molar. Separate values can be given for the inner and outer buffer regions.
Diffusion coefficient, D_B^n	m ² a ⁻¹	Either the pore diffusion coefficient (D_{pore}) or effective diffusion coefficients (D_{eff}) for each radionuclide are required. If the pore diffusion coefficient is specified, then the effective diffusion is calculated as $D_{eff}^n = \epsilon_B^n D_{pore}$, where the porosity is scaled by the radionuclide-specific porosity factor.
Effective mixing cell flow rate, Q_{GW}	m ³ a ⁻¹	Required if the mixing cell condition is specified. The rate can be time-varying (piecewise constant).
Incoming water concentrations, C_{GW}^n	TBq m ⁻³ or mol m ⁻³	For the outer boundary. Default is zero. Either the activity concentration in TBq m ⁻³ or the concentration in mol m ⁻³ can be specified.

A1.3.5 Verification

Verification of the STMAN suite of codes has been carried out at two levels. Firstly, full scale comparisons of the results calculated using STMAN have been compared with other codes and analytic solutions. Secondly, detailed confirmation of the behaviour of new capabilities has been carried out as the code has developed.

Moreover, the codes were completely rewritten in 1999, the earlier versions being written in Fortran and the later (and current) versions being written in C++. Because there is no common code between the versions, the successful cross-comparison between them at that time provides strong confirmation of their correct functioning. The new versions have more accurate discretisation than the older ones, so the results were not identical; a range of discretisations was tested to confirm that this was the cause of any differences.

The STMAN codes differ only in their treatment of the waste and associated processes. The major part of the codes, involving transport through the buffer and interfacing to the host rock, is common. Verification of any of the codes is, in this regard, verification of all of them. In the case of a strongly solubility limited radionuclide, which maintains a constant concentration in the waste form, all of the codes will produce the same release profiles, since the waste form aspects are irrelevant.

The original version of the SPENT code was verified by cross-comparison with the PAGODA code. PAGODA was an integrated performance assessment tool used for strategic and training purposes, but was capable of producing a good approximation to the spent-fuel release and buffer transport aspects in SPENT. Good agreement was obtained for a full decay chain.

A detailed cross comparison was undertaken between SPENT and AMBER in the context of a larger cross-comparison exercise in 2001. This took a full suite of radionuclides and two types of spent fuel (with different properties). AMBER is a general-purpose compartment modelling tool that can be used to create compartment models for transport of passive radioactive contaminants. A compartment model was constructed to reproduce the SPENT model, so that good agreement would be expected. A mixing tank model was used for the outer buffer boundary.

Fig. A1.3-1 shows the STMAN and AMBER results for the release of the key radionuclides from the buffer into the host rock for one of the waste types.

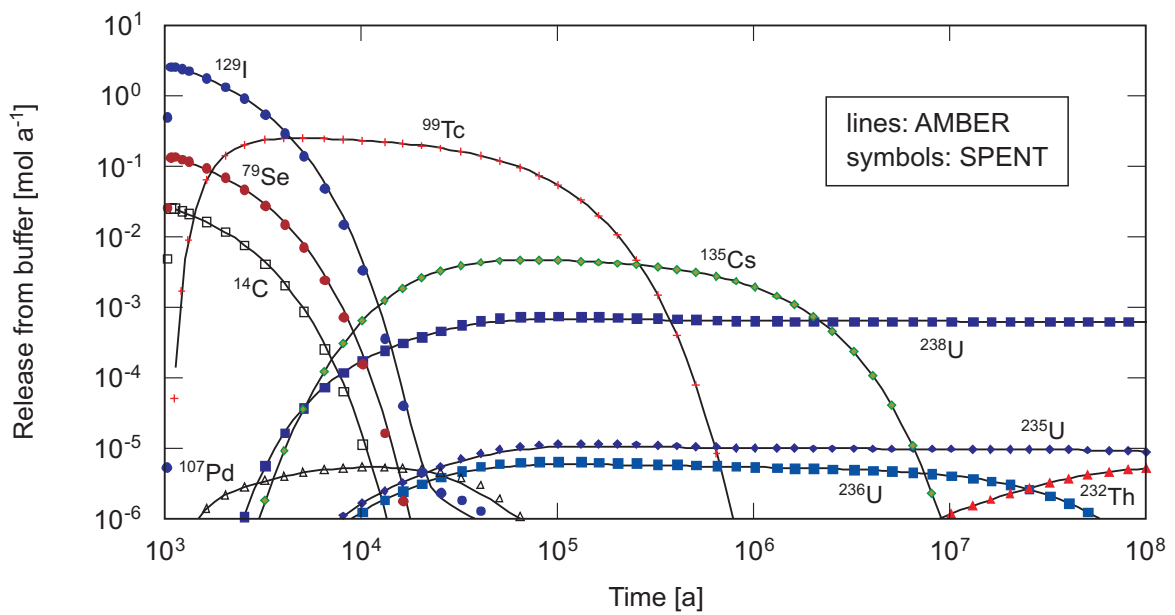


Fig. A1.3-1: Comparison of SPENT and AMBER results in a code comparison verification test

Other results were in similarly good agreement. The comparison exercise actually went further than verification of SPENT, because it included a far-field component. It was therefore possible to verify SPENT and PICNIC linked together against an integrated compartment model of the full system. Both results were converted to doses using the same equilibrium biosphere conversion factors. Figs. A1.3-2 and A1.3-3 show the results. They are in good agreement (a few percent difference in the peak doses).

Verification of new capabilities of the STMAN suite of codes has been undertaken with each new release. This has generally involved hand calculations to confirm the correct behaviour. A test of this kind, for the split-buffer capability, is described in the STALLION verification section but is applicable to STMAN as a whole.

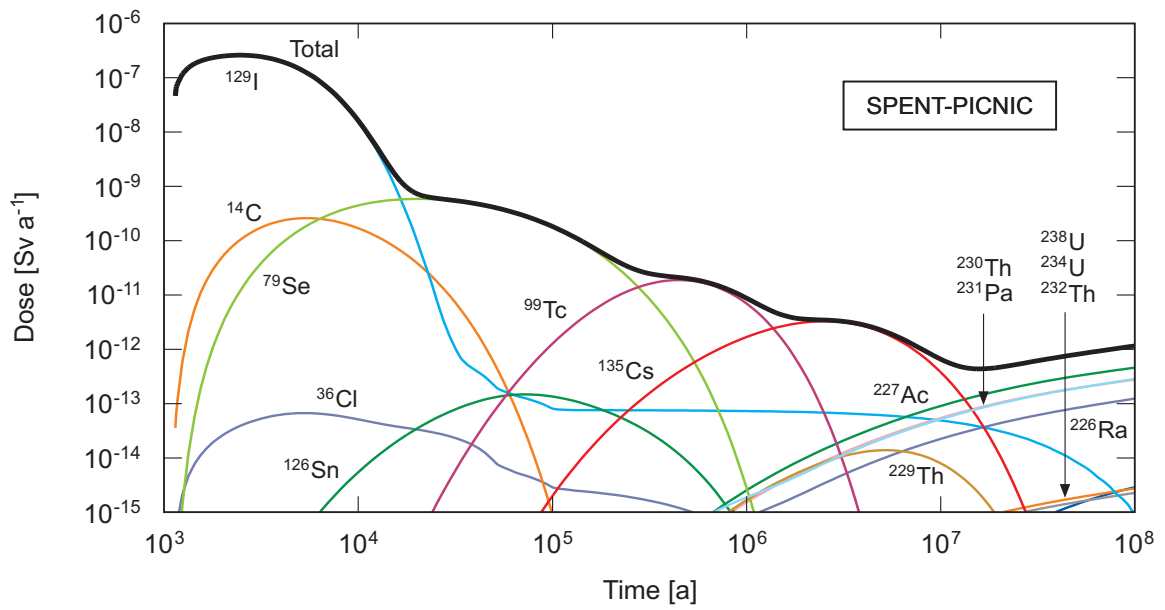


Fig. A1.3-2: Doses calculated using SPENT and PICNIC in a code comparison verification test

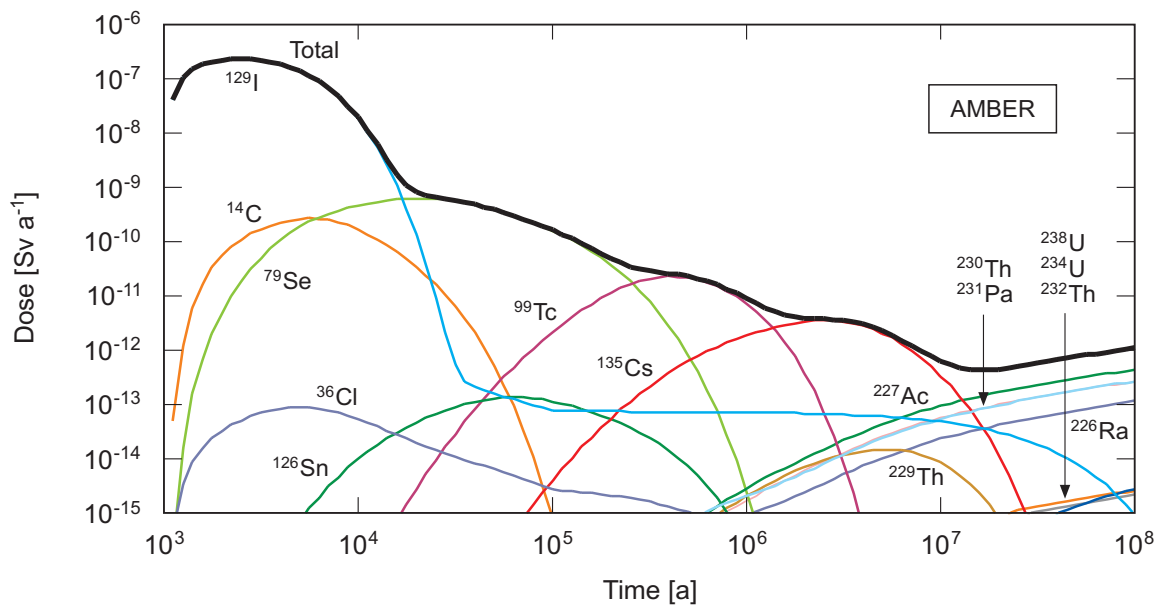


Fig. A1.3-3: Doses calculated using AMBER in a code comparison verification test

A1.4 STRENG

A1.4.1 Scope and purpose

STRENG is that part of the STMAN suite of codes for the near field release and transport of radionuclides from an HLW canister. STRENG represents the cylindrical canister containing the waste and an annular buffer region around this. The outer boundary of the region considered in STRENG is the interface to the geosphere and is handled through the use of an appropriate boundary condition (generally a mixing cell condition).

The STMAN suite of codes all treat the buffer and outer boundary in the same way, differing only in their treatment of the waste form. Thus, these aspects of the description are not repeated here.

The primary output is a flux to the near field for use in the geosphere but current concentrations and other intermediate results can also be output for use in other calculations, for example human intrusion consequence analysis.

A1.4.2 Phenomena included in STRENG

A1.4.2.1 Overview

An overview of the representation of Super-FEPs in the various safety assessment computer codes is given in Section A1.2-3 (Tab. A1.2-2). Tab. A1.4-1 describes in more detail how STRENG represents the different Super-FEPs that fall into its model domain, namely the HLW near field. The symbols used in Tab. A1.4-1 are explained in Section A1.2-3. The following model features are considered separately:

- The containment period and canister breaching modes;
- The release mechanisms for radionuclides from the waste form and the reservoir;
- Transport through the buffer; and
- The interface with the host rock.

The final two aspects are common to all codes in the STMAN family and the relevant sections in the description of SPENT (Appendix A.1.3) should therefore be consulted. An earlier version of STRENG was fully described by Grindrod et al. (1990).

Some safety-relevant aspects of the Super-FEPs (indicated by large bold ticks in Tab. A1.4-1) are either modelled explicitly by STRENG, or their magnitude, timing, rate, spatial extent and performance directly determine one or more input parameters. These aspects or phenomena are summarised in Tab. A1.4-2 and discussed in more detail in the following sections, where they are highlighted in bold. The table also notes radioactive decay and ingrowth as included phenomena. Shaded boxes are used since these phenomena are not directly related to the Super-FEPs. STRENG (and the other STMAN codes) models these phenomena, including the branching and rejoining of chains, in all parts of the system. The suite of radionuclides considered is specified as part of the input so that the STMAN codes can be configured to any situation.

Tab. A1.4-1: Super-FEPs, their safety-relevant aspects (as taken from Tab. A5.2.1 of Nagra 2002d) and the ways in which they are represented by the code STRENG

Symbols: see Section A1.2.3

Super-FEPs	Safety-relevant aspects to be represented by models	Model features				Explanatory comments
		Containment period and breaching modes	Glass release mechanisms and the reservoir	Transport through the buffer	Interface with the host rock	
HLW						
Quantities of glass and associated radionuclide inventories	Waste inventory in a single package and number of packages	✓				Directly provides input parameters.
Dissolution rate of glass	Dissolution rate		✓			Fractured glass is modelled as equivalent spheres. Glass dissolution rate and glass spherical radius must be input as parameter values.
HLW canisters						
Breaching of steel canisters	Distribution of breaching times	●				Not included, but canister breaching time can be selected such that results err on the side of pessimism.
	Time of occurrence of breaching	✓				Time of breaching (containment) time is input as a parameter value – see, however, "the long resaturation time of the repository and its surroundings", below.
Gas generation by steel canister corrosion	Gas generation rate for SF / HLW			▶	▶	No transport of radionuclides in volatile form considered; gas generation assumed to be irrelevant (see Gas Model).
Canister material	Time of occurrence of breaching (time of occurrence affected by canister material)	✓				Canister material affects evaluation of breaching time, which must be input as parameter.
	Presence of initial defects (likelihood affected by canister material)	✓				Canister material affects the possibility of localised defects, with associated transport resistances, which are characterised by input parameters.
HLW near field						
The long resaturation time of the repository and its surroundings	The rate of the resaturation process	✓				The resaturation process and its transient effects on the transport-relevant properties of the buffer are not modelled by STRENG. However, the period of complete containment can, if required, be extended beyond canister breaching time to account for a long resaturation time (this is not done in the present assessment).

Tab. A1.4-1: (Cont.)

Super-FEPs	Safety-relevant aspects to be represented by models	Model features				Explanatory comments
		Containment period and breaching modes	Glass release mechanisms and the reservoir	Transport through the buffer	Interface with the host rock	
HLW near field						
Geochemical immobilisation and retardation in the near field	Solubility limitation (reservoir)		✓			Solubility limits for the reservoir are input as parameter values.
	Solubility limitation (buffer)			✓		Solubility limits for the buffer are input as parameter values.
	Linear, equilibrium sorption			✓		Sorption coefficients for the buffer are input as parameter values.
	Colloid filtration by bentonite			✓		Precipitated solids are assumed to be immobile.
	The extent of co-precipitation with secondary minerals		✓	✓		Can be taken into account via the setting of the solubility limits.
	The extent of sorption on canister corrosion products		●			Sorption on canister corrosion products not included, but omission is conservative.
	The effects on solubility limitation of the natural concentrations of isotopes		●	●		Natural background concentrations not included, but omission is conservative.
Thermal alteration of the bentonite buffer adjacent to the HLW canisters	Proportion of the buffer affected and the magnitude of the effects on buffer transport properties			○		Extent of thermal alteration must be evaluated separately. Diffusion coefficients appropriate to altered buffer can be input, if required, as parameter values for all or part of the buffer.
Transport resistances provided by internal spaces (fractures) within the waste forms, by the breached HLW canisters and by corrosion products	The magnitude of transport resistance of initial defects		✓			Transport resistance of breached canisters can be considered via the "pinhole model" built into STRENG.
	The magnitude and time-dependence of other transport resistances		●			Other transport resistances not included, but omission is conservative.
Tunnel liner	The requirement for a liner				●	Requirement for a liner ruled out by supplementary studies.
Hydraulic transport characteristics of bentonite	Effective flow rate at outer boundary				✓	Input parameter.
	Aqueous diffusion			✓		Aqueous diffusion is assumed to convey radionuclides across the bentonite buffer; element-specific diffusion coefficients are input as parameter values.
	Compaction of bentonite by tunnel convergence			○		Compaction during tunnel convergence can be taken into account in setting the tunnel radius and bentonite transport properties.

Tab. A1.4-1: (Cont.)

Super-FEPs	Safety-relevant aspects to be represented by models	Model features				Explanatory comments
		Containment period and breaching modes	Glass release mechanisms and the reservoir	Transport through the buffer	Interface with the host rock	
HLW near field						
Gas transport characteristics of bentonite	Gas-induced release of dissolved radionuclides			○		Expulsion of the IRF by repository gas can be simulated, if required, by neglecting the transport resistance of the bentonite for the IRF.
	Dilatant gas pathway formation (SF / HLW near field)			▶		Not considered in STRENG (see Gas Model).
	Gas dissolution and diffusion			▶		See above.
The barrier system (general)						
Future human actions	Borehole penetration of the repository				○	The nature and timing of future human actions cannot be evaluated using STRENG. The consequences of hypothetical actions that may influence the near field can, however, be bounded in some cases (e.g. the possibility of future drilling of a borehole inadvertently affecting the barrier system can be modelled by interfacing STRENG directly with the biosphere model).

Tab. A1.4-2: Phenomena explicitly included in the STRENG model

Model features	Phenomena explicitly included in the STRENG model
All	Radionuclide decay and ingrowth
The containment period and canister breaching modes	Waste inventory in a single package and number of packages
	Time of occurrence of HLW canister breaching
	Presence of initial defects
	Transport resistance of initial defects
Glass release mechanisms and the reservoir	Dissolution rate of glass
	Solubility limitation
Transport through the buffer	Aqueous diffusion
	Linear equilibrium sorption
	Solubility limitation
Interface with the host rock	Effective flow rate at outer boundary

Some other safety-relevant aspects of the Super-FEPs (indicated by smaller ticks in Tab. A1.4-1) are only partly represented or are built into the SPENT model assumptions, and are also described in detail in later sections.

The possibility of time dependent system properties associated with some Super-FEPs cannot be directly represented by the code (as indicated by the symbol \circ in Tab. A1.3-1). Parameter sets can, however, be chosen that represent steady-state system properties corresponding, for example, to the end-state of the system once the process is complete or one of a number of possible transient states, as explained in the discussions of individual conceptualisations in Chapters 3 to 8.

Gas-related phenomena (indicated by the symbol \blacktriangleright) require the use of an alternative code if they are to be modelled. Where no qualified code exists, this is indicated using the symbol \bullet .

A1.4.2.2 Containment and canister breaching

Containment and canister breaching are treated in the same way in STRENG as in SPENT. Prior to some specified **time of occurrence of HLW canister breaching**, the canister is assumed to be completely intact. Complete containment of radionuclides is provided up to this time, although the initial inventory, specified via the **waste inventory in a single package and the number of packages**, is altered by **radioactive decay and ingrowth**.

When the canister is breached, the usual assumption is that the canister breaching is instant and complete, so the canister plays no further role in preventing water ingress or radionuclide release. Releases are then controlled by the behaviour of the glass matrix and the properties of the radionuclides and the buffer. An alternative breaching mode can also be modelled, where the possible **presence of initial defects**, termed **pinholes**, is considered. In this situation, the **transport resistance of the defects** also affect release rates. Processes leading to breaching are not modelled in STRENG; the breaching time is an input parameter.

A1.4.2.3 Glass release mechanisms and the reservoir

Following canister breaching, water is assumed to enter the canister and instantly saturate any void spaces in the canister interior. These saturated void spaces are collectively termed the reservoir.

Water entering the reservoir comes into contact with the vitrified waste surfaces, and glass dissolution begins. Radionuclides and stable isotopes are considered to be uniformly distributed within the vitrified waste, and thus release from the waste to the reservoir occurs congruently with glass dissolution. The **dissolution rate of glass** is assumed to be proportional to the exposed surface area of the glass. Fracturing of the glass is assumed to have taken place during cooling, so that the exposed area is higher than the external area of an unfractured vitrified waste block. The glass fragments are modelled as a number of spheres of equal size, with an initial total volume equal to that of the glass. The number of spheres is set such that the initial surface area of the spheres also equals that of the fractured glass. The surface area of the spheres decreases with time as they dissolve at a specified rate per unit surface area.

Radionuclides and stable isotopes are assumed to be uniformly mixed within the reservoir. The transport resistances experienced by radionuclides migrating through the reservoir (including, for example, the transport resistances of cracks within the fuel pellets) are thus neglected. Sorption on the solid surfaces with which reservoir water is in contact (including the canister and canister corrosion products) is also not modelled by STRENG. Aqueous concentrations are, however, constrained by **solubility limitation**; the solubility limits of each element in the reservoir are input as parameters. Concentrations of all isotopes of the same element, including stable isotopes, are taken into account when evaluating whether the solubility limit has been reached. Co-precipitation with, for example, corrosion products, is not modelled explicitly, but can be taken into account if the necessary data are available when setting solubility limits. Solids are precipitated or re-dissolved at rates that maintain aqueous concentrations at or below the solubility limits. Dissolved radionuclides and stable isotopes can diffuse from the reservoir into the buffer (via the pinhole if that model is used), but solids, including colloids, are assumed to be retained within the reservoir (filtration by the buffer).

A1.4.2.4 Transport through the buffer and the interface with the host rock

The assumptions and model for the buffer and outer boundary conditions in STRENG are the same as SPENT (see Sections A1.4.2.4 and A1.4.2.5).

A1.4.3 Mathematical representation

Mathematically, the only difference between STRENG and SPENT is in the release of radionuclides to the reservoir. For the rest of the system refer to Appendix 1.3.3.

A1.4.3.1 Glass release mechanisms

Following canister breaching, the release of radionuclides to the reservoir begins. At the same time losses from the reservoir to the buffer also begin. The radionuclide amounts in the reservoir, denoted M^n are governed by

$$\frac{dM^n}{dt} = -\lambda^n M^n + \lambda^{n-1} M^{n-1} + \mu_G N_G^n - B^n, \quad (\text{A1.4-1})$$

where

μ_G [a^{-1}] is the time-dependent glass dissolution rate and B^n [mol a^{-1}] is the rate at which radionuclides are lost from the reservoir to the buffer. All the terms are the same as those that appear in equation (A1.3-3) except for the glass dissolution term that replaces the cladding and fuel matrix terms.

This equation applies for times after the canister breaching time. The decayed inventory is governed by the decay and ingrowth equation

$$\frac{dN_G^n}{dt} = -\lambda^n N_G^n + \lambda^{n-1} N_G^{n-1}. \quad (\text{A1.4-2})$$

In common with the approach used in SPENT, this inventory is not the actual inventory left in the glass, but is the total decayed inventory whether still in the glass or not. The glass dissolution rate μ_G is derived as follows (Hartley 1985):

The glass is represented as a set of equally-sized spheres. The radius of the spheres, r_f [m], is fixed by the requirement that the initial ratio of glass volume to surface area is the same for the spheres as for the real fractured glass blocks,

$$r_f = \frac{3V_0}{A_0}. \quad (\text{A1.4-3})$$

where V_0 is the total volume of the blocks and A_0 is the total surface area. In order that the total volume of the spheres is equal to the total volume of the blocks, the number of spheres is given by:

$$n_f = \frac{3V_0}{4\pi r_f^3}. \quad (\text{A1.4-4})$$

The assumption of a constant glass-corrosion rate per unit surface area leads to a decrease in the radius of the spheres which is proportional to time, so that the lifetime of the blocks is given by τ [years]:

$$\tau = \frac{\rho_g r_f}{R}, \quad (\text{A1.4-5})$$

where ρ_g is the glass density [kg m^{-3}] and R is the dissolution rate. Note that the units of R in this equation are [$\text{kg m}^{-2} \text{a}^{-1}$] but the input value is in [$\text{g cm}^{-2} \text{d}^{-1}$]. V [m^3], the time-dependent volume of glass summed over all glass blocks, is then:

$$V = \begin{cases} V_0 & : t \leq t_C \\ V_0 \left(1 - \frac{(t-t_C)}{\tau} \right)^3 & : t_C < t < \tau + t_C \\ 0 & : t \geq \tau + t_C \end{cases} \quad (\text{A1.4-6})$$

and from this the dissolution rate is simply given by

$$\mu_G = -\frac{1}{V_0} \frac{dV}{dt} . \quad (\text{A1.4-7})$$

Note that this is fully determined by the dissolution time, τ , and this is therefore fundamental to the behaviour of the glass in the STRENG model.

Given the amounts of each radionuclide, the concentrations can be calculated for the reservoir. These are subject to solubility limitation in precisely the same way as in the SPENT model.

The pinhole release model can be used, again as in the SPENT model.

A1.4.4 Input parameters

The input parameters required to specify a STRENG calculation can be split into categories:

- Radionuclides and decays;
- Inventory data;
- Physical data for the glass and canister;
- Chemical data for the glass and canister;
- Physical data for the buffer, including the outer boundary condition;
- Chemical data for the buffer.

Of these, only the physical and chemical properties of the glass and canister are specific to STRENG, the others applying to all STMAN codes. Only these specific inputs are presented here, the others are presented in the section on SPENT, Tabs. A1.3-2 and A1.3-4.

In addition, output specifications are needed and control parameters may be modified. These do not form part of the input data listed here, but will be commented on in the description of the individual cases.

The units of inputs to STMAN used are fixed within the code and are quoted here.

Tab. A1.4-3: STRENG input data requirements for the glass and canister

Input	Units	Requirements
<i>Canister Properties</i>		
Breaching time	a	
Number of canisters	dimensionless	This is used to scale the relevant outputs.
Length	m	
Initial diameter of waste form	m	This is generally set to be twice the inner buffer radius, but can be less than this. It is only used to calculate a reservoir volume if none is set explicitly. In the present study, the reservoir volume is set directly and so the waste diameter is not used.
<i>Release Properties</i>		
Glass density, ρ_g	kg m ⁻³	Used in determining the glass dissolution time.
Glass dissolution rate	g cm ⁻² d ⁻¹	Used in determining the glass dissolution time.
Equivalent spherical radius, r_f	m	Used in determining the glass dissolution time. Should be determined to give the required surface area per unit volume of the fragmented glass.
Reservoir volume, V	m ³	A non-zero volume is needed, but this can be set to be small if required.
Solubility limits	mol l ⁻¹	For each element in the reservoir. Note that the units are molar.
Pinhole radius	m	If the pinhole option is used.
Number of pinholes	dimensionless	If the pinhole option is used.

A1.4.5 Verification

Verification of the STMAN suite of codes has been carried out at two levels. Firstly, full scale comparisons of the results calculated using STMAN have been compared with other codes and analytic solutions. Secondly, detailed confirmation of the behaviour of new capabilities has been carried out as the code has developed.

Moreover, the codes were completely rewritten in 1999, the earlier versions being written in Fortran and the later (and current) versions being written in C++. Because there is no common code between the versions, the successful cross-comparison between them at that time provides strong confirmation of their correct functioning. The new versions have more accurate discretisation than the older ones, so the results were not identical; a range of discretisations was tested to confirm that this was the cause of any differences.

The STMAN codes differ only in their treatment of the waste and associated processes. The major part of the codes, involved in transport through the buffer and interfacing to the host rock, is common. Verification of any of the codes is, in this regards, verification of all of them. In the case of a strongly solubility limited radionuclide, which maintains a constant concentration in the waste form, all of the codes will produce the same release profiles, since the waste-form aspects are irrelevant. The verification tests presented in the SPENT description can thus be regarded as verifying most of the STRENG code.

Verification cases for the original version of STRENG were documented by Grindrod et al. (1990). These involved comparison with analytic cases for single solubility-limited radionuclides and internal cross-checks for chain cases.

The key difference between STRENG and SPENT is in the waste dissolution model. These models are sufficiently simple that hand checks can be carried out on the reported amounts of radionuclides in the various locations distinguished by the model (glass and reservoir).

A1.5 STALLION

A1.5.1 Scope and purpose

STALLION is that part of the STMAN suite of codes for the near field release and transport of radionuclides from a cementitious waste form. STALLION represents the waste as a cylindrical region surrounded by an annular buffer region. The buffer region thickness can be set to an arbitrarily small value if, as in the present study, no such region is present. This geometry is the same as that for the SF and vitrified waste and is used simply for convenience. Since there is no spatial variation within the part of the STALLION system representing the waste form, the precise geometry is not important. The outer boundary of the region considered in STALLION is the interface to the geosphere and is handled through the use of an appropriate boundary condition (generally a mixing cell condition).

The STMAN suite of codes all treat the buffer and outer boundary in the same way, differing only in their treatment of the waste form. Thus, these aspects of the description are not repeated here. Note, however that, because the application of STALLION for the current project uses a very thin buffer layer, this aspect of the model is redundant.

The primary output is a flux to the near field for use in the geosphere but current concentrations and other intermediate results can also be output for use in other calculations, for example human intrusion consequence analysis.

A1.5.2 Phenomena included in STALLION

A1.5.2.1 Overview

An overview of the representation of Super-FEPs in the various safety assessment computer codes is given in Section A1.2.3 (Tab. A1.2-2). Tab. A1.5-1 describes in more detail how STALLION represents the different Super-FEPs that fall into its model domain, namely the ILW near field. The symbols used in Tab. A1.5-1 are explained in Section A1.2.3. The following model features are considered separately:

- The containment period;
- The behaviour of radionuclides in the cementitious region;
- Transport through the buffer (redundant in the present study and so not included in Tab. 1.5-1); and
- The interface with the host rock.

The final two aspects are common to all codes in the STMAN family and the relevant sections in the description of SPENT (Appendix A.1.3) should therefore be consulted.

Tab. A1.5-1: Super-FEPs, their safety-relevant aspects (as taken from Tab. A5.2.1 of Nagra 2002d) and the ways in which they are represented by the code STALLION

Symbols: see Section A1.2.3

Super-FEPs	Safety-relevant aspects to be represented by models	Model features			Explanatory comments
		Containment period	The behaviour of radionuclides in the cementitious region	Interface with the host rock	
ILW					
Quantities of waste and associated radionuclide inventories	Waste inventory in a single package and number of packages	✓			Directly provides input parameters.
Breaching of ILW steel drums and emplacement containers	Time of occurrence of breaching	✓			Time of breaching (containment) time is input as a parameter value – see, however, "the long resaturation time of the repository and its surroundings", below.
Corrosion / dissolution of ILW	Corrosion rate of metallic components		✓		Delayed release of radionuclides due to the slow corrosion rate of ILW metallic components can be modelled (although conservatively omitted in the present assessment).
	Corrosion / dissolution rate of remaining ILW components		●		Corrosion / dissolution of ILW conservatively assumed to be instantaneous.
Immobilisation and retardation in the ILW near field	Linear, equilibrium sorption and solubility limitation		✓		Sorption coefficients and solubility limits are input as parameter values.
Gas generation	Gas generation rates for ILW		▶	▶	No transport of radionuclides in volatile form considered; gas generation assumed to be irrelevant (see Gas Model).
Hydraulic and gas transport characteristics of ILW near field	Effective flow rate at outer boundary			✓	Input parameter.
	Gas dissolution and diffusion			▶	Not considered in STALLION (see Gas Model).
	Porewater displacement by gas			▶ or ○	The displacement of water by gas can be simulated by selecting an appropriate effective flow rate at the interface with the geosphere model.
Compaction of waste / mortar	Timing of convergence arising from void reduction of breached, corroded canisters			○	Compaction of waste / mortar is not modelled explicitly by STALLION. Its transient effects in terms of the expulsion of water from the near field must be evaluated separately. The effects on radionuclide release can then be bounded by assuming an increased effective flow rate assumed at near-field / geosphere interface (as in Cases 1.7a-b).
The long resaturation time of the ILW tunnels	The rate of the resaturation process	✓			The resaturation process and its transient effects on the transport-relevant properties of the ILW tunnels are not modelled by STALLION. However, the period of complete containment can, if required, be extended beyond the steel drum / emplacement container breaching time to account for a long resaturation time.

Tab. A1.5-1: (Cont.)

Super-FEPs	Safety-relevant aspects to be represented by models	Model features			Explanatory comments
		Containment period	The behaviour of radionuclides in the cementitious region	Interface with the host rock	
The barrier system (general)					
Future human actions	Borehole penetration of the repository			○	The nature and timing of future human actions cannot be evaluated using STALLION. The consequences of hypothetical actions that may influence the near field can, however, be bounded in some cases (e.g. the possibility of future drilling of a borehole inadvertently affecting the barrier system can be modelled by interfacing STALLION directly with the biosphere model).

Tab. A1.5-2: Phenomena explicitly included in the STALLION model

Model features	Phenomena explicitly included in the STALLION model
All	Radionuclide decay and ingrowth
The containment period	Waste inventory in a single package and number of packages
	Time of occurrence of breaching (ILW steel drums and emplacement containers)
The behaviour of radionuclides in the cementitious region	Corrosion rate of metallic components
	Linear equilibrium sorption
	Solubility limitation
Interface with the host rock	Effective flow rate

Some safety-relevant aspects of the Super-FEPs (indicated by large bold ticks in Tab. A1.5-1) are either modelled explicitly by STALLION, or their magnitude, timing, rate, spatial extent and performance directly determine one or more input parameters. These aspects or phenomena are summarised in Tab. A1.5-2 and discussed in more detail in the following sections, where they are highlighted in bold. The table also notes radioactive decay and ingrowth as included phenomena. Shaded boxes are used since these phenomena are not directly related to the Super-FEPs. STALLION (and the other STMAN codes) models these phenomena, including the branching and rejoining of chains, in all parts of the system. The suite of radionuclides considered is specified as part of the input so that the STMAN codes can be configured to any situation.

Some other safety-relevant aspects of the Super-FEPs (indicated by smaller ticks in Tab. A1.5-1) are only partly represented or are built into the STALLION model assumptions, and are also described in detail in later sections.

The possibility of time dependent system properties associated with some Super-FEPs cannot be directly represented by the code (as indicated by the symbol \circ in Tab. A1.3-1). Parameter sets can, however, be chosen that represent steady-state system properties corresponding, for example, to the end-state of the system once the process is complete or one of a number of possible transient states, as explained in the discussions of individual conceptualisations in Chapters 3 to 8.

Gas-related phenomena (indicated by the symbol \blacktriangleright) require the use of an alternative code if they are to be modelled. Where no qualified code exists, this is indicated using the symbol \bullet .

A1.5.2.2 Containment

Prior to some specified **time of occurrence of breaching**, ILW steel drums and emplacement containers are assumed to be completely intact. Complete containment of radionuclides is provided up to this time⁴⁸, although the initial inventory, specified via the **waste inventory in a single package and the number of packages**, is altered by **radioactive decay and ingrowth**.

Following this period, it is assumed that the system is completely saturated and that the waste containers play no further role in preventing water ingress or radionuclide release. Release is controlled by the properties of the cementitious region in which the waste is embedded and by the properties of the buffer. The possibility of localised defects in the waste containers is not considered in STALLION.

A1.5.2.3 The behaviour of radionuclides in the cementitious region

The interior of an ILW disposal tunnels (in the absence of a clay buffer lining the tunnel walls) is treated as a single homogeneous porous medium, termed the cementitious region. Following the containment period, radionuclides and stable isotopes contained in waste forms are generally assumed to be released instantly to the pore water of the cementitious region, although a fraction of the inventory can be modelled as being subject to slow release, controlled by, for example, the **corrosion rate of metallic components** of the waste.

Released radionuclides and stable isotopes are uniformly mixed with the pore water of the cementitious region. The transport resistances experienced by radionuclides migrating through the cementitious region are thus neglected. Aqueous concentrations are, however, affected by **linear equilibrium sorption** on pore surfaces. The constant of proportionality is the element-specific sorption coefficient K_d . The quantification of retardation also requires the porosity and density of the buffer to be specified. Density can be expressed either as grain density, i.e. the mass of solid material per unit volume of buffer, not including the volume occupied by pores, or bulk dry density, i.e. the mass of solid material per unit volume of buffer, including pore volume.

Aqueous concentrations of radionuclides are also constrained by **solubility limitation**; the solubility limits of each element in the cementitious region are input as parameters. Concentrations of all isotopes of the same element, including stable isotopes, are taken into account when evaluating whether the solubility limit has been reached. Solids, including colloids, are precipitated or re-dissolved at rates that maintain aqueous concentrations at or below the solubility limits, and are assumed to be contained within the cementitious region.

⁴⁸ In fact, in the present assessment, the containment period is determined by the prolonged resaturation time, more than by the physical containment period provided by steel drums and emplacement containers.

A1.5.2.4 Interface with the host rock

Radionuclides can migrate by aqueous diffusion into a clay buffer, if one is present. Otherwise, radionuclides migrate directly into the host rock at a rate determined by their aqueous concentration in the cementitious region and the **effective flow rate** at the interface with the host rock (see Appendix 3).

A1.5.3 Mathematical representation

Mathematically, the only difference between STALLION and SPENT is in the release of radionuclides to the buffer. For the rest of the system refer to Appendix 1.3.3.

A1.5.3.1 Cementitious region

Following the containment period, some radionuclides are instantly released to the cementitious region and release from the slow-release fraction begins. At the same time losses from the cementitious region to the buffer also begin. The radionuclide amounts in the cementitious region, denoted M^n are governed by

$$\frac{dM^n}{dt} = -\lambda^n M^n + \lambda^{n-1} M^{n-1} + \mu_s N_s^n - B^n, \quad (\text{A1.5-1})$$

where

μ_s [a^{-1}] is the slow-release rate and B^n [mol a^{-1}] is the rate at which radionuclides are lost from the reservoir to the buffer. All the terms are the same as those that appear in equation (A1.3-3) except for the slow-release term that replaces the cladding and matrix terms. The instantly released fraction provides the initial value for the amount at the end of the containment period.

This equation applies for times after the containment period. The decayed inventory is governed by the decay and ingrowth equation, both for the instantly released part, N_I and the slow release part, N_S .

$$\frac{dN_I^n}{dt} = -\lambda^n N_I^n + \lambda^{n-1} N_I^{n-1} \quad t < t_C, \quad (\text{A1.5-2})$$

$$\frac{dN_S^n}{dt} = -\lambda^n N_S^n + \lambda^{n-1} N_S^{n-1} - \mu_s N_S^n. \quad (\text{A1.5-3})$$

Here, the slow-release inventory is the remaining amount in the waste form. The slow-release rate μ_s is an input parameter. It given the constant release rate relative to the inventory at any particular time. With this model, the slow release continues indefinitely with an exponentially decreasing release to the cementitious region.

The buffer diffusion is driven by the aqueous concentration within the cementitious region, which is constrained by sorption and solubility.

Two cases must be considered, depending on whether the total over all isotopes exceeds a solubility limiting value or not.

Let m^e be the total mass summed over isotopes of element e (one of which is radionuclide n). Then, the aqueous concentration is given by

$$C_{CR}^n = M^n / \varepsilon_{CR} R_{CR}^e V_{CR} \quad \text{if } m^e \leq \varepsilon_{CR} R_{CR}^e V_{CR} C_{sol}^e, \quad (\text{A1.5-4a})$$

$$C^n = \frac{M^n}{m^e} C_{sol}^e \quad \text{if } m^e > \varepsilon_{CR} R_{CR}^e V_{CR} C_{sol}^e. \quad (\text{A1.5-4b})$$

Here, V_R [m³] is the volume of the cementitious region, ε_{CR} [-] is the porosity, R_{CR}^e [-] is the retention factor and C_{sol}^e [mol m⁻³] is the solubility limit for element e .

The retention factor is calculated from

$$R_{CR}^e = 1 + \frac{(1 - \varepsilon_{CR}) \rho_{CR} K_{d,CR}^e}{\varepsilon_{CR}}, \quad (\text{A1.5-5})$$

with ρ_{CR} the solid density of the cement (mass per volume of solid in the region), and $K_{d,CR}^e$ the cement sorption coefficient. Note that the model does not include porosity scaling factors since the cement is assumed to be an open structure in which anion exclusion is not important.

A1.5.4 Input parameters

The input parameters required to specify a STALLION calculation can be split into categories:

- Radionuclides and decays;
- Inventory data;
- Physical data for the cement and containers;
- Chemical data for the cement;
- Physical data for the buffer, including the outer boundary condition;
- Chemical data for the buffer.

Of these, only the physical and chemical properties of the cement and containers are specific to STALLION, the others applying to all STMAN codes. Only these specific inputs are presented here, the others are presented in the section on SPENT, Tabs. A1.3-2 and A1.3-4.

In addition, output specifications are needed and control parameters may be modified. These do not form part of the input data listed here, but will be commented on in the description of the individual cases.

The units of inputs to STMAN used are fixed within the code and are quoted here.

Tab. A1.5-3: STALLION input data requirements for the cement and container

Input	Units	Requirements
<i>Slow Release Properties</i>		
Fraction of the inventory or each radionuclide that is subject to slow release	dimensionless	
Slow release rate, μ_S	a ⁻¹	Time-independent congruent rate.
<i>Container Properties</i>		
Containment time	a	
Number of containers	dimensionless	This is used to scale the relevant outputs. May be set to one if, as in the present study, the whole cementitious region is treated as a single container.
Length	m	Of the region treated as a single container. Note that the volume of the region is calculated by taking the radius to be equal to the inner buffer radius.
<i>Cementitious Region Properties</i>		
Porosity, ϵ_{CR}	dimensionless	
Density	kg m ⁻³	Either solid density, ρ_{CR} , or bulk dry density, ρ_{CR}^{dry} , may be specified for the cement.
Sorption coefficient, $K_{d,CR}^e$	m ³ kg ⁻¹	Equilibrium sorption coefficients, for each element, for the cement.
Solubility limits, C_{sol}^e	mol l ⁻¹	For each element in the reservoir. Note that the units are molar.

A1.5.5 Verification

Verification of the STMAN suite of codes has been carried out at two levels. Firstly, full scale comparisons of the results calculated using STMAN have been compared with other codes and analytic solutions. Secondly, detailed confirmation of the behaviour of new capabilities has been carried out as the code has developed.

Moreover, the codes were completely rewritten in 1999, the earlier versions being written in Fortran and the later (and current) versions being written in C++. Because there is no common code between the versions, the successful cross-comparison between them at that time provides strong confirmation of their correct functioning. The new versions have more accurate discretisation than the older ones, so the results were not identical; a range of discretisations was tested to confirm that this was the cause of any differences.

The STMAN codes differ only in their treatment of the waste and associated processes. The major part of the codes, involved in transport through the buffer and interfacing to the host rock, is common. Verification of any of the codes is, in this regard, verification of all of them. In the case of a strongly solubility limited radionuclide, which maintains a constant concentration in the waste form, all of the codes will produce the same release profiles, since the waste-form

aspects are irrelevant. The verification tests presented in the SPENT description can thus be regarded as verifying most of the STALLION code.

Verification cases for the original version of STALLION involved comparison with analytic cases for single solubility-limited radionuclides and internal cross-checks for chain cases. In addition, some comparisons were made using a general-purpose differential equation code, SPADE.

The key difference between STALLION and SPENT is in the waste model. The STALLION model is a uniformly mixed model, and simple hand checks can therefore be carried out on the concentrations, sorbed and precipitated amounts. Some radionuclides can have a slow-release fraction. A specific test case for two example radionuclides, ^{14}C and ^{36}Cl , was set up to test this case, in conjunction with a thin buffer giving rapid release to the geosphere.

With a release rate of 10^{-4} a^{-1} , the remaining unreleased inventory at 1 000, 10 000 and 50 000 a was compared to the analytic result. Tab. A1.5-4 shows that good agreement was obtained.

Tab. A1.5-4: Results of a verification test for slow release with STALLION

Time [a]	Unreleased inventory of ^{14}C [mol]		Unreleased inventory of ^{36}Cl [mol]	
	STALLION	Analytic	STALLION	Analytic
1 000	6.07350×10^{-3}	6.07350×10^{-3}	4.55911×10^{-4}	4.55911×10^{-4}
10 000	8.30920×10^{-4}	8.31289×10^{-4}	1.81539×10^{-4}	1.81545×10^{-4}
50 000	1.20723×10^{-7}	1.20543×10^{-7}	3.03185×10^{-6}	3.03158×10^{-6}

Verification of new capabilities of the STMAN suite of codes has been undertaken with each new release. This has generally involved hand calculations to confirm the correct behaviour. In the case of the split-buffer capability, a comparison test was run against the AMBER compartmental modelling tool. This used a single, hypothetical radionuclide that was solubility limited throughout. The outer part of the buffer had higher porosity and diffusion coefficient.

Fig. A1.5-1 shows a direct comparison. In this case, the AMBER compartment model was tuned to match the numerical discretisation used in STALLION. The resulting agreement is excellent (4 significant figures except at very early times when the release is tiny).

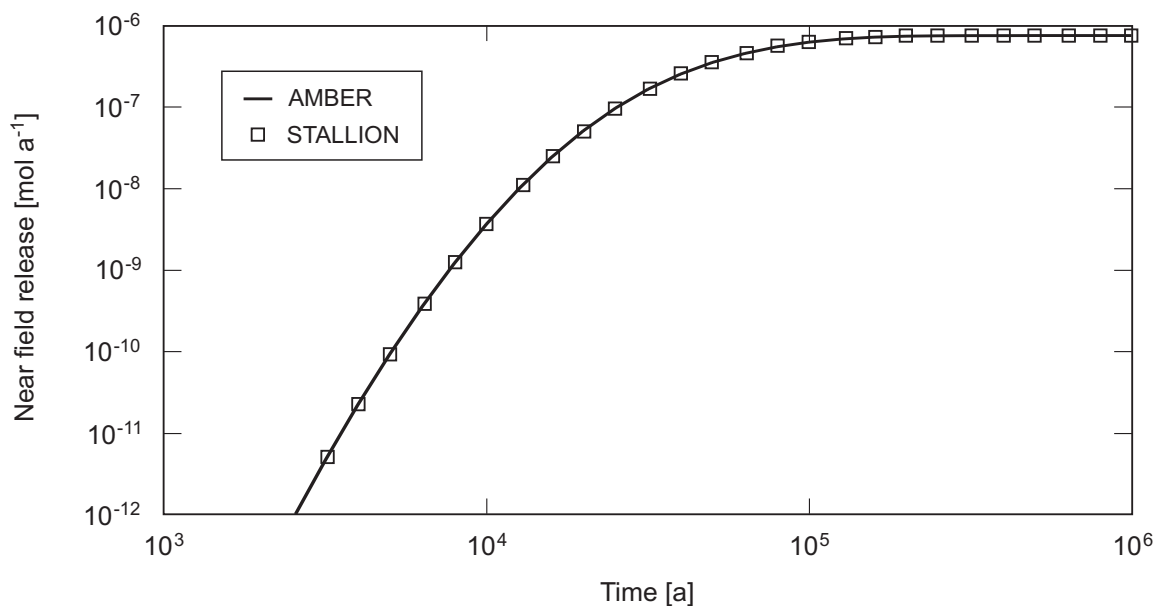


Fig. A1.5-1: Comparison of STALLION and AMBER buffer release rates in a code comparison verification test

A1.6 PICNIC

A1.6.1 Scope and purpose

PICNIC is a computer code that models transport of dissolved radionuclides through the geosphere. PICNIC allows the geosphere to be modelled as a network of one-dimensional transport paths (called legs in PICNIC), which may represent porous media or discrete features like fractures, cracks, or channels. PICNIC can also represent a single one-dimensional geosphere transport path; this is the primary use to which it has been put in assessment calculations for Project *Entsorgungsnachweis*.

Two main aspects distinguish PICNIC from other codes. These are relevant mainly to its use in modelling transport through fractured media.

- (i) The transport paths may be in contact with so-called matrix zones of variable geometry and heterogeneous properties that contain stagnant pore water.
- (ii) Different types of transport paths in contact with rock matrix can be combined in series or in parallel to mimic a network of fractures with heterogeneous properties with respect to flow, matrix diffusion, and sorption.

Thus, PICNIC has the capability to describe transport influenced by heterogeneities of the geosphere at two different scales. These are the local scale, where matrix diffusion is an important feature, and the larger scale, where the network of transport paths between sources and the output location may significantly influence the breakthrough of solutes.

In the context of this study, PICNIC has been used to model situations in which diffusion along transport paths is a key phenomenon. When PICNIC is used in such cases, the assumptions that

are made about coupling between legs in a network would be invalid if two diffusion-dominated legs were connected together. Thus, the diffusion-dominated path through the Opalinus Clay has to be treated as a single leg.

A1.6.2 Phenomena included in PICNIC

A1.6.2.1 Overview

An overview of the representation of Super-FEPs in the various safety assessment computer codes is given in Section A1.2.3 (Tab. A1.2-2). Tab. A1.6-1 describes in more detail how PICNIC represents the different Super-FEPs that fall into its model domain, namely the (i), the access tunnels / ramp / shaft and their associated excavation disturbed zones, (ii), the undisturbed Opalinus Clay and (iii), the confining units and regional aquifers. The symbols used in Tab. A1.6-1 are explained in Section A1.2.3. The following model features are considered separately.

1. Phenomena in a single leg; and
2. Network structure and properties.

Some safety-relevant aspects of the Super-FEPs (indicated by large bold ticks in Tab. A1.6-1) are either modelled explicitly by PICNIC, or their magnitude, timing, rate, spatial extent and performance directly determine one or more input parameters. These aspects or phenomena are summarised in Tab. A1.6-2 and discussed in more detail in the following sections, where they are highlighted in bold. The table also notes radioactive decay and ingrowth as included phenomena. Shaded boxes are used since these phenomena are not directly related to the Super-FEPs. A range of other phenomena can also be included if required by appropriate parameter selection (e.g. the effects on transport of radionuclide-bearing colloids and high-pH solutes), although this has not been necessary in the present assessment.

The transport resistance of the seals and the surrounding rock (indicated by a smaller tick in Tab. A1.6-1) is not represented explicitly by PICNIC, but can be taken into account in evaluating flow along the repository tunnels / shafts / seals.

The possibility of time dependent system properties associated with some Super-FEPs cannot be directly represented by the code (as indicated by the symbol \circ in Tab. A1.6-1). Parameter sets can, however, be chosen that represent steady-state system properties corresponding, for example, to the end-state of the system once the process is complete or one of a number of possible transient states, as explained in the discussions of individual conceptualisations in Chapters 3 to 8.

Gas-related phenomena and processes giving rise to transient groundwater flow (indicated by the symbol \blacktriangleright) require the use of an alternative code if they are to be modelled. Where no alternative qualified code exists for a phenomenon, this is indicated using the symbol \bullet .

A PICNIC model is built up from single legs, and the phenomena that can be represented in each leg are described first. In some cases a model may consist of a single leg only (e.g. in cases where only transport through the Opalinus Clay is of concern). In any case, each leg has boundary conditions, linking it to other legs and to the external situation (typically to the near field and to the biosphere). The PICNIC network capability allows large-scale heterogeneity to be represented (at least in advection-dominated systems), either within a single medium or as a representation of transport through a collection of different media. It also allows transport paths

to be considered, for example, though the repository access tunnels / ramp / shaft as well as through the Opalinus Clay.

PICNIC has no built-in list of radionuclides or decays and all properties are specified in an input file. Output can be obtained at junctions or in legs.

Tab. A1.6-1: Super-FEPs, their safety-relevant aspects (as taken from Tab. A5.2.1 of Nagra 2002d) and the ways in which they are represented by the code PICNIC

Symbols: see Section A1.2.3

Super-FEPs	Safety-relevant aspects to be represented by models	Model features		Explanatory comments
		Phenomena in a single leg	Network structure and properties	
Tunnels / ramp / shaft and seals				
Low groundwater flow rate along the sealed tunnels / ramp / shaft, and through the surrounding excavation disturbed zones (EDZs)	Transport paths provided by the tunnels / ramp / shaft		✓	The situation of negligible flow through the tunnels / ramp / shaft can be modelled by using a single leg to represent transport through the intact Opalinus Clay only. Uncertainties (e.g. due to reduced performance of seals) can be handled by choosing an appropriate network of legs to represent transport paths through the tunnel / ramp / shaft / host rock, and selecting appropriate parameters for the transport/retention properties of backfilled tunnels / ramp / shaft/ host rock, as well as flow.
	Stationary flow	✓		Darcy velocity provided as input parameter.
	Transient flow	○		Transient flow cannot be modelled using PICNIC, but the effects can be bounded by assuming an increased steady-state flow field.
	Advection / dispersion	✓		Modelled explicitly.
	Aqueous diffusion	✓		Modelled explicitly.
The seals and the surrounding rock	Transport resistance of the seals and the surrounding rock	✓		The performance (effectiveness and longevity) of the seals affects the groundwater flow rate along the sealed tunnels / ramp / shaft/ host rock, and through the surrounding excavation disturbed zones (EDZs) (see above).

Tab. A1.6-1: (Cont.)

Super-FEPs	Safety-relevant aspects to be represented by models	Model features		Explanatory comments
		Phenomena in a single leg	Network structure and properties	
Opalinus Clay and confining units				
Low groundwater flow rate through undisturbed Opalinus Clay	Stationary flow	✓		Darcy velocity provided as input parameter.
	Transient flow	▶ or ○		Transient flow cannot be modelled using PICNIC, but the effects can be bounded by assuming an increased steady-state flow field. Explicit representation of transient flow in the Opalinus Clay requires the use of FRAC3DVS.
	Advection / dispersion	✓		Modelled explicitly.
	Aqueous diffusion	✓		Modelled explicitly.
	Long-term changes (e.g. due to erosion of overburden)	●		Long-term changes in physical and chemical properties of the transport paths are not modelled using PICNIC, but significant effects of, for example, uplift and erosion are ruled out within the one million year period of primary interest in the safety assessment.
Length of vertical transport path from emplacement tunnels to overlying and underlying formations	Transport paths provided by the Opalinus Clay and confining units		✓	The situation of homogeneous Opalinus Clay can be modelled by using a single leg, with advective / dispersive / diffusive transport only.
Geochemical immobilisation and retardation in the Opalinus Clay and confining units	Linear, equilibrium sorption	✓		Sorption constants input as parameter values.
	Immobilisation processes	●		Irreversible immobilisation processes not modelled, but omission is conservative.
Homogeneity	Transport paths provided by transmissive discontinuities, faults and repository-induced fractures in the clay		✓	The situation of a transmissive feature affecting a part of the near-field release can be modelled by introducing a second leg, with advective / dispersive / diffusive transport along the feature, and matrix diffusion into the adjoining undisturbed rock.
Migration of high-pH plume from ILW backfill into Opalinus Clay	The depth of migration, and associated physical and chemical changes in the clay	○		The migration of high-pH plume from ILW backfill into Opalinus Clay must be evaluated separately. Transport properties appropriate to Opalinus Clay affected by such a plume could be input, if required, as a parameter values for all or part of the Opalinus Clay.
Radionuclide transport through the confining units and regional aquifers	Transport paths provided by the confining units and regional aquifers		✓	Radionuclide transport through the confining units and regional aquifers can either be conservatively neglected, or modelled by choosing an appropriate network of legs to represent transport paths through these features.

Tab. A1.6-1: (Cont.)

Super-FEPs	Safety-relevant aspects to be represented by models	Model features		Explanatory comments
		Phenomena in a single leg	Network structure and properties	
The barrier system (general)				
The migration of repository induced gas	Gas dissolution and diffusion in the Opalinus Clay (incl. tunnel EDZs)	▶	▶	No transport of radionuclides in volatile form considered (see Gas Model).
	Capillary leakage in the Opalinus Clay	▶	▶	See above.
	Pathway dilation in the Opalinus Clay	▶	▶	See above.
	Porewater displacement in the Wedelsandstein	▶	▶	See above.
	Gas dissolution and diffusion in the low-permeability upper confining units	▶	▶	See above.
	Capillary leakage through low-permeability upper confining units	▶	▶	See above.
Future human actions	Abandonment of repository before backfilling / sealing	○	○	The nature and timing of future human actions cannot be evaluated using PICNIC. The consequences of hypothetical actions that may influence the repository system can, however, be bounded in some cases (e.g. the possibility of the repository being abandoned before it is backfilled and sealed can be modelled by choosing an appropriate network of legs to represent transport paths through the tunnel / ramp / shaft/ host rock, and selecting appropriate parameters for the transport/retention properties of backfilled tunnels / ramp / shaft/ host rock, as well as flow).

Tab. A1.6-2: Phenomena explicitly included in the PICNIC model

Model features	Phenomena explicitly included in the PICNIC model
All	Radionuclide decay and ingrowth
Phenomena in a single leg: retardation processes	Stationary flow
	Advection / dispersion
	Aqueous diffusion (incl. matrix diffusion where the leg represents a fractured medium)
	Linear equilibrium sorption
Network structure and properties	Transport paths provided by: <ul style="list-style-type: none"> - the tunnels / ramp / shaft; - the Opalinus Clay and confining units; - by transmissive discontinuities, faults and repository-induced fractures in the clay; - the confining units and regional aquifers; as required by the assessment case under consideration

A1.6.2.2 Phenomena in a single leg

In the code, all parameters of a leg are considered time and space invariant. The porosity structure of a leg is specified in general terms to allow both homogeneous and fractured situations to be modelled. Fig. A1.6-1 shows a cross section of a leg with the various aspects indicated. Note that in the present study the Opalinus Clay is represented by the central section (the transport path) alone.

Within each leg, PICNIC considers the following transport and interaction mechanisms:

- **Advection / dispersion / diffusion**, with **matrix diffusion** normal to the flow direction if the leg represents a fractured medium;
- retardation by **linear equilibrium sorption** on infill material, in the adjacent matrix, and at the interface between these; and
- **Ingrowth and decay** of radionuclides (decay chains).

Advective transport is governed by water flow through the leg. PICNIC can calculate a flow rate from given hydraulic properties and boundary conditions, or can accept an imposed flow rate.

Dispersion is specified through a Peclet number, enabling a dispersion coefficient to be derived from the flow velocity and path length. Diffusion in the transport path and in the matrix zones may be specified as a radionuclide-independent pore diffusion coefficient or as a radionuclide-dependent effective diffusion coefficient. Dispersion and diffusion are driven by aqueous concentration gradients along the transport path or in the buffer.

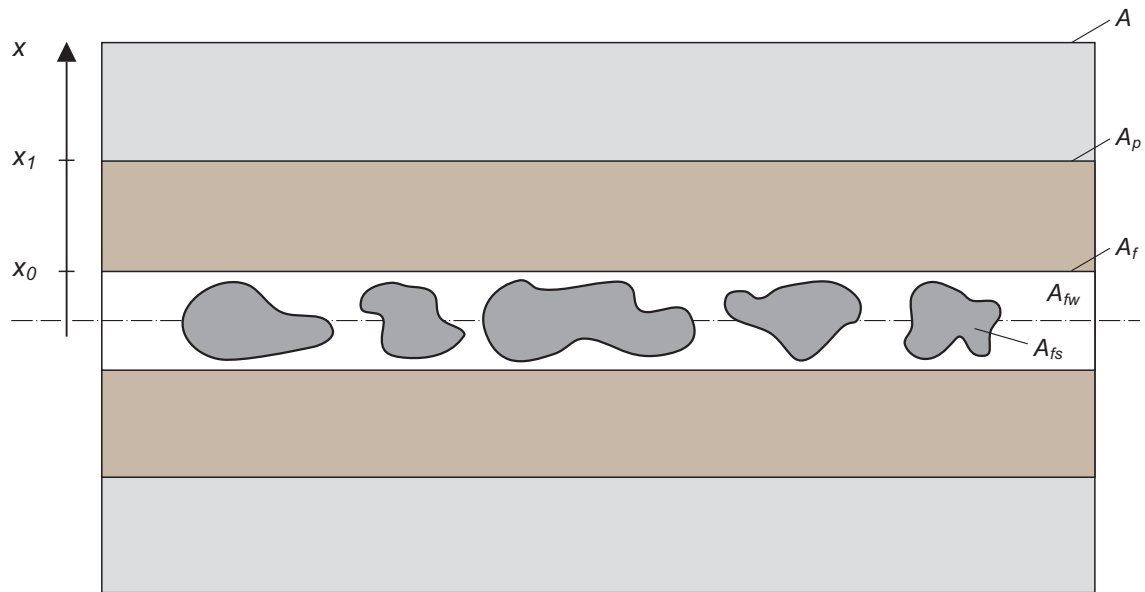


Fig. A1.6-1: Areas defining the properties of a PICNIC leg

Sorption on infill and matrix pore surfaces and (if required) on the boundary surfaces of the transport path is represented as an instantaneous, reversible process, with the amount sorbed on pore surfaces proportional to aqueous concentration. The constants of proportionality are the element-specific sorption coefficients K_d and K_a for sorption on pore surfaces and on the boundary surfaces of the transport path, respectively. The quantification of retardation due to sorption on pore surfaces also requires the grain density of the buffer to be specified.

Throughout the modelled region, radionuclide decay and ingrowth are modelled, including allowance for branching and rejoining chains. The decay properties apply to all legs and associated matrix regions.

Matrix diffusion can be modelled with a variety of geometries. Within this study, only the simple planar geometry has been used. This allows radionuclides to diffuse away from the transport paths into stagnant matrix pores up to some specified distance.

In order to allow anion exclusion effects to be modelled, radionuclide-specific porosity scaling factors can be applied to the infill and matrix porosities.

Each leg has a boundary condition at each end. These are referred to as the "upstream" and "downstream" boundaries, even though, in the present study, flow is often assumed to be very slow.

At the upstream end, the total flux of radionuclides entering the leg is controlled. For a single leg (or a leg in a network linked to a source), this flux represents the material entering the model from outside and would generally represent material leaving the near field. The time-dependent flux is either specified in an input file, or may be set using simple functions (such as a top hat).

At the downstream end, PICNIC offers a choice of boundary conditions. These are appropriate for different situations. The default condition is to treat the leg as being semi-infinite (this is possible because PICNIC uses analytic solutions for the spatial aspects of transport in a leg).

This boundary condition is appropriate when there is no significant change in material properties at the end of the leg. In advection-dominated cases, it gives very similar behaviour to the alternative zero-gradient condition.

For diffusion-dominated situations, the zero-concentration condition is appropriate when the leg discharges into a material with more rapid transport (e.g. an aquifer).

PICNIC cannot accurately handle situations where one diffusion-dominated leg discharges into another (except by combining them into one), because it does not allow any mass to be transported from the upstream end of one leg to the downstream end of its predecessor. In this study, no such cases have been required. The case where a diffusion-dominated leg discharges to a fast flowing leg (for example an aquifer), on the other hand, can be handled.

Every leg discharges its total flux at the downstream end.

A1.6.2.3 Network structure and properties

PICNIC networks can be used to represent **transport paths** through a heterogeneous geosphere, and also the repository tunnels / ramp / shaft and seals. The user defines the geometrical arrangement (structure) of legs. For advection-dominated situations, the structure may be based on a water flow model. Coupling between different legs is done by considering continuity of water flux and continuity of solute flux at the junctions between legs, assuming that downstream legs do not affect concentrations of upstream legs, and that solutes are distributed at junctions according to the water flows of outgoing legs. Where a source is linked to several legs, the user may override the distribution according to water flows – this is important for cases where one or more of the legs are diffusion dominated.

In this study, limited use has been made of the network capabilities of PICNIC. Where it has been used, it has represented distinct transport paths, provided for example by the repository tunnels and shafts and their associated disturbed zones, rather than large-scale heterogeneity of the geosphere itself.

A1.6.3 Mathematical representation

This section presents the governing equations of the model encoded in PICNIC (Barten & Robinson 2001). The basic equations are formulated for a single leg. A network may then be constructed from joining weighted solutions for single legs with appropriate boundary conditions. This is possible since it is assumed that downstream legs do not influence upstream legs.

A1.6.3.1 Leg areas and porosities

The parameters for specifying the geometric properties of a leg allow for both fractured and homogeneous media to be represented.

In the case of fracture transport, the total cross section of a single leg, A [m^2], encloses the actual fracture area, A_f , the area of the adjacent rock matrix that is accessible through diffusion, A_p , and inaccessible matrix area, A_s (see Fig. A1.6-1). The fracture may contain porous infill material. Thus, the fracture area A_f can be split up into the area of the flowing water, A_{fw} , and the area of solid infill, A_{fs} . The accessible matrix area A_p is composed of the area with stagnant water, A_{pw} , and the area with solids, A_{ps} . It is important to distinguish between the following porosities:

$$\text{flow porosity } \varepsilon_f = \frac{A_{fw}}{A}, \quad (\text{A1.6-1})$$

$$\text{fracture porosity } \varepsilon_i = \frac{A_{fw}}{A_f}, \quad (\text{A1.6-2})$$

$$\text{matrix porosity } \varepsilon_p = \frac{A_{pw}}{A_p}. \quad (\text{A1.6-3})$$

In the homogeneous case, the situation is simpler. The total area, A , and the area of the transport path, A_f , are the same. Thus the flow porosity⁴⁹ and infill porosity are also the same. There is no matrix.

A1.6.3.2 Transport equations in a single leg

In the following, we will present equations for a single radionuclide – the general case for a decay chain is obtained by linking several such equations together. The governing equation for transport in the water flowing in the fracture in the z -direction is

$$\varepsilon_f^n R_f^n \frac{\partial C_f^n}{\partial t} = D_f^n \frac{\partial^2 C_f^n}{\partial z^2} - v_D \frac{\partial C_f^n}{\partial z} - \lambda^n \varepsilon_f^n R_f^n C_f^n + \lambda^{n-1} \varepsilon_f^{n-1} R_f^{n-1} C_f^{n-1} - \varepsilon_f^n \delta_f j_m^n, \quad (\text{A1.6-4})$$

where C_f^n [mol m⁻³] is the concentration of the radionuclide n in the flowing water, R_f^n [-] the retardation factor in the fracture or transport path, $D_f^n = v_D L / Pe + D_{eff}^n$ the summed dispersion and effective diffusion coefficient [m² a⁻¹], ε_f^n [-] is the flow porosity which can be radionuclide-specific (e.g. to account for ion exclusion), v_D [m a⁻¹] the Darcy velocity, λ^n [a⁻¹] the decay constant, δ_f [m⁻¹] the surface area of matrix per unit volume of flowing water, and j_m^n [mol m⁻² a⁻¹] the solute flux of radionuclide n from the transport path to the adjacent matrix per unit area of the matrix interface (zero in the case of a homogeneous medium). Note that R_f^n , ε_f^n , D_f^n and λ^n are specific for each radionuclide. The effective diffusion coefficient is either specified directly or calculated from the pore-water coefficient as $D_{eff}^n = \varepsilon_f^n D_{pore}$. The term $\lambda^{n-1} R_f^{n-1} C_f^{n-1}$ represents radioactive ingrowth. The superscript $n-1$ indicates the parent radionuclide (it is assumed here that there is a single parent; there may be none, in which case the term is omitted, or more than one, in which case there are several ingrowth terms).

The retardation factor is defined in a slightly different way than usual to facilitate input, namely as the sum of a base retardation coefficient, $R_{0,f}^n$, and terms depending on sorption coefficients for the transport path boundaries (fracture walls) and for the infill material:

⁴⁹ The term flow porosity is retained, even though flow may be slow and transport may be diffusion dominated.

$$R_f^n = R_{0,f}^n + \frac{(1-\varepsilon_i)}{\varepsilon_i^n} \rho_f K_{d,f}^n + \delta_f (1-\varepsilon_p) K_{a,f}^n. \quad (\text{A1.6-5})$$

In the above equation, ρ_f is the solid density of the infill, $K_{d,f}^n$ the mass-based infill sorption coefficient, $K_{a,f}^n$ [m^3/kg] the surface-based sorption coefficient at the fracture-matrix interface, and ε_i [-] and ε_p [-] are the fracture and matrix porosities as defined above. In the case of a fractured medium, if the fracture contains no infill, $\varepsilon_i = 1$. Recall that for a homogeneous leg references to infill should be thought of as referring to the entire porous medium, $\varepsilon_i = \varepsilon_f$ and $\delta_f = 0$.

In the above equations some of the porosities are denoted as being radionuclide specific. These are calculated from the basic value times a porosity scaling factor, allowing anion exclusion to be modelled. It is also possible to specify dry bulk densities directly rather than specifying solid densities, $\rho^{dry} = (1-\varepsilon)\rho^{solid}$.

The flux from transport path to matrix, j_m^n , depends on structure and properties of the matrix. Specific forms can be calculated from the matrix diffusion equations presented in the following subsection.

Initially, the leg is assumed to contain no radionuclides. The solute fluxes in the flow network are coupled through response functions for the individual legs. The corresponding boundary condition at the inlet of the leg may be stated as:

$$A \left(v_D C_f^n - D_f^n \frac{\partial C_f^n}{\partial z} \right)_{z=0} = \gamma_i I^n(t). \quad (\text{A1.6-6})$$

Here, γ_i [-] is the fraction of water flow entering leg i , and $I^n(t)$ is the mass flux of radionuclide n entering the upstream boundary of leg i . At the outlet of the leg, one of the following conditions may be chosen:

$$C_f^n \rightarrow 0 \quad \text{as} \quad z \rightarrow \infty \quad (\text{semi-infinite}), \quad (\text{A1.6-7a})$$

$$\left. \frac{\partial C_f^n}{\partial z} \right|_{z=L} = 0 \quad (\text{zero gradient}), \quad \text{or} \quad (\text{A1.6-7b})$$

$$C_f^n(L, t) = 0 \quad (\text{zero concentration}). \quad (\text{A1.6-7c})$$

A1.6.3.3 Rock matrix transport equations

PICNIC can treat various degrees of matrix heterogeneity for fractured media (“matrix geometries”), but in this study the only one that has been used is the one-dimensional planar form, which is homogeneous out to some specified distance from the two surfaces of the fracture.

The equation for matrix diffusion for planar geometry is

$$\varepsilon_p^n R_p^n \frac{\partial C_p^n}{\partial t} = D_p^n \frac{\partial^2 C_p^n}{\partial x^2} - \lambda^n \varepsilon_p^n R_p^n C_p^n + \lambda^{n-1} \varepsilon_p^{n-1} R_p^{n-1} C_p^{n-1}. \quad (\text{A1.6-8})$$

In the above equation, C_p^n is the radionuclide concentration in the pores of the matrix, ε_p^n [-] is the a radionuclide-specific matrix porosity (equal to the physical porosity, ε_p , times a radionuclide-specific factor), D_p^n [$\text{m}^2 \text{a}^{-1}$] the effective diffusion coefficient in the matrix region, and x the spatial co-ordinate along which diffusion takes place (normal to the fracture plane). The matrix retardation factor R_p^n is defined as

$$R_p^n = R_{0,p}^n + \frac{(1 - \varepsilon_p)}{\varepsilon_p^n} \rho_p K_{d,p}^n, \quad (\text{A1.6-9})$$

with ρ_p [kg/m^3] the solid density of matrix (mass per volume of solid matrix in the accessible region), and $K_{d,p}^n$ [m^3/kg] the matrix sorption coefficient, and ε_p the matrix porosity as defined above.

It is assumed that the matrix region is initially free of radionuclides. The boundary conditions at the interface between fracture and matrix ($x=0$) and at the outer boundary of the accessible region ($x=d$) are:

$$C_p^n(0, z, t) = C_f^n(z, t), \quad (\text{A1.6-10})$$

$$\left. \frac{\partial C_p^n}{\partial x} \right|_{x=d} = 0. \quad (\text{A1.6-11})$$

The solute flux j_m^n from fracture to matrix per unit area of matrix interface, which couples the transport in the matrix with transport in the fracture, is

$$j_m^n = -D_p^n \left. \frac{\partial C_p^n}{\partial x} \right|_{x=0}. \quad (\text{A1.6-12})$$

A1.6.3.4 Coupling of solute flux at junctions through response functions

Solutions for the leg or matrix equations can be obtained in the form of so-called input response (or transfer) functions. They represent the solution obtained in case of a delta-input function. For transport in a leg, the input response function may be interpreted as a travel time distribution function. A convolution of the input response function with the input function of interest gives the required output function in terms of solute flux. For transport in a network the corresponding equations are as defined in the next paragraph.

If we denote the upstream junction for leg i as j , the mass flux $I_i^n(t)$ of radionuclide n leaving the leg i and entering the downstream junction can be written as

$$I_i^n(t) = \sum_{m=1}^n \gamma_i \int_0^t P_i^{nm}(\tau) I_j^m(t-\tau) d\tau \quad (\text{A1.6-13})$$

where γ_i is the proportion of water flow from upstream junction j entering leg i , P_i^{nm} is the response function matrix for leg i , that is the output at the downstream junction of radionuclide n for a delta-function input of radionuclide m at the upstream junction, and $I_j^m(t)$ is the specific input of radionuclide m at the upstream junction j . The sum over radionuclides appears because of decay. Note that P_i^{nm} is only non-zero for $n \geq m$, since daughter radionuclides do not affect their parent's flux. The weight γ_i is determined from the values of the Darcy velocities v_D and the areas F of all legs leaving the upstream junction. For source junctions, we have

$$I_o^n(t) = S(t), \quad (\text{A1.6-14})$$

where $S(t)$ is the time-dependent source term for radionuclide n . Note that γ_i can be specified directly by the user in the case of a source entering several legs.

A1.6.3.5 Methods of solution

In general, the transport equations are Laplace transformed, solved in Laplace space, and then inverted back numerically using the Talbot algorithm. The convolutions become simple products in the transformed equations. A slightly different approach has to be used in case of time dependent source functions, when the response function of the whole network is calculated and the convolution is performed in the time-domain.

A1.6.4 Input parameters

The input parameters required to specify a PICNIC calculation can be split into categories (Tab. A1.6-3):

- Radionuclides and decays;
- Network structure;
- Leg data:
 - Basic data;
 - Properties of transport path;
 - Properties of matrix;
- Network flow data;
- Source information.

In addition, output specifications are needed and control parameters may be modified. These do not form part of the input data listed here, but will be commented on in the description of the individual cases.

The units of inputs to PICNIC need only be self-consistent. Here, however, specific units used in this study are quoted.

Tab. A1.6-3: PICNIC input data requirements

Input	Units	Requirements
Radionuclides and Decays		
Radionuclides and decays to be used.	Half lives are specified in years.	Table of parent, daughter and half-life. Where a parent has more than one daughter, the half-life for each decay is the total half-life of the parent divided by the fraction decaying to the particular daughter.
Network Structure (only needed when there is more than one leg)		
List of junction names. Inlet and outlet junctions for each leg.	N/A	The leg and junction names are use to reference the relevant data in later sections.
Leg Data – Basic Data (for each leg, identified by name if more than one)		
Length	m	Transport distance from inlet to outlet.
Cross sectional area	m ²	Total area for the leg, A .
Darcy velocity, v_D	m a ⁻¹	Darcy velocity, v_D , equal to the total flow through the leg divided by the area. May be omitted if flows are calculated.
Hydraulic conductivity	m a ⁻¹	Not required if Darcy velocity given. Hydraulic conductivity and heads must be specified for all legs if flows are calculated.
Peclet number	dimensionless	Peclet number, Pe , characterising hydrodynamic dispersion in the leg. A default value of 10 can be used.
Diffusion	m ² a ⁻¹	Either the pore diffusion coefficient (D_{pore}) or effective diffusion coefficients (D_{eff}) for each radionuclide are required. The default value is zero. If the pore diffusion value is specified, then the effective diffusion is calculated as $D_{eff}^n = \epsilon_f^n D_{pore}$, where the porosity is scaled by the radionuclide-specific porosity factor (see below).
Leg Data – Properties of Transport Path (for each leg, identified by name if more than one)		
Retardation factor, R_p^n	dimensionless	May be specified directly for each radionuclide, or calculated from the other parameters.
Density, ρ_p	kg m ⁻³	Either solid density, ρ_f , or bulk dry density, ρ_f^{dry} , may be specified for the infill material (or for the bulk porous medium for the homogeneous case).
Flow porosity	dimensionless	Porosity, ϵ_f , for the flowing pores of the leg. This is the total flowing porosity of the medium. For a porous medium this will equal the infill porosity. For a fracture system it is equal to the infill porosity multiplied by the fraction of the system that is in a fracture. See section A1.6.3.1.
Infill porosity	dimensionless	Porosity, ϵ_i , for infill in the part of the leg where there is flow. For a porous medium, this is equal to ϵ_f , the total flowing porosity of the medium. For a fracture system it is the porosity of material within the fractures.
Porosity factors	dimensionless	Factor to scale porosity for some radionuclides. Default is 1, so only needed for radionuclides that are affected. The factors are less than one and represent constraints on the accessible porosity for some radionuclides (e.g. due to anion exclusion). The factors scale both the infill and flow porosity. The scaled porosities are denoted by ϵ_i^n and ϵ_f^n respectively.

Input	Units	Requirements
Sorption coefficient,	$\text{m}^3 \text{kg}^{-1}$	Equilibrium sorption coefficients, for each radionuclide, for the fracture infill material or bulk porous medium.
Leg Data – Properties of Matrix (for each leg with an associated rock matrix, identified by name if more than one). The following assumes a planar matrix, which is homogeneous out to some specified distance.		
Specific surface area	$\text{m}^2 \text{m}^{-3}$	The surface area of the matrix per unit volume of flowing water. Denoted as δ_f . May be set to zero for the homogeneous case.
Maximum penetration depth	m	The maximum distance from a fracture surface that radionuclides can penetrate into the matrix. This will be constrained by geometric considerations (fracture separation) but also by properties of the rock which might indicate that a smaller distance is appropriate.
Surface sorption coefficient	$\text{m}^3 \text{m}^{-2}$	Surface equilibrium sorption coefficient, for each radionuclide, used in determining the total retardation in the fracture. Default value of zero, so may be omitted.
Retardation factor	dimensionless	May be specified directly for each radionuclide, or calculated from the other parameters.
Density	kg m^{-3}	Either solid density, ρ_f , or bulk dry density, ρ_f^{dry} , may be specified for the matrix material.
Matrix porosity	dimensionless	Porosity, \mathcal{E}_p , for the matrix.
Porosity factors	dimensionless	Factor to scale porosity for some radionuclides. Default is 1, so only needed for radionuclides that are affected. The factors are less than one and represent constraints on the accessible porosity for some radionuclides (e.g. due to anion exclusion). The scaled porosities are denoted by \mathcal{E}_p^n .
Sorption coefficient, $K_{d,p}^n$	$\text{m}^3 \text{kg}^{-1}$	Equilibrium sorption coefficients, for each radionuclide, for the matrix material.
Diffusion coefficient	$\text{m}^2 \text{a}^{-1}$	Either the pore diffusion coefficient (D_{pore}) or effective diffusion coefficients (D_{eff}) for each radionuclide are required. The default value is zero. If the pore diffusion value is specified, then the effective diffusion calculated as $D_{eff}^n = \mathcal{E}_p^n D_{pore}$, where the porosity is scaled by the radionuclide-specific porosity factor.
Network Flow Data (for networks with more than one leg, or where the flow is calculated, one item per junction, identified by name)		
Flows in and out	$\text{m}^3 \text{a}^{-1}$	Water flow entering and/or leaving the system at the junction.
Head	m	Head (metres of water) for calculating flows.
Source Information (for each source)		
Source flux	mol a^{-1}	Specified as a file of data or via a simple function. Data for each radionuclide.
Fraction to each leg	dimensionless	If more than one leg leaves the source and the flow rates are not used to split the source flux.

A1.6.5 Verification

To ensure the reliability of PICNIC, the code has been extensively verified in a series of seven steps with increasing complexity of rock matrix (Barten & Robinson, 2001). Transport of single radionuclides or radionuclide chains in single legs, in single pathways (several legs in sequence) and in networks of pathways was carefully tested and analysed. Different sources and boundary

conditions were considered. Quantitative estimates of the accuracy of the code were derived from comparisons with analytical solutions and other computer codes.

Cross-comparison with other codes was only possible for one-dimensional matrix diffusion into homogeneous and heterogeneous rock matrices (Barten & Robinson, 2001). Tab. A1.6-4 lists the verification steps performed (Barten & Robinson, 2001). Verification of more complex rock matrix geometries was also undertaken, but is irrelevant for the present study.

Tab. A1.6-4: PICNIC verification steps and codes used for cross-comparisons

See Barten & Robinson (2001) for references.

Step	System	Methods, codes for cross-comparison
1	Homogeneous one-dimensional planar rock matrix	Analytical solution for rock matrix response; codes RANCHMD, GIMRT, PAWorks/LTG
2	Homogeneous cylindrical rock matrix	Code RANCHMD
3	Homogeneous one-dimensional planar rock matrix, represented with two-dimensional finite-element model	Analytical solution for rock matrix response; codes RANCHMD, GIMRT, PAWorks/LTG; discretisation tests
4	Two-layer one-dimensional planar rock matrix	Code RIP
5	Heterogeneous one-dimensional planar rock matrix	Codes PAWorks/LTG, RIP; discretisation tests

In a further verification exercise, analytical calculations of the Reference Case radionuclide release rates from the near field and geosphere were performed for those radionuclides that are known to be dose dominating (Gribi 2003). The results were in good agreement with those calculated numerically with the codes STMAN/PICNIC.

A1.7 TAME

A1.7.1 Scope and purpose

TAME is a general purpose biosphere model to convert releases of radionuclides from the geosphere into the biosphere into measures of radiological impact (in this case individual dose) for comparison with the regulatory guidelines.

A1.7.2 Phenomena included in TAME

A1.7.2.1 Overview

An overview of the representation of Super-FEPs in the various safety assessment computer codes is given in Section A1.2.3 (Tab. A1.2-2). Tab. A1.7-1 describes in more detail how *TAME* represents the different Super-FEPs that fall into its model domain, namely the biosphere. The symbols used in Tab. A1.7-1 are explained in Section A1.2.3.

The safety-relevant aspects of the Super-FEPs listed in the table are not modelled explicitly by TAME. The time dependent system properties associated with climatic and geomorphological evolution cannot, for example, be directly represented by the code (as indicated by the symbol ○ in Tab. A1.7-1). Parameter sets can, however, be chosen that represent steady-state system properties corresponding to alternative, stylised steady-state situations, as explained in the discussions of individual conceptualisations in Chapters 3 to 8. As indicated by the symbol ►, the possibility of drinking water extraction from the Malm aquifer is evaluated using a simple drinking water model, rather than TAME.

Tab. A1.7-1: Super-FEPs, their safety-relevant aspects (as taken from Tab. A5.2.1 of Nagra 2002d) and the ways in which they are represented by the code TAME

Symbols: see Section A1.2.3

Super-FEPs	Safety-relevant aspects to be represented by models	Model features						Explanatory comments
		Interface with geosphere model	Conceptual model objects (CMOs)	Material flows	Contaminant transport / accumulation	Exposure modes	Receivers of dose / critical group	
Opalinus Clay and confining units								
Future human actions	Borehole penetration of the repository	○						The nature and timing of future human actions cannot be evaluated using TAME. The consequences of hypothetical actions that may influence the repository system can, however, be bounded in some cases (e.g. the possibility of future drilling of a borehole inadvertently affecting the barrier system can be modelled by interfacing TAME directly with the near-field model).
	Drinking water extraction from the Malm aquifer	►						A simple drinking water model is used, based on a hypothetical pumping rate and capture efficiency of the deep well.
The surface environment								
Climatic evolution	The nature and timing of climate change		○	○	○			Climatic evolution is not modelled directly. Rather, alternative future climate states can be postulated and assumed to exist throughout the modelled period.
Geomorphological evolution	Properties of the exfiltration area for groundwater conveying radionuclides		○	○	○			Geomorphological evolution is not modelled directly. Rather, alternative geomorphological situations can be postulated and assumed to exist throughout the modelled period.

Environmental concentrations of radionuclides released from the geosphere into the biosphere are likely to be so low that system dynamics are not perturbed by their presence. The focus in TAME is therefore on the biosphere movement of water and solid material that potentially contain radionuclides. This means that the movements of solids and liquids determine radionuclide transport. Radionuclides enter the biosphere in solution and so water (as solvent) is the principal means of transport. Interactions of radionuclides with both fixed solid material and mobile solids are also potentially important for sorbing species. Transport in the gas phase is of

minor importance. Tab. A1.7-2 lists the phenomena that are explicitly included in the TAME model. These phenomena are also highlighted in bold text in the following paragraphs.

The role of the transport model is to determine the distribution of radionuclides in those parts of the system with which the **exposed population** is assumed to come into contact. The resulting exposure pathways are determined by the three exposure modes: **ingestion**, **inhalation** and **external radiation** (see, for example, BIOMASS, 2001). Concentrations in **foodstuffs**, **water supplies** and the **atmosphere** are therefore important, as well as the possibility of direct exposure to accumulations in soils.

Tab. A1.7-2: Phenomena explicitly included in the TAME model

Model features	Phenomena explicitly included in the TAME model
All	Radionuclide decay and ingrowth
Interface with geosphere model	Contaminated groundwater
Conceptual model objects (CMOs)	Soils
	Surface water bodies / water supplies
	Near-surface water bodies / water supplies / irrigation
	Atmosphere / airborne particulates
	Flora and fauna / foodstuffs
Material flows	Bulk water movement
	Deposition / erosion
Contaminant transport / accumulation	Partitioning (between solid, liquid and gas phases)
Exposure modes	Ingestion
	Inhalation
	External radiation
Receivers of dose / critical group	Exposed population / subsistence agriculture

A1.7.2.2 Key model assumptions

The biosphere is conceptualised as part of a catchment system with flow of water and solids into and out of the modelled area. Material flows are principally associated with **bulk water movements** in the aquifer and surface water although there is the possibility of **deposition** and **erosion** at exposed surfaces. Solid material can also be transported by bulk surface water movements. The atmosphere above the modelled region exchanges air (including **airborne particulates**) with the environment outside the modelled biosphere. These represent the major external interactions of the system. It is possible to indicate other external interactions, but they are generally smaller in magnitude and so, conservatively, these are set to zero as an imposed set of boundary conditions. These assumptions act to retain contaminants in the model biosphere compartments. All losses from the system are therefore described by interactions involving bulk transport from aquifer, surface water and atmosphere.

The focus is on radionuclides entering the biosphere in contaminated groundwater. Solid material transport is involved in internal interactions. In the sub-model describing transport the **partitioning of contaminants** between solid and liquid phases in **soils** and **surface water bodies** is important.

A second sub-model represents accumulation in the biotic parts of the system and the interaction of the human population with radionuclide containing components. The aquifer, which may contain **contaminated groundwater**, provides drinking water for humans and animals and may be used as a source of **irrigation water**. The interactions between **flora, fauna** and humans represent the food chain. **Subsistence agriculture** is conservatively assumed. The two sub-models are expanded in Figs. A1.7-1 and A1.7-2.

Material released to the downstream components of the biosphere (denoted by *Elsewhere*) cannot return to the rest of the system.

Exposures to the environmental concentrations of radionuclides give rise to doses to the exposed individuals. Dose is calculated via the pathways summarised in Tab. A1.7-3, with the arrangement of pathways shown in Fig. A1.7-2. The main focus is on the ingestion pathways since, in most cases, it is via these routes that the greatest exposure to radionuclides in the environment occurs (see BIOMOVs II, 1996). Inhalation doses can also be significant for radionuclides with high dose coefficients for inhalation. Some radionuclides also have a significant γ -ray exposure factor and this is addressed by the external radiation pathway.

A1.7.3 Mathematical representation

The two sub-models have straightforward mathematical descriptions. In the transport sub-model contaminant transfers between the compartments are represented by first-order linear dynamics. The content of each of the compartments is then linked to the critical group on the assumption of equilibrium concentration in foodstuffs.

The amount of radionuclide N in the i^{th} compartment is denoted by N_i [Bq]. The transfer interactions are then denoted by a set of fractional transfer rates from this compartment to the other j compartments in the system – λ_{ij} [a^{-1}] and to this compartment from the others – λ_{ji} [a^{-1}]. The rate of change of the contents of compartment i is therefore

$$\frac{dN_i}{dt} = \left(\sum_{j \neq i} \lambda_{ji} N_j + \lambda_N M_i + S_i(t) \right) - \left(\sum_{j \neq i} \lambda_{ij} N_i + \lambda_N N_i \right) \quad [\text{Bq a}^{-1}] \quad (\text{A1.7-1})$$

where

N_i, N_j [Bq] are the contents of compartments i and j respectively (where $i = L, D, T, W, S$, see Fig. A.1.7-1 for definition of these symbols);

$\lambda_{ji}, \lambda_{ij}$ [a^{-1}] are the transfer coefficients into and out of compartment i , respectively;

M_i [Bq] is the amount of the precursor radionuclide of N in compartment i ;

λ_N [a^{-1}] is the decay constant of radionuclide N ; and

$S_{N,i}(t)$ [Bq a^{-1}] is the external source term of radionuclide N into compartment i .

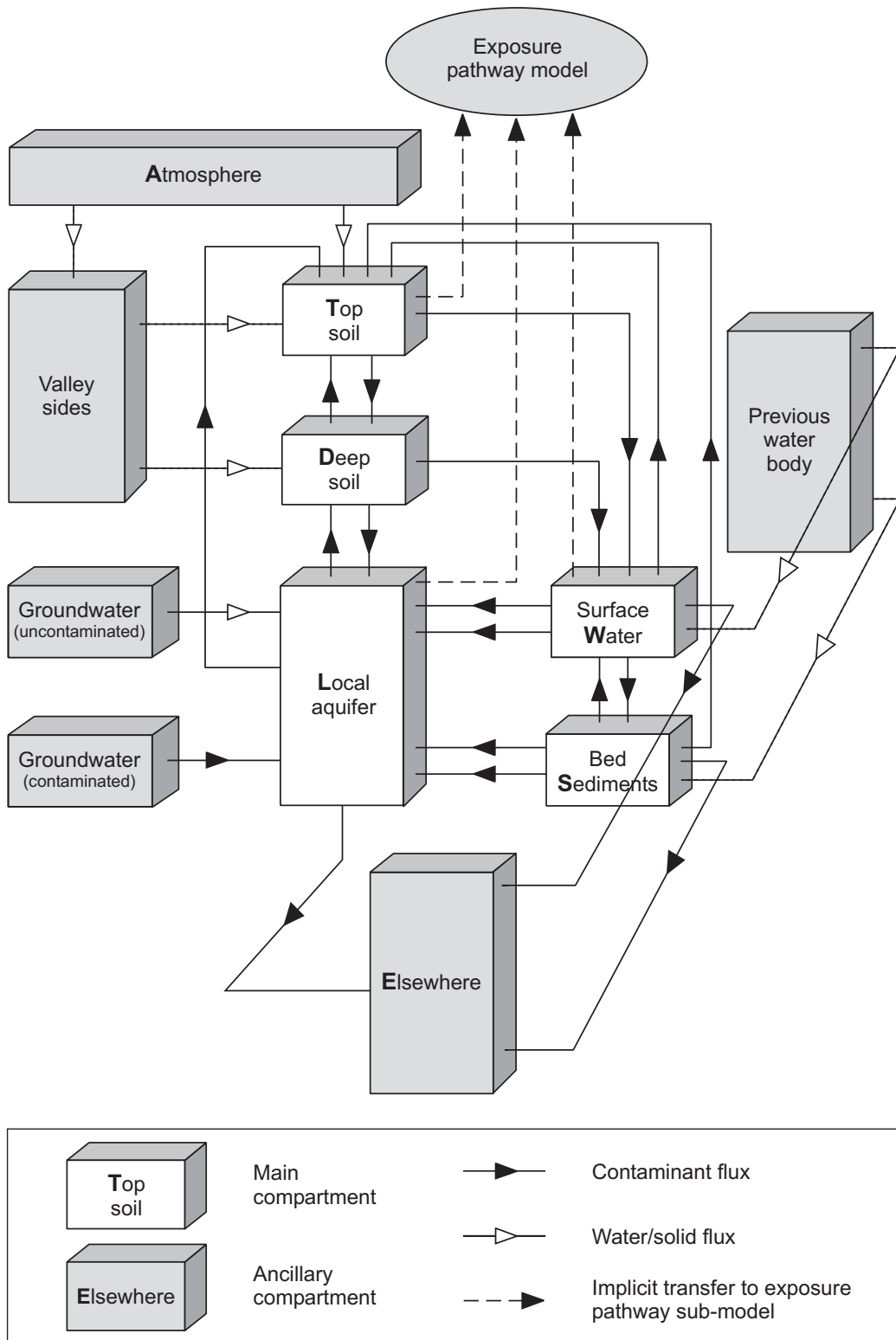


Fig. A1.7-1: Structure of the TAME transport and accumulation model of the biosphere (Klos *et al.* 1996)

Focus is on modelling the five main compartments: *L* – local aquifer, *D* – deep soil, *T* – top soil, *W* – surface water, *S* – bed sediment. Additionally, *A* – atmosphere, *U* – uncontaminated material, *C* – contaminated material and *E* – elsewhere.

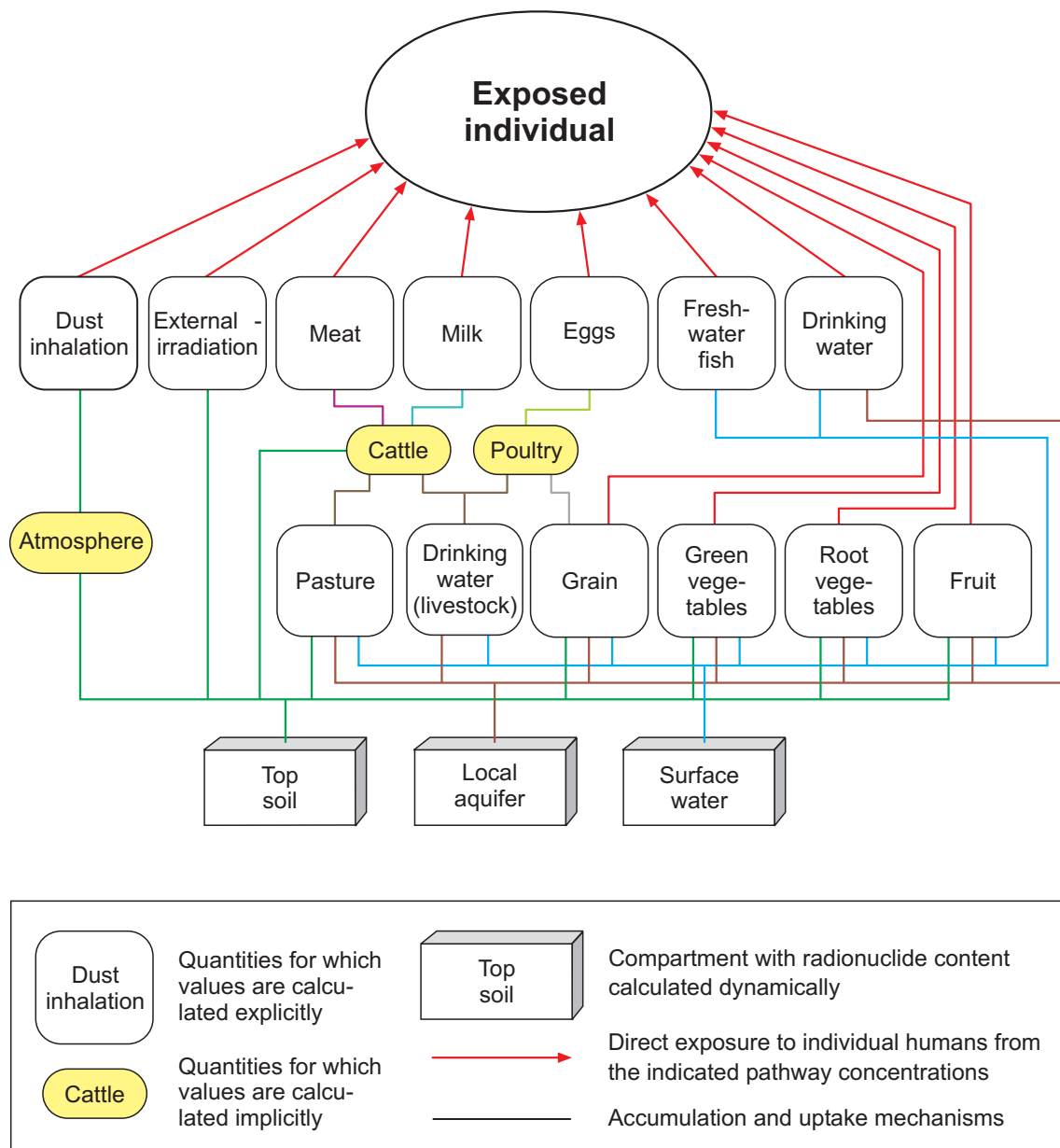


Fig. A1.7-2: The TAME exposure pathway sub-model showing the relationship between pathways and the physical environment

Tab. A1.7-3: Summary of exposure pathways modelled in TAME

ingestion	inhalation	external radiation
consumption: <i>drinking water</i> <i>meat</i> <i>milk</i> <i>eggs</i> <i>fish</i> <i>grain</i> <i>green vegetables</i> <i>root vegetables</i> <i>fruit</i>	inhalation of atmospheric dust: <i>normal dust loading</i> <i>enhanced dust loading</i>	γ -irradiation from <i>occupancy of contaminated land</i>

With the conceptual model of the system described above, the transfer coefficients are linked to water (in which soluble radionuclides are transported) and solid material fluxes (the driving forces of radionuclide transport between compartments). Klos *et al.* (1996) show that the generic form of transfers is given by

$$\lambda_{ij} = \frac{1}{\theta_i + (1 - \varepsilon_i)\rho_i k_i} \cdot \frac{F_{ij} + k_i M_{ij}}{l_i A_i} + D_{ij} \quad [\text{a}^{-1}] \quad (\text{A1.7-2})$$

where

- F_{ij} [$\text{m}^3 \text{a}^{-1}$] are the water fluxes leaving compartment i ;
 M_{ij} [kg a^{-1}] are the solid material fluxes leaving compartment i ; and
 D_{ij} [a^{-1}] are the effective diffusion rates for dissolved radionuclides leaving compartment i .

These are linked to the physical properties of the system:

- l_i [m] is the depth of compartment i ;
 A_i [m^2] is the surface (plan) area of compartment i ;
 θ_i [-] is the volumetric moisture content of compartment i ;
 ε_i [-] is the porosity of compartment i ; and

ρ_i [kg m⁻³] is the solid density of compartment i .

The amount of radionuclides in solution is determined by compartment-specific sorption values:

k_i [Bq kg⁻¹][Bq m⁻³]⁻¹ is the sorption value for compartment i , which describes the internal chemistry of the compartment in relation to the chemistry of the radionuclide. The K_d approach is valid here since radionuclide concentrations are low.

The input parameters are derived from the (case-specific) water and solid material transfers between compartments. These are balanced so that no gains or losses of water and solid material occur.

The exposure pathway sub-model relates environmental concentrations to doses to the exposed group. This means that the dose, $D_p^{(N)}$ [Sv a⁻¹], from pathway p arising from environmental concentrations of radionuclide N , determined by the integration of Equation (A1.7-1), is

$$D_p^{(N)}(t) = \sum_{i,exp} E_p H_{exp}^{(N)} P_{p,i} N_i(t) \text{ [Sv a}^{-1}\text{]} \quad (\text{A1.7-3})$$

i.e., a linear combination of the content of the biosphere compartments.

Conversion of radionuclide inventories into expressions of dose requires:

$H_{exp}^{(N)}$ the dose coefficient for N via exposure mode exp (ingestion, inhalation or external radiation);

E_p the exposure rate for pathway p – the amount of consumption for ingestion pathways, the amount inhaled for inhalation or the duration of exposure in the case of external radiation;

$P_{p,i}$ the pathway *processing* factor for pathway p from all compartments, i . Its role is to convert the radionuclide content of compartment i into a form by which the exposure takes place.

This latter factor may represent a large number of features and processes. As shown in Fig. A1.7-2, there are many ways in which radionuclides can be concentrated in the exposure pathways. The following paragraphs give examples of equations for exposure pathways. To simplify the notation, the dependency on radionuclide N and time t are omitted in these equations. A full description of the exposure pathway equations is given in Klos *et al.* (1996).

Dose from the consumption of contaminated surface water:

The parameters used in evaluation of the dose from consumption of contaminated drinking water from both the surface water and aquifer compartments are given in Tab. A.1.7-4. Using this nomenclature Equation (A1.7-3) translates into

$$D_{wat} = H_{ing} I_{wat} (1 - f_{well}) \frac{1 + (1 - f_{filter}) \alpha_w k_w}{1 + \alpha_w k_w} \cdot \frac{N_w}{l_w w_w d_w} \quad [\text{Sv a}^{-1}], \quad (\text{A1.7-4})$$

for the doses received from consumption of contaminated surface water. Here the dose per unit intake is defined as the value appropriate for the ingestion of the radionuclide. The intake rate $I_{wat} (1 - f_{well})$ involves the fraction of the total drinking water intake taken from the well, f_{well} , which is an alternative source of water. The concentration in the river water including the radionuclides sorbed onto suspended solid material is $\frac{N_w}{l_w w_w d_w}$, but the concentration in the consumed drinking water is reduced if the particulates are first filtered. The fraction of the drinking water which is thus processed is f_{filter} .

Dose from the consumption of contaminated well water:

The dose from the well water pathway is given by

$$D_{well} = H_{ing} I_{wat} f_{well} \frac{1 + (1 - f_{filter}) \alpha_L k_L}{\theta_L + (1 - \varepsilon_L) \rho_L k_L} \cdot \frac{N_L}{l_L A_f} \quad [\text{Sv a}^{-1}]. \quad (\text{A1.7-5})$$

Again the filtered fraction is evident and the porewater concentration is used.

Dose from the consumption of contaminated meat products

In the case of the livestock pathways, the parallel nature of the exposure pathways produces greater complexity. The dose to the human consumer of meat is given by

$$D_{meat} = H_{ing} I_{meat} K_{meat} \left\{ I_{water}^{livestock} + I_{water-irrigation-pasture}^{livestock} + I_{soil-pasture}^{livestock} + I_{soil}^{livestock} \right\} \quad [\text{Sv a}^{-1}] \quad (\text{A1.7-6})$$

H_{ing} [Sv Bq^{-1}] is again the dose per unit intake, I_{meat} [kg d^{-1}] is the consumption rate of meat and K_{meat} [$(\text{Bq kg}^{-1})/(\text{Bq d}^{-1})$] is the transfer factor for meat. The remaining terms define the concentration in the consumed meat:

$$C_{meat} = K_{meat} \left\{ I_{water}^{livestock} + I_{water-irrigation-pasture}^{livestock} + I_{soil-pasture}^{livestock} + I_{soil}^{livestock} \right\} [\text{Bq kg}^{-1}]. \quad (\text{A1.7-7})$$

The concentration in the consumed animal tissue therefore depends on the biochemical properties of the element and the intake by the animal. This occurs via four intake pathways:

- water consumption by the animal
- consumption of pasture contaminated by the foliar interception of irrigation water
- consumption of pasture contaminated by root uptake
- intake of soil on the surface of the pasture or directly with the pasture.

These intakes can be written in terms of the compartment inventories as follows:

Livestock intake via drinking water:

$$I_{water}^{livestock} = I_{wc} \left[f_A \frac{1}{\theta_L + (1 - \varepsilon_L) \rho_L k_L} \cdot \frac{N_L}{l_L A_f} + (1 - f_A) \frac{N_W}{l_W d_W w_W} \right] [\text{Bq d}^{-1}]. \quad (\text{A1.7-8})$$

I_{wc} [$\text{m}^3 \text{d}^{-1}$] is the daily water consumption by the animal and

f_A [-] is the fraction of that water obtained from the well.

Tab. A1.7-4: Parameters used to characterise the dose from the drinking water pathways
In these expressions, the subscripts *W* and *L* refer to the surface water and local aquifer.

Parameter	Units	Description
α_W	[kg m ⁻³]	suspended solid load in the surface water
α_L	[kg m ⁻³]	suspended solid load in the aquifer porewater
k_W	[(Bq kg ⁻¹) (Bq m ⁻³) ⁻¹]	nuclide specific solid - liquid distribution coefficient in the water compartment (K_d value)
k_L	[(Bq kg ⁻¹) (Bq m ⁻³) ⁻¹]	nuclide specific solid - liquid distribution coefficient in the local aquifer (K_d value)
θ_L and ε_L	[-]	volumetric moisture content and porosity of the local aquifer
f_{filter}	[-]	fraction between 0 and 1 which determines the amount of suspended solid material filtered out of the water before consumption
f_{well}	[-]	fraction of drinking water obtained from a well in the local aquifer; this is used to partition I_{wat}
I_{wat}	[m ³ a ⁻¹]	<i>exposure factor</i> , the total annual consumption of drinking water via each of the two pathways
H_{ing}	[Sv Bq ⁻¹]	dose coefficient for ingestion

Livestock consumption of pasture contaminated by irrigation:

$$I_{\substack{\text{livestock} \\ \text{water-} \\ \text{irrigation-} \\ \text{pasture}}} = Z I_{pc} \left[\frac{1 - e^{-\mu_p Y_p}}{Y_p (W_p + H_{pc})} \right] \left[\frac{\frac{1}{\theta_L + (1 - \varepsilon_L) \rho_L k_L} \cdot \frac{N_L}{l_L A_f} F_{LT} + \frac{N_W}{l_W d_w w_W} F_{WT}}{A_f} \right] \quad [\text{Bq d}^{-1}] \quad (\text{A1.7-9})$$

The intake of pasture is defined by the parameters

Z	[-]	ratio by weight of fresh pasture to hay
I_{pc}	[kg d ⁻¹]	daily consumption of dry fodder by the animal

which give the equivalent weight of wet pasture consumed daily.

The amount of radionuclide retained by the crop depends on the irrigation interception factor and the removal from the crop as a result of weathering and cropping. These factors are given in the first square brackets, using

μ_p	[m ² kg ⁻¹]	pasture irrigation mass-interception factor
Y_p	[kg m ⁻²]	yield of pasture
W_p	[a ⁻¹]	weathering rate for the radionuclide on pasture
H_{pc}	[a ⁻¹]	harvesting rate for the crop as a result of grazing by cattle and for cattle consumption as hay.

The second square bracket in Equation (A1.7-9) deals with the radionuclide concentration in irrigation water (including sorption on suspended solids) and the amount of irrigation water taken from each source - aquifer or surface water. These factors are defined in terms of the parameters used in the transport sub-model.

Livestock consumption of pasture contaminated by root uptake:

$$I_{\text{soil-pasture}}^{\text{livestock}} = I_{pc} Z K_p \frac{1}{(1 - \varepsilon_T) \rho_T} \cdot \frac{N_T}{l_T A_f} \quad [\text{Bq d}^{-1}] \quad (\text{A1.7-10})$$

Here, the concentration in the pasture is derived from the concentration in the top soil using K_p [(Bq kg⁻¹ crop, fresh weight)(Bq kg⁻¹ soil, dry weight)⁻¹], the soil - pasture concentration ratio.

Livestock ingestion of soil during grazing:

$$I_{\text{soil}}^{\text{livestock}} = S_{pc} Z I_{pc} \frac{1}{(1 - \varepsilon_T) \rho_T + \varepsilon_T \rho_W} \cdot \frac{N_T}{l_T A_f} \quad [\text{Bq d}^{-1}]. \quad (\text{A1.7-11})$$

In this form, S_{pc} is the fraction of the weight of pasture made up of wet soil.

A1.7.4 Input parameters

A large number of parameters are required for biosphere modelling using TAME, many of which are generic in the sense that they can be taken as applying to a range of sites and environmental conditions. Among these are half-lives, dose coefficients, concentration ratios, sorption data, food processing factors and parameters characterising the human diet and practices. A number of parameters are site-dependent, i.e. they depend on the specific conditions at the discharge area under investigation. For example, input parameters characterising biosphere compartments and water and solid material fluxes between the compartments are site-dependent. Sorption data can be chosen according to the composition of the solid material in the compartments (e.g. coarse = sandy, fine = containing clay or organics).

The data used in the present assessment are fully documented in Appendix 3 of the present report. Section A3.7 contains the input parameters for TAME used in the model calculations for the Reference Case biosphere. In Section A3.8, the input parameters for TAME for a number of alternative biosphere cases are listed.

A1.7.5 Verification

As discussed in the previous sections, TAME calculations are performed in three steps:

- derivation of transfer coefficients;
- integration of Equation (A1.7-1);
- calculation of environmental and foodstuff concentrations and calculation of doses (Equation A1.7-3).

Each of these stages has been subjected to different verification checks.

TAME representations of the physical biosphere rely on a system of mass balance to drive contaminant transport. Water fluxes (contaminants in solution) and solid material fluxes (transporting sorbed species) are determined on the basis of site characteristics. Transfer coefficients are calculated as linear combinations of these matrices, including radionuclide-specific properties, such as compartment-specific K_d -values. The resulting transfer matrix has been verified by hand, using spreadsheet techniques. The method of calculating transfer coefficients in TAME was also discussed in some detail in the BIOMOVs II (1996) Complementary Studies Exercise.

Numerical integration in TAME has been verified with respect to the calculations carried out in the *Kristallin – I* assessment (Nagra, 1994a). The *Kristallin – I* implementation of TAME employed a different set of numerical integration routines taken from the *BIOPATH* code (Bergström *et al.*, 1982). *BIOPATH* has been independently checked over a number of years in international intercomparison exercises, including BIOMOVs II (1996), in which TAME also participated, using both the original integration method as well as the new TAME 3c specific routines. In addition, an independent benchmarking of the TAME 3c routines against the results of TAME calculations in *Kristallin – I* has been performed.

Coding of the exposure pathway calculations in TAME was also discussed in detail in the Complementary Studies report (BIOMOVs II, 1996). A set of detailed spreadsheets were developed to verify the coding of this part of TAME. Using the distribution of radionuclides in the physical biosphere compartment calculated by the integration routines, exact agreement between the TAME codes and the spreadsheets was achieved.

In addition to the above verification measures, the biosphere dose conversion factors (BDCFs) have been independently calculated using a simplified analytical model for the Reference Case biosphere area (Gribi 2003). As shown in Fig. A1.7-3, the BDCFs are in good agreement with those calculated with TAME.

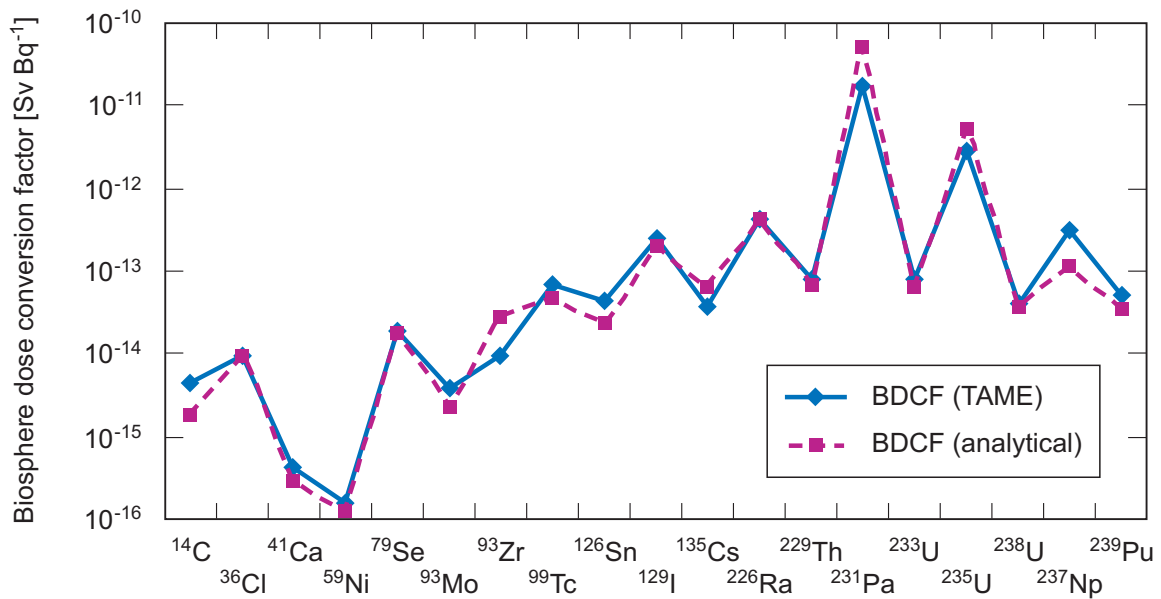


Fig. A1.7-3: Comparison of biosphere dose conversion factors (BDCFs) calculated by TAME and by the simplified analytical model discussed in Gribi (2003)

A1.8 FRAC3DVS

A1.8.1 Scope and purpose

FRAC3DVS is a general purpose flow and transport model. Like PICNIC (see Section A1.6.1), the numerical code FRAC3DVS can be used to calculate the transport of dissolved radionuclides through the geosphere. Some aspects of the near field can also be included in FRAC3DVS, for example the buffer region. The code is described in detail in Therrien & Sudicky (1996) and in Therrien et al. (1999). Unlike PICNIC, it is a three-dimensional code. In particular, it solves the three-dimensional groundwater flow and solute transport equations in discretely fractured and porous media. FRAC3DVS may also be applied to one- or two-dimensional model geometries. Processes and phenomena explicitly included in FRAC3DVS are given in the following sections.

A1.8.2 Phenomena included in FRAC3DVS

A1.8.2.1 Overview

An overview of the representation of Super-FEPs in the various safety assessment computer codes is given in Section A1.2.3 (Tab. A1.2-2). Tab. A1.8-1 describes in more detail how FRAC3DVS represents the different Super-FEPs that fall into its model domain. The symbols used in Tab. A1.8-1 are explained in Section A1.2.3. The following model features are considered separately.

1. Geometric features;
2. Flow phenomena; and
3. Transport and retention phenomena.

The safety-relevant aspects of the Super-FEPs are either modelled explicitly by FRAC3DVS, or their magnitude, timing, rate, spatial extent and performance directly determine one or more input parameters. These aspects or phenomena are summarised in Tab. A1.8-2 and discussed in more detail in the following sections, where they are highlighted in bold. The table also notes radioactive decay and ingrowth as included phenomena. Shaded boxes are used since these phenomena are not directly related to the Super-FEPs. Other flow and transport processes are included implicitly, for example through the selection of appropriate parameter values and boundary conditions. Where no alternative qualified code exists for a phenomenon, this is indicated using the symbol ●.

FRAC3DVS needs as input boundary conditions the radionuclide release rates from the near field models, and provides radionuclide release rates, which are used for the biosphere transport modelling. Fig. A1.8-1 shows the types of input data that are needed in a FRAC3DVS model. Further discussion of the phenomena that FRAC3DVS can consider is provided in the following three sections, and these are picked up in the subsequent discussion on the mathematical approach.

Tab. A1.8-1: Super-FEPs, their safety-relevant aspects (as taken from Tab. A5.2.1 of Nagra 2002d) and the ways in which they are represented by the code FRAC3DVS

Symbols: see Section A1.2.3

Super-FEPs	Safety-relevant aspects to be represented by models	Model features			Explanatory comments
		Geometric features	Flow phenomena	Transport and retention phenomena	
SF / HLW near field					
Geochemical immobilisation and retardation in the near field	Linear, equilibrium sorption			✓	Sorption coefficients used to calculate retardation factors, which are input as FRAC3DVS parameters.
Hydraulic transport characteristics of bentonite	Stationary flow		✓		Explicitly represented by FRAC3DVS.
	Transient flow		✓		See above.
	Advection / dispersion			✓	See above.
	Aqueous diffusion			✓	Aqueous diffusion is assumed to convey radionuclides across the bentonite buffer; element-specific diffusion coefficients are input as parameter values.

Tab. A1.8-1: (Cont.)

Super-FEPs	Safety-relevant aspects to be represented by models	Model features			Explanatory comments
		Geometric features	Flow phenomena	Transport and retention phenomena	
Opalinus Clay and confining units					
Low groundwater flow rate through undisturbed Opalinus Clay	Stationary flow		✓		Determined by hydraulic conductivity and hydraulic head boundary conditions.
	Transient flow		✓		Time dependent hydraulic head boundary conditions can be imposed to model transient effects (e.g. due to gas pressure build-up in the near field, tunnel convergence and ice loads).
	Advection / dispersion			✓	Aqueous diffusion, together with some advection / dispersion, is assumed to convey radionuclides across the Opalinus Clay and confining units.
	Aqueous diffusion			✓	
	Long-term changes (e.g. due to erosion of overburden)				●
Length of vertical transport path from emplacement tunnels to overlying and underlying formations	Transport paths provided by the Opalinus Clay and confining units	✓			Directly affects geometry of modelled domain.
Geochemical immobilisation and retardation in the Opalinus Clay and confining units	Linear, equilibrium sorption			✓	Sorption coefficients used to calculate retardation factors, which are input as FRAC3DVS parameters.
	Immobilisation processes				●
Homogeneity	Transport paths provided by transmissive discontinuities, faults and repository-induced fractures in the clay	✓			Homogeneity of the Opalinus Clay is assumed in modelling this as a single matrix zone with no transmissive discontinuities. Transmissive discontinuities and multiple matrix zones with different properties can be included as necessary.

Tab. A1.8-2: Phenomena explicitly included in the FRAC3DVS model

Model features	Phenomena explicitly included in the FRAC3DVS model
All	Radionuclide decay and ingrowth
Geometric features	Transmissive discontinuities, faults and repository-induced fractures in the clay
	Path length
Flow phenomena	Stationary flow
	Transient flow
Transport and retention phenomena	Advection / dispersion
	Aqueous diffusion
	Linear equilibrium sorption

A1.8.2.2 Geometric features

Due to its modular design, FRAC3DVS allows the use of different modelling strategies for dealing with geometric complexity, as shown in Fig. A1.8-2.

Three main model concepts are possible, continuum models, discrete fractured porous-medium models and discrete fracture models. The appropriate model concept for a problem depends on the model scale, the significance of inhomogeneities, including the possible existence of **transmissive discontinuities, faults and repository-induced fractures in the clay**, and of course of the knowledge about the system under consideration, including, for example, the **path length** from emplacement tunnels to overlying and underlying formations.

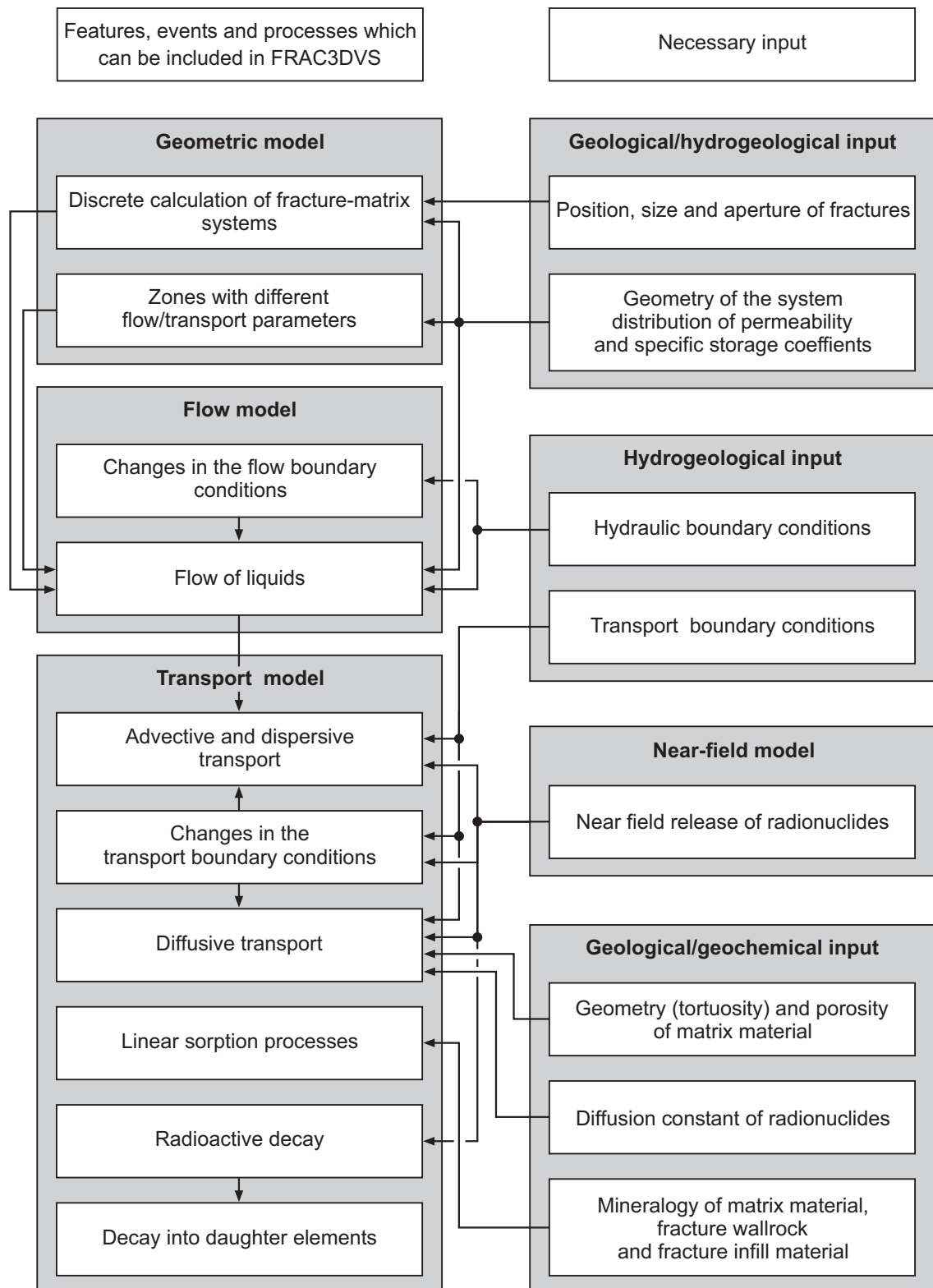


Fig. A1.8-1: Input data requirements in a FRAC3DVS model

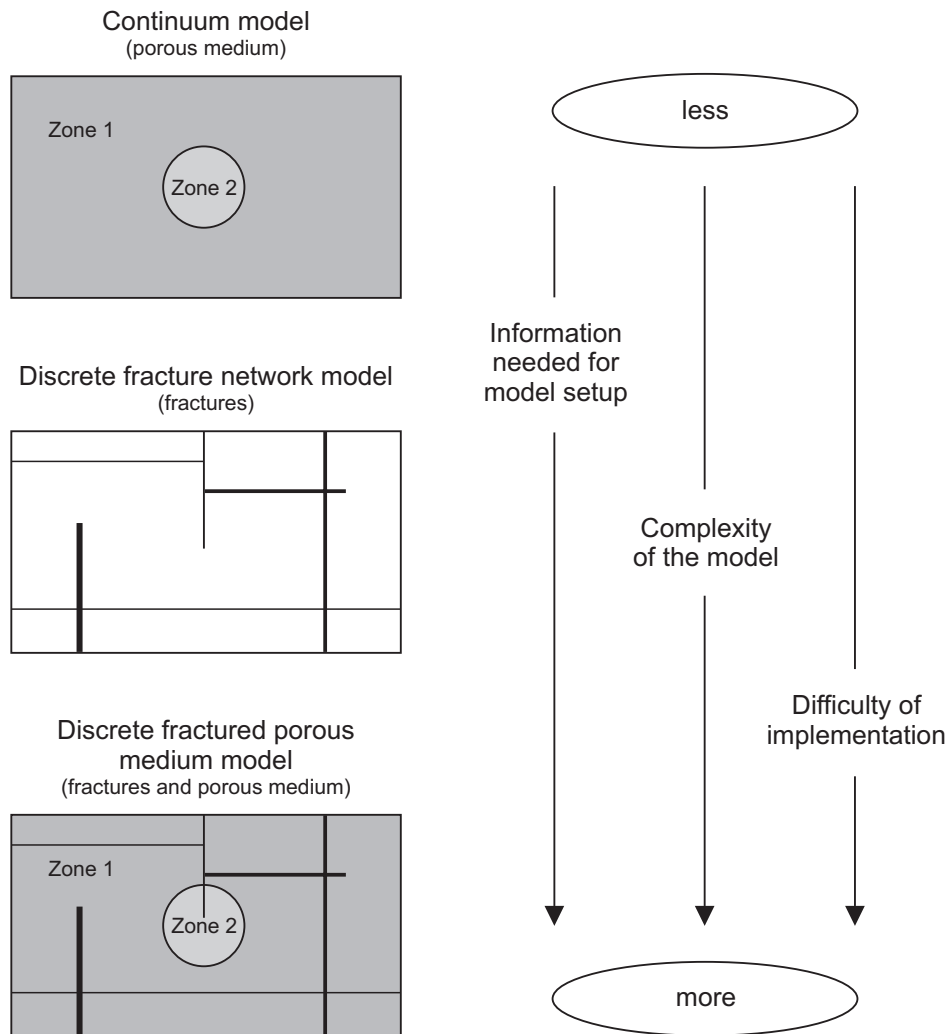


Fig. A1.8-2: Modelling strategies with FRAC3DVS

Continuum models are applied if it is possible to divide the inhomogeneous domain into homogeneous subdomains (for example, Zone 1 and Zone 2 represent the geosphere and near field). This is based on the concept of the representative elementary volume (REV). On the one hand, the size of the homogeneous subdomains should be large enough to average over local minor fluctuations of the physical parameters, on the other hand the subdomains should be small enough to allow the explicit inclusion of significant heterogeneities.

Discrete fracture network models can be applied if large scale and approximately linear heterogeneities dominate the flow and/or transport in the overall model domain. In this case it is not possible to approximate single connected fractures as porous media and the REV is larger than the model domain. These models allow separate radionuclide transport paths to be represented.

Discrete fractured porous medium models are applied if the exchange processes between fractures and matrix are important. In such hybrid models, discrete fractures are placed into the porous matrix which is itself treated as a continuum model.

It is important to mention that the knowledge required about the real system is much greater when using a discrete fractured porous medium model than when using a continuum model. This goes hand in hand with the effort needed for the model setup, numerical calculations and data analysis for the different models (see Fig. A1.8-2).

On the scale of the geosphere model, the emplacement tunnels can be described as line sources (long cylinders) for the radionuclides. Because of the cylindrical geometry, transport need only be considered in a plane normal to the tunnel axis and so a two-dimensional representation is appropriate.

A1.8.2.3 Flow phenomena

Flow is treated as being governed by Darcy's law. The modelled region is assumed to be saturated and the properties are assumed to be constant in time.

The time-independence of parameters in FRAC3DVS places some limitations on its application. In particular, for cases where mechanical opening (fracturing) of high conductivity pathways (for example due to high gas pressures) is relevant, FRAC3DVS cannot be used. Similarly, the restriction to saturated cases does not allow FRAC3DVS to be used directly to model interacting gas and water flows.

The three-dimensional flow equation is solved for **stationary flow** or **transient flow** boundary conditions.

A1.8.2.4 Transport and retention phenomena

Solutes are transported and dispersed with fluids due to hydraulic potentials and gradients in the host rock. Based on the flow solution the three-dimensional **advection / dispersion** equation is solved. **Aqueous diffusion** is also considered.

Transport is retarded by **linear equilibrium sorption**. Sorption constants can be selected conservatively to account for any non-linearity. The assumption of reversibility is conservative. Radioactive decay and ingrowth can be considered.

Hydrodynamic dispersion is modelled as being proportional to the advection velocity and is quantified by longitudinal and transversal dispersion lengths. This assumption is supported by many experimental measurements (see, e.g., Fig. 2.5.1 in Kinzelbach, 1992). The value for the longitudinal dispersion length is scale-dependent and is often taken to be 10 % of the length scale of the problem.

A1.8.3 Mathematical representation

The mathematical representation of flow and transport is based on mass balance, carried out over a representative elementary volume (REV) (see e.g. Bear, 1972). Additional assumptions are described in the previous sub-section. The idea is to replace a heterogeneous medium with a hypothetical medium consisting of one or more homogeneous sub-regions which mimics the behaviour of the real heterogeneous medium. The number of regions represented depends on the size and structure of the heterogeneities in the medium. The size of the heterogeneities should be much smaller than the size of the regions. Where a fracture provides a fast pathway across a region it may need to be modelled explicitly.

The following sub-sections are a simplified version of the program description by Therrien and Sudicky (1996). First the basic equations for the flow of water in porous media and in fractures are presented. Based on their solutions the equations for the transport of solutes can be formulated. A very short presentation of the numerical implementation of these equations is then given.

A1.8.3.1 Flow in porous medium

For the calculation of flow in porous media the groundwater flow equation is used

$$\nabla \cdot (\mathbf{K} \nabla h) + q_s = S_s \frac{\partial h}{\partial t} \quad . \quad (\text{A1.8-1})$$

The hydraulic head h is defined as the elevation of the piezometric water level. q_s is a fluid sink or source term, or volumetric rate at which the fluid is added to or removed from the system per unit volume of the porous medium. S_s is the specific storage, or volume of fluid released from storage in a unit volume of the porous medium per unit decline of head. \mathbf{K} is the hydraulic conductivity tensor. In a porous medium the hydraulic conductivity tensor is defined via Darcy's law

$$v_D = -\mathbf{K} \nabla h \quad . \quad (\text{A1.8-2})$$

The components of the Darcy velocity v_D are discharges per unit bulk area of the porous medium. Normally it is possible to choose a co-ordinate system in such a way that the axes are pointing in the same direction as the main components of the hydraulic conductivity tensor. This makes all components of the conductivity tensor, except the principal components, equal to zero.

The seepage or average water velocity v_f is defined by dividing the Darcy velocity by the flow (kinematic) porosity ε_f :

$$v_f = \frac{v_D}{\varepsilon_f} \quad . \quad (\text{A1.8-3})$$

The true microscopic fluid velocity in the matrix is highly variable due to the local pore structure, and v_f represents a macroscopic average. It corresponds to the average velocity of a passive tracer in the water.

A1.8.3.2 Flow in fractures

The fractures are idealised as two-dimensional parallel plates. This implies that the hydraulic head is uniform across the fracture width. It is now possible to formulate the flow equation for fractures by analogy with equation A1.8-1:

$$\nabla \cdot (\mathbf{K} \nabla h) - q_{n|I^-} + q_{n|I^+} + q_s = S_{sf} \frac{\partial h}{\partial t} \quad . \quad (\text{A1.8-4})$$

Equation (A1.8-1) and (A1.8-4) are linked via the fluid leakage fluxes $q_{n|I^-}$ and $q_{n|I^+}$ across the two surfaces I and I^+ , respectively, of a fracture. Here we assume, that there is no pressure discontinuity at the interface between a fracture and the adjacent rock matrix. The hydraulic head at the matrix side of the interface equals the hydraulic head at the fracture side for all fracture surfaces.

$S_{sf} [\text{L}^{-1}]$ is the specific storage coefficient for the fractures. Because it is assumed here that the fractures are not deformable and completely filled with fluid, there is no contribution to the storage term from the fracture compressibility. Thus the storage term is related to the fluid compressibility $\beta_f [\text{M}^{-1} \text{L} \text{T}^2]$ according to:

$$S_{sf} = \rho_f g \beta_f \quad . \quad (\text{A1.8-5})$$

Here g (9.81 m s^{-2}) is the gravitational acceleration and ρ_f is the fluid density.

In the case of two-dimensional laminar flow between smooth walls with constant aperture $2b$ it is possible to derive the law of Hagen-Poiseuille (often called cubic law) from the Navier-Stokes equations. The specific mass flow rate v_F between parallel plates, which is equivalent to the Darcy velocity, and which in case of open fractures is also equal to an average water velocity, can be expressed as:

$$v_F = \frac{-\rho_f g (2b)^2}{12\mu_f} \nabla h \quad , \quad (\text{A1.8-6})$$

where μ_f is the dynamic viscosity of the fluid. For equation (A1.8-6) it is possible to define a hydraulic fracture conductivity tensor by analogy with Darcy's law. In FRAC3DVS, it is assumed that fractures are homogeneous and isotropic, therefore the hydraulic conductivity tensor is reduced to a scalar fracture conductivity K_F :

$$K_F = \frac{\rho_f g (2b)^2}{12\mu_f} \quad . \quad (\text{A1.8-7})$$

Note that the cubic law discussed earlier is derived directly from this when total flow rather than Darcy velocity is considered.

A1.8.3.3 Transport in porous medium

In order to describe transport in a discretely fractured porous medium, two transport equations are needed, one for the porous medium, and one for the fractures.

Three-dimensional transport in a porous medium is described by the following equation:

$$\varepsilon_p R_p \frac{\partial C}{\partial t} + v_D \cdot \nabla C - \nabla \cdot (\varepsilon_p \mathbf{D}_h \nabla C) + \varepsilon_p R_p \lambda C + \Omega_s = 0 \quad . \quad (\text{A1.8-8})$$

Here $C=C(x,y,z,t)$ is the solute concentration, \mathbf{D}_h is the hydrodynamic dispersion tensor, ε_p is the matrix porosity and λ is a first-order (radioactive) decay constant. Ω_s is a general source or sink term representing an addition or a loss of mass. This term includes the addition of mass by ingrowth from a parent radionuclide and mass transfer from fractures.

The retardation factor for a porous medium R_p is given by

$$R_p = 1 + \frac{\rho_p}{\varepsilon_p} K_d \quad . \quad (\text{A1.8-9})$$

ρ_p is the dry bulk density of the rock and K_d is the volume-based sorption coefficient.

The components of the hydrodynamic dispersion tensor $D_{h,ij}$ are given by:

$$D_{h,ij} = (\alpha_L - \alpha_T) \frac{v_{f,i} v_{f,j}}{|v_f|} + \alpha_T |v_f| \delta_{ij} + \varepsilon_p \tau D_w \delta_{ij}, \quad i, j = 1, 2, 3 \quad . \quad (\text{A1.8-10})$$

α_L and α_T are the longitudinal and transverse dispersion length, respectively. $|v_f|$ is the magnitude of the seepage velocity and $v_{f,i}$ are the components of the seepage velocity vector, τ is the matrix tortuosity, D_w is the diffusion coefficient in free water, and δ_{ij} is the Kronecker delta.

The transport equation (A1.8-8) for porous media is coupled via the Darcy equation to the flow equation (A1.8-1).

A1.8.3.4 Transport in fractures

By analogy with equation A1.8-8 a two-dimensional transport equation for open fractures can be formulated:

$$R_f \frac{\partial C}{\partial t} + v_F \cdot \nabla C - \nabla \cdot (\mathbf{D}_h \nabla C) + R_f \lambda C - \Omega_{n|l^-} + \Omega_{n|l^+} + \Omega_S = 0 \quad . \quad (\text{A1.8-11})$$

Here $C=C(x,y,t)$ is the solute concentration in the fracture. \mathbf{D}_h is the two-dimensional hydrodynamic dispersion tensor of the fracture. The components can be derived from equation (A1.8-10) by inserting the fluxes and dispersivities for the fracture and setting the fracture porosity to unity. We do not need a special porosity term, because it is assumed that the fracture is open and fully saturated with water. The terms with $\Omega_{n|l^+}$ and $\Omega_{n|l^-}$ represent advective-

dispersive losses of solute mass across the surfaces I and I^+ , respectively, of the fracture due to fluid leakage. Ω_s is a general source or sink term representing an addition or a loss of mass. This term includes the addition of mass by ingrowth from a parent radionuclide. The retardation factor R_f in the fracture is defined as

$$R_f = 1 + \frac{2K_a}{2b} . \quad (\text{A1.8-12})$$

K_a is a surface-based sorption coefficient.

The transport equation (A1.8-11) for fractures is coupled to the flow equation (A1.8-4) for fractures via the fluid velocity in equation (A1.8-6).

A1.8.3.5 Boundary conditions

FRAC3DVS supports two types of flow boundary conditions:

Dirichlet (first-type) boundary conditions are implemented by assigning hydraulic heads h to appropriate nodes. It is possible to assign time-variable heads

$$h = h(x, t) . \quad (\text{A1.8-13})$$

Neumann (second-type) boundary conditions are implemented by assigning fluid fluxes normal to the boundary.

$$n \cdot (K \nabla h) = q = q(x, t) . \quad (\text{A1.8-14})$$

$q_i(x, t)$ is a given arbitrary function representing the fluid flux normal to the boundary and n is a unit vector in the normal direction.

FRAC3DVS supports three types of transport boundary conditions:

Dirichlet (first-type) boundary conditions are implemented by assigning a concentration to the appropriate nodes. It is possible to assign time-variable concentrations.

$$C = C(x, t) . \quad (\text{A1.8-15})$$

Neumann (second-type) boundary conditions are implemented by assigning additional mass fluxes to selected nodes.

$$\Omega_s = \Omega_s(x, t) , \quad (\text{A1.8-16})$$

where $\Omega_s(x, t)$ is a given arbitrary function representing the mass flux for a domain.

Cauchy (third-type) boundary conditions are implemented by assigning third-type concentration values to the selected faces. Normally the mass fluxes are calculated by FRAC3DVS from the flow solution. Only positive fluxes (i.e. into the domain) are possible.

$$-n \cdot \left(\mathbf{D} \nabla c + c \frac{v_D}{\varepsilon_p} \right) = h(x, t) \quad . \quad (\text{A1.8-17})$$

A1.8.3.6 Numerical implementation

The detailed description of the numerical implementation can be found in Therrien & Sudicky (1996). Here we only give a summary of the implementation and some more information, which is important for the calculation of radionuclide transport in fractured porous media.

A1.8.3.7 Solution of the flow and transport equations

The solution of the coupled flow and transport equations is based on the control volume finite-element approach (sometimes also called finite volume approach). In this method, the volume of the domain, or area of the fracture domain, is discretised by a numerical grid. Around each node a control volume is defined. The differential equations are solved by direct calculation of the fluxes through each control volume. This procedure ensures fluid conservation both locally and globally.

The transport equation is solved in a similar way to the flow equation. The type of elements used for transport are identical to those used for the flow problem. There are no explicit (solute) mass exchange terms formulated, because the two-dimensional elements representing the fractures are superposed on the faces of three-dimensional matrix elements and share the same nodes.

Full details of the numerical solution can be found in Therrien & Sudicky (1996).

A1.8.4 Input parameters

The input parameters required to specify a FRAC3DVS calculation can be split into categories (Tab. A1.8-3):

- Radionuclides and decays;
- Transport properties:
 - Basic data;
 - Properties of the transport path;
- Flow data;
- Source information.

In addition, output specifications are needed and control parameters may be modified. These do not form part of the input data listed here, but will be commented on in the description of the individual cases.

The units of inputs to FRAC3DVS need only be self-consistent. Here, however, specific units used in this study are quoted.

Tab. A1.8-3: FRAC3DVS input data requirements

Input	Units	Requirements
<i>Radionuclides and Decays</i>		
Radionuclides and decays to be used.	Half lives are specified in years.	Table of parent, daughter and half-life. Where a parent has more than one daughter, the half-life for each decay is the total half-life of the parent divided by the fraction decaying to the particular daughter.
<i>Basic Data</i>		
Length	m	Not used; instead, the dimensions of the model domain are specified (see Fig. 3.4-1).
Cross sectional area	m ²	Not used. Instead, the width and depth of the model domain are specified.
Darcy velocity, v_D	m a ⁻¹	Not used.
Hydraulic conductivity	m a ⁻¹	For each material type, anisotropic values may be used for the hydraulic conductivity.
Peclet number	dimensionless	Not used.
Diffusion	m ² a ⁻¹	The effective diffusion coefficients (D_{eff}) for each radionuclide is defined by specifying the diffusion constant in free water and the tortuosity and the porosity for each material type.
Specific storage coefficient, S_s	m ⁻¹	For each material type, the specific storage coefficient is specified.
<i>Properties of Transport Path</i>		
Retardation factor, R_p^n	dimensionless	This is calculated from the other parameters.
Density, ρ_p	kg m ⁻³	Bulk dry density, ρ_f^{dry} , is specified for the bulk of each material type.
Flow porosity, ε_f	dimensionless	Porosity corresponding to the part of the volume where water can flow, specified for each material type.
Infill porosity	dimensionless	Same as flow porosity.
Porosity factors	dimensionless	Not used (different runs for different porosities must be performed).
Sorption coefficient	m ³ kg ⁻¹	Equilibrium sorption coefficients, for each radionuclide and each material type.
<i>Flow Data</i>		
Flows in and out	m ³ a ⁻¹	Water flow entering and/or leaving the system at the boundary. No-flow may be specified. Time-dependent water flows may be prescribed at all (or a selection of) nodes or calculated using initial conditions and specific storage coefficients for each material type.
Head	m	Head (metres of water) at boundaries for calculating flows.
<i>Source Information</i>		
Source flux	mol a ⁻¹	Specified as a file of data for each source. Data for each radionuclide.
Fraction to each leg	dimensionless	Not used.

A1.8.5 Verification

The accuracy of the FRAC3DVS code has been verified by comparison with analytical solutions (where available) and by comparison with other codes. Tab. A1.8-4 gives an overview of the test cases.

Tab. A1.8-4: Overview of test cases for FRAC3DVS

Case	Process, features, events	Comparisons/Author
1D-consolidation driven flow in a porous medium	Time variable hydraulic head boundary function, time dependent fluid flow in a homogeneous medium including aquifer storativity	Analytical solution, Kosakowski (2000)
Drawdown in a 2D-Theis aquifer	Time variable fluid flow boundary function, time dependent fluid flow in a homogeneous porous medium including aquifer storativity	Analytical solution, Therrien et al. (1999)
Chain decay and transport in a 1D porous medium	Advection, dispersion, retardation, radioactive chain decay	Analytical solution, Therrien et al. (1999)
1D diffusion dominated transport in porous media	Advection, dispersion, diffusion, decay	Analytical solution and numerical solutions with MCOTAC, Pfingsten (2000)
Chain decay and transport in a single fracture	Advection, dispersion, diffusion, retardation, decay in fracture Diffusion, decay, retardation in matrix	Analytical solution, Therrien et al. (1999)
Chain decay and transport in a single fracture	Advection, dispersion, diffusion, retardation, decay in fracture Diffusion, decay, retardation in matrix	Numerical solutions with RANCHMD, PICNIC, Pfingsten (2000)
Time-variable source condition for transport in 1D porous medium	Time-variable source concentration, advection, dispersion	Analytical solution, Therrien et al. (1999)
Heterogeneous 2D diffusion dominated transport	Advection, diffusion, dispersion, decay, retardation, heterogeneous distribution of hydraulic conductivities	Numerical solution with MCOTAC, Pfingsten (2000)

A1.9 The Gas Model

A1.9.1 Scope and purpose

The Gas Model is used to perform simplified calculations for the pressure evolution and gas migration in the SF/HLW/ILW repository in Opalinus Clay and dose calculations for the release of volatile radionuclides in the gas phase from the repository. The pressure build-up caused by gas generation is mitigated by gas dissolution and gas diffusion, gas-induced porewater displacement and capillary leakage by 2-phase flow from the emplacement tunnel walls into the Opalinus Clay or along the EDZ into the access tunnel system. If the gas pressure exceeds a threshold pressure of about 13 MPa, dilatant gas pathways in the Opalinus Clay are created, which increase the efficiency of gas release and limit the maximal gas pressure in the repository. Gas transported through the host rock will accumulate in the Wedelsandstein formation (lateral extension due to higher permeability compared to Opalinus Clay and low-permeability upper confining units), from which gas release takes place through the low-permeability upper confining units to the Malm aquifer. Dose calculations are performed for ^{14}C only, because ^{14}C is the only relevant volatile radionuclide in SF and ILW. For HLW, the contribution of volatile radionuclides to the total dose is insignificant.

A1.9.2 Phenomena included in the Gas Model

An overview of the representation of Super-FEPs in the various safety assessment computer codes is given in Section A1.2.3 (Tab. A1.2-2). Tab. A1.9-1 describes in more detail how the Gas Model represents the different Super-FEPs that fall into its model domain. The symbols used in Tab. A1.9-1 are explained in Section A1.2.3. The following model features are considered separately.

1. Pressure evolution and gas migration - this feature is discussed in detail in Section A1.9.3 - and
2. Dose due to volatile ^{14}C in the gas phase - this feature is discussed in detail in Section A1.9.4.

Some safety-relevant aspects of the Super-FEPs (indicated by large bold ticks in Tab. A1.9-1) are either modelled explicitly by the Gas Model, or their magnitude, timing, rate, spatial extent and performance directly determine one or more input parameters. These aspects or phenomena are summarised in Tab. A1.9-2 and discussed in more detail in the following sections, where they are highlighted in bold. The table also notes radioactive decay as an included phenomenon, as well as phenomena related to dilution in the surface environment and exposure by ingestion, although these are not directly related to the Super-FEPs. Shaded boxes are used to distinguish these phenomena from those directly related to the Super-FEPs.

Some other safety-relevant aspects of the Super-FEPs (indicated by smaller ticks in Tab. A1.9-1) are only partially represented by the Gas Model or only indirectly affect input parameters. The waste inventory, for example, is represented only in so far as it affects the amount of ^{14}C released as volatile species. These aspects are also described in detail in later sections.

Tab. A1.9-1: Super-FEPs, their safety-relevant aspects (as taken from Tab. A5.2.1 of Nagra 2002d) and the ways in which they are represented by the Gas Model

Symbols: see Section A1.2.3

Super-FEPs	Safety-relevant aspects to be represented by models	Model features		Explanatory comments
		Pressure evolution and gas migration	Release of volatile ¹⁴ C in the gas phase	
SF				
Quantities and burnup of fuel and associated radionuclide inventories, including the instant release fraction (IRF)	Waste inventory in a single package and number of packages	✓	✓	Inventory partially represented by model (¹⁴ C only); number of SF packages affects gas generation rate and ¹⁴ C inventory.
	Partitioning between fuel matrix, cladding and IRF		✓	See above.
	¹⁴ C in organic and inorganic form upon release		✓	See above.
	Proportion of organic ¹⁴ C in volatile form upon release		✓	All organic ¹⁴ C assumed to be released in volatile form.
Corrosion of cladding	Corrosion rate		✓	Directly provides input parameter.
Dissolution of fuel matrix	Dissolution rate		✓	Directly provides input parameter (not used in the safety assessment because all ¹⁴ C in the fuel matrix is assumed to be present in inorganic form).
HLW glass				
Quantities of glass and associated radionuclide inventories	Waste inventory in a single package and number of packages	✓		It is assumed that radionuclides originating from the HLW near field are not released and transported in the gas phase. Gas generation in the HLW near field does, however, contribute to overall gas generation in the repository and thus provides input to the Gas Model.
SF / HLW canisters				
Breaching of steel canisters	Time of occurrence of breaching		✓	Time of breaching (containment) time is input as a parameter value.
Gas generation by steel canister corrosion	Gas generation rate for SF / HLW	✓		Directly provides input parameter.
SF / HLW near field				
The long resaturation time of the repository and its surroundings	The rate of the resaturation process	✓		While gas pressure in the repository is below the formation pore pressure of 6.5 MPa, slow inflow of water from the Opalinus Clay occurs and water saturation in the emplacement tunnels gradually increases.
Gas transport characteristics of bentonite	Dilatant gas pathway formation (SF / HLW near field)	✓		Assumption underlying calculation of gas pressure build-up.
	Gas dissolution and diffusion	✓		Directly provides input parameters.

Tab. A1.9-1:(Cont.)

Super-FEPs	Safety-relevant aspects to be represented by models	Model features		Explanatory comments
		Pressure evolution and gas migration	Release of volatile ¹⁴ C in the gas phase	
ILW				
Quantities of waste and associated radionuclide inventories	Waste inventory in a single package and number of packages	✓	✓	Directly provides input parameters. ILW inventory affects gas generation rate and provides inventories of radionuclides that form volatile species (¹⁴ C only).
Gas generation rates for ILW	Gas generation rates for ILW	✓		Directly provides input parameter.
Hydraulic and gas transport characteristics ILW near field	Gas dissolution and diffusion	✓		Explicitly included process.
	Porewater displacement by gas	✓		Explicitly included process.
Tunnels / ramp / shaft and seals				
The seals and the surrounding rock	Formation of gas pathways through the sealing zone (EDZ, sealing material)	✓		Process implicitly considered in a separate calculational case by increasing the total length of the ILW emplacement tunnels from 180 m to 360 m with the purpose to include the additional gas storage volume available in the Operations Tunnel following gas escape through the ILW tunnel plugs (incl. EDZ).
Opalinus Clay and confining units				
Length of vertical transport path from emplacement tunnels to overlying and underlying formations	Transport paths provided by the Opalinus Clay and confining units	✓		Path length affects capillary leakage of gas (and hence radionuclides as volatile species) through Opalinus Clay via the parameter "distance over which hydraulic gradient is maintained". It also affects the amount of gas that can be stored in the Opalinus Clay.
The barrier system (general)				
The migration of repository induced gas	Gas dissolution and diffusion in the Opalinus Clay (incl. tunnel EDZs)	✓		Explicitly included process.
	Capillary leakage in the Opalinus Clay	✓		Explicitly included process.
	Pathway dilation in the Opalinus Clay	✓		Explicitly included process.
	Porewater displacement in the Wedelsandstein	✓		Explicitly included process.
	Gas dissolution and diffusion in the low-permeability upper confining units	✓		Explicitly included process.
	Capillary leakage through low-permeability upper confining units	✓		Explicitly included process, although this process does not contribute to gas transport in practice because the threshold pressure for capillary leakage through low-permeability upper confining units is not reached.

Tab. A1.9-2: Safety-relevant aspects of the Super-FEPs and other phenomena explicitly included in the Gas Model

Note: Radioactive decay and phenomena associated with the dilution in the surface environment and dose are not directly related to the Super-FEPs and are placed in shaded boxes.

Model features	Safety-relevant aspects of the Super-FEPs explicitly included in the Gas Model
General	Radionuclide decay
Pressure evolution and gas migration	Gas generation rate for SF / HLW
	Gas generation rate for ILW
	Gas dissolution and diffusion (SF / HLW near field; ILW near field; Opalinus Clay, incl. tunnel EDZs)
	Porewater displacement by gas (ILW near field)
	Capillary leakage into the Opalinus Clay
	Dilatant gas pathway formation in the Opalinus Clay
	Porewater displacement in the Wedelsandstein
	Gas dissolution and diffusion in the low-permeability upper confining units
Dose due to volatile ^{14}C in the gas phase	Organic ^{14}C in volatile form upon release
	Corrosion rate (cladding)
	Dissolution rate (fuel matrix)
	Time of occurrence of breaching (SF canisters)
	Dilution in the Quaternary aquifer
	Ingestion of drinking water from Quaternary aquifer

A1.9.3 Pressure evolution and gas migration

A1.9.3.1 Conceptual model

In the following, the relevant processes governing the pressure evolution and gas migration in the SF/HLW/ILW repository in Opalinus Clay are listed and the conceptual assumptions discussed (see Tab. A1.9-3 and Figs. A1.9-1 and A1.9-2):

- Resaturation of tunnels

While gas pressure in the repository is below the formation pore pressure of 6.5 MPa, slow inflow of water from the Opalinus Clay occurs and water saturation in the emplacement tunnels gradually increases. In the case of the ILW emplacement tunnels, full saturation is, however, not likely to be reached before the start of gas generation and a free gas phase will remain.

- Gas generation

Gas generation is caused by anaerobic corrosion of SF/HLW steel canisters (the **gas generation rate for SF / HLW** is determined by the corrosion rate - a realistic corrosion rate is $1 \mu\text{m a}^{-1}$, but may be as low as $0.1 \mu\text{m a}^{-1}$) and - for ILW - other metals, producing

hydrogen, and by microbial degradation of organic compounds, producing CH₄ and CO₂. Realistic **gas generation rates for ILW** are used for the Base Case (Nagra 2003a). There is the possibility that hydrogen may be reduced to methane by microbial activity, leading to a reduction in the total gas volume, but this process is not considered in the calculations.

- **Gas dissolution and diffusion**

Gases generated by the above mechanisms, as well as gas entrapped at the time of closure, dissolve in the near-field pore water until the gas solubility in the near field at repository pressure is reached. Dissolved gas diffuses through the tunnel walls into the Opalinus Clay.

- **Pressure build-up and porewater displacement by gas**

The pressure of the free gas phase increases as a result of the ongoing generation of gas. In the case of ILW and for pressures exceeding the formation pore pressure of 6.5 MPa, water is displaced from the emplacement tunnels into the Opalinus Clay. In the case of SF/HLW, the pressure increases until gas pathways through the bentonite are created. The resulting gas storage volume in the near field is significantly smaller than for ILW and the amount of displaced porewater is expected to be small. If the gas generation rate exceeds the rate of gas removal (dissolution/diffusion) and gas volume increase (porewater displacement), then the gas pressure further rises until capillary leakage and/or pathway dilation occurs (see next two bullet points).

- **Capillary leakage into the Opalinus Clay**

When the gas pressure exceeds the threshold for capillary leakage (formation pore pressure of 6.5 MPa plus gas entry pressure of approximately 5 MPa), leakage of gas into the Opalinus Clay takes place. Leakage is proportional to the product of the gas permeability times the hydraulic gradient (Darcy's law).

- **Formation of gas pathways through the sealing zone (ILW only)**

If the gas pressure exceeds the threshold pressure for the formation of gas pathways through the sealing zone (including EDZ), gas escapes to the operations tunnel where significant pore volumes are provided for additional gas storage. These processes have not been fully included in the Gas Model, but their mitigating effect is illustrated in a parameter variation in which the total length of the ILW tunnels is doubled from 180 m to 360 m, thus providing additional volume for gas accumulation.

- **Dilatant gas pathway formation in the Opalinus Clay (pathway dilation)**

Pressure may further increase until the threshold pressure for the formation of dilatant gas pathways in the Opalinus Clay is eventually reached (approximately 13 MPa). Based on the prevailing stress conditions, dilatant gas pathways penetrate along the bedding planes into the formation, thus increasing the surface over which capillary leakage and gas diffusion vertically into the Opalinus Clay matrix take place. Gas pathway propagation stops when the combined effect of capillary leakage / porewater displacement / gas diffusion over the available surfaces (tunnel wall and gas pathway) balances the gas generation rate. In the conceptual model, the gas pathways are represented by a single feature with an effective aperture. The effective aperture is determined by the number and apertures of individual pathways as well as by the extent of a desaturated zone along the pathways, the formation of which is assumed to occur in equilibrium with the propagation of the pathways. The growth of the feature is dynamically modelled by considering the mass balance for gas and by assuming a constant pressure inside the pathway, which equals the threshold pressure for gas pathways.

- Gas accumulation in and loss from the Wedelsandstein

Gas transported through the host rock and/or through the ramp/shaft accumulates in the Wedelsandstein formation. A gas-filled pore volume develops radially at a rate determined by the gas release rate to the Wedelsandstein and by the gas release from the Wedelsandstein due to **gas dissolution** followed by **gas diffusion** back into the Opalinus Clay and into the low-permeability upper confining units, transporting gas to the Malm aquifer. Note that **capillary leakage** does not contribute to the loss of gas because, with the parameters used to evaluate assessment cases, the gas pressure in the Wedelsandstein formation always remains below the threshold pressure for capillary leakage into the low-permeability formations of the upper confining units.

Tab. A1.9-3: Summary of transport processes considered in the conceptual models for the different transport pathways and waste types

Transport processes considered	Tunnel seals (incl. EDZ)		Opalinus Clay (incl. EDZ)		Wedelsandstein	Low-permeability upper confining units
	ILW	SF/HLW	ILW	SF/HLW	SF/HLW/ILW	SF/HLW/ILW
Gas dissolution and diffusion	(✓) ¹	-	✓	✓	-	✓
Displacement of porewater		-	✓	-	✓	-
Capillary leakage		-	✓	✓	✓	✓
Pathway dilation		-	✓	✓	-	-
Gas frac	-	-	-	-	-	-

¹ Process implicitly considered in a separate calculational case for ILW by increasing the total length of the tunnels from 180 m to 360 m with the purpose to include the additional gas storage volume available in the Operations Tunnel following gas escape through the ILW tunnel plugs (incl. EDZ).

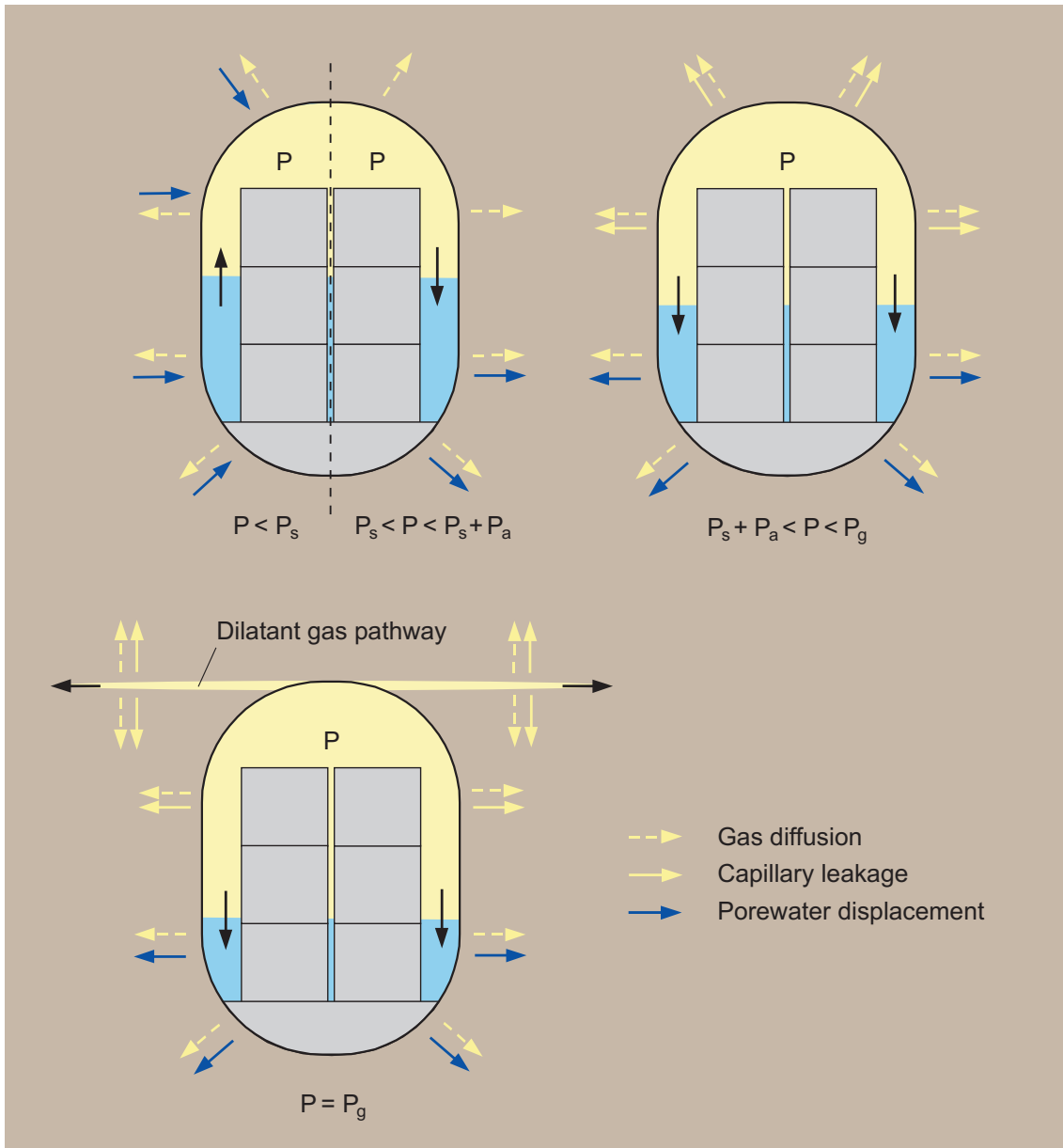


Fig. A1.9-1a: Scheme of the conceptual model for pressure build-up in the ILW emplacement tunnels, mitigated by gas diffusion, capillary leakage, porewater displacement and by the formation of dilatant gas pathways

P_s , P_a , P_g formation pore pressure (6.5 MPa), gas entry pressure (5 MPa) and threshold pressure for the creation of dilatant gas pathways (13 MPa), respectively.

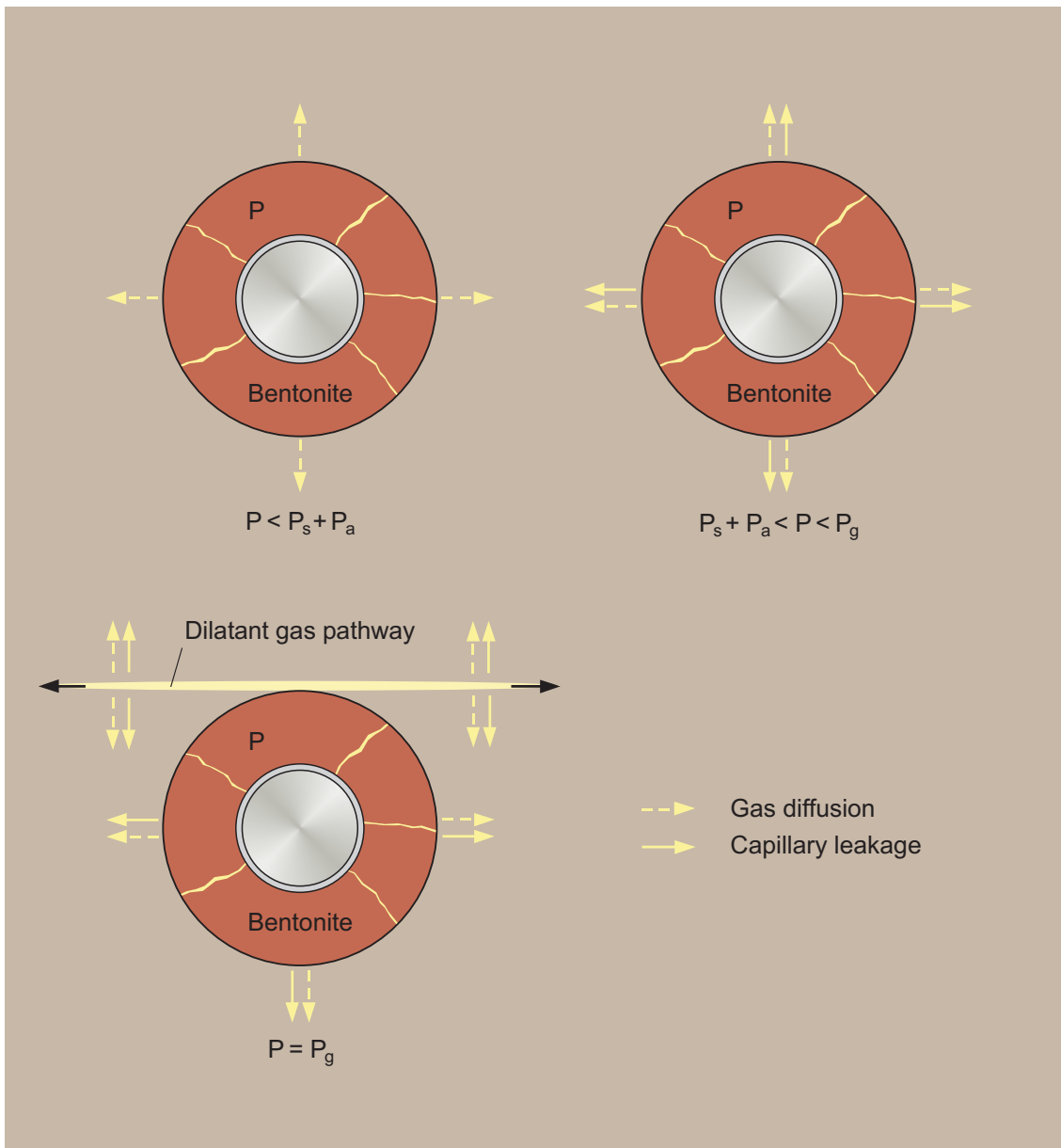


Fig. A1.9-1b: Scheme of the conceptual model for pressure build-up in the SF/HLW emplacement tunnels, mitigated by gas diffusion, capillary leakage and by the formation of dilatant gas pathways

P_s , P_a , P_g denote formation pore pressure (6.5 MPa), gas entry pressure (5 MPa) and threshold pressure for the creation of dilatant gas pathways (13 MPa), respectively.

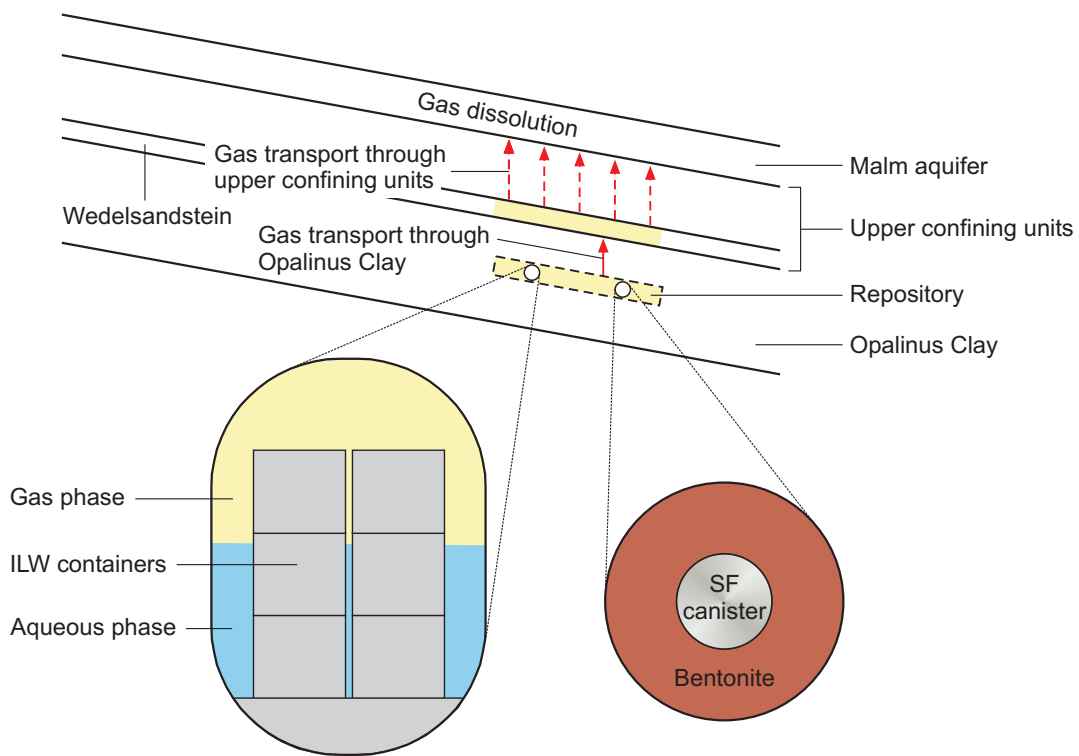


Fig. A1.9-2: Scheme of the conceptual model for gas release from the SF/HLW/ILW emplacement tunnels through Opalinus Clay, Wedelsandstein and low-permeability upper confining units

The formation of macroscopic gas fracs in the Opalinus Clay is not considered in this investigation because capillary leakage / porewater displacement / gas diffusion occurs at such a rate that the frac-pressure of the host rock will never be reached (Nagra 2003a).

A1.9.3.2 Mathematical Representation

The following mathematical model is a simplified representation of the processes shown in Figs. A1.9-1 and A1.9-2. All input parameters, with the exception of the gas generation rate, are assumed to be constant in time. In particular, the lengths over which the gas-induced hydraulic gradient and the concentration gradient for dissolved gas in the Opalinus Clay are non-zero are assumed to be time-independent. Furthermore, the gas permeability of the Opalinus Clay is assumed to be constant in time and space, but is varied over a relatively large parameter range in the framework of parameter variations.

Case with gas pressure below threshold for pathway formation in Opalinus Clay ($P < P_g$):

The gas pressure is governed by

$$P(t) = n(t) \frac{RT}{V_g(t)} \quad (\text{A1.9-1})$$

with the gas volume in the emplacement tunnels being changed, in the case of ILW, by water inflow from the Opalinus Clay into the tunnels ($P < P_s$) and by gas-induced porewater displacement from the tunnels into the Opalinus Clay ($P > P_s$):

$$\begin{aligned} V_g(t) &= \min(V_p; V_g(0) + \int_0^t Q_w(t') dt') \\ &= \min(V_p; V_g(0) + \frac{\pi KrH}{2l_i \rho g} \int_0^t (P(t') - P_s) dt') \quad (\text{ILW}) \\ V_g(t) &= V_g(0) \quad (\text{SF / HLW}) \end{aligned} \quad (\text{A1.9-2})$$

with

$$\begin{aligned} V_g(0) &= V_p S_{ILW} = \pi r^2 H \varepsilon_{ILW} S_{ILW} \quad (\text{total ILW}) \\ V_g(0) &= \pi r^2 p \varepsilon_{ben} S_{ben} \quad (\text{per SF / HLW canister}) \end{aligned}$$

$P(t)$	gas pressure in tunnel at time t [Pa]
P_s	formation pore pressure in Opalinus Clay [Pa]
$n(t)$	amount of gas in tunnel [mol]
R	universal gas constant [$\text{J K}^{-1} \text{mol}^{-1}$]
T	temperature [K]
V_p	total pore volume in tunnel [m^3]
$V_g(t)$	storage volume available to gas [m^3]
$Q_w(t)$	water inflow/outflow rate to/from tunnel [$\text{m}^3 \text{a}^{-1}$]
K	hydraulic conductivity of Opalinus Clay [m s^{-1}]
r	tunnel radius [m]
H	total tunnel length [m]
p	canister pitch (SF/HLW) [m]
ε_{ILW}	bulk porosity of ILW emplacement tunnel [-]
S_{ILW}	initial gas saturation of pore space in emplacement tunnel [-]
ε_{ben}	bentonite porosity [-]
S_{ben}	mean gas saturation of pore space in bentonite [-]
l_i	distance over which hydraulic gradient due to gas generation is non-zero [m]

ρ	density of water [kg m ⁻³]
g	gravitational acceleration [m s ⁻²]

$V_g(t)$ in (Eq. A1.9-2, ILW case) cannot be greater than the total pore volume in the tunnels, V_p . For $V_g(t) = V_p$, full water expulsion from the ILW tunnel is achieved. To simplify the numerical treatment, the surface over which porewater displacement takes place is assumed to be constant and equal to a quarter of the total ILW tunnel circumference (average between initially half saturated tunnels and fully dewatered tunnels).

The mass balance for gas contained in the free gas phase of the tunnel is expressed as:

$$\dot{n} = \begin{cases} \dot{n}_p - \dot{n}_{sol} - \dot{n}_{diff} & (P < P_s + P_a) \\ \dot{n}_p - \dot{n}_{sol} - \dot{n}_{diff} - \dot{n}_{leak} & (P_s + P_a < P < P_g) \end{cases} \quad (\text{A1.9-3})$$

where

\dot{n}	rate of change of gas contained in free gas phase [mol a ⁻¹]
\dot{n}_p	gas generation rate [mol a ⁻¹]
\dot{n}_{sol}	gas dissolution rate in near field porewater [mol a ⁻¹]
\dot{n}_{diff}	gas diffusion rate from tunnel walls into Opalinus Clay [mol a ⁻¹]
\dot{n}_{leak}	capillary leakage rate from tunnel walls into Opalinus Clay [mol a ⁻¹]

Note that in this chapter, the time derivative of a quantity n is denoted by a dot (\dot{n}). In Eq. A1.9-3, loss terms due to gas migration along the tunnel system are not taken into account, i.e. the plugs and sealing zones are assumed to be impermeable. In the case of ILW, the different terms in Eq. A1.9-3 are calculated in a one-dimensional approximation as follows (similar expressions are derived for SF/HLW, assuming that dissolution takes place in the tunnel backfill and assuming diffusion and capillary leakage to take place from the tunnel wall into the Opalinus Clay):

$$\dot{n}_{sol} = \frac{1}{4} \pi r^2 H \varepsilon_{ILW} \frac{C(P_0)}{P_0} \dot{P} \quad (\text{A1.9-4})$$

$$\dot{n}_{diff} = 2\pi r H \varepsilon_{OPA} D_p \frac{C(P_0)}{P_0} \frac{P}{l_d} \quad (\text{A1.9-5})$$

$$\dot{n}_{leak} = \frac{3}{2} \pi r H \frac{k_g}{\mu_g RT} \frac{P^2 - (P_s + P_a)^2}{2l_l} \quad (P > P_s + P_a) \quad (\text{A1.9-6})$$

ε_{OPA}	porosity of Opalinus Clay [-]
D_p	pore diffusion constant of Opalinus Clay (non-anions) [$\text{m}^2 \text{s}^{-1}$]
$C(P_0)$	hydrogen solubility at pressure $P_0 = 0.1 \text{ MPa}$ [mol m^{-3}]
l_d	distance over which gradient of dissolved gas concentration is maintained [m]
$k_g = k_a k_r$	gas permeability of Opalinus Clay (=intrinsic \times relative permeability) [m^2]
μ_g	dynamic viscosity of hydrogen gas [Pa s]
P_a	threshold pressure for capillary leakage into Opalinus Clay [Pa]

In Eq. A1.9-4, the volume of pore water in which gas dissolution takes place is assumed to be time-independent and corresponds to a quarter of the total pore space in the ILW emplacement tunnels (average between initially half saturated tunnels and fully dewatered tunnels). Similarly, the surface over which capillary leakage takes place is assumed to be constant and equal to three quarters of the total ILW tunnel circumference (Eq. A1.9-6). In contrast, gas diffusion (as dissolved gas) is assumed to occur across the entire surface of the emplacement tunnels.

Eqs. (A1.9-1) to (A1.9-6) are integrated numerically using a backward time-stepping procedure. The time-dependent gas generation rate for ILW has been fitted to the original data (Nagra 2003a) in the time period $10 \text{ a} < t < 10^4 \text{ a}$ using an exponential law and extrapolated beyond 10^4 a , under the condition that the total volume of gas generated is reproduced (see Fig. A1.9-3). For the time period $1 \text{ a} < t < 10 \text{ a}$, the original data is used in the calculations.

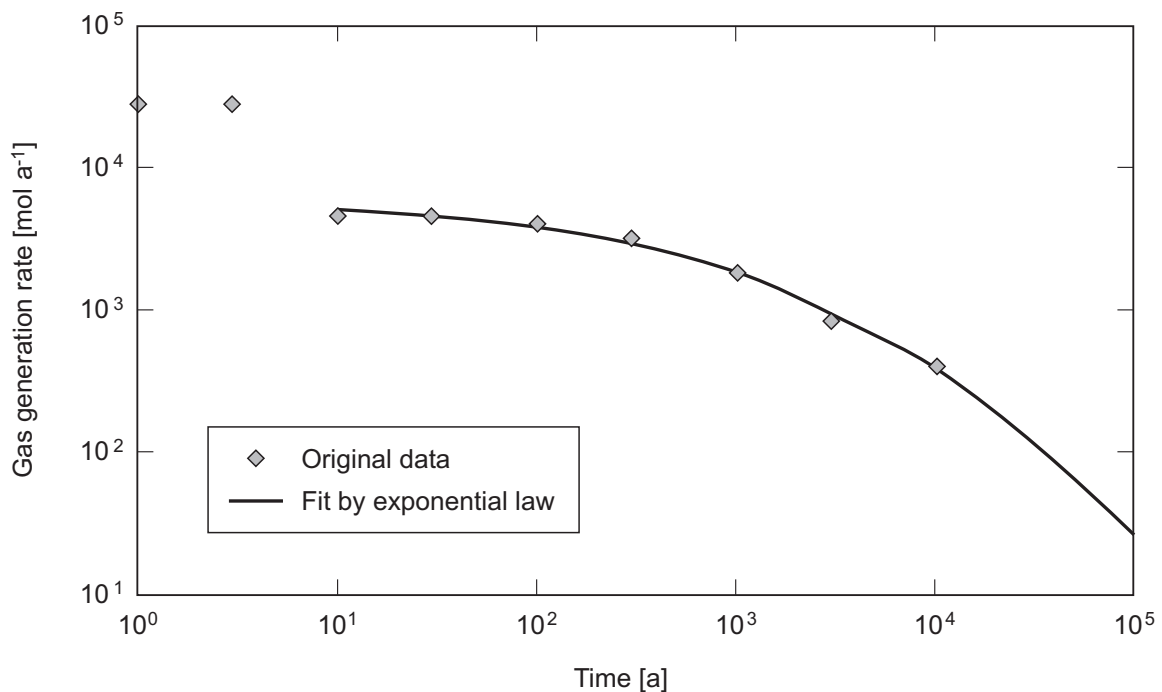


Fig. A1.9-3: Fit of time-dependent gas generation rate for ILW using an exponential law in the time period $10 \text{ a} < t < 10^5 \text{ a}$

Exponential law: $\exp[8.55 - 0.00217 (\log_e t)^{3.20}]$. Original data from Nagra (2003a).

Case with gas pressure equal to threshold pressure for dilatant gas pathway formation in Opalinus Clay ($P=P_g$):

Once the threshold pressure for dilatant gas pathway formation has been reached ($t = t_g$), the pressure is assumed to be constant, i.e. $P(t \geq t_g) = P_g$. For this situation, the governing equation is

$$\dot{V}_g(t) = n(t) \frac{RT}{P_g}; \quad t \geq t_g \quad (\text{A1.9-7})$$

with

$$\dot{V}_g(t) = \frac{\pi KrH}{2l_1 \rho g} (P_g - P_s) + 2wH\dot{L}(t) \quad (\text{ILW}) \quad (\text{A1.9-8})$$

$$\dot{V}_g(t) = 2wp\dot{L}(t) \quad (\text{SF / HLW})$$

$n(t)$ Mass of gas contained in free gas phase [mol]

$L(t)$ length (tunnel-to-tip) of effective dilatant gas pathway from top of tunnel into Opalinus Clay [m]

w effective aperture of representative dilatant gas pathway [m]

In Eq. A1.9-8 (ILW case), the first term is set to zero when full dewatering of the pore space in the ILW emplacement tunnels is achieved. In the case of SF/HLW, the length of gas pathways is limited, by geometrical consideration, to half of the separation between neighbouring emplacement tunnels. The effective aperture of the representative gas pathway, representing the gas storage volume provided by a network of microscopic dilatant gas pathways within the Opalinus Clay, including a zone of the Opalinus Clay matrix in which gas saturation is assumed to be in equilibrium with the nearby gas pathways, is calculated as follows:

$$w = W(\Delta\varepsilon + \varepsilon_{OPA}S_{OPA}) \quad (\text{A1.9-9})$$

w effective aperture of representative gas pathway [m]

W extent of gas saturated zone assumed to be in equilibrium with microscopic gas pathways [m]

$\Delta\varepsilon$ dilatancy of Opalinus Clay [-]

ε_{OPA} porosity of Opalinus Clay [-]

S_{OPA} gas accessible porosity fraction in Opalinus Clay [-].

The mass balance for gas contained in the free gas phase (tunnel + dilatant gas pathway) is:

$$\dot{n} = \dot{n}_p - \dot{n}_{sol} - \dot{n}_{diff} - \dot{n}_{leak} \quad (P = P_g) \quad (A1.9-10)$$

The leakage/diffusion rates from the ILW tunnels are calculated over the total available surface (tunnel walls + surface of dilatant gas pathway; for SF/HLW, similar expressions are derived):

$$\dot{n}_{sol} = 0 \quad (P = P_g)$$

$$\dot{n}_{diff} = (2\pi rH + 4LH)\varepsilon_{OPA}D_p \frac{C(P_0) P_g}{P_0 l_d} \quad (A1.9-11)$$

$$\dot{n}_{leak} = \left(\frac{3}{2}\pi rH + 4LH\right) \frac{k_g}{\mu_g RT} \frac{P_g^2 - (P_s + P_a)^2}{2l_1} \quad (A1.9-12)$$

Eqs. (A1.9-7) to (A1.9-12) are integrated numerically using a forward time-stepping procedure.

Accumulation of gas in the Wedelsandstein:

Gas flow into the Wedelsandstein is assumed to start as soon as 10 % of the gas accessible pore space in the Opalinus Clay is filled with gas (for the definition of gas accessible porosity, see Tab. A3.3-4e in Appendix 3). Mathematically, this is expressed as follows:

$$\frac{V_{cum}(t_w) - V_g(t_w)}{\varepsilon_{OPA} S_{OPA} V_{OPA}} = 0.1 \quad (\text{for SF/HLW and ILW, whichever is fulfilled first}) \quad (A1.9-13)$$

t_w	start of gas flow into the Wedelsandstein [a]
$V_{cum}(t)$	cumulated volume of gas generated until time t [$\text{m}^3 (P_g)$]
$V_g(t)$	gas storage volume, [m^3], created in near field (including gas pathways) until time t , calculated by Eq. A1.9-8
ε_{OPA}	porosity of Opalinus Clay [-]
S_{OPA}	gas accessible porosity fraction in Opalinus Clay [-]
V_{OPA}	$=H d_{sep} d_{OPA}$ is the bulk volume of Opalinus Clay, [m^3], spanned by the total emplacement tunnel length, H [m], tunnel separation, d_{sep} [m], and thickness of Opalinus Clay, d_{OPA} [m].

Alternatively, when gas migration takes place through the ramp/shaft or by way of a direct gas-filled pathway through the Opalinus Clay (see definition of cases 2.2 and 4.6, respectively, in Chapter 4 and Tab. A1.9-4), gas flow into the Wedelsandstein is hypothetically assumed to start immediately after the threshold pressure for the creation of dilatant gas pathways has been reached ($P=P_g$). In these cases, no network of dilatant gas pathways is created and no storage of gas is assumed to take place in the Opalinus Clay.

After gas breakthrough, gas accumulates in the Wedelsandstein above the repository and a free gas phase is assumed to develop radially. This gas phase is assumed to be fed from both the gas generated in the SF/HLW and ILW facility, at a rate equal to the total gas generation rate after the start of gas flow (“overflow” criterion according to Eq. A1.9-13). For constant pressure in the gas phase accumulated in the Wedelsandstein, P_w , the governing equation is

$$V_w(t) = n(t) \frac{RT}{P_w} \quad (\text{A1.9-14})$$

with

$$V_w(t) = \pi R_w^2(t) d_w \varepsilon_w S_w$$

$$P_w = P_{s,w} + P_{a,w}$$

P_w	gas pressure in Wedelsandstein [Pa]
$P_{s,w}$	pore pressure in Wedelsandstein [Pa]
$P_{a,w}$	gas entry pressure for horizontal gas migration in Wedelsandstein [Pa]
$V_w(t)$	volume of gas accumulated in Wedelsandstein [m ³]
$R_w(t)$	radius of gas accumulated in Wedelsandstein [m]
$d_w/\varepsilon_w/S_w$	thickness [m], gas accessible porosity [-] and gas saturation [-] of Wedelsandstein, respectively

The mass balance for the free gas phase in the Wedelsandstein is:

$$\dot{n} = \dot{n}_p - \dot{n}_{sol} - \dot{n}_{diff} - \dot{n}_{leak} \quad (P = P_w) \quad (\text{A1.9-15})$$

The capillary leakage rate from the gas volume accumulated in the Wedelsandstein is calculated over the available surface upwards only, whereas diffusion of dissolved gas is assumed to take place upwards and downwards (back into those areas of Opalinus Clay where gas solubility in the porewater has not been reached previously):

$$\dot{n}_{sol} = 0 \quad (P = P_w) \quad (\text{A1.9-16})$$

$$\dot{n}_{diff} = 2\pi R_w^2 \varepsilon_{cu} D_{p,cu} \frac{C(P_0)}{P_0} \frac{P_w}{l_{w,d}} \quad (\text{A1.9-17})$$

$$\dot{n}_{leak} = \begin{cases} \pi R_w^2 \frac{k_{g,cu}}{\mu_g RT} \frac{P_w^2 - (P_{s,cu} + P_{a,cu})^2}{2l_{cu,l}} & (P_w > P_{s,cu} + P_{a,cu}) \\ 0 & (P_w \leq P_{s,cu} + P_{a,cu}) \end{cases} \quad (\text{A1.9-18})$$

The quantities with the index *cu* are defined for the low-permeability upper confining units. Because P_w is always smaller than $P_{s,cu} + P_{a,cu}$ (see Section 4.2.3), no capillary leakage takes place from the Wedelsandstein through the low-permeability upper confining units. Eqs. (A1.9-14) to (A1.9-18) are integrated numerically using a forward time-stepping procedure.

A1.9.4 Dose due to volatile ^{14}C in the gas phase

A1.9.4.1 Conceptual model

The conceptual assumptions for the model calculations related to the release of volatile ^{14}C are as follows (see also Fig. A1.9-4):

- Dose calculations for the gaseous release are performed only for **organic ^{14}C in volatile form upon release**. Tritium (half-life 12.3 years) decays to insignificant levels before it is released from the near field. Volatile chemical compounds containing I, Cl and Se (e.g. I_2 , HI, CH_3I , etc.) immediately hydrolyse under reducing conditions, i.e. they are not transported in the gas phase (Nagra 2003a). Radioactive noble gases from chain decay (Rn) may contribute to the total dose if their precursor decays in the biosphere, but they are not long-lived enough to survive transport from the near-field to the biosphere.
- In spent fuel, ^{14}C exists as an activation product in the cladding and in the fuel matrix. The instant release fraction (IRF) is approximately 20 % for the cladding and 10 % for the fuel matrix. The remainder of ^{14}C is embedded in the Zircaloy and fuel matrix and will be congruently released at rates controlled by the **corrosion rate of the cladding** and the **dissolution rate of the fuel matrix**. It is pessimistically assumed that 100 % of the ^{14}C inventory in the cladding is released in the form of low molecular weight volatile organic compounds (methane, see Chapter 4). ^{14}C originating from the fuel matrix is inorganic and will not be transformed to volatile species. The calculations are based on 935 BWR UO_2 canisters, 450 mixed PWR canisters (3 UO_2 and 1 MOX fuel elements) and 680 PWR UO_2 canisters, all with a burnup of 48 GWd/t_{HM} (NPP operation of 60 years).
- No significant amounts of radionuclides that can form volatile species exist in HLW.
- In ILW, ^{14}C exists in Zircaloy hulls and ends (WA-BNF-4, WA-COG-4, see Chapter 4). The IRF of ^{14}C is 20 %, which corresponds to the radionuclides contained in the oxide layer. The remainder of ^{14}C is embedded in the Zircaloy matrix and will be congruently released by cladding corrosion. Some additional ^{14}C exists in WA-BNF-2 (MEB crud, barium carbonate slurry) in inorganic form, but will not be converted to volatile organic form at alkaline pH. It is pessimistically assumed that 100 % of the ^{14}C inventory in WA-BNF-4 and WA-COG-4 is released in the form of low molecular weight volatile organic compounds (methane).
- Gas generation takes place predominantly by anaerobic metal corrosion (hydrogen) and microbial degradation of organics (methane, carbon dioxide). For SF, the hydrogen gas generation rate lies in the range of 0.4 - 4 mol a^{-1} per canister, corresponding to anaerobic

steel corrosion rates of 0.1 - 1 $\mu\text{m a}^{-1}$. In the case of ILW, the gas generation rate is high in an initial phase ($t \leq 10$ years) and slowly decreases in the time domain $t > 10$ years, with time-dependent contributions from hydrogen and methane.

- The release of volatile ^{14}C from SF is assumed to start at the **time of occurrence of canister breaching** (10 000 a). All canisters are assumed to be breached simultaneously. For ILW, the times needed for waste package failure and near-field saturation are conservatively neglected. i.e. release of ^{14}C is assumed to start after the end of waste emplacement.
- Released volatile ^{14}C is assumed to be instantaneously mixed with non-radioactive gases in gas-filled pore space present in the near field (backfill), in and around dilatant gas pathways created in the Opalinus Clay (gas layer), in the access tunnel system and in the Wedel-sandstein formation. The spatial distribution and evolution of gas-filled pore space in the repository system is modelled in a simplified way by considering three characteristic calculational cases (Tab. A1.9-4). For each case, the gas release rate to the Malm aquifer is calculated separately, considering vertical gas diffusion through the low-permeability formations of the upper confining units (see Section A1.9.3), but neglecting horizontal transport of dissolved gas by advection and diffusion through the Wedelsandstein formation into the biosphere.
- Sorption of dissolved ^{14}C on the solid phase is neglected in all parts of the system.
- All gases (including all volatile radionuclides) released from the upper confining units are assumed to remain completely dissolved in the Malm aquifer and to be transported instantaneously to the reference biosphere area. There is further **dilution in the Quaternary aquifer** of the reference biosphere. No degassing and atmospheric dilution of these radionuclides is considered.
- Human exposure occurs by **ingestion of drinking water from the Quaternary aquifer** (see Fig. A1.9-4 and Fig. A1.9-5); no consideration of exposures by inhalation and external radiation). In all cases, the dose contribution of non-volatiles radionuclides is not taken into account.

Tab. A1.9-4: Pore space available for gas considered in the different assessment cases (numbering of cases according to Chapter 2)

Values for gas storage volumes are given in Chapter 4.Assessment case	Backfill	EDZ	Dilatant gas pathways in Opalinus Clay	Access Tunnels	Wedel-sandstein
Case 2.1 Release of volatile ^{14}C from SF and ILW in the gas phase not affected by ramp/shaft ("tight seals")	✓	✓	✓	-	✓
Case 2.2 Release of volatile ^{14}C from SF and ILW in the gas phase affected by ramp/shaft ("leaky seals")	✓	✓	-	✓	✓
Case 4.6 Unretarded transport of volatile ^{14}C from SF and ILW through host rock ("what if")	✓	✓	-	-	✓

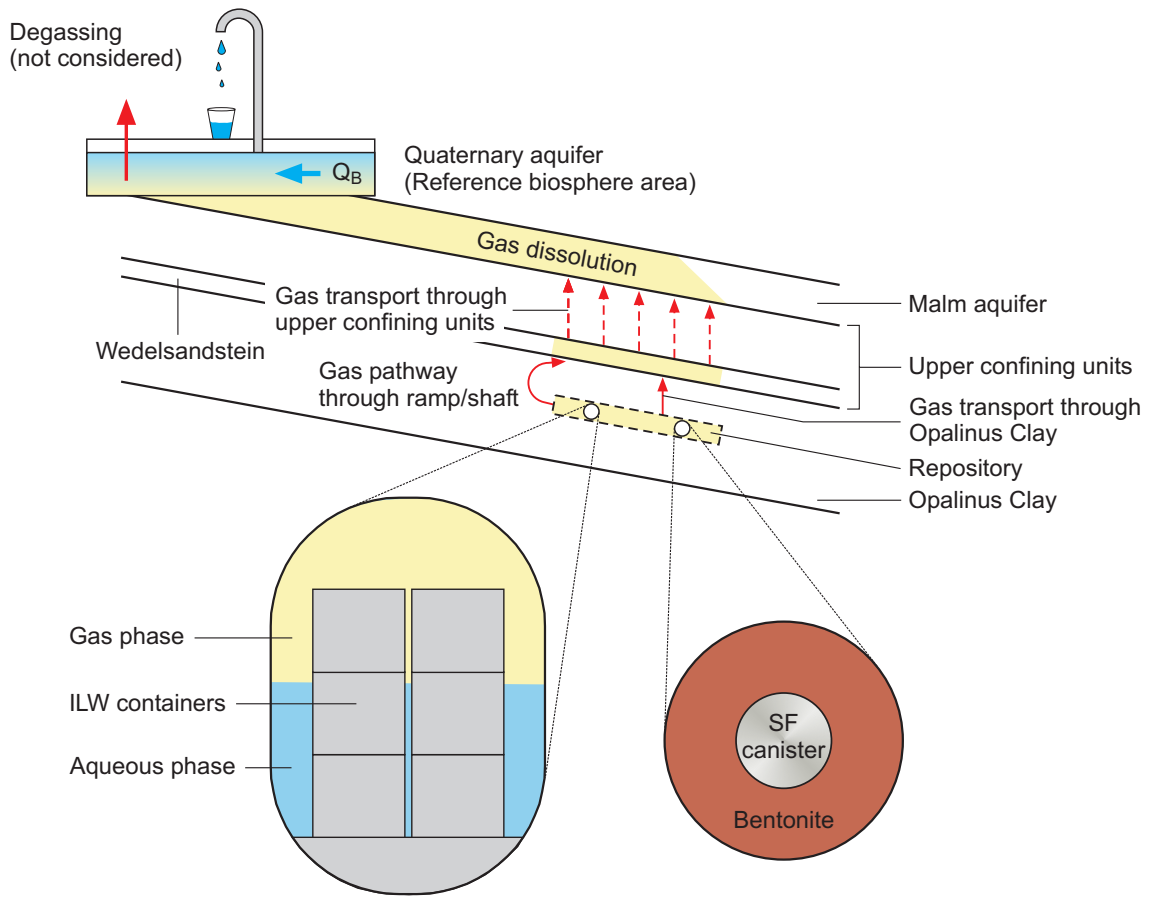


Fig. A1.9-4: Illustration of the conceptual model for the release of volatile ¹⁴C from the SF and ILW parts of the repository in Opalinus Clay

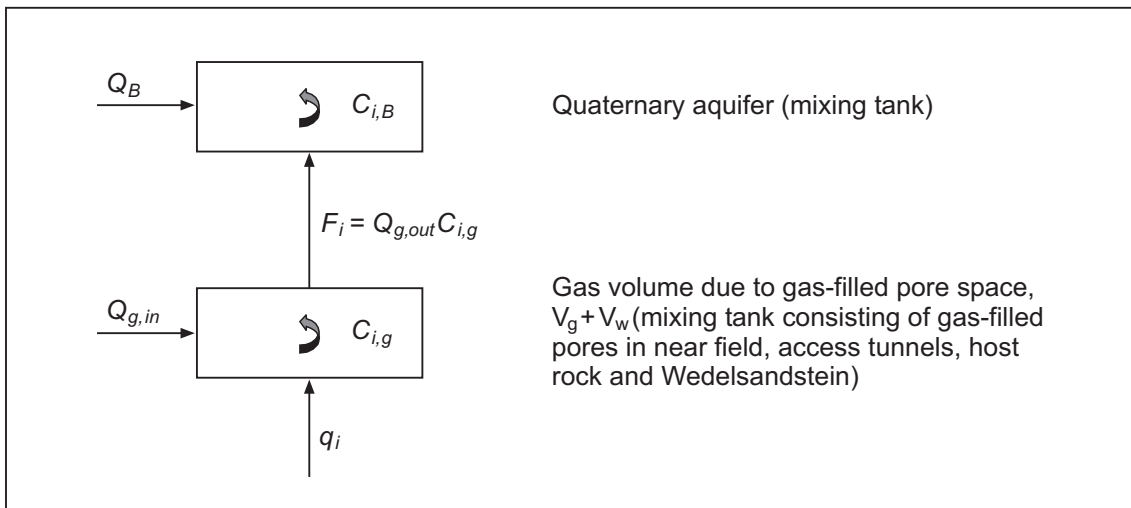


Fig. A1.9-5: Scheme of compartment model used for the calculation of the activity concentration in the gas phase and in the biosphere (Quaternary aquifer)

A1.9.4.2 Mathematical model

The activity concentrations in the gas phase in the available storage volume (consisting of gas-filled pore space in near field, Opalinus Clay, access tunnel system and Wedelsandstein) and in the aqueous phase in the Quaternary aquifer are calculated using a simple compartment model (Fig. A1.9-5). In the gas storage volume, the mobilised volatile radionuclide i enters at a rate q_i and is instantaneously mixed with non-radioactive gas generated by metal corrosion and microbial degradation at a rate $Q_{g,in}$ [$\text{m}^3 \text{a}^{-1}$].

The gaseous activity concentration of radionuclide i in the gas storage volume, $C_{i,g}$ [Bq m^{-3}], is governed by the equation

$$\frac{d}{dt}[C_{i,g}(V_g + V_w)] = q_i - \lambda_i(V_g + V_w)C_{i,g} - Q_{g,out}C_{i,g} \quad (t \geq t_0)$$

with

$$C_{i,g}(t_0) = \frac{I_i(t_0)IRF_i}{V_g(t_0) + V_w(t_0)}$$

$$q_i = q_i(t_0) \exp(-\lambda_i(t - t_0)) = \begin{cases} I_i(t_0) (F_{i,c} \frac{2r_c}{d_c} + F_{i,m}f) \exp(-\lambda_i(t - t_0)) & (SF) \\ I_i(t_0) F_{i,c} \frac{2r_c}{d_c} \exp(-\lambda_i(t - t_0)) & (ILW) \end{cases}$$

t_0	breaching time for SF canisters (for ILW $t_0 = 0$) [a]
V_g	gas storage volume in near field (including dilatant gas pathways) [m^3]
V_w	gas storage volume in Wedelsandstein [m^3]
$Q_{g,in}$	gas generation rate in near field [$\text{m}^3(\text{P}_w) \text{a}^{-1}$]
$Q_{g,out}$	gas flow rate from Wedelsandstein formation to Malm aquifer [$\text{m}^3(\text{P}_w) \text{a}^{-1}$]
P_w	gas pressure in Wedelsandstein [MPa]
q_i	activity release rate of volatile ^{14}C from waste [Bq a^{-1}]
I_i	inventory of volatile ^{14}C [Bq]
$F_{i,c}$	inventory fraction in cladding [-]
IRF_i	instant release fraction [-]
$F_{i,m}$	inventory fraction in SF matrix (= 0 in cases 2.1, 2.2, 4.6) [-]
f	fractional release rate from SF matrix (not used in cases 2.1, 2.2, 4.6) [a^{-1}]
r_c	corrosion rate of cladding [m a^{-1}]
d_c	thickness of cladding [m]
λ_i	decay constant of ^{14}C [a^{-1}]

From this equation:

$$(V_g + V_w) \frac{dC_{i,g}}{dt} + C_{i,g} \frac{d}{dt}(V_g + V_w) = q_i - \lambda_i (V_g + V_w) C_{i,g} - Q_{g,out} C_{i,g} \quad (t \geq t_0)$$

The second term on the left-hand side of this equation is assumed to be small compared to the first, and thus:

$$(V_g + V_w) \frac{dC_{i,g}}{dt} = q_i - \lambda_i (V_g + V_w) C_{i,g} - Q_{g,out} C_{i,g} \quad (t \geq t_0) \quad (\text{A1.9-19})$$

The consequences of this approximation are that the resulting solution (Eq. A1.9-22) errs on the side of conservatism. This is discussed in detail in Chapter 5 of Nagra (2003a).

For SF, no release of volatile radionuclides to the gas storage volume occurs before the canisters are breached, i.e. for $t < t_0$. In the case of ILW, t_0 is set to zero⁵⁰. Note that in Eq. A1.9-19, the gaseous activity concentration within the entire volume of the free gas phase ($V_g + V_w$) is assumed to be uniform, and the gas pressure is taken to be equal to the pressure in the Wedelsandstein, P_w . This simplification leads to a slightly overestimated gas release rate to the biosphere.

Furthermore, the gas storage volume provided by gas-filled pore space in the near field and by the pore space of the dilatant gas pathways in Opalinus Clay, V_g (Eqs. A1.9-2 and A1.9-8), and the gas storage volume within the Wedelsandstein, V_w (Eq. A1.9-14), are slowly varying with time, but are assumed to be step-wise constant in the present conceptualisation. The gas flow rate from the Wedelsandstein through the low-permeability formations of the upper confining units, $Q_{g,out}$ [$\text{m}^3(P_w) \text{a}^{-1}$], is governed by gas diffusion (diffusive flow of dissolved gas). This quantity depends on the gas generation rate and on transport properties in near field, Opalinus Clay and upper confining units, and is a time-dependent function (see Chapter 4). The analytical solution to Eq. A1.9-19 is:

$$C_{i,g} = \left(C_{i,g}(t_0) + \frac{q_i(t_0)}{V_g + V_w} \int_{t_0}^t dt' \exp\left(\frac{\bar{Q}_{g,out}(t')(t'-t_0)}{V_g + V_w}\right) \right) \exp\left(-\lambda_i(t-t_0) - \frac{\bar{Q}_{g,out}(t)(t-t_0)}{V_g + V_w}\right) \quad (t \geq t_0)$$

with

$$\bar{Q}_{g,out}(t) = \frac{1}{t-t_0} \int_{t_0}^t dt' Q_{g,out}(t')$$

⁵⁰ In the Reference Conceptualisation, the containment time for ILW (start of radionuclide dissolution) is assumed to be 100 years. In contrast to this treatment of dissolved radionuclides, here it is assumed that volatile radionuclides start to be mobilised right after the end of emplacement, in parallel with the onset of gas generation.

$\bar{Q}_{g,out}$ is a slowly varying function with time⁵¹. In this model it is treated as a step-wise constant quantity, to be applied both to SF and ILW. The simplified analytical solution may thus be written:

$$C_{i,g} = \left(C_{i,g}(t_0) \exp\left(-\frac{\bar{Q}_{g,out}}{V_g + V_w}(t - t_0)\right) + \frac{q_i(t_0)}{\bar{Q}_{g,out}} \left(1 - \exp\left(-\frac{\bar{Q}_{g,out}}{V_g + V_w}(t - t_0)\right)\right) \right) \times \exp(-\lambda_i(t - t_0)) \quad (t \geq t_0) \quad (\text{A1.9-20})$$

The aqueous activity concentration in the Quaternary aquifer, $C_{i,B}$ [Bq m⁻³], is governed by the equation

$$V_B \frac{dC_{i,B}}{dt} = F_i - \lambda_i V_B C_{i,B} - Q_B C_{i,B} \quad (t \geq t_0) \quad (\text{A1.9-21})$$

$$C_{i,B}(t_0) = 0$$

V_B pore volume of Quaternary aquifer [m³]

$F_i = Q_{g,out} C_{i,g}$ activity release rate into Quaternary aquifer [Bq a⁻¹]

Q_B dilution rate in Quaternary aquifer [m³ a⁻¹].

The analytical solution to Eqs. A1.9-20 and A1.9-21 is

$$C_{i,B} = \left(\frac{(C_{i,g}(t_0) \bar{Q}_{g,out} - q_i(t_0)) \exp\left(-\frac{\bar{Q}_{g,out}}{V_g + V_w}(t - t_0)\right) - \exp\left(-\frac{Q_B}{V_B}(t - t_0)\right)}{\left(\frac{Q_B}{V_B} - \frac{\bar{Q}_{g,out}}{V_g + V_w}\right) V_B} + \frac{q_i(t_0)}{Q_B} \left(1 - \exp\left(-\frac{Q_B}{V_B}(t - t_0)\right)\right) \right) \times \exp(-\lambda_i(t - t_0)) \quad (t \geq t_0) \quad (\text{A1.9-22})$$

⁵¹ In evaluating this function in the safety assessment calculations reported in Nagra (2002c), t_0 was set to zero not only for ILW, but also for SF. Subsequent calculations for SF taking $t_0 = 10\,000$ a showed that this simplification leads to an underestimate of the calculated dose maxima, for Case 2.1, of 23 %, 16 % and 13 % for Opalinus Clay gas permeabilities of 10^{-22} m², 10^{-23} m² and 0, respectively. For Case 2.2, the corresponding figures are 39 %, 37 % and 37 % and, for Case 4.6, 36 %, 33 % and 34 %.

Finally, the drinking water dose rate, D_i [mSv a⁻¹], is given by

$$D_i = C_{i,B} \delta_i U DF_i^{ing} \quad (\text{A1.9-23})$$

U drinking water consumption rate [m³ a⁻¹]

DF_i^{ing} dose coefficient for ingestion [mSv Bq⁻¹]

δ_i degassing factor (fraction of radionuclides not degassed into the atmosphere) [-]

A1.9.5 Input parameters

The parameters that are required for the Gas Model are listed in tables in Chapter 4.

A1.9.6 Verification

An independent code for solving the governing equations has been developed that confirms the adequacy of the Gas Model for the purpose of the present safety assessment (Smith 2003).

A1.10 Execution of model calculations with the Reference Model Chain

A1.10.1 Objectives and tools

In total, several hundred different deterministic model calculations were conducted to cope with the comprehensive list of scenarios, conceptualisations and parameter variations investigated in the framework of the Opalinus Clay safety assessment. Each assessment case is associated with a unique set of conceptual assumptions and input parameters (see Appendix 3), and is evaluated by means of separate "calculational cases" for each SF reference canister type (BWR-UO₂-48, PWR-UO₂-48, and PWR-MOX-48), for HLW and for each ILW waste group (ILW-1, ILW-2). Most of the calculations are performed using the Reference Model Chain (STMAN, PICNIC and TAME). For example, the Reference Case requires an STMAN near-field calculation to be carried out for each SF reference canister type, for HLW and for each ILW group. The STMAN calculations for SF, HLW and ILW each provide input to a PICNIC geosphere calculation. PICNIC in turn provides input to a TAME biosphere calculation.

The large number of calculational cases requires a system of operational elements and procedures which handles the calculations efficiently and meets all requirements regarding quality management (see Appendix 8). Furthermore, the procedures must be flexible enough to allow calculational cases to be revisited and modified if necessary.

The basic operational elements and procedures of the implemented system are:

- three Excel workbooks⁵², each consisting of:
 - a database to manage the raw data, references and data clearances in data tables;
 - a table of calculational cases to select the individual parameter sets which make up the input file(s) for a specific calculational case;
 - a pre-processor to automatically generate input files using the table of calculational cases and the database of raw data;
- a Job Starter, encompassing:
 - a graphical user interface to initiate calculations, to keep track of the current status of each calculation, to trace modifications in input files by communicating with the Revision Control System, and to create plots of key results;
 - a continuous record of all model calculations performed to log relevant information such as operator, date of calculation, as well as names, dates and version of input files, output files and computer codes.

An overview of this system is shown in Fig. A1.10-1. Detailed descriptions of these operational elements and procedures are provided in the following sections.

⁵² Excel file consisting of tables and programs (macros) written in Visual Basic for Applications.

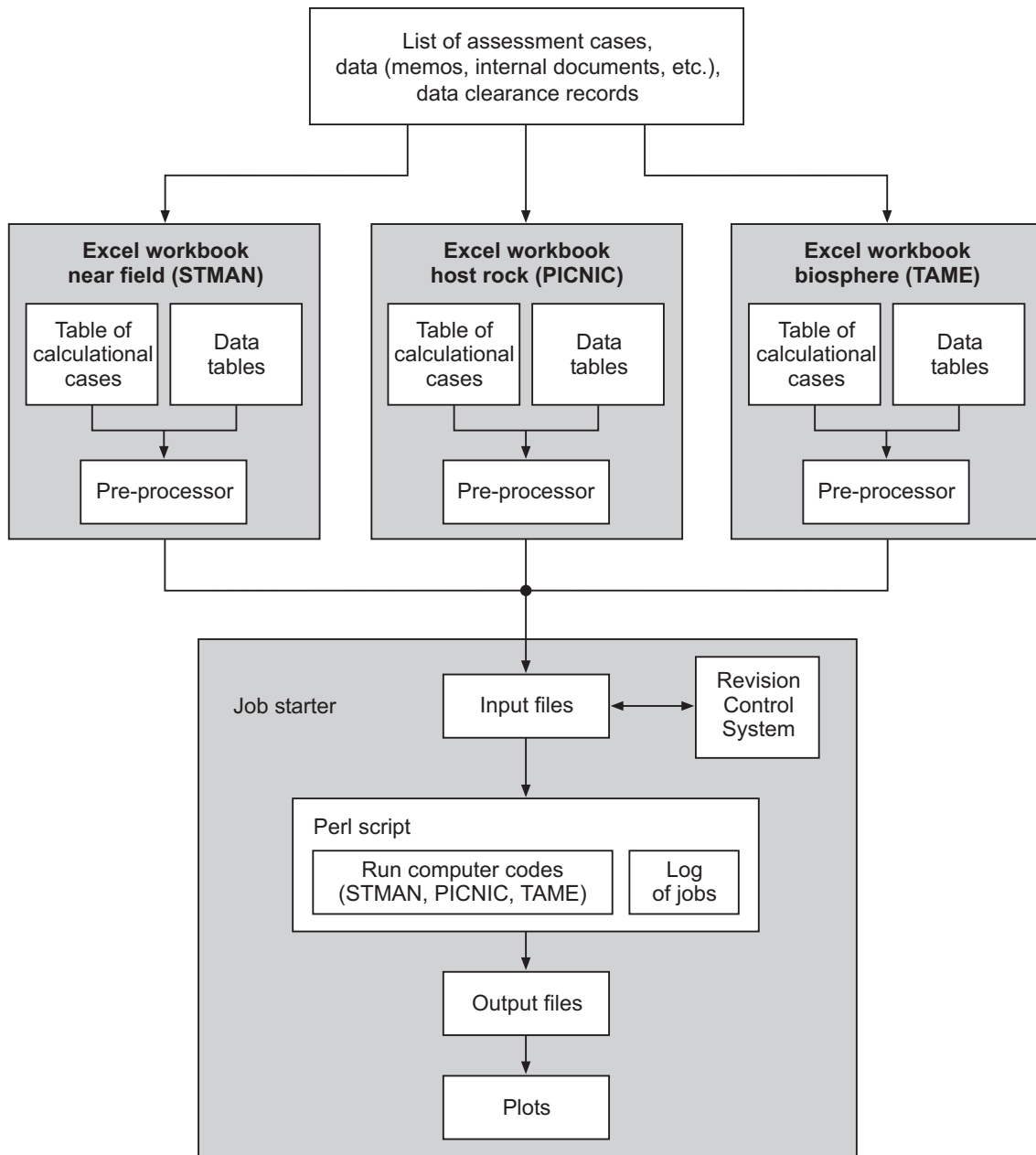


Fig. A1.10-1: Overview of the basic operational elements and procedures of the system implemented to run the model calculations with STMAN, PICNIC and TAME

A1.10.2 Excel workbooks

Three Excel workbooks were used, related to near field, geosphere and biosphere calculations. It should be noted that, in comparison to the alternative method of creating the input files manually with a text editor, the system based on Excel workbooks bears a significantly smaller risk of errors related to data handling.

A1.10.2.1 Excel workbook for near field calculations with STMAN

The Excel workbook is named opa0702_nah.xls. It consists of a table of calculational cases (called "cases") which is used for the definition of input parameters, and a series of data tables which make up the database of raw input data. Further, it contains a macro for the generation of input files.

Database of raw input data

The input files required by STMAN to perform a near field calculation are simple ASCII text files consisting of a series of sections or blocks. Each block starts with a unique title and ends with an end keyword. For example, the block enclosed in the keywords RELEASE and END holds release rates of radionuclides from the waste matrix and cladding as functions of time; the block enclosed by BUFFER_SOLUBILITY and END holds a list of elements present in the repository together with the solubility limit of the element in mol l⁻¹.

The raw input data required to construct such blocks of the input file are held in the data tables of the Excel workbook. For example, the table "release" (Fig. A1.10-2a) holds release rates for different spent fuel canister types and various chemical conditions as a function of time, all organised in separate columns. The column headers provide a short name to identify the type of data contained. Additional detail such as parameter units and the source of the data are found in cells below the header. Fig A1.10-2b shows an excerpt of the table "solubility" with the element-dependent solubility limits for various chemical conditions. Starting from line 6, the solubility limits for the elements are listed. The highlighted column in Fig. A1.10-2b shows the solubility limits in the SF / HLW bentonite buffer for the Reference Case. Similarly, there are tables for sorption constants, inventories, decay constants etc., corresponding to the data blocks of an STMAN input file.

	A	B	C
1	PMIX (Reference Values)	BUO/PUO (Reference values)	PMIX (10-fold fuel dissolution rate)
2	# Für Inventar SF-BE-2 (PWR-MOX/UO2)	# Für Inventar SF-BE1 (BUO) und SF-BE-3 (PUO)	# Für Inventar SF-BE-2 (PWR-MOX/UO2)
3	# AN 02-153, 04.07.02, Tab. 2, Sp. 1 & 3; t<1000a: Tab. 3; Tab. 1, Zeile 4	# AN 02-153, 04.07.02, Tab.2, Sp. 1 & 2, t<1000a: Tab. 3; Tab. 1, Zeile 4	# 10-fache Werte von AN 02-153, 04.07.02, Tab. 2, Sp. 1 & 3; t<1000a: Tab. 3; Tab. 1, Zeile 4
4	# Freigabe: EN/078/002	# Freigabe: EN/078/002	# Freigabe: EN/078/002
5	# Zeit [a], Matrix release rate [1/a], Cladding release rate [1/a]	# Zeit [a], Matrix release rate [1/a], Cladding release rate [1/a]	# Zeit [a], Matrix release rate [1/a], Cladding release rate [1/a]
6	RELEASE	RELEASE	RELEASE
7	START 1.00E-04 3.0E-5	START 1.00E-04 3.0E-5	START 1.00E-03 3.0E-5
8	5.00E+01 2.00E-05 3.0E-5	5.00E+01 2.00E-05 3.0E-5	5.00E+01 2.00E-04 3.00E-05
9	1.00E+02 1.50E-05 3.0E-5	1.00E+02 1.50E-05 3.0E-5	1.00E+02 1.50E-04 3.00E-05
10	2.00E+02 1.30E-05 3.0E-5	2.00E+02 1.30E-05 3.0E-5	2.00E+02 1.30E-04 3.00E-05
11	3.00E+02 9.30E-06 3.0E-5	3.00E+02 9.30E-06 3.0E-5	3.00E+02 9.30E-05 3.00E-05
12	5.00E+02 7.20E-06 3.0E-5	5.00E+02 7.20E-06 3.0E-5	5.00E+02 7.20E-05 3.00E-05
13	7.00E+02 5.30E-06 3.0E-5	7.00E+02 5.30E-06 3.0E-5	7.00E+02 5.30E-05 3.00E-05
14	1.00E+03 3.80E-06 3.0E-5	1.00E+03 2.40E-06 3.0E-5	1.00E+03 3.80E-05 3.00E-05
15	2.00E+03 2.00E-06 3.0E-5	2.00E+03 1.30E-06 3.0E-5	2.00E+03 2.00E-05 3.00E-05
16	3.00E+03 1.40E-06 3.0E-5	3.00E+03 8.90E-07 3.0E-5	3.00E+03 1.40E-05 3.00E-05
17	5.10E+03 1.00E-06 3.0E-5	5.10E+03 6.70E-07 3.0E-5	5.10E+03 1.00E-05 3.00E-05
18	7.60E+03 8.90E-07 3.0E-5	7.60E+03 5.90E-07 3.0E-5	7.60E+03 8.90E-06 3.00E-05
19	1.00E+04 7.90E-07 3.0E-5	1.00E+04 5.30E-07 3.0E-5	1.00E+04 7.90E-06 3.00E-05
20	1.50E+04 6.10E-07 3.0E-5	1.50E+04 4.20E-07 3.0E-5	1.50E+04 6.10E-06 3.00E-05

Fig. A1.10-2a: Table "release" listing release rates for two spent fuel canister types as a function of time

	A	C	D	E	F	G
1	# kurz:	SF/HLW (reference values)	SF/HLW (lower limit)	SF/HLW (upper limit)	SF/HLW (oxidising conditions)	ILV-1 (reference values)
2	# Werte:	Reference case solubility limits (reducing conditions) for bentonite near field of SF/HLW repository	Lower limit solubility limits (optimistic, reducing conditions) for bentonite near field of SF/HLW repository	Upper limit solubility limits (pessimistic, reducing conditions) for bentonite near field of SF/HLW repository	Solubility limits (oxidising conditions) for bentonite near field of SF/HLW repository	Reference case solubility limits cementitious near field of waste group II
3	# Einheit:	[mol L ⁻¹]	[mol L ⁻¹]	[mol L ⁻¹]	[mol L ⁻¹]	[mol L ⁻¹]
4	# Referenz:	AN 02-174, table 1, col 2	AN 02-174, table 1, col 3	AN 02-174, table 1, col 4	AN 02-174, table 1, col 5	AN 02-174, table 1, col 2
5	# Freigabe:	EN/072/005	EN/072/005	EN/072/005	EN/072/005	EN/072/005
6	Ac	1.00E-06	5.00E-08	3.00E-05	1.00E-06	2.00E-06
7	Ag	3.00E-06	1.00E-10	3.00E-06	3.00E-06	-
8	Am	1.00E-06	5.00E-08	3.00E-05	1.00E-06	2.00E-09
9	Be	1.00E-06	1.00E-06	-1	1.00E-06	-
10	C	3.00E-03	6.00E-04	7.00E-03	3.00E-03	2.00E-04
11	Ca	1.00E-02	1.00E-02	1.00E-02	1.00E-02	-
12	CH	-1	-1	-1	-1.00E+00	-1
13	Cl	-1	-1	-1	-1.00E+00	-1
14	Cm	1.00E-06	5.00E-08	3.00E-05	1.00E-06	2.00E-09
15	Co	-	-	-	-	7.00E-07
16	Cs	-1	-1	-1	-1.00E+00	-1
17	Eu	-	-	-	-	2.00E-06
18	H	-1	-1	-1	-1.00E+00	-1
19	Ho	5.00E-07	3.00E-07	9.00E-07	5.00E-07	-
20	I	-1	-1	-1	-1.00E+00	-1
21	Mo	1.00E-06	1.00E-06	1.00E-05	1.00E-06	3.00E-05
22	Nb	3.00E-05	1.00E-08	1.00E-04	3.00E-05	-1
23	Ni	3.00E-05	1.00E-05	8.00E-05	3.00E-05	3.00E-07

Fig. A1.10-2b: Table "solubility" listing element-dependent solubility limits for various chemical conditions

Note: The element CH denotes organic carbon, a value of -1 denotes unlimited solubility, and a hyphen means no value available.

Definition of calculational cases

The table of calculational cases, termed "cases", is used to define the set of input parameters for each calculational case and to generate the input files for STMAN. Each row of the table holds all data and links required to create a complete input file for one calculational case. Fig. A1.10-3 shows an excerpt of the table "cases". Columns D to L are used to input basic data required to uniquely identify a calculational case, e.g. the type of inventory (SF), canister type (BUO), code and option used for calculation (STMAN, SPENT), as well as other supplementary information. The case name in Column A (e.g. S01-BUO) is constructed automatically with an Excel command connecting text elements (=VERKETTEN(...)), based on a pre-defined naming convention for input files. Similar commands are used to construct the name of the input file and the title of the calculational case as it appears on the output plots. The text elements are taken primarily from cells in the same row of the table, thereby guaranteeing consistency between file names, titles and input data.

CaseName	ProjectDirectory	Inventory	Number	Abfalltyp	Description	Code	Code-Option	Other	BaseDirectory	Inputfile	Outputfile	TITEL
S01-BUO	opa0702	SF	01	BUO	Reference Case SF: BE-1 (BvR-UO2)	Stman	SPENT	Vd+2E-14	fgsafoa0702nahf/SI/	fgsafoa0702nahf/SI/data/S01-BUO.prb	fgsafoa0702nahf/SI/resu/S01-BUO.*	ID=S01-BUO, Projekt=OPA0702, Nahfeldrechenfall: SF-01, Abfalltyp=BUO, Vd+2E-14, Code=STMAN, CodeOption=SPENT
S01-PMIX	opa0702	SF	01	PMIX	Reference Case SF: BE-2 (PVR-MOX/UO2)	Stman	SPENT	Vd+2E-14	fgsafoa0702nahf/SI/	fgsafoa0702nahf/SI/data/S01-PMIX.prb	fgsafoa0702nahf/SI/resu/S01-PMIX.*	ID=S01-PMIX, Projekt=OPA0702, Nahfeldrechenfall: SF-01, Abfalltyp=PMIX, Vd+2E-14, Code=STMAN, CodeOption=SPENT
S01-PUO	opa0702	SF	01	PUO	Reference Case SF: BE-3 (PVR-UO2)	Stman	SPENT	Vd+2E-14	fgsafoa0702nahf/SI/	fgsafoa0702nahf/SI/data/S01-PUO.prb	fgsafoa0702nahf/SI/resu/S01-PUO.*	ID=S01-PUO, Projekt=OPA0702, Nahfeldrechenfall: SF-01, Abfalltyp=PUO, Vd+2E-14, Code=STMAN, CodeOption=SPENT
S02a-BUO	opa0702	SF	02a	BUO	Comparison of different canister loadings: PVR-UO2-48	Stman	SPENT	Vd+2E-14	fgsafoa0702nahf/SI/	fgsafoa0702nahf/SI/data/S02a-BUO.prb	fgsafoa0702nahf/SI/resu/S02a-BUO.*	ID=S02a-BUO, Projekt=OPA0702, Nahfeldrechenfall: SF-02a, Abfalltyp=BUO, Vd+2E-14, Code=STMAN, CodeOption=SPENT
S02b-PUO	opa0702	SF	02b	PUO	Comparison of different canister loadings: PVR-UO2-48	Stman	SPENT	Vd+2E-14	fgsafoa0702nahf/SI/	fgsafoa0702nahf/SI/data/S02b-PUO.prb	fgsafoa0702nahf/SI/resu/S02b-PUO.*	ID=S02b-PUO, Projekt=OPA0702, Nahfeldrechenfall: SF-02b, Abfalltyp=PUO, Vd+2E-14, Code=STMAN, CodeOption=SPENT
S02c-PMIX	opa0702	SF	02c	PMIX	Comparison of different canister loadings: PVR-mixed-48	Stman	SPENT	Vd+2E-14	fgsafoa0702nahf/SI/	fgsafoa0702nahf/SI/data/S02c-PMIX.prb	fgsafoa0702nahf/SI/resu/S02c-PMIX.*	ID=S02c-PMIX, Projekt=OPA0702, Nahfeldrechenfall: SF-02c, Abfalltyp=PMIX, Vd+2E-14, Code=STMAN, CodeOption=SPENT

Fig. A1.10-3: Excerpt of table "cases"

This section of the table illustrates the definition of the names of individual calculational cases. Note: The cell content is automatically set in bold font if it differs from the corresponding cell content in the reference case "S01-BUO".

Fig. A1.10-4 shows a different section of the same table "cases", defining the parameter sets for the various blocks of an input file. Instead of containing single data values, these cells contain links to specific data tables and columns as required to define any particular calculational case. Each link has the structure *tablename column header*, i.e. the name of the data table referenced, followed by two colons, followed by the header of a specific column in that data table. For example, for the calculational case S01-BUO (row 4) the reference "solubility SF/HLW (reference values)" is a link to the column labelled "SF/HLW (reference values)" in data table "solubility" (see Fig. A1.10-2b).

CaseName	RESERVOIR_SOLUBILITY	CEMENT_SORPTION	BUFFER_SOLUBILITY	BUFFER_SORP	BUFFER_DIFFUSION	BUFFER_POROSITY_FACTOR	OUTER_BUFFER_SOLUBILITY	OUTER_BUFFER_POROSITY_FACTOR
S01-BUO	solubility:SF/HLW (reference values)		solubility:SF/HLW (reference values)	sorption:Bentonite (reference values for SF/HLW)	diffusion:Bentonite (reference values for SF/HLW)	porosity:Bentonite (reference values for SF/HLW)		
S01-PMIX	solubility:SF/HLW (reference values)		solubility:SF/HLW (reference values)	sorption:Bentonite (reference values for SF/HLW)	diffusion:Bentonite (reference values for SF/HLW)	porosity:Bentonite (reference values for SF/HLW)		
S01-PUO	solubility:SF/HLW (reference values)		solubility:SF/HLW (reference values)	sorption:Bentonite (reference values for SF/HLW)	diffusion:Bentonite (reference values for SF/HLW)	porosity:Bentonite (reference values for SF/HLW)		
S02a-BUO	solubility:SF/HLW (reference values)		solubility:SF/HLW (reference values)	sorption:Bentonite (reference values for SF/HLW)	diffusion:Bentonite (reference values for SF/HLW)	porosity:Bentonite (reference values for SF/HLW)		
S02b-PUO	solubility:SF/HLW (reference values)		solubility:SF/HLW (reference values)	sorption:Bentonite (reference values for SF/HLW)	diffusion:Bentonite (reference values for SF/HLW)	porosity:Bentonite (reference values for SF/HLW)		
S02c-PMIX	solubility:SF/HLW (reference values)		solubility:SF/HLW (reference values)	sorption:Bentonite (reference values for SF/HLW)	diffusion:Bentonite (reference values for SF/HLW)	porosity:Bentonite (reference values for SF/HLW)		

Fig. A1.10-4: Excerpt of the table "cases" showing links to certain columns in the data tables as required for the creation of input files

For example, the solubility limits provided in the block BUFFER_SOLUBILITY of case S01-BUO are taken from the column labelled "SF/HLW (reference values)" in data table "solubility" (see Fig. A1.10-2b).

Generation of input files

In addition to data tables, the Excel workbook opa0702_nah.xls also incorporates a macro, i.e. a program written in the MS office programming language Visual Basic for Applications used for the generation of input files for STMAN. The macro runs only in the table of calculational cases where its execution is initiated by selecting any cell in the row of a particular calculational case and then clicking on the red button labelled "Make Input" in the upper left hand corner of the table.

The macro starts by creating a new file with the name and directory path specified in the column entitled "Inputfile" and writing introductory identifier lines and the title of the calculational case. The macro continues by writing a series of blocks, each consisting of the contents of the referenced column in one of the data tables. The first block written into the input file is the block DECAY. From that block the macro extracts a list of safety-relevant elements or nuclides which is used subsequently to create other blocks with element- or nuclide-dependent data.

For QA purposes, the macro also conducts consistency checks and communicates the results, if inconsistencies are detected. For example, in the course of creating the block BUFFER_SOLUBILITY for the Reference Case of spent fuel (S01-BUO), an error message is prompted in case there is one or more radionuclides in the DECAY block for which no data are available in column "SF/HLW (reference values)" of table "solubility".

A1.10.2.2 Excel workbook for geosphere calculations with PICNIC

The Excel workbook named opa0702_geo.xls has a similar structure as the workbook for near field calculations. It contains several data tables making up the database of raw input data. A main difference with respect to STMAN stems from the fact that PICNIC models a network of one-dimensional transport legs whose structure depends on the problem to be solved. To retain clarity and simplicity despite the varying degree of complexity of the investigated networks, the workbook for geosphere calculations relies on several tables of calculational cases, namely GeoCases, Geo1e2Cases, Geo3Cases and TunCases, and an additional table called "Vorlage" with templates of PICNIC input files (see Fig. A1.10-6). The data tables with element-dependent information are similar to those described above. A macro is also incorporated which functions in all tables of calculational cases to automatically generate the input files for PICNIC.

Database of raw input data

The Excel workbook contains data tables with element-dependent raw input data, e.g. table "sorption" or table "diffusion". The structure of those tables is identical to those used in the Excel workbook for near field calculations with STMAN.

Database of templates for PICNIC input files

The table named "Vorlage" contains different templates of the PICNIC input files (see Fig. A1.10-5). The differences between templates are related to differences in the structural network of transport legs. A PICNIC template looks just like a normal PICNIC input file, except that it contains a number of special tags instead of parameter values. The general format of these tags is ">columnheader<", i.e. the symbol ">", followed by the header of a column in the table of calculational cases in which that particular template is called up, followed by the symbol "<". These tags are eventually replaced with single parameter values or series of data values when the macro for the generation of an input file is executed. As the tags are replaced with appropriate data contents, a single template may be used to generate several different input files. This process is discussed below.

1	Geo1	LMA_Geo1	Geot1	Ge
2	#PICNIC Case File	#PICNIC Case File	#PICNIC Case File	#F
3	VERSION V2.3	VERSION V2.3	VERSION V2.3	VE
4	TITLE	TITLE	TITLE	TI
5	>TITEL<	>TITEL<	>TITEL<	>T
6	END	END	END	EA
7	# \$Header\$	# \$Header\$	# \$Header\$	# \$
8	# moreinfo: >Description<	# moreinfo: >Description<	# moreinfo: >Description<	# \$
9			# AN 02-151, Variante A2, Fig. 6.5-1, Tab. 3.4-4b, 3.07.2002	# /
10	>DECAYS<	>DECAYS<	# Freigabe: ENJ088/001	# F
11				
12	CONTROLS	CONTROLS	>DECAYS<	>E
13	CALCULATE-FLOWS	CALCULATE-FLOWS	CONTROLS	
14	NPDEC 40	NPDEC 40	NPDEC 40	CC
15	TRSTRT 0.1	TRSTRT 0.1	TRSTRT 0.1	N
16	NTALB 33	NTALB 33	NTALB 33	TI
17	ANU 15	ANU 15	NTALB 33	N
18	SIGMA 0	SIGMA 0	ANU 15	A
19	REFINE 0	REFINE 0	SIGMA 0	SI
20	END	END	REFINE 0	R
21			END	EA
22				
23	# Leg Data	# Leg Data	# Leg Data	# L
24			# AN 02-151, Tab. 3.4-4b	# /
25	LEG Opa	LEG OpaLma1	# Freigabe: ENJ088/001	# F
26	# AN 02-151, Tab. 3.4-4a	# AN 02-151, Tab. 3.4-4a		
27	# Freigabe: ENJ088/001	# Freigabe: ENJ088/001	LEG OpaGest	LE
28	FROM Repository	FROM RepositoryLma1	FROM Repository	F
29	TO IfaceGeoBio	TO IfaceGeoBio	TO IfaceGeoBio	T
30	# in [m]	# in [m]	# in [m]	II
31	LENGTH> Path.Length<	LENGTH> Path.Length<	LENGTH 200	L
32	# CSA: Anzahl Tunnel x Laenge x Abstand, in [m2]	# CSA: Anzahl Tunnel x Laenge x Abstand, in [m2]	# CSA spielt keine Rolle, da Randbedingung = Nuklidfluss, in [m2]	# C
33	# CSA spielt jedoch keine Rolle, da Randbedingung = Nuklidfluss	# CSA spielt jedoch keine Rolle, da Randbedingung = Nuklidfluss	CSA 1	C
34	CSA > CSA<	REFINE 0	DARCY-VELOCITY & 3.115E-07	# II
35	HYDRAULIC-CONDUCTIVITY > HydraulicConductivity<	HYDRAULIC-CONDUCTIVITY > HydraulicConductivity<	ROCK-TYPE Opalinuston	C
36	ROCK-TYPE Opalinuston	ROCK-TYPE Opalinuston	BC-TYPE Zero-Concentration	F
37	BC-TYPE Zero-Concentration	BC-TYPE Zero-Concentration	# Default wert	E
38	# Default wert	# Default wert	# Freigabe: ENJ095/001	# C
39	# Freigabe: ENJ095/001	# Freigabe: ENJ095/001	PECLET > Peolet<	# F
40	PECLET > Peolet<	PECLET > Peolet<	EFFECTIVE-DIFFUSION > Effective_Diffusion<	F
41	EFFECTIVE-DIFFUSION > Effective_Diffusion<	EFFECTIVE-DIFFUSION > Effective_Diffusion<	END	E
42	END	END	LEG OpaGest	EA
43		LEG OpaLma2		LE
44		# AN 02-151, Tab. 3.4-4a	# AN 02-151, Tab. 3.4-4b	F
45		# Freigabe: ENJ088/001	# Freigabe: ENJ088/001	T
46		FROM RepositoryLma2	FROM Repository	# II

Fig. A1.10-5: Section of table "Vorlage" with excerpts of templates for PICNIC input files
 The tags in bold font enclosed in ">" and "<" are references to specific columns in one of the tables of calculational cases (see Fig. A1.10-7).

Definition of calculational cases

As discussed above, the Excel workbook contains several tables of calculational cases, i.e. GeoCases, Geo1e2Cases, Geo3Cases and TunCases. Each table defines all the parameters required for the creation of PICNIC input files for calculational cases of a particular group of scenarios. The table "TunCases", for example, contains calculational cases related to the release of radionuclides affected by the ramp/shaft. Fig. A1.10-6 shows the leftmost section of the "GeoCases" table of calculational cases with general project information, an identifier of model geometry, information on the near field calculational cases which enter the PICNIC input files as source terms, as well as the template to be used (column R "VORLAGE").

Case	Projekt	Geometrie	Rechenfall	Inventarklass	Inventarnucl1	Inventarnucl2	Inventarnucl3	MakridRechenfallnr	Description	Code	Diber	BaseDirecto	Inputfile	Outputfile	VORLAGE	TITEL
G01a_S01	opa0702	01	a	S	BUO	PMIX	PUO	01	Reference Case	picnic	Vd:2E-14	IgsaIopa0702IgeoI01SIdataIa_S01.in	IgsaIopa0702IgeoI01SIdataIa_S01.out	Vorlage::Geo1	ID: G01 Vd: 2E Geosp Code:	
G01a_H01	opa0702	01	a	H	BNFL	COG		01	Reference Case	picnic	Vd:2E-14	IgsaIopa0702IgeoI01HIdataIa_H01.in	IgsaIopa0702IgeoI01HIdataIa_H01.out	Vorlage::Geo1	ID: G1 Proje Geos; 01a, C	
G01a_I01	opa0702	01	a	I	ILV1	ILV2		01	Reference Case	picnic	Vd:2E-14	IgsaIopa0702IgeoI01IIdataIa_I01.in	IgsaIopa0702IgeoI01IIdataIa_I01.out	Vorlage::LMA_Geo1	ID: G1 Proje Geos; 01a, C	

Fig. A1.10-6: Excerpt of the "GeoCases" table of calculational cases showing a matrix of cases (rows) and parameters (columns)

In this part of the table the case names are defined.

Generation of input files

A macro contained in the Excel workbook is used to create the PICNIC input files. It is started by selecting any cell in the row defining a particular case in any one of the tables of calculational cases and pressing the red button labelled "Make Input" in the upper left hand corner of that table.

The macro starts by creating a new file with the name and directory path specified in the column entitled "Inputfile". Then the macro reads the template referenced under "VORLAGE" one line at a time and writes it into the new file. When the macro finds a line containing a tag of the format ">columnheader<", it analyses the content of the cell under that column header in the table of calculational cases. Depending on the content of the cell, the macro starts one of the following actions:

- If the cell content has the format "tablename columnheader", the tag is replaced by radionuclide-dependent data. For example, "diffusion Opalinus Clay (reference values)" is replaced by data found in column "Opalinus Clay (reference values)" of table "diffusion".
- In all other cases, the tag is directly replaced by the cell content. For example, the value "7.04E+5" replaces the tag ">CSA<" when creating the case G01a_S01 (see Fig. A1.10-7).

When processing the tag ">DECAYS<" the DECAYS block of the PICNIC file is created by inserting the referenced column of the table "decays". From this a list of safety-relevant radionuclides is created for later use in the generation of other blocks with radionuclide-dependent data.

Case	VORLAGE	TITEL	DECAYS	CSA	uity	Hydraulic Conductivity	Path Length	Head	Peck	Effective Diffusion	Porosity Factor	Kd
G01a_S01	Vorlage::Geo1	ID=G01a_S01, Projekt=OPA0702, Vd=2E-14, Geosphaerenrechenfall=GEO-01a, Code=PICNIC	decays::SF-HLV-ILV	7.04E+05	6.31E-07	40	40	10	diffusion::Opalinus clay (reference values)	porosityfactor::Opalinus clay (reference values)	sorption::Opalinus clay (reference values)	
G01a_H01	Vorlage::Geo1	ID=G01a_H01, Projekt=OPA0702, Vd=2E-14, Geosphaerenrechenfall=GEO-01a, Code=PICNIC	decays::SF-HLV-ILV	160000	6.31E-07	40	40	10	diffusion::Opalinus clay (reference values)	porosityfactor::Opalinus clay (reference values)	sorption::Opalinus clay (reference values)	
G01a_I01	Vorlage::LMA_Geo1	ID=G01a_I01, Projekt=OPA0702, Vd=2E-14, Geosphaerenrechenfall=GEO-01a, Code=PICNIC	decays::SF-HLV-ILV		6.31E-07	40	40	10	diffusion::Opalinus clay (reference values)	porosityfactor::Opalinus clay (reference values)	sorption::Opalinus clay (reference values)	

Fig. A1.10-7: Excerpt of the "GeoCases" table of calculational cases showing a matrix of cases (rows) and parameters (columns)

The parameter values of individual cases defined here are used by the template to create the input file. For example, when creating the input file of case "G01a_S01", the highlighted value 7.04E+05 in column "CSA" replaces the tag ">CSA<" for cross-sectional area in the template "Geo1" of table "VORLAGE" (see Fig. A1.10-5).

A1.10.2.3 Excel workbook for biosphere calculations with TAME

The biosphere model TAME (version 3c) is a package including the computer codes make_nuc, tameexec, siemexec and doseexec. These codes are run in series, controlled by the perl script tsd_3c.pl. The inputs required for the perl script are the following:

- Names of files containing parameters which define a particular biosphere model. The file name extensions are *.bio, *.bal, *.int, *.sol, *.dse and *.rel where the wildcard * substitutes for a unique name of a biosphere scenario. For example, the file "rspd.bio" holds biosphere parameters for the reference scenario for present day climate. Other data common to all scenarios, such as the decay constants, are stored in other files.
- The name of a file containing radionuclide-dependent release rates for the above defined biosphere, i.e. an output file from calculations performed with PICNIC or STMAN.

The Excel workbook named opa0702_bio.xls is structured and handled similarly to the workbooks for near field and geosphere calculations.

Definition of calculational cases

The parameters required to create an input file for the perl script tsd_3c.pl are listed in the table of calculational cases "tamecases" (Fig. A1.10-8). Input is provided in columns D to M. The contents of column A and columns N to S are generated automatically with Excel commands based on the data entered in columns D to M.

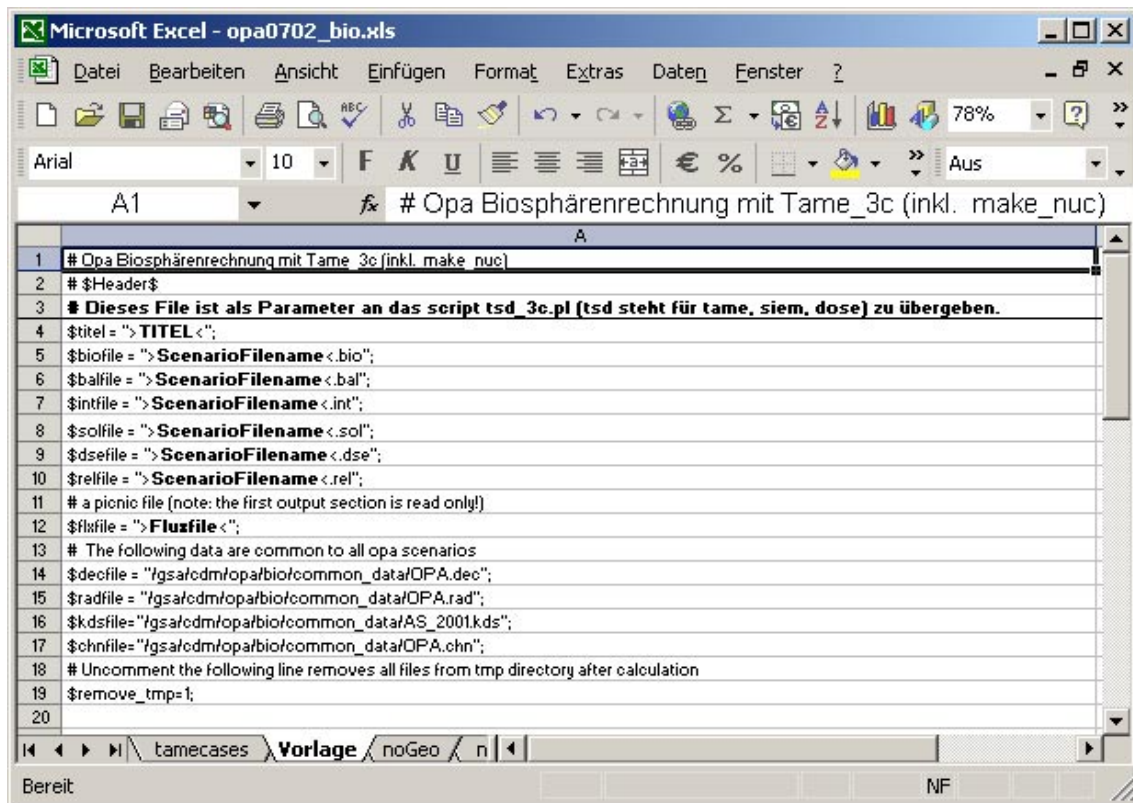


Fig. A1.10-9: Table "Vorlage" is used to create the input file required to run TAME 3c

Any tags of the format ">columnheader<" are replaced by the corresponding cell content in the table "tamecases".

A1.10.3 Job Starter

The computer codes STMAN, PICNIC and TAME are program codes designed to be started on the command line. For example, the command:

```
>STMAN SPENT S01-BUO.prb
```

starts the program STMAN with the option SPENT and the input file S01-BUO.prb. Similar commands start PICNIC and TAME.

The program code Job Starter is a graphical user interface (GUI) initiating the execution of the program codes STMAN, PICNIC and TAME with specified input files. At the same time, Job Starter provides information about the available input files and their status. To start a job or retrieve such information, one first selects one of the codes STMAN, PICNIC or TAME at the top of the main window of Job Starter (Fig. A1.10-10). The next two input fields are used to select a directory in which file names may be searched for a specified character pattern. Job Starter then searches for input files corresponding to the selected program code in the specified directory and all its subdirectories and displays the input files matching the specified character pattern. As an example, Fig. A1.10-10 shows the STMAN input files of the Reference Case as searched for with the pattern "S01-". The displayed information on the input files and the available operations activated by the buttons on the right hand side are as follows:

- The window within the scroll bars provides the complete name as well as information on the revision status of the input files matching the prescribed character pattern. For example, "/gsa/opa0702/nah/S/data/S01-BUO.prb v 1.13" is revision 1.13 of that specific input file (see section on Revision Control System below).
- The colour of the switch to the left of the file name indicates whether the file will be submitted for (re-)calculation with the computer code selected at the top of the window when the button "Submit" is pressed. Red means yes, gray means no.
- By pressing the "Refresh" button, all switches are set automatically. The switch is set to red if there is no matching output file or if at least one of the input files is younger than the output file.
- The first line below the name of the input file indicates whether the latest modification to the file involved either a change in data and possibly comment lines ("Letzte Änderung: Daten (und Kommentare) modifiziert"), or a change in the comment lines only ("Letzte Änderung: Kommentare modifiziert"). In the latter case, no re-calculation is required and the switch will not automatically be set to red upon pushing the button "refresh". However, if modifications in the data have occurred, any differences with respect to the previous version are displayed along with an input field for a mandatory entry into the log file and a button labelled "ci" (check in). The comment entered into this field reflects the reason for and / or the type of the modifications made in the input file. Pressing the check in button registers the modification in the Revision Control System (see Section A1.10.3.1).
- All switches to the left of the file names can also be set manually. The button "Select all" sets all switches in the window to red. In other words, all input files will be (re-)calculated when the button "Submit" is pressed. Likewise, the button "Deselect all" sets all switches in the window to gray. Instead of using these two buttons, individual switches can be set to red or gray when clicked on directly.
- In case an input file has been submitted and is in the process of being executed, the last few lines of the log file are displayed, thereby showing the progress of the job. An error message is prompted, should the execution be unsuccessful.
- Once the calculation with a specific input file has been executed successfully, the revision of the processed input file, together with the date of calculation is displayed as a link (see Fig. A1.10-10). Clicking on the link initiates a plotting routine which generates a plot with a summary of the results.
- The button "Exit" is used to leave Job Starter and to close the window.

A1.10.4 Revision Control System

An input file may be subject to modifications due to changes in model parameters or as a result of errors being detected in the QA process. The Revision Control System (RCS) as introduced by Tichy (1985) is used to keep track of all changes made in the input files in the course of time.

The RCS manages multiple revisions of files and automates the storing, retrieval, logging, and identification of revisions. The RCS is, in general, useful for text that is revised frequently such as computer codes and documentation. The basic user interface is simple. The function ci, short for "check in", deposits the contents of a file into an archives file called an RCS file. An RCS file contains all revisions of a particular file. The function co, short for "check out", retrieves revisions from a RCS file. The complete reference material for the freely available RCS can be found in the internet. The functions of the RCS which are used by Job Starter are the following:

- Store and retrieve multiple revisions of text such as input files: RCS saves all old revisions in a memory saving way. Changes do not destroy the original and the previous revisions remain accessible. Revisions can be retrieved according to ranges of revision numbers, symbolic names, dates, authors, and states.
- Maintain a complete history of changes: RCS logs all changes automatically. Besides the text of each revision, RCS stores the author, the date and time of check-in, and a log message summarizing the change. The logging facilitates control of a file's history.
- Automatically identify each revision with name, revision number, creation time, author, etc. The identification is like a stamp that can be embedded at an appropriate place in the text of a revision. The identification facilitates the controlled use of revisions.
- A function to compare different versions of a file.

A1.10.5 QA of Excel workbooks and input file generator

The tables comprising the database in the Excel workbooks were verified by comparing the entries in the data tables with the reference documents. After the verification, the data in the data tables were write-protected in order to avoid inadvertent modifications. The input file generation functionality of the Excel workbooks was verified (i) by QA of the Visual Basic for Applications code used and (ii) by systematically checking whether the parameters in sample input files were identical to those in the corresponding data tables.

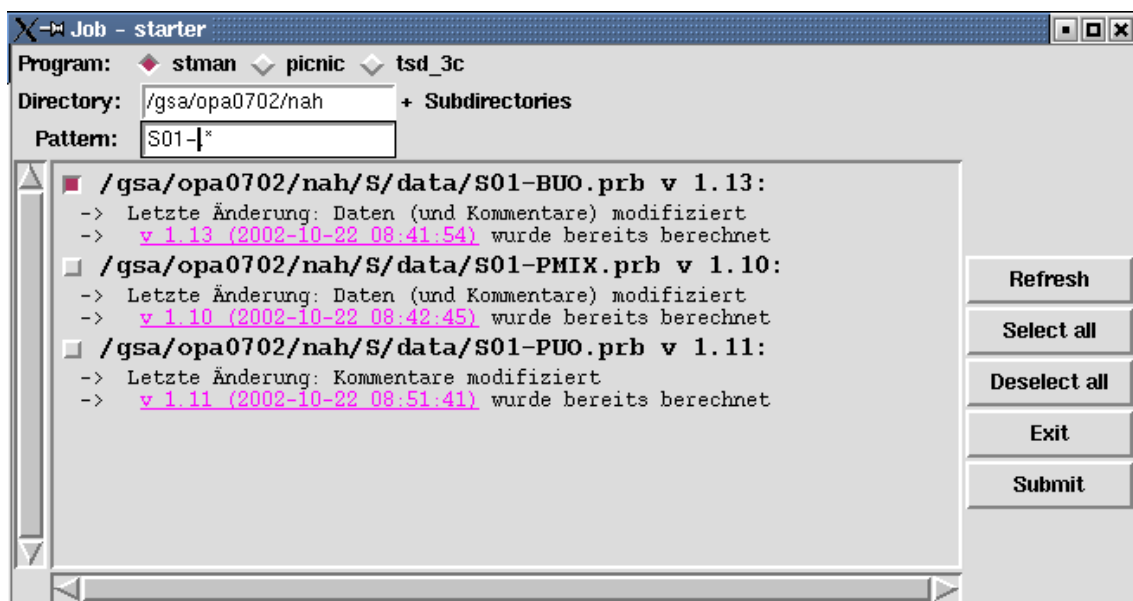


Fig. A1.10-10: Example of the interactive window of Job Starter

Note: The selection of input files is defined with the three identifiers at the top of the window, i.e. the computer code (= program) with which the file is processed, the directory and subdirectories to be searched, and the character pattern in the input file name.

Appendix 2: Probabilistic calculations

A2.1 Scope and purpose

GIPC (General Input Processing Code) is a simple general purpose tool that allows uncertainty or sensitivity analysis to be undertaken by automatically generating multiple runs of STMAN and PICNIC (and other codes), with parameter values sampled according to user-specified distributions. Because it is general, there is no built-in knowledge of STMAN and PICNIC.

GIPC can be used for any codes that are driven by free-format ASCII input files with a command-line instruction. It allows control over the values of input parameters and allows files to be directed to appropriate directories and/or given names that indicate the sequence number of the run. GIPC does not currently undertake any post-processing. For a more detailed description of GIPC, see Robinson & Benbow (2003).

A2.2 Methodology (GIPC)

The basic input approach in GIPC is to automatically generate input files by taking a specially annotated file and replacing placeholders with numeric values that are generated according to specified distributions or formulae. This basic capability is coupled with control commands that can be used to create directories and files and to execute programs.

Three types of file are used as input in a GIPC run:

- the Control File, which sets the number of samples to be created, controls the files that are generated and indicates which programs are run;
- the Processed Files, which are the annotated versions of the input files; and
- the Specification File, which indicates how the values should be generated for each sample.

Also, four types of file are generated as output in a GIPC run:

- the Log File, which reports on the actions taken during the run;
- the Report File, which reports on the values for all sampled parameters;
- the Target Files, which are generated from the Processed Files by substituting numeric values for the placeholders, and are generally used as input to one or more programs; and
- the Program Output Files, which are the normal output of the programs, and can be named to record the sequence number of the run that generated them.

A2.2.1 The Control File

The Control File has two sections. The first specifies sampling controls (number of samples and seed), and names the Specification File and Report File to be used. The valid sampling controls are shown in Tab. A2.2-1a. The second section lists the actions to be taken for each sample. The valid actions are shown in Tab. A2.2-1b.

Tab. A2.2-1a: Valid sampling controls of the code GIPC

Control	Purpose
SAMPLES num	Specifies the number of samples to be run. The default is 1.
SEED seed	Specifies a starting seed. This allows the same sequence of random numbers to be generated. If omitted, the seed will set from the system time.
SPEC spec-file	Names the specification file to use. The file name is relative to the working directory and must be in quotes if it has any special characters. The contents of the specification file are discussed later. If several specification files are used then they act as if they had been concatenated in the order given and treated as a single file. Note that duplicate names are not allowed, so the files must not both define the same item.
REPORT report-file	Names a file for the values of the variables to be written to as a table in comma-separated form. If no file is named then this output is not written, although the values will be written to a log file.

Tab. A2.2-1b: Valid actions in the Control File of the code GIPC

Action	Purpose
PROCESS subfile TO targetfile	Process a file by replacing the variables (%name%) with their values for the current sample. It specifies the name of a file to use as a starting point for substituting values and the name of the target file to be written – this will probably use %sample% in its name or directory (otherwise it would be overwritten) This line can be repeated (e.g. for STMAN then PICNIC).
CD directory	Directory to change to for subsequent commands. The directory name is relative to the previous directory. The directory will be created if it does not exist. Note that the code reverts to the top directory at the start of each sample loop.
MD directory	Make a directory. The directory will be created if it does not exist.
RUN command-line	Command to run. The command line is a quoted string giving the command and its arguments. This can be repeated (e.g. to run STMAN then PICNIC). The line is passed to the operating system as is, so valid inputs are determined by the system.
COPY file TO tofile	To give more portability than using a system command in RUN. Copies the named file to the named tofile. The tofile name may include %sample%.
DELETE file	To give more portability than using a system command in RUN. Used to remove unwanted files after a command has run (e.g. large log or diagnostic files that would waste disk space if left for every sample).

The most important of these actions is the PROCESS action, which creates the Target Files from the Processed Files.

A2.2.2 The Processed Files

Processed Files are just the usual input files for the codes with some numeric values (and strings if required) replaced by special fields that GIPC recognises.

Two types of field are available. The simplest is just replaced by a value and takes the form %name%. This will correspond to an entry in the specification file described in the next section.

A more powerful field allows a formula to be used. This takes the form %=formula% where formula can itself refer to the simple field types. The same types of formulae are allowed as in the specification file. This field allows, for instance, a series of release rates all to be scaled by the same, sampled, value.

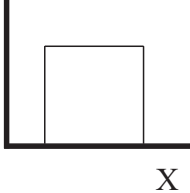
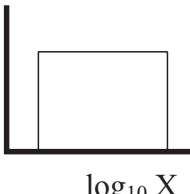
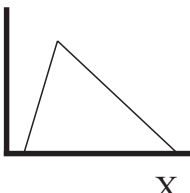
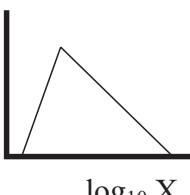
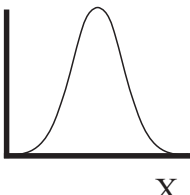
A2.2.3 The Specification File

The specification file provides the master list of known variables and indicates how these are to be generated. Three types of specification are supported:

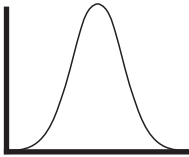
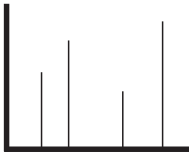
- PDF, which specifies a probability distribution;
- FORMULA, which gives a formula, usually incorporating variables that have already appeared;
- STRING, which allows character strings to be created.

Two built-in names can be used in the formula or strings, %sample%, which is the current sample number, and %topdir%, which is the directory that execution started in. These can also be used in the control file. Tab. A2.2-2 shows the types of probability density functions that can be used.

Tab. A2.2-2: Types of probability density functions available in GIPC

PDF-type	Description
<p data-bbox="459 465 568 499">Uniform</p> 	<p data-bbox="815 465 1273 533">Uniformly distributed between a given minimum and maximum.</p>
<p data-bbox="432 786 596 819">Log-uniform</p> 	<p data-bbox="815 786 1342 887">The logarithm value is uniformly distributed between the logarithms of a given minimum and maximum.</p>
<p data-bbox="443 1106 585 1140">Triangular</p> 	<p data-bbox="815 1106 1302 1207">Triangular-shaped distribution between a given minimum and maximum with a given peak.</p>
<p data-bbox="419 1426 609 1460">Log-triangular</p> 	<p data-bbox="815 1426 1326 1561">Logarithm of the value has a triangular-shaped distribution between the logarithms of a given minimum and maximum with a given peak.</p>
<p data-bbox="464 1747 564 1780">Normal</p> 	<p data-bbox="815 1747 1347 1879">Normal distribution with specified mean and standard deviation. Optionally truncated symmetrically or asymmetrically at a given number of standard deviations.</p>

Tab. A2.2-2: (Cont.)

PDF-type	Description
<p data-bbox="437 468 588 499">Log-normal</p>  <p data-bbox="501 692 596 723">$\log_{10} X$</p>	<p data-bbox="817 468 1347 629">The logarithm has a normal distribution with specified median and standard deviation. Optionally truncated symmetrically or asymmetrically at a given number of standard deviations.</p>
<p data-bbox="461 788 564 819">Discrete</p>  <p data-bbox="571 1016 596 1048">X</p>	<p data-bbox="817 788 1347 853">Distribution with only a fixed set of possible outcomes each with a given probability.</p>

The formulae can include a full set of operators and functions. Using formulae allows correlations to be created between inputs. For example the following input might be used.

```

%s1%: PDF Uniform MIN 0.0 MAX 1.0;
%s2%: PDF Uniform MIN -1.0 MAX 1.0;
%v1%: FORMULA 1.0 + %s1%*3.0;
%v2%: FORMULA 7.0 - %s1%*2.0 + 0.5*%s2%;

```

This gives a slightly (negatively) correlated relationship, as shown in Fig. A2.2-1.

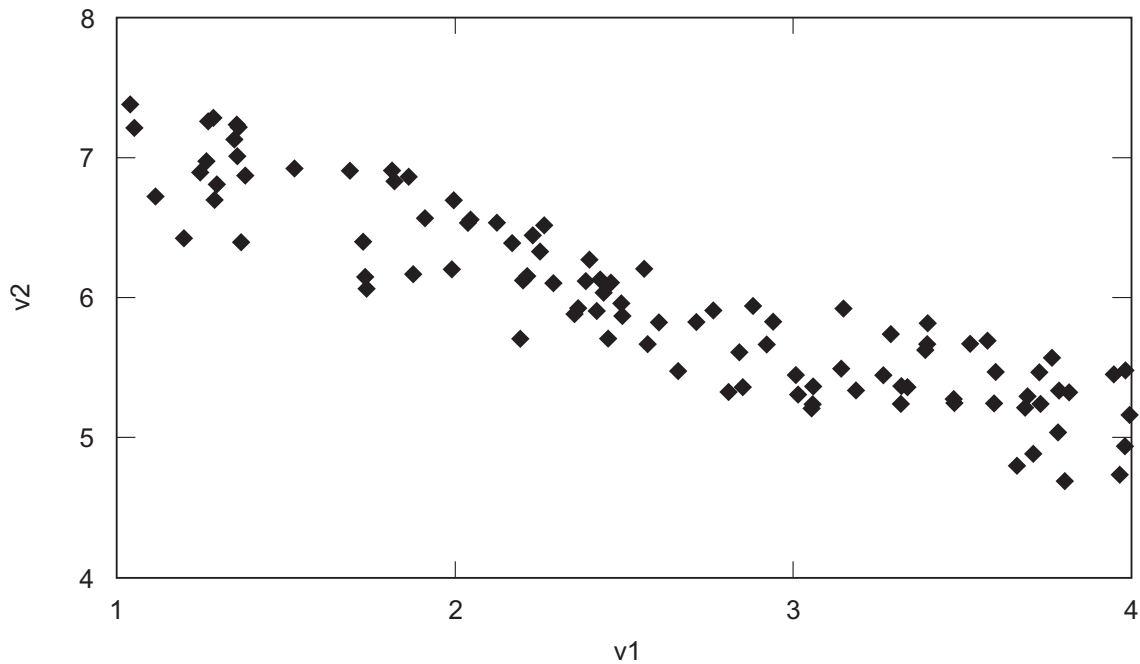


Fig. A2.2-1: Typical scatter plot of two (slightly negatively) correlated parameters

A2.3 Mathematical representation

The mathematical aspects of GIPC are in its random number generation, including the generation of samples from particular distributions, and the use of formulae in the specifications.

Both of these are handled in GIPC by making use of standard Perl modules (Perl is the computer language in which GIPC is written).

A2.4 Input parameters

Input to a GIPC run consists of the Control, Specification and Processed Files. Describing a GIPC calculation therefore requires a description for the inputs of each program that is run, with the probabilistic aspects described.

A2.5 Post processing of probabilistic sensitivity analysis

Having performed the model calculations with GIPC, the results of all samples are analysed and processed with scripts written in the programming language Python⁵³ (see, for example, Lutz & Ascher (1999) and / or Beazley (1999)).

⁵³ Python is a general purpose object oriented Open Source scripting language (www.python.org). A selection of features are used in the present safety assessment, including libraries for numerical computations, statistics and plotting.

Complementary cumulative density function⁵⁴

For each sample the radionuclide-specific release rate to the biosphere (output of the PICNIC calculation, in units of mol a^{-1}) is read in. The evolution of radionuclide-specific dose (in units of mSv a^{-1}) and the summed dose (sum of radionuclide-specific doses) are calculated using the biosphere dose conversion factors for the Reference Case biosphere (see Tab. A3.9-1 in Appendix 3). Then, for each sample, the dose maximum is evaluated for each radionuclide as well as for the summed dose. Finally, the probability of exceeding a given dose as a function of that dose is calculated for each key radionuclide as well as for the summed dose. This quantity is termed the complementary cumulative density function (CCDF).

Evolution of the median, the 95th percentile and highest / lowest dose maxima of all samples⁵⁵

The Python script used for this purpose performs the following steps: For each sample, the radionuclide-specific release rate to the biosphere (output of the PICNIC calculation, in units of mol a^{-1}) is read in. The evolution of the radionuclide-specific dose (in units of mSv a^{-1}) is calculated using the biosphere dose conversion factors for the Reference Case biosphere (see Tab. A3.9-1 in Appendix 3). A summary file is created which holds the summed dose (i.e. the sum of the radionuclide-specific doses) as a function of time. Based on the evolution of the summed dose of each sample, for each point in time the following values are evaluated and plotted:

- Minimum dose (the summed dose of the sample having the lowest dose at that point in time),
- Maximum dose (the summed dose of the sample having the highest dose at that point in time),
- Median dose (the dose in the middle of the series of all samples, i.e. one half of the samples have a summed dose lower than the median, and the other half of the samples have a summed dose which is higher than the median dose),
- 95th percentile (the summed dose, which is exceeded by only 5 % of all samples at that point in time).

A2.6 Verification

Detailed testing of the random number generation modules was undertaken during the development of GIPC. This confirmed both that the correct distributions were being created, but also that no spurious correlations were created.

Testing of the formulae was undertaken by working through some examples. Since the widely-used Perl language is directly used in this evaluation, the numerical accuracy of the evaluation is not in doubt.

⁵⁴ See, for example, Fig. 7.4-3a in Nagra (2002c).

⁵⁵ See, for example, Fig. 7.4-3b in Nagra (2002c).

Appendix 3: Datasets

A3.1 Introduction

One of the aims of the methodology to develop the safety case is to provide documentation that is *traceable* and *transparent*. This appendix is designed to provide traceability and, in particular, to ensure that the input parameter values that are used to evaluate specific assessment cases can be readily identified and traced back to their sources.

Attention is restricted in this appendix to cases that are evaluated using the reference model chain consisting of the STMAN and PICNIC near field and geosphere release and transport codes and the TAME biosphere code. Parameters for the evaluation of other cases are described in the relevant sections of the main part of this report.

Section A3.2 identifies the different parameter combinations that are used for each assessment case. In order to present the entire set of combinations in concise tables, unique numbers and letters are used to identify each parameter and parameter value (or set of values – see below), respectively. The numbering scheme for parameters and lettering scheme for parameter values is described in Section A3.3. In some cases, an assessment case requires more than one value to be assigned to a particular parameter. For example, radionuclide inventory is a single parameter that requires values to be assigned for each radionuclide and for each waste form. In such cases, the letters refer to sets of parameters. Tables of values for such parameters are given in Sections A3.4 (radionuclide-dependent parameters, such as inventory), A3.5 (element-dependent parameters, such as solubility limits) and A3.6. More detailed discussions of some specific parameter values are also given in Section A3.6.

For most cases, the distribution of radionuclides in the biosphere and the resultant doses are calculated using the code TAME, with parameter values identical to those of the Reference Case. The Reference Case input parameters for TAME are given in Section A3.7. Biosphere parameters for other cases are given in Section A3.8. Finally, biosphere dose conversion factors (BDCFs) for all biosphere cases are given in Section A3.9.

A3.2 Parameter combinations for the evaluation of assessment cases

A3.2.1 Near-field parameter combinations

Tab. A3.2-1a-d give the different parameter combinations that are used for the STMAN calculations to evaluate near-field release and transport in the various assessment cases:

- Tab. A3.2-1a gives parameter combinations for assessment cases within the Reference Scenario,
- Tab. A3.2-1b gives parameter combinations for assessment cases within Alternative Scenario 2: release of radionuclides affected by human actions,
- Tab. A3.2-1c gives parameter combinations for "what if?" assessment cases, and
- Tab. A3.2-1d gives parameter combinations for STMAN calculations to investigate design and system options.

Assessment cases within Alternative Scenario 1, in which the release of ^{14}C as volatile species is investigated, are not evaluated using STMAN and are therefore not discussed here. These cases are evaluated using the Gas Model (Chapter 4).

The first column gives an identifying number for each assessment case (see Tab. 2.2-1). For example, Case 1.1a is the Reference Case. The second column gives the waste type to which the parameter values in subsequent columns refer, i.e:

- SF: spent fuel, with radionuclide release and near-field transport evaluated using the SPENT module of STMAN,
- HLW: vitrified high-level waste, with radionuclide release and near-field transport evaluated using the STRENG module of STMAN, and
- ILW: long-lived intermediate-level waste, with radionuclide release and near-field transport evaluated using the STALLION module of STMAN.

The remaining numbered columns each correspond to a particular parameter, with parameter values indicated by letters. For all parameters, the letter *A* corresponds to values for the Reference Case. Dark shading indicates parameters that are not relevant for a particular waste type. In the case of ILW, parameters related to the bentonite buffer are shaded in this way, since no bentonite buffer layer is present for this waste form. In practice, the calculations for ILW have been carried out assuming a buffer layer of 1 cm thickness, with geochemical parameters, porosity and diffusion coefficients identical to those for Opalinus Clay, as explained in Appendix A3.6.

In all of the alternative cases, only parameter values that differ from the Reference Case values are indicated explicitly by letter codes in the tables. Light shading indicates where parameters take identical values to the Reference Case.

A3.2.2 Geosphere parameter combinations

Tabs. A3.2-2a-c give the different parameter combinations that are used for the PICNIC calculations to evaluate geosphere transport in the various assessment cases:

- Tab. A3.2-2a gives parameter combinations for assessment cases within the Reference Scenario,
- Tab. A3.2-2b gives parameter combinations for assessment cases within Alternative Scenario 2: release of radionuclides affected by human actions, and
- Tab. A3.2-2c gives parameter combinations for "what if?" assessment cases.

Assessment cases within Alternative Scenario 1, in which the release of ^{14}C as volatile species is investigated, are not evaluated using PICNIC; these cases are treated using the Gas Model (Chapter 4). The PICNIC calculations to investigate design and system options are identical to the Reference Case PICNIC calculations.

The format of the tables is, in most respects, identical to Tabs. A3.2-1a-d. The second column, however, gives the PICNIC "leg" to which the parameter values in the following columns refer. In most cases, a single leg is used (L_1). In a few cases, however, multiple legs are used, and references are given to figures in the main text that define the names and the network structure of such legs.

Dark shading indicates parameters that are not relevant. These parameters (PICNIC Parameters 19 and 20) are the hydraulic heads at the upstream and downstream ends of the legs. PICNIC has the option of deriving the Darcy velocities in the legs from the head gradient and the hydraulic conductivity. In all the assessment cases considered, however, the Darcy velocity is specified directly as PICNIC Parameter 5. As before, light shading indicates where parameters take identical values to the Reference Case.

Tab. A3.2-2a: (Cont.)

Reference Scenario																				
Case	Leg	Parameter combination																		
		1	2	3	4	5	6	7	8	9	10	11	12	13	14	15	16	17	18	19
1.7 Convergence-induced release affected by ramp/shaft																				
1.7a	L_1		E	I	D	M		D	C		E	E								
	L_7																			
1.7b	evaluated using FRAC3DVS (see Section 3.7)																			
1.8 Gas-induced release of dissolved radionuclides affected by ramp/shaft																				
1.8a	L_1		D	G	C	J		D	C		E	E								
	L_2							D	C		E	E								
	L_3							D	C		E	E								
	L_4							D	C		E	E								
	L_5							E	D		D									
	L_6																			
	L_7																			
1.8b	L_1		D	G	C	K		D	C		E	E								
	L_7																			

Tab. A3.2-2b: Parameter combinations in the PICNIC calculations for assessment cases within Alternative Scenario 2 (release of radionuclides affected by human actions)

For a definition of the parameters and the parameter values, see Tab. A3.3-3.

Alternative Scenario 2: Release of radionuclides affected by human actions																				
Case	Leg	Parameter combination																		
		1	2	3	4	5	6	7	8	9	10	11	12	13	14	15	16	17	18	19
3.1 Borehole penetration																				
		no calculation – direct release from near field to biosphere																		
3.2 Deep groundwater extraction from Malm aquifer (production of well as dilution)																				
3.2a	L_1																			
3.2b																				
3.3 Abandoned repository																				
3.3a	L_1		D	H	C	L		D	C		E	E								
	L_2							D	C		E	E								
	L_3							D	C		E	E								
	L_4							D	C		E	E								
	L_5							E	D		D									
	L_6																			
	L_7																			

A3.2.3 Biosphere parameter combinations

Tab. A3.2-3 shows the assessment cases for which the code TAME has been used, with parameter values identical to those of the Reference Case, to evaluate the distribution of radionuclides in the biosphere and the resultant doses. As mentioned in the introduction to this appendix, most cases fall into this category. The Reference Case biosphere parameter values used in TAME are compiled in Tabs. A3.7-1 to A3.7-5. Alternative biosphere parameter values used in TAME are summarised in Tab. A3.8-1. The calculations of drinking water doses are documented in the corresponding sections in the main text of this report. Note that for this exposure pathway, a drinking water consumption rate of 2 litres per day ($0.73 \text{ m}^3 \text{ a}^{-1}$) is chosen (Tab. A3.7-3). A semi-quantitative dose estimate for the periglacial climate state is discussed in Appendix 6.

Tab. A3.2-3: Parameter combinations in the TAME calculations

For parameter values, see Sections A3.7 and A3.8.

Scenario	Conceptualisation	Cases	Biosphere model
1. Reference Scenario Release of dissolved radionuclides	1.1 Reference Conceptualisation	1.1a - k	Reference Case biosphere
	1.2 Solubility-limited dissolution of SF	1.2a	
	1.3 Bentonite thermal alteration	1.3a	
	1.4 Glacially-induced flow in the Opalinus Clay	1.4a	
	1.5 Additional barrier provided by confining units	1.5a - b	
	1.6 Radionuclide release affected by ramp/shaft	1.6a - b	
	1.7 Convergence-induced release affected by ramp (ILW)	1.7a - b	
	1.8 Gas-induced release of dissolved radionuclides affected by ramp/shaft	1.8a - b	
2. Alternative Scenario 1 Release of volatile radionuclides along gas pathways	2.1 Release of ^{14}C from SF and ILW as volatile species in the gas phase not affected by ramp/shaft ("tight seals")	2.1a - c	Drinking water model (see Section A1.9.4.2)
	2.2 Release of ^{14}C from SF and ILW as volatile species in the gas phase affected by ramp/shaft ("leaky seals")	2.2a - c	
3. Alternative Scenario 2 Release of radionuclides affected by human actions	3.1 Borehole penetration	3.1a - g	Reference Case biosphere
	3.2 Deep groundwater extraction from Malm aquifer (production of well as dilution)	3.2a - b	Drinking water model (see Section 5.2)
	3.3 Abandoned repository	3.3a	Reference Case biosphere

Tab. A3.2-3: (Cont.)

4. "What if?" cases to investigate robustness of the disposal system	4.1	High water flow rate	4.1a	Reference Case biosphere
	4.2	Transport along transmissive discontinuities	4.2a - f	
	4.3	SF: Increased fuel dissolution rate	4.3a - b	
	4.4	Redox front (SF / ILW compacted hulls)	4.4a	
	4.5	ILW: Gas-induced release of dissolved radionuclides through ramp only	4.5a - b	
	4.6	Unretarded transport of ¹⁴ C released as volatile species through host rock; retardation in confining units taken into account	4.6a - c	Drinking water model (see Section 6.6)
	4.7	Poor near field and pessimistic near-field / geosphere geochemical dataset	4.7a - c	Reference Case biosphere
	4.8	No advection in geosphere (diffusive transport only)	4.8a	
	4.9	SF: Increased cladding corrosion rate	4.9a	
	4.10	K _d (I) for NF and geosphere = 0	4.10a	
	4.11	Decreased transport distance in Opalinus Clay (30 m)	4.11a	
5. Design and system options	5.1	Increased waste arisings (300 GWa(e))	5.1a	Reference Case biosphere
	5.2	ILW high force compacted waste option	5.2a	
	5.3	SF canister with Cu shell	5.3a - b	
6. Illustration of effects of biosphere uncertainty	6.1	Reference and alternative geomorphology	6.1a	Reference Case biosphere
			6.1b	Alternative TAME parameters (see Tab. A3.8-1)
			6.1c	Alternative TAME parameters (see Tab. A3.8-1)
			6.1d	Drinking water model (see Section 8.3)
	6.2	Reference and alternative climates	6.2a	Reference Case biosphere
			6.2b	Alternative TAME parameters (see Tab. A3.8-1)
			6.2c	Alternative TAME parameters (see Tab. A3.8-1)
			6.2d	Semi-quantitative dose estimate (see Appendix 6)

A3.3 Parameter values for the evaluation of assessment cases

A3.3.1 Parameter values for STMAN calculations

Tab. A3.3-1 presents parameter values for STMAN calculations. Each of the 35 parameters is assigned a number, which is given in the first column and corresponds to the parameter numbering scheme in Tabs. 3.2-1a-d. The parameters are described in words in the second column. Specific values assigned to each parameter are identified by code letters (A, B, C, ...), which are given in the third column. The fourth column either gives the values themselves, or a reference to another table where values can be found. Some parameters are specific to a particular waste form (SF, HLW or ILW), or take different values according to the waste form or type

under consideration. Waste type refers to the type of spent fuel within a canister (e.g. BWR-UO₂-48), to the origin of vitrified high-level waste (BNFL or COGEMA) or the type of ILW (ILW-1 and ILW-2). The waste forms and types to which specific parameters apply are given in the fifth and sixth columns. The seventh column gives comments on the parameter values, or refers to source documentation allowing the origins of the parameter values to be traced. Where the symbol ► is shown, further explanatory notes on the parameter are given in Section A3.6.

In Tab. A3.3-2a-c, key parameters for the SF, HLW and ILW near field are summarised and referenced.

Tab. A3.3-1: Parameter values for STMAN calculations

Parameter	Letter code and value	Waste		Comments / source			
		Form	Type				
Radionuclides and inventory							
1	Nuclides and decays to be used	A	Tab. A3.4-1	All	All	Selection of safety-relevant radionuclides described in Appendix 5.	
		B	²³⁸ U only	SF			
		C	¹⁴ C (org.), ³⁶ Cl, ⁴¹ Ca, ¹²⁹ I, ⁷⁹ Se	SF			Analysis limited to a few example radionuclides.
		D	¹⁴ C (org.), ¹²⁹ I	ILW			Analysis limited to two example radionuclides.
2	Inventory of each nuclide in a single package	A	Tabs. A3.4-2a-c	All	All	The inventory varies between waste forms and waste type. Parameter 6 defines the numbers of waste packages containing particular waste types.	
		B	Tabs. A3.4-2a, but with all ¹⁴ C in SF assumed to be in organic form				
		C	Tab. A3.4-2a, but IRF only	SF	All		
		D	Tab. A3.4-2c	ILW	ILW-1	High force compacted waste option	
		E	0.25 × inventory for ILW-1 (cemented waste option) in Tab. A3.4-2c	ILW	ILW-1	Borehole penetration	
Waste form and Canister							
3	Percentage of the inventory for each nuclide assigned to fuel matrix, cladding and instant release fraction	A	Tab. A3.4-2a	SF	All	Entire reference inventory hypothetically assigned to instant release fraction (IRF).	
		B	Tab. A3.4-2b				
		C	100 % to IRF				

Tab. A3.3-1: (Cont.)

Parameter	Letter code and value	Waste		Comments / source			
		Form	Type				
Waste form and Canister							
4	Fraction of the inventory that is subject to slow release	A	0	ILW	All	Not used in any of the assessment cases.	
5	Containment time	A	10 ⁴ a	SF / HLW	All	Tab. A3.3-2a (SF), Tab. A3.3-2b (HLW), Tab. A3.3-2c (ILW)	
			100 a	ILW			
		B	0 a	SF			
		C	10 ³ a	SF / HLW			
		D	10 ⁵ a	SF			
		E	10 ² a	SF / HLW			
			0 a	ILW			
F	500 a	ILW	ILW-1	Borehole penetration			
6	Number of waste packages	A	935	SF	9 BWR-UO ₂ -48	Applies to the 192 GWa(e) power generation scenario. These are rounded values; the exact values, which were used in the calculations, cannot be disclosed because of confidentiality agreements (see also Tab. A3.3-2a).	
			680		4 PWR-UO ₂ -48		
			450		3 PWR UO ₂ -48 + 1 PWR MOX-48		
			270		HLW		BNFL
			460				COGEMA
		1	ILW	ILW-1	ILW-1 and ILW-2 tunnels each treated as a single "waste package".		
		1		ILW-2			
		B	1630	SF	9 BWR-UO ₂ -48	Applies to the 300 GWa(e) power generation scenario. These are rounded values; the exact values, which were used in the calculations, cannot be disclosed because of confidentiality agreements (see also Tab. A3.3-2a).	
			1500		4 PWR-UO ₂ -48		
			450		3 PWR UO ₂ -48 + 1 PWR MOX-48		

Tab. A3.3-1: (Cont.)

Parameter	Letter code and value	Waste		Comments / source		
		Form	Type			
Waste form and Canister						
6	Number of waste packages	C	1		PWR-UO ₂ -55	Calculations for single SF / HLW canisters only – alternative canister inventories.
			1		3 PWR UO ₂ -55 + 1 PWR UO ₂ -65	
			1		3 PWR UO ₂ -55 + 1 PWR UO ₂ -75	
			1		3 PWR UO ₂ -48 + 1 PWR MOX-65	
			1	HLW	BNFL	
			1		COGEMA	
		D	75 % of reference values (A)	SF / HLW	All	
	E	25 % of reference values (A)			Zones A & C of Fig. 3.6-1, corresponding to tunnel segments of 100 m each.	
	F	10 % of reference values (A) × 10 000	SF	All	Only 10 % of the SF canisters are assumed to be affected (Case 1.8). By up-scaling the number of waste packages by the arbitrary number of 10 000, the depletion of the radionuclide inventory in the emplacement tunnel is conservatively prevented. ►	
		Reference values (A) × 10 000	ILW	All		
	G	22	SF	BWR-UO ₂ -48	Assumes one discontinuity intersects all the tunnels, with one SF / HLW canister per tunnel affected, the remaining radionuclides being released through the Opalinus Clay matrix (as in the Reference Case).	
		5	HLW	COGEMA		

Tab. A3.3-1: (Cont.)

Parameter	Letter code and value	Waste		Comments / source		
		Form	Type			
Waste form and Canister						
6	Number of waste packages	H	88	SF	BWR-UO ₂ -48	Assumes two discontinuities intersect all the tunnels, with four SF / HLW canisters per tunnel affected, the remaining radionuclides being released through the Opalinus Clay matrix (as in the Reference Case).
			20	HLW	COGEMA	
		I	2	SF	3 PWR UO ₂ -48 + 1 PWR MOX-48	Borehole assumed to penetrate SF/HLW tunnel, affecting 2 canisters (near hit).
			2	HLW	COGEMA	
		J	4	SF	3 PWR UO ₂ -48 + 1 PWR MOX-48	Borehole assumed to penetrate SF/HLW tunnel, affecting 4 canisters (near hit).
			4	HLW	COGEMA	
		K	1	SF	3 PWR UO ₂ -48 + 1 PWR MOX-48	Borehole assumed to penetrate SF canister (direct hit).
		7	Waste package length	A	4.6 m	SF
1.03 m	HLW				All	Tab. A3.3-2b
180 m	ILW				ILW-1	Tab. A3.3-2c
60 m					ILW-2	
B	150 m			ILW	ILW-1	High force compacted waste option.
C	90 m			ILW	ILW-1	Borehole penetration of one ILW-1 emplacement tunnel.
8	Initial diameter of waste	A	1.05 m	SF	All	2 × inner radius of buffer (Parameter 23).
			0.43 m	HLW		McGinnes (2002)
9	Matrix release rate	A	Tab. A3.6-1 / col. 1	SF	BWR-UO ₂ -48	►
					PWR-UO ₂ -48	
			Tab. A3.6-1 / col. 2		PWR-mixed-48	
		B	Tab. A3.6-1 / col. 3		All higher burn-up cases	

Tab. A3.3-1: (Cont.)

Parameter	Letter code and value	Waste		Comments / source		
		Form	Type			
Waste form and Canister						
9	Matrix release rate	C	Reference values (A) × 10	SF	All	▶
		D	Reference values (A) × 100			
		E	Rate based on separate calculation using ²³⁸ U			
10	Cladding release rate	A	$3 \times 10^{-5} \text{ a}^{-1}$	SF	All	Reference value (A) discussed in Johnson & McGinnes (2002).
		B	$3 \times 10^{-4} \text{ a}^{-1}$			
11	Glass grain density	A	$2\,750 \text{ kg m}^{-3}$	HLW	All	McGinnes (2002).
12	Glass dissolution rate	A	$5.5 \times 10^{-4} \text{ kg m}^{-2} \text{ a}^{-1}$	HLW	BNFL	Values A and B are from Curti (2003). Variation (B) represents an extremely pessimistic glass dissolution rate. See also Tab. A3.3-2b.
			$7.3 \times 10^{-5} \text{ kg m}^{-2} \text{ a}^{-1}$		COGEMA	
		B	$4.0 \times 10^{-2} \text{ kg m}^{-2} \text{ a}^{-1}$		All	
		C	Reference values (A) × 10			
13	Glass spherical radius	A	$1.8 \times 10^{-2} \text{ m}$	HLW	All	Evaluated using Eq. 5.2.4 in Nagra (1994a), but using a factor of 15 (rather than 12.5) to account for the increase in surface area due to fracturing. See also Tab. A3.3-2b.
14	Slow release rate	A	-	ILW	All	Not used in any of the assessment cases.
15	Reservoir thickness	A	0.041 m	SF	All	Reservoir thickness is based on internal void volumes of SF and HLW packages (Tabs. A3.3-2a/b) ▶
			0.025 m	HLW		
16	Solubility limits in reservoir	A	Tab. A3.5-1 / col. 1	SF / HLW	All	
		B	Tab. A3.5-1 / col. 2			
		C	Tab. A3.5-1 / col. 3			

Tab. A3.3-1: (Cont.)

Parameter	Letter code and value	Waste		Comments / source			
		Form	Type				
Waste form and Canister							
16	Solubility limits in reservoir	D	Unlimited solubility	SF	3 PWR UO ₂ -48 + 1 PWR MOX-48		
17	Pinhole radius	A	-	All	All	Tab. A3.3-2a	
		B	1.1 mm	SF	3 PWR UO ₂ -48 + 1 PWR MOX-48		
		C	4.0 mm	SF			
18	Number of pinholes	A	not used	All	All		
		B	1 pinhole in a single canister	SF	3 PWR UO ₂ -48 + 1 PWR MOX-48		
ILW cementitious region							
19	Porosity	A	0.3	ILW	All	Tab. A3.3-2c	
20	Grain density	A	700 kg m ⁻³	ILW	ILW-1	Tab. A3.3-2c	
			400 kg m ⁻³		ILW-2		
21	Sorption K_d	A	Tab. A3.5-4 / col. 1	ILW	ILW-1		
			Tab. A3.5-4 / col. 2		ILW-2		
		B	Tab. A3.5-4 / col. 3		ILW-1		
			Tab. A3.5-4 / col. 4		ILW-2		
		C	Tab. A3.5-4 / col. 2		ILW-1		Assume the same sorption for ILW-1 as for ILW-2.
		D	$K_d(I) = 0$		All		
22	Solubility limits	A	Tab. A3.5-3 / col. 1	ILW	ILW-1		
			Tab. A3.5-3 / col. 2		ILW-2		
		B	Tab. A3.5-3 / col. 3		ILW-1		
			Tab. A3.5-3 / col. 4		ILW-2		
		C	Tab. A3.5-3 / col. 2		ILW-1		Assume the same solubilities for ILW-1 as for ILW-2.

Tab. A3.3-1: (Cont.)

Parameter	Letter code and value	Waste		Comments / source		
		Form	Type			
Buffer						
23	Inner radius	A	0.525 m	SF	All	Tab. A3.3-2a
			0.47 m	HLW		Tab. A3.3-2b
			4.5 m	ILW	ILW-1	Tab. A3.3-2c
			2.9 m		ILW-2	
24	Outer radius	A	1.15 m	SF / HLW	All	Tab. A3.3-4d
			4.51 m	ILW	ILW-1	Appendix 3.6 ►
			2.91 m		ILW-2	
		B	0.525	SF	All	No buffer.
25	Split radius	A	not used	SF / HLW	All	Homogeneous buffer properties.
			B	0.84 m		SF
			0.81 m	HLW		
26	Porosity for inner buffer region	A	Tab. A3.5-2 / col. 1	SF / HLW	All	
27	Porosity for outer buffer region	A	Tab. A3.5-2 / col. 1	SF / HLW	All	Same as inner region.
28	Grain density	A	2 760 kg m ⁻³	SF / HLW	All	Tabs. A3.3-2a/b
29	Sorption K_d for inner buffer	A	Tab. A3.5-2 / col. 1	SF / HLW	All	
		B	Tab. A3.5-2 / col. 2			
		C	Tab. A3.5-2 / col. 3			
		D	$K_d(I) = 0$			
30	Sorption K_d for outer buffer	A	Tab. A3.5-2 / col. 1	SF / HLW	All	
		B	Tab. A3.5-2 / col. 2			
		C	Tab. A3.5-2 / col. 3			
		D	$K_d(I) = 0$			

Tab. A3.3-1: (Cont.)

Parameter		Letter code and value		Waste		Comments / source	
				Form	Type		
Buffer							
31	Solubility limits for inner buffer	A	Tab. A3.5-1 / col. 1	SF / HLW	All		
		B	Tab. A3.5-1 / col. 2				
		C	Tab. A3.5-1 / col. 3				
32	Solubility limits for outer buffer	A	Tab. A3.5-1 / col. 1	SF / HLW	All		
		B	Tab. A3.5-1 / col. 2				
		C	Tab. A3.5-1 / col. 3				
33	Effective diffusion coefficients for inner buffer	A	Tab. A3.5-2 / col. 1	SF / HLW	All		
	Pore diffusion coefficients for inner buffer	B	$6.3 \times 10^{-2} \text{ m}^2 \text{ a}^{-1}$	SF / HLW			Diffusion coefficient for free water (Fetter 1993).
34	Effective diffusion coefficients for outer buffer	A	Tab. A3.5-2 / col. 1	SF / HLW	All	Same as inner region.	
35	Mixing cell flow rate per waste package	A	$6.0 \times 10^{-3} \text{ m}^3 \text{ a}^{-1}$	SF	All	Reference flowrate and effective diffusivity in Opalinus Clay ►	
			$4.0 \times 10^{-3} \text{ m}^3 \text{ a}^{-1}$	HLW			
			$2.2 \times 10^{-3} \text{ m}^3 \text{ a}^{-1}$	ILW			ILW-1
			$1.6 \times 10^{-3} \text{ m}^3 \text{ a}^{-1}$				ILW-2
		B	$6.0 \times 10^{-3} \text{ m}^3 \text{ a}^{-1}$	SF	All	Diffusion only in the Opalinus Clay, with reference effective diffusivity ►	
			$4.0 \times 10^{-3} \text{ m}^3 \text{ a}^{-1}$	HLW			
			$2.2 \times 10^{-3} \text{ m}^3 \text{ a}^{-1}$	ILW			ILW-1
			$1.5 \times 10^{-3} \text{ m}^3 \text{ a}^{-1}$				ILW-2

Tab. A3.3-1: (Cont.)

Parameter	Letter code and value	Waste		Comments / source				
		Form	Type					
Buffer								
35	Mixing cell flow rate per waste package	C	$6.0 \times 10^{-3} \text{ m}^3 \text{ a}^{-1}$	SF	All	0.1 × reference flowrate in Opalinus Clay, with reference effective diffusivity ►		
			$4.0 \times 10^{-3} \text{ m}^3 \text{ a}^{-1}$	HLW				
			$2.2 \times 10^{-3} \text{ m}^3 \text{ a}^{-1}$	ILW	ILW-1			
			$1.5 \times 10^{-3} \text{ m}^3 \text{ a}^{-1}$		ILW-2			
		D	$6.2 \times 10^{-3} \text{ m}^3 \text{ a}^{-1}$	SF	All		10 × reference flowrate in Opalinus Clay, with reference effective diffusivity ►	
			$4.1 \times 10^{-3} \text{ m}^3 \text{ a}^{-1}$	HLW				
			$2.3 \times 10^{-3} \text{ m}^3 \text{ a}^{-1}$	ILW	ILW-1			
			$1.6 \times 10^{-3} \text{ m}^3 \text{ a}^{-1}$		ILW-2			
		E	$7.9 \times 10^{-3} \text{ m}^3 \text{ a}^{-1}$	SF	All			100 × reference flowrate in Opalinus Clay, with reference effective diffusivity ►
			$5.2 \times 10^{-3} \text{ m}^3 \text{ a}^{-1}$	HLW				
			$2.9 \times 10^{-3} \text{ m}^3 \text{ a}^{-1}$	ILW	ILW-1			
			$2.0 \times 10^{-3} \text{ m}^3 \text{ a}^{-1}$		ILW-2			
	F^I	$6.0 \times 10^{-2} \text{ m}^3 \text{ a}^{-1}$	SF	All	Reference flowrate in Opalinus Clay, with 10 × reference effective diffusivity ►			
		$4.0 \times 10^{-2} \text{ m}^3 \text{ a}^{-1}$	HLW					
		$2.2 \times 10^{-2} \text{ m}^3 \text{ a}^{-1}$	ILW	ILW-1				
		$1.5 \times 10^{-2} \text{ m}^3 \text{ a}^{-1}$		ILW-2				
	G	∞	SF / HLW	SF: only BWR-UO ₂ -48 HLW: only COGEMA		Zero concentration boundary condition.		
	H	$1.0 \times 10^{-5} \text{ m}^3 \text{ a}^{-1}$	ILW	ILW-1		0.1 m ³ a ⁻¹ divided by 10 000 (see note on parameter 6F), conveying 3% of total mobile radionuclide inventory. Pulse duration = 1 000 years. ►		

Tab. A3.3-1: (Cont.)

Parameter	Letter code and value	Waste		Comments / source		
		Form	Type			
Buffer						
35	Mixing cell flow rate per waste package	I	$5.8 \times 10^{-6} \text{ m}^3 \text{ a}^{-1}$	ILW	ILW-1	For ILW-1, $\approx 0.05 \text{ m}^3 \text{ a}^{-1}$ divided by 10 000 (see note on parameter 6F), conveying 50% of total mobile radionuclide inventory. Pulse duration = 30 000 years. ► For ILW-1, $\approx 0.3 \text{ m}^3 \text{ a}^{-1}$ divided by 10 000 (see note on parameter 6F), conveying 100% of total mobile radionuclide inventory. Pulse duration = 10 000 years. ► See note on parameter 6F. Pulse duration = 1 000 years. ► See Section 6.2.4. These values are for the entire ILW-1 and ILW-2 tunnel lengths, in contrast to the other ILW mixing cell flow rates, which are per m of tunnel length. Borehole penetration: Water flow rate partitioned between affected SF/HLW canisters.
			$8.0 \times 10^{-7} \text{ m}^3 \text{ a}^{-1}$		ILW-2	
		J	$3.5 \times 10^{-5} \text{ m}^3 \text{ a}^{-1}$	ILW	ILW-1	
			$4.8 \times 10^{-5} \text{ m}^3 \text{ a}^{-1}$		ILW-2	
		K	$6.5 \times 10^{-8} \text{ m}^3 \text{ a}^{-1}$	SF	All	
		L	$0.14 \text{ m}^3 \text{ a}^{-1}$	ILW	ILW-1	
			$0.05 \text{ m}^3 \text{ a}^{-1}$		ILW-2	
		M	$1.4 \text{ m}^3 \text{ a}^{-1}$	ILW	ILW-1	
			$0.5 \text{ m}^3 \text{ a}^{-1}$		ILW-2	
		N ²	$0.01 \text{ m}^3 \text{ a}^{-1}$	SF / HLW ILW	SF: only 3 PWR UO ₂ -48 + 1 PWR MOX-48 HLW: only COGEMA ILW: only ILW-1	
		O ³	$1 \text{ m}^3 \text{ a}^{-1}$			
		P ⁴	$0.0001 \text{ m}^3 \text{ a}^{-1}$			

¹ These are the suggested values for the mixing cell flow rate corresponding to the calculated effective flow rates for pessimistic geosphere diffusion constants, as discussed in Chapter 3. However, in the calculations for Case 1.1j, the Reference Case values (A) were used instead. Employing the suggested values as given in Tab. A3.3-1 yields a resulting summed dose maximum for SF that is increased by about 20 % with respect to that shown in Tab. 7.10-1 of Nagra (2002c).

² This is the suggested value for the mixing cell flow rate as discussed in Chapter 3. However, in the calculations for HLW, a pessimistic mixing cell flow rate per waste package of $0.04 \text{ m}^3 \text{ a}^{-1}$ was used instead. Employing the suggested value as given in Tab. A3.3-1 yields a slightly lower resulting summed dose maximum than that shown in Tab. 7.10-1 of Nagra (2002c).

³ This is the suggested value for the mixing cell flow rate as discussed in Chapter 3. However, in the calculations for HLW, a pessimistic mixing cell flow rate per waste package of $2 \text{ m}^3 \text{ a}^{-1}$ was used instead. Employing the suggested value as given in Tab. A3.3-1 yields a slightly lower resulting summed dose maximum than that shown in Tab. 7.10-1 of Nagra (2002c).

⁴ This is the suggested value for the mixing cell flow rate as discussed in Chapter 3. However, in the calculations for HLW, a pessimistic mixing cell flow rate per waste package of $0.0002 \text{ m}^3 \text{ a}^{-1}$ was used instead. Employing the suggested value as given in Tab. A3.3-1 yields a slightly lower resulting summed dose maximum than that shown in Tab. 7.10-1 of Nagra (2002c).

Tab. A3.3-2a: SF near field parameter values

Parameter	Reference value	Variations	Comments / References
Containment time	10 ⁴ a	10 ² a, 10 ³ a, 10 ⁵ a	10 ² a: "what if?" case; 10 ³ a: parameter variation; 10 ⁵ a: Cu canister case (also with initial pinhole defect, see below) Johnson & King (2003)
Number of pinholes	0	1	Based on the discussion in Nagra (2002c), Section 5.3.4.4.
Pinhole area	4 mm ²	50 mm ²	Assumption
Number of canisters	2065 (192 GWa(e) scenario) 935 BWR 680 PWR 450 mixed (3 UO ₂ + 1 MOX)	3580 (300 GWa(e) scenario) 1630 BWR 1500 PWR 450 mixed	These are rounded values; the exact values, which were used in the calculations, cannot be disclosed because of confidentiality agreements (McGinnes 2002).
Canister radius r	0.525 m		Johnson & King (2003)
Canister length L	4.6 m		The canister length of 4.6 m is the weighted average of all PWR and BWR canisters, based on the numbers and types of canisters in McGinnes (2002). Canister lengths for PWR and BWR canisters are from Johnson & King (2003).
Thickness, d, of reservoir ("volume for dissolution")	0.041 m		Derived from internal void volume V = 0.65 m ³ of canister loaded with spent fuel. Dissolution is assumed to occur in an annular water reservoir of thickness d, length L and radius r, with: $V = L * 2\pi * (r+d/2) * d$
Inner bentonite radius	0.525 m	0.84 m	Variation value based on half-thickness, assuming clay reaching >100 °C is altered and is a poor diffusion barrier (Johnson et al. 2002).
Outer bentonite radius	1.15 m		Radius after tunnel convergence (Section 5.3.3.1 of Nagra 2002c).
Bentonite porosity	0.36		Porosity at saturated density of 2150 kg m ⁻³ (Section 5.3.3.1 of Nagra 2002c).
Bentonite grain density	2760 kg m ⁻³		Nagra (1994a)

Tab. A3.3-2b: HLW near field parameter values

Parameter	Reference value	Variations	Comments / References
Containment time	10^4 a	10^2 a, 10^3 a	10^2 a: "what if?" case; 10^3 a: parameter variation Johnson & King (2003)
Glass corrosion rate			
SON-68 glass (WA-COG-1)	7.3×10^{-5} $\text{kg m}^{-2} \text{a}^{-1}$	4.0×10^{-2} $\text{kg m}^{-2} \text{a}^{-1}$	Curti (2003)
MW glass (WA-BNF-1)	5.5×10^{-4} $\text{kg m}^{-2} \text{a}^{-1}$	4.0×10^{-2} $\text{kg m}^{-2} \text{a}^{-1}$	Curti (2003)
Number of canisters	460 (Cogema) 270 (BNFL)		These are rounded values; the exact values, which were used in the calculations, cannot be disclosed because of confidentiality agreements (McGinnes 2002).
Length of glass blocks, h	752 m (1.03 m for each block, 730 blocks)		McGinnes (2002)
Initial diameter of glass blocks, d_0	0.43 m		McGinnes (2002)
Glass density	2750 kg m^{-3}		McGinnes (2002)
Factor of glass surface area increase due to fracturing	15		Pessimistic assumption, adjusted upwards from value of 12.5 used in Nagra (1994a).
Thickness, d, of reservoir ("volume for dissolution", V_R)	d = 0.025 m $V_R = 24.6 \text{ m}^3$ (0.037 m^3 for each block)		$V_R = h \cdot (d_0/2 + d/2) \cdot 2\pi \cdot d$
Canister radius	0.47 m		Steag & Motor Columbus (1985)
Inner bentonite radius	0.47 m	0.81 m	Variation value based on half-thickness, assuming clay reaching >100 °C is altered and is a poor diffusion barrier (Johnson et al. 2002).
Outer bentonite radius	1.15 m		Radius after tunnel convergence (Section 5.3.3.1 of Nagra 2002c).
Bentonite porosity	0.36		Porosity at saturated density of 2150 kg m^{-3} (Section 5.3.3.1 of Nagra 2002c).
Bentonite grain density	2760 kg m^{-3}		Nagra (1994a)

Tab. A3.3-2c: ILW near field parameter values

Parameter	Reference value	Variations / Comments / References
Containment time	100 a	Assumption: incomplete resaturation of the near field and immobilisation of radionuclides in the waste forms prevent radionuclide release at earlier times. A containment time of 0 a is assumed in a "what if?" case.
Tunnel length (2 ILW-1 tunnels)	180 m	Reference value is for "cemented waste option" and corresponds to 2 × 90 m (Nagra 2002b, Beilage 3-1). Alternative value of 150 m for "high force compacted waste option" is based on the reduced conditioned waste volume for this option (McGinnes 2002).
Tunnel length (ILW-2 tunnel)	60 m	Nagra (2002b), Beilage 3-1. The amount of ILW-2 waste (WA-COG-2) is not affected by the different waste arising scenarios (McGinnes 2002).
Tunnel radius	4.5 m (ILW-1) 2.9 m (ILW-2)	See Tab. A3.3-4d
Outer tunnel radius	4.51 m (ILW-1) 2.91 m (ILW-2)	Represents a diffusion layer of 1 cm thickness of Opalinus Clay surrounding the ILW tunnels, see Appendix 3.6
Cement content in solid of cement matrix	700 kg m ⁻³ (ILW-1) 400 kg m ⁻³ (ILW-2)	Schwyn et al. (2003)
Average porosity of cement matrix (cement plus waste) for ILW-1 and ILW-2	0.3	Schwyn et al. (2003)

A3.3.2 Parameter values for PICNIC calculations

Tab. A3.3-3 presents parameter values for PICNIC calculations. Each of the 20 parameters is assigned a number, which is given in the first column and corresponds to the parameter numbering scheme in Tabs. 3.2-2a-c. The parameters are described in words in the second column. Specific values assigned to each parameter are identified by code letters (A, B, C, ...), which are given in the third column. The fourth column either gives the values themselves, or a reference to another table where the values can be found (e.g. Tabs. A3.3-4a-e). Some parameters are specific to a particular leg within a PICNIC network. In the cases of the lengths, cross-sectional areas and Darcy velocities of legs (Parameter 3, 4 and 5), the fourth column is split so that values for each leg are presented in a single row. The fifth column gives comments on the parameter values, or refers to source documentation allowing the origins of the parameter values to be traced. Again, where the symbol ► is shown, further explanatory notes on the parameter are given in Section A3.6.

In Tabs. A3.3-4a-e, various parameters related to the properties of the geosphere and the access tunnel system including ramp and shaft are given and referenced, including:

- parameters for host rock (Tab. A3.3-4a);
- key hydrogeological parameters for alternative radionuclide transport pathways within the host rock and confining units (Tab. A3.3-4b);
- parameters for alternative radionuclide transport pathways within / along the ramp / shaft (Tab. A3.3-4c);
- effective radii for various repository elements (Tab. A3.3-4d);
- parameters used for the gas model (Tab. A3.3-4e).

Tab. A3.3-3: Parameter values for PICNIC calculations

Parameter		Letter code and value		Comments / source					
Radionuclides and inventory									
1	Nuclides and decays to be used	A	Tab. A3.4-1	Selection of safety-relevant radionuclides described in Appendix 5.					
Network structure									
2	Description of network	A	Single leg	Single leg either representing the Opalinus Clay or a single tunnel segment as a homogeneous porous medium.					
		B	2 legs	Fig. 3.5-2a or Fig. 6.2-1					
		C	4 legs	Fig. 3.5-2b					
		D	7 legs	Fig. 3.6-5					
		E	2 legs <i>L₁</i> : operations tunnel ILW <i>L₇</i> : upwards through Opalinus Clay	Fig. 3.6-5					
Leg data – basic data									
3	Length of legs within a given network structure		Letter codes and values for each leg [m]			Comments / source			
	Network (A)	Single leg	A	40			Tab. A3.3-4a		
			B	30			Decreased transport distance in Opalinus Clay.		
			C	1000			Tab. A3.3-4c		
	Network (B)	2 legs	D	<i>L₁</i>		<i>L₂</i>	Tabs. A3.3-4a-c		
				140		200			
				40		40			
	Network (C)	4 legs	F	<i>L₁₁</i>		<i>L₁₂</i>	<i>L₂₁</i>	<i>L₂₂</i>	
				40		25 000	100	15 000	
	Network (D)	7 legs	G	<i>L₁</i>	<i>L₂</i>	<i>L₃</i>	<i>L₄</i>	<i>L₅</i>	<i>L₆</i>
1 000				1 000	800	100	40	40	40
100				100	800	100	40	40	40
Network (E) ⁵⁶	2 legs	I	<i>L₁</i>			<i>L₇</i>			
			1 000			40			
4	Cross-sectional area of legs within a given network structure		Letter codes and values for each leg [m ²]				Comments / source		
	Networks (A) and (B)	Single leg and 2 legs	A	Irrelevant (single leg cases) or identical for all legs originating at repository (magnitude irrelevant)					
	Network (C)	4 legs	B	<i>L₁₁</i>		<i>L₁₂</i>	<i>L₂₁</i>	<i>L₂₂</i>	
				= <i>L₂₁</i>		1	= <i>L₁₁</i>	1	
	Network (D)	7 legs	C	<i>L₁</i>	<i>L₂</i>	<i>L₃</i>	<i>L₄</i>	<i>L₅</i>	<i>L₆</i>
23				23	23	23	13	A, C: 2.0 × 10 ⁴ B: 1.2 × 10 ⁵	4 000
Network (E)	2 legs	D	<i>L₁</i>			<i>L₇</i>			
			23			4 000			

⁵⁶ Network E is a sub-system of network D, corresponding to the ILW part of the repository, including the operations tunnel and the ramp.

Tab. A3.3-3: (Cont.)

5	Darcy velocity of legs within a given network structure		Letter codes and values for each leg [$\times 10^{-7} \text{ m a}^{-1}$]						Comments / source
Network (A)	Single leg	A	6.3						Tab. A3.3-4a
		B	0						Diffusive transport only
		C	0.63						Parameter variations
		D	63						
		E	630						
		V	2.2×10^4						Gas-induced release through ramp only (Section 6.5).
		W	1.3×10^5						
		X	3.2×10^7						Values (X) and (Y) correspond to 1 mm aperture features of transmissivity 10^{-10} and $10^{-9} \text{ m}^2 \text{ s}^{-1}$ (Section 6.2).
		Y	3.2×10^8						
		Network (B)	2 legs	F	L_1			L_2	
			32			6.3			
Network (C)	4 legs	G	L_{11}		L_{12}		L_{21}		L_{22}
			6.3		160		16		32 000
Network (D)	7 legs	H	L_1	L_2	L_3	L_4	L_5	L_6	L_7
			280	87	34	110	260	5.5	5.0
		I	1 300	430	480	3 200	6 500	5.1	4.0
		J	1 800	-1 000	70	230	540	8.8	80
		K	9 100	-	-	-	-	-	450
		L	SF: 830 ILW: 650	830	22	83	180	5.4	2.8
Network (E)	2 legs	M	L_1			L_7			
			5 700			160			
6	Peclet number	A	10				The Peclet number is the ratio of transport distance to longitudinal dispersion length. A review of field-scale dispersion in porous and fractured media has been reported in Gelhar et al. (1992), on the basis of which a Peclet number of 10 is adopted in the present study.		
		B	dispersion neglected						
7	Effective diffusion coefficient	A	Tab. A3.5-5 / col. (1)						
		B	Tab. A3.5-5 / col. (2)						
	Pore diffusion coefficient	C	$6.3 \times 10^{-2} \text{ m}^2 \text{ a}^{-1}$						Diffusion coefficient for free water (Fetter 1993).
		D	$1.6 \times 10^{-2} \text{ m}^2 \text{ a}^{-1}$						Pore diffusion coefficient for tunnel backfill (Tab. A3.3-4c)
		E	$1.6 \times 10^{-3} \text{ m}^2 \text{ a}^{-1}$						Tab. A3.3-4c

Tab. A3.3-3: (Cont.)

Parameter		Letter code and value		Comments / source
Leg data – properties of flowing region				
8	Grain density	A	2 720 kg m ⁻³	Tab. A3.3-4a
		B	Irrelevant	Fractured geosphere cases with no fracture infill.
	Bulk dry density	C	558 kg m ⁻³	Mass of bentonite per m ³ of backfill material, Tab. A3.3-4c
		D	2 120 kg m ⁻³	Corresponding to EDZ of Opalinus Clay, Tab. A3.3-4c
9	Flow porosity	A	Equal to infill porosity	Required for modelling Opalinus Clay as a homogeneous porous medium .
		B	10 ⁻³	Fractured Wedelsandstein formation, Tab. A3.3-4b
		C	1	Fractured geosphere cases with no fracture infill.
10	Infill porosity	A	0.12 × porosity factors in Tab. A3.5-5	A3.3-4a
		B	1	Fractured geosphere cases with no fracture infill.
		C	0.05 × porosity factors in Tab. A3.5-5	Sandsteinkeuper formation, A3.3-4b
		D	0.22	Tab. A3.3-4c (EDZ)
		E	0.3	Tab. A3.3-4c
11	Sorption K_d	A	Tab. A3.5-5 / col. (1)	
		B	Tab. A3.5-5 / col. (2)	
		C ^f	Tab. A3.5-5 / col. (1) × 0.05	Clay content (Sandsteinkeuper) = 0.05 × clay content (Opalinus Clay), see Chapter 9 of Nagra (2002a)
		D	Irrelevant	Fractured geosphere cases with no fracture infill.
		E	Tab. A3.5-2/ col. (1)	Bentonite values.
		F	$K_d(I) = 0$	
Leg data – properties of matrix (relevant only in the case of a fractured geosphere)				
12	Specific surface area	A	Irrelevant	Non-fractured geosphere.
		B	2 000 m ⁻¹	1 mm apertures assumed for discontinuities.
13	Maximum penetration depth	A	0 m	No matrix diffusion.
		B	0.5 m	Fractured Wedelsandstein formation.
		C	Limited to half the canister pitch in the case of SF/HLW and unlimited in the case of ILW	
14	Surface sorption coefficient	A	Irrelevant or 0 m	Non-fractured geosphere or no surface sorption on the surfaces of discontinuities.
15	Grain density	A	Irrelevant	Non-fractured geosphere.
		B	2 720 kg m ⁻³	Reference value for Opalinus Clay - equivalent to Parameter 8, value (A).

Tab. A3.3-3: (Cont.)

Parameter		Letter code and value		Comments / source
Leg data – properties of matrix (relevant only in the case of a fractured geosphere)				
16	Matrix porosity	A	Irrelevant	Non-fractured geosphere.
		B	$0.12 \times$ porosity factors in Tab. A3.5-5	Matrix (Wedelsandstein), Tab. A3.3-4b
		C	$0.12 \times$ porosity factors in Tab. A3.5-5	Matrix (Opalinus Clay), Tab. A3.3-4a
17	Sorption K_d	A	Irrelevant	Non-fractured geosphere.
		B ¹	Tab. A3.5-5 / col. (1) $\times 0.1$	Clay content (Wedelsandstein) = $0.1 \times$ clay content (Opalinus Clay), see Chapter 9 of Nagra (2002a)
		C	Tab. A3.5-5 / col. (1)	
18	Pore diffusion coefficient	A	Irrelevant	Non-fractured geosphere.
		B ¹	$8.3 \times 10^{-11} \text{ m}^2 \text{ s}^{-1}$ (anions) $4.2 \times 10^{-10} \text{ m}^2 \text{ s}^{-1}$ (non-anions)	Identical to pore diffusion constant parallel to strata in Opalinus Clay, Tab. A3.3-4a
Network flow data				
19	Head at upstream end of leg	-	-	Irrelevant because flows in each leg are specified via the Darcy velocity (Parameter 5) and the cross-sectional area (Parameter 4).
20	Head at downstream end of leg	-	-	

¹ These are the values suggested by Nagra (2002a). However, in the calculations for Case 1.5b, the Reference Case sorption values for Opalinus Clay (Tab. A3.5-5 / col. 1) and a pore diffusion constant for anions of $4.2 \times 10^{-11} \text{ m}^2 \text{ s}^{-1}$ were used. Employing the values suggested by Nagra (2002a) leads to a slightly (3 %) higher summed dose maximum than that shown in Tab. 7.10-1 of Nagra (2002c).

Tab. A3.3-4a: Parameters for host rock

Parameter	Value	Source / comments
Grain density [kg m ⁻³]	2 720	Nagra 2002a, Tab. 9.4-1
Porosity for non-anions [-]	0.12	Nagra 2002a, Tab. 9.4-1
Porosity for anions [-]	0.06	Nagra 2002a, Tab. 9.4-1
Effective diffusion constant for non-anions, perpendicular to bedding planes [m ² s ⁻¹]	1 × 10 ⁻¹¹ (best guess) 1 × 10 ⁻¹⁰ (pessimistic)	Nagra 2002a, Tab. 9.4-3
Effective diffusion constant for anions, perpendicular to bedding planes [m ² s ⁻¹]	1 × 10 ⁻¹² (best guess) 3 × 10 ⁻¹² (pessimistic)	Nagra 2002a, Tab. 9.4-3
Effective diffusion constant for non-anions, parallel to bedding planes [m ² s ⁻¹]	5 × 10 ⁻¹¹	Nagra 2002a, Tab. 9.4-3
Effective diffusion constant for anions, parallel to bedding planes [m ² s ⁻¹]	5 × 10 ⁻¹²	Nagra 2002a, Tab. 9.4-3
Darcy velocity [m s ⁻¹]	2 × 10 ⁻¹⁴	Nagra 2002a, Tab. 9.4-4a: Obtained by multiplying K _v (the vertical hydraulic conductivity) by 1 (the best guess for the hydraulic gradient).
Vertical transport path length (upwards / downwards) [m]	40	Nagra 2002a, Tab. 9.4-4a: Includes variability of the thickness of the host rock and vertical extent of the emplacement tunnels and their EDZ.
Specific storage coefficient S _s [m ⁻¹]	1 × 10 ⁻⁵	Nagra 2002a, Tab. 9.4-2

Tab. A3.3-4b: Key hydrogeological parameters for alternative radionuclide transport pathways within the host rock and confining units

Parameter	Value	Source / comments
Vertical transport path length (upwards); corresponds to leg L ₁ of network (B) in Tab. A3.3-3. [m]	140	Nagra 2002a, Tab. 9.4-4b: 40 m in host rock and 100 m in upper confining units (see Figs. 3.5-1/2).
Hydraulic conductivity for L ₁ [m s ⁻¹]	1 × 10 ⁻¹³	Nagra 2002a, Tab. 9.4-4b.
Vertical transport path length (downwards); corresponds to leg L ₂ of network (B) in Tab. A3.3-3. [m]	200	Nagra 2002a, Tab. 9.4-4b: 40 m in host rock and 160 m in lower confining units (see Figs. 3.5-1/2).
Hydraulic conductivity for L ₂ [m s ⁻¹]	2 × 10 ⁻¹⁴	Nagra 2002a, Tab. 9.4-4b.
Vertical transport path length in host rock (upwards); corresponds to leg L ₁₁ of network (C) in Tab. A3.3-3. [m]	40	Nagra 2002a, Tab. 9.4-4a: Includes variability of the thickness of the host rock and vertical extent of the emplacement tunnels and their EDZ; part of transport pathway upwards through host rock and laterally in the Wedelsandstein (see Figs. 3.5-1/2).
Hydraulic conductivity for L ₁₁ [m s ⁻¹]	2 × 10 ⁻¹⁴	Nagra 2002a, Tab. 9.4-4a.
Lateral transport in Wedelsandstein; corresponds to leg L ₁₂ of network (C) in Tab. A3.3-3. [m]	25 000	Nagra 2002a, Tab. 9.4-4a: Part of transport pathway upwards through host rock and laterally in the Wedelsandstein (see Fig. 3.5-1).
Hydraulic conductivity for L ₁₂ [m s ⁻¹]	5 × 10 ⁻¹⁰	Nagra 2002a, Tab. 9.4-4a.
Hydraulic gradient for L ₁₂ [-]	1 × 10 ⁻³	Nagra 2002a, Tab. 9.4-4a.
Hydraulic head in Wedelsandstein [m]	342	Nagra 2002a, Tab. 9.4-4a.
Flow porosity in Wedelsandstein [-]	1 × 10 ⁻³	Derived from trace length per unit surface perpendicular to flow of 1 m m ⁻² as given in Nagra 2002, Tab. 9.4-4a, and an assumed fracture aperture of 1 mm.
Matrix porosity in Wedelsandstein, non-anions [-]	0.12	Taken to be identical to the values for Opalinus Clay (Nagra 2002a, Chapter 9).
Matrix porosity in Wedelsandstein, anions [-]	0.06	
Vertical transport path length (downwards); corresponds to leg L ₂₁ of network (C) in Tab. A3.3-3. [m]	100	Nagra 2002a, Fig. 6.5-1a: Part of transport pathway downwards through host rock / lower confining units and laterally in the Sandsteinkeuper (see also Figs. 3.5-1/2).
Hydraulic conductivity for L ₂₁ [m s ⁻¹]	5 × 10 ⁻¹⁴	Nagra 2002a, Tab. 9.4-4a.
Lateral transport in Sandsteinkeuper; corresponds to leg L ₂₂ of network (C) in Tab. A3.3-3. [m]	15 000	Nagra 2002a, Tab. 9.4-4a: Part of transport pathway downwards through host rock / lower confining units and laterally in the Sandsteinkeuper (see also Figs. 3.5-1/2).

Tab. A3.3-4b: (Cont.)

Parameter	Value	Source / comments
Hydraulic conductivity for L ₂₂ [m s ⁻¹]	2×10^{-8}	Nagra 2002a, Tab. 9.4-4a.
Hydraulic gradient for L ₂₂ [-]	5×10^{-3}	Nagra 2002a, Tab. 9.4-4a.
Hydraulic head in Sandsteinkeuper [m]	465	Nagra 2002a, Tab. 9.4-4a.
Flow porosity in Sandsteinkeuper [-]	5×10^{-2}	Nagra 2002a, Tab. 9.4-4a.
Transmissivity of hypothetical transmissive discontinuities in the host rock [m ² s ⁻¹]	1×10^{-10}	Nagra 2002a, Tab. 9.4-5c. Note that in a parameter variation, a hypothetical hydraulic transmissivity of 10^{-9} m ² s ⁻¹ is postulated.
Hydraulic gradient for transport along hypothetical transmissive discontinuities [-]	1	Nagra 2002a, Tab. 9.4-5c. The gradient is upwardly directed and corresponds to the head difference between the Wedelsandstein and the Stubensandstein formations at Benken.

Tab. A3.3-4c: Parameters for alternative radionuclide transport pathways within / along the ramp / shaft

Parameter	Value	Source / comments
Transport distance in backfilled tunnel / ramp from parts A, C and D of the repository in Fig. 3.6-1; corresponds to length of legs L ₁ and L ₂ of network (D) in Tab. A3.3-3. [m]	1 000	Nagra 2002b, Beilagen 3-1 and 3-2: Approximate transport distance in the backfilled tunnel / ramp up to the point where the ramp intersects the boundary between the host rock and the upper confining units.
Transport distance in backfilled ventilation tunnel from part A of the repository to the shaft; corresponds to leg L ₃ of network (D) in Tab. A3.3-3. [m]	800	Nagra 2002b, Beilage 3-1 (approximate value)
Transport distance in backfilled tunnel from part C of the repository to the shaft; corresponds to leg L ₄ of network (D) in Tab. A3.3-3. [m]	100	Nagra 2002b, Beilage 3-1 (approximate value)
Tunnel backfill, part bentonite [wt-%]	30	design requirement
Tunnel backfill, part sand [wt-%]	70	design requirement
Porosity of tunnel backfill [-]	0.3	assumption

Tab. A3.3-4c: (Cont.)

Parameter	Value	Source / comments
Pore diffusion constant for tunnel backfill [m ² s ⁻¹]	5×10^{-10}	assumption
Hydraulic conductivity for tunnels backfilled with bentonite / sand mixture [m s ⁻¹]	5×10^{-11}	assumption
Dry density of bentonite in tunnel backfill [kg m ⁻³]	558	derived from dry density of bentonite (Tab. A3.3-2a), dry density of sand (1900 kg m ⁻³ assumed), and mixing ratio bentonite / sand
Vertical transport distance in EDZ of shaft; corresponds to leg L ₅ of network (D) in Tab. A3.3-3. [m]	40	The same arguments apply as for the vertical transport path length in the host rock (Tab. A3.3-4a).
Hydraulic conductivity for EDZ [m s ⁻¹]	1×10^{-12}	Nagra 2002a, Tab. 9.4-5b
Porosity for EDZ [-]	0.22	Nagra 2002a, Tab. 9.4-5b
Pore diffusion constant for EDZ parallel to bedding planes perp. to bedding planes [m ² s ⁻¹]	2×10^{-10} 5×10^{-11}	Corresponds to an effective diffusion constant of 5×10^{-11} m ² s ⁻¹ (value for non-anions parallel to bedding planes) or 1×10^{-11} m ² s ⁻¹ (value for non-anions perp. to bedding planes) as given in Nagra (2002a), Tab. 9.4-3.
Dry density for EDZ [kg m ⁻³]	2 120	derived from grain density of Opalinus Clay (2720 kg m ⁻³ , see Tab. A3.3-4a) and EDZ porosity
Vertical transport distance upwards through host rock; corresponds to length of legs L ₆ and L ₇ of network (D) in Tab. A3.3-3. [m]	40	see Tab. A3.3-4a
Hydraulic conductivity for bentonite (backfilled SF/HLW tunnels, seals) [m s ⁻¹]	1×10^{-13}	assumption, based on discussion in Nagra (2002c), Section 5.3.3.1

Tab. A3.3-4d: Effective radii for various repository elements

Parameter	Value	Source / comments
SF/HLW emplacement tunnels		
radius after convergence [m]	1.15	Nagra 2002a, Tab. 9.4-5a
radius for EDZ [m]	1.85	Nagra 2002a, Tab. 9.4-5a proposes to add 0.7 m to the unconverged tunnel radius of 1.25 m to obtain the radius for the inner EDZ. For the simplified analytical flow calculations in the present report, the converged tunnel radius of 1.15 m and an EDZ radius of 1.15 m + 0.7 m = 1.85 m was used.
ILW emplacement tunnels		
radius ¹ for ILW-1 (including liner) [m]	4.5	Nagra 2002b, Beilage 3-8 (Schnitt L-L)
radius for EDZ for ILW-1 [m]	5.5	Nagra 2002a, Tab. 9.4-5b
radius ¹ for ILW-2 (including liner) [m]	2.9	Nagra 2002b, Beilage 3-7
radius for EDZ for ILW-2 [m]	3.9	Nagra 2002a, Tab. 9.4-5b
Ramp		
radius ² (excluding liner) [m]	3.1	Nagra 2002b, Beilage 3-3 (Zugangstunnel einschalig)
radius for EDZ [m]	4.4	Nagra 2002a, Tab. 9.4-5b
Shaft		
radius ² (excluding liner) [m]	1.8	Nagra 2002b, Beilage 3-9 (Schachtscheibe einschalig)
radius for EDZ [m]	2.7	Nagra 2002a, Tab. 9.4-5b
Construction and operations tunnels		
radius ² (excluding liner) [m]	2.7	Nagra 2002b, Beilage 3-6 (Betriebstunnel: Schnitt C-C)
radius for EDZ [m]	3.9	Nagra 2002a, Tab. 9.4-5b

¹ Effective radii r_a **including** the liner are calculated from the cross-sectional area A using the expression $r_a = (A/\pi)^{1/2}$

² Effective radii r_i **excluding** the liner of thickness d are calculated using the expression $r_i = r_a - d$

Tab. A3.3-4e: Parameters used for the Gas Model

RV: reference value (best guess); AV: alternative value (pessimistic). Taken from Tab. 9.4-7 of Nagra (2002a)

Parameter	RV	AV	Comments
Host rock			
Pore pressure at repository depth [MPa]	6.5	7.5	
Intrinsic permeability [m ²]	1×10^{-20}	2×10^{-21}	
Gas permeability [m ²]	1×10^{-21}	1×10^{-24}	
Gas entry pressure [MPa]	5	-	
Gas accessible porosity [-]	0.024	0.006	Only AV is used in safety assessment calculations. This value is calculated by assuming that of the total porosity of Opalinus Clay (0.12), only 5 % is gas accessible due to in-situ stress conditions at repository depth.
Threshold pressure for creation of dilatant gas pathways [MPa]	13	-	
EDZ			
Gas entry pressure [MPa]	2	-	
Gas accessible porosity [-]	0.011	-	This value is obtained by multiplying the porosity of the EDZ of 0.22 (Tab 9.4-5a of Nagra 2002a) by 5 % (the fraction of the total porosity that is gas accessible, which is assumed to be the same as that for undisturbed host rock, see comment above).
Wedelsandstein formation			
Gas accessible porosity [-]	0.001	-	
Gas entry pressure [MPa]	0.2	-	

A3.4 Nuclide-dependent parameters

This section presents tables of nuclide-dependent parameter values that are referenced by Tabs. A3.3-1 and A3.3-3 of the previous section.

Tab. A3.4-1 gives a list of all safety-relevant radionuclides considered in the evaluation of assessment cases, together with relevant properties directly related to radioactivity, namely half lives, conversion factors from moles to becquerels, dose coefficients for inhalation and ingestion and exposure factors for external radiation from surface contamination in the biosphere. For the selection of safety-relevant radionuclides and the treatment of decay chains, see Appendix 5.

Tabs. A3.4-2a-c give the inventories of radionuclides in the different waste packages. Tab. A3.4-2a gives the inventories of each spent fuel canister containing one of the three reference spent fuel types, with the abbreviated names BWR-UO₂-48, PWR-mixed-48 and PWR-UO₂-48. These spent fuel types are described in Chapter 4 of Nagra (2002c). The table also indicates how the inventories are distributed between the fuel matrix, the fuel cladding and the instant release fraction (IRF). Tab. A3.4-2b gives the inventories of each spent fuel canister containing one of the four alternative spent fuel types, with the abbreviated names PUO55, PUO55/65, PUO55/75 and PMIX48/65. These spent fuel types are described in Tab. 7.4-1 of Nagra (2002c). Tab. A3.4-2b again indicates how the inventories are distributed between the fuel matrix, the fuel cladding and the IRF. Tab. A3.4-2c gives the inventories of each high-level waste canister containing waste from reprocessing by BNFL and by COGEMA. It also shows the inventories of the ILW-1 and ILW-2 tunnels. In the case of ILW-1, the inventories are shown for both the cemented waste option and the high force compacted waste option. The inventories for ILW-2 are identical for both options.

Tab. A3.4-1: Safety-relevant radionuclides and properties related to radioactivity

Half-lives are taken from McGinnes (2000), dose coefficients from StSV (1994) or, where this reference does not present a value for a given nuclide, from ICRP (1996), and exposure factors for external radiation from Svensson (1979).

Radionuclide and daughters	Half-life [a]	Conversion factor from moles to Bq [Bq mol ⁻¹]	Dose coefficient		γ -ray exposure factor [Sv/(Bq m ⁻³) a]
			for inhalation [Sv Bq ⁻¹]	for ingestion [Sv Bq ⁻¹]	
³ H	1.2×10^1	1.1×10^{15}	2.6×10^{-10}	4.2×10^{-11}	0.0
¹⁰ Be	1.6×10^6	8.3×10^9	3.5×10^{-8}	1.1×10^{-9}	0.0
¹⁴ C	5.7×10^3	2.3×10^{12}	5.8×10^{-9}	5.8×10^{-10}	0.0
³⁶ Cl	3.0×10^5	4.4×10^{10}	7.3×10^{-9}	9.3×10^{-10}	0.0
⁴¹ Ca	1.0×10^5	1.3×10^{11}	1.8×10^{-10}	1.9×10^{-10}	0.0
⁵⁹ Ni	7.5×10^4	1.8×10^{11}	4.4×10^{-10}	6.3×10^{-11}	0.0
⁶⁰ Co → Ni (stable)	5.3×10^0	2.5×10^{15}	3.1×10^{-8}	3.4×10^{-9}	2.47×10^{-9}
⁶³ Ni	1.0×10^2	1.3×10^{14}	1.3×10^{-9}	1.5×10^{-10}	0.0
⁷⁹ Se	1.1×10^6	1.2×10^{10}	6.8×10^{-9}	2.9×10^{-9}	0.0
⁹⁰ Sr → Zr (stable)	2.9×10^1	4.6×10^{14}	1.6×10^{-7}	3.1×10^{-8}	0.0
⁹³ Mo → ^{93m} Nb	4.0×10^3	3.3×10^{12}	2.3×10^{-9}	3.1×10^{-9}	0.0
^{93m} Nb → Nb (stable)	1.6×10^1	8.2×10^{14}	1.8×10^{-9}	1.2×10^{-10}	0.0
⁹³ Zr → ^{93m} Nb (95%), ⁹³ Nb (5%)	1.5×10^6	8.8×10^9	2.5×10^{-8}	1.1×10^{-9}	0.0
⁹⁴ Nb	2.0×10^4	6.6×10^{11}	4.9×10^{-8}	1.7×10^{-9}	1.44×10^{-9}
⁹⁹ Tc	2.1×10^5	6.3×10^{10}	1.3×10^{-8}	6.4×10^{-10}	0.0
¹⁰⁷ Pd → Ag (stable)	6.5×10^6	2.0×10^9	5.9×10^{-10}	3.7×10^{-11}	0.0
^{108m} Ag → Pd (stable)	4.2×10^2	3.2×10^{13}	3.7×10^{-8}	2.3×10^{-9}	1.38×10^{-9}
^{121m} Sn	5.5×10^1	2.4×10^{14}	4.7×10^{-9}	5.6×10^{-10}	2.05×10^{-12}
¹²⁶ Sn	2.3×10^5	5.6×10^{10}	2.8×10^{-8}	5.1×10^{-9}	2.65×10^{-11}
¹²⁹ I	1.6×10^7	8.4×10^8	3.6×10^{-8}	1.1×10^{-7}	3.08×10^{-12}
¹³⁵ Cs	2.3×10^6	5.8×10^9	8.6×10^{-9}	2.0×10^{-9}	0.0
¹³⁷ Cs	3.0×10^1	4.4×10^{14}	3.9×10^{-8}	1.3×10^{-8}	4.91×10^{-10}
¹⁵¹ Sm	9.3×10^1	1.4×10^{14}	4.0×10^{-9}	9.8×10^{-11}	2.16×10^{-13}
^{166m} Ho	1.2×10^3	1.1×10^{13}	1.2×10^{-7}	2.0×10^{-9}	1.43×10^{-9}
¹⁵⁴ Eu	8.8	1.5×10^{15}	5.3×10^{-8}	2.0×10^{-9}	1.10×10^{-9}
²²⁸ Ra → ²²⁸ Th	5.8	2.3×10^{15}	1.6×10^{-5}	6.9×10^{-7}	0.0
²²⁸ Th → Pb (stable)	1.9	6.9×10^{15}	4.4×10^{-5}	1.4×10^{-7}	1.83×10^{-12}
²³² Th → ²²⁸ Ra	1.4×10^{10}	9.4×10^5	1.1×10^{-4}	2.3×10^{-7}	1.31×10^{-13}
²³² U → ²²⁸ Th	6.9×10^1	1.9×10^{14}	3.7×10^{-5}	3.3×10^{-7}	5.29×10^{-13}
²³⁶ U → ²³² Th	2.3×10^7	5.6×10^8	8.7×10^{-6}	4.7×10^{-8}	0.0
²⁴⁰ Pu → ²³⁶ U	6.6×10^3	2.0×10^{12}	1.2×10^{-4}	2.5×10^{-7}	0.0
²⁴⁴ Cm → ²⁴⁰ Pu	1.8×10^1	7.3×10^{14}	5.7×10^{-5}	1.2×10^{-7}	3.91×10^{-14}

Tab. A3.4-1: (Cont.)

Radionuclide and daughters	Half-life [a]	Conversion factor from moles to Bq [Bq mol ⁻¹]	Dose coefficient		γ -ray exposure factor [Sv/(Bq m ⁻³) a]	
			for inhalation [Sv Bq ⁻¹]	for ingestion [Sv Bq ⁻¹]		
4N+1 chain	²²⁹ Th → Pb (stable)	7.9×10^3	1.7×10^{12}	2.6×10^{-4}	6.1×10^{-7}	1.77×10^{-11}
	²³³ U → ²²⁹ Th	1.6×10^5	8.3×10^{10}	9.6×10^{-6}	5.1×10^{-8}	5.29×10^{-13}
	²³⁷ Np → ²³³ U	2.1×10^6	6.2×10^9	5.0×10^{-5}	1.1×10^{-7}	1.62×10^{-11}
	²⁴¹ Am → ²³⁷ Np	4.3×10^2	3.1×10^{13}	9.6×10^{-5}	2.0×10^{-7}	9.48×10^{-12}
	²⁴¹ Pu → ²⁴¹ Am	1.4×10^1	9.2×10^{14}	2.3×10^{-6}	4.8×10^{-9}	0.0
	²⁴⁵ Cm → ²⁴¹ Pu	8.5×10^3	1.6×10^{12}	9.9×10^{-5}	2.1×10^{-7}	2.78×10^{-11}
4N+2 chain	²¹⁰ Pb → ²¹⁰ Po	2.2×10^1	5.9×10^{14}	5.7×10^{-6}	6.9×10^{-7}	6.20×10^{-13}
	²¹⁰ Po → Pb (stable)	3.8×10^{-1}	3.5×10^{16}	4.3×10^{-6}	1.2×10^{-6}	5.54×10^{-14}
	²²⁶ Ra → ²¹⁰ Pb	1.6×10^3	8.3×10^{12}	9.5×10^{-6}	2.8×10^{-7}	5.49×10^{-12}
	²³⁰ Th → ²²⁶ Ra	7.5×10^4	1.8×10^{11}	1.0×10^{-4}	2.1×10^{-7}	3.02×10^{-13}
	²³⁴ U → ²³⁰ Th	2.5×10^5	5.4×10^{10}	9.4×10^{-6}	4.9×10^{-8}	2.70×10^{-13}
	²³⁸ Pu → ²³⁴ U	8.8×10^1	1.5×10^{14}	1.1×10^{-4}	2.3×10^{-7}	1.16×10^{-13}
	²³⁸ U → ²³⁴ U	4.5×10^9	3.0×10^6	8.0×10^{-6}	4.8×10^{-8}	0.0
	^{242m} Am → ²³⁸ Pu (82.7 %), ²⁴² Pu (17.3%)	1.4×10^2	9.4×10^{13}	9.7×10^{-5}	2.0×10^{-7}	0.0
	²⁴² Pu → ²³⁸ U	3.8×10^5	3.5×10^{10}	1.1×10^{-4}	2.4×10^{-7}	0.0
	²⁴⁶ Cm → ²⁴² Pu	4.7×10^3	2.8×10^{12}	9.8×10^{-5}	2.1×10^{-7}	0.0
4N+3 chain	²²⁷ Ac → Pb (stable)	2.2×10^1	6.1×10^{14}	5.7×10^{-4}	1.2×10^{-6}	0.0
	²³¹ Pa → ²²⁷ Ac	3.3×10^4	4.0×10^{11}	1.4×10^{-4}	7.1×10^{-7}	1.60×10^{-11}
	²³⁵ U → ²³¹ Pa	7.0×10^8	1.9×10^7	8.5×10^{-6}	4.7×10^{-8}	9.49×10^{-11}
	²³⁹ Pu → ²³⁵ U	2.4×10^4	5.5×10^{11}	1.2×10^{-4}	2.5×10^{-7}	5.75×10^{-14}
	²⁴³ Am → ²³⁹ Pu	7.4×10^3	1.8×10^{12}	9.6×10^{-5}	2.0×10^{-7}	2.56×10^{-11}
	²⁴³ Cm → ²³⁹ Pu	2.9×10^1	4.5×10^{14}	6.9×10^{-5}	1.5×10^{-7}	3.91×10^{-14}

Tab. A3.4-2a: Inventories and their distributions – reference SF packages

Inventory data taken from McGinnes (2002). Distribution data taken from Johnson & McGinnes (2002) and summarised in Tab. A3.4-2d.

Radionuclides and stable isotopes		Inventory per waste package after 40 years decay [mol] and distribution [%]								
		BWR-UO ₂ -48			PWR-mixed-48			PWR-UO ₂ -48		
		matrix	clad.	IRF	matrix	clad.	IRF	matrix	clad.	IRF
Activation / fission products	³ H	6.53 × 10 ⁻³			6.10 × 10 ⁻³			6.38 × 10 ⁻³		
		98	0	2	98	0	2	98	0	2
	¹⁰ Be	2.12 × 10 ⁻³			2.03 × 10 ⁻³			2.07 × 10 ⁻³		
		90	0	10	90	0	10	90	0	10
	¹⁴ C _{inorg}	2.89 × 10 ⁻²			2.41 × 10 ⁻²			2.70 × 10 ⁻²		
		90	0	10	90	0	10	90	0	10
	¹⁴ C _{org}	2.48 × 10 ⁻²			1.36 × 10 ⁻²			1.55 × 10 ⁻²		
		0	80	20	0	80	20	0	80	20
	³⁶ Cl	5.17 × 10 ⁻²			3.16 × 10 ⁻²			3.70 × 10 ⁻²		
		33	62	5	44	51	5	45	50	5
	⁴¹ Ca	2.28 × 10 ⁻³			1.70 × 10 ⁻³			2.01 × 10 ⁻³		
		76	24	0	84	16	0	84	16	0
	⁵⁹ Ni	7.20 × 10 ⁻¹			6.62 × 10 ⁻¹			6.91 × 10 ⁻¹		
		1	99	0	1	99	0	1	99	0
	⁶³ Ni	1.03 × 10 ⁻¹			9.45 × 10 ⁻²			1.01 × 10 ⁻¹		
		1	99	0	1	99	0	1	99	0
	⁷⁹ Se	1.32 × 10 ⁻¹			1.21 × 10 ⁻¹			1.29 × 10 ⁻¹		
		91	0	9	94	0	6	96	0	4
	⁹⁰ Sr	4.83			4.07			4.72		
		99	0	1	99	0	1	99	0	1
⁹³ Mo	1.26 × 10 ⁻⁴			2.36 × 10 ⁻⁴			2.44 × 10 ⁻⁴			
	20	80	0	9	91	0	9	91	0	
^{93m} Nb	1.61 × 10 ⁻⁴			1.38 × 10 ⁻⁴			1.53 × 10 ⁻⁴			
	89	11	0	93	7	0	93	7	0	
⁹³ Zr	1.90 × 10 ²			1.61 × 10 ²			1.80 × 10 ²			
	90	10	0	93	7	0	93	7	0	
⁹⁴ Nb	2.00 × 10 ⁻²			5.46 × 10 ⁻²			5.67 × 10 ⁻²			
	2	98	0	0	100	0	0	100	0	
⁹⁹ Tc	1.77 × 10 ¹			1.65 × 10 ¹			1.73 × 10 ¹			
	98	0	2	98	0	2	98	0	2	
¹⁰⁷ Pd	5.00			5.62			4.74			
	98	0	2	98	0	2	98	0	2	
^{108m} Ag	4.58 × 10 ⁻⁵			3.89 × 10 ⁻⁵			4.23 × 10 ⁻⁵			
	100	0	0	100	0	0	100	0	0	
¹²⁶ Sn	5.36 × 10 ⁻¹			5.89 × 10 ⁻¹			5.24 × 10 ⁻¹			
	91	0	9	92	0	8	96	0	4	

Tab. A3.4-2a: (Cont.)

Radionuclides and stable isotopes		Inventory per waste package after 40 years decay [mol] and distribution [%]								
		BWR-UO ₂ -48			PWR-mixed-48			PWR-UO ₂ -48		
		matrix	clad.	IRF	matrix	clad.	IRF	matrix	clad.	IRF
Activation / fission products	¹²⁹ I	3.21			3.17			3.14		
		91	0	9	93	0	7	96	0	4
	¹³⁵ Cs	6.37			7.56			6.76		
		95	0	5	94	0	6	96	0	4
	¹³⁷ Cs	7.99			7.49			7.79		
		95	0	5	95	0	5	96	0	4
¹⁵¹ Sm	1.12 × 10 ⁻¹			1.32 × 10 ⁻¹			1.10 × 10 ⁻¹			
	100	0	0	100	0	0	100	0	0	
^{166m} Ho	1.88 × 10 ⁻⁴			1.83 × 10 ⁻⁴			1.70 × 10 ⁻⁴			
	100	0	0	100	0	0	100	0	0	
Stable isotopes	Ag	1.60			1.92			1.56		
		100	0	0	100	0	0	100	0	0
	Ca	2.31			1.99			2.08		
		78	22	0	85	15	0	85	15	0
	Ho	5.89 × 10 ⁻³			6.85 × 10 ⁻³			5.75 × 10 ⁻³		
		100	0	0	100	0	0	100	0	0
	Nb	1.39			6.16			6.35		
		1	99	0	0	100	0	0	100	0
	Ni	2.63 × 10 ²			3.98 × 10 ²			4.12 × 10 ²		
		0	100	0	0	100	0	0	100	0
	Pb	4.35 × 10 ⁻¹			2.61 × 10 ⁻¹			2.75 × 10 ⁻¹		
		2	98	0	3	97	0	3	97	0
	Pd	2.43 × 10 ¹			2.61 × 10 ¹			2.34 × 10 ¹		
		98	0	2	98	0	2	98	0	2
	Se	1.40			1.25			1.38		
		91	0	9	94	0	6	96	0	4
	Sm	6.91			6.48			6.58		
		100	0	0	100	0	0	100	0	0
	Sn	8.68 × 10 ¹			5.20 × 10 ¹			5.48 × 10 ¹		
		1	99	0	2	98	0	1	99	0
Sr	8.28			7.09			8.24			
	99	0	1	99	0	1	99	0	1	
Zr	7.38 × 10 ³			4.46 × 10 ³			4.71 × 10 ³			
	1	99	0	1	99	0	2	98	0	

Tab. A3.4-2a: (Cont.)

Radionuclides and stable isotopes		Inventory per waste package after 40 years decay [mol] and distribution [%]								
		BWR-UO ₂ -48			PWR-mixed-48			PWR-UO ₂ -48		
		matrix	clad.	IRF	matrix	clad.	IRF	matrix	clad.	IRF
4N chain	²²⁸ Ra	1.38 × 10 ⁻¹⁴			1.03 × 10 ⁻¹⁴			1.35 × 10 ⁻¹⁴		
		100	0	0	100	0	0	100	0	0
	²²⁸ Th	2.76 × 10 ⁻⁸			2.40 × 10 ⁻⁸			2.92 × 10 ⁻⁸		
		100	0	0	100	0	0	100	0	0
	²³² Th	4.40 × 10 ⁻⁵			3.29 × 10 ⁻⁵			4.29 × 10 ⁻⁵		
		100	0	0	100	0	0	100	0	0
	²³² U	9.12 × 10 ⁻⁷			8.65 × 10 ⁻⁷			1.05 × 10 ⁻⁶		
		100	0	0	100	0	0	100	0	0
	²³⁶ U	3.67 × 10 ¹			2.74 × 10 ¹			3.58 × 10 ¹		
		100	0	0	100	0	0	100	0	0
	²⁴⁰ Pu	1.97 × 10 ¹			3.25 × 10 ¹			1.78 × 10 ¹		
		100	0	0	100	0	0	100	0	0
²⁴⁴ Cm	1.09 × 10 ⁻¹			2.49 × 10 ⁻¹			1.02 × 10 ⁻¹			
	100	0	0	100	0	0	100	0	0	
4N+1 chain	²²⁹ Th	8.46 × 10 ⁻⁹			6.79 × 10 ⁻⁹			8.46 × 10 ⁻⁹		
		100	0	0	100	0	0	100	0	0
	²³³ U	8.04 × 10 ⁻⁵			6.51 × 10 ⁻⁵			7.86 × 10 ⁻⁵		
		100	0	0	100	0	0	100	0	0
	²³⁷ Np	5.15			4.47			5.04		
		100	0	0	100	0	0	100	0	0
	²⁴¹ Am	9.87			1.60 × 10 ¹			9.15		
		100	0	0	100	0	0	100	0	0
	²⁴¹ Pu	1.66			2.67			1.58		
		100	0	0	100	0	0	100	0	0
	²⁴⁵ Cm	3.58 × 10 ⁻²			1.13 × 10 ⁻¹			3.20 × 10 ⁻²		
		100	0	0	100	0	0	100	0	0
4N+2 chain	²¹⁰ Pb	1.58 × 10 ⁻¹⁰			1.40 × 10 ⁻¹⁰			1.70 × 10 ⁻¹⁰		
		100	0	0	100	0	0	100	0	0
	²¹⁰ Po	2.60 × 10 ⁻¹²			2.30 × 10 ⁻¹²			2.81 × 10 ⁻¹²		
		100	0	0	100	0	0	100	0	0
	²²⁶ Ra	3.46 × 10 ⁻⁸			3.15 × 10 ⁻⁸			3.76 × 10 ⁻⁸		
		100	0	0	100	0	0	100	0	0
	²³⁰ Th	1.81 × 10 ⁻⁴			1.71 × 10 ⁻⁴			1.95 × 10 ⁻⁴		
		100	0	0	100	0	0	100	0	0
	²³⁴ U	1.80			1.77			1.85		
		100	0	0	100	0	0	100	0	0
	²³⁸ Pu	1.69			2.13			1.55		
		100	0	0	100	0	0	100	0	0
²³⁸ U	6.45 × 10 ³			5.54 × 10 ³			5.78 × 10 ³			
	100	0	0	100	0	0	100	0	0	

Tab. A3.4-2a: (Cont.)

Radionuclides and stable isotopes		Inventory per waste package after 40 years decay [mol] and distribution [%]								
		BWR-UO ₂ -48			PWR-mixed-48			PWR-UO ₂ -48		
		matrix	clad.	IRF	matrix	clad.	IRF	matrix	clad.	IRF
4N+2 chain	^{242m} Am	6.06 × 10 ⁻³			2.48 × 10 ⁻²			6.58 × 10 ⁻³		
		100	0	0	100	0	0	100	0	0
	²⁴² Pu	5.41			8.68			4.85		
		100	0	0	100	0	0	100	0	0
	²⁴⁶ Cm	4.33 × 10 ⁻³			1.17 × 10 ⁻²			4.11 × 10 ⁻³		
		100	0	0	100	0	0	100	0	0
4N+3 chain	²²⁷ Ac	5.50 × 10 ⁻¹⁰			5.00 × 10 ⁻¹⁰			6.40 × 10 ⁻¹⁰		
		100	0	0	100	0	0	100	0	0
	²³¹ Pa	1.89 × 10 ⁻⁶			1.74 × 10 ⁻⁶			2.23 × 10 ⁻⁶		
		100	0	0	100	0	0	100	0	0
	²³⁵ U	4.83 × 10 ¹			4.46 × 10 ¹			5.69 × 10 ¹		
		100	0	0	100	0	0	100	0	0
	²³⁹ Pu	4.06 × 10 ¹			5.23 × 10 ¹			3.97 × 10 ¹		
		100	0	0	100	0	0	100	0	0
	²⁴³ Am	1.24			2.21			1.13		
		100	0	0	100	0	0	100	0	0
	²⁴³ Cm	1.47 × 10 ⁻³			4.33 × 10 ⁻³			1.44 × 10 ⁻³		
		100	0	0	100	0	0	100	0	0

Tab. A3.4-2b: Inventories and their distributions – alternative SF packages

Inventory data taken from McGinnes (2002). Distribution data taken from Johnson & McGinnes (2002) and summarised in Tab. A3.4-2d.

Radio-nuclides and stable isotopes		Inventory per waste package after 40 years decay [mol] and distribution [%]											
		PUO55			PUO55/65			PUO55/75			PMIX48/65		
		matrix	clad.	IRF	matrix	clad.	IRF	matrix	clad.	IRF	matrix	clad.	IRF
Activation / fission products	³ H	7.39 × 10 ⁻³			7.68 × 10 ⁻³			7.94 × 10 ⁻³			6.55 × 10 ⁻³		
		99	0	1	99	0	1	99	0	1	98	0	2
	¹⁰ Be	2.45 × 10 ⁻³			2.54 × 10 ⁻³			2.64 × 10 ⁻³			2.15 × 10 ⁻³		
		90	0	10	90	0	10	90	0	10	90	0	10
	¹⁴ C _{inorg}	3.10 × 10 ⁻²			3.28 × 10 ⁻²			3.37 × 10 ⁻²			2.54 × 10 ⁻²		
		90	0	10	90	0	10	90	0	10	90	0	10
	¹⁴ C _{org}	1.95 × 10 ⁻²			2.05 × 10 ⁻²			2.12 × 10 ⁻²			1.48 × 10 ⁻²		
		0	80	20	0	80	20	0	80	20	0	80	20
	³⁶ Cl	4.51 × 10 ⁻²			4.77 × 10 ⁻²			4.85 × 10 ⁻²			3.32 × 10 ⁻²		
		42	52	5	41	52	6	40	52	7	43	51	6
	⁴¹ Ca	2.63 × 10 ⁻³			2.71 × 10 ⁻³			2.84 × 10 ⁻³			1.76 × 10 ⁻³		
		83	17	0	83	17	0	83	17	0	84	16	0
	⁵⁹ Ni	7.09 × 10 ⁻¹			7.43 × 10 ⁻¹			7.77 × 10 ⁻¹			6.90 × 10 ⁻¹		
		1	99	0	1	99	0	1	99	0	1	99	0
	⁶³ Ni	1.01 × 10 ⁻¹			1.05 × 10 ⁻¹			1.09 × 10 ⁻¹			9.99 × 10 ⁻²		
		1	99	0	1	99	0	1	99	0	1	99	0
	⁷⁹ Se	1.55 × 10 ⁻¹			1.61 × 10 ⁻¹			1.68 × 10 ⁻¹			1.30 × 10 ⁻¹		
		89	0	11	87	0	13	85	0	15	92	0	8
	⁹⁰ Sr	5.38			5.56			5.82			4.22		
		99	0	1	99	0	1	99	0	1	96	0	4
	⁹³ Mo	2.56 × 10 ⁻⁴			2.68 × 10 ⁻⁴			2.79 × 10 ⁻⁴			2.48 × 10 ⁻⁴		
		10	90	0	10	90	0	10	90	0	10	90	0
	^{93m} Nb	1.78 × 10 ⁻⁴			1.83 × 10 ⁻⁴			1.90 × 10 ⁻⁴			1.46 × 10 ⁻⁴		
		93	7	0	92	8	0	92	8	0	93	7	0
	⁹³ Zr	2.08 × 10 ²			2.14 × 10 ²			2.23 × 10 ²			1.71 × 10 ²		
		93	7	0	93	7	0	93	7	0	93	7	0
	⁹⁴ Nb	5.45 × 10 ⁻²			5.74 × 10 ⁻²			5.98 × 10 ⁻²			5.65 × 10 ⁻²		
		1	99	0	1	99	0	1	99	0	1	99	0
⁹⁹ Tc	1.88 × 10 ¹			1.96 × 10 ¹			2.01 × 10 ¹			1.75 × 10 ¹			
	92	0	8	91	0	9	89	0	11	93	0	7	
¹⁰⁷ Pd	5.66			6.08			6.35			6.44			
	92	0	8	90	0	10	89	0	11	90	0	10	
^{108m} Ag	4.61 × 10 ⁻⁵			4.93 × 10 ⁻⁵			5.06 × 10 ⁻⁵			4.14 × 10 ⁻⁵			
	100	0	0	100	0	0	100	0	0	100	0	0	
¹²⁶ Sn	6.06 × 10 ⁻¹			6.49 × 10 ⁻¹			6.76 × 10 ⁻¹			6.63 × 10 ⁻¹			
	89	0	11	87	0	13	84	0	16	90	0	10	

Tab. A3.4-2b: (Cont.)

Radio-nuclides and stable isotopes		Inventory per waste package after 40 years decay [mol] and distribution [%]											
		PUO55			PUO55/65			PUO55/75			PMIX48/65		
		matrix	clad.	IRF	matrix	clad.	IRF	matrix	clad.	IRF	matrix	clad.	IRF
Activation / fission products	¹²⁹ I	3.51			3.70			3.83			3.47		
		89	0	11	87	0	13	85	0	15	91	0	9
	¹³⁵ Cs	7.03			7.37			7.92			8.28		
		89	0	11	87	0	13	84	0	16	90	0	10
	¹³⁷ Cs	8.87			9.31			9.67			8.09		
		89	0	11	87	0	13	85	0	15	92	0	8
	¹⁵¹ Sm	1.42×10^{-1}			1.36×10^{-1}			1.48×10^{-1}			1.37×10^{-1}		
		100	0	0	100	0	0	100	0	0	100	0	0
	^{166m} Ho	2.11×10^{-4}			2.33×10^{-4}			2.43×10^{-4}			2.24×10^{-4}		
		100	0	0	100	0	0	100	0	0	100	0	0
Stable isotopes	Ag	1.87			1.99			1.83			2.11		
		100	0	0	100	0	0	100	0	0	100	0	0
	Ca	2.11			2.11			2.11			2.00		
		83	17	0	83	17	0	83	17	0	84	16	0
	Ho	6.84×10^{-3}			7.35×10^{-3}			6.76×10^{-3}			7.88×10^{-3}		
		100	0	0	100	0	0	100	0	0	100	0	0
	Nb	5.31			5.27			5.27			5.86		
		0	100	0	0	100	0	0	100	0	0	100	0
	Ni	3.65×10^2			3.61×10^2			3.61×10^2			3.86×10^2		
		0	100	0	0	100	0	0	100	0	0	100	0
	Pb	3.00×10^{-1}			3.00×10^{-1}			3.00×10^{-1}			2.70×10^{-1}		
		3	97	0	3	97	0	3	97	0	3	97	0
	Pd	2.81×10^1			3.05×10^1			2.78×10^1			3.00×10^1		
		92	0	8	90	0	10	90	0	10	91	0	9
	Se	1.56			1.62			1.55			1.33		
		89	0	11	87	0	13	86	0	14	92	0	8
	Sm	7.67			7.98			7.61			7.00		
		100	0	0	100	0	0	100	0	0	100	0	0
	Sn	6.18×10^1			6.18×10^1			6.18×10^1			5.42×10^1		
		1	98	0	1	98	0	1	98	0	2	98	0
Sr	9.34			9.61			9.30			7.38			
	99	0	1	99	0	1	99	0	1	96	0	4	
Zr	5.20×10^3			5.20×10^3			5.19×10^3			4.62×10^3			
	2	98	0	2	98	0	2	98	0	2	98	0	

Tab. A3.4-2b: (Cont.)

Radio-nuclides and stable isotopes		Inventory per waste package after 40 years decay [mol] and distribution [%]											
		PUO55			PUO55/65			PUO55/75			PMIX48/65		
		matrix	clad.	IRF	matrix	clad.	IRF	matrix	clad.	IRF	matrix	clad.	IRF
4N chain	²²⁸ Ra	1.49 × 10 ⁻¹⁴			1.49 × 10 ⁻¹⁴			1.54 × 10 ⁻¹⁴			1.04 × 10 ⁻¹⁴		
		100	0	0	100	0	0	100	0	0	100	0	0
	²²⁸ Th	9.23 × 10 ⁻⁸			8.16 × 10 ⁻⁸			1.16 × 10 ⁻⁷			2.56 × 10 ⁻⁸		
		100	0	0	100	0	0	100	0	0	100	0	0
	²³² Th	4.62 × 10 ⁻⁵			4.62 × 10 ⁻⁵			4.79 × 10 ⁻⁵			3.29 × 10 ⁻⁵		
		100	0	0	100	0	0	100	0	0	100	0	0
	²³² U	3.24 × 10 ⁻⁶			2.85 × 10 ⁻⁶			4.05 × 10 ⁻⁶			9.17 × 10 ⁻⁷		
		100	0	0	100	0	0	100	0	0	100	0	0
²³⁶ U	3.86 × 10 ¹			3.86 × 10 ¹			3.98 × 10 ¹			2.76 × 10 ¹			
	100	0	0	100	0	0	100	0	0	100	0	0	
²⁴⁰ Pu	2.00 × 10 ¹			2.06 × 10 ¹			2.08 × 10 ¹			3.41 × 10 ¹			
	100	0	0	100	0	0	100	0	0	100	0	0	
²⁴⁴ Cm	1.61 × 10 ⁻¹			1.96 × 10 ⁻¹			2.33 × 10 ⁻¹			4.47 × 10 ⁻¹			
	100	0	0	100	0	0	100	0	0	100	0	0	
4N+1 chain	²²⁹ Th	1.11 × 10 ⁻⁸			1.07 × 10 ⁻⁸			1.20 × 10 ⁻⁸			6.91 × 10 ⁻⁹		
		100	0	0	100	0	0	100	0	0	100	0	0
	²³³ U	1.05 × 10 ⁻⁴			1.02 × 10 ⁻⁴			1.16 × 10 ⁻⁴			6.63 × 10 ⁻⁵		
		100	0	0	100	0	0	100	0	0	100	0	0
	²³⁷ Np	7.05			6.87			7.81			4.54		
		100	0	0	100	0	0	100	0	0	100	0	0
	²⁴¹ Am	9.64			9.77			9.90			1.67 × 10 ¹		
		100	0	0	100	0	0	100	0	0	100	0	0
²⁴¹ Pu	1.64			1.65			1.69			2.77			
	100	0	0	100	0	0	100	0	0	100	0	0	
²⁴⁵ Cm	4.50 × 10 ⁻²			5.87 × 10 ⁻²			6.88 × 10 ⁻²			2.52 × 10 ⁻¹			
	100	0	0	100	0	0	100	0	0	100	0	0	
4N+2 chain	²¹⁰ Pb	1.60 × 10 ⁻¹⁰			1.60 × 10 ⁻¹⁰			1.62 × 10 ⁻¹⁰			1.49 × 10 ⁻¹⁰		
		100	0	0	100	0	0	100	0	0	100	0	0
	²¹⁰ Po	2.58 × 10 ⁻¹²			2.60 × 10 ⁻¹²			2.63 × 10 ⁻¹²			2.44 × 10 ⁻¹²		
		100	0	0	100	0	0	100	0	0	100	0	0
	²²⁶ Ra	3.57 × 10 ⁻⁸			3.57 × 10 ⁻⁸			3.67 × 10 ⁻⁸			3.39 × 10 ⁻⁸		
		100	0	0	100	0	0	100	0	0	100	0	0
	²³⁰ Th	2.04 × 10 ⁻⁴			2.00 × 10 ⁻⁴			2.10 × 10 ⁻⁴			1.89 × 10 ⁻⁴		
		100	0	0	100	0	0	100	0	0	100	0	0
²³⁴ U	2.12			2.08			2.25			2.04			
	100	0	0	100	0	0	100	0	0	100	0	0	
²³⁸ Pu	2.37			2.45			2.87			2.83			
	100	0	0	100	0	0	100	0	0	100	0	0	

Tab. A3.4-2b: (Cont.)

Radio-nuclides and stable isotopes		Inventory per waste package after 40 years decay [mol] and distribution [%]											
		PUO55			PUO55/65			PUO55/75			PMIX48/65		
		matrix	clad.	IRF	matrix	clad.	IRF	matrix	clad.	IRF	matrix	clad.	IRF
4N+2 chain	²³⁸ U	5.78×10^3			5.78×10^3			5.78×10^3			5.54×10^3		
		100	0	0	100	0	0	100	0	0	100	0	0
	^{242m} Am	6.09×10^{-3}			6.17×10^{-3}			6.41×10^{-3}			2.74×10^{-2}		
		100	0	0	100	0	0	100	0	0	100	0	0
	²⁴² Pu	6.18			6.72			6.95			1.16×10^1		
		100	0	0	100	0	0	100	0	0	100	0	0
²⁴⁶ Cm	6.11×10^{-3}			9.58×10^{-3}			1.22×10^{-2}			3.19×10^{-2}			
	100	0	0	100	0	0	100	0	0	100	0	0	
4N+3 chain	²²⁷ Ac	4.86×10^{-10}			4.35×10^{-10}			4.41×10^{-10}			4.95×10^{-10}		
		100	0	0	100	0	0	100	0	0	100	0	0
	²³¹ Pa	1.66×10^{-6}			1.49×10^{-6}			1.50×10^{-6}			1.73×10^{-6}		
		100	0	0	100	0	0	100	0	0	100	0	0
	²³⁵ U	4.22×10^1			3.80×10^1			3.83×10^1			4.42×10^1		
		100	0	0	100	0	0	100	0	0	100	0	0
	²³⁹ Pu	3.68×10^1			3.68×10^1			3.68×10^1			4.99×10^1		
		100	0	0	100	0	0	100	0	0	100	0	0
	²⁴³ Am	1.64			1.84			2.02			3.18		
		100	0	0	100	0	0	100	0	0	100	0	0
²⁴³ Cm	1.85×10^{-3}			2.04×10^{-3}			2.20×10^{-3}			6.53×10^{-3}			
	100	0	0	100	0	0	100	0	0	100	0	0	

Tab. A3.4-2c: Reference inventories of HLW packages and ILW tunnels and inventory of ILW-1 for the high force compacted waste option

Data taken from McGinnes (2002).

Radionuclides and stable isotopes		Inventory per waste package after 40 years decay [mol]		Total inventory after 40 years decay [mol]		
		Reference inventory (ILW: Cemented waste option) (1)				High force compacted waste option (2)
		COGEMA	BNFL	ILW-1	ILW-2	ILW-1
Activation / fission products	³ H	-	-	2.01	3.92×10^{-5}	2.01
	¹⁴ C _{inorg}	8.23×10^{-5}	3.08×10^{-5}	4.00	-	4.00
	¹⁴ C _{org}	-	-	3.94	3.48×10^{-4}	3.93
	³⁶ Cl	-	-	1.43	3.56×10^{-4}	1.42
	⁵⁹ Ni	1.36×10^{-2}	3.80×10^{-3}	6.96×10^2	3.91×10^{-3}	6.94×10^2
	⁶⁰ Co	-	-	1.61×10^{-1}	7.94×10^{-6}	1.69×10^{-1}
	⁶³ Ni	1.99×10^{-3}	5.42×10^{-4}	1.11×10^2	5.26×10^{-4}	1.11×10^2
	⁷⁹ Se	9.98×10^{-2}	1.33×10^{-1}	1.12×10^{-1}	7.64×10^{-4}	1.10×10^{-1}
	⁹⁰ Sr	2.81	3.46	4.45	1.66×10^{-2}	4.49
	⁹³ Mo	1.54×10^{-5}	1.51×10^{-5}	4.30×10^{-1}	8.16×10^{-7}	4.31×10^{-1}
	^{93m} Nb	9.39×10^{-5}	1.34×10^{-4}	7.33×10^{-3}	1.03×10^{-4}	7.34×10^{-3}
	⁹³ Zr	1.07×10^2	1.47×10^2	6.70×10^3	1.17×10^2	6.69×10^3
	⁹⁴ Nb	1.03×10^{-3}	1.50×10^{-5}	4.78×10^1	9.83×10^{-6}	4.77×10^1
	⁹⁹ Tc	1.33×10^1	1.49×10^1	2.54×10^1	6.08×10^{-2}	2.53×10^1
	¹⁰⁷ Pd	3.19	3.69	-	-	-
	^{108m} Ag	1.71×10^{-5}	1.49×10^{-5}	-	-	-
	^{121m} Sn	-	-	1.09	1.75×10^{-6}	1.09
	¹²⁶ Sn	6.56×10^{-1}	9.04×10^{-1}	2.79×10^{-1}	5.23×10^{-2}	2.83×10^{-1}
	¹²⁹ I	1.90×10^{-3}	2.49×10^{-3}	5.13×10^1	4.55	5.12×10^1
	¹³⁵ Cs	3.48	6.78	2.08×10^1	5.13×10^{-2}	2.05×10^1
¹³⁷ Cs	4.33	5.25	9.76	7.34×10^{-2}	9.89	
¹⁵¹ Sm	9.84×10^{-2}	1.20×10^{-1}	3.72×10^{-1}	1.80×10^{-3}	3.51×10^{-1}	
¹⁵⁴ Eu	-	-	2.09×10^{-2}	1.63×10^{-4}	2.09×10^{-2}	
^{166m} Ho	1.63×10^{-5}	1.36×10^{-5}	-	-	-	
Stable is.	Ni	1.07×10^1	5.71	-	-	-
	Pd	1.74×10^1	1.94×10^1	-	-	-
	Se	8.88×10^{-1}	1.22	-	-	-
	Sn	1.08	9.71×10^{-1}	-	-	-

Tab. A3.4-2c: (Cont.)

Radionuclides and stable isotopes		Inventory per waste package after 40 years decay [mol]		Total inventory after 40 years decay [mol]		
		Reference inventory (ILW: Cemented waste option) (1)				High force compacted waste option (2)
		COGEMA	BNFL	ILW-1	ILW-2	ILW-1
4N chain	²²⁸ Ra	1.17×10^{-17}	2.43×10^{-18}	0	0	0
	²²⁸ Th	1.59×10^{-10}	3.33×10^{-11}	2.30×10^{-8}	0	2.34×10^{-8}
	²³² Th	3.61×10^{-8}	7.54×10^{-9}	0	0	0
	²³² U	5.21×10^{-9}	1.20×10^{-9}	8.14×10^{-7}	0	8.04×10^{-7}
	²³⁶ U	3.01×10^{-2}	6.55×10^{-3}	1.35×10^1	2.17	1.35×10^1
	²⁴⁰ Pu	9.43×10^{-2}	1.14×10^{-1}	1.17×10^1	3.80×10^{-1}	1.18×10^1
	²⁴⁴ Cm	2.05×10^{-2}	1.64×10^{-2}	7.35×10^{-3}	1.36×10^{-4}	7.23×10^{-3}
4N+1 chain	²²⁹ Th	3.28×10^{-9}	3.75×10^{-9}	2.06×10^{-9}	0	2.07×10^{-9}
	²³³ U	3.73×10^{-5}	4.21×10^{-5}	2.18×10^{-5}	9.22×10^{-7}	2.05×10^{-5}
	²³⁷ Np	2.76	3.24	1.20	8.07×10^{-2}	1.19
	²⁴¹ Am	1.01	3.27	5.37	2.25×10^{-1}	5.31
	²⁴¹ Pu	9.66×10^{-4}	2.39×10^{-3}	6.27×10^{-1}	3.37×10^{-2}	6.32×10^{-1}
	²⁴⁵ Cm	3.79×10^{-3}	4.18×10^{-3}	9.73×10^{-4}	2.36×10^{-5}	9.72×10^{-4}
	²¹⁰ Pb	3.88×10^{-11}	1.37×10^{-10}	7.93×10^{-11}	1.03×10^{-11}	7.98×10^{-11}
	²¹⁰ Po	6.30×10^{-13}	2.26×10^{-12}	1.30×10^{-12}	1.76×10^{-13}	1.30×10^{-12}
4N+2 chain	²²⁶ Ra	6.53×10^{-9}	2.30×10^{-8}	1.85×10^{-8}	2.41×10^{-9}	1.86×10^{-8}
	²³⁰ Th	1.77×10^{-5}	6.27×10^{-5}	1.05×10^{-4}	1.33×10^{-5}	1.05×10^{-4}
	²³⁴ U	1.86×10^{-3}	1.84×10^{-3}	1.02	1.21×10^{-1}	1.02
	²³⁸ Pu	2.06×10^{-3}	5.11×10^{-3}	5.06×10^{-1}	2.54×10^{-2}	5.06×10^{-1}
	²³⁸ U	6.42	2.03	3.68×10^3	4.91×10^2	3.67×10^3
	^{242m} Am	6.35×10^{-3}	1.27×10^{-2}	1.09×10^{-3}	1.62×10^{-4}	1.11×10^{-3}
	²⁴² Pu	3.12×10^{-3}	9.92×10^{-3}	2.16	1.19×10^{-1}	2.16
	²⁴⁶ Cm	3.93×10^{-4}	4.29×10^{-4}	1.10×10^{-4}	2.33×10^{-6}	1.09×10^{-4}
4N+3 chain	²²⁷ Ac	1.04×10^{-9}	2.63×10^{-9}	6.05×10^{-10}	6.93×10^{-11}	6.04×10^{-10}
	²³¹ Pa	2.06×10^{-6}	4.95×10^{-6}	2.06×10^{-6}	2.37×10^{-7}	2.06×10^{-6}
	²³⁵ U	6.38×10^{-2}	1.60×10^{-2}	5.30×10^1	5.91	5.30×10^1
	²³⁹ Pu	3.83×10^{-2}	1.22×10^{-1}	3.10×10^1	1.19	3.10×10^1
	²⁴³ Am	4.23×10^{-1}	4.90×10^{-1}	2.01×10^{-1}	2.05×10^{-2}	2.03×10^{-1}
	²⁴³ Cm	5.94×10^{-4}	6.38×10^{-4}	2.03×10^{-4}	3.54×10^{-6}	2.07×10^{-4}

Tab. A3.4-2d: IRF values of key radionuclides for BWR and PWR UO₂ fuel and PWR MOX fuel

In all cases, the IRF is applied to the radionuclide inventory present in the fuel matrix. In the case of ¹⁴C, there is an additional IRF of 20 % assumed for the inventory of the cladding. Data taken from Johnson & McGinnes (2002).

Nuclide	t _{1/2} [a]	IRF Value [%]			
		BWR UO ₂ Fuel (48 GWd/t _{IHM})	PWR UO ₂ Fuel (48 GWd/t _{IHM})	PWR UO ₂ Fuel (75 GWd/t _{IHM})	PWR MOX Fuel (48 GWd/t _{IHM})
³ H ^{*)}	1.23 × 10 ¹	1	1	1	1
¹⁰ Be	1.6 × 10 ⁶	10	10	10	10
¹⁴ C	5.73 × 10 ³	10	10	10	10
³⁶ Cl	3.0 × 10 ⁵	13	10	25	15
⁷⁹ Se	1.1 × 10 ⁶	9	4	25	15
⁹⁰ Sr	2.86 × 10 ¹	1	1	1	1
⁹⁹ Tc	2.1 × 10 ⁵	2	2	17	2
¹⁰⁷ Pd	6.5 × 10 ⁶	2	2	17	2
¹²⁶ Sn	2.3 × 10 ⁵	9	4	25	15
¹²⁹ I	1.57 × 10 ⁷	9	4	25	15
¹³⁵ Cs	2.3 × 10 ⁶	5	4	25	10
¹³⁷ Cs	3.02 × 10 ¹	5	4	25	10

*) Assessment calculations were performed using an IRF of 2 %.

A3.5 Element-dependent parameters

This section presents the tables of the element-dependent parameter values that are referenced by Tabs. A3.3-1 and A3.3-3 of Section A3.3. Column numbers referenced by these tables are given in parentheses.

Tab. A3.5-1 gives a list of solubility limits for the SF / HLW near field for both reducing and oxidising conditions. In the case of reducing conditions, both optimistic and pessimistic values are given in addition to the reference values. The data for Tab. A3.5-1 are taken from Berner (2002).

Tab. A3.5-1: Solubility limits and associated uncertainties for the SF / HLW near field, for reference case (pH = 7.25, Eh = -194 mV) and for oxidising conditions ("what if?" case); "high" denotes a solubility limit that is assumed to be never attained
Data taken from Berner (2002).

Element	Solubility limits [mol l ⁻¹]			
	Reducing conditions			Oxidising conditions ¹
	Reference values (1)	Pessimistic values (2)	Optimistic values	(3)
H	high	high	high	
Be	1×10^{-6}	high	1×10^{-6}	
C _{inorg}	3×10^{-3}	7×10^{-3}	6×10^{-4}	
C _{org}	high	high	high	
Cl	high	high	high	
Ca	1×10^{-2}	1×10^{-2}	1×10^{-2}	
Ni	3×10^{-5}	8×10^{-5}	1×10^{-5}	
Se	5×10^{-9}	1×10^{-5}	2×10^{-11}	high
Sr	2×10^{-5}	1×10^{-4}	3×10^{-6}	
Zr	2×10^{-9}	2×10^{-9}	3×10^{-11}	
Nb	3×10^{-5}	1×10^{-4}	1×10^{-8}	
Mo	1×10^{-6}	1×10^{-5}	1×10^{-6}	
Tc	4×10^{-9}	1×10^{-8}	1×10^{-9}	high
Pd	5×10^{-8}	2×10^{-7}	1×10^{-10}	
Ag	3×10^{-6}	3×10^{-6}	1×10^{-10}	
Sn	1×10^{-8}	1×10^{-7}	5×10^{-9}	
I	high	high	high	
Cs	high	high	high	
Sm	5×10^{-7}	9×10^{-7}	3×10^{-7}	
Ho	5×10^{-7}	9×10^{-7}	3×10^{-7}	
Pb	2×10^{-6}	8×10^{-5}	2×10^{-8}	
Po	high	high	high	
Ra	2×10^{-11}	5×10^{-8}	4×10^{-12}	
Ac	1×10^{-6}	3×10^{-5}	5×10^{-8}	
Th	7×10^{-7}	3×10^{-6}	2×10^{-7}	
Pa	1×10^{-8}	1×10^{-5}	1×10^{-8}	1×10^{-5}
U	3×10^{-9}	5×10^{-7}	3×10^{-10}	3×10^{-4}
Np	5×10^{-9}	1×10^{-8}	3×10^{-9}	1×10^{-5}
Pu	5×10^{-8}	1×10^{-6}	3×10^{-9}	3×10^{-8}
Am	1×10^{-6}	3×10^{-5}	5×10^{-8}	
Cm	1×10^{-6}	3×10^{-5}	5×10^{-8}	

¹ Only given when different from reducing conditions

Tab. A3.5-2 gives a list of sorption coefficients, effective diffusion coefficients and accessible porosities in compacted bentonite for both reducing and oxidising conditions. In the case of the sorption coefficients for reducing conditions, both optimistic and pessimistic values are given in addition to the reference values. The data for Tab. A3.5-2 are taken from Bradbury & Bayens (2003a). Porosities are those of the buffer after tunnel convergence (Chapter 5 in Nagra 2002c).

Tab. A3.5-3 gives a list of solubility limits for the ILW cementitious near field. Both optimistic and pessimistic values are given for ILW-1 and ILW-2, in addition to the reference values. The derived ILW-2 reference values may also be used as conservative estimates for a “what if?” case that assumes oxidising conditions in ILW-1. The data for Tab. A3.5-3 are taken from Berner (2003).

Tab. A3.5-4 gives a list of sorption coefficients for the ILW cementitious near field. Both optimistic and pessimistic values are given for ILW-1 and ILW-2, in addition to the reference values. The ILW-2 reference values may also be used as conservative estimates for a “what if?” case that assumes oxidising conditions in ILW-1. The data for Tab. A3.5-4 are taken from Wieland and Van Loon (2002).

Tab. A3.5-2: Sorption constants, effective diffusion coefficients and accessible porosities in compacted bentonite

Reference Case (pH = 7.25, Eh = -194 mV) incl. lower (pessimistic) and upper (optimistic) limits, and "what if?" case for oxidising conditions. Data taken from Bradbury & Baeyens (2003a).

Element	Sorption coefficients [m ³ kg ⁻¹]			Effective diffusion coefficients [m ² s ⁻¹]		Accessible porosities		
	Reducing			Oxidising ¹	Reducing	Oxidising ¹	Reducing	Oxidising ¹
	Reference (1)	Pessimistic (2)	Optimistic	(3)	(1)	(3)	(1)	(3)
H	0	0	0		2 × 10 ⁻¹⁰		0.36	
Be	0.2	0.009	5		2 × 10 ⁻¹⁰		0.36	
C _{inorg}	6 × 10 ⁻⁵	2 × 10 ⁻⁵	3 × 10 ⁻⁴		3 × 10 ⁻¹²		0.05	
C _{org}	0	0	0		2 × 10 ⁻¹⁰		0.36	
Cl	0	0	0		3 × 10 ⁻¹²		0.05	
Ca	0.003	5 × 10 ⁻⁴	0.02		2 × 10 ⁻¹⁰		0.36	
Ni	0.2	0.009	5		2 × 10 ⁻¹⁰		0.36	
Se	0	0	0	0.06	3 × 10 ⁻¹²		0.05	
Sr	0.003	5 × 10 ⁻⁴	0.02		2 × 10 ⁻¹⁰		0.36	
Zr	80	1	4000		2 × 10 ⁻¹⁰		0.36	
Nb	30	1	900		2 × 10 ⁻¹⁰		0.36	
Mo	0	0	0		3 × 10 ⁻¹²		0.05	
Tc	60	0.5	600	0	2 × 10 ⁻¹⁰	3 × 10 ⁻¹²	0.36	0.05
Pd	5	0.2	100		2 × 10 ⁻¹⁰		0.36	
Ag	0	0	0		2 × 10 ⁻¹⁰		0.36	
Sn	800	1	10000		2 × 10 ⁻¹⁰		0.36	
I ²	5 × 10 ⁻⁴	5 × 10 ⁻⁵	0.005		3 × 10 ⁻¹²		0.05	
Cs	0.1	0.03	0.3		2 × 10 ⁻¹⁰		0.36	
Sm	4	0.1	100		2 × 10 ⁻¹⁰		0.36	
Ho	4	0.1	100		2 × 10 ⁻¹⁰		0.36	
Pb	7	0.5	100		2 × 10 ⁻¹⁰		0.36	
Po	0.06	0.008	0.5		3 × 10 ⁻¹²		0.05	
Ra	0.002	3 × 10 ⁻⁴	0.01		2 × 10 ⁻¹⁰		0.36	
Ac	20	1	300		2 × 10 ⁻¹⁰		0.36	
Th	60	10	200		2 × 10 ⁻¹⁰		0.36	
Pa	5	0.2	100		2 × 10 ⁻¹⁰		0.36	
U	40	2	400	0.01	2 × 10 ⁻¹⁰		0.36	
Np	60	6	600	0.01	2 × 10 ⁻¹⁰		0.36	
Pu	20	1	300	10	2 × 10 ⁻¹⁰		0.36	
Am	20	1	300		2 × 10 ⁻¹⁰		0.36	
Cm	20	1	300		2 × 10 ⁻¹⁰		0.36	

¹ Only given when different from reducing conditions

² The possibility of K_d(I) = 0 is considered in a "what if?" case

Tab. A3.5-3: Solubility limits and associated uncertainties for the cementitious near field of the waste groups ILW-1 and ILW-2

"High" denotes a solubility limit that is assumed to be never attained. The ILW-2 reference values may also be used as conservative estimates for a "what if?" case that assumes oxidising conditions in ILW-1. Data taken from Berner (2003).

Element	ILW-1			ILW-2		
	Reference [mol l ⁻¹] (1)	Pessimistic [mol l ⁻¹] (3)	Optimistic [mol l ⁻¹]	Reference [mol l ⁻¹] (2)	Pessimistic [mol l ⁻¹] (4)	Optimistic [mol l ⁻¹]
H	high	high	high	high	high	high
C _{inorg}	2 × 10 ⁻⁴	4 × 10 ⁻⁴	1 × 10 ⁻⁴	2 × 10 ⁻⁴	4 × 10 ⁻⁴	1 × 10 ⁻⁴
C _{org}	high	high	high	high	high	high
Cl	high	high	high	high	high	high
Co	7 × 10 ⁻⁷	7 × 10 ⁻⁶	7 × 10 ⁻⁷	high	high	high
Ni	3 × 10 ⁻⁷	8 × 10 ⁻⁶	1 × 10 ⁻⁸	high	high	high
Se	1 × 10 ⁻⁵	7 × 10 ⁻⁴	7 × 10 ⁻⁶	high	high	high
Sr	3 × 10 ⁻³	6 × 10 ⁻³	2 × 10 ⁻³	3 × 10 ⁻³	6 × 10 ⁻³	2 × 10 ⁻³
Zr	6 × 10 ⁻⁶	6 × 10 ⁻⁵	6 × 10 ⁻⁷	6 × 10 ⁻⁶	6 × 10 ⁻⁵	6 × 10 ⁻⁷
Nb	high	high	high	high	high	high
Mo	3 × 10 ⁻⁵	2 × 10 ⁻³	3 × 10 ⁻⁶	3 × 10 ⁻⁵	2 × 10 ⁻³	3 × 10 ⁻⁶
Tc	high	high	3 × 10 ⁻⁷	high	high	high
Sn	1 × 10 ⁻⁷	8 × 10 ⁻⁶	1 × 10 ⁻⁷	1 × 10 ⁻⁷	8 × 10 ⁻⁶	1 × 10 ⁻⁷
I	high	high	high	high	high	high
Cs	high	high	high	high	high	high
Sm	2 × 10 ⁻⁶	2 × 10 ⁻⁵	2 × 10 ⁻⁷	2 × 10 ⁻⁶	2 × 10 ⁻⁵	2 × 10 ⁻⁷
Eu	2 × 10 ⁻⁶	2 × 10 ⁻⁵	2 × 10 ⁻⁷	2 × 10 ⁻⁶	2 × 10 ⁻⁵	2 × 10 ⁻⁷
Pb	3 × 10 ⁻³	high	3 × 10 ⁻³	3 × 10 ⁻³	high	3 × 10 ⁻³
Po	high	high	high	high	high	high
Ra	1 × 10 ⁻⁵	2 × 10 ⁻⁵	1 × 10 ⁻⁶	1 × 10 ⁻⁵	2 × 10 ⁻⁵	1 × 10 ⁻⁶
Ac	2 × 10 ⁻⁶	2 × 10 ⁻⁵	2 × 10 ⁻⁷	2 × 10 ⁻⁶	2 × 10 ⁻⁵	2 × 10 ⁻⁷
Th	3 × 10 ⁻⁹	1 × 10 ⁻⁸	8 × 10 ⁻¹⁰	3 × 10 ⁻⁹	1 × 10 ⁻⁸	8 × 10 ⁻¹⁰
Pa	1 × 10 ⁻⁸	high	1 × 10 ⁻⁸	1 × 10 ⁻⁸	high	1 × 10 ⁻⁸
U	1 × 10 ⁻⁸	5 × 10 ⁻⁷	1 × 10 ⁻⁸	1 × 10 ⁻⁸	5 × 10 ⁻⁷	1 × 10 ⁻⁸
Np	5 × 10 ⁻⁹	1 × 10 ⁻⁸	3 × 10 ⁻⁹	high	high	high
Pu	4 × 10 ⁻¹¹	1 × 10 ⁻¹⁰	1 × 10 ⁻¹¹	6 × 10 ⁻¹¹	6 × 10 ⁻¹⁰	2 × 10 ⁻¹¹
Am	2 × 10 ⁻⁹	1 × 10 ⁻⁸	3 × 10 ⁻¹⁰	2 × 10 ⁻⁹	1 × 10 ⁻⁸	3 × 10 ⁻¹⁰
Cm	2 × 10 ⁻⁹	1 × 10 ⁻⁸	3 × 10 ⁻¹⁰	2 × 10 ⁻⁹	1 × 10 ⁻⁸	3 × 10 ⁻¹⁰

Tab. A3.5-4: Sorption constants for the ILW cementitious near field

The ILW-2 reference values may also be used as conservative estimates for a "what if?" case that assumes oxidising conditions in ILW-1. Data taken from Wieland & Van Loon (2002).

Element	ILW-1			ILW-2		
	Reference [m ³ kg ⁻¹] (1)	Pessimistic [m ³ kg ⁻¹] (3)	Optimistic [m ³ kg ⁻¹]	Reference [m ³ kg ⁻¹] (2)	Pessimistic [m ³ kg ⁻¹] (4)	Optimistic [m ³ kg ⁻¹]
H	1 × 10 ⁻⁴	7 × 10 ⁻⁵	1 × 10 ⁻⁴	1 × 10 ⁻⁴	7 × 10 ⁻⁵	1 × 10 ⁻⁴
C _{inorg}	0	0	0	0	0	0
C _{org}	0	0	0	0	0	0
Cl	0.005	0.003	0.007	0.005	0.003	0.007
Co	0	0	0	0	0	0
Ni	0	0	0	0	0	0
Se	0.03	0.02	0.04	0.001	7 × 10 ⁻⁴	0.001
Sr	0.001	7 × 10 ⁻⁴	0.001	0.001	7 × 10 ⁻⁴	0.001
Zr	10	2	30	10	2	30
Nb	1	0.7	1	1	0.7	1
Mo	0	0	0	0	0	0
Tc	0.001	7 × 10 ⁻⁴	1	0.001	7 × 10 ⁻⁴	0.001
Sn	10	2	30	10	2	30
I ¹	0.001	7 × 10 ⁻⁴	0.001	0.001	7 × 10 ⁻⁴	0.001
Cs	5 × 10 ⁻⁴	3 × 10 ⁻⁴	7 × 10 ⁻⁴	5 × 10 ⁻⁴	3 × 10 ⁻⁴	7 × 10 ⁻⁴
Sm	80	20	300	80	20	300
Eu	80	20	300	80	20	300
Pb	0.5	0.3	0.7	0.5	0.3	0.7
Po	0	0	0	0	0	0
Ra	0.05	0.03	0.07	0.05	0.03	0.07
Ac	80	20	300	80	20	300
Th	80	20	300	80	20	300
Pa	0.1	0.07	0.1	0.1	0.07	0.1
U	2	1	2	2	1	2
Np	80	20	300	0.1	0.07	0.1
Pu	80	20	300	0.1	0.07	0.1
Am	80	20	300	80	20	300
Cm	80	20	300	80	20	300

¹ The possibility of K_d(I) = 0 is considered in a "what if?" case

Tab. A3.5-5 gives a list of sorption constants, effective diffusion coefficients and accessible porosities in Opalinus Clay.

Tab. A3.5-5: Sorption coefficients, effective diffusion coefficients and accessible porosities in Opalinus Clay

Reference values (pH = 7.25, Eh = -167 mV) incl. pessimistic and optimistic values for K_d and pessimistic values for $D_{e\perp}$ (perpendicular to bedding). In addition, effective diffusion coefficients parallel to bedding ($D_{e\parallel}$) and accessible porosities (ϵ) are given. Data taken from Bradbury & Baeyens (2003b) and Nagra (2002a), Tab. 9.4-3.

Element	K_d			$D_{e\perp}$		$D_{e\parallel}$	ϵ	Porosity factor ²
	Reference [m ³ kg ⁻¹] (1)	Pessimistic [m ³ kg ⁻¹] (2)	Optimistic [m ³ kg ⁻¹]	Reference [m ² s ⁻¹] (1)	Pessimistic [m ² s ⁻¹] (2)			
H	0	0	0	1×10^{-11}	1×10^{-10}	5×10^{-11}	0.12	1
Be	0.9	0.03	20	1×10^{-11}	1×10^{-10}	5×10^{-11}	0.12	1
C _{inorg}	0.001	1×10^{-4}	0.006	1×10^{-12}	3×10^{-12}	5×10^{-12}	0.06	0.5
C _{org}	0	0	0	1×10^{-11}	1×10^{-10}	5×10^{-11}	0.12	1
Cl	0	0	0	1×10^{-12}	3×10^{-12}	5×10^{-12}	0.06	0.5
Ca	0.001	1×10^{-4}	0.007	1×10^{-11}	1×10^{-10}	5×10^{-11}	0.12	1
Co	0.4	0.01	20	1×10^{-11}	1×10^{-10}	5×10^{-11}	0.12	1
Ni	0.9	0.03	20	1×10^{-11}	1×10^{-10}	5×10^{-11}	0.12	1
Se	0	0	0	1×10^{-12}	3×10^{-12}	5×10^{-12}	0.06	0.5
Sr	0.001	1×10^{-4}	0.007	1×10^{-11}	1×10^{-10}	5×10^{-11}	0.12	1
Zr	10	0.3	300	1×10^{-11}	1×10^{-10}	5×10^{-11}	0.12	1
Nb	4	0.1	100	1×10^{-11}	1×10^{-10}	5×10^{-11}	0.12	1
Mo	0.01	0.001	0.2	1×10^{-12}	3×10^{-12}	5×10^{-12}	0.06	0.5
Tc	50	0.5	500	1×10^{-11}	1×10^{-10}	5×10^{-11}	0.12	1
Pd	5	0.2	100	1×10^{-11}	1×10^{-10}	5×10^{-11}	0.12	1
Ag	0	0	0	1×10^{-11}	1×10^{-10}	5×10^{-11}	0.12	1
Sn	100	0.2	1000	1×10^{-11}	1×10^{-10}	5×10^{-11}	0.12	1
I ^I	3×10^{-5}	3×10^{-6}	4×10^{-4}	1×10^{-12}	3×10^{-12}	5×10^{-12}	0.06	0.5
Cs	0.5	0.09	3	1×10^{-11}	1×10^{-10}	5×10^{-11}	0.12	1
Sm	50	5	600	1×10^{-11}	1×10^{-10}	5×10^{-11}	0.12	1
Eu	50	5	600	1×10^{-11}	1×10^{-10}	5×10^{-11}	0.12	1
Ho	50	5	600	1×10^{-11}	1×10^{-10}	5×10^{-11}	0.12	1
Pb	2	0.02	300	1×10^{-11}	1×10^{-10}	5×10^{-11}	0.12	1
Po	0.1	0.04	0.7	1×10^{-12}	3×10^{-12}	5×10^{-12}	0.06	0.5
Ra	7×10^{-4}	1×10^{-4}	0.005	1×10^{-11}	1×10^{-10}	5×10^{-11}	0.12	1
Ac	10	1	200	1×10^{-11}	1×10^{-10}	5×10^{-11}	0.12	1

Tab. A3.5-5:(Cont.)

Element	K_d			$D_{e\pm}$		$D_{e=}$ [m ² s ⁻¹]	ε [-]	Porosity factor ² [-]
	Reference [m ³ kg ⁻¹] (1)	Pessimistic [m ³ kg ⁻¹] (2)	Optimistic [m ³ kg ⁻¹]	Reference [m ² s ⁻¹] (1)	Pessimistic [m ² s ⁻¹] (2)			
Th	50	10	200	1×10^{-11}	1×10^{-10}	5×10^{-11}	0.12	1
Pa	5	0.2	100	1×10^{-11}	1×10^{-10}	5×10^{-11}	0.12	1
U	20	0.5	200	1×10^{-11}	1×10^{-10}	5×10^{-11}	0.12	1
Np	50	5	500	1×10^{-11}	1×10^{-10}	5×10^{-11}	0.12	1
Pu	20	1	300	1×10^{-11}	1×10^{-10}	5×10^{-11}	0.12	1
Am	10	1	200	1×10^{-11}	1×10^{-10}	5×10^{-11}	0.12	1
Cm	10	1	200	1×10^{-11}	1×10^{-10}	5×10^{-11}	0.12	1

¹ The possibility of $K_d(I) = 0$ is considered in a "what if?" case.

² The porosity factor is 0.5 for anions and 1 for non-anions.

A3.6 Specific explanatory notes on the derivation of parameters

Number of waste packages (STMAN Parameter 6)

In the case of ILW, a water pulse (water flow of limited duration and constant rate), originating from the cementitious near field and containing dissolved radionuclides, is simulated by means of the following parameters and settings:

- the starting time t_0 [a] and ending time t_1 [a] of the water pulse are set by the canister breaching time and the time the STMAN calculation stops, respectively;
- by setting the buffer thickness equal to zero (NUMBER_OF_CELLS 0), the aqueous concentration in the mixing cell is set equal to the porewater concentration of the cementitious region;
- the number of waste packages is multiplied by a large number (here an arbitrary scaling factor f_{scale} [-] of 10 000 is used) to assure that leaching by groundwater does not significantly reduce the aqueous concentration within the cementitious region;
- the groundwater flow rate per waste package (i.e. the effective mixing cell flow rate Q_{GW} [m³ a⁻¹]), to be specified in STMAN, is set equal the total volume of porewater displaced per waste package (V_{disp} [m³]) divided by the duration of the water pulse ($t_1 - t_0$, [a]) and by the scaling factor (f_{scale} [-]):

$$Q_{GW} = \frac{V_{disp}}{(t_1 - t_0) \cdot f_{scale}} \quad (\text{A3.6-1})$$

In the case of SF, a water pulse, originating from the reservoir and containing dissolved radionuclides from the instant release fraction, is simulated by means of an analogous set of parameters and settings as in the case of ILW. In addition,

- the radionuclide release rates from the fuel matrix and the cladding are set to zero (transport of instant release fraction only);
- the displaced volume V_{disp} , required to calculate the groundwater flowrate per waste package, is calculated from the reservoir volume V_r multiplied by the fraction of the IRF p_{IRF} which is assumed to be displaced by the water pulse:

$$V_{disp} = V_r \cdot p_{IRF} \quad (\text{A3.6-2})$$

Waste package length (STMAN Parameter 7)

In the case of spent fuel, the value is the weighted average length of all PWR and BWR canisters, based on the numbers and types of canisters in McGinnes (2002). For 60 years power plant operation (the Reference Case), there are 935 BE-1 canisters with a length of 4.92 m, 450 BE-2 canisters with a length of 4.40 m and 680 BE-3 canisters with a length of 4.40 m.

Reservoir thickness (STMAN Parameter 15)

The reservoir is assumed to surround the SF waste forms and HLW glass blocks. Its thickness is selected to give a volume of 0.65 m^3 and 0.037 m^3 per waste package for SF and HLW, respectively, which is equal to the internal void volume within the canisters (the values used for HLW are also given in Tab. 3.7.2 of Nagra (1994a)). The relationship between void volume, V [m^3], and reservoir thickness, d [m], is:

$$V = \pi d l (d_0 + d) \quad (\text{A3.6-3})$$

where d_0 [m] is the initial diameter of the SF or HLW waste form (STMAN Parameter 8) and l is its length (STMAN Parameter 7).

Matrix release rate (STMAN Parameter 9)

Tab. A3.6-1 gives the fuel matrix fractional dissolution rate as a function of time. Values are based on the results of Johnson & Smith (2000), which presents a model based on alpha radiolysis, where the dissolution rate is proportional to the time-dependent alpha decay energy of the fuel (Tab. 1 of Johnson & Smith (2000)). For UO_2 with a burnup of $48 \text{ GWd}/t_{\text{IHM}}$, the alpha energy outputs agree with values from McGinnes (2002). For MOX fuel with a burnup of $65 \text{ GWd}/t_{\text{IHM}}$, the rates used are those for the MOX $55 \text{ GWd}/t_{\text{IHM}}$ case in Tab. 2 of Johnson & Smith (2000). These will tend to overestimate the rate slightly, as ^{239}Pu is progressively burned out as burnup increases. For cases in which dissolution rates for higher burnup UO_2 fuels are required, the MOX 65 rates are used, which again overestimates rates. In addition, a fuel dissolution rate is required for the initial canister defect case for times prior to 1000 years. These rates are given in Tab. A3.6-1 for the case of the UO_2 / MOX canister, and are based on the extrapolation of the later rates to short times, using the time-dependent alpha energy output of fuel with a burnup of $48 \text{ GWd}/t_{\text{IHM}}$ given in Johnson & Smith (2000). The rate in the 1 to 50 year timeframe is based on rates for aerated conditions. Thus, it is significantly higher than the rates for longer time frames, which are for oxidative dissolution caused solely by radiolytic oxidants.

Tab. A3.6-1: Fuel matrix fractional dissolution rate as a function of time, evaluated assuming two different canister loadings

Data taken from Johnson & Smith (2000).

Time [a]	Fuel matrix fractional dissolution rate [a ⁻¹]		
0	1.0×10^{-4}		
50	2.0×10^{-5}		
100	1.5×10^{-5}		
200	1.3×10^{-5}		
300	9.3×10^{-6}		
500	7.2×10^{-6}		
700	5.3×10^{-6}		
	Values based on UO ₂ fuel elements with a burn-up of 48 GWd/t _{HIM}	Values based on a weighted average of 1 MOX fuel element and 3 UO ₂ fuel elements, each with a burn-up of 48 GWd/t _{HIM}	Values based on MOX fuel elements with a burn-up of 65 GWd/t _{HIM}
	(1)	(2)	(3)
1.0×10^3	2.4×10^{-6}	3.8×10^{-6}	8.6×10^{-6}
2.0×10^3	1.3×10^{-6}	2.0×10^{-6}	4.4×10^{-6}
3.0×10^3	8.9×10^{-7}	1.4×10^{-6}	3.1×10^{-6}
5.1×10^3	6.7×10^{-7}	1.0×10^{-6}	2.3×10^{-6}
7.6×10^3	5.9×10^{-7}	8.9×10^{-7}	1.9×10^{-6}
1.0×10^4	5.3×10^{-7}	7.9×10^{-7}	1.7×10^{-6}
1.5×10^4	4.2×10^{-7}	6.1×10^{-7}	1.3×10^{-6}
2.0×10^4	3.3×10^{-7}	4.7×10^{-7}	9.3×10^{-7}
3.0×10^4	2.1×10^{-7}	2.8×10^{-7}	5.3×10^{-7}
5.1×10^4	1.1×10^{-7}	1.4×10^{-7}	2.3×10^{-7}
6.4×10^4	7.6×10^{-8}	9.8×10^{-8}	1.7×10^{-7}
8.1×10^4	5.6×10^{-8}	7.3×10^{-8}	1.3×10^{-7}
1.1×10^5	4.0×10^{-8}	5.4×10^{-8}	1.0×10^{-7}
1.5×10^5	3.0×10^{-8}	4.2×10^{-8}	8.3×10^{-8}
2.1×10^5	2.7×10^{-8}	3.7×10^{-8}	7.4×10^{-8}
3.1×10^5	2.5×10^{-8}	3.4×10^{-8}	6.6×10^{-8}
5.2×10^5	2.2×10^{-8}	2.9×10^{-8}	5.5×10^{-8}
8.2×10^5	1.8×10^{-8}	2.4×10^{-8}	4.5×10^{-8}
1.0×10^6	1.6×10^{-8}	2.1×10^{-8}	4.0×10^{-8}
1.6×10^6	1.3×10^{-8}	1.8×10^{-8}	3.2×10^{-8}
2.1×10^6	1.2×10^{-8}	1.6×10^{-8}	2.7×10^{-8}
3.1×10^6	1.1×10^{-8}	1.3×10^{-8}	2.1×10^{-8}
4.9×10^6	1.0×10^{-8}	1.1×10^{-8}	1.5×10^{-8}
7.0×10^6	1.0×10^{-8}	1.1×10^{-8}	1.2×10^{-8}
$\geq 1.0 \times 10^7$	1.0×10^{-8}	1.0×10^{-8}	1.0×10^{-8}

Outer buffer radius for STALLION (STMAN Parameter 24)

As discussed in Appendix A1.4, the STALLION model assumes that, following access of water to the waste, radionuclides are instantaneously released and uniformly mixed in a cylindrical zone corresponding to the backfilled interior of an emplacement cavern. Here, they may either sorb on the cementitious backfill, precipitate if the solubility limit of the corresponding element is exceeded, or diffuse into the surrounding rock. Diffusion into the surrounding rock is modelled explicitly in STALLION, out to a certain distance that has to be supplied by the user. Beyond this distance, a geosphere transport code (e.g. PICNIC) is used. Migration between the STALLION model domain and the geosphere model domain is represented using an effective flow rate, Q [$\text{m}^3 \text{a}^{-1}$], to simulate both diffusion and a very small (in the Reference Case) advective component (see next section). The issue addressed here is the choice of a sensible value for the distance that the STALLION model extends into the host rock.

Consider a radionuclide that is, as assumed in the STALLION model, uniformly mixed in a cylindrical zone corresponding to the backfilled interior of an emplacement tunnel, with an aqueous concentration C_0 [mol m^{-3}]. Considering the situation of diffusion across the annular rock zone surrounding the tunnel, with inner radius r_a [m] and outer radius r_b [m], and neglecting radioactive decay, the solution to the steady-state diffusion equation is:

$$C = \frac{C_0 \ln\left(\frac{r_b}{r}\right) + C_1 \ln\left(\frac{r}{r_a}\right)}{\ln\left(\frac{r_b}{r_a}\right)},$$

where C_1 [mol m^{-3}] is the concentration at the outside of the zone. The steady-state diffusive release across a cylindrical surface within the zone of length L [m] (the length of the tunnel) is:

$$F = 2\pi r L D_e \frac{dC}{dr} = \frac{2\pi r L D_e}{\ln\left(\frac{r_b}{r_a}\right)} (C_0 - C_1).$$

In the STALLION model, at the outer boundary of the zone:

$$F = Q C_1.$$

Eliminating C_1 from these two equations,

$$F = Q C_0 \frac{1}{1 + \frac{Q}{2\pi L D_e} \ln\left(\frac{r_b}{r_a}\right)}. \quad (\text{A3.6-4})$$

Note that $F \rightarrow Q C_0$ as the annular zone becomes small ($r_b \rightarrow r_a$). Eq. A3.6-4 has to be evaluated to test whether F is sensitive to the choice of $r_b - r_a$, i.e. the arbitrary distance that the STALLION model extends into the rock.

The following parameters were used to evaluate Eq. A3.6-4 (ILW-1):

$$\begin{aligned} r_a &= 4.5 \text{ m} \\ Q &= 0.4 \text{ m}^3 \text{ a}^{-1} \\ L &= 180 \text{ m} \\ D_e &= 10^{-11} \text{ m}^2 \text{ s}^{-1} \text{ (value for non-anions).} \end{aligned}$$

Eq. A3.6-4, together with the above data, is used to plot F/QC_0 as a function of $r_b - r_a$ in Fig. A3.6-1.

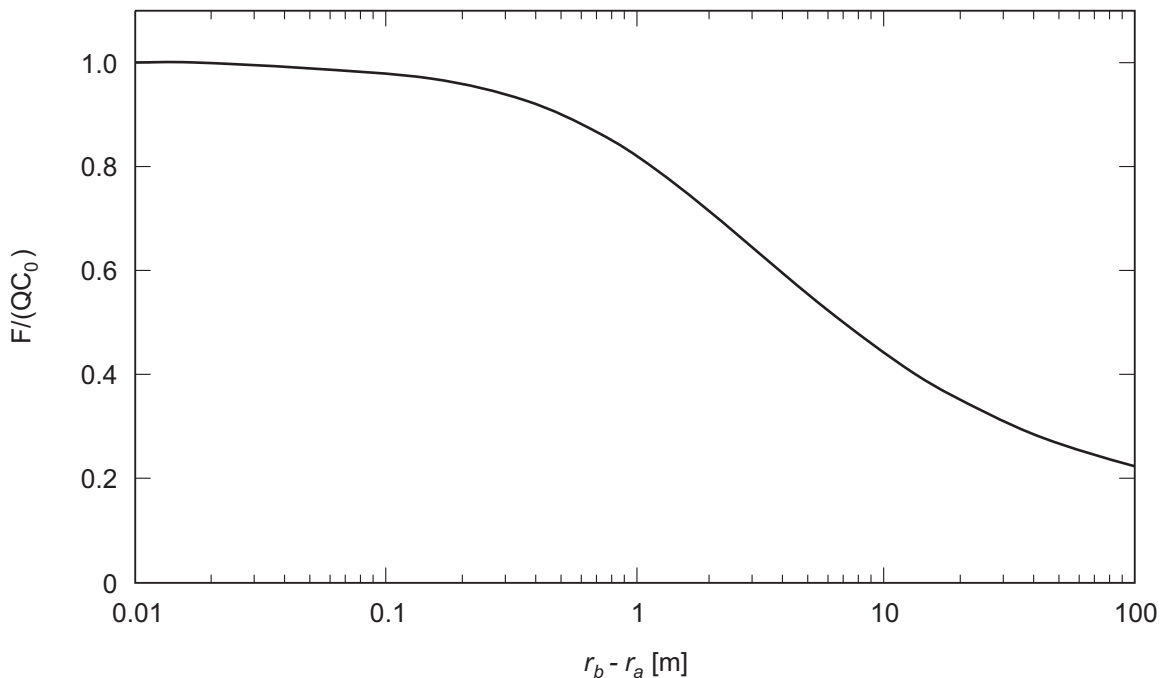


Fig. A3.6-1: Normalised release, as a function of thickness of the diffusive barrier (Opalinus Clay) around the cementitious ILW-1 tunnel

Fig. A3.6-1 shows that in order not to underpredict the release of a long-lived radionuclide, the value for the distance that the STALLION model extends into the rock should be set to well below 1 m. Consequently a value of 1 cm was chosen for all calculations presented in Nagra (2002c).

Mixing cell flow rate per waste package (STMAN Parameter 35)

The governing equations for the STMAN code incorporate the assumption that transport in the excavation-disturbed zone (EDZ) is advection dominated and, at the interface between the

repository engineered barriers and the EDZ, a "mixing-tank" boundary condition can be applied in which the rate at which radionuclides are released to the zone by diffusion from the engineered barriers is equal to the rate of radionuclide advection out of the zone. In many of the assessment cases, however, both diffusion and advection are important transport mechanisms in the EDZ (and in the Opalinus Clay as a whole). In order to apply STMAN, it is thus necessary to define an "effective flowrate" at the boundary that accounts for diffusion as well as advection in the EDZ. It has to be recognised that such an approach is only an approximation, since diffusion in the EDZ can result in radionuclides reentering the engineered barriers, whereas advection cannot – radionuclides are always transported away from the engineered barriers. The "effective flowrate" can, however, be assigned a value that is conservative for all radionuclides with the potential to migrate to the surface environment.

The effective flowrate per waste package, Q_{eff} [$\text{m}^3 \text{a}^{-1}$] is obtained using the equation:

$$Q_{eff} = 2r_{EDZ} p \left(v_D + \frac{\pi D_e}{L} \right) \quad (\text{A3.6-5})$$

where p [m] is the tunnel length per waste package (the canister pitch in the case of SF / HLW and the tunnel length in the cases of ILW-1 and ILW-2), r_{EDZ} [m] is the EDZ radius, v_D [m a^{-1}] is the Darcy velocity in the Opalinus Clay and D_e [$\text{m}^2 \text{a}^{-1}$] is the effective diffusion coefficient in the Opalinus Clay. L [m] is an equivalent length for diffusion, i.e. a measure of the "diffusive transport distance" through the Opalinus Clay. In the case of a steady-state release of a non-decaying radionuclide, when there is a uniform concentration gradient across the Opalinus Clay, this distance is equal to 40 m (the geosphere transport distance in the Reference Case). Before a steady state is reached, however, and more generally if radioactive decay is taken into account, the concentration gradient at the boundary can be higher and L smaller than 40 m. In the present study, a value $L = 5$ m is assumed. This approach is conservative for long-lived radionuclides that are transported across the Opalinus Clay without substantial decay. It can be non-conservative for some shorter-lived radionuclides, but these, in any case, do not reach the surface environment. As shown by analytical calculations, the geosphere release rates of those radionuclides that dominate dose are well reproduced by this simplified approach (Gribi 2003).

Tab. A3.6-2 shows the effective flowrate per waste package for different combinations of Darcy velocity and effective diffusion coefficient in the Opalinus Clay. These values are assigned to STMAN Parameter 35, as described in Section A3.3.1.

In case of a water pulse (water flow of limited duration and constant rate) modelled using STMAN, the mixing cell flow rate per waste package is divided by a scale factor f_{scale} [-] to conservatively avoid depletion of the aqueous concentration of radionuclides within the near field (see note on number of waste packages, STMAN Parameter 6).

Tab. A3.6-2: The effective flowrate per waste package for different combinations of Darcy velocity and effective diffusion coefficient (D_e) in the Opalinus Clay

Data calculated by use of Eq. A3.6-5.

Waste form	Tunnel length per waste package [m] ¹	EDZ diameter [m] ²	Effective flowrate per waste package [m ³ a ⁻¹]					
			Darcy velocity [m s ⁻¹]:					
			0	2×10^{-15}	2×10^{-14}	2×10^{-13}	2×10^{-12}	2×10^{-14}
			$D_e = 10^{-11} \text{ m}^2 \text{ s}^{-1}$					$10^{-10} \text{ m}^2 \text{ s}^{-1}$
SF	7.6	4	6.0×10^{-3}	6.0×10^{-3}	6.0×10^{-3}	6.2×10^{-3}	7.9×10^{-3}	6.0×10^{-2}
HLW	5	4	4.0×10^{-3}	4.0×10^{-3}	4.0×10^{-3}	4.1×10^{-3}	5.2×10^{-3}	4.0×10^{-2}
ILW-1	1	11	2.2×10^{-3}	2.2×10^{-3}	2.2×10^{-3}	2.3×10^{-3}	2.9×10^{-3}	2.2×10^{-2}
ILW-2	1	7.8	1.5×10^{-3}	1.5×10^{-3}	1.6×10^{-3}	1.6×10^{-3}	2.0×10^{-3}	1.5×10^{-2}

Notes: ¹ From Fig. 4.5-7, Nagra (2002c).

² From Tab. A3.3-4d. For the SF / HLW tunnels, the EDZ diameter has been rounded from 3.7 m to 4 m.

Cross-sectional area and Darcy velocity of legs within a given network structure (PICNIC Parameters 4 & 5)

For cases that are more complex than a single leg, the cross-sectional areas of PICNIC legs and their Darcy velocities are calculated on a case-by-case basis from the geometrical and hydro-geological properties of the system under consideration.

The case 1.5 (additional barrier provided by confining units) is discussed in detail in Section 3.5. In this case, the areas for legs originating at the repository are chosen to be identical. The magnitude of the leg area is irrelevant, because the transport rate for radionuclides in the leg is determined by the activity flux imposed at the upstream boundary of the leg and by the transport properties of the leg. The Darcy velocities for cases 1.5a and 1.5b are calculated using the parameter values listed in Tabs. 3.5-1 to 3.5-3 and Tabs. 3.5-4 to 3.5-8, respectively.

Cases 1.6, 1.7, 1.8, 3.3 and 4.5 are dealing with a release of radionuclides affected by the ramp / shaft. The PICNIC network structure is depicted in Fig. 3.6-5. Note that in cases 1.7 (convergence-induced release affected by ramp) and 4.5 (gas-induced release of dissolved radionuclides through the ramp only), the ILW part of the repository including the ILW operations tunnel and ramp is considered only. The calculation of leg areas and Darcy velocities is discussed in detail in the corresponding sections (Sections 3.6, 3.7, 3.8, 5.3 and 6.5, respectively).

A3.7 Reference Case input parameters for biosphere modelling

In Tabs. A3.7-1 to A3.7-5, the input parameters for TAME used in the model calculations for the Reference Case biosphere are compiled. The abbreviated parameter names in these tables correspond to variable names in the code TAME (Klos et al. 1996). A short parameter description is given where needed. A detailed justification of all biosphere parameter values used in the present assessment is given in Nagra (2003b).

The TAME dataset is structured as follows:

- definition of biosphere compartments and input parameters determining water and solid material fluxes between the compartments (Tab. A3.7-1),
- biosphere sorption database (Tab. A3.7-2),
- parameter values characterising the human diet and practices (Tab. A3.7-3),
- transfer factors and concentration ratios for foodstuffs (Tab. A3.7-4),
- food processing factors, turnover times for weathering losses and other rate factors (Tab. A3.7-5).

Tab. A3.7-1: Definition of biosphere compartments and input parameters determining water and solid material fluxes between the compartments

Data taken from Nagra (2003b).

Category	Parameter name	Description	Unit	Reference Case
GENERAL	AF	Surface area of the biosphere region	m ²	2.3×10^6
GENERAL	A_LE	Area of interface between local aquifer and Elsewhere compartment	m ²	not used
GENERAL	D0	Ionic diffusion constant in pure water	m ² a ⁻¹	3.8×10^{-2}
GENERAL	ETP	Evapotranspiration	m a ⁻¹	0.6
GENERAL	RAINFALL	Precipitation	m a ⁻¹	1.0
GENERAL	CAPIL_R	Capillary rise	m a ⁻¹	0
GENERAL	IRRI_L	Irrigation with groundwater	m a ⁻¹	0.5
GENERAL	IRRI_W	Irrigation with surface water (incl. flooding)	m a ⁻¹	0
GENERAL	ME	Erosion	kg m ⁻² a ⁻¹	0.27
GENERAL	M_DEP	Sedimentation (only part not connected with water fluxes)	kg m ⁻² a ⁻¹	0
GENERAL	ALPHA_P	Suspended solid concentration in water from previous river section	kg m ⁻³	0.1
GENERAL	V_A	Average windspeed in biosphere region	m a ⁻¹	4.1×10^7
GENERAL	L_A	Mixing depth for the atmosphere - inhalation of volatile nuclides	m	2
DEEPSOIL	ALPHA_D	Suspended solid concentration in deep soil porewater	kg m ⁻³	1×10^{-3}
DEEPSOIL	EPS_D	Porosity of deep soil	-	0.4
DEEPSOIL	L_D	Thickness of deep soil	m	2.0
DEEPSOIL	M_D	Biomass in deep soil	kg m ⁻²	0.1
DEEPSOIL	RHO_D	Dry density of deep soil material	kg m ⁻³	2.65×10^3
DEEPSOIL	THETA_D	Volumetric moisture content of deep soil	-	0.3
DEEPSOIL	T_D	Tortuosity of deep soil material	-	3.9
DEEPSOIL	W_D	Activity of earthworms: number of round trips between deep soil and top soil	a ⁻¹	20
LOCAL	ALPHA_L	Suspended solid concentration in local aquifer porewater	kg m ⁻³	1×10^{-3}
LOCAL	EPS_L	Porosity of local aquifer	-	0.2
LOCAL	L_L	Thickness of local aquifer	m	20
LOCAL	RHO_L	Dry density of local aquifer material	kg m ⁻³	2.65×10^3
LOCAL	THETA_L	Volumetric moisture content of local aquifer	-	0.2
LOCAL	T_L	Tortuosity of local aquifer material	-	8.6
WATER	ALPHA_W	Suspended solid concentration in surface water	kg m ⁻³	0.1
WATER	D_W	Depth of surface water	m	3.3
WATER	L_W	Length of surface water compartment	m	3.5×10^3

Tab. A3.7-1: (Cont.)

Category	Parameter name	Description	Unit	Reference Case
WATER	RHO_W	Density of water	kg m ⁻³	1 × 10 ³
WATER	W_W	Width of surface water compartment	m	1 × 10 ²
SEDIMENT	EPS_S	Porosity of bed sediment	-	0.5
SEDIMENT	KAPPA_SW	Turnover rate: bed sediment to suspended solid in water column	a ⁻¹	1
SEDIMENT	D_S	Thickness of bed sediment layer	m	0.1
SEDIMENT	SL	Application rate: mass of bed sediment to land area	kg m ⁻² a ⁻¹	0
SEDIMENT	RHO_S	Dry density of bed sediment material	kg m ⁻³	2.65 × 10 ³
SEDIMENT	THETA_S	Volumetric moisture content of bed sediment	-	0.5
SEDIMENT	T_S	Tortuosity of bed sediment material	-	2.9
TOPSOIL	ALPHA_T	Suspended solid concentration in top soil porewater	kg m ⁻³	1 × 10 ⁻³
TOPSOIL	EPS_T	Porosity of top soil	-	0.4
TOPSOIL	L_T	Thickness of top soil	m	0.25
TOPSOIL	RHO_T	Dry density of top soil material	kg m ⁻³	2.65 × 10 ³
TOPSOIL	THETA_T	Volumetric moisture content of top soil	-	0.3
TOPSOIL	T_T	Tortuosity of top soil material	-	3.9
BAL-File	F_CL	Flux of contaminated deep groundwater into local aquifer	m ³ a ⁻¹	1.3 × 10 ⁵
BAL-File	F_CW	Flux of contaminated deep groundwater into surface water	m ³ a ⁻¹	0
BAL-File	F_UL	Flux of uncontaminated water into local aquifer	m ³ a ⁻¹	1.5 × 10 ⁶
BAL-File	F_UW	Flux of uncontaminated water into surface water	m ³ a ⁻¹	1.2 × 10 ¹⁰
REL-File	REL_L	Fraction of release into local aquifer	-	1
REL-File	REL_W	Fraction of release into surface water	-	0
SOL-File	SOL_L	Classification of grain size in local aquifer	-	Coarse
SOL-File	SOL_D	Classification of grain size in deep soil	-	Fine
SOL-File	SOL_T	Classification of grain size in top soil	-	Fine
SOL-File	SOL_W	Classification of grain size in surface water	-	Fine
SOL-File	SOL_S	Classification of grain size in bed sediment	-	Coarse

Tab. A3.7-2: Biosphere sorption database (K_d)

Data taken from Nagra (2003b).

Element	Sorption coefficients (K_d) [m ³ kg ⁻¹]		
	coarse	fine	organics
H	0	0	0
Be	1×10^{-2}	0.1	0.2
C	5×10^{-3}	5×10^{-3}	5×10^{-3}
Cl	0	0	0
Ca	1×10^{-2}	0.1	0.2
Co	0.1	1	2
Ni	0.1	1	2
Se	1×10^{-3}	1×10^{-2}	2×10^{-2}
Sr	1×10^{-2}	0.1	0.2
Zr	1	10	20
Nb	5×10^{-2}	0.5	1
Mo	5×10^{-4}	5×10^{-3}	1×10^{-2}
Tc	1×10^{-2}	0.1	0.2
Pd	0.1	1	2
Ag	2×10^{-4}	2×10^{-3}	4×10^{-3}
Sn	0.1	1	2
I	1×10^{-4}	1×10^{-3}	2×10^{-3}
Cs	0.3	3	3
Sm	1	10	20
Eu	1	10	20
Ho	1	10	20
Pb	0.1	1	2
Po	1	10	20
Ra	0.1	1	2
Ac	1	10	20
Th	1	10	20
Pa	1	10	20
U	0.1	1	2
Np	1	10	20
Pu	1	10	20
Am	1	10	20
Cm	1	10	20

Tab. A3.7-3: Parameter values characterising human diet and practices
Data taken from Nagra (2003b).

Category	Parameter name	Description	Unit	Value
HUMAN	ENERGY	Calorific value of food consumed annually	kJ a^{-1}	2.9×10^6
HUMAN	F_MILK	Fraction of annual food energy intake obtained from milk	-	0.46
HUMAN	I_FLUID	Annual intake of liquids from all sources ¹	$\text{m}^3 \text{a}^{-1}$	1.1
HUMAN	FILTER	Filtration factor for water consumption	-	0
HUMAN	H_DRINK	Fraction of water taken from the well in the local aquifer	-	1
HUMAN	F_EGG	Fraction of annual food energy intake obtained from eggs	-	0.018
HUMAN	F_FF	Fraction of annual food energy intake obtained from fish	-	0.012
HUMAN	P_VEG	Fraction of annual food energy intake obtained from vegetables, after milk, eggs, fish, and fruits have been taken into account	-	0.72
HUMAN	P_G	Fraction of energy intake from vegetable consumption coming from grain	-	0.79
HUMAN	P_GV	Fraction of energy intake from vegetable consumption coming from green vegetables	-	6.6×10^{-2}
HUMAN	P_RV	Fraction of energy intake from vegetable consumption coming from root vegetables	-	0.15
HUMAN	P_FRUIT	Fraction of annual food energy intake obtained from fruit	-	4.5×10^{-2}
HUMAN	I_AIR	Annual inhalation rate of air, i.e. breathing rate	$\text{m}^3 \text{a}^{-1}$	8.0×10^3
HUMAN	O_F	Fraction of year spent at high dust concentrations	-	0
FOODS	ETA_MILK	Food energy content of milk	kJ m^{-3}	2.8×10^6
FOODS	ETA_EGG	Food energy content of one egg	kJ	3.1×10^2
FOODS	ETA_FF	Food energy content of fish	kJ kg^{-1}	5.7×10^3
FOODS	ETA_GV	Food energy content of green vegetables	kJ kg^{-1}	1.1×10^3
FOODS	ETA_RV	Food energy content of root vegetables	kJ kg^{-1}	3.0×10^3
FOODS	ETA_G	Food energy content of grain	kJ kg^{-1}	1.4×10^4
FOODS	ETA_MEAT	Food energy content of meat	kJ kg^{-1}	8.7×10^3
FOODS	ETA_FRUIT	Food energy content of fruits	kJ kg^{-1}	2.2×10^3
GRAIN	S_G	Surface contamination factor for grain	kg kg^{-1}	9.0×10^{-5}
GRAIN	MU_G	Spray irrigation interception factor for grain	$\text{m}^2 \text{kg}^{-1}$	0.66
GRAIN	Y_G	Yield of grain	kg m^{-2}	0.61
GRAIN	H_G	Harvesting rate for grain	a^{-1}	1

¹ Note that this corresponds to a drinking water consumption rate of $0.6 \text{ m}^3 \text{a}^{-1}$ and a milk consumption rate of $0.5 \text{ m}^3 \text{a}^{-1}$. In some assessment cases, the dose calculations are restricted to the drinking water exposure pathway (see Tab. A3.2-3). These cases are based on a drinking water consumption rate of 2 l d^{-1} ($0.73 \text{ m}^3 \text{a}^{-1}$), which is slightly higher than the value used in TAME.

Tab. A3.7-3: (Cont.)

Category	Parameter name	Description	Unit	Value
GREENVEG	S_GV	Surface contamination factor for green vegetables	kg kg ⁻¹	2.0×10^{-4}
GREENVEG	MU_GV	Spray irrigation interception factor for green vegetables	m ² kg ⁻¹	0.14
GREENVEG	Y_GV	Yield of green vegetables	kg m ⁻²	3.0
GREENVEG	H_GV	Harvesting rate for green vegetables	a ⁻¹	2
ROOT_VEG	S_RV	Surface contamination factor for root vegetables	kg kg ⁻¹	0
ROOT_VEG	MU_RV	Spray irrigation interception factor for root vegetables	m ² kg ⁻¹	0.10
ROOT_VEG	Y_RV	Yield of root vegetables	kg m ⁻²	4.0
ROOT_VEG	H_RV	Harvesting rate for root vegetables	a ⁻¹	1
FRUIT	S_FRUIT	Surface contamination factor for fruits	kg kg ⁻¹	2.5×10^{-4}
FRUIT	MU_FRUIT	Spray irrigation interception factor for fruits	m ² kg ⁻¹	0.16
FRUIT	Y_FRUIT	Yield of fruits	kg m ⁻²	2.5
FRUIT	H_FRUIT	Harvesting rate for fruits	a ⁻¹	1
CATTLE	CATTLEFRAC	Fraction of farmed area devoted to cattle, i.e. for pasture	-	not used
CATTLE	N_CATTLE	Stocking density of cattle	m ⁻²	not used
CATTLE	I_WC	Water consumption rate for cattle	m ³ d ⁻¹	3×10^{-2}
CATTLE	I_PC	Pasture consumption rate for cattle, calculated as hay, not grass	kg d ⁻¹	20
CATTLE	A_DRINK	Fraction of cattle water consumption taken from the well in the local aquifer	-	1
PASTURE	Z	Ratio of weight of fresh pasture (i.e. grass) to hay	-	5
PASTURE	S_CP	Surface contamination factor for pasture	kg kg ⁻¹	0.1
PASTURE	MU_P	Spray irrigation interception factor for pasture	m ² kg ⁻¹	0.33
PASTURE	Y_P	Yield of pasture, calculated as hay, not grass	kg m ⁻²	1.2
POULTRY	I_WH	Water consumption rate for poultry	m ³ d ⁻¹	2×10^{-4}
POULTRY	I_GH	Grain consumption rate for poultry	kg d ⁻¹	7×10^{-2}
POULTRY	P_DRINK	Fraction of poultry water consumption taken from the well in the local aquifer	-	1
ENVIRON	A_R	Airborne dust concentration: value for normal background conditions	kg m ⁻³	5×10^{-8}
ENVIRON	A_F	Airborne dust concentration: value for high and/or occupational background conditions	kg m ⁻³	1×10^{-5}

Tab. A3.7-4: Transfer factors and concentration ratios for foodstuffs

K_FF = concentration ratio between fish and water; K_G = concentration ratio between grain and soil (root uptake); K_GV = concentration ratio between green vegetables and soil (root uptake); K_MEAT = transfer factor for meat; K_MILK = transfer factor for milk; K_P = concentration ratio between pasture (i.e. grass) and soil (root uptake); K_RV = concentration ratio between root vegetables and soil (root uptake); K_EGG = transfer factor for eggs; K_FRUIT = concentration ratio between fruit and soil. Data taken from Nagra (2003b).

Element	K_FF	K_G	K_GV	K_MEAT	K_MILK	K_P	K_RV	K_EGG	K_FRUIT
	(Bq/kg)/ (Bq/m ³)	(Bq/kg fresh weight)/ (Bq/kg dry soil)	(Bq/kg fresh weight)/ (Bq/kg dry soil)	(Bq/kg)/ (kg/day fresh weight)	(Bq/kg)/ (kg/day fresh weight)	(Bq/kg fresh weight)/ (Bq/kg dry soil)	(Bq/kg fresh weight)/ (Bq/kg dry soil)	(Bq/egg)/ (kg/day fresh weight)	(Bq/kg fresh weight)/ (Bq/kg dry soil)
H	1.0 × 10 ⁻³	4.8	4.8	1.2 × 10 ⁻²	1.0 × 10 ⁻²	2.4 × 10 ¹	4.8	0.0	4.8
Be	2.0 × 10 ⁻³	4.7 × 10 ⁻⁴	4.7 × 10 ⁻⁴	8.0 × 10 ⁻⁴	2.0 × 10 ⁻⁵	2.4 × 10 ⁻³	4.7 × 10 ⁻⁴	1.0 × 10 ⁻³	4.7 × 10 ⁻⁴
C	4.6	3.0 × 10 ¹	2.0	3.1 × 10 ⁻²	1.2 × 10 ⁻²	1.0	1.0	1.0 × 10 ⁻¹	1.0
Cl	1.0 × 10 ⁻²	4.5 × 10 ¹	5.0	8.0 × 10 ⁻²	5.0 × 10 ⁻²	1.3 × 10 ¹	7.5	1.0	7.5
Ca	3.0 × 10 ⁻²	1.2 × 10 ⁻¹	1.5 × 10 ⁻¹	8.1 × 10 ⁻⁴	1.4 × 10 ⁻³	5.8 × 10 ⁻¹	1.4 × 10 ⁻¹	1.6 × 10 ⁻²	1.4 × 10 ⁻¹
Co	3.0 × 10 ⁻¹	1.3 × 10 ⁻²	7.4 × 10 ⁻³	1.3 × 10 ⁻²	1.0 × 10 ⁻³	9.0 × 10 ⁻²	8.2 × 10 ⁻²	5.0 × 10 ⁻³	8.2 × 10 ⁻²
Ni	1.0 × 10 ⁻¹	4.2 × 10 ⁻²	1.7 × 10 ⁻²	2.0 × 10 ⁻³	1.0 × 10 ⁻³	5.0 × 10 ⁻²	1.6 × 10 ⁻²	5.2 × 10 ⁻²	1.6 × 10 ⁻²
Se	2.0 × 10 ⁻¹	3.6 × 10 ⁻²	3.5 × 10 ⁻²	3.2 × 10 ⁻¹	4.0 × 10 ⁻³	2.5 × 10 ⁻¹	3.8 × 10 ⁻²	4.8 × 10 ⁻¹	0.5
Sr	3.0 × 10 ⁻²	1.2 × 10 ⁻¹	1.5 × 10 ⁻¹	8.1 × 10 ⁻⁴	1.4 × 10 ⁻³	5.8 × 10 ⁻¹	1.4 × 10 ⁻¹	1.6 × 10 ⁻²	1.4 × 10 ⁻¹
Zr	2.0 × 10 ⁻¹	2.7 × 10 ⁻²	3.4 × 10 ⁻³	2.0 × 10 ⁻²	3.0 × 10 ⁻⁵	2.0 × 10 ⁻²	2.1 × 10 ⁻³	1.0 × 10 ⁻⁴	2.1 × 10 ⁻³
Nb	1.0 × 10 ⁻²	9.4 × 10 ⁻³	9.4 × 10 ⁻³	3.0 × 10 ⁻⁷	2.5 × 10 ⁻³	4.7 × 10 ⁻²	9.4 × 10 ⁻³	6.0 × 10 ⁻⁵	5.0 × 10 ⁻³
Mo	2.0 × 10 ⁻⁷	4.0	4.5 × 10 ⁻¹	6.8 × 10 ⁻³	1.4 × 10 ⁻³	1.1	7.0 × 10 ⁻¹	2.6 × 10 ⁻²	7.0 × 10 ⁻¹
Tc	1.5 × 10 ⁻²	4.5	1.0	1.0 × 10 ⁻³	2.5 × 10 ⁻²	2.5	1.5	9.8 × 10 ⁻²	2.0 × 10 ¹
Pd	1.0 × 10 ⁻¹	5.0 × 10 ⁻²	1.7 × 10 ⁻²	2.0 × 10 ⁻³	1.0 × 10 ⁻³	5.0 × 10 ⁻²	1.6 × 10 ⁻²	5.2 × 10 ⁻²	1.6 × 10 ⁻²
Ag	2.0 × 10 ⁻³	4.0 × 10 ⁻²	4.0 × 10 ⁻²	1.0 × 10 ⁻³	3.0 × 10 ⁻²	4.0 × 10 ⁻²	4.0 × 10 ⁻²	5.0 × 10 ⁻²	4.0 × 10 ⁻²
Sn	3.0	3.6 × 10 ⁻¹	4.0 × 10 ⁻²	4.0 × 10 ⁻⁴	1.2 × 10 ⁻³	1.0 × 10 ⁻¹	6.0 × 10 ⁻²	4.6 × 10 ⁻²	6.0 × 10 ⁻²
I	5.0 × 10 ⁻²	3.6 × 10 ⁻¹	1.9 × 10 ⁻²	3.6 × 10 ⁻³	9.9 × 10 ⁻³	1.0 × 10 ⁻¹	5.6 × 10 ⁻³	1.5 × 10 ⁻¹	5.0 × 10 ⁻²
Cs	1.0	1.3 × 10 ⁻²	1.3 × 10 ⁻²	2.6 × 10 ⁻²	7.1 × 10 ⁻³	2.0 × 10 ⁻²	8.0 × 10 ⁻³	2.5 × 10 ⁻²	5.0 × 10 ⁻²
Sm	1.0 × 10 ⁻¹	1.8 × 10 ⁻⁴	2.0 × 10 ⁻⁴	6.0 × 10 ⁻²	5.0 × 10 ⁻⁶	5.0 × 10 ⁻⁴	3.0 × 10 ⁻⁴	5.0 × 10 ⁻²	3.0 × 10 ⁻⁴
Eu	1.0 × 10 ⁻¹	1.8 × 10 ⁻⁴	2.0 × 10 ⁻⁴	6.0 × 10 ⁻²	5.0 × 10 ⁻⁶	5.0 × 10 ⁻⁴	3.0 × 10 ⁻⁴	5.0 × 10 ⁻²	3.0 × 10 ⁻⁴
Ho	1.0 × 10 ⁻¹	1.8 × 10 ⁻⁴	2.0 × 10 ⁻⁴	6.0 × 10 ⁻²	5.0 × 10 ⁻⁶	5.0 × 10 ⁻⁴	3.0 × 10 ⁻⁴	5.0 × 10 ⁻²	3.0 × 10 ⁻⁴
Pb	1.0 × 10 ⁻¹	1.7 × 10 ⁻²	1.8 × 10 ⁻³	4.0 × 10 ⁻⁴	2.6 × 10 ⁻⁴	4.5 × 10 ⁻³	2.7 × 10 ⁻³	4.6 × 10 ⁻²	1.0 × 10 ⁻²
Po	0.5	2.0 × 10 ⁻⁴	2.0 × 10 ⁻⁴	4.0 × 10 ⁻³	3.0 × 10 ⁻⁴	2.0 × 10 ⁻⁴	2.0 × 10 ⁻⁴	5.0 × 10 ⁻⁵	2.0 × 10 ⁻⁴
Ra	2.5 × 10 ⁻²	1.4 × 10 ⁻²	1.6 × 10 ⁻³	9.0 × 10 ⁻⁴	4.0 × 10 ⁻⁴	4.0 × 10 ⁻³	3.0 × 10 ⁻³	4.6 × 10 ⁻²	4.0 × 10 ⁻²
Ac	1.0 × 10 ⁻¹	1.8 × 10 ⁻⁴	2.0 × 10 ⁻⁴	6.0 × 10 ⁻²	5.0 × 10 ⁻⁶	5.0 × 10 ⁻⁴	3.0 × 10 ⁻⁴	5.0 × 10 ⁻²	5.0 × 10 ⁻⁴
Th	3.0 × 10 ⁻²	7.1 × 10 ⁻⁴	3.8 × 10 ⁻⁴	2.0 × 10 ⁻⁴	5.0 × 10 ⁻⁶	9.5 × 10 ⁻⁴	5.7 × 10 ⁻⁴	5.0 × 10 ⁻²	5.0 × 10 ⁻⁴
Pa	1.0 × 10 ⁻²	1.7 × 10 ⁻²	2.7 × 10 ⁻²	8.0 × 10 ⁻²	5.0 × 10 ⁻⁶	9.4 × 10 ⁻³	6.0 × 10 ⁻²	5.0 × 10 ⁻²	4.0 × 10 ⁻²
U	2.0 × 10 ⁻³	1.3 × 10 ⁻³	3.8 × 10 ⁻⁴	3.4 × 10 ⁻⁴	3.7 × 10 ⁻⁴	9.5 × 10 ⁻⁴	5.7 × 10 ⁻⁴	5.1 × 10 ⁻²	1.0 × 10 ⁻⁴
Np	1.0 × 10 ⁻²	1.5 × 10 ⁻²	2.7 × 10 ⁻³	2.0 × 10 ⁻⁴	5.0 × 10 ⁻⁶	2.4 × 10 ⁻³	6.0 × 10 ⁻²	4.4 × 10 ⁻⁴	3.0 × 10 ⁻⁴
Pu	5.0 × 10 ⁻³	1.8 × 10 ⁻³	1.4 × 10 ⁻⁴	2.0 × 10 ⁻⁶	1.0 × 10 ⁻⁷	9.5 × 10 ⁻⁵	3.0 × 10 ⁻⁴	3.9 × 10 ⁻⁴	1.0 × 10 ⁻⁴
Am	2.5 × 10 ⁻²	2.2 × 10 ⁻⁵	2.0 × 10 ⁻⁴	2.0 × 10 ⁻⁴	4.1 × 10 ⁻⁷	5.0 × 10 ⁻⁴	3.0 × 10 ⁻⁴	4.4 × 10 ⁻⁴	1.0 × 10 ⁻³
Cm	2.5 × 10 ⁻²	1.1 × 10 ⁻³	2.0 × 10 ⁻⁴	2.0 × 10 ⁻⁴	5.0 × 10 ⁻⁶	5.0 × 10 ⁻⁴	3.0 × 10 ⁻⁴	4.4 × 10 ⁻⁴	3.0 × 10 ⁻⁴

Tab. A3.7-5: Food processing factors, turnover times for weathering losses and other rate factors

F_i = food processing factor which gives the fraction of activity retained after food processing; W_i = turnover time for weathering losses from the external surfaces of crops; T_i = a rate constant describing the transfer of the element from external plant surfaces to the edible portions; G = grain; P = pasture; GV = green vegetables; RV = root vegetables. Data taken from Nagra (2003b).

Element	F_G	W_G	W_P	F_GV	W_GV	F_RV	W_RV	T_RV	F_FRUIT	W_FRUIT	T_FRUIT
	-	a ⁻¹	a ⁻¹	-	a ⁻¹	-	a ⁻¹	a ⁻¹	-	a ⁻¹	a ⁻¹
H	0.15	8.4	18	0.5	18	0.5	18	1.8×10^4	0.5	18	1.8×10^4
Be	0.15	8.4	18	0.5	18	0.5	18	0.0	0.5	18	0.0
C	0.15	8.4	18	0.5	18	0.5	18	1.8×10^4	0.5	18	1.8×10^4
Cl	0.15	8.4	18	0.5	18	0.5	18	2.0	0.5	18	2.0
Ca	0.15	8.4	18	0.5	18	0.5	18	0.0	0.5	18	0.0
Co	0.15	8.4	18	0.5	18	0.5	18	0.95	0.5	18	0.95
Ni	0.15	8.4	18	0.5	18	0.5	18	0.95	0.5	18	0.95
Se	0.15	8.4	18	0.5	18	0.5	18	2.0	0.5	18	0.12
Sr	0.15	8.4	18	0.5	18	0.5	18	0.18	0.5	18	0.18
Zr	0.15	8.4	18	0.5	18	0.5	18	0.18	0.5	18	0.18
Nb	0.15	8.4	18	0.5	18	0.5	18	0.18	0.5	18	0.62
Mo	0.15	8.4	18	0.5	18	0.5	18	0.0	0.5	18	0.0
Tc	0.5	8.4	18	0.5	18	0.5	18	2.0	0.5	18	0.12
Pd	0.15	8.4	18	0.5	18	0.5	18	0.0	0.5	18	0.0
Ag	0.15	8.4	18	0.5	18	0.5	18	0.95	0.5	18	0.95
Sn	0.15	8.4	18	0.5	18	0.5	18	0.95	0.5	18	0.95
I	0.5	8.4	18	0.5	18	0.5	18	2.0	0.5	18	0.33
Cs	0.5	8.4	18	0.5	18	0.5	18	2.0	0.5	18	9.8×10^{-2}
Sm	0.15	8.4	18	0.5	18	0.5	18	0.38	0.5	18	0.38
Eu	0.15	8.4	18	0.5	18	0.5	18	0.38	0.5	18	0.38
Ho	0.15	8.4	18	0.5	18	0.5	18	0.0	0.5	18	0.0
Pb	0.15	8.4	18	0.5	18	0.5	18	0.0	0.5	18	0.11
Po	0.15	8.4	18	0.5	18	0.5	18	0.18	0.5	18	0.11
Ra	0.15	8.4	18	0.5	18	0.5	18	0.18	0.5	18	7.3×10^{-2}
Ac	0.15	8.4	18	0.5	18	0.5	18	0.18	0.5	18	0.21
Th	0.15	8.4	18	0.5	18	0.5	18	0.18	0.5	18	0.13
Pa	0.15	8.4	18	0.5	18	0.5	18	0.0	0.5	18	0.21
U	0.15	8.4	18	0.5	18	0.5	18	0.18	0.5	18	0.19
Np	0.1	51	18	0.5	51	0.5	18	0.0	0.5	18	0.21
Pu	0.1	51	18	0.5	51	0.5	18	0.0	0.5	18	0.19
Am	0.1	51	18	0.5	51	0.5	18	0.0	0.5	18	0.13
Cm	0.15	8.4	18	0.5	18	0.5	18	0.0	0.5	18	0.0

A3.8 Input parameters for biosphere modelling of alternative cases

In this section, input parameters for alternative biosphere cases are listed where their values differ from the Reference Case values. Tab. A3.8-1 thus contains a subset of the parameters listed in Tab. A3.7-1. All parameters compiled in Tabs. A3.7-2 to A3.7-5 are identical in the Reference Case and in all alternative cases analysed with TAME. A detailed justification of the biosphere parameter values used in the safety assessment for Project *Entsorgungsnachweis* is given in Nagra (2003b).

Tab. A3.8-1: List of biosphere input parameters for alternative biosphere cases

Parameters not listed are identical to those for the Reference Case. Data taken from Nagra (2003b).

Category	Parameter name	Description	Unit	Reference Case	Alternative Cases			
					Case 1	Case 2	Case 3	Case 4
		Short characterisation of climate and geomorphological unit		Present-day, eroding river	Present-day, sedimentation area	Present-day, wetland	Dry climate, eroding river	Wet climate, eroding river
Case number in Nagra 2002c	6.1a / 6.2a	6.1b	6.1c	6.2b	6.2c			
GENERAL	AF	Surface area of the biosphere region	m ²	2.3×10^6	2.3×10^6	1.0×10^6	2.3×10^6	2.3×10^6
GENERAL	ETP	Evapotranspiration	m a ⁻¹	0.6	0.6	0.6	1.0	1.0
GENERAL	RAIN-FALL	Precipitation	m a ⁻¹	1.0	1.0	1.0	0.5	2.0
GENERAL	CAPIL_R	Capillary rise	m a ⁻¹	0	0.1	0	0	0
GENERAL	IRRI_L	Irrigation with groundwater	m a ⁻¹	0.5	0.25	0	0.6	0.25
GENERAL	IRRI_W	Irrigation with surface water (incl. flooding)	m a ⁻¹	0	0.5	1.0	0	0
GENERAL	ME	Erosion	kg m ⁻² a ⁻¹	0.27	1.6	0	0.27	0.27
GENERAL	ALPHA_P	Suspended solid concentration in water from previous river section	kg m ⁻³	0.1	3.5	0.01	0.1	0.1
DEEPSOIL	THETA_D	Volumetric moisture content of deep soil	-	0.3	0.3	0.4	0.3	0.3
WATER	ALPHA_W	Suspended solid concentration in surface water	kg m ⁻³	0.1	3.5	0.01	0.1	0.1
WATER	D_W	Depth of surface water	m	3.3	1	2	3.3	3.3
WATER	L_W	Length of surface water compartment	m	3 500	3 000	3 000	3 500	3 500
WATER	W_W	Width of surface water compartment	m	100	20	20	100	100
TOPSOIL	EPS_T	Porosity of top soil	-	0.4	0.4	0.5	0.4	0.4

Tab. A.3.8-1 (Cont.)

Category	Parameter name	Description	Unit	Reference Case	Alternative Cases			
					Case 1	Case 2	Case 3	Case 4
					Present-day, eroding river	Present-day, sedimentation area	Present-day, wetland	Dry climate, eroding river
		Short characterisation of climate and geomorphological unit		6.1a / 6.2a	6.1b	6.1c	6.2b	6.2c
		Case number in Nagra 2002c						
TOPSOIL	RHO_T	Dry density of top soil material	kg m ⁻³	2 650	2 650	1 400	2 650	2 650
TOPSOIL	THETA_T	Volumetric moisture content of top soil	-	0.3	0.3	0.5	0.3	0.3
BAL-File	F_CL	Flux of contaminated deep groundwater into local aquifer	m ³ a ⁻¹	1.3 × 10 ⁵	8.0 × 10 ⁴	0	1.3 × 10 ⁵	1.3 × 10 ⁵
BAL-File	F_CW	Flux of contaminated deep groundwater into surface water	m ³ a ⁻¹	0	0	8.0 × 10 ⁴	0	0
BAL-File	F_UL	Flux of uncontaminated water into local aquifer	m ³ a ⁻¹	1.5 × 10 ⁶	1.3 × 10 ⁶	1.3 × 10 ⁶	1.3 × 10 ⁶	1.8 × 10 ⁶
BAL-File	F_UW	Flux of uncontaminated water into surface water	m ³ a ⁻¹	1.2 × 10 ¹⁰	5.0 × 10 ⁷	5.0 × 10 ⁷	5.9 × 10 ⁹	2.3 × 10 ¹⁰
REL-File	REL_L	Fraction of release into local aquifer	-	1	1	0	1	1
REL-File	REL_W	Fraction of release into surface water	-	0	0	1	0	0
SOL-File	SOL_T	Classification of grain size in top soil	-	fine	fine	organics	fine	fine

A3.9 Biosphere dose conversion factors

The sensitivity to assumptions regarding the surface environment is illustrated in Fig. A3.9-1. The quantity on the vertical axis of the figure is the ratio of the dose to an exposed individual due to a given nuclide to the corresponding release rate of that nuclide to the biosphere, termed biosphere dose conversion factor (BDCF). BDCFs are given for a range of safety-relevant radionuclides and biosphere cases.

In Fig. A3.9-1, the presented set of radionuclides, a sub-set of all safety-relevant radionuclides⁵⁷, is selected by expert judgement based on a consideration of their properties (half-lives, geochemical behaviour, etc.) and the relative importance of their contribution to dose. The BDCFs for the complete set of safety-relevant radionuclides are listed in Tab. A3.9-1.

The range of considered biosphere cases includes:

- The combination of the reference area and the present-day climate, i.e. Reference Case assumptions.
- Alternative areas: the characteristics of the surface environment based on a sedimentation area and on an area of wetlands.
- Alternative climates: drier/warmer and wetter/warmer than present-day climate.
- Drinking water (Reference Case dilution): i.e. drinking water doses, based on the assumption that drinking water is obtained from a shallow Quaternary aquifer in the reference area, with an assumed dilution rate of $10^6 \text{ m}^3 \text{ a}^{-1}$.
- Drinking water (spring at valley side): i.e. drinking water doses, based on the assumption that drinking water is obtained from a spring at the side of a larger river valley, with an assumed discharge of 60 l min^{-1} ($3.2 \times 10^4 \text{ m}^3 \text{ a}^{-1}$) and a capture efficiency of 10 %⁵⁸.
- Drinking water (Malm aquifer): i.e. doses are drinking water doses, based on the assumption that drinking water is obtained from a deep well, with an extraction rate of 300 l min^{-1} ($1.6 \times 10^5 \text{ m}^3 \text{ a}^{-1}$), which represents a minimal rate for a viable exploitation of a drinking water well, and an assumed capture efficiency of 10 %.

Fig. A3.9-1 indicates that the variability in BDCFs for individual radionuclides is, with a few exceptions, less than three orders of magnitude. This is to a large extent related to variability in the degree of dilution in the surface environment. For most radionuclides, the highest BDCFs are obtained for the biosphere case considering the effects of a dry climate, whereas the Reference Case BDCFs are typically near the middle of the variability range. The lowest BDCFs are obtained for the cases involving high dilution (wetland) or ingestion of drinking water only. It is worthwhile noting that for ^{129}I , which determines the dose maximum in most cases (see Chapter 7 in Nagra 2002c), the BDCF for the dry climate case is only about one order of magnitude higher than that for the Reference Case. For other important radionuclides, such as ^{14}C , ^{79}Se and ^{36}Cl , the BDCF is increased by up to a factor of 40, when comparing the dry climate case and the Reference Case. Drinking water BDCFs depend on the ratio of the capture efficiency to the dilution rate. For this reason, the drinking water BDCFs for the reference biosphere area and the deep well in the Malm aquifer are similar, whereas the drinking water BDCFs for the spring at a valley side are higher by about a factor of 5.

⁵⁷ The procedure for the selection of safety-relevant radionuclides is discussed in Appendix 5.

⁵⁸ The capture efficiency is the fraction of radionuclides released from the repository to the Malm aquifer that is captured by a spring or well.

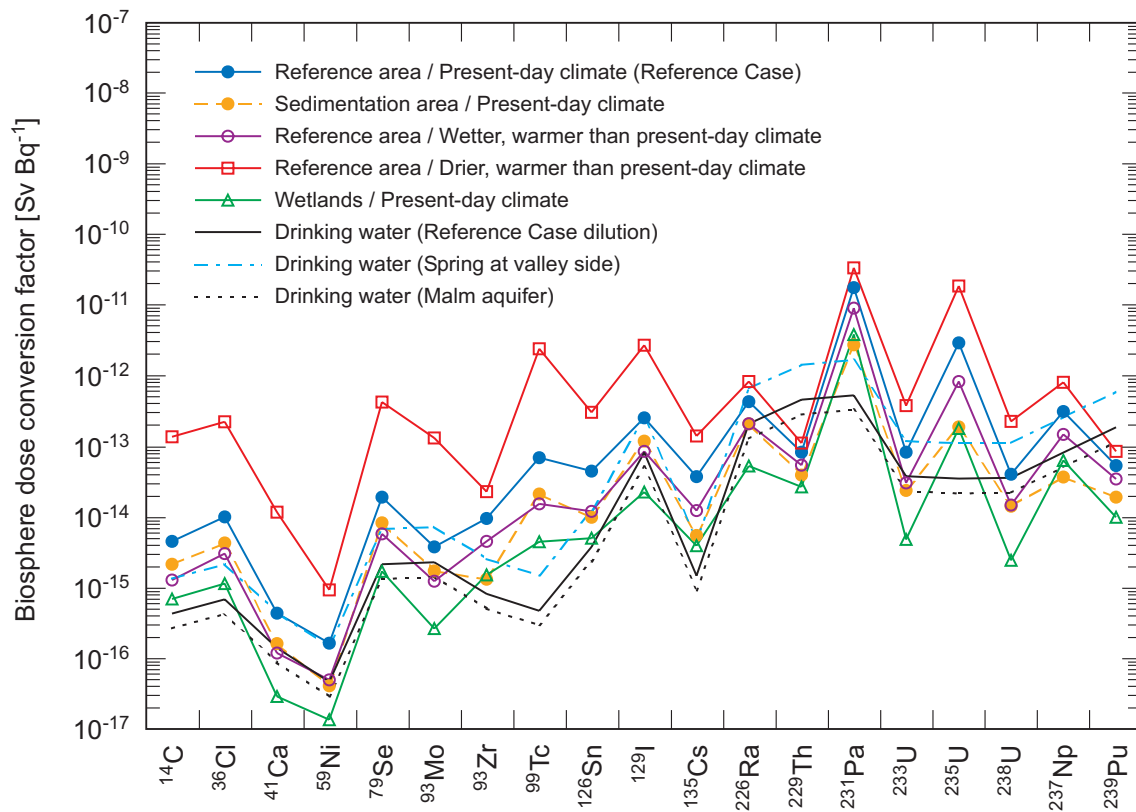


Fig. A3.9-1: Biosphere dose conversion factors (BDCF) for various cases related to uncertainty in conditions in the surface environment

The BDCF for a given radionuclide is the ratio of the corresponding steady-state annual dose [Sv a^{-1}] to the input value of 1 Bq a^{-1} .

Tab. A3.9-1: Biosphere dose conversion factors (BDCFs) in Sv Bq⁻¹ for all safety-relevant radionuclides and for the various cases shown in Fig. A3.9-1

The BDCF for a given radionuclide is the ratio of the corresponding steady-state annual dose [Sv a⁻¹] to the input value of 1 Bq a⁻¹.

Radio-nuclide and daughters	Reference area / Present-day climate (Reference Case)	Sedimentation area / Present-day climate	Reference area / Wetter, warmer than present-day climate	Reference area / Drier, warmer than present-day climate	Wetlands / Present-day climate	Drinking water / Reference Case dilution	Drinking water / Spring at valley side	Drinking water / Malm aquifer	
Activation / fission products	³ H	1.7 × 10 ⁻¹⁶	7.7 × 10 ⁻¹⁷	5.6 × 10 ⁻¹⁷	9.6 × 10 ⁻¹⁶	2.2 × 10 ⁻¹⁷	3.1 × 10 ⁻¹⁷	9.7 × 10 ⁻¹⁷	1.9 × 10 ⁻¹⁷
	¹⁰ Be	4.8 × 10 ⁻¹⁶	2.8 × 10 ⁻¹⁶	2.2 × 10 ⁻¹⁶	2.5 × 10 ⁻¹⁵	2.7 × 10 ⁻¹⁷	8.0 × 10 ⁻¹⁶	2.5 × 10 ⁻¹⁵	5.0 × 10 ⁻¹⁶
	¹⁴ C	4.5 × 10 ⁻¹⁵	2.1 × 10 ⁻¹⁵	1.3 × 10 ⁻¹⁵	1.3 × 10 ⁻¹³	6.9 × 10 ⁻¹⁶	4.2 × 10 ⁻¹⁶	1.3 × 10 ⁻¹⁵	2.6 × 10 ⁻¹⁶
	³⁶ Cl	9.9 × 10 ⁻¹⁵	4.2 × 10 ⁻¹⁵	3.0 × 10 ⁻¹⁵	2.2 × 10 ⁻¹³	1.1 × 10 ⁻¹⁵	6.8 × 10 ⁻¹⁶	2.2 × 10 ⁻¹⁵	4.2 × 10 ⁻¹⁶
	⁴¹ Ca	4.3 × 10 ⁻¹⁶	1.6 × 10 ⁻¹⁶	1.2 × 10 ⁻¹⁶	1.2 × 10 ⁻¹⁴	2.9 × 10 ⁻¹⁷	1.4 × 10 ⁻¹⁶	4.4 × 10 ⁻¹⁶	8.7 × 10 ⁻¹⁷
	⁵⁹ Ni	1.6 × 10 ⁻¹⁶	4.0 × 10 ⁻¹⁷	4.9 × 10 ⁻¹⁷	9.2 × 10 ⁻¹⁶	1.3 × 10 ⁻¹⁷	4.6 × 10 ⁻¹⁷	1.5 × 10 ⁻¹⁶	2.9 × 10 ⁻¹⁷
	⁶⁰ Co	3.4 × 10 ⁻¹⁷	2.0 × 10 ⁻¹⁷	1.8 × 10 ⁻¹⁷	4.1 × 10 ⁻¹⁷	1.6 × 10 ⁻¹⁵	2.5 × 10 ⁻¹⁵	7.9 × 10 ⁻¹⁵	1.6 × 10 ⁻¹⁵
	⁶³ Ni	6.2 × 10 ⁻¹⁸	3.7 × 10 ⁻¹⁸	3.6 × 10 ⁻¹⁸	7.8 × 10 ⁻¹⁸	1.6 × 10 ⁻¹⁷	1.1 × 10 ⁻¹⁶	3.5 × 10 ⁻¹⁶	6.8 × 10 ⁻¹⁷
	⁷⁹ Se	1.9 × 10 ⁻¹⁴	8.2 × 10 ⁻¹⁵	5.7 × 10 ⁻¹⁵	4.2 × 10 ⁻¹³	1.7 × 10 ⁻¹⁵	2.1 × 10 ⁻¹⁵	6.7 × 10 ⁻¹⁵	1.3 × 10 ⁻¹⁵
	⁹⁰ Sr	4.0 × 10 ⁻¹⁵	2.3 × 10 ⁻¹⁵	2.1 × 10 ⁻¹⁵	6.7 × 10 ⁻¹⁵	3.6 × 10 ⁻¹⁵	2.3 × 10 ⁻¹⁴	7.2 × 10 ⁻¹⁴	1.4 × 10 ⁻¹⁴
	⁹³ Mo	3.7 × 10 ⁻¹⁵	1.7 × 10 ⁻¹⁵	1.2 × 10 ⁻¹⁵	1.3 × 10 ⁻¹³	2.6 × 10 ⁻¹⁶	2.3 × 10 ⁻¹⁵	7.2 × 10 ⁻¹⁵	1.4 × 10 ⁻¹⁵
	^{93m} Nb	1.4 × 10 ⁻¹⁸	9.4 × 10 ⁻¹⁹	8.8 × 10 ⁻¹⁹	1.7 × 10 ⁻¹⁸	9.5 × 10 ⁻¹⁸	8.8 × 10 ⁻¹⁷	2.8 × 10 ⁻¹⁶	5.5 × 10 ⁻¹⁷
	⁹³ Zr	9.4 × 10 ⁻¹⁵	1.3 × 10 ⁻¹⁵	4.4 × 10 ⁻¹⁵	2.2 × 10 ⁻¹⁴	1.5 × 10 ⁻¹⁵	8.0 × 10 ⁻¹⁶	2.5 × 10 ⁻¹⁵	5.0 × 10 ⁻¹⁶
	⁹⁴ Nb	2.0 × 10 ⁻¹³	4.4 × 10 ⁻¹⁴	5.0 × 10 ⁻¹⁴	1.8 × 10 ⁻¹²	7.1 × 10 ⁻¹⁵	1.2 × 10 ⁻¹⁵	3.9 × 10 ⁻¹⁵	7.8 × 10 ⁻¹⁶
	⁹⁹ Tc	6.8 × 10 ⁻¹⁴	2.1 × 10 ⁻¹⁴	1.5 × 10 ⁻¹⁴	2.4 × 10 ⁻¹²	4.4 × 10 ⁻¹⁵	4.7 × 10 ⁻¹⁶	1.5 × 10 ⁻¹⁵	2.9 × 10 ⁻¹⁶
	¹⁰⁷ Pd	1.0 × 10 ⁻¹⁶	2.3 × 10 ⁻¹⁷	3.0 × 10 ⁻¹⁷	6.4 × 10 ⁻¹⁶	7.8 × 10 ⁻¹⁸	2.7 × 10 ⁻¹⁷	8.6 × 10 ⁻¹⁷	1.7 × 10 ⁻¹⁷
	^{108m} Ag	1.2 × 10 ⁻¹⁴	5.4 × 10 ⁻¹⁵	3.8 × 10 ⁻¹⁵	1.3 × 10 ⁻¹³	1.1 × 10 ⁻¹⁵	1.7 × 10 ⁻¹⁵	5.3 × 10 ⁻¹⁵	1.0 × 10 ⁻¹⁵
	^{121m} Sn	2.1 × 10 ⁻¹⁷	1.6 × 10 ⁻¹⁷	1.1 × 10 ⁻¹⁷	2.6 × 10 ⁻¹⁷	2.9 × 10 ⁻¹⁶	4.1 × 10 ⁻¹⁶	1.3 × 10 ⁻¹⁵	2.6 × 10 ⁻¹⁶
	¹²⁶ Sn	4.4 × 10 ⁻¹⁴	9.8 × 10 ⁻¹⁵	1.2 × 10 ⁻¹⁴	3.0 × 10 ⁻¹³	5.0 × 10 ⁻¹⁵	3.7 × 10 ⁻¹⁵	1.2 × 10 ⁻¹⁴	2.3 × 10 ⁻¹⁵
	¹²⁹ I	2.5 × 10 ⁻¹³	1.2 × 10 ⁻¹³	8.3 × 10 ⁻¹⁴	2.6 × 10 ⁻¹²	2.2 × 10 ⁻¹⁴	8.0 × 10 ⁻¹⁴	2.5 × 10 ⁻¹³	5.0 × 10 ⁻¹⁴
¹³⁵ Cs	3.6 × 10 ⁻¹⁴	5.4 × 10 ⁻¹⁵	1.2 × 10 ⁻¹⁴	1.4 × 10 ⁻¹³	3.9 × 10 ⁻¹⁵	1.5 × 10 ⁻¹⁵	4.6 × 10 ⁻¹⁵	9.1 × 10 ⁻¹⁶	
¹³⁷ Cs	1.9 × 10 ⁻¹⁶	1.2 × 10 ⁻¹⁶	1.0 × 10 ⁻¹⁶	2.3 × 10 ⁻¹⁶	6.2 × 10 ⁻¹⁵	9.5 × 10 ⁻¹⁵	3.0 × 10 ⁻¹⁴	5.9 × 10 ⁻¹⁵	
¹⁵¹ Sm	7.7 × 10 ⁻¹⁹	4.9 × 10 ⁻¹⁹	4.3 × 10 ⁻¹⁹	9.1 × 10 ⁻¹⁹	2.0 × 10 ⁻¹⁷	7.2 × 10 ⁻¹⁷	2.3 × 10 ⁻¹⁶	4.5 × 10 ⁻¹⁷	
¹⁵⁴ Eu	4.3 × 10 ⁻¹⁸	2.5 × 10 ⁻¹⁸	2.3 × 10 ⁻¹⁸	5.2 × 10 ⁻¹⁸	1.1 × 10 ⁻¹⁵	1.5 × 10 ⁻¹⁵	4.6 × 10 ⁻¹⁵	9.1 × 10 ⁻¹⁶	
^{166m} H	1.7 × 10 ⁻¹⁴	1.1 × 10 ⁻¹⁴	1.0 × 10 ⁻¹⁴	2.1 × 10 ⁻¹⁴	1.7 × 10 ⁻¹⁴	1.5 × 10 ⁻¹⁵	4.6 × 10 ⁻¹⁵	9.1 × 10 ⁻¹⁶	
4N chain	²²⁸ Ra	8.0 × 10 ⁻¹⁶	6.1 × 10 ⁻¹⁶	5.8 × 10 ⁻¹⁶	8.9 × 10 ⁻¹⁶	2.3 × 10 ⁻¹⁴	5.0 × 10 ⁻¹³	1.6 × 10 ⁻¹²	3.1 × 10 ⁻¹³
	²²⁸ Th	4.5 × 10 ⁻¹⁸	3.6 × 10 ⁻¹⁸	3.4 × 10 ⁻¹⁸	5.0 × 10 ⁻¹⁸	3.2 × 10 ⁻¹⁵	1.0 × 10 ⁻¹³	3.2 × 10 ⁻¹³	6.4 × 10 ⁻¹⁴
	²³² Th	4.6 × 10 ⁻¹²	1.0 × 10 ⁻¹²	2.4 × 10 ⁻¹²	1.0 × 10 ⁻¹¹	4.7 × 10 ⁻¹³	1.7 × 10 ⁻¹³	5.3 × 10 ⁻¹³	1.0 × 10 ⁻¹³
	²³² U	4.8 × 10 ⁻¹⁵	3.5 × 10 ⁻¹⁵	3.4 × 10 ⁻¹⁵	5.5 × 10 ⁻¹⁵	1.0 × 10 ⁻¹⁴	2.4 × 10 ⁻¹³	7.6 × 10 ⁻¹³	1.5 × 10 ⁻¹³
	²³⁶ U	3.5 × 10 ⁻¹⁴	1.4 × 10 ⁻¹⁴	1.4 × 10 ⁻¹⁴	1.5 × 10 ⁻¹³	2.3 × 10 ⁻¹⁵	3.4 × 10 ⁻¹⁴	1.1 × 10 ⁻¹³	2.1 × 10 ⁻¹⁴
	²⁴⁰ Pu	2.1 × 10 ⁻¹⁴	1.1 × 10 ⁻¹⁴	1.5 × 10 ⁻¹⁴	2.8 × 10 ⁻¹⁴	6.3 × 10 ⁻¹⁵	1.8 × 10 ⁻¹³	5.8 × 10 ⁻¹³	1.1 × 10 ⁻¹³
	²⁴⁴ Cm	9.4 × 10 ⁻¹⁷	5.9 × 10 ⁻¹⁷	6.9 × 10 ⁻¹⁷	1.1 × 10 ⁻¹⁶	2.6 × 10 ⁻¹⁵	8.8 × 10 ⁻¹⁴	2.8 × 10 ⁻¹³	5.5 × 10 ⁻¹⁴

Tab. A3.9-1: (Cont.)

Radio-nuclide and daughters		Reference area / Present-day climate (Reference Case)	Sedimentation area / Present-day climate	Reference area / Wetter, warmer than present-day climate	Reference area / Drier, warmer than present-day climate	Wetlands / Present-day climate	Drinking water / Reference Case dilution	Drinking water / Spring at valley side	Drinking water / Malm aquifer
4N+1 chain	²²⁹ Th	8.1×10^{-14}	3.9×10^{-14}	5.3×10^{-14}	1.1×10^{-13}	2.6×10^{-14}	4.5×10^{-13}	1.4×10^{-12}	2.8×10^{-13}
	²³³ U	8.1×10^{-14}	2.3×10^{-14}	3.0×10^{-14}	3.7×10^{-13}	4.8×10^{-15}	3.7×10^{-14}	1.2×10^{-13}	2.3×10^{-14}
	²³⁷ Np	3.0×10^{-13}	3.6×10^{-14}	1.5×10^{-13}	7.9×10^{-13}	6.2×10^{-14}	8.0×10^{-14}	2.5×10^{-13}	5.0×10^{-14}
	²⁴¹ Am	1.2×10^{-15}	1.0×10^{-15}	9.9×10^{-16}	1.4×10^{-15}	3.2×10^{-15}	1.5×10^{-13}	4.6×10^{-13}	9.1×10^{-14}
	²⁴¹ Pu	4.2×10^{-17}	3.4×10^{-17}	3.4×10^{-17}	4.9×10^{-17}	7.5×10^{-17}	3.5×10^{-15}	1.1×10^{-14}	2.2×10^{-15}
	²⁴⁵ Cm	5.7×10^{-14}	2.5×10^{-14}	3.8×10^{-14}	8.0×10^{-14}	1.3×10^{-14}	1.5×10^{-13}	4.9×10^{-13}	9.6×10^{-14}
4N+2 chain	²¹⁰ Pb	3.8×10^{-15}	3.1×10^{-15}	2.7×10^{-15}	4.3×10^{-15}	3.3×10^{-14}	5.0×10^{-13}	1.6×10^{-12}	3.1×10^{-13}
	²¹⁰ Po	9.1×10^{-18}	7.3×10^{-18}	6.6×10^{-18}	1.0×10^{-17}	9.1×10^{-14}	8.8×10^{-13}	2.8×10^{-12}	5.5×10^{-13}
	²²⁶ Ra	4.2×10^{-13}	2.1×10^{-13}	2.0×10^{-13}	8.1×10^{-13}	5.2×10^{-14}	2.0×10^{-13}	6.5×10^{-13}	1.3×10^{-13}
	²³⁰ Th	5.1×10^{-12}	9.9×10^{-13}	2.0×10^{-12}	1.5×10^{-11}	2.3×10^{-13}	1.5×10^{-13}	4.9×10^{-13}	9.6×10^{-14}
	²³⁴ U	2.6×10^{-13}	3.7×10^{-14}	6.6×10^{-14}	1.8×10^{-12}	7.8×10^{-15}	3.6×10^{-14}	1.1×10^{-13}	2.2×10^{-14}
	²³⁸ Pu	3.5×10^{-16}	2.4×10^{-16}	2.4×10^{-16}	9.1×10^{-16}	2.8×10^{-15}	1.7×10^{-13}	5.3×10^{-13}	1.0×10^{-13}
	²³⁸ U	4.0×10^{-14}	1.4×10^{-14}	1.5×10^{-14}	2.2×10^{-13}	2.4×10^{-15}	3.5×10^{-14}	1.1×10^{-13}	2.2×10^{-14}
	^{242m} A	5.0×10^{-16}	3.9×10^{-16}	3.9×10^{-16}	7.1×10^{-16}	2.9×10^{-15}	1.5×10^{-13}	4.6×10^{-13}	9.1×10^{-14}
	²⁴² Pu	9.0×10^{-14}	2.3×10^{-14}	5.2×10^{-14}	1.9×10^{-13}	1.3×10^{-14}	1.8×10^{-13}	5.6×10^{-13}	1.1×10^{-13}
	²⁴⁶ Cm	1.8×10^{-14}	9.5×10^{-15}	1.2×10^{-14}	2.3×10^{-14}	7.4×10^{-15}	1.5×10^{-13}	4.9×10^{-13}	9.6×10^{-14}
4N+3 chain	²²⁷ Ac	1.5×10^{-15}	9.7×10^{-16}	8.7×10^{-16}	1.7×10^{-15}	1.7×10^{-13}	8.8×10^{-13}	2.8×10^{-12}	5.5×10^{-13}
	²³¹ Pa	1.7×10^{-11}	2.7×10^{-12}	8.9×10^{-12}	3.3×10^{-11}	3.7×10^{-12}	5.2×10^{-13}	1.6×10^{-12}	3.2×10^{-13}
	²³⁵ U	2.8×10^{-12}	1.8×10^{-13}	8.1×10^{-13}	1.8×10^{-11}	1.8×10^{-13}	3.4×10^{-14}	1.1×10^{-13}	2.1×10^{-14}
	²³⁹ Pu	5.2×10^{-14}	1.9×10^{-14}	3.4×10^{-14}	8.3×10^{-14}	9.7×10^{-15}	1.8×10^{-13}	5.8×10^{-13}	1.1×10^{-13}
	²⁴³ Am	3.6×10^{-14}	1.4×10^{-14}	2.3×10^{-14}	5.4×10^{-14}	8.0×10^{-15}	1.5×10^{-13}	4.6×10^{-13}	9.1×10^{-14}
	²⁴³ Cm	1.3×10^{-16}	8.0×10^{-17}	9.5×10^{-17}	1.8×10^{-16}	3.3×10^{-15}	1.1×10^{-13}	3.5×10^{-13}	6.8×10^{-14}

A3.10 Input parameters for probabilistic analysis

This section documents the input parameters used in the probabilistic analysis of Chapter 6 and 7 in Nagra (2002c). As discussed in Section 6.7.4 of Nagra (2002c), probabilistic calculations allow an investigation of the sensitivity of calculated doses to reference model chain input parameters in a comprehensive manner, including the effects of varying all parameters at the same time.

In the probabilistic analysis, input parameters for individual runs are selected from probability density functions (PDFs), some of which are correlated, and a large number of runs are carried out, in order to obtain a distribution of results. The selection of PDFs and the correlations considered between parameters / waste types / radionuclides / species (anions, non-anions) are discussed in the following sections.

A3.10.1 Input PDFs

The PDFs in Tab. A.3-10 for the most important parameters that determine release and transport of radionuclides were developed based on discussions with various Nagra experts. Explanations for the PDF attributes (shape and truncation values) are provided below.

Cladding dissolution rate – The truncation limits were set at 5 times greater and less than the reference value. The reference value is based on review of reported measurements of Zircaloy corrosion rates by Johnson & McGinnes (2002) and represents a rate of $\sim 10 \text{ nm a}^{-1}$. This value is pessimistic (about 2 to 10 times the reported values), thus the upper truncation limit is considered very unlikely (2σ of a log-normal distribution).

IRF – The reference IRF values are for SF with an average burnup of $48 \text{ GWd/t}_{\text{HM}}$. The PDF is log-uniform, with the lower truncation limit at the reference value, because this reflects the most probable situation (it is based on real burnup data for a large quantity of SF, thus the average cannot realistically be lower). The upper truncation limit adopts IRF values for SF with a burnup of $75 \text{ GWd/t}_{\text{HM}}$. It is considered extremely improbable that such an average burnup could be reached, thus the low assigned probability.

SF matrix dissolution rate – The reference value is considered to be the maximum value, because the effects of H_2 are expected to produce even lower dissolution rates (Johnson & Smith 2000). The lower truncation limit is defined by a rate controlled by solubility-limited dissolution. A log-normal distribution was arbitrarily selected.

HLW dissolution rate – The upper truncation limit adopts very pessimistic values (almost 100 times the reference rates for the two glasses). The use of a triangular distribution reflects the view that such high rates are very unlikely, because they are based on the early (transient) dissolution rate, not the measured lower rates that occur once steady state has been reached (Curti 2003). The lower truncation represents the possibility that a protective gel layer continues to grow, progressively lowering the rate.

Radionuclide solubilities for SF/HLW and ILW near field – The optimistic and pessimistic values given in Tab. A3.5-1 and A3.5-3 were adopted as truncation values. The discrete distribution ($P = 0.7$ for the reference value, with $P = 0.15$ for the optimistic and pessimistic values) was selected to give sufficient weight to the reference value, while acknowledging that the limiting values have a significant likelihood.

K_d values for SF/HLW and ILW near field – As for solubilities.

D_e in bentonite – The upper truncation limit, which is only twice the reference value, reflects the view that values greater than this are physically unrealistic, because the reference value is itself only about 10 to 20 times lower than the value in free water. The lower truncation, set at ten times lower than the reference value, is consistent with the lowest D_e value discussed in compilations of diffusion data such as Yu & Neretnieks (1997). The log-normal distribution was an arbitrary choice.

Transport path length in Opalinus Clay - The reference case value of 40 m was pessimistically selected (the host rock is 105 to 125 m thick, thus a realistic path length is about 50 m). The PDF chosen is uniform, thus giving equal weight to all values between 40 m and 60 m.

D_e in Opalinus Clay – An upper truncation of 3 times the reference value was selected for D_e 's for all species, corresponding to the alternative pessimistic value proposed for anions and neutral species in the geosynthesis report (Nagra 2002a). Based on observations in other rocks, where laboratory experiments indicate a higher diffusion coefficient for some cations (Andra 2001), a pessimistic alternative value of 10 times the reference value is proposed for non-anions (specifically for cations) in the geosynthesis report. In order to keep operational procedures simple, this was not taken into account in the probabilistic analysis; however, a 10 times higher diffusion coefficient for all non-anions was considered in the deterministic analysis. The lower truncation is set to half the reference value for all species, because lower values would be inconsistent with values derived from laboratory measurements on Opalinus Clay core material from Benken and from in-situ field experiments at Mont Terri.

Darcy velocity in Opalinus Clay - The reference value for the Darcy velocity reflects the reference hydraulic gradient of 1 and the reference vertical hydraulic conductivity K_v of $2 \times 10^{-14} \text{ m s}^{-1}$. The upper truncation value (10 times the reference value) assumes that sustained overpressures (gradient 5 times the reference value) in the near field drive flow and takes into account further uncertainties. The lower cutoff (20 times lower than the reference value) represents the possibility of a threshold gradient. The log-normal distribution gives a significant weighting to the truncation values (1σ for the upper truncation).

A3.10.2 Correlations

In the probabilistic calculations, some parameters are correlated, representing a "linked" treatment of waste types, radionuclides, species (anions, non-anions). In all investigated cases, the chosen correlation coefficients are either 1 (fully correlated parameters) or 0 (uncorrelated parameters). Although the code GIPC (Appendix 2) has full flexibility with regard to parameter correlations, no partial correlations ($0 < \text{correlation coefficient} < 1$) have been introduced.

SF/HLW near field

- For SF, to simplify the calculations, a single "weighted average canister" is defined based on the three reference case canister types, and their reference case numbers, with a weighted average inventory, IRF and SF matrix dissolution rate (see Tab. A3.10-1);
- the HLW matrix dissolution rates for COGEMA and BNFL are fully correlated;
- the radionuclide solubilities and K_d values for different elements are uncorrelated, reflecting uncertainty in the measurement and derivation of these values;
- the bentonite D_e for anions and non-anions are fully correlated, reflecting a common state of the bentonite microstructure affecting all species in a similar manner.

ILW near field

- The radionuclide solubilities and K_d values for different elements are uncorrelated, reflecting uncertainty in the measurement and derivation of these values.

Opalinus Clay

- Generally, all Opalinus Clay parameter values sampled for SF, HLW and ILW are taken to be uncorrelated;
- the K_d values for Opalinus Clay for different elements are uncorrelated, reflecting uncertainty in the measurement and derivation of the K_d values;
- the Opalinus Clay D_e for anions and non-anions are fully correlated, reflecting a common state of the Opalinus Clay microstructure affecting all species in a similar manner;
- a special correlation is adopted in case 4.2 ("Transport along transmissive discontinuities", see Section 6.2) for SF/HLW: The effective diffusion constant parallel to the bedding planes, used in leg L2 to model radionuclide diffusion from the discontinuity horizontally into the Opalinus Clay matrix (Fig. 6.2-1), is assumed to be fully correlated with the effective diffusion constant perpendicular to the bedding planes, used in leg L1 to model radionuclide diffusion from the emplacement tunnels vertically through the undisturbed Opalinus Clay. Likewise, the K_d values for the Opalinus Clay used in legs L1 and L2 are taken to be fully correlated.

Tab. A3.10-1: Probability density functions (PDF's) for probabilistic analysis

SF/HLW near field			
Model parameter	Reference Case values	PDF attributes	"What if?" values
Cladding dissolution rate	$3 \times 10^{-5} \text{ a}^{-1}$	Log-normal median = Reference Case value, (log) = 0.35 upper truncation = $1.5 \times 10^{-4} \text{ a}^{-1}$ (2) lower truncation = $6 \times 10^{-6} \text{ a}^{-1}$ (2)	$3 \times 10^{-4} \text{ a}^{-1}$
IRF	Tab. A3.4-2a (weighted average of the three canister types)	Log-uniform lower cut-off - values for 48 GWd/t _{IHM} PWR fuel (best estimate); upper cut-off - values for 75 GWd/t _{IHM} PWR fuel	-
SF matrix dissolution rate ¹	Tab. A3.6-1 (weighted average of the three canister types)	Log-uniform maximum = reference rate (t), minimum = solubility limited rate (t)	10 × and 100 × Reference Case value
HLW dissolution rate	Tab. A3.3-2b	Triangular maximum = pessimistic variation values (Tab. A3.3-2b) minimum = 0.05 × reference value	See highly pessimistic variations (Tab. A3.3-2b)
Radionuclide solubilities	Tab. A3.5-1	Discrete Probability (P) = 0.7 for reference value, P = 0.15 for optimistic and pessimistic values	Values for oxidising conditions in Tab. A3.5-1
K _d values	Tab. A3.5-2	Discrete P = 0.7 for reference value, P = 0.15 for optimistic and pessimistic values	Values for oxidising conditions in Tab. A3.5-2 "What if?" case for ¹²⁹ I K _d = 0
D _e	Tab. A3.5-2	Log-normal median – reference values, (log) = 0.3 upper truncation = 2 × reference values (1), lower truncation = 0.1 × reference values (3.3)	-

Tab. A3.10-1: (Cont.)

ILW near field			
Model parameter	Reference Case values	PDF attributes	"What if?" values
Radionuclide solubilities	Tab. A3.5-3	Discrete Probability (P) = 0.7 for reference value, P = 0.15 for optimistic and pessimistic values	Values for oxidising conditions in Tab. A3.5-3
K_d values	Tab. A3.5-4	Discrete P = 0.7 for reference value, P = 0.15 for optimistic and pessimistic values	"What if?" case for ^{129}I $K_d = 0$
Opalinus Clay			
Model parameter	Reference Case values	PDF attributes	"What if?" values
K_d values	Tab. A3.5-5	Discrete P = 0.7 for reference value, P = 0.15 for optimistic and pessimistic values	"What if?" case for ^{129}I $K_d = 0$
Transport path length	40 m	Uniform minimum = 40 m maximum = 60 m	30 m
D_e	Tab. A3.5-5	Log-normal median = reference values, $(\log) = 0.24$ upper truncation = $3 \times$ reference values (2), lower truncation = $0.5 \times$ reference values (1.26)	-
Darcy velocity	$2 \times 10^{-14} \text{ m s}^{-1}$	Log-normal median = reference values, $(\log) = 1$ upper truncation = $2 \times 10^{-13} \text{ m s}^{-1}$ (1), lower truncation = $1 \times 10^{-15} \text{ m s}^{-1}$ (1.3)	100-fold increase in flow rate
Transmissivity of hypothetical transmissive discontinuity	-	-	10^{-9} and $10^{-10} \text{ m}^2 \text{ s}^{-1}$

¹ In Nagra (2002c), Tab. A2.13, it is indicated that the reference rate is that for a UO_2 48 GWd/ t_{HM} canister, whereas in reality, the weighted average rate (which is essentially identical to that for a UO_2 48 GWd/ t_{HM} canister) was used.

Appendix 4: Solving the Governing Equations for Steady-State Transport Through Opalinus Clay Intersected by Discontinuities

The governing equations and boundary conditions for steady-state radionuclide transport through Opalinus Clay intersected by discontinuities are given in Section 9.4 (Eqs. 9.4-3 to 9.4-11). This appendix describes the semi-analytical approach used to solve these equations.

For convenience, Eq. 9.4-3 is written in the form:

$$0 = \frac{d^2 P}{dx^2} + \alpha_1 \frac{dP}{dx} + \alpha_2 C + \alpha_3 \left. \frac{\partial C}{\partial z} \right|_{z=b}, \quad (\text{A4-1})$$

where:

$$\alpha_1 = -\frac{u'}{(a'_L u' + D')}, \quad (\text{A4-2})$$

$$\alpha_2 = -\frac{\lambda}{(a'_L u' + D')}, \quad (\text{A4-3})$$

and

$$\alpha_3 = \frac{\varepsilon D}{b(a'_L u' + D')}. \quad (\text{A4-4})$$

Eq. 9.4-5 is written in the form:

$$0 = \frac{d^2 C}{dx^2} + \frac{d^2 C}{dz^2} - \mu C, \quad (\text{A4-5})$$

where

$$\mu = \frac{\lambda R}{D}. \quad (\text{A4-6})$$

In order to satisfy the boundary condition given by Eq. 9.4-11, solutions to Eq. A4-5 of the form:

$$C = \sum_{n=0}^{\infty} C_n(x) \cos \lambda_n z' \quad (\text{A4-7})$$

are sought, where

$$z' = z - B, \quad (\text{A4-8})$$

n is a set of integers (≥ 0) and λ_n is a set of eigenvalues that must be determined.

Substitution of Eq. A4-7 in Eq. A4-5 leads to the equation:

$$\frac{d^2 C_n}{dx^2} - (\lambda_n^2 + \mu) C_n = 0. \quad (\text{A4-9})$$

The solution of Eq. A4-9 that satisfies the condition given by Eq. 9.4-9 is:

$$C_n = A_n \exp(-x \sqrt{\lambda_n^2 + \mu}). \quad (\text{A4-10})$$

where A_n are constants.

Similarly, solutions to Eq. A4-1 of the form:

$$P = \sum_{n=0}^{\infty} P_n \exp(-x \sqrt{\lambda_n^2 + \mu}) \quad (\text{A4-11})$$

are sought.

The condition given by Eq. 9.4-10 leads to:

$$P_n = A_n \cos[\lambda_n (B - b)]. \quad (\text{A4-12})$$

Substitution of Eqs. A4-7, A4-10 and A4-11 in Eq. A4-1 gives:

$$(\mu + \lambda_n^2) P_n - \sqrt{\mu + \lambda_n^2} \alpha_1 P_n + \alpha_2 P_n + \alpha_3 A_n \lambda_n \sin[\lambda_n (B - b)] = 0. \quad (\text{A4-13})$$

Combining Eq. A4-12 and A4-13 leads to the following equation for the λ_n :

$$(\mu + \lambda_n^2)P_n - \sqrt{\mu + \lambda_n^2} \alpha_1 P_n + \alpha_2 P_n + \alpha_3 P_n \lambda_n \tan[\lambda_n (B - b)] = 0. \quad (\text{A4-14})$$

In order to evaluate the λ_n , it is noted that, if λ_n is a root, then so too is $-\lambda_n$, although because of the inherent symmetries, just one of these needs to be employed. A detailed numerical study has revealed that generally there exists a solitary λ_n on the positive imaginary axis, and many real, positive λ_n . Indeed replacement of the trigonometric function in Eq. A4-14 by its corresponding series representation confirms that λ_n^2 must be either real or complex conjugate pairs (the only exception being the degenerate case when $u' = 0$ and $D' + a_L u' = D$ (in effect, the case of a homogeneous Opalinus Clay), which leads to $\lambda_0 = 0$).

Using these features, a code has been written to obtain a user-specified number (N) of eigenvalues, λ_n .

Once the λ_n have been evaluated, it is then necessary to evaluate the coefficients C_n . These are evaluated by imposing the boundary condition at $x = 0$ (Eq. 9.4-8), namely that:

$$C|_{x=0} = \sum_{n=0}^{\infty} A_n \cos \lambda_n z' = C_0. \quad (\text{A4-15})$$

Eq. A4-15 does not have the orthogonality property of a standard Fourier expansion, and so no explicit expressions for the A_n are, in general, possible. Instead, the A_n are determined by the numerical solution of an $N \times N$ set of linear equations. These are derived using the collocation method, imposing the condition given by Eq. A4-15 at N selected points along the z' -direction.

Having obtained the λ_n and the A_n , the concentrations C and P can be obtained using Eqs. A4-7, A4-10, A4-11 and A4-12.

Appendix 5: Selection of Safety-Relevant Radionuclides

In the safety assessment, it is necessary to consider all radionuclides with the potential to give rise to significant radiation doses following disposal of waste in the repository, or the parents of such radionuclides. The number of radionuclides present in the inventory is prohibitively large for detailed model-chain calculations to be performed for all of them. A set of radionuclides for consideration in the present assessment has therefore been selected by means of a simple screening analysis which takes account of:

- a period of complete containment of radionuclides;
- a generic duration of near field release;
- dilution in the Quaternary aquifer;
- ingestion of contaminated aquifer water (drinking water dose).

The solubility limitation in the near field, transport and sorption of radionuclides in bentonite (SF/HLW) and cementitious materials (ILW), retardation in the geological barriers, accumulation of radionuclides in the surface environment and dose pathways other than ingestion of drinking water are neglected. The selection of safety-relevant radionuclides is an iterative process. In a first step, the set of safety-relevant radionuclides is selected on the basis of provisional datasets (inventory, dilution rate, etc.) and, thereafter, provisional model calculations are performed for the selected radionuclides. In a second step, the selection is revised and finalised, based on definitive datasets and on the results of provisional model calculations. Only then are the definitive model calculations performed for the final selection of safety-relevant radionuclides.

The safety-relevant radionuclides are selected according to their drinking water dose, $D^{(i)}$ [mSv a^{-1}] calculated by:

$$D^{(i)} = \frac{N^{(i)} I_{\text{wat}} D_{\text{ing}}^{(i)}}{T_c Q}$$

where:

- $N^{(i)}$ [Bq] is the inventory of radionuclide i at failure time (i.e. end of complete containment). For SF/HLW and ILW, the failure time is set at 1 000 years and 100 years, respectively.
- T_c is a generic duration of near field release. In the case of SF/HLW, the generic release duration is taken to be 1000 years, based on extremely pessimistic assumptions regarding waste dissolution and near field transport times. In the case of ILW, a generic near field release duration of 100 years is assumed.
- Q is the water flow in Quaternary aquifer, set at $10^6 \text{ m}^3 \text{ a}^{-1}$;
- I_{wat} is the total annual drinking water intake by an individual, set at $0.73 \text{ m}^3 \text{ a}^{-1}$;
- $D_{\text{ing}}^{(i)}$ is the effective dose per unit ingestion of radionuclide i , [mSv Bq^{-1}].

All activation and fission products for which the dose is greater than $10^{-5} \text{ mSv a}^{-1}$ are selected as being relevant to safety. This value is four orders of magnitude below the regulatory guideline of 0.1 mSv a^{-1} . Additionally, ^3H , ^{90}Sr and ^{137}Cs are included in the list of safety-relevant radio-

nuclides. They serve as indicators for phenomena that occur at relatively early times after the end of emplacement (e.g. pinhole release for defective SF/HLW canisters). The selection of safety-relevant activation and fission products for SF/HLW/ILW are summarised in Tab. A5-1. Short-lived daughter radionuclides not appearing in Tab. A5-1 are implicitly taken into account by adding their dose coefficients to the longer-lived parent radionuclide (see Tab. A5-3). This corresponds to the assumption of equilibrium between daughter and parent radionuclide. The dose contributions of some daughter radionuclides are negligible, because their dose coefficients are very small relative to the parent (e.g. ^{108}Ag , ^{137}Ba).

The actinide chains $4N$, $4N+1$, $4N+2$ and $4N+3$ are considered to be safety-relevant, irrespective of any safety criterion (Tab. A5-2). Decay-chain branching ($4N+2$) and recombination ($4N$, $4N+2$) are explicitly taken into account in the codes STMAN, PICNIC and TAME. Short-lived daughter radionuclides not appearing in Tab. A5-2 are implicitly taken into account by adding their dose coefficients to the longer-lived parent radionuclides (see Tab. A5-3).

The basis of Nagra's database of dose coefficients is the revised Swiss "Strahlenschutzverordnung" (StSV 1994). Data not available in StSV (1994) are taken from ICRP (1996), because ICRP (1996) is the original source from which the values in StSV (1994) were derived.

A potential source of bias arises in the treatment of ^{222}Rn in the $4N + 2$ chain, which is assumed to be in radioactive equilibrium with its parent throughout the assessment model chain. ^{222}Rn is the immediate daughter of ^{226}Ra and is a noble gas with a half-life of about 4 days; it decays through a series of very short-lived radionuclides (half-lives 27 minutes or less) to ^{210}Pb (half-life 22.3 years). The assumption of radioactive equilibrium effectively ignores any transport of ^{222}Rn from its point of origin to its point of decay. This assumption is valid in the near field and geosphere, and between the majority of biosphere compartments, where transport times are considerably greater than 4 days. If ^{226}Ra is present in the soil, then a fraction of the ^{222}Rn produced could escape to the air before decaying. This could have either favourable or unfavourable consequences for safety, depending on whether the ^{222}Rn is quickly dispersed in the atmosphere, or accumulates, for example, in buildings. It is currently estimated that the net bias due to the assumption of ^{222}Rn equilibrium in biosphere modelling is small, but this is an issue that might deserve attention in future assessment calculations.

Tab. A5-1: (Cont.)

Nuclide	OPA (this assessment)			KRI-I	NGB	Nagra 91	B	D		F		FIN	GB	J	NL	S		USA
	SF	HLW	ILW	HLW	HLW	ILW	1	HLW	ILW	HLW	ILW	SF	ILW	HLW	2	SF	ILW	3
¹³⁷ Cs	✓	✓	✓			✓	✓	✓	✓			✓	✓	✓	✓	✓	✓	
¹³³ Ba																	✓	
¹³⁷ Ba																✓		
¹⁴⁶ Pm																✓		
¹⁴⁷ Pm																✓	✓	
¹⁴⁷ Sm							✓	✓	✓					✓	✓			
¹⁵¹ Sm	✓	✓	✓				✓					✓		✓	✓	✓	✓	
¹⁵² Eu																✓	✓	
¹⁵⁴ Eu			✓				✓								✓	✓	✓	
¹⁵⁵ Eu																✓	✓	
^{166m} Ho	✓	✓														✓	✓	

Note: 1 HLW + ILW
 2 HLW + ILW + L / ILW
 3 SF + HLW

Tab. A5-2: List of safety-relevant actinide decay chain members for the present assessment

Decay-chain branching (4N+2) and recombination (4N, 4N+2) are explicitly taken into account. Short-lived daughter radionuclides not appearing in the table are implicitly taken into account by adding their dose coefficients to their longer-lived parent radionuclides.

4N	4N+1	4N+2	4N+3
²⁴⁴ Cm	²⁴⁵ Cm	²⁴⁶ Cm	²⁴³ Cm
²⁴⁰ Pu	²⁴¹ Pu	^{242m} Am	²⁴³ Am
²³⁶ U	²⁴¹ Am	²⁴² Pu	²³⁹ Pu
²³² U	²³⁷ Np	²³⁸ Pu	²³⁵ U
²³² Th	²³³ U	²³⁸ U	²³¹ Pa
²²⁸ Ra	²²⁹ Th	²³⁴ U	²²⁷ Ac
²²⁸ Th		²³⁰ Th	
		²²⁶ Ra	
		²¹⁰ Pb	
		²¹⁰ Po	

Tab. A5-3: Dose conversion factors (ingestion/inhalation) for activation and fission products and actinide decay chains, compiled from StSV (1994) and supplemented with ICRP (1996)

Short-lived daughter radionuclides are implicitly taken into account by adding their dose conversion factor to the longer-lived parent radionuclide. The dose contributions of some daughter radionuclides (in brackets) are negligible, either because their dose conversion factors are very small relative to the parent or because they are nearly stable.

Nuclide	Dose conversion factors for inhalation [Sv/Bq]	Dose conversion factors for ingestion [Sv/Bq]	Daughters included in the dose conversion factors (negligible contributions from daughters in brackets)
³ H	2.6×10^{-10}	4.2×10^{-11}	none
¹⁰ Be	3.5×10^{-8}	1.1×10^{-9}	none
¹⁴ C	5.8×10^{-9}	5.8×10^{-10}	none
³⁶ Cl	7.3×10^{-9}	9.3×10^{-10}	none
⁴¹ Ca	1.8×10^{-10}	1.9×10^{-10}	none
⁶⁰ Co	3.1×10^{-8}	3.4×10^{-9}	none
⁵⁹ Ni	4.4×10^{-10}	6.3×10^{-11}	none
⁶³ Ni	1.3×10^{-9}	1.5×10^{-10}	none
⁷⁹ Se	6.8×10^{-9}	2.9×10^{-9}	none
⁹⁰ Sr	1.6×10^{-7}	3.1×10^{-8}	⁹⁰ Y
⁹³ Zr	2.5×10^{-8}	1.1×10^{-9}	none
^{93m} Nb	1.8×10^{-9}	1.2×10^{-10}	none
⁹⁴ Nb	4.9×10^{-8}	1.7×10^{-9}	none
⁹³ Mo	2.3×10^{-9}	3.1×10^{-9}	none
⁹⁹ Tc	1.3×10^{-8}	6.4×10^{-10}	none
¹⁰⁷ Pd	5.9×10^{-10}	3.7×10^{-11}	none
^{108m} Ag	3.7×10^{-8}	2.3×10^{-9}	none (¹⁰⁸ Ag)
^{121m} Sn	4.7×10^{-9}	5.6×10^{-10}	¹²¹ Sn
¹²⁶ Sn	2.8×10^{-8}	5.1×10^{-9}	^{126m} Sb, (¹²⁶ Sb)
¹²⁹ I	3.6×10^{-8}	1.1×10^{-7}	none
¹³⁵ Cs	8.6×10^{-9}	2.0×10^{-9}	none
¹³⁷ Cs	3.9×10^{-8}	1.3×10^{-8}	none (^{137m} Ba)
¹⁵¹ Sm	4.0×10^{-9}	9.8×10^{-11}	none
¹⁵⁴ Eu	5.3×10^{-8}	2.0×10^{-9}	none
^{166m} Ho	1.2×10^{-7}	2.0×10^{-9}	none
²¹⁰ Pb	5.7×10^{-6}	6.9×10^{-7}	²¹⁰ Bi (²⁰⁶ Hg, ²⁰⁶ Tl)
²¹⁰ Po	4.3×10^{-6}	1.2×10^{-6}	none
²²⁶ Ra	9.5×10^{-6}	2.8×10^{-7}	²¹⁴ Pb, ²¹⁴ Bi (²¹⁸ Po, ²¹⁸ At, ²¹⁴ Po, ²¹⁰ Tl)
²²⁸ Ra	1.6×10^{-5}	6.9×10^{-7}	²²⁸ Ac

Tab. A5-3: (Cont.)

Nuclide	Dose conversion factors for inhalation [Sv/Bq]	Dose conversion factors for ingestion [Sv/Bq]	Daughters included in the dose conversion factors (negligible contributions from daughters in brackets)
²²⁷ Ac	5.7×10^{-4}	1.2×10^{-6}	²²⁷ Th, ²²³ Ra, ²¹⁵ Po (²¹⁹ At, ²¹⁵ Bi, ²¹¹ Pb, ²¹¹ Bi, ²⁰⁷ Tl, ²¹¹ Po)
²²⁸ Th	4.4×10^{-5}	1.4×10^{-7}	²²⁴ Ra, ²¹² Pb, ²¹² Bi (²¹⁶ Po, ²⁰⁸ Tl, ²¹² Po)
²²⁹ Th	2.6×10^{-4}	6.1×10^{-7}	²²⁵ Ra, ²²⁵ Ac, ²¹³ Bi (²²¹ Fr, ²¹⁷ At, ²¹³ Po, ²⁰⁹ Tl, ²⁰⁹ Pb)
²³⁰ Th	1.0×10^{-4}	2.1×10^{-7}	none
²³² Th	1.1×10^{-4}	2.3×10^{-7}	none
²³¹ Pa	1.4×10^{-4}	7.1×10^{-7}	none
²³² U	3.7×10^{-5}	3.3×10^{-7}	none
²³³ U	9.6×10^{-6}	5.1×10^{-8}	none
²³⁴ U	9.4×10^{-6}	4.9×10^{-8}	none
²³⁵ U	8.5×10^{-6}	4.7×10^{-8}	²³¹ Th
²³⁶ U	8.7×10^{-6}	4.7×10^{-8}	none
²³⁸ U	8.0×10^{-6}	4.8×10^{-8}	²³⁴ Th (²³⁴ Pa, ^{234m} Pa)
²³⁷ Np	5.0×10^{-5}	1.1×10^{-7}	²³³ Pa
²³⁸ Pu	1.1×10^{-4}	2.3×10^{-7}	none
²³⁹ Pu	1.2×10^{-4}	2.5×10^{-7}	none
²⁴⁰ Pu	1.2×10^{-4}	2.5×10^{-7}	none
²⁴¹ Pu	2.3×10^{-6}	4.8×10^{-9}	none (²³⁷ U)
²⁴² Pu	1.1×10^{-4}	2.4×10^{-7}	none
²⁴¹ Am	9.6×10^{-5}	2.0×10^{-7}	none
^{242m} Am	9.7×10^{-5}	2.0×10^{-7}	²³⁸ Np, ²⁴² Am, ²⁴² Cm
²⁴³ Am	9.6×10^{-5}	2.0×10^{-7}	²³⁹ Np
²⁴³ Cm	6.9×10^{-5}	1.5×10^{-7}	none
²⁴⁴ Cm	5.7×10^{-5}	1.2×10^{-7}	none
²⁴⁵ Cm	9.9×10^{-5}	2.1×10^{-7}	none
²⁴⁶ Cm	9.8×10^{-5}	2.1×10^{-7}	none

Appendix 6: Semi-Quantitative Dose Estimate for the Periglacial Climate

A6.1 Introduction

There is strong evidence that within the next one million years, the climate in northern Switzerland will continue to change between glacial and interglacial periods ("icehouse", Nagra 2002c). This expectation is based on the assumption that past and future human activities may perturb, but not completely alter, the long-term major climatic cycles. During the transition between interglacial and glacial periods, a periglacial climate (e.g. tundra climate) may develop in northern Switzerland (Burga & Perret 1998). This note evaluates potential effects of periglacial conditions on the calculated doses.

Under a periglacial climate different ecosystems may develop, e.g. polar desert, steppe, tundra, boreal forest. Periglacial conditions as presently found in the arctic region are used as an example for situations which could occur in northern Switzerland during glacial periods.

Early studies concerning radioactive fallout from nuclear bomb testing already showed that the doses of populations in the arctic region from caesium isotopes were significantly higher than the doses received by populations in temperate climates (see review by Wicker & Pinder, 2002). A large number of recent studies have provided new information and better understanding of the behaviour of radionuclides in the arctic region. Several conferences have been held. Three articles presented at a recent conference are used as a basis to evaluate the effects of periglacial conditions on biosphere modelling (Strand et al. 2002, Travnikova et al. 2002, Howard et al. 2002).

A6.2 Specific features of arctic biospheres

Low temperatures, low precipitation rates and permafrost are some of the characteristics of arctic environments. Technological agricultural production as practised in Western Europe is of no or only of minor importance. The diets of populations in the arctic region depend to a significant extent on vegetation and fauna of natural and semi-natural environments, e.g. berries, mushrooms, fish and reindeer. The products from technological agriculture and in particular from arable production methods (e.g. potatoes, grain) are all imported (Strand et al. 2002).

The net annual production rate of vegetation (e.g. in kg dry matter per m²) in natural and semi-natural ecosystems is significantly lower than the production rate of modern technological agriculture. These ecosystems are characterised by low input rates of major and sometimes also of minor nutritional elements. These nutrients are recycled within the ecosystem to minimise losses (e.g. leaching from the rooting zone). In such environments also the losses of the radionuclides of caesium and strontium are much smaller than in environments in which technological agriculture is practised. As a consequence, the doses from a radioactive contamination are higher and stay longer at a high level in such environments than under technological agricultural production methods (for the same level of contamination per m²).

In addition to the generic characteristics of natural and semi-natural environments discussed in the previous paragraph, another important food chain in arctic environments is the atmospheric deposition → lichen → animal (e.g. reindeer) → humans pathway. Lichens are efficient collectors of atmospheric deposition and can, because of their longevity, integrate this deposition over several years. Especially in winter, lichens often serve as a major food supply for herbivores.

A6.3 Comparison of release and biosphere transport processes in the arctic region

As discussed in section A6.2, natural and semi-natural environments are of major importance as locally produced food in the diet of humans living in the arctic region. Transfer of radionuclides through food chains in these environments are discussed in this section.

Most of the information about radionuclide behaviour in the arctic region is from releases from bomb testing and from Chernobyl. The contamination occurs through atmospheric dispersion and deposition (fallout) on vegetation or soil. Important pathways are: atmospheric deposition → vegetation (→ animals) → humans and atmospheric deposition → soil → vegetation (→ animals) → humans. Other releases of importance for present arctic environments are releases to the marine environment. For future periglacial conditions in Switzerland these are not relevant and therefore they are not discussed here.

The major release mechanism of radionuclides from a deep radioactive waste repository into the biosphere is through the exfiltration of deep groundwater from geological aquifers into either surface water or into Quaternary aquifers. Under arctic conditions both infiltration and exfiltration may be limited by permafrost. Nevertheless exfiltration of deep groundwater can occur through unfrozen surface water or groundwater into the biosphere. Thus the release of radionuclides into an arctic biosphere environment is possible, but is expected to be limited. Important exposure pathways are groundwater → soil → vegetation (→ animals) → humans and direct consumption of water by animals and humans.

Under periglacial conditions precipitation is significantly reduced. Due to the low temperatures and the low precipitation, large areas may be bare of vegetation. Therefore a secondary mechanism of contamination may become significant: soil material originally contaminated through groundwater may be transported by wind through the atmosphere. The soil → atmosphere → lichen → animal → humans pathway could so become significant, in addition to the pathways groundwater → soil → vegetation (→ animals) → humans.

Contamination of lichens from the atmosphere leads to higher doses than atmospheric deposition onto soil under natural or semi-natural conditions. A contamination originating from groundwater release would probably cause locally higher doses through the groundwater → soil pathways. However, as these might be significantly reduced due to the frozen ground, the pathways through lichen might still be significant, in particular, if contamination through groundwater is totally stopped and the contamination in the soil is caused by radionuclides released during previous warmer climates.

Tab. A6.3-1: Overview of different contamination mechanisms

	Fallout from bomb testing and Chernobyl	Release from radioactive waste repository	
release / input into biosphere	atmospheric deposition	groundwater release	contaminated soil transported by wind
duration of the input	years	centuries	centuries
radioactive elements	Cs, Sr	large range (e.g. I, Cl, Cs, actinides)	
area of input	world wide	order of km ²	order of 10 to 100 km ²

A6.4 Comparison of critical groups in a periglacial climate with the reference biosphere

Transfer of radionuclides in the biosphere and through the different exposure pathways will strongly depend on the type of environment including the climate and the type of foods produced and consumed. For different climates different critical groups can be defined. The Reference Case biosphere (described in Chapter 8) is based on a critical group living in the area in which the highest concentration of radionuclides released into the biosphere occur. A present-day diet and present-day agricultural practices are assumed, but a conservative assumption is that all food and drinking water is produced locally in the area with the highest concentrations. For a periglacial climate two critical groups can be defined: 1) a community consuming a relatively large amount of products from natural and semi-natural environments and 2) a community which consumes also a large amount of products from natural and semi-natural environments but which, in addition, breeds reindeer and consumes reindeer products.

Tab. A6.4-1: Characteristics of different communities / critical groups (in the framework of the assessment of radioactive waste disposal)

	Present agricultural production methods	Relying on products from natural and semi-natural environments	Lichen → reindeer → humans
Supply of nutrient elements	high	low	low
Losses of nutrient elements	high	low	low
Area required for food for one person (rough estimate)	in the order of 0.01 km ²	in the order of 0.1 km ²	in the order of 1 km ²
Transfer of radionuclides to consumed products	relatively low	relatively high	relatively high
Major transfer pathways of contamination	soil to plant transfer	soil to plant transfer	atmospheric deposition

A6.5 Semi-quantitative evaluation

Using information given in the review of Strand et al. (2002) doses can be compared for (1) populations with significant input from the lichen → reindeer → humans pathway, (2) populations with a major input from natural and semi-natural environments and (3) general populations in Western Europe and North America, assuming the same level of contamination with caesium and strontium radionuclides.

Tab. A6.5-1: Relative doses for different populations for the same level of contamination

Technological agricultural production	1
Major contribution from natural and semi-natural environments	2 - 30
Major contribution from atmosphere → lichen → reindeer → humans pathway	10 - 40

The net production rate of vegetation in arctic environments is significantly lower than of crops produced with technological agricultural methods under a temperate climate. Also a larger area of primary production is required when the fraction of animal products in the diet is larger as is the case for a population raising reindeer. For the other biosphere scenarios, critical groups or communities of approximately 100 persons have been defined. Such a group would, under a temperate climate and present-day agricultural production methods (the Reference Case biosphere), require an area of a few square kilometres for food production. Under a periglacial climate, the same amount of food production would require a few hundred square kilometres.

In the other biosphere areas discussed in Chapter 8, it is assumed that the area in which the highest accumulation of radionuclides occurs is in the order of 1 km². Assuming that, under periglacial conditions, the primary contamination also occurs in an area of 1 km², this area could only provide about 1 % of the food required for a community of about 100 persons and the rest of the food would be uncontaminated. An average individual of the critical group or community would thus only receive 1 % of the dose which would be calculated for an individual consuming only contaminated food.

Whereas, under a periglacial climate, the transfer to food products might be significantly higher than under a temperate climate and with present technological agricultural production methods, concentrations in drinking water for humans and animals would only be affected by the hydrological regime. Variations in the hydrological regime due to different climates have been studied as parameter variation of the Reference Case biosphere and are not further discussed here (see Chapter 8).

Tab. A6.5-2: Comparison of biosphere scenarios (Strand et al. 2002)

Biosphere scenario	Reference Case biosphere	Periglacial biosphere scenario
Transfer of radionuclides to humans for the same concentration in the biosphere (relative units)	1	2 - 40
Net productivity of vegetation (relative units)	1	0.005 - 0.02
Total amount of radioactivity released into the modelled biosphere (relative units)	1	< or = 1
Average concentration in food for the same total amount of released radioactivity (relative units)	1	0.01 - 0.8
Dose to an average individual of the critical group (relative units)	1	0.01 - 0.8

The highest rate of transfer of radionuclides to humans might occur for the pathway atmosphere → lichen → reindeer → humans. Atmospheric transfer of radionuclides is only possible under very dry conditions and would involve a further dilution of the radioactivity introduced into the biosphere by groundwater.

Appendix 7: The Applicability of the One-Dimensional Approximation for Modelling Transport through the Opalinus Clay

A7.1 Introduction

In order to evaluate radionuclide release and transport, the geometry of the repository near-field/geosphere system is simplified. The purpose of this appendix is to assess whether the simplifications used can have significant effects on calculated releases.

For model chain calculations using the STMAN suite of codes and PICNIC, as well as for the barrier efficiency models described in Section 9.3, the Opalinus Clay is treated as a one-dimensional layer. Releases from the bentonite surrounding the SF / HLW packages and from the ILW cementitious region occur along the lower boundary of this layer and releases across the top boundary are evaluated. The bentonite surrounding the SF / HLW packages is treated as a homogeneous annular cylinder.

This geometrical simplification means, in effect, that the only transport path that is explicitly considered through the Opalinus Clay is one that starts at the uppermost point of the bentonite annulus and extends for 40 m vertically upwards to the top boundary of the Opalinus Clay. In reality, the vertical transport distance varies slightly according to the point of release from the bentonite annulus. It should also be noted that perturbations to groundwater flow in the Opalinus Clay caused by the presence of the repository near field are neglected when carrying out the geometrical simplification. Furthermore, in cases where diffusive transport is dominating over advective transport, some radionuclides will migrate downwards, even if the hydraulic gradient drives advective transport in the opposite direction, and will be released from the lower boundary of the Opalinus Clay.

Since the models are required to evaluate releases that are spatially integrated in the horizontal plane, the neglect of horizontal diffusion and transverse dispersion is unimportant.

A7.2 Method to evaluate the applicability of the one-dimensional approximation

The code FRAC3DVS is used to assess the effects of the simplifications described above. FRAC3DVS is applied over the two-dimensional domain illustrated in Fig. A7.2-1, which includes both the Opalinus Clay and the SF / HLW bentonite annulus. FRAC3DVS is not used in this way to model the assessment cases because it cannot take account of solubility limits, which are important for many safety-relevant radionuclides.

The code SPENT (a member of the STMAN suite of codes used to model near field release and transport in the case of spent fuel, see Appendix 1) is used to calculate radionuclide release rates of some example radionuclides at the inner boundary of the FRAC3DVS model domain, which corresponds approximately to the canister outer surface⁵⁹. The resulting release rates across the boundaries *AA'* and *BB'* (Fig. A7.2-1) are evaluated as functions of time using FRAC3DVS and summed together. The example radionuclides that are chosen are not expected to reach their solubility limits anywhere within the modelled system.

⁵⁹ In order to apply FRAC3DVS to this problem, radionuclides are, in fact, released at a small distance outside the canister and inside the bentonite annulus.

In the Reference Case, SPENT is used to calculate radionuclide release rates at the outer boundary of the bentonite annulus, and, by applying the one-dimensional approximation, PICNIC is used to evaluate the release rates from the Opalinus Clay. A comparison of results calculated using FRAC3DVS and PICNIC gives an indication of the magnitude of the effects of the one-dimensional approximation.

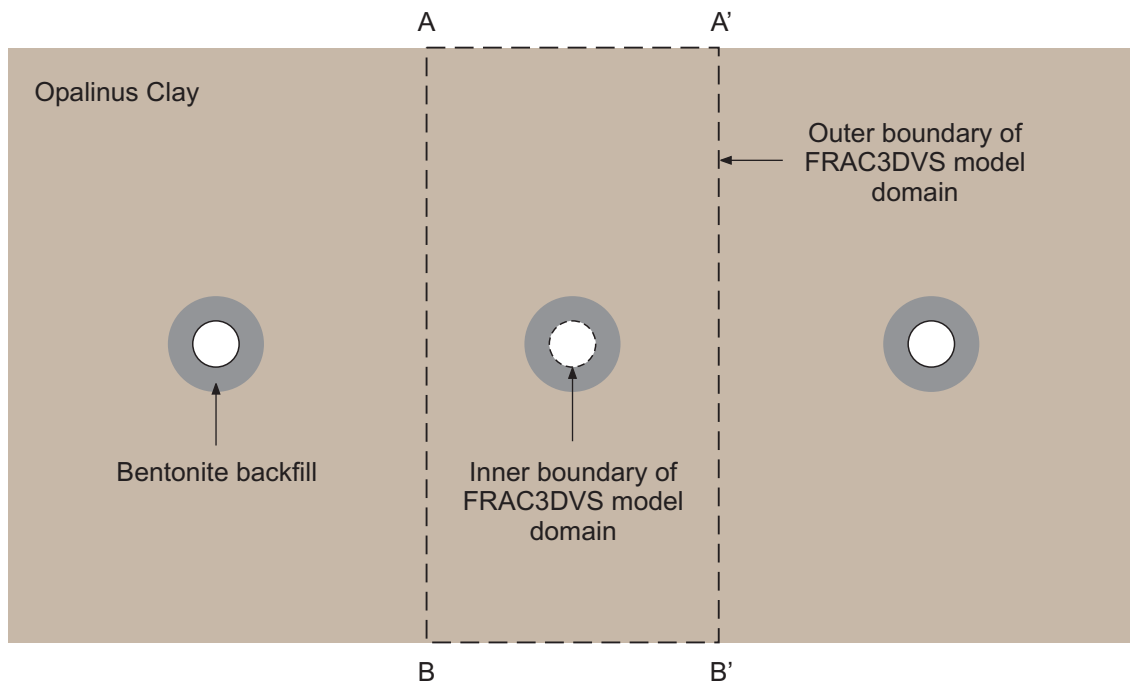


Fig. A7.2-1: The two-dimensional domain modelled using FRAC3DVS

A7.3 Boundary conditions and data

The physico-chemical data used for this exercise are the same as those of the Reference Case. Boundary conditions and geometrical parameters for the FRAC3DVS calculation are summarised in Tab. A7.3-1.

Tab. A7.3-1: Boundary conditions and geometrical parameters for FRAC3DVS

Boundary	Length [m]	Hydraulic boundary condition	Mass transport boundary condition
<i>AA'</i> and <i>BB'</i>	40 m	fixed head	zero concentration
<i>AB</i> and <i>A'B'</i>	80 m	no flow	zero gradient normal to boundary
inner boundary of FRAC3DVS domain	1.05 m (diameter)	no flow	mass flow from SPENT calculation

A7.4 Results and conclusion

Tab. A7.4-1 gives the maximum release rates for a single canister and times of these maxima for the example radionuclides, evaluated using PICNIC (i.e. applying the one-dimensional approximation) and using FRAC3DVS.

Tab. A7.4-1: Maximum release rates and times of these maxima for some example radionuclides, evaluated using PICNIC and using FRAC3DVS

Radionuclide	PICNIC results		FRAC3DVS results	
	max. release rate [mol a ⁻¹]	time of max. [a]	max. release rate [mol a ⁻¹]	time of max. [a]
¹⁴ C _{org}	5.9×10^{-8}	4.5×10^4	4.5×10^{-8}	4.5×10^4
⁴¹ Ca	2.8×10^{-10}	6.3×10^5	2.6×10^{-10}	6.3×10^5
³⁶ Cl	1.9×10^{-5}	3.2×10^5	1.4×10^{-5}	3.6×10^5
¹²⁹ I	2.3×10^{-4}	1.3×10^6	2.2×10^{-4}	1.3×10^6
⁷⁹ Se	6.3×10^{-7}	1.3×10^6	5.3×10^{-7}	1.4×10^6

The one-dimensional approximation gives similar results to the geometrically more realistic FRAC3DVS model. FRAC3DVS release maxima are, however, slightly lower and occur at slightly later times. This modelling exercise thus gives strong support for the applicability of the one-dimensional approximation. Discrepancies introduced by the approximation are shown to be small and to err on the side of conservatism.

Appendix 8: Quality Assurance Measures

The performance assessment calculations and the corresponding preparatory work are conducted within the framework of the Nagra Quality Management (QM) System and take into account the requirements defined by the quality assurance guidelines discussed below. The Nagra Quality Management System is based on the following principles and corresponding general Quality Assurance Procedures:

1. The starting point to ensure sufficient quality (i.e. no unacceptable deviations from the planned scope of work) is based on a **Company Policy** that ensures that the work is conducted by persons that are sufficiently qualified for their work and have the necessary tools, that are fully aware of the expectations and take full responsibility for their work. The requirement of sufficiently qualified persons applies both to the Nagra staff involved as well as to personnel of contractors.
2. Through a **Project Plan** developed at the start of the project, all persons involved in the project are fully aware of the aims and boundary conditions of their work (definition and analysis of mission of project and identification of sub-projects), are clear about the responsibility they have within the project (organisation of project), and know the interrelations between the different activities/sub-projects within the project, the timing of these activities and the expected deliverables. The Project Plan also defines the need for Project Plans for sub-projects and identifies for which activities/(sub-)projects a Quality Assurance Plan is needed. If needed, the Project Plan is updated.
3. With the **Quality Assurance Plan** developed early in the project, it is clearly defined what QA measures are required for which activity/(sub-)project by whom and at what stage in the project (a priori definition) and the QA measures conducted are clearly documented (a posteriori documentation). The need for a (a priori) Quality Assurance Plan for (sub-)projects is defined in the Project Plan. The quality assurance measures identified in the Quality Assurance Plan can either be defined by specific Quality Assurance Guidelines or can specifically be defined. If needed, the Quality Assurance Plan is updated. An integral part of the QA measures is the requirement of a peer review for all Nagra Technical Reports.
4. Thanks to a **Project Documentation** that is continuously updated all persons involved are fully aware of the relevant documents for the project. For this purpose a documentation structure is defined, a centralised catalogue of all relevant documents is maintained and all those documents catalogued that are not readily available (e.g. Nagra internal notes) are archived. At the end of the project all documents entered into the project documentation are checked for their relevance to ensure that the documents needed for traceability of the project are properly catalogued and available for any future use.
5. With a rigorous **Data Clearance Process** it is ensured that throughout the whole Project *Entsorgungsnachweis* suitable and consistent data are used. Data are always cleared for a certain purpose and for specific (sub-)projects/users. It is the duty of a data user to initiate the clearance process for a specific purpose and to ask the data producer to deliver the data in a suitable document, together with a Data Clearance Form, to the clearance group for processing. The clearance group ensures (by expert judgement) that the data are adequate for the intended purpose. If the data are especially important, additional QM measures (e.g. peer review) are implemented in the process of compiling / producing the data to be cleared. Whenever any planned updates, new findings or errors detected in the course of the project need to be considered, a revised Data Clearance Form and supporting document is issued

and submitted again to the clearance group for processing (see above). The Data Clearance Process ensures that all data users are made aware of such a revision. This forms the basis for further actions; e.g. a re-calculation of the affected assessment cases. Such further actions are, however, not part of the Data Clearance Process. If required, they are initiated by the project manager in charge.

6. To ensure the effectiveness of the QM system, **Audits** are performed to check if the procedures are followed and if there is a need to modify or enhance the existing QM system. If any deficiencies are detected, appropriate measures are taken by the project manager in charge.
7. For individual working steps **Specific Working Procedures** are defined that may include **Specific Quality Assurance Measures** (defined in specific **Quality Assurance Guidelines**). For the performance assessment calculations within Project *Entsorgungsnachweis* the following specific quality assurance guidelines were included:
 - 7.1 **Performing PA Calculations:** The adequacy of the codes for the calculations at hand needs to be checked (explicit/implicit consideration of FEPs, acceptable simplifications) and the codes need to be verified to the extent required by the problem. Additionally, the system for storing / archiving of all the files needs to be defined; this includes a clear strategy for the use of file-identifiers. Where appropriate, computer runs should also produce log-files to ensure traceability of the calculations performed. The input data to the computer calculations must have passed the Data Clearance Process.
 - 7.2 **Checking PA Calculations:** This includes checking the appropriateness of conceptual models, of mathematical models (e.g. equations, initial and boundary conditions), of numerical solution techniques, of input data and of results and arguments. This involves plausibility checks (e.g. comparison with information from other performance assessment studies and for numerical results comparison with results from other analyses or other cases) and can additionally require independent calculations (simplified or equally complex), considerations based on the same method / on the same approach, or - in the extreme case - a calculation with a different method or considerations based on a different approach. The checks may be done by the same person that has done the original work, by another person of the same organisation, or by an independent "third" person.
 - 7.3 **Maintenance of PA Computer Programmes:** With specific measures it is ensured that the compiled version of a code operates as defined. Specific checks are needed when the code has been modified (e.g. adaptations for new computer system) or modifications e.g. to the input-/output procedures have been made. For this purpose, for each important code a log-book is maintained in which the person responsible for the code is identified, in which modifications to the code are documented and in which the results of benchmark tests, e.g. after modifications to the code, are documented.